



University of Banja Luka
Faculty of Mechanical Engineering



DEMI 2021

**15th International Conference on
Accomplishments in Mechanical and
Industrial Engineering**

PROCEEDINGS



Banja Luka, 28 - 29 May 2021

University of Banja Luka
Faculty of Mechanical Engineering

**PROCEEDINGS
DEMI 2021**

Banja Luka, May 2021

**15th INTERNATIONAL CONFERENCE ON ACCOMPLISHMENTS IN
MECHANICAL AND INDUSTRIAL ENGINEERING**

DEMI 2021

Supported by:

MINISTRY OF SCIENTIFIC AND TECHNOLOGICAL DEVELOPMENT,
HIGHER EDUCATION AND INFORMATION SOCIETY OF THE REPUBLIC OF SRPSKA

Organizer and publisher:

FACULTY OF MECHANICAL ENGINEERING
UNIVERSITY OF BANJA LUKA

Co-organizer:

FACULTY OF MECHANICAL ENGINEERING,
UNIVERSITY OF NIŠ, SERBIA

FACULTY OF MECHANICAL ENGINEERING PODGORICA,
UNIVERSITY OF MONTENEGRO, MONTENEGRO

FACULTY OF ENGINEERING,
HUNEDOARA, ROMANIA

FACULTY OF ENGINEERING RESITA,
BABEŞ-BOLYAI UNIVERSITY, ROMANIA

For publisher:

Full. Prof. Aleksandar Milašinović, PhD

Editor in chief:

Assoc. Prof. Stevo Borojević, PhD

Executive editor:

Biljana Prochaska, MSc

ORGANIZING COMMITTEE

Chairman of the Organizing Committee: Assoc. Prof. Stevo Borojević, PhD, PhD, Faculty of Mechanical Engineering, University of Banja Luka

Full. Prof. Darko Knežević, PhD

Full. Prof. Aleksandar Milašinović, PhD

Assoc. Prof. Zorana Tanasić, PhD

Full. Prof. Igor Vušanović, PhD (Podgorica),

Assoc. Prof. Dejan Mitrović, PhD (Niš),

Assoc. Prof. Sorin Ioan Deaconu PhD, (Hunedoara, Rumunija),

Lecturer Relu Costel Ciubotariu, PhD (Rešica, Rumunija),

Assist. Prof. Branislav Sredanović, PhD

Assist. Prof. Bojan Knežević, PhD

Assist. Prof. Milovan Kotur, PhD

Sen. Assist. Saša Laloš, MSc

Sen. Assist. Danijela Kardaš, MSc

Sen. Assist. Gordana Tošić, MSc

Assist. Saša Tešić, MSc

EFL Lecturer Sanja Maglov, MSc

Biljana Prochaska, MSc

Boro Marić, BSc

Nedeljka Sladojević Putnik, BSc

Milivoj Stipanović.

SCIENTIFIC COMMITTEE

Chairman of the Scientific Committee: Prof. Đorđe Čiča, PhD, Faculty of Mechanical Engineering, University of Banja Luka

Prof. Darko Knežević, PhD, Faculty of Mechanical Engineering, University of Banja Luka; Prof. Radivoje Mitrović, PhD, Faculty of Mechanical Engineering, University of Belgrade; Prof. Vlastimir Nikolić, PhD, Faculty of Mechanical Engineering, University of Niš; Prof. Nenad D. Pavlović, PhD, Faculty of Mechanical Engineering, University of Niš; Prof. Igor Vušanović, PhD, Faculty of Mechanical Engineering Podgorica, University of Montenegro; Prof. Gelu Ovidiu Tirian, PhD, University Politehnica Timisoara, Romania; Prof. Gilbert-Rainer GILLICH, PhD, Faculty of Engineering Resita, Babeş-Bolyai University; Prof. Dejan Lukić, PhD, Faculty of Technical Sciences, University of Novi Sad; Prof. Saša Živanović, PhD, Faculty of Mechanical Engineering, University of Belgrade; Prof. Mijodrag Milošević, PhD, Faculty of Technical Sciences, University of Novi Sad; Prof. Aleksandar Milašinović, PhD, Faculty of Mechanical Engineering, University of Banja Luka; Prof. Izet Bjelonja, PhD, Faculty of Mechanical Engineering, University of Sarajevo; Senior Researcher Aleksander Michailov, PhD, OAO NPO "Saturn", Russia; Prof. Dorian Nedelcu, PhD, Faculty of Engineering Resita, Babeş-Bolyai University; Assist. Prof. Alexander Remizov Evgenyevich, PhD, Rybinsk State Aviation Technical University, Russia; Prof. Milan Zeljković, PhD, Faculty of Technical Sciences, University of Novi Sad; Prof. Franci Pušavec, PhD, Faculty of Mechanical Engineering, University of Ljubljana; Prof. Miodrag Manić, PhD, Faculty of Mechanical Engineering, University of Niš; Prof. Mileta Janjić, PhD, Faculty of Mechanical Engineering Podgorica, University of Montenegro; Assist. Prof. Davorin Kramar, PhD, University of Ljubljana, Slovenia; Prof. Simo Jokanović, PhD, Faculty of Mechanical Engineering, University of Banja Luka; Prof. Gordana Globočki-Lakić, PhD, Faculty of Mechanical Engineering, University of Banja Luka; Prof. Ardelean Erika, PhD, University Politehnica Timisoara, Romania; Prof. Petar Gvero, PhD, Faculty of Mechanical Engineering, University of Banja Luka; Prof. Slobodan Lubura, PhD, Faculty of Electrical Engineering, University of East Sarajevo; Prof. Sanda Midžić – Kurtagić, PhD, Faculty of Mechanical Engineering, University of Sarajevo; Assist. Prof. Srđan Vasković, PhD, Faculty of Mechanical Engineering, University of East Sarajevo; Prof. Dragica Milenković, PhD, Faculty of Mechanical Engineering, University of Niš; Prof. Bratislav Blagojević, PhD, Faculty of Mechanical Engineering University of Niš; Prof. Milan Radovanović, PhD, Faculty of Mechanical Engineering, University of Belgrade; Prof. Dragoslava Stojiljković, PhD, Faculty of Mechanical Engineering, University of Belgrade; Prof. Nebojša Manić, Ph, Faculty of Mechanical Engineering, University of Belgrade; Prof. Dunja Martinović, PhD, Faculty of Mechanical Engineering, University of Sarajevo; Prof. Milan Lečić, PhD, Faculty of Mechanical Engineering, University of Belgrade; Prof. Neven Duić, PhD, Faculty of Mechanical Engineering and Naval Architecture, University of Zagreb; Prof. Vojislav Novaković, PhD, NTNU, Norway;

Prof. Milan Rackov, PhD, Faculty of Technical Sciences, University of Novi Sad; Prof. Mirko Blagojević, PhD, Faculty of Engineering Sciences, University of Kragujevac; Prof. Nataša Trišović, PhD, Faculty of Mechanical Engineering, University of Belgrade; Prof. Mladimir Milutinović, PhD, Faculty of Technical Science, University of Novi Sad; Prof. Dražan Kozak, PhD, University of Josip Juraj Strossmayer in Osijek, Croatia; Prof. Predrag Kozić, PhD, Faculty of Mechanical Engineering, University of Niš; Prof. Dragan Milčić, PhD Faculty of Mechanical Engineering; University of Niš; Prof. Radoslav Tomović, PhD; Faculty of Mechanical Engineering Podgorica; University of Montenegro; Prof. Janko Jovanović, PhD; Faculty of Mechanical Engineering Podgorica; University of Montenegro; Prof. Nebojša Radić, PhD; Faculty of Mechanical Engineering; University of East Sarajevo; Prof. Valentina Golubović – Bugarski, PhD; Faculty of Mechanical Engineering; University of Banja Luka; Prof. Strain Posavljak, PhD; Faculty of Mechanical Engineering; University of Banja Luka; Prof. Dong Leiting, PhD; Beijing University of Aeronautics & Astronautics; China; Prof. Atul Bhaskar, PhD; University of Southampton; United Kingdom; Assist. Prof. Milan Rakita, PhD; Perdue University; USA; Prof. Halil Caliskan, PhD; Bartin University; Turkey; Prof. Socalici Ana, PhD; University Politehnica Timisoara; Romania; Prof. Milan Tica, PhD; Faculty of Mechanical Engineering; University of Banja Luka; Prof. Milan Bajić, PhD; Faculty of Mechanical Engineering; University of Niš; Prof. Zoran Bučevac, PhD; Faculty of Mechanical Engineering; University of Belgrade; Prof. Radiša Jovanović, PhD; ; Faculty of Mechanical Engineering; University of Belgrade; Prof. Aleksandar Sedmak, PhD; Faculty of Mechanical Engineering; University of elgrade; Prof. Branko Blanuša, PhD; Faculty of Electrical Engineering; University of Banja Luka; Prof. Marina Mijanović Markuš, PhD; Faculty of Mechanical Engineering Podgorica; University of Montenegro; Prof. Miroslav Rogić, PhD; Faculty of Mechanical Engineering; University of Banja Luka; Prof. Dejan Mitrović, PhD; Faculty of Mechanical Engineering; University of Niš; Prof. Goran Janevski, PhD; Faculty of Mechanical Engineering; University of Niš; Prof. Uroš Karadžić, PhD Faculty of Mechanical Engineering Podgorica; University of Montenegro; Prof. Milan Petrović, PhD; Faculty of Mechanical Engineering; University of Belgrade; Prof. Predrag Cosić, PhD; University of Zagreb; Croatia; Prof. Deaconu Sorin, PhD; University Politehnica Timisoara; Romania; Prof. Bordeasu Ilare, PhD; University Politehnica Timisoara; Romania; Prof. Zdravko Milovanović, PhD; Faculty of Mechanical Engineering; University of Banja Luka; Prof. dr Vinko Babić, PhD; Faculty of Mechanical Engineering; University of Banja Luka; Prof. Jovanka Lukić, PhD; Faculty of Engineering Sciences; University of Kragujevac; Prof. Dragan Taranović, PhD; Faculty of Engineering Sciences; University of Kragujevac; Prof. Goran Petrović, PhD; Faculty of Mechanical Engineering; University of Niš; Prof. Radoje Vujadinović, PhD; Faculty of Engineering Sciences; University of Kragujevac; Prof. Snežana Petković, PhD; Faculty of Mechanical Engineering; University of Banja Luka; Prof. Miodrag Hadžistević, PhD; Faculty of Technical Sciences; University of Novi Sad; Prof. Milorad Pantelić, PhD; Technical Faculty Čačak; University of Kragujevac; Prof. Bratislav Blagojević, PhD; Faculty of Mechanical Engineering; University of Niš; Prof. Peđa Milosavljević, PhD; Faculty of Mechanical Engineering; University of Niš; Prof.

Jelena Jovanović, PhD; Faculty of Mechanical Engineering Podgorica; University of Montenegro; Prof. Mladen Todić, PhD;; Faculty of Mechanical Engineering University of Banja Luka; Prof. Milija Krajišnik, PhD; Faculty of Mechanical Engineering; University of East Sarajevo; Prof. Ilija Ćosić, Emeritus; Faculty of Technical Sciences; University of Novi Sad; Prof. Zorana Tanasić, PhD; Faculty of Mechanical Engineering; University of Banja Luka; Prof. Mirko Soković, PhD, University of Ljubljana, Slovenia; Prof. Miroslav Bobrek, PhD; Faculty of Mechanical Engineering; University of Banja Luka; Prof. Goran Janjić, PhD; Faculty of Mechanical Engineering; University of Banja Luka; Prof. Igor Budak, PhD; Faculty of Technical Sciences; University of Novi Sad; Prof. Tiomir Latinović, PhD; Faculty of Mechanical Engineering; University of Banja Luka; Prof. Sead Pašić, PhD; Faculty of Mechanical Engineering, "Džemal Bijedić"; University in Mostar; Prof. Borut Kosec, PhD; Faculty of Natural Sciences and Engineering; University of Ljubljana; Prof. Darko Bajić, PhD; Faculty of Mechanical Engineering Podgorica; University of Montenegro; Prof. Dragoslav Dobraš, PhD; Faculty of Mechanical Engineering; University of Banja Luka; Prof. Kiss Imre, PhD; University Politehnica Timisoara; Romania; Senior Scient.Eng. Milica Grahovac, PhD; Lawrence Berkeley National Laboratory USA; Prof. Doina Frunzaverde, PhD; Faculty of Engineering Resita; Babeş-Bolyai niversity; Prof. Calin Octavian Miclosina, PhD; Faculty of Engineering Resita; Babeş-Bolyai University; Prof. Gordana Stefanovic, PhD; Faculty of Mechanical Engineering; University of Niš.

CONTENT

KEYNOTE LECTURE	1
1. PROGRAMMING OF MACHINE TOOLS AND ROBOTS FOR MACHINING USING STEP-NC IN THE ERA OF INDUSTRY 4.0 Saša Živanović, Nikola Slavković	3
2. RECENT TRENDS IN ENERGY EFFICIENT AC MOTOR DRIVES Darko Marčetić	27
3. COMPARATIVE STUDIES ON THE MICROSTRUCTURE AND CORROSION BEHAVIOUR OF FORGED AND SLM PROCESSED 316L STAINLESS STEEL D. Woelk, N. Kazamer, G. Margineana	36
<hr/>	
PRODUCTION AND COMPUTER-AIDED TECHNOLOGIES	43
1. IRONING PROCESS IN CONDITIONS OF CONSTANT AND VARIABLE LATERAL FORCE S. Djacic, S. Aleksandrovic, D. Arsic, M. Delic, V. Lazic	45
2. POROSITY DISTRIBUTION IN METAL INJECTION MOLDED PARTS Samir Butković, Emir Šarić, Muhamed Mehmedović	51
3. 3D PRINTING: TECHNOLOGY, MATERIALS, AND APPLICATIONS IN THE MANUFACTURING INDUSTRY S. Đurović, D. Lazarević, Ž. Šarkoćević, M. Blagojević, J. Stanojković	55
4. EFFECTS OF SHAPE OPTIMIZATION ON THE 10 BAR TRUSS EXAMPLE N. Petrovic, N. Kostic, N. Marjanovic	61
5. EXPERIMENTAL RESEARCH OF SURFACE ROUGHNESS IN POWDER MIXED ELECTRIC DISCHARGE MACHINING D. Rodic, M. Gostimirovic, M. Sekulic, B. Savkovic, N. Kulundzic, A. Aleksic	65
6. ANALYSIS OF CUTTING FORCES IN HYBRID TURNING AIDED BY GAS COMBUSTION HEATING OF WORKPIECE B. Sredanović, Đ. Čiča, S. Borojević, S. Tešić, D. Kramar	71
7. ADVANCED METAL FORMING TOOLS AS A MAIN LINK OF DIGITAL MANUFACTURING Ilić Jovica, Milutinović Mladomir, Kraišnik Milija, Marković Milisav	77

8.	IMPROVEMENT OF BRAKE TRIANGLE THROUGH APPLICATION OF REVERSE ENGINEERING AND RAPID PROTOTYPING P. Đekić, B. Milutinović, M. Ristić, M. Pavlović, M. Nikolić	81
9.	ENERGY CONSUMPTION MODEL OF THE FACE MILLING S. Tesic, Dj. Cica, M. Zeljkovic, S. Borojevic, B. Sredanovic , G. Jotic	89
10	MODERN APPROACH IN PROCESS PLANNING AND OPTIMIZATION OF THE PRODUCT MANUFACTURING D. Lukić, M. Milošević, R. Čep, I. Kuric, M. Kljunović, M. Zagoričnik	94
11	EFFECT OF VARIOUS FLUID FLOW ON TEMPERATURE OF AN ANGULAR CONTACT BALL BEARINGS IN MOTORIZED SPINDLE M. Knežev, M. Zeljković, C. Mladenović, H. Smajić, A. Stekolschik, A. Živković	102
12	KNEE PROSTHESIS BIOMATERIAL SELECTION BY USING MCDM SOLVER D. Petković, M. Madić, G. Radenković	107
13	AN OPEN ARCHITECTURE CONTROL SYSTEM FOR MULTI-AXIS WOOD CNC MACHINING CENTER S. Živanović, Z. Dimić, A. Rakić, M. Knežević, S. Mitrović	113

	ENERGETICS AND THERMAL ENGINEERING	121
1.	MONITORING OF THERMAL STRESSES OF HOT WATER BOILER TUBE PLATE IN REGIME OF STARTING UP Dragoljub Živković, Milena Rajić, Milan Banić, Marko Mančić	123
2.	PERSPECTIVES OF HYDROPOWER POTENTIALS IN REPUBLIKA SRPSKA O. Kašiković, D. Golubović, D. Milić	133
3.	COMPUTATIONAL INVESTIGATION OF HOT AIR GENERATION SYSTEM USING PELLETS FOR DRIVING AN ABSORPTION PROCESS M. Ilić, V. Stefanović, S. Pavlović, M. Grozdanović, G. Ilić	141
4.	REVIEW OF SOLAR DISH STIRLING ENGINES FOR MICRO-COGENERATION M. Grozdanović, V. Stefanović, S. Pavlović, M. Laković-Paunović, M. Ilić, N. Tomić	147
5.	INFLUENCE OF BUILDING ENVELOPE ON BUILDING ENERGY CONSUMPTION J. Skerlić, D. Nikolić, J. Radulović, A. Radojević, M. Djordjević, A. Mišković	153

6.	EXPERIMENTAL INVESTIGATION OF HYDROGEN ENGINE WORKING CYCLE WITH A LEAN MIXTURE I. Grujić, N. Stojanović, A. Davinić, R. Pešić	159
7.	INTEGRATION OF LARGE-SCALE HEAT PUMPS IN THE DISTRICT HEATING SYSTEM OF SKOPJE Igor Shesho, Done Tashevski, Risto Filkoski, Monika Uler-Zefikj	163
8.	POSSIBILITY FOR ENERGY SAVING IN SERBIAN BUILDING WITH PHOTOVOLTAIC-THERMAL COLLECTORS D. Nikolić, J. Skerlić, J. Radulović, V. Šušteršič, A. Radojević, I. Terzić	173
9.	EXPERIMENTAL INVESTIGATIONS OF FSI MECHANISMS IN PIPELINE SYSTEMS R. Brđanin, U. Karadžić, A. Bergant, J. Ilić	180
10.	THE USE OF PASSIVE TECHNIQUES TO IMPROVE HEAT TRANSFER IN PELLET STOVE M. Jovčevski, M. Laković, F. Stojkovski, M. Jovčevski, M. Mančić, S. Pavlović	185
11.	THE IMPACT OF THERMAL POWER PLANTS ON RIVER THERMAL POLLUTION -A CASE STUDY M. Laković, M. Jovčevski, F. Stojkovski, V. Stefanović, M. Mančić, M. Rajić	192
12.	NUMERICAL INVESTIGATION OF CENTRIFUGAL PUMP WITH CYLINDRICAL BLADES AND DIFFERENT BLADE WRAP ANGLE J. Bogdanović Jovanović, Ž. Stamenković, M. Kocić, J. Petrović	199
13.	DESIGN OF THE AIR CONDITIONING SYSTEM IN THE DATA CENTER S. Stavreva, M. Serafimov, C. Dimitrieska, K. Popovski	205
14.	THE USE FLAT PLATE COLLECTORS IN A PUMPED THERMAL ENERGY STORAGE LATENT SYSTEM S. Pavlović, E. Bellos, V. Stefanović, M. Ilić, M. Grozdanović, C. Tzivanidis	210
15.	ENERGY MANAGEMENT TO LOW-CARBON CITIES: THE EXAMPLE OF THE CITY OF KRAGUJEVAC A. Radojević, D. Nikolić, J. Skerlić, J. Radulović	216
16.	ANALYSIS OF SEASONAL DEVIATIONS INFLUENCE ON AIR-COOLED CONDENSER PERFORMANCES J. Škundrić, P. Živković, D. Mitrović, M. Vukić, D. Đurica, B. Bačić	222

17. DOMESTIC WASTEWATER TREATMENT IN THE RURAL AREAS OF THE REPUBLIC OF SERBIA N. Aleksić, V. Šušteršič, J. Nikolić, N. Rakić, D. Gordić	229
18. OPTIMIZATION OF THE COOLING SYSTEM OF THE REFRIGERATED DISPLAY CASE IN THE SUPERMARKET Ivan Rajič, Diana Bogdan, Petar Gvero	237
19. INFLUENCES ON URBAN AIR QUALITY IN THE CITY OF NIŠ P. Živković, M. Tomić, J. Janevski, M. Vukić, B. Radovanović	242
<hr/>	
MECHANICS AND DESIGN	251
1. COMPARATIVE FREE VIBRATION ANALYSIS OF FG PLATE AND FG PLATE RESTING ON AN ELASTIC FOUNDATION D. Čukanović, D. Milosavljević, G. Bogdanović, A. Radaković, N. Velimirović	253
2. PROPAGATION OF ELASTIC WAVES IN ISOTROPIC AND ANISOTROPIC MEDIA A. Radaković, D. Milosavljević, G. Bogdanović, D. Čukanović, N. Velimirović	258
3. SOLVING NONLINEAR PROBLEMS IN MECHANICS USING SIMULATION I. Terzic, M. Todorovic, S. Aleksandrov, G. Miodragovic	265
4. GEARS REPLACEMENT OF MINUTEMAN COVER DRIVE PLANETARY GEAR TRAIN J. Stefanović-Marinović, S. Troha, Ž. Vrcan, K. Marković, A. Šoljić	271
5. ESTIMATION OF THE REMAINING LIFE OF THE HIGH PRESSURE PIPELINE IN THE THERMAL POWER PLANT K. Maksimović, S. Posavljak, M. Maksimović, I. Vasović Maksimović	276
6. INFLUENCE OF CYCLOID DISK PROFILE CORRECTION ON CONTACT FORCE T. Mačkić, N. Marjanović, G. Jotić, M. Tica, Ž. Đurić	282
7. UPRIGHT AND FRAME PROTECTIVE COMPONENTS OF PALLET RACKING R. Vujanac, N. Miloradovic, L. Petrovic, P. Zivkovic	286
8. STRUCTURAL FEM ANALYSIS OF AN AIRCRAFT PISTON ENGINE CYLINDER ASSEMBLY AT ELEVATED TEMPERATURE N. Vučetić, R. Antunović, B. Krstić, D. Jeremić	291
9. FATIGUE ENDURANCE ANALYSIS OF A SURFACE STRESS RAISER Slobodanka Boljanović, Strain Posavljak, Stevan Maksimović	299

MECHATRONICS	305
1. UPGRADING OF THE HYDRAULIC SYSTEM BY INSTALLING A FREQUENCY CONVERTER J. Eric Obucina, S. Stankovski, G. Ostojic, S. Aleksandrov	307
2. A NEW CONCEPT OF ROBOTIC PLANT PROTECTION IN GREENHOUSES B. Z. Knezevic, A. Gojkovic, Z. Gajic, S. Mitric	313
AUTOMOTIVE AND TRANSPORTATION ENGINEERING	321
1. EXPERIMENTAL DETERMINATION OF THERMAL STRESSES DISK BRAKES IN DEPENDING FROM THE BRAKING PRESSURE AND VEHICLE SPEED N. Stojanović, I. Grujić, J. Glišović	323
2. POSSIBILITY OF IMPLEMENTING THE LEAN SIX SIGMA CONCEPT ON LOGISTICS PROCESSES N. Simić, A. Stanković, I. Mačužić, G. Petrović	330
3. AN OVERVIEW OF NON-EXHAUST BRAKE EMISSION MEASURING METHODS S. Vasiljević, J. Glišović, N. Stojanović, I. Grujić	339
4. APPLICATION OF HYBRID COMPOSITES BASED ON ZA27 ALLOY IN AUTOMOTIVE INDUSTRY D. Miloradović, N. Miloradović, J. Glišović, B. Stojanović, R. Vujanac	349
MATERIALS SCIENCE	355
1. OPTIMIZATION OF HYBRID ZA-27 NANOCOMPOSITES USING ANOVA AND ANN ANALYSIS S. Gajević, S. Miladinović, O. Güler, H. Çuvalcı, N. Miloradović, B. Stojanović	357
2. THERMAL PROPERTIES OF ARMOUR STEEL PROTAC 600 M. Lešnjak, B. Kosec, B. Karpe, G. Janjić, M. Gojić, J. Bernetič, G. Kosec	363
3. THE MATERIAL SELECTION OF THE HEATING PLATES USED IN THE VULCANIZATION PROCESS OBTAINED USING DIFFERENT MCDM METHODS J. Mihajlović, G. Petrović, D. Ćirić, M. Madić	367

4.	HIGH STRENGTH LOW-ALLOY STEELS IMPACT TOUGHNESS ASSESSMENT AT DIFFERENT TEST TEMPERATURES S. Bulatović, V. Aleksić, Lj. Milović, B. Zečević	375
5.	CAVITATION EROSION BEHAVIOR OF ALUMINIUM BASED ALLOYS M. Ćosić, S. Boljanović, M. Dojčinović	379
6.	INFLUENCE OF THE POLYMER MATRIX TYPE ON CAVITATION RESISTANCE OF COMPOSITES M. Dojčinović, M. Pavlović, S. Jezdimirović, B. Purić, A. Cvetković	383
<hr/>		
	QUALITY AND ECOLOGY	387
1.	ENERGY MANAGEMENT SYSTEM APPLICATION IN HEALTHCARE Milena Rajić, Rado Maksimović, Peđa Milosavljević, Dragan Pavlović	389
2.	DUST PARTICLES EMISSIONS AT STEEL CUTTING AND WELDING PROCESSES L. Cigić, B. Kosec, M. Ilić Mićunović, D. Klobčar, Z. Tanasić, B. Karpe, A. Nagode	399
3.	ANALYSIS OF ENERGY SAVING OPPORTUNITIES IN THE BUILDING, TRANSPORT AND PUBLIC LIGHTING SECTORS IN LOCAL COMMUNITIES H. Muratović, S. Midžić Kurtagić, S. Arnaut, F. Ćorović, E. Manić	405
4.	STRATEGIC ANALYSIS OF THE POSSIBILITY OF STARTING THE PRODUCTION OF FAST - GROWING PAULOWNIA TREE G. Janjić, M. Radaković, Z. Tanasić, B. Kosec, D. Kardaš Ančić	415
5.	BUSINESS PROCESS IMPROVEMENT IN THE AUTOMOTIVE INDUSTRY - QUALITY METHODS AND TOOLS Z. Tanasić, A. Jokić, G. Janjić, M. Bobrek, B. Kosec	423
6.	COMPARATIVE STUDY OF DIFFERENT OPTICAL COORDINATE MEASUREMENT SYSTEMS G. Jotić, B. Štrbac, S. Tešić, M. Hadžistević	431
7.	KNOWLEDGE MANAGEMENT AS A TOOL FOR MANAGEMENT QUALITY IMPROVEMENT M. Bobrek, Z. Tanasic, G. Janjic, K. Macanović	436
8.	CONTAMINANTS IN USED ENGINE OIL AND THEIR IMPACT ON THE ENVIRONMENT AND HUMAN HEALTH S. Rațiu, A. Josan, V.G. Cioată, I. Kiss	440

MAINTENANCE OF ENGINEERING SYSTEMS AND OCCUPATIONAL SAFETY ENGINEERING	445
1. THE INFLUENCE OF THE APPLICATION OF TECHNICAL DIAGNOSTIC ON THE EFFICIENCY OF THE INDUSTRIAL SYSTEM D. Branković, Z. Milovanović	447
2. OCCUPATIONAL INJURY ANALYSIS ACCORDING TO THE INJURED PART OF THE BODY IN THE FUNCTION OF RISK MANAGEMENT Msc Mile Vajkić, PhD Biljana Vranješ, PhD Evica Stojiljković	451
3. EXPOSURE OF PRODUCTION WORKERS TO STRESS K. Mijanović, M. Jukić, J. Mijanović-Jukić, J. Kopač	458
4. ANALYSIS OF THE CAUSES OF OCCUPATIONAL INJURIES IN A PRODUCTION SYSTEM – A CASE STUDY A. Helvida, L. Haznadarević, B. Vranješ, D. Adamović, E. Stojiljković	464

PREFACE

Dear colleagues,

The first DEMI Conference was established and held in 1998 as a scientific-professional conference at the Faculty of Mechanical Engineering Banjaluka. Year after year the DEMI Conference matured into a relevant scientific and professional event in the field of mechanical engineering. That is how our conference became recognized first locally, then regionally, and afterwards internationally. Starting as a local conference, DEMI has grown to become the international scientific conference of first category. Besides that, our plenary speakers included some of the notable professors and scientists in mechanical engineering. Also, a great deal of research papers from a number of countries, as well as interesting social events have placed DEMI on the list of the most significant conferences in the field of mechanical engineering. These results were achieved primarily by all those employed at the Faculty of Mechanical Engineering Banjaluka, but also all participants, authors and co-authors of scientific and professional papers, as well as those who provided support for the conference.

In these challenging times it is very important to recognize and keep what we have accomplished. Nothing is ever all too easy and we always face new challenges and new problems. Mechanical engineering is a field that specifically focuses on overcoming the problems, solving them and finding answers to sometimes very difficult questions.

In that regard, the forthcoming fifteenth DEMI Conference faces the most difficult challenges and requirements so far. However, we need to follow in our predecessors' steps, meet expectations, improve events and make a leap forward towards excellence. It is up to us to meet the requirements and deal with any challenges along the way.

The following 15th DEMI Conference will be held from 28 to 29 May in Banjaluka, in line with the recommendations of the Public Health Institute of the Republic of Srpska. We will stick to what our Conference has been recognized for, both in respect to its organization and scientific-professional scope. The only change, which remains as an option, may be online presentation of papers, which, we sincerely hope, will not happen.

Dear colleagues, I hope that the 15th DEMI Conference we will find us in good health and that we will be able to present our research results at the Faculty of Mechanical Engineering in Banjaluka. In that case you can expect to have a good time with us.

In Banjaluka, 20 May 2021

Chair of Organizing Committee
of the 15th DEMI Conference

Assoc. Prof. Stevo Borojević, PhD

Keynote Lectures



Banja Luka
28-29 May 2021.

DEMI 2021

15th International Conference on
Accomplishments in Mechanical and
Industrial Engineering

www.demi.mf.unibl.org



Programming of machine tools and robots for machining using STEP-NC in the era of Industry 4.0

Saša Živanović^a, Nikola Slavković^a

^aUniversity of Belgrade, Faculty of Mechanical Engineering, Serbia

Abstract This paper presents a method for applying the ISO 10303-238 (AP-238) standard for programming CNC machine tools and robots for machining operations. The method encompasses programming, simulation, and machining by machine tools and industrial robots as part of current and future research at the University of Belgrade Faculty of Mechanical Engineering. Application and validation of methodology for programming according to STEP-NC protocol are performed using available CNC machine tools and industrial robots, with the following tools: (a) commercial CAD/CAM software, (b) STEP-NC Machine software with configured virtual machine tools and virtual robots, as well as (c) developed translators for generation of G-code and/or robotic programming language. STEP-NC provides new opportunities to support high-level information from design to CNC controller. This implies further evolution of the CNC system they will act using STEP-NC standards as an interface between CAD and CNC in the era of Industry 4.0.

Keywords STEP-NC, Machine tools, robots for machining, virtual machines and robots, Industry 4.0

1. INTRODUCTION

This paper discusses the programming of the CNC machine tools and industrial robots for machining, based on ISO 10303-238 (AP-238) known as STEP-NC (Standard for Product Model Data Exchange for Numerical Control) in the era of Industry 4.0. The article also presents research results at the Faculty of Mechanical Engineering from Belgrade on the application of a new programming method in actual production conditions.

Corresponding author

Prof. dr Saša Živanović
szivanovic@mas.bg.ac.rs

University of Belgrade, Faculty of Mechanical
Engineering, Belgrade, Serbia

Industry 4.0 has an initiative that aims to digitalize industrial manufacturing via the exploitation of innovative technologies. The transformation goal is to enable and enhance the flexibility, individualization, and customization abilities of the production system. In order to meet the challenges of Industry 4.0, the current manufacturing system requires a significant transformation in the information handling between CAD/CAPP/CAM - CNC [1].

Machine tools have evolved from simple machines to today's highly sophisticated Computer Numerically Controlled (CNC) machine tools [2]. Much like the different stages of industrialization, machine tools have also gone through different stages of technological advancements. Industry 4.0 pleads for a new generation of machines-Machine Tool 4.0 [3,4]. Machine Tool 4.0, otherwise known as Cyber-

Physical Machine Tool (CPMT), is the integration of machine tool, machining processes, computerization, and networking, where embedded computers and networks can monitor and control the machining processes, with feedback loops in which machining processes can affect computations and vice versa [5].

In this new industrial world, everything will be connected through the internet and the cloud, enabling factories to function as a system rather than individual parts. Many jobs will shift from physically operating to operating them via computers, monitoring data, and providing monitoring to automated CNC machining operations [6].

Although the machine tools have changed rapidly, the programming language has basically remained the same with programming in G-code (ISO 6983) [7].

Machine tool programming by G-code is characterized by low-level information content. This low-level information describes elementary actions and tool moves, strongly reducing possibilities at the CNC level. It also breaks the CAD-CAM-CNC numerical chain and disables easily gathering feedback information from the shop floor [8].

It is necessary to prepare the tool path for each type of CNC machine tool individually using the appropriate postprocessor. It requires a large number of different postprocessors for each type of machine tool, Fig.1. Therefore, the classical programs for CNC machine tools (G-code) do not include any useful information about the product, such as data about the geometric primitives of the model, tolerances, material properties, setting up the fixture, and other information created during the design and planning of manufacturing technology. All this information will disappear when converting the tool path in G-code [2].

Today a new standard, STEP-NC, is being used as the basis for the development of the next generation of CNC controller. The new STEP compliant NC standard (STEP-NC) is based on the Standard for Exchange of Product data model (STEP) and has been developed to overcome the shortcomings of G-code [9].

In the field of machine tool programming, an open challenge is the new programming method based on STEP-NC standards, for different machining systems.

The STEP-NC provides new opportunities to support high-level information from design to CNC controller. It allows bi-directional data flow between CAD/CAM and CNC without any information loss, Fig.1.

STEP-NC is a new interface that has been developed for the exchange of information between CAD/CAM systems and CNC controllers, and various users who exchange technology or monitoring machining processes over the Internet, which is in line with Industry 4.0.

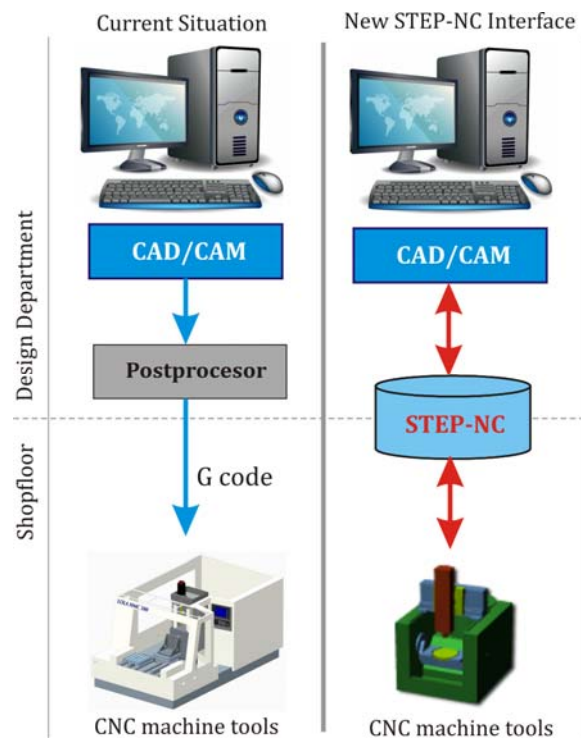


Fig. 1. Comparison of current G-code and new STEP-NC interface for programming CNC machine tools

In this regard, this paper will present the possibilities of applying the new programming method for different CNC machine tools (milling, turning, Wire EDM, additive manufacturing, CMM, etc.) and the example of robots for machining in the era of Industry 4.0.

2. STEP-NC LITERATURE REVIEW

The STEP-NC, as a new standard, provides a new breed of intelligence to the CNC controller in terms of interoperability, flexibility, adaptability, and extensibility [10].

The STEP-NC standard has been developed to challenge the standardization of the exchange of

product data along the manufacturing digital chain (CAD-CAPP-CAM-CNC), which includes simulation, optimization, and convert or export code capabilities, Fig.2.

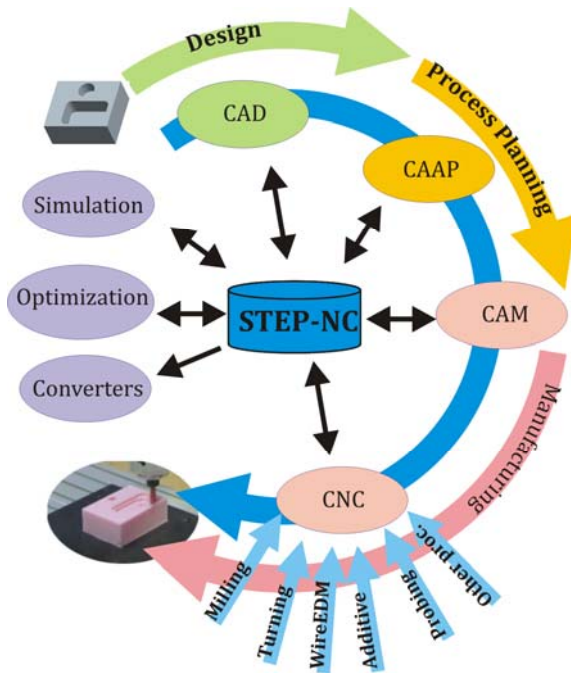


Fig. 2. Digital chains based on STEP-NC

Digital thread for manufacturing is considered for various CNC machine tools used in milling, turning, electro-erosion, additive manufacturing, and other processes, and also in machining operations where is used industrial robot. Many studies have been conducted to promote STEP-NC as an upcoming generation of data model interface for CNC systems.

The developing STEP-NC standards are the result of an international effort to replace the G-code ISO6983 standard with a modern associative language that connects the CAD design data used to determine the machining requirements for an operation with the CAM process data that solves those requirements [11]. Thus the migration of G-code programming to STEP-NC calls for time, funding, and changes to the industrial mindset [8].

These new standards are ISO 14649 and ISO 10303-238. These standards can be viewed as two different implementation methods of the STEP-NC standard. The ISO 14649 standard is more likely to be used in an environment in which CAM systems have exact information from the shop floor, whereas ISO 10303-238, as

a part of the STEP standard, is more suitable for a complete design and manufacturing integration [2].

The STEP-NC provides a comprehensive model of the manufacturing process. It is object and feature-oriented and describes the machining operations executed on the workpiece, and not machine-dependent axis motions. It will be running on different machine tools or controllers [12]. If old NC programs in G-code are to be used on such controllers, the corresponding translators or converters will be able to postprocess the STEP-NC program into different NC program types.

Due to the fluctuation in market needs and trends, digitization, data exchange between virtual companies around the world, CNC industrial companies are facing a big challenge to integrate all levels in product lifecycle management. In this regard, it can be said that the old method of programming using G-code, got an alternative in the powerful standard called STEP-NC.

2.1 Research project overview

The STEP-NC has been developed as a result of several research projects carried out by companies, university institutes, research institutes and associations, manufacturers of CAM systems, controls, and machine tools.

Different studies were carried around the world by major research groups which dealt with the application of STEP-NC for the integration of CAD, CAPP, CAM, and CNC systems. Within these studies the following projects are implemented [13,14]:

- European strategic program on research in information technology - ESPRIT STEP-NC.
- Intelligent manufacturing systems based on STEP-NC - IMS STEP-NC.
- Supermodel project – Model-driven intelligent control of manufacturing (MDICM).
- STEP manufacturing suite – SMS project,
- Rapid acquisition of manufactured parts – RAMP project.
- Intelligent manufacturing for STEP-supported machining and inspection.

One of the earliest international research projects is the European ESPRIT III project, OPTIMAL (Optimized Preparation of Manufacturing Information with Multi-Level CAM-CNC Coupling) for the development of

STEP-supported systems is the optimized preparation of manufacturing information with multi-level CAM-CNC coupling project which is based on information about features and machining strategies [13,14]. This project includes twenty industrial and academic partners with rich experience in the fields of CAD/CAM (Dassault, Open Mind), control (Siemens, OSAI), machine tools (CMS), and end-users (Daimler-Chrysler, Volvo) in Europe formed the European STEP-NC consortium [14]. The global research in the areas of STEP-NC has been primarily coordinated under a single IMS (Intelligent Manufacturing System) project that effectively entails an international package of actions. Partners from four regions participate in the project: EU, Korea, Switzerland, and the USA. The regional coordinators are Siemens (EU), CADCAMation (Switzerland), STEP Tools (USA), and ERC-ACI (Korea) [2,14].

The Super Model Project awarded in October 1999 to STEP Tools, Inc. (USA), working with a team of sub-contractors. It was a project funded by the National Institute of Standards and Technology (NIST). The goal of this project is to build a database that contains all the information required to make a part.

The result is STEP-NC as a modern, associative communications protocol that connects computer numerically controlled (CNC) process data to a product description of the part being machined. Integration of the CNC model into STEP to produce ISO 10303-238 was done in the United States, with the funding of the MDICM project by the NIST and led and work performed by STEP Tools, Inc. [15].

Results presented in this paper are based on ISO 10303-238, and software STEP-NC Machine. The STEP-NC Machine software can export files either in P21 (clear text) or P28 (XML). Used software STEP-NC Machine can export files in P21 (clear text) format that is currently the most popular implementation method, although P28 files, in format XML, are increasingly used today [16-18].

2.2 Levels of research strategies related to STEP-NC

STEP-NC promises new opportunities for machine tool programming, but also requires the development of the next generation of intelligent CNC systems [8,19]. Changes in the digital chain CAD-CAM-CNC are necessary,

including high-level object-oriented information from STEP-NC files has to be interpreted and executed on the machine tool or robot axis commands.

Levels of research strategies, Fig.3, related to STEP-NC advanced programming is possible define at four levels [8,19,20]:

- At the first level, the use of STEP-NC with CNC controllers, which are only able to read only G-code files, by developing converters STEP-NC to G-code, is made possible. This level is indirect STEP-NC programming.

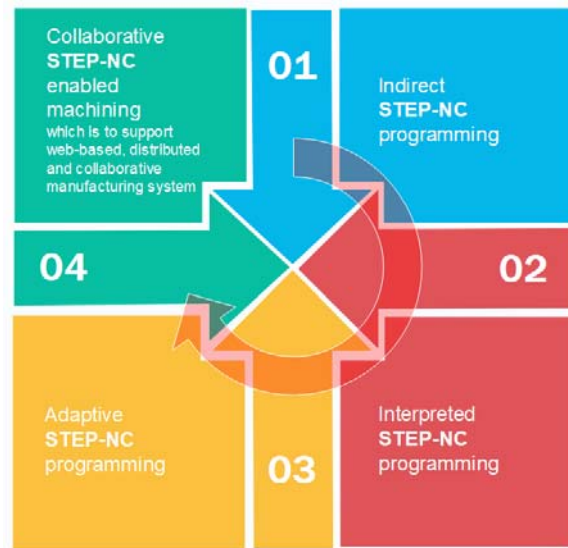


Fig. 3. Levels of research strategies related to STEP-NC advanced programming

- The second level is Interpreted STEP-NC programming where axis command is directly executed from STEP-NC file. This level is required a new open architecture controller where the external data can be integrated into the tool-path generation process with embedded CAM function inside the controller system.
- The third level is Adaptive STEP-NC programming where the CNC controller estimates online process data and optimizes machining parameters and tool paths in real-time.
- The fourth level is the ultimate goal is Collaborative STEP-NC enabled machining which is to support web-based, distributed, and collaborative manufacturing systems.

The aims are parallel with the e-manufacturing paradigm DA-BA-SA [19,21]: Design-Anywhere, Build-Anywhere, Support-Anyways, where is possible. These aims for collaborative manufacturing providing a digital thread for CNC manufacturing running in the STEP-NC System world via the Internet is achievable. Today's digital communication technologies have solved some critical problems of reliably transferring information across global networks. The STEP-NC is an available interface for exchange information about technology that enabled machining and a new model of data transfer between CAD/CAM systems and CNC machines [22].

2.3 STEP-NC based platforms for robotic machining

The new programming method that uses STEP-NC protocol ISO 10303-238, is increasingly applied in the field of CNC machine tool programming and given that industrial robots are getting more and more capable of taking on machining operations, it is necessary considering to couple the robot for machining towards with STEP-NC protocol [17, 23].

Examples of the applications of STEP-NC standards in programming robots for machining can be found in several research works [23-26]. In paper [23] a computer-aided manufacturing (CAM) system for industrial robot machining operations is introduced. The system is based on the new machining standard STEP-NC which is rapidly making its way into the world of CNC machines. Developed Robot CAM module for industrial robot machining operations based on a STEP-NC input file that can interpret, translate and transfer the manufacturing orders to an industrial robot. The experimental verification was carried out without any material cutting. The generated toolpath was drawn by the robot on millimeter-scale paper.

In research [24] authors proposed the RoboCAD INFELT STEP platform that enables the product designers to program the movement of the robot for a product process plans by means of that product CAD STEP data structure. The RoboCAD INFELT is an interoperable and collaborative platform for CAD/CAPP/CAM applications and integrates the programming data based on ISO 10303 (STEP) standards while supporting the data structures related to robot applications.

The paper [25] represents presented the unified data models of industrial robots under the STEP standard to exchange information between different CAx and robot off-line programming systems. A presented prototype of a robot off-line programming system with a 3D virtual environment (like the function of STEP-NC Machine) will not only benefit the robot simulation systems, but also the improvement of traditional industrial robot controllers. In the developing progress of STEP-CNC, the STEP-NC technology is firstly implemented in a virtual environment. Once the corresponding CAD/CAM and CNC technologies are mature, the STEP-CNC controller will definitely emerge.

The research work [26] proposed a procedure that uses forward and inverse kinematics methods applicable to serial and hybrid robots, allowing STEP-NC compliant information to be received and generates the path along which the robot should move, reducing the time for setup and integration of robots in manufacturing. These paths were tested on three robots with different configurations (AdeptOne, 4-DOF serial robot, ABB IRB-140, 6-DOF serial robot, and Comau Tricept-806, 6-DOF hybrid robot), in a virtual environment, confirming the feasibility of the method.

As above mentioned, STEP-NC promises new opportunities for machine tools and robots programming and according to this, it is useful that high-level object-oriented information in STEP-NC files has to be treated and executed on the machine tool and industrial robot for machining. Levels of research strategies related to STEP-NC presented in section 2.2, could be applicable likewise for programming of industrial robots in machining tasks.

The papers [21,27] is a result of a collaboration between researchers from Brazil and Serbia through a method for applying the ISO 10303-238 (AP-238) standard in robotic machining operations by using two industrial robots (ASEA IRB6-S2 in Brazil and LOLA 50 in Serbia) which use the LinuxCNC control. This collaboration is achievable by using STEP and STEP-NC with aims at providing a digital thread for CNC manufacturing running in the STEP-NC System world via the Internet, thus realizing the paradigm known as e-Manufacturing.

3. METHODOLOGY FOR THE APPLICATION OF PROGRAMMING BASED ON THE STEP-NC PROTOCOL

At the Faculty of Mechanical Engineering, the University of Belgrade, current research in the field of STEP-NC programming based on the ISO10303-238 standard has been going on for more than ten years.

A STEP compliant CNC interface is proposed and developed by the STEP Tools Company [15]. This software, known as STEP-NC Machine, generates ISO 10303-238 files (Application Integrated Model) and works as a front application on a current CNC controller [8]. For our research and application of a new programming method, the licensed software STEP-NC Machine is used.

In this paper, we propose an integrated methodology, as a result of our experiences, for the first level of indirect programming that involves the use of STEP-NC with CNC controllers of machine tools, which are only able to read-only G-code files. Also, this research includes robots for machining that are programmed with either G-code or robotic language, based on their own developed Robot language converters (RLC).

Generated STEP-NC programs that can be shared as data for technology exchange between many organizations and reused on many different CNC machine tools (milling machine, Lathe, Wire EDM, 3D printers, etc.) and robots for machining, where is possible.

One of the common ways to describe the methodology for CNC machining based on STEP-NC is using the IDEF0 diagram [12,17,28,29]. IDEF0 is used to describe a programming method as a structured representation of the activities within the considered programming methodology. This methodology is a structural representation of activity, which can be viewed at several different levels, where each level consists of a set of hierarchical diagrams with text descriptions [17,28].

A special case of one box IDEF0 context diagram, containing the top-level function (A0: Programming method for CNC machining based on STEP-NC) that is modeled with its inputs, controls, outputs, and mechanisms are resented in Fig. 4. Each function or activity in the IDEF0 diagram may be decomposed into its major sub-

functions by creating its child diagrams which contain the child boxes and arrows that provide additional details about the parent box.

The basic activities for the programming method for CNC machining based on STEP-NC are:

- A1-Process planning and generating of STEP files, and tool path in CAD/CAM system;
- A2-Machining simulation in CAD/CAM system;
- 4A3-STEP-NC Machine program generator;
- A4-CNC Machining simulation in STEP-NC Machine;
- A5-Web interface for the virtual machine/robots (Digital twin) based on STEP-NC;
- A6-Postprocessing and/or program converter; A7-Virtual machine or robots for machining in the control system;
- A8-CNC machining.

According to the proposed basic flow of activities, shown by the IDEF0 diagram in Fig.4, Process planning and generating of STEP files, and tool path are prepared in the licensed CAD/CAM system (PTC Creo). Results of activity A1 are CAD models of the workpiece, raw piece, tool, fixture in STEP format, as well as toolpath (CLF) for each working step, and are represents an input for activity A2 and activity A3. Activity A2 is used for verification of toolpath and involves simulation of the obtained toolpath, material removal simulation in CAD/CAM environment, with the possibility of simulation by applying configured virtual machine tools, and virtual robots for machining. After that, activity A3, the thus prepared results from previous activities are integrated by loading in the STEP-NC Machine software, where the program is generated in STEP-NC format (*.238, *.p21, *.p28, *.stpnc), according to ISO 10303-238. The advantage of software STEP-NC Machine is that it can combine toolpaths CLF/APT from different CAD/CAM systems (Pro/Engineer, CATIA, UGS NX) and make an integrated program in P21 format, which is of importance if different CAD/CAM environments are used for programming the machining tasks of some complex part [17]. The generated STEP-NC program from activity A3 is an input for activity A4, A5, and A6.

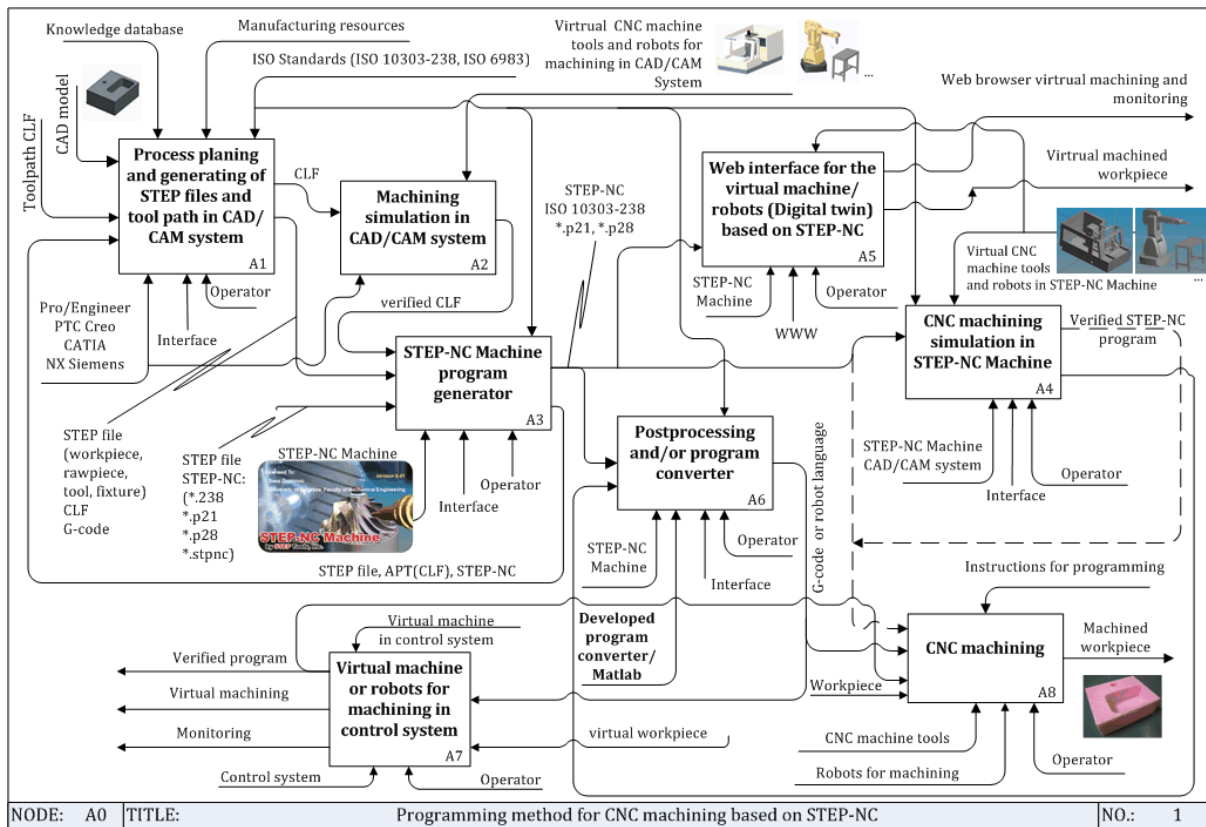


Fig. 4. An integrated methodology for programming method for CNC machining based on STEP-NC

Activity A4 implies performing the Machine simulation based on STEP-NC on available or configured virtual machine tools and virtual robots for machining in order to verify the program. In the era of industry 4.0, activity A5 is especially important, which enables virtual processing and monitoring via the web environment.

Activity A6 is realized as part of software STEP-NC, and with developed program converter, especially for robots for machining. This activity allows post-processing of the STEP-NC program into G-code for machining on the most existing CNC machine tools. Special cases need used developed converter. Activity A7 is optional and is used if the control system has integrated virtual machine tools and virtual robots as a paradigm of the digital twin in Industry 4.0. Finally, in activity A8 is performed program execution and real machining.

3.1 Scenarios for STEP-NC based programming

At the moment, for most users, this new method of programming based on STEP-NC cannot be

completely used with all the benefits provided by STEP-NC, because the resources for its development are not available to everyone [28]. This section proposed two possible scenarios (Sc1, Sc2) [13,28,30,31] for indirect programming method based on STEP-NC on existing CNC machine tools and robots for machining using the available and developed software, Fig. 5. These scenarios are:

- Scenario Sc1 - using the native STEP-NC program, post-processing or converting STEP-NC program into G-code and executing on the machine tool or robot for machining which is only able to read-only G-code files.
- Scenario Sc2 - enables the generation of STEP-NC programs based on the available CAD/CAM system and licensed software STEP-NC Machine, in order to exchange technology and machining capabilities on machines that can directly interpret STEP-NC programs, but also those that execute only G-code.

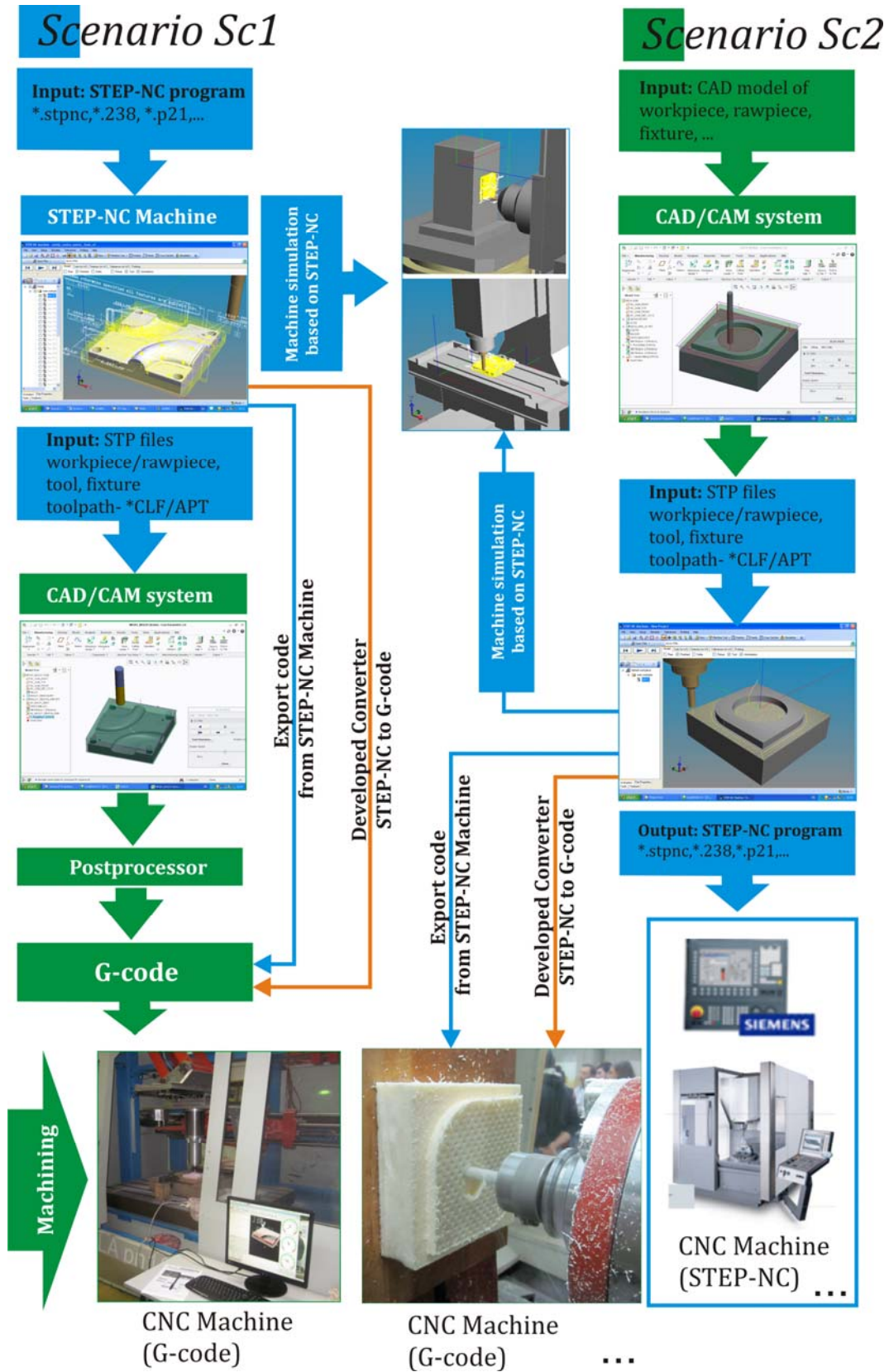


Fig. 5. Scenarios for the application indirect STEP-NC programming method

For now, the first scenario is realistic, for most users, and feasible in three ways. The first way is using CLF, which is specifically imported into the available CAD/CAM system and post-processed for the selected machine tool. CAD system takes reference model and workpiece in STEP format and CL File. Verification of material removal is done in a CAD/CAM system in the module (NC Check). CAD/CAM system uses configured postprocessor to generate G-code for the available CNC machine tools [28]. The second way uses an export code option of STEP-NC Machine which can directly export STEP-NC program into G-code from the available control units, offered by software (Fanuc, Siemens, Okuma, Haas, etc.). The third way is parsing the STEP-NC file and converted into G-code using developed converters.

Scenario Sc2 is primarily intended for the possibility to generate our own STEP-NC program and for the exchange of technology between users to be based on STEP-NC.

Scenario Sc2 involves importing geometry elements of the reference model, workpiece, tool, fixture, measuring probe, and adequate tool path from common CAD/CAM system (Creo, Catia, NX Siemens, ...) into STEP-NC Machine software. The procedure of this scenario can be described through the following steps: (i) CAD models of reference model, workpiece, rawpiece, tool, fixture is prepared in the CAD/CAM system; (ii) technology for machining are planned and implemented; (iii) tool path CLF - Cutter Location File (*.ncl) is generated; (iv) tool path and material removal simulations (NC Check) is done; (v) the inputs for software STEP-NC Machine are prepared by exporting reference model, workpiece and tool from CAD/CAM System in STEP format; (vi) the reference model, model of the workpiece and rawpiece, model of tool in STEP format, and CLF (*.ncl) are loaded in software STEP-NC Machine; (vii) program is saved in the format of STEP-NC AP238 (*.stpnc, *.238, *.p21); (viii) program is tested by simulations on different machines available or configured in the software STEP-NC Machine; (ix) program for machining is directly interpreted on CNC machine which can read STEP-NC programs, or translated into G-code in one of the three described ways in scenario Sc1; (x) workpiece is machined on available CNC machine tools.

These scenarios completely cover the field of application of robots for machining. There are two possibilities of preparing programs that can be either in the format of G-code or robot programming language (using developed RLC [17]).

4. CONFIGURING OF VIRTUAL MACHINE TOOLS AND ROBOTS IN STEP-NC ENVIRONEMNT

STEP-NC Machine can display and simulate the machining or measuring process within a STEP-NC file, including the simulation of virtual machine tool, or virtual robots, or virtual measuring machine and it can be extended as needed to simulate new machines. Thus, the STEP-NC Machine environment allows configuring its own virtual CNC machine tools and virtual robots for machining. In this way, it is possible to perform a simulation based on the generated STEP-NC programs in order to verify them.

Virtual CNC machine tool or robot for machining is able to interpret the STEP-NC program in the software STEP-NC Machine environment. To load the new machine in the STEP-NC environment, it is necessary to follow the next procedure: (i) configuring a CAD model of the CNC machine tool or robot for machining; (ii) make an export model of the CNC machine tool or robot for machining in the STEP format by the protocol AP203, AP214 or AP224; (iii) configuring virtual machine or robot in STEP-NC Machine environment; (iv) prepare XML file which includes characteristics of a machine tool or robot; (v) include both files for the machine (STEP file and XML file) in folder machine in software STEP-NC Machine; (vi) start STEP-NC Machine and in the Machine tool drop-down menu it will appear the new configured machine tool or robot ready for Virtual machining, based on STEP-NC program [32].

In the process of configuring a virtual machine, a description of the structure defined by the XML file is very important. The characteristic structure of the XML file for machine tools or robots for machining is given in Fig. 6. This figure shows fragments of XML files for one Horizontal machining center LOLA HMC500, and for one robot for machining LOLA 50.

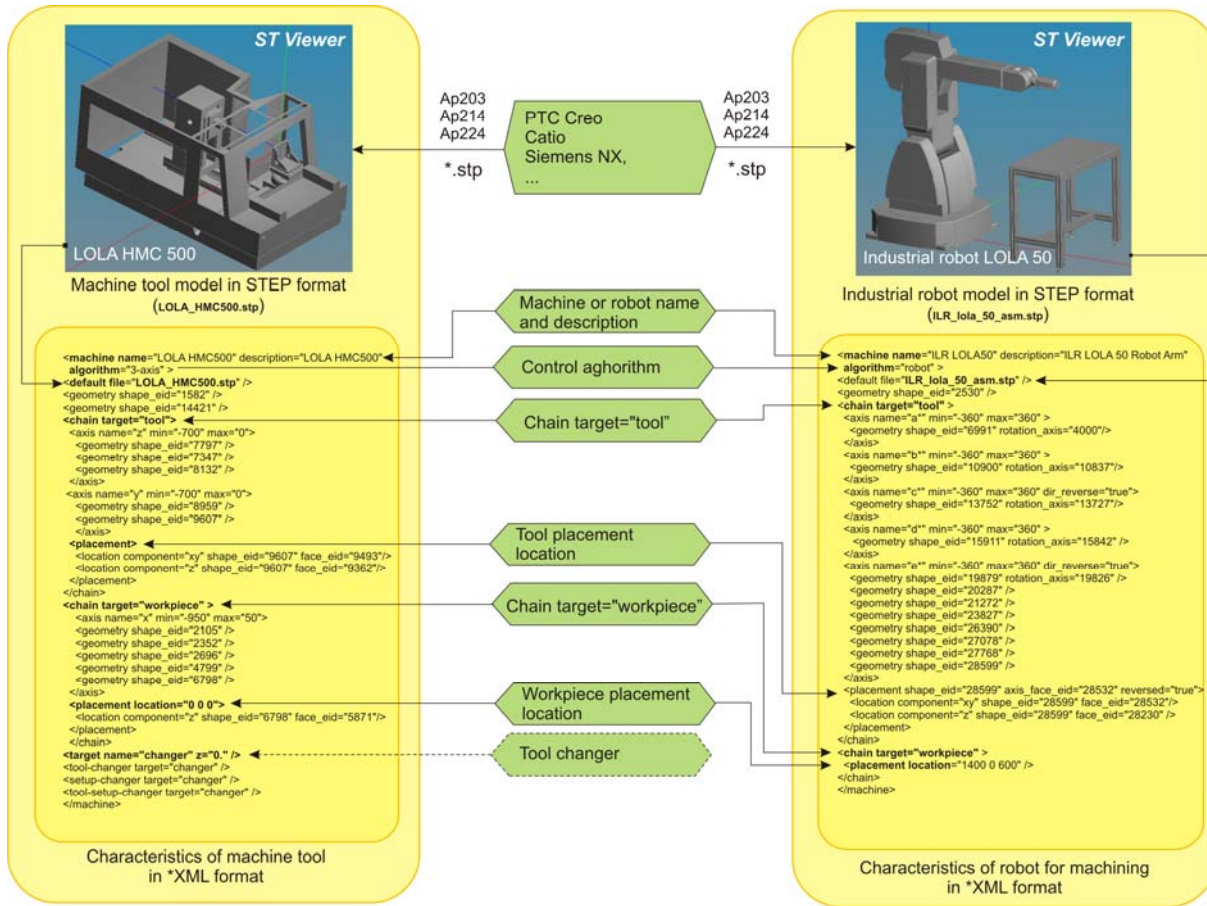


Fig. 6. Configuring virtual machine and robots for machining in STEP-NC Machine environment [32]

The usual XML file structure for description structure of machine tools and robots for machining has the following parts [32]: (i) machine or robot name, (ii) control algorithm, (iii) name of the STEP file of machine or robot, (iv) description of the machine or robot base structure, which is stationary, (v) description of tool side structure, (vi) defining placement location for tool, (vii) description of workpiece side structure, (viii) defining placement location for workpiece, (ix) description of NC axes and their feeds, or description rotating joints of robots (name a, b, c, d and e, constraints, mutual position, as well as the sequence of rotary axes). Thus, the configured own virtual machine tool and robot for machining can be loaded in the STEP-NC Machine environment, where they will appear as new machines in a dropdown menu of Machine Tool. Upon selecting the machine from the menu, it is loaded and can execute STEP-NC programs. This is important for training in a new method of programming because it is now possible to check STEP-NC programs by

simulating work on own configured virtual machines or robots for machining.

4.1 Configured virtual machine tools

The configured types of CNC machine tools so far are shown in Fig. 7. The available machines for which the first level of indirect programming based on STEP-NC was applied were considered.

The types of machines considered in Fig. 7 are: (i) CNC machine tools - (1-5) for milling operations with serial kinematics (3 to 5 axes), PKM (Parallel kinematic machines) - (6) Hybrid Kinematic Machines - (7); (ii) CNC lathe for turning operations - (8,9); (iii) Wire EDM for electrical discharge machining - (10); (iv) 3D printers, for additive manufacturing - (11,12); (v) CMM (Coordinate Measuring Machine) for measuring - (13).

A more detailed procedure for configuring new machine tools in STEP-NC machine is given in [33], and some results also can be seen in

[13,32,34-36]. The existing database of available machines in the STEP-NC machine software has been significantly upgraded with new machines.

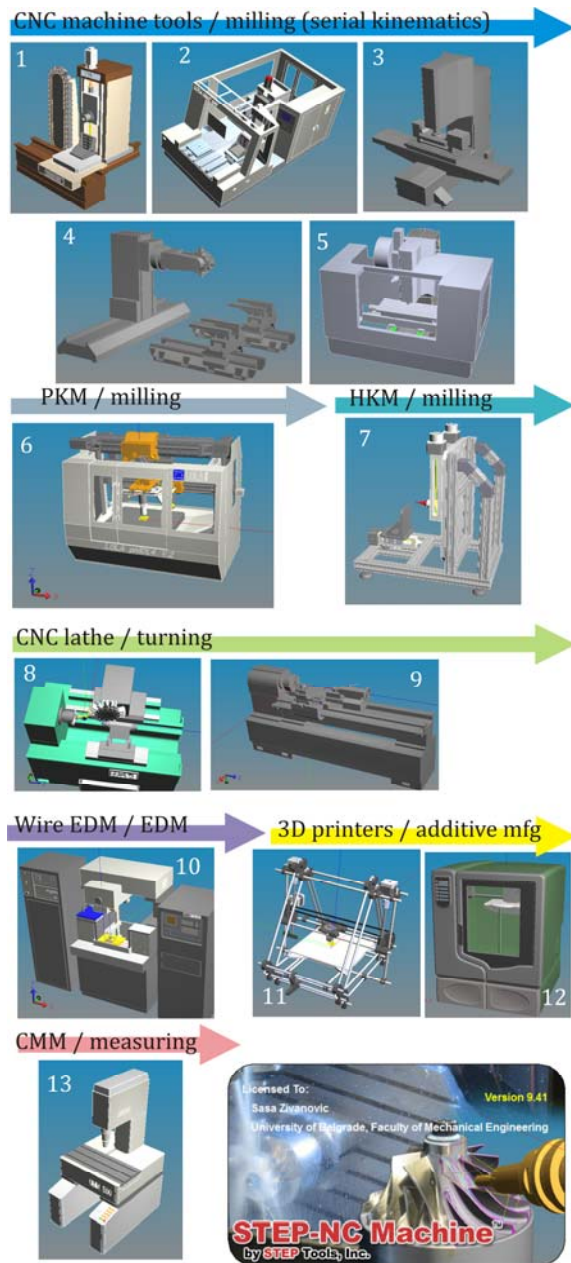


Fig. 7. Example of configured machine tools in STEP-NC Machine

4.2 Configured virtual robots

Used own methodology for configuring robot is described in more detail in [16,37,38]. So far, a number of robots have been configured, such as: LOLA, Mitsubishi, Fanuc, Asea, ABB robots.

Some of the configured robots are shown in Fig.8.



Fig. 8. Example of configured virtual robots for machined in STEP-NC Machine

In Fig. 8 the following robots are shown: (1) - ASEA Irb-S2, (2) - Gosko, (3) - LOLA50, (4) - LOLA15, (5) - Mitsubishi rv6s1, (6) - Mitsubishi Movemaster EX, (7) - ABB irb140, (8) - Fanuc LR Mate 200iD.

As already shown, an example of the XML files description for the 5-axis machining robot LOLA50, with comments and illustrations are given in Fig. 6-right. In order to correctly create the XML file structure and the description of the assembly components, the robot model in STEP format is loaded in the software ST Viewer which is used to define geometry shape_eid for each part and face_eid for corresponding surfaces. Three elementary entities can be distinguished in a structure: robot stationary components (base, working table), chain target tool, and chain target workpiece. All movable rotational joints are placed here on the side of the tool. For each axis, the elements that have to be defined are: name (a, b, c, d, e), constraints, mutual position, as well as the sequence of rotary axes. The placement location for the workpiece is defined with respect to a specified coordinate system of the robot (robot zero-configuration).

Configured machine tools and robots can also be used in a WEB interface which is shown in more detail in the next chapter.

4.3 Web interface for the virtual machine tools and robots for machining

A configured virtual machines and robots in a STEP-NC Machine environment can through a Web interface and local server enable accessibility on a cloud platform for simulation and monitoring.

Web interface based on STEP-NC is used NC.js. The NC.js package is implemented in JavaScript. The web interface on the local server can use the STEP Tools Machine commercial software [15] which can display the 3D models for the machining workpiece, tools, measuring probes, CNC, robots for machining, or CMM as well as material removal simulation, measuring path simulation, etc.

Procedures for build and run server can be viewed at [39]. The NC.js package is built from the source using the Node Package Manager. This will assemble all of the dependencies, including a pre-built version of the STEPNode plugin, and then start the server on a STEP-NC

file that you specify. First, it needs to install Node, and after it is installed, it is necessary to download the NC.js source code from GitHub. In the top-level directory of the NC.js package, the file "config.js" and the STEP-NC file can be edit, as also the machine tool model sample which is used in the STEP-NC Machine desktop software package. After successfully install Node and NC.js packages, a build and run server is available. When the server is running, start the web browser to address <http://localhost:8080/>, and you will see a machining setup shown in Fig.9 and Fig.10. After virtual machining, it is possible to download the virtual machined part as an STL file, for further qualitative analysis.

Two examples of virtual horizontal machining center LOLA HMC500, and industrial robot Gosko in WEB environment, where execute STEP-NC program and doing virtual machining, are shown on Figs. 9 and 10.

Web interface and local server can enable accessibility on a cloud platform STEP-NC environment for simulation and monitoring using a laptop computer, tablets, Smart Phones, and other mobile devices on any type of web browser (Fig.9 d, e, f).

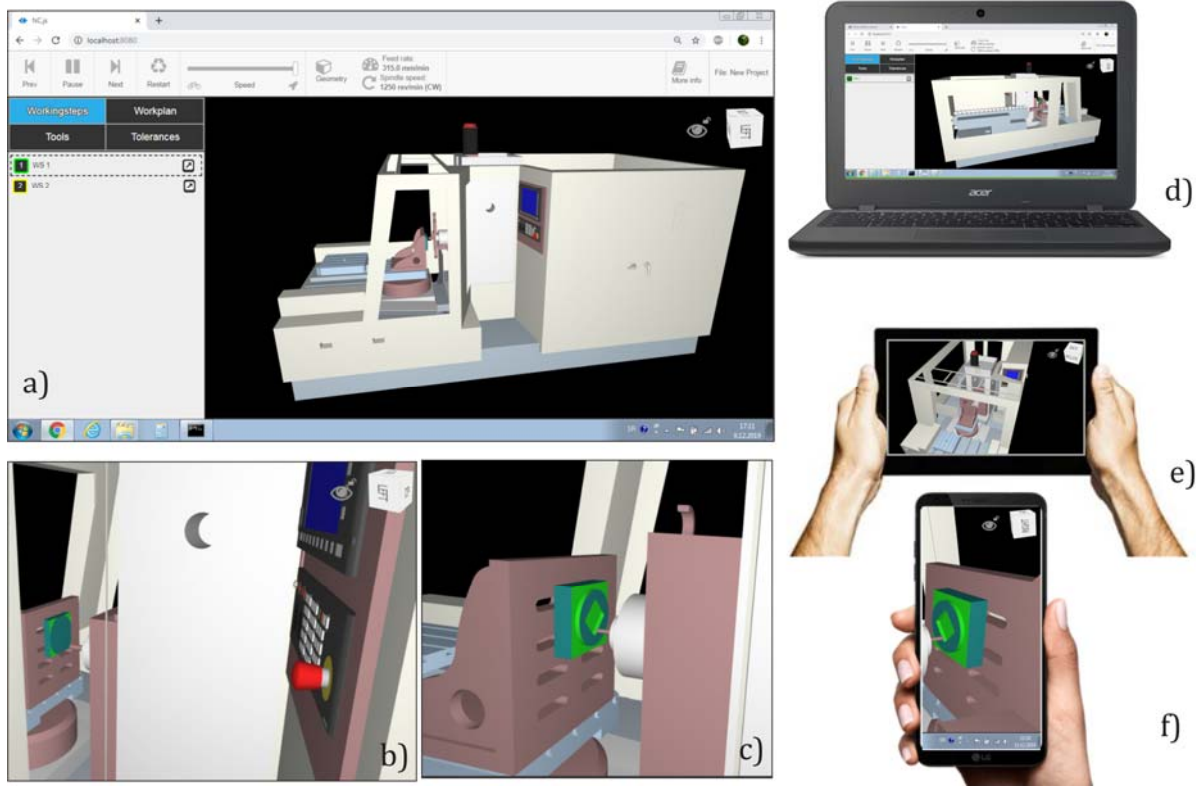


Fig. 9. Examples of configured machine tool in a WEB interface on local server

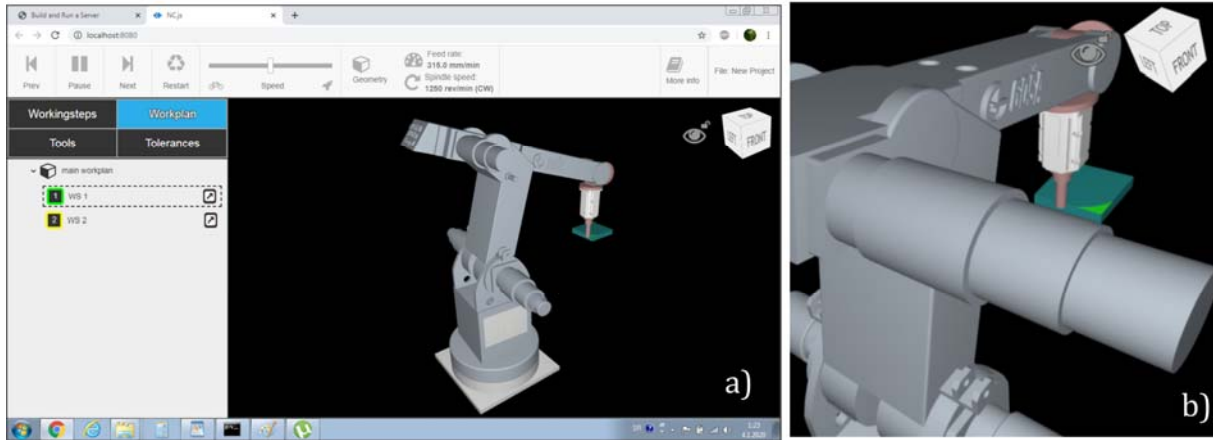


Fig. 10. Examples of configured virtual robot in a WEB interface on local server

In this way, it is possible to create interactive websites to share machining programs to get feedback. This is an example of the application of STEP-NC in the era of Industry 4.0 through Collaborative manufacturing, which would include here connect product design, manufacturing, and inspection with a digital twin, built-in real-time while machining with a new 3D model-based simulator [15,39].

5. PROGRAMMING ROBOT FOR MACHINING BASED ON STEP-NC

It can be said there are not many researches works on the application of STEP-NC in generating programs for industrial robots for machining. One of the reasons for the difficulty in applying STEP-NC to robots is that the controller needs to receive commands in a specific language imposed by each manufacturer, resulting in a large number of robot programming languages and difficulty in achieving standardization [26].

The focus of our research work is to contribute to the implementation of STEP-NC in the generation of native programs for industrial robots, without making changes in the robot control system [17].

The application of such a programming method does not involve additional costs and aids the integration of currently active industrial robots with the STEP-NC standard, which can be extended very easily to the existing robot controller even though it cannot currently benefit from all the innovations of STEP-NC [17].

Nowadays programming of industrial robots in machining tasks can be done in several ways [17,38]: (i) using CAD/CAM systems for programming of the multi-axis machine tool with the use of appropriate converters of CAM data (Cutter Location File – CLF and G-code) in native robot language, (ii) by postprocessing CLF, from current CAD/CAM systems for multi-axis machining to G-code if the robot controller can directly interpret G-code, and (iii) using specialized CAM software for programming of robot for machining that generates directly native robot language using appropriate postprocessors for robots, Fig.11.

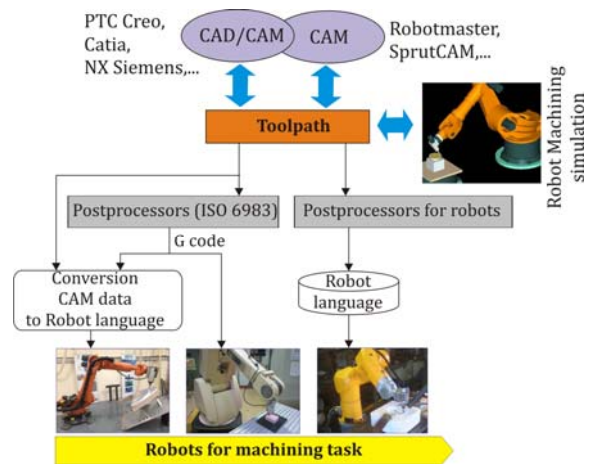


Fig. 11. G-code or robot language manufacturing data chain [17]

As already stated, the STEP-NC provides bi-directional data flow between CAD/CAM and CNC machine tools or robots for machining without losing information if they can directly interpret the STEP-NC program, i.e., if they have

a control unit that supports a new method of programming. There are practically no such commercial robots.

As it is presented in Fig.12, this research topic is to indirectly use the STEP-NC program on robots for machining. This can be done in two ways: (i) using the export option in STEP-NC software to export the program into G-code if the robot controller can directly interpret G-code, or (ii) by using appropriate converter in order to translate the STEP-NC program into a native robot language [17].

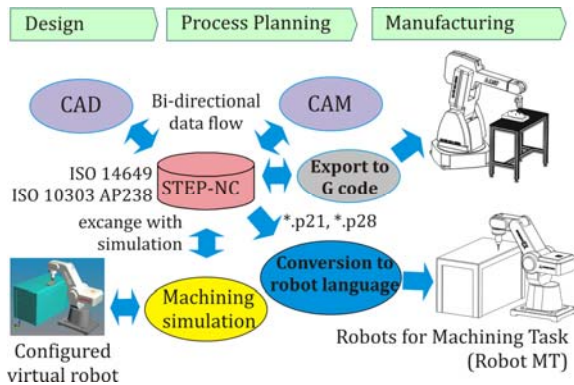


Fig. 12. G-code or robot language manufacturing data chain based on STEP-NC [17]

The developed programming method is applicable directly by CNC machine tool programmers by using the existing available CAD/CAM systems. Also, the methodology includes the developed procedure of configuring and integrating virtual robots for program simulation and verification. In order to realize real machining tasks, and considering that there are no robot controllers that can integrate STEP-NC programs directly, the methodology employs an indirect STEP-NC programming method to translate the program based on the ISO 10303–238 standard, using a developed converter for the STEP-NC program translation to robotic programming language [17].

Programming robots for machining based on STEP-NC is used to create machining programs that can be shared between many organizations and reused on many different machines and robots. With STEP-NC Machine, the execution of a STEP-NC program can be directly simulated on the configured virtual robots for machining, to make sure it will execute correctly using adequate modeled tools and fixtures. Also, in this way is a possible directly interpreted STEP-

NC program on available or configured virtual robots which is an integrated part of the software. This option is important for the purpose of verifying programmed tool paths, as well as for training and education.

6. DEVELOPED CONVERTORS FOR MACHINE TOOLS AND ROBOTS FOR MACHINING

Our research presented in paper [16,17,38] considers an Indirect programming method, based on standard ISO 10303–238, using the developed Robo STEP-NC converter i.e. Robot language converter (RLC), Fig. 13, which is employed for translating the exported STEP-NC *.p21 file into robot programming language in two ways: (i) G-code, or (ii) robot programming language.

This converter can be used for both industrial robots and machine tools with appropriate customization of the program output format, Fig.13.

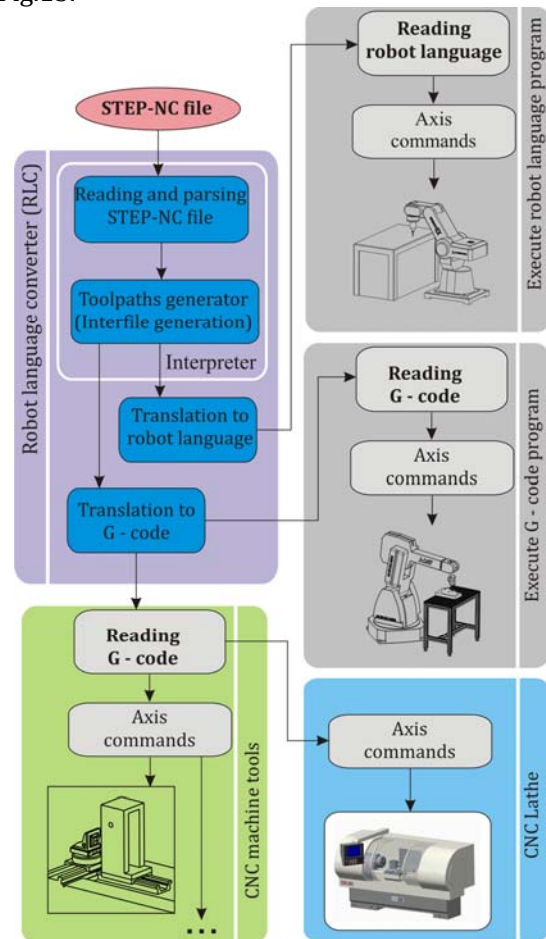


Fig. 13. Indirect STEP-NC programming method for machine tools and industrial robot for machining

The complete procedure of STEP-NC program conversion to G-code or robot language can be seen in [16,17]. This procedure should involve a STEP-NC program interpreter and its translation into an appropriate language. Main activities during translation STEP-NC program are: (i) reading and parsing P21 file, (ii) toolpath generator (Interfile generation), (iii) translation to G-code or robot language, (iv) toolpath simulation of generated G-code or robot language, and (v) execution of program on the real robot or CNC machine tool.

During further research, it is planned further development of the converter for different robot languages and specific G-codes.

7. DIGITAL THREAD FOR MANUFACTURING CAD-CAM-STEP-NC-CNC

The digital thread for manufacturing refers to the communication framework between CAD-CAM-STEP-NC-CNC that allows a connected data flow and integrated view of the product data throughout its lifecycle [40].

Primary trends of digitalization in the manufacturing industry are increasing efficiency, productivity, and the quality of products. As a base of the modern manufacturing industry, CNC machine tools and industrial robots play an essential role in industrial digitalization in the era of Industry 4.0 [3].

In this regard, the key link that forms the digital thread is STEP-NC as the interface between CAD/CAM and CNC. Nowadays, when the development of complex products involves the participation of different teams working in different environments, it is necessary to have an environment that can connect this work into an efficient integrated whole for the needs of manufacturing that product. For example, STEP-NC Machine can combine toolpaths APT/CLF from different CAD/CAM systems (Pro/Engineer, CATIA, UGS NX), Fig. 14, and form an integrated program in format P21, which is of importance if different CAD/CAM environments are used for programming the machining of some complex part.

On the other hand, the integrated technology thus obtained can be converted into the desired output, Fig.14, according to the available resources of the machine tool or the robot for machining. Desired output is possible using the export code option of STEP-NC Machine (Fanuc,

Siemens, Okuma, Haas, Heidenhain, ..., APT, ...) or using developed converters.

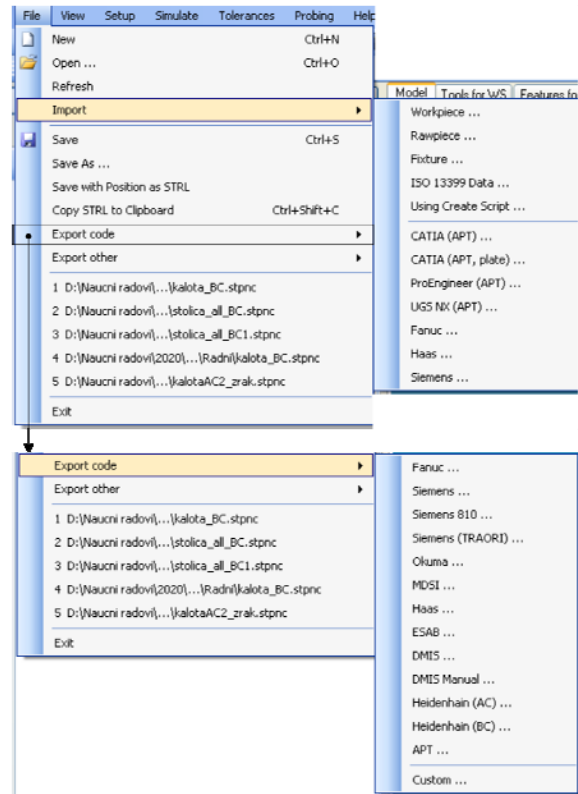


Fig. 14. Import and Export STEP-NC interfaces

Figure 15 shows an integrated digital thread for manufacturing based on STEP-NC. This is a demonstration of research at the Faculty of Mechanical Engineering in Belgrade, which is prepared in a similar way as demonstrations which organized STEP Tools [15] in order to promote this method of programming.

This figure shows mainly the application of STEP-NC programming methods on available machines and robots at the Faculty of Mechanical Engineering University of Belgrade, and the results of cooperation with the Faculty of Technical Science University of Novi Sad [13,41,423], Faculty of Mechanical Engineering University of Banja Luka [13], and the Mechanic and Mechatronic Engineering Department, University of Brasilia [21,27].

The Fig. 15 shows all the elements of the digital thread for manufacturing based on the STEP-NC Machine software and the ISO 10303-238 standard as data flow and integrated view of the product data throughout its lifecycle, both in virtual and real world.

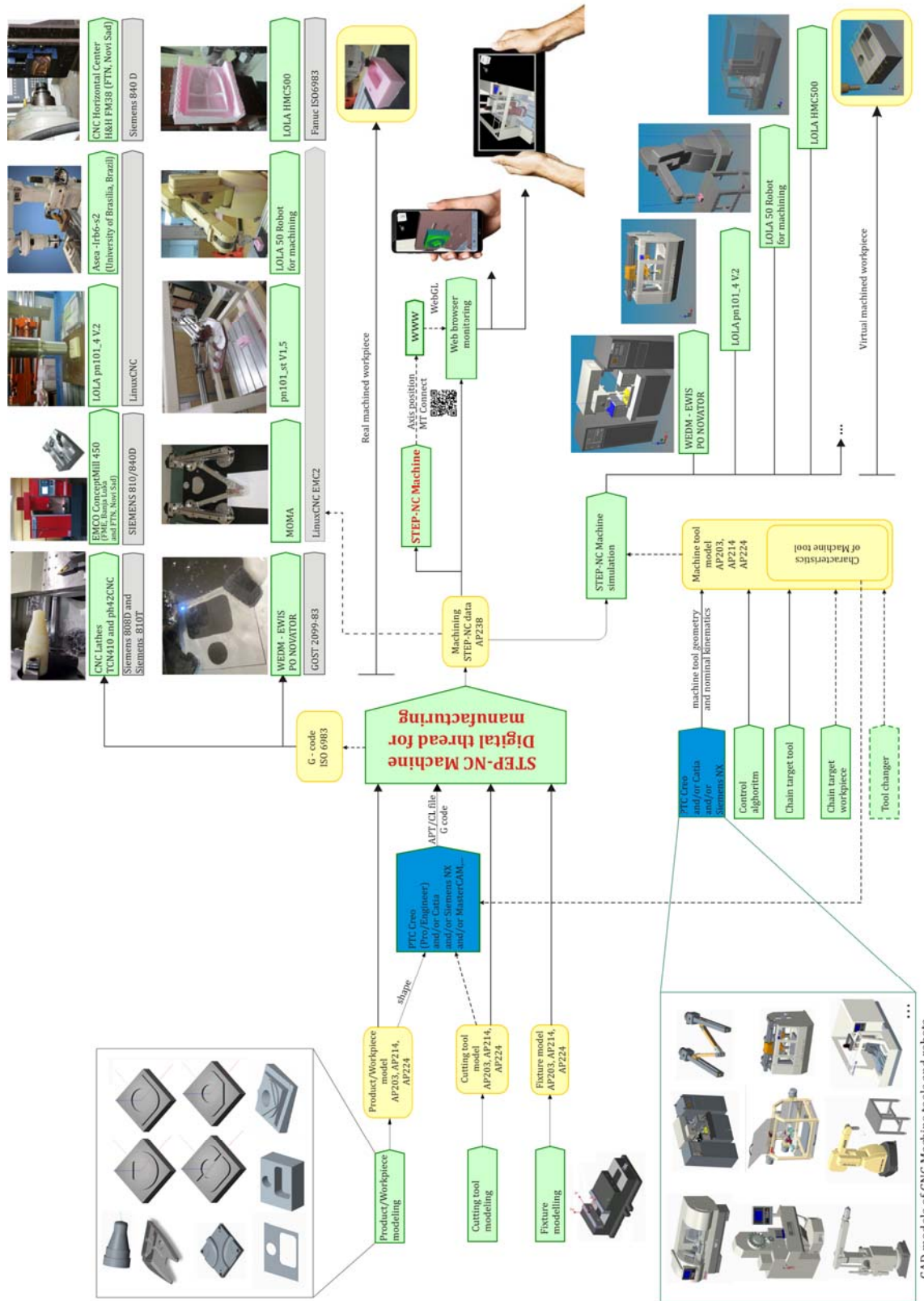


Fig. 15. Digital thread for manufacturing based on STEP-NC

8. EXPERIMENTAL VERIFICATION OF STEP-NC PROGRAMING IN ACTUAL PRODUCTION CONDITIONS

The aim of machining experiments is to test the methodology for the application of programming based on STEP-NC standards, for configured CNC machine tools and robots for machining. CAD/CAM system PTC Creo and STEP-NC Machine software are used to prepare the program and models of virtual machines or robots. After the simulation process is completed, the postprocessing or converting of STEP-NC programs in G-code or robot language follows.

In mostly where the available machines and robots cannot directly interpret STEP-NC, two approaches can be applied: (i) choosing an internal application for direct export of STEP-NC program to G-code in the STEP-NC Machine software, Fig.14, (ii) using developed converters for specific G-code format, or robot programming language.

Verification of the programming method and virtual machining workpieces using the STEP-NC is realized through several machining experiments.

8.1 Benchmark test

The first experimental verification was realized by processing a benchmark workpiece based on the original STEP-NC program according to ISO 14649-11 (ARM model). There are five machining working steps in the original file: milling the top surface of the workpiece; drilling and reaming the hole; and rough and finish milling the pocket.

NIST has built two STEP-NC interpreters [15,43] for milling operations, one using STEP-NC AIM (ISO10303-AP238), and the other using STEP-NC ARM (ISO14649-10-11). The system outputs Canonical Machining Commands (CMCs) [43,44].

Original STEP-NC program according to ISO 14649-11 is translated using STEP-NC interpreter [15] in Canonical Machining Commands (CMCs), and then these CMCs are translated into G-code. Machining was realized on a vertical 3-axis machine with parallel kinematics LOLA pn101_4 V2, Fig.16a. The scaled benchmark workpiece was also machined on the desktop variant of the vertical

3-axis machine with parallel kinematics pn101_st V1.5 [45], Fig.16b.

In the following, we used the proposed methodology to generate a STEP-NC file for this benchmark test, but according to the ISO 10303-238 standard (AIM model), while the tool path was achieved using a developed converter to the appropriate G-code. Figure 16c shows the machining of a benchmark workpiece on a robot for machining LOLA 50 [16], which is programmed in G-code [46]. G-code is obtained using a developed Robo STEP-NC converter.

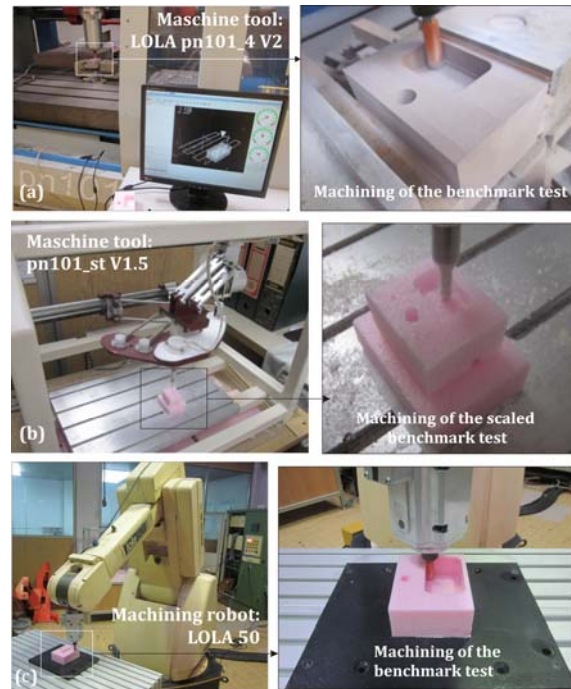


Fig. 16. Examples of machining 3D benchmark test

We also provide examples that refer to the machining 2D benchmark workpiece based on the STEP-NC program according to ISO 10303 AP238, Fig.17, for the 2 axis Wire EDM machine [35], and reconfigurable 2-axis parallel kinematic machine MOMA [47].

For preparing all inputs for generating STEP-NC file, used CAD/CAM system PTC Creo, were also performed tool path verification, Fig.17a. A generated STEP-NC file in P21 format and an example of its tool path simulation in STEP-NC Machine is shown in Figure 17b.

The 2D benchmark workpiece has 3 machining features: two inner contours of the circle and a rectangle with rounded edges and an outer contour of a rectangle shape [32]. The contour of the workpiece was cut in aluminum sheet

with 2 mm thickness on WEDM machine Ewis. This 2D benchmark workpiece contours on the second 2-axis reconfigurable parallel kinematic machine (MOMA) were plotted on the paper, Fig.17c.

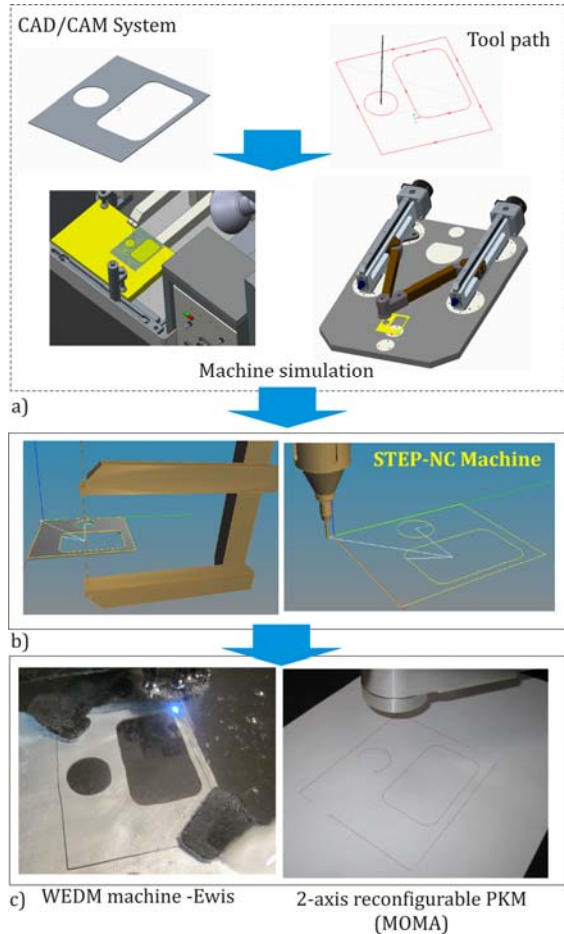


Fig. 17. Examples of machining 2D benchmark test

8.2 Mill machining experiments

For a group of experiments related to the machining of original STEP-NC files from STEP Tools [15], machining of parts Fishhead, NAS979, and Moldy part was performed. The first example is Fishhead, and for this example is used scenario Sc1, where the original STEP-NC program (AIM model) is translated into the G-code and then it was machined on three different machines, with three different control system: (i) LOLA HMC 500, FANUC (FME-BG), (ii) 3 axis vertical milling machine with parallel kinematics LOLA pn101_4 V2, LinuxCNC (FME-BG), and (iii) CNC Horizontal center, H&H FM38 Siemens 840D (FTN-NS), Fig. 18.



Fig. 18. Examples of mill machining based on STEP-NC

Example of machining test workpiece NAS 979 (circle/diamond/square test) according to the scenario Sc1, use original STEP-NC program translated into the G-code and then it is machined on the 3-axis vertical milling machine with parallel kinematics LOLA pn101_4 V2, Fig.19a.

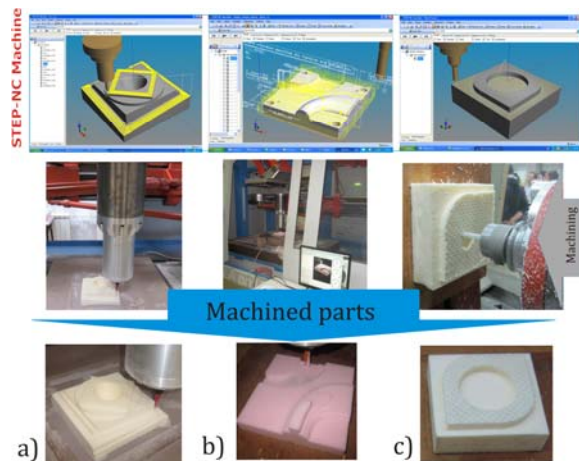


Fig. 19. Examples of mill machining

Previously necessary simulations were made (in STEP-NC Machine) for the reconstruction of

machining technology for a test workpiece NAS 979. File format STEP-NC for part NAS979 is directly translated into Fancu G-code using the Export option of software STEP-NC Machine [2]. As a part of the promotion activities on the STEP-NC [48], the test workpiece NAS979 is machined during a presentation in Orlando (Florida, USA, 2005.) [49].

The machined part in Fig.19b is the Moldy part which is also the original STEP-NC program translated into the G-code and then it was machined on the 3-axis vertical milling machine with parallel kinematics LOLA pn101_4 V2. Moldy mold test part was used on demonstration the STEP Manufacturing team met in Renton, Washington to demonstrate and discuss advanced use of the STEP-NC AP238 standard. The key goals for this round of demonstrations were to have multiple sites machine the same part from the same AP-238 data, and to show AP-238 can be used for molds [50].

To verify the Sc2 scenario, a set of parts was prepared, one of which as an example of machining is shown in Fig. 19c. Scenario Sc2 enables importing geometry elements of the reference model (Fig.5), workpiece, tool, and tool path from common CAD/CAM system into STEP-NC Machine software where STEP-NC file is generated in P21 format. After that is used option export to G-code for Fancu CNC control, and machining result on horizontal machining center LOLA HMC500 is shown in Fig. 19c.

8.3 Machining experiments on lathe

Verification of the developed programming methodology using STEP-NC protocol, through machining of parts on available CNC lathes was performed in the laboratory with programming, simulation, and translation of the STEP-NC program in format P21 into G-code [51,52].

The software STEP-NC Machine was used to generate the STEP-NC program in P21 format where the simulation was performed on the configured virtual CNC lathes. After that, the translation of the STEP-NC program into G-code was performed.

Figure 20 shows an example related to the complete machining of a workpiece (including roughing and finishing) on a TCN410 CNC lathe, based on STEP-NC protocol.

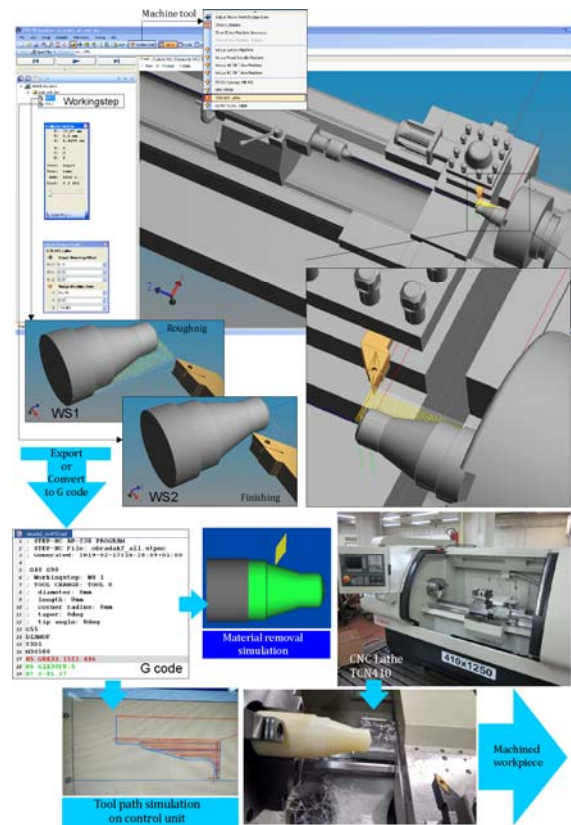


Fig. 20. Example of machining on CNC lathe

During the machining on the CNC lathe, two working steps were performed: roughing and finishing. After generating the STEP-NC program in P21 format and simulating on the TCN410 virtual lathe in the STEP-NC Machine software, the program was translated to G-code for the Siemens control unit. The program obtained in this way in the G-code was additionally tested in the CIMCO program environment, as well as on the control unit of the Siemens Sinumerik 808D, after which the workpiece on the machine was machined.

By machining the selected trial part, the possibility of applying a new programming method based on the STEP-NC protocol was confirmed, using a hybrid programming method which at this stage is reduced to translating the STEP-NC program to G-code using the Export option of STEP-NC Machine software or using developed converters for the specific format of G - code.

8.4 Robot machining experiments

The first results in the application of the indirect programming method based on the

STEP-NC standard ISO 10303-238, applicable on robots for machining were achieved on the LOLA 50 robot [16], and then on the Mitsubishi Movemaster EX robot [17].

The first example, presented here, refers to the machining of a typical STEP-NC benchmark project, which already shown in Fig. 16c. Although this example is provided in ISO14649-11, in this example it has been remodeled according to ISO10303-238, because the proposed programming methodology for robots includes software STEP-NC Machine, which cannot read the P21 file according to standard ISO 14649. For this example, we prepared a CAD model in STEP format for the workpiece, tool (diameter 12 mm), and tool path in APT/CLF. There are three machining working steps. They are for milling the top surface of the workpiece, drilling, and milling of the pocket (rough and finish).

By applying the proposed methodology from Section 3, models of the workpiece, tool, and toolpath were loaded in software STEP-NC Machine, and STEP-NC file was generated in format P21. For the thus obtained program, the configured virtual robots are available for machining simulation according to this program. After successful machining simulations, the obtained P21 file was translated, using the developed module RoboSTEP-NC [16], whereby G-code is obtained and adapted to direct application on available 5-axis machining robot LOLA50.

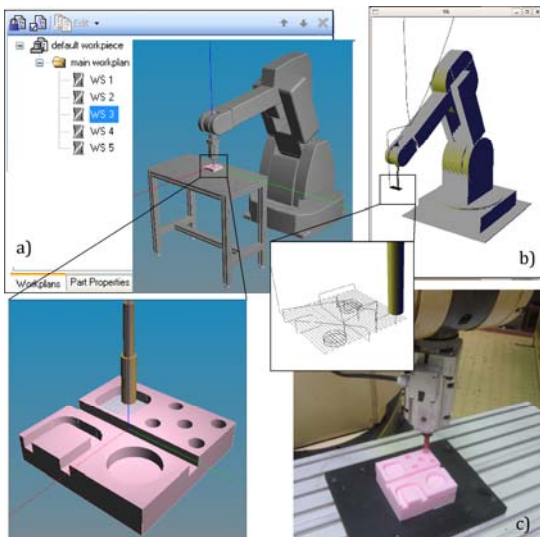


Fig. 20. Example of machining on robot LOLA50

The second example refers to the machining of a specially designed test workpiece, which includes trajectory milling, pocket milling, and drilling. The procedure of program preparation and verification is identical to the one presented for the first example. Simulation results in the STEP-NC Machine software for the program in P21 format are shown in Fig. 20a. The robot control and programming system are based on the LinuxCNC for which a virtual robot was also developed to meet the needs of off-line machining simulation [53]. The G-code obtained by applying the developed module RoboSTEP-NC [17] is verified once again, on a virtual robot integrated with the control system, Fig.20b, and thereafter the machining of a workpiece is executed on the robot, Fig. 20c.

The third example refers to experiments on the 5-axis robot Mitsubishi Movemaster EX was to verify the proposed methodology for indirect programming that includes: generating the program in P21 format, machining simulation on a configured virtual robot (Fig.21a,c), and translating STEP-NC *.p21 file to native robot language by applying the, developed converter [17].

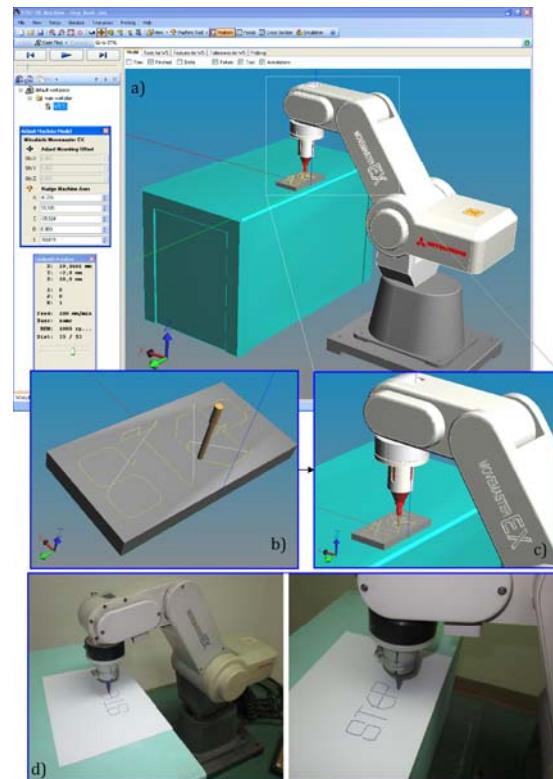


Fig. 21. Example of contour drawing on Mitsubishi Movemaster EX robot

Verification of this indirect method for robot programming using the STEP-NC is realized through drawing contours. The presented example, Fig.21b, refers to the programming of drawn contours, which includes linear and circular segments. This contour is a specially designed word "STEP". The drawing of this contour on a robot is shown in Fig.20d.

STEP-NC based machining architecture applied to industrial robots is a topic of cooperation between the Faculty of Mechanical Engineering University of Belgrade and the Mechanic and Mechatronic Engineering Department, University of Brasilia. DA-BA-SA concept of collaboration between researchers from Brazil and Serbia [21,27] through method for applying the ISO 10303-238 in robotic machining is shown in Fig.22a. The method encompasses programming based on STEP-NC, simulation, and machining by industrial robots in Serbia and in Brazil. Application and validation of robotized machining are performed using two industrial robots (ASEA IRB6-S2 and LOLA50) using the LinuxCNC control system, Fig.22b.

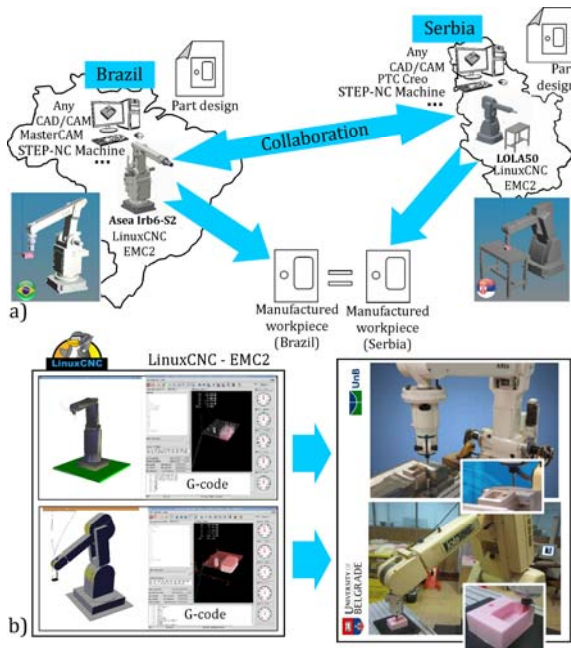


Fig.22. E-manufacturing context using STEP-NC

Initially, a 3D part is designed using any CAD system, and it is sent through the Internet to a CAM specialist who uses an adequate available software to generate a process plan in a STEP-NC format. Then, machine operators in Brazil or Serbia download the part design and its process

plan in a STEP-NC format and simulate machining based on working steps data. Finally, machining with real robots in Brazil and in Serbia is carried out [21]. The ISO 10303-238 is the first step toward smart manufacturing and concept for Industry 4.0 which allows cloud manufacturing possibility, which is demonstrated through this collaboration.

9. CONCLUSION

In order to contribute to efficient applications of a new method of programming based on STEP-NC protocol (ISO10303-238), the focus of our current research is related to applying STEP-NC, for programming different kinds of CNC machine tools, as well as a robots for machining. This paper presents the results of ten years of research in this field, which does not lose its relevance. Through developed methodology and experimental validation through machining based on STEP-NC, our research and collaboration are presented.

STEP-NC (ISO10303-238) is an object-oriented standard that is well adapted for exchanging high-level manufacturing data. It provides a new vision of the numerical chain with multidirectional exchange possibilities. For now, the application of STEP-NC-based programming methods is limited and is applied mainly at the first indirect level that applies to machines that can only execute G-code. It can be said that companies cannot get rid of their existing CNC controller and CAD/CAM solutions, so the implementation of STEP-NC has to be achieved step by step. In order to fully realize the STEP-NC concept, the development of a STEP-NC compliant controller is crucial.

A new vision of CAD/CAM/CNC data chain, with STEP-NC as the interface, has large benefits for the manufacturing industry in terms of efficiency and interoperability. The applying STEP-NC protocol is also compliant with the developments of Industry 4.0, concepts of digitalization such as virtual machine tools and robots as a paradigm known as a digital twin, cyber-physical systems, and cloud computing. The suggestion of future works includes the further development of converters for specific G-code and new robotic language, as well as the transition to the second level of direct interpreted STEP-NC programming where axis command is directly executed from STEP-NC file.

Acknowledgement

The presented research was supported by the Ministry of Education, Science and Technological Development of the Republic of Serbia through the project “Integrated research in macro, micro, and nano mechanical engineering” (contract no. 451-03-9/2021-14/200105 dated 5 February 2021).

REFERENCES

- [1] Kamran L., Aini Z. A. K., Yusri Y. (2019). The Importance of STEP-NC in the IR 4.0 Manufacturing Systems, *International Journal of Advanced Trends in Computer Science and Engineering*, vol. 8, no.4, p. 1568-1570.
- [2] Zivanovic, S., Vasilic, G. (2017). A New CNC Programming Method using STEP-NC Protocol. *FME Transactions*, vol. 45, no. 1, p. 149-158. DOI: [10.5937/fmet1701149Z](https://doi.org/10.5937/fmet1701149Z)
- [3] Živanović, S., Tabaković, S., Zeljković, M. (2018). Machine tools and Industry 4.0 - trends of development, 4th International Scientific Conference on Mechanical Engineering Technologies and Applications COMETA2018, Conference Proceedings, Invited paper - Plenary lectures, p.2-19.
- [4] Xu, X. (2017). Machine Tool 4.0 for the new era of manufacturing, *International Journal of Advanced Manufacturing Technology*, vol.92, no.5-8, p.1893–1900. DOI: [10.1007/s00170-017-0300-7](https://doi.org/10.1007/s00170-017-0300-7)
- [5] Liu, C., Xu, X. (2017). Cyber-Physical Machine Tool – the Era of Machine Tool 4.0, *Procedia CIRP, The 50th CIRP Conference on Manufacturing Systems*, vol. 63, p. 70-75. DOI: [10.1016/j.procir.2017.03.078](https://doi.org/10.1016/j.procir.2017.03.078)
- [6] 6 Ways Industry 4.0 Is Changing Machine Tools. From: <https://www.manufacturingtomorrow.com/article/2017/12/6-ways-industry-40-is-changing-machine-tools/10787>, accessed on: March 25, 2021.
- [7] ISO 6983-1:1982. (1982). *Numerical control of machines – Program format and definition of address words – Part 1: Data format for positioning, line motion and contouring control systems*. International Organization for Standardization. Geneva.
- [8] Rauch M., Laguionie R., Hascoet J.Y., Suh S.H. (2012). An advanced STEP-NC controller for intelligent machining processes. *Robotics and Computer-Integrated Manufacturing*, vol. 28, no.3, p. 375–384. DOI: [10.1016/j.rcim.2011.11.001](https://doi.org/10.1016/j.rcim.2011.11.001)
- [9] Bonnard R., Hascoët J.Y., Mognol P. Stroud I. (2018). STEP-NC digital thread for additive manufacturing: data model, implementation and validation. *International Journal of Computer Integrated Manufacturing*, p. 1–20. DOI: [10.1080/0951192X.2018.1509130](https://doi.org/10.1080/0951192X.2018.1509130)
- [10] Ahmad M.I., Yusof Y., Daud M. E. (2019). An overview of the current status on STEP-NC. *IOP Conf. Series: Journal of Physics: Conf. Series* 1150, 012015, DOI: [10.1088/1742-6596/1150/1/012015](https://doi.org/10.1088/1742-6596/1150/1/012015)
- [11] Randelović S., Živanović S. (2007). CAD-CAM Data Transfer as a Part of Product Life Cycle. *Facta Universitatis, Series: Mechanical Engineering* vol.5, no.1, p. 87-96.
- [12] Sääski, J., Salonen, T., Paro, J. (2005). Integration of CAD/CAM and NC with STEP-NC, VTT Information Service, Finland. From: http://www.engineering108.com/Data/Engineering/Mechanical/CAD_CAM/CAD-CAM_integration.pdf, accessed on: April 9, 2021.
- [13] Lukic, D., Zivanovic, S., Vukman, J., Milosevic, M., Borojevic, S., Antic, A. (2018). The possibilities for application of STEP-NC in actual production conditions. *Journal of Mechanical Science and Technology*, vol. 32, no. 7, p. 1-12. DOI: [10.1007/s12206-018-0634-6](https://doi.org/10.1007/s12206-018-0634-6)
- [14] Xu, X. W., Wang, H., Mao, J., Newman, S. T., Kramer, T. R., Proctor, F. M., Michaloski, J. L. (2005). STEP-compliant NC research: the search for intelligent CAD/CAPP/CAM/CNC integration. *International Journal of Production Research*, vol.43, no.17, p. 3703–3743. DOI: [10.1080/00207540500137530](https://doi.org/10.1080/00207540500137530)
- [15] Step Tools, Inc., From: <http://www.steptools.com/>, accessed on: March 31, 2020.
- [16] Zivanovic, S., Slavkovic, N., Milutinovic, D. (2018). An approach for applying STEP-NC in robot machining. *Robotics and Computer-Integrated Manufacturing*, vol.49, p. 361–373. DOI: [10.1016/j.rcim.2017.08.009](https://doi.org/10.1016/j.rcim.2017.08.009)
- [17] Slavkovic, N., Zivanovic, S., Milutinovic, D. (2019). An indirect method of industrial robot programming for machining tasks based on STEP-NC. *International Journal of Computer Integrated Manufacturing*, vol.32, no.1, p.43-57. DOI: [10.1080/0951192X.2018.1543952](https://doi.org/10.1080/0951192X.2018.1543952)
- [18] Xiao, W., L. Zheng, J. Huan, and P. Lei. (2015). A Complete CAD/CAM/CNC Solution for STEP-compliant Manufacturing. *Robotics and Computer-Integrated Manufacturing*, vol.31, p. 1–10. DOI: [10.1016/j.rcim.2014.06.003](https://doi.org/10.1016/j.rcim.2014.06.003)
- [19] Othman M. A., Minhat M., Jamaludin, Z. (2017). An overview on STEP-NC compliant controller development. *IOP Conference Series: Materials*

- Science and Engineering, vol. 257, p.012048. DOI: [10.1088/1757-899X/257/1/012048](https://doi.org/10.1088/1757-899X/257/1/012048)
- [20] Rauch, M., Hascoët, J-Y., Simoes, V., Hamilton, K. (2014). Advanced programming of machine tools: interests of an open CNC controller within a STEP-NC environment. *International Journal of Machining and Machinability of Materials*, vol.15, no.1-2, p.2-17. DOI: [10.1504/IJMMM.2014.059184](https://doi.org/10.1504/IJMMM.2014.059184)
- [21] Toquica, J., S., Zivanovic, S., Bonnard, R., Rodriguez, E., Alvares, A. J., Ferreira, J.C.E. (2019). STEP-NC-based machining architecture applied to industrial robots. *Journal of the Brazilian Society of Mechanical Sciences and Engineering*, vol. 41, p.314. DOI: [10.1007/s40430-019-1811-y](https://doi.org/10.1007/s40430-019-1811-y)
- [22] Xu, X.W. (2006). Realization of STEP-NC enabled machining. *Robotics and Computer-Integrated Manufacturing*, vol.22, no.2, p.144-153. DOI: [10.1016/j.rcim.2005.02.009](https://doi.org/10.1016/j.rcim.2005.02.009)
- [23] Solvang, B., Refsahl, L. K., Sziebig, G. (2009). "STEP-NC Based Industrial Robot CAM System, in Preprints of the 9th International Symposium on Robot Control (SYROCO'09)." The International Federation of Automatic Control, Gifu, Japan, p.361-366.
- [24] Valilai, O. F., Nodeh, M. J., Houshmand, M. (2010). Robocad INFELT STEP, Interoperable Platform to Manage Collaboration among CAD and Robot Programming Agents Integrated Based on STEP (ISO 10303) Standard. In Proceedings of the World Congress on Engineering and Computer Science, San Francisco, CA: International Association of Engineers (IAENG), p.350-356.
- [25] Xiao, W., Huan, J., Dong, S. (2014). A STEP-compliant Industrial Robot Data Model for Robot Off-Line Programming Systems. *Robotics and Computer-Integrated Manufacturing*, vol.30, p. 114-123. DOI: [10.1016/j.rcim.2013.09.007](https://doi.org/10.1016/j.rcim.2013.09.007)
- [26] Rea Minango, S. N., Ferreira, J., Carlos, E. (2017). Combining the STEP-NC standard and forward and inverse kinematics methods for generating manufacturing tool paths for serial and hybrid robots. *International Journal of Computer Integrated Manufacturing*, p.1-21. DOI: [10.1080/0951192X.2017.1305507](https://doi.org/10.1080/0951192X.2017.1305507)
- [27] Toquica, J.S, Živanović, S., Alvares, A.J., Bonnard, R. (2018). A STEP-NC compliant robotic machining platform for advanced manufacturing. *The International Journal of Advanced Manufacturing Technology*, vol. 95,p. 3839-3854. DOI: [10.1007/s00170-017-1466-8](https://doi.org/10.1007/s00170-017-1466-8)
- [28] Živanović, S., Glavonjić, M. (2014). Methodology for implementation scenarios for applying protocol STEP-NC. *Journal of Production Engineering*, vol.17, no.1, p. 71-74.
- [29] Zhang, Y., Bai X-L., Xu, X., Liu, Y-X. (2012). STEP-NC based high-level machining simulations integrated with CAD/CAPP/CAM. *International Journal of Automation and Computing*, vol. 9, no.5, p.506-517. DOI: [10.1007/s11633-012-0674-9](https://doi.org/10.1007/s11633-012-0674-9)
- [30] Glavonjic, M., Zivanovic, S. (2012). A new CNC programming method using STEP-NC. 38th JUPITER Conference, 34th Symposium "NC-ROBOTS-FMS", Conference Proceedings (in Serbian), p. 3.112-3.117.
- [31] Glavonjic, M., Zivanovic, S. (2012). STEP-NC protocol for programming CNC machine tools. *TECHNICS- Magazine of the union of engineers and technicians of Serbia (in Serbian)*, vol.6, p.937-942.
- [32] Zivanovic, S., Slavkovic, N., Dimic, Z., Vasilic, G., Puzovic, R., Milutinovic, D. (2017). Virtual machine tools and robots for machining simulation based on STEP-NC program, 6th International Conference on Manufacturing Engineering ICMEN 2017 Conference Proceedings, p.41-51.
- [33] Zeljkovic, M., Tabakovic, C., Zivkovic, A., Zivanovic, C., Mladjenovic, C., Knezev, M. (2018) *Basics of CAD/CAE/CAM technology*. University of Novi Sad, Faculty of Technical Sciences.
- [34] Zivanovic S., Glavonjic M. (2013). Simulations of machining based on STEP-NC. 11th Anniversary International Conference on Accomplishments in Electrical and Mechanical Engineering and Information Technology DEMI 2013 Conference Proceedings, p. 513-521.
- [35] Zivanovic, S., Puzovic, R.(2016). Wire EDM machining simulations based on STEP-NC program. *Tehnički vjesnik / Technical Gazette*, vol. 23, no. 6, p.1831-1838. DOI: [10.17559/TV-20151122180547](https://doi.org/10.17559/TV-20151122180547)
- [36] Živanović, S., Vorkapić, N., Slavković, N., Kokotović, B. (2020). Analysis of the application of a new programming method of CNC lathes by application of the STEP-NC protocol. 42nd JUPITER Conference, 38th Symposium "NC-ROBOTS-FMS", Conference Proceedings (in Serbian), p. 3.129-3.134.
- [37] Slavkovic, N., Zivanovic, S., Milutinovic, D., Kokotovic, B. (2017). Robot machining simulation in STEP-NC machine environment. 13th International Conference on Accomplishments in Electrical and Mechanical Engineering and Information Technology DEMI 2017 Conference Proceedings, p. 43-50.
- [38] Živanović, S., Slavković, N., Milutinović, D., Methodology of programming robots based on STEP-NC protocol, 41st JUPITER Conference, 37th Symposium "NC-ROBOTS-FMS",

- Conference Proceedings (in Serbian), p. 3.60-3.67.
- [39] STEP Tools, Inc, Build and run server. From: <https://steptools.github.io/NC.js/build.html>, accessed on: April 13,2021.
- [40] What is the Digital Thread in Manufacturing? Definition & Benefits. From: <https://www.ibaset.com/what-is-the-digital-thread/>, accessed on: April 15, 2021.
- [41] Lukić, D., Vukman, J., Živanović, S., Milošević, M., Borojević, S., Jovičić, G., Mladenović, C. (2016). Application of STEP-NC in the integration CAX and CNC systems: Case studies. *Machine Design*, vol.8, no.1, p.23 -26.
- [42] Zivanovic, S., Tabakovic, S., Zeljkovic, M., Mladjenovic, C., Košarac, A. Machining simulation and verification of tool path for CNC machine tools with serial and hybrid kinematics. *Proceedings of the IX International Conference Heavy Machinery-HM 2017*, July, 2017, Faculty of mechanical and civil engineering in Kraljevo University of Kragujevac, Zlatibor p.B.63-B.68.
- [43] Toolkit for ISO 14649 / STEP-NC, From: <http://code.google.com/p/iso-14649-toolkit/downloads/list>, accessed on: April 7, 2020.
- [44] Zhao, Y. F., Habeeb, S., Xu, X. (2008). Research into integrated design and manufacturing based on STEP. *The International Journal of Advanced Manufacturing Technology*, vol.44., no. 5-6, p.606–624. DOI: [10.1007/s00170-008-1841-6](https://doi.org/10.1007/s00170-008-1841-6)
- [45] Zivanovic, S., Glavonjic, M., Milutinovic, D., Slavkovic, N. (2014). Programming methods for mini laboratory and desktop 3-axis parallel kinematic milling machine. 5th International Conference on Manufacturing Engineering ICMEN Conference Proceedings, p.153-162.
- [46] Milutinovic, D., Glavonjic, M., Slavkovic, N., Dimic, Z., Zivanovic, S., Kokotovic, B., Tanovic, L. (2010). Reconfigurable robotic machining system controlled and programmed in a machine tool manner. *The International Journal of Advanced Manufacturing Technology*, vol. 53, no. 9-12, p. 1217–1229. DOI: [10.1007/s00170-010-2888-8](https://doi.org/10.1007/s00170-010-2888-8)
- [47] Vasilic, G., Zivanovic, S. Kokotovic, B. Dimic, Z. (2019). Configuring and analysis of a class of generalized reconfigurable 2-axis parallel kinematic machine. *Journal of Mechanical Science and Technology*, vol.33, no.7, p.1-15. DOI: [10.1007/s12206-019-0636-z](https://doi.org/10.1007/s12206-019-0636-z)
- [48] Hardwick, M., Zhao, Y. F., Proctor, F. M. (2013). A roadmap for STEP-NC-enabled interoperable manufacturing. *International Journal of Advanced Manufacturing Technology*, vol. 68, no. 5-8, p.1023–1037. DOI: [10.1007/s00170-013-4894-0](https://doi.org/10.1007/s00170-013-4894-0)
- [49] STEP-NC Pilot Demonstration OMAC STEP-NC Working Group Meeting, Orlando, Florida, USA, 2005. From: http://www.steptools.com/stds/stepnc/2005_orlando/, accessed on: April 18, 2021.
- [50] International STEP-NC Demonstration, Renton, WA 2009. From: http://www.steptools.com/stds/stepnc/2009_renton/, accessed on: April 18, 2021.
- [51] Živanović, S., Slavković, N. (2018). Application of the STEP-NC standard ISO 10303 AP238 for turning operations, 13th International Scientific Conference mma 2018 – Flexible Technologies, Conference Proceedings, Invited paper, p. 49-52.
- [52] Živanović, S., Vorkapić, N., Slavković, N., Kokotović, B. (2020). Analysis of the application of a new programming method of CNC lathes by application of the STEP-NC protocol, 42nd JUPITER Conference, 38th Symposium "NC-ROBOTS-FMS", Conference Proceedings (in Serbian), p. 3.129-3.134.
- [53] Dimic Z., Milutinovic, D., Zivanovic, S., Kvrjic, V. (2016). Virtual environment in control and programming system for reconfigurable machining robot. *Technical Gazette*, vol. 23, no. 6, p.1821-1829. DOI: [10.17559/TV-20150210133556](https://doi.org/10.17559/TV-20150210133556)



Banja Luka
28–29 May 2021.

DEMI 2021

15th International Conference on
Accomplishments in Mechanical and
Industrial Engineering

www.demi.mf.unibl.org



Recent Trends in Energy Efficient AC Motor Drives

Darko Marčetić^a

^aUniversity of Novi Sad, Faculty of Technical sciences, Trg Dositeja Obradovića 6, Novi Sad

Abstract

This paper deals with the recent trends in the development of energy efficient drives with alternating current (AC) motors, both three phase squirrel cage induction motor (IM) and three phase synchronous motor with permanent magnets (PMSM) mounted on the rotor. Beside the denoted motor types (IM and PMSM), two quite opposite AC motor applications are considered: low-cost appliance drives and high-performance drives for electrical vehicles. First, the difference between relatively cheap and mass production-ready general-purpose appliance drive and high-performance drive for electrical vehicles is highlighted. Special attention is given to the similarity of the models and model based methods used for improving the energy efficiency of both motor and AC drive types. Next, different model based methods for improvement of the energy efficiency of PMSM drive are given and discussed in more details. Finally, it will be shown that only with drive self-commissioning (automatic estimation of motor parameters and control loops gains) one can get the most from the model-based methods, resulting in robust AC drive performance and peak efficiency. At the end of the paper one example of PMSM drive self-commissioning procedure of low voltage PMSM drive powered by 48V battery in the electrical golf-cart application is described.

Keywords AC motors, Energy efficiency, Self-Commissioning

1. INTRODUCTIONS

During the recent decades, the energy efficiency arose as an essential paradigm within the modern alternating current (AC) power drives [1]-[3]. Different drive applications, starting from low-cost low-performance appliance drives (pumps, compressors, etc.), all the way to the high-performance high-fidelity drives for electrical vehicles, all require peak efficiency and/or extension of the motor torque dynamic capacity.

Depending on the AC motor type, IM (Three phase Induction Motor) or PMSM (Three phase permanent magnet synchronous motor) different control algorithms are suggested to adapt the motor flux level to achieve maximum efficiency at a given loading point. All energy efficient control techniques for AC drives could be classified as model based [4]-**Error! Reference source not found.**, and search based [16]-[19]. Search controller methods have zero

parametric uncertainty but exhibits undesired torque oscillations as well as slow convergence to the peak efficiency point. Model based approaches, upgraded with parameter identification algorithms, impose small parametric uncertainty, no torque ripple, are suitable for both steady and quasi-steady state drive operation and have no convergence problems. For the enlisted reasons, model based techniques are better candidate for construction of optimal AC drive in most of drive applications.

Model based techniques can be further classified to loss model controller (LMC) and techniques related to maximization of motor torque (MT). Both adapt the flux level of IM or PMSM with torque and speed reference, however LMC insures minimum overall losses, while MT strategies provide torque enhancement as well as partial loss minimization (only copper loss component is minimized).

This paper gives an overview of modern energy efficient AC drives for both low-cost appliance

market and high-performance high-fidelity electrical drives. In chapter two, dynamic models of IM and PMSM, and their respective energy balances are presented. Chapter three provides an overview of typical model based control strategies for PMSM that insure higher efficiency in both steady state and quasi-steady state. Finally, in chapter four, one example of PMSM drive self-commissioning is presented. The chapter contains the drive block diagram, typical signals achieved during the self-commissioning phases, and finally attained results which are needed to set proper parameters of model based techniques for power losses minimization.

2. DYNAMIC MODELS OF AC MOTORS INCLUDING IRON LOSSES

Most of the control algorithms for AC motors are based on their dynamic models. AC motor models all have similar electrical subsystem that is usually represented in rotating dq reference frame, which rotation is synchronized with the rotation of rotor flux vector. In that case, all three phase AC signals (voltages, currents, fluxes), can be represented as rotating vectors, with dq coordinates that are constant in steady state and can be easily controlled by optimization algorithm.

The inputs in every AC motor models are voltage vector dq coordinates, and the outputs are dq coordinates of stator current and rotor flux vectors, as well as and the electromagnetic torque T_e produced by the motor. The produced torque is an excitation input to the mechanical subsystem from which the rotor speed ω_r can be calculated:

$$\frac{d\omega_r}{dt} = \frac{P}{J} (T_e - T_l) \quad (1)$$

where P denotes drive pole pairs, T_l load torque and J as mechanical inertia.

2.1 Dynamic model of IM

Due to its robustness, low cost and simple installation and maintenance, the three phase induction motor (IM) is often used within low cost AC drive applications. Upgraded with the proper control algorithm, IM becomes linear torque convertor and for that reason is frequently used also in the high-performance high-efficiency drive applications, such are electrical vehicles.

Most of the control algorithms for IM are based on its dynamic model. The electrical subsystem of IM model is comprised from stator and rotor voltage equations:

$$v_{ds} = R_s i_{ds} + \frac{d\psi_{ds}}{dt} - \omega_e \psi_{qs} \quad (2)$$

$$v_{qs} = R_s i_{qs} + \frac{d\psi_{qs}}{dt} + \omega_e \psi_{ds} \quad (3)$$

$$0 = R_r i_{dr} + \frac{d\psi_{dr}}{dt} - (\omega_e - \omega_r) \psi_{ds} \quad (4)$$

$$0 = R_r i_{qr} + \frac{d\psi_{qr}}{dt} + (\omega_e - \omega_r) \psi_{qs} \quad (5)$$

flux linkage equations:

$$\psi_{ds} = L_{\gamma s} i_{ds} + L_m i_{dm}, \psi_{qs} = L_{\gamma s} i_{qs} + L_m i_{qm} \quad (6)$$

$$\begin{aligned} \psi_{dr} &= L_{\gamma r} i_{dr} + L_m i_{dm}, \psi_{qr} \\ &= L_{\gamma r} i_{qr} + L_m i_{qm} \end{aligned} \quad (7)$$

and the electromagnetic torque equation:

$$T_e = \frac{3}{2} P \frac{L_m}{L_{\gamma r}} \Psi_{dr} (i_{qs} - i_{qFe}) \quad (8)$$

Described dynamic model of IM, including iron losses, is given in Fig. 1, [7].

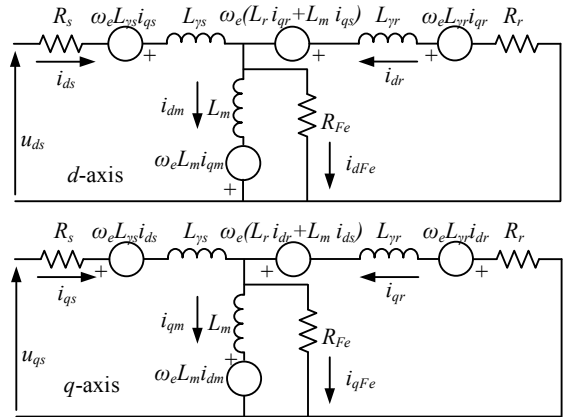


Fig. 1. Dynamic model of IM with included iron losses

Presented model has the following parameters: L_m as magnetizing inductance, R_s i $L_{\gamma s}$ stator resistance and leakage inductance, respectively, R_r i $L_{\gamma r}$ equivalent rotor resistance and leakage inductance and R_{Fe} equivalent active resistance of magnet circuit which models the iron (core) losses.

The total losses of an IM, P_{loss} , consist of stator and rotor copper losses P_{cu} , core losses P_{Fe} and mechanical losses P_m :

$$P_{loss} = P_{cu} + P_{Fe} + P_m \quad (9)$$

The mechanical losses are mostly rotor speed dependent, where k_m is mechanical loss coefficient:

$$P_m = k_m \omega_r^2 \quad (10)$$

As a consequence, mechanical losses are not

controllable by altering the parameters of voltage or current supplied to the motor.

On the other hand, copper and iron losses are controllable losses since they can be altered by utilizing appropriate voltage or current vector.

Therefore, to maximize the AC drive efficiency, the sum of copper and iron losses has to be minimized at given speed and loading conditions. To achieve that goal, trade-off has to be attained between the current and voltage amplitude because copper losses are a function of current amplitudes,

$$P_{cu} = R_s(i_{ds}^2 + i_{qs}^2) + R_r(i_{dr}^2 + i_{qr}^2) \quad (11)$$

while, the iron losses, in the first approximation, are the function of the stator voltage amplitude, U_s :

$$P_{Fe} \approx k_e \omega^2 \psi_m^2 = \frac{(\omega \psi_m)^2}{\frac{1}{k_e}} \approx \frac{U_s^2}{R_{Fe}} \quad (12)$$

where $U_s^2 = u_{ds}^2 + u_{qs}^2$.

Thus, the goal is to supply the IM with optimal current and voltage vectors which result with minimum controllable power losses, while IM is still delivering the mechanical power with corresponding mechanical speed and load torque.

2.2 Dynamic model of PMSM

The three phase permanent magnet synchronous motor (PMSM) can impose more efficiency comparing to the IM triggering the trend of IM replacement in both low-cost and high performance AC drive applications. The PMSM control algorithm is based on PMSM model and can transform PMSM as linear torque convertor with maximum efficiency. Similarly, the PMSM model is comprised with stator voltage balance equations in dq frame [13]:

$$u_{ds} = R_s i_{ds} + \frac{d\psi_{ds}}{dt} - \omega_{dq} \psi_{qs} \quad (13)$$

$$u_{qs} = R_s i_{qs} + \frac{d\psi_{qs}}{dt} + \omega_{dq} \psi_{ds} \quad (14)$$

$$u_{ds} = R_s i_{ds} + R_{Fe} i_{dFe} \quad (15)$$

$$u_{qs} = R_s i_{qs} + R_{Fe} i_{qFe} \quad (16)$$

and with stator flux linkage equations:

$$\psi_{ds} = L_d i_{do} + \psi_{PM} \cos(\theta_{dq} - \theta_{PM}) \quad (17)$$

$$\psi_{qs} = L_q i_{qo} - \psi_{PM} \sin(\theta_{dq} - \theta_{PM}) \quad (18)$$

where θ_{dq} and θ_{PM} define synchronous reference frame and permanent magnet angle coordinates. Model is completed with conservation of current:

$$i_{ds} = i_{do} + i_{dFe} \quad i_{qs} = i_{qo} + i_{qFe} \quad (19)$$

Finally, the PMSM electromagnetic torque is:

$$T_e = (3/2)P(\psi_{ds} i_{qo} - \psi_{qs} i_{do}) \quad (20)$$

Iron loss effects in the case of PMSM are also included

in the orthogonal branch of model, Fig. 2.

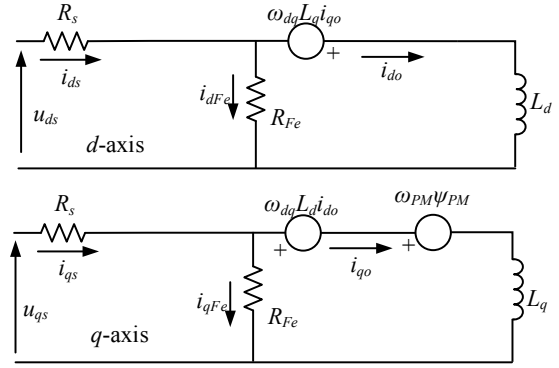


Fig. 2. Dynamic model of PMSM with included iron losses

In PMSM drive, the copper losses are directly related to stator current amplitude only.

$$P_{cu} = R_s(i_{ds}^2 + i_{qs}^2) \quad (21)$$

On the other hand, in the first approximation, core losses are related to the stator voltage amplitude:

$$P_{Fe} \approx \frac{u_{ds}^2}{R_{Fe}} + \frac{u_{qs}^2}{R_{Fe}} = \frac{U_s^2}{R_{Fe}} \quad (22)$$

3. FIELD-ORIENTED CONTROL OF AC MOTORS

The most popular algorithm used for energy efficient control of AC drives is field oriented control (FOC). The main result of FOC is linear control of AC motor torque production and improvement of AC drive dynamics. The second important result of FOC strategy is the ability of independent and decoupled control of flux level in the machine regarding the torque, which has the direct impact on AC motor efficiency.

FOC has the same structure for all AC drives types. FOC is based on the control of AC motor current vector which is typically achieved with two current regulators placed in the rotating dq reference frame. Based on the stator current coordinate errors, dq current regulators provide voltage references for space vector pulse width modulation (SVPWM) block which generates three phase PWM output signals for inverter.

The typical block diagram of high performance AC drive using FOC is given in Fig. 3. FOC uses two current sensors to establish stator current control, and one shaft sensor to measure rotor flux angle needed for FOC orientation [2]. Information from speed sensor is also used as a feedback signal in speed control loop. The scheme is similar for IM and PMSM, the only difference is in the FOC orientation block. In the case of PMSM the flux angle is directly measured, while in the case of IM rotor flux angle is estimated based on rotor position and rotor slip angle calculation [2].

Very similar block diagram of control scheme suitable for low cost AC drive using FOC is given in Fig. 4. The only difference is in the absence of the mechanical

sensor and the replacement of two expensive current sensors with one cheap shunt sensor, directly resulting in the overall drive cost reduction. However, cheap shunt sensor requires the additional phase current calculation

algorithm [20] and with appropriate sensorless algorithm, the one can estimate rotor flux angle and rotor speed as outputs [21].

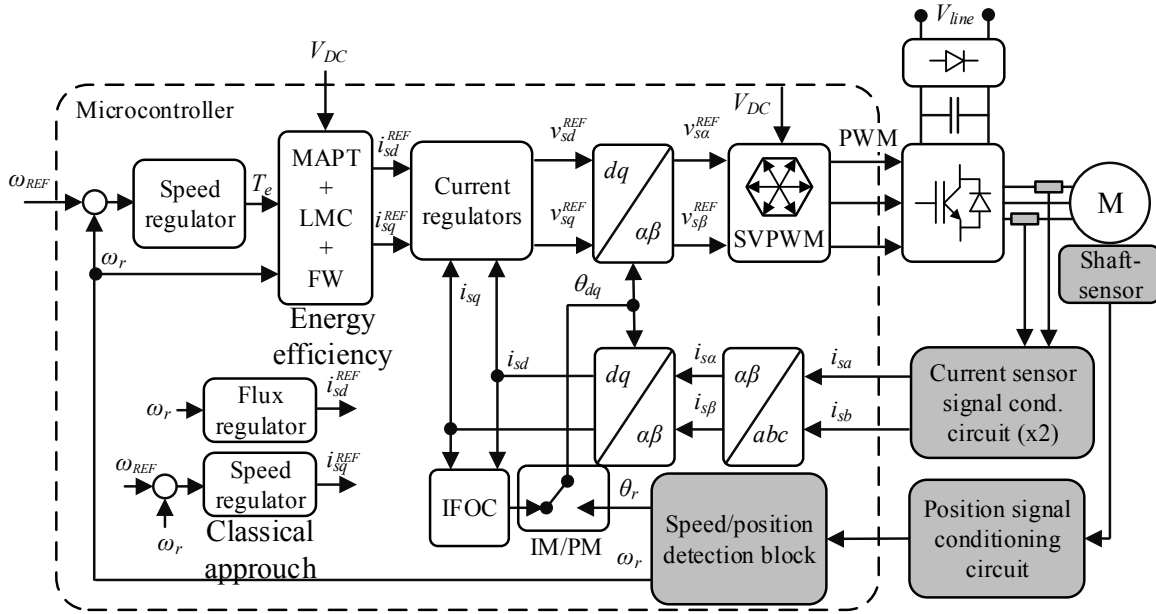


Fig. 3. Block diagram of high performance FOC AC drive with shaft sensor and two current Hall effect sensors, [21]

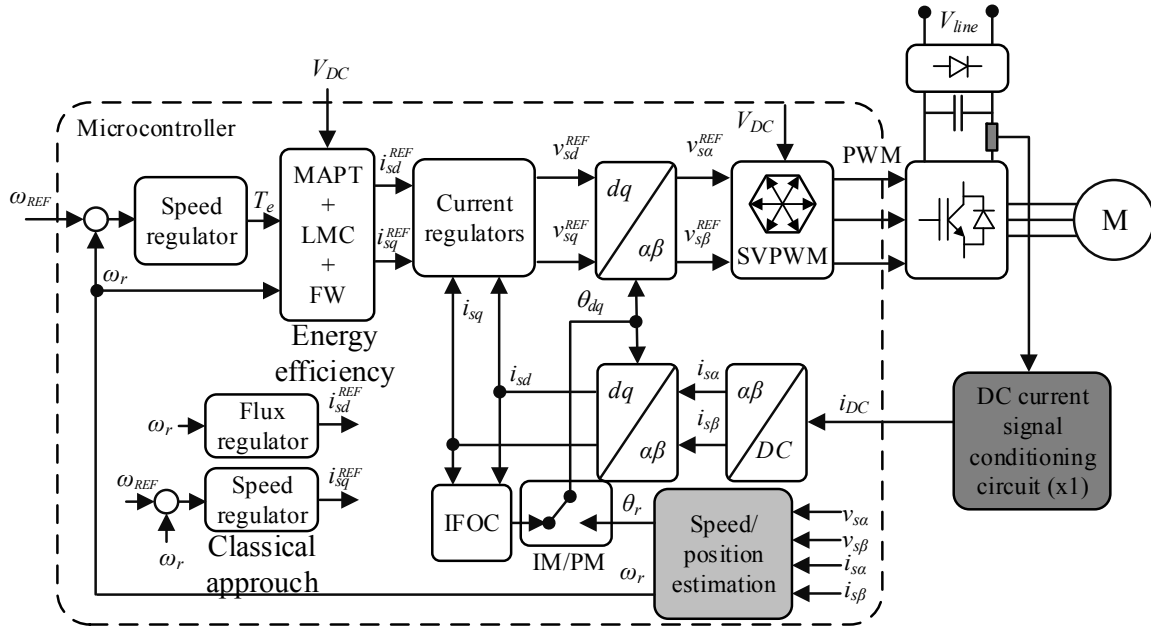


Fig. 4. Block diagram of low-cost FOC AC drive with minimum sensors (shaft-sensorless with single dc shunt), [20]

In the classical AC drive control approach, reference torque and flux production mechanisms are decoupled. Speed regulator is responsible for producing the torque reference, while the flux regulator block is controlling the flux reference, essentially performing rotor speed based field weakening (FW). Presented scheme is basically the analogous of the control scheme used for separately

excited direct current (DC) motor. However, in modern energy efficient drives the flux production has to be closely related with the torque demand, in order to insure the optimal control for given torque load and speed. For that reason, appropriate energy efficient control algorithm (like MAPT - Minimum Ampere per Torque or LMC- Loss Model Controller) has to be implemented in order to provide optimal dq

current pair for given torque demand. The only exception case is when the drive enters the voltage limit, in which the optimal strategy is canceled, and replaced with FW - field weakening.

4. ENERGY EFFICIENT CONTROL STRATEGIES FOR PMSM

In this chapter the optimal control strategies for PMSM are discussed. Very similar strategies are available for IM also [4].

2.1 Optimal control of PMSM at low speeds

At low speed region, iron losses can be neglected and the optimal control strategy transforms to keeping the remaining controllable copper losses at minimum. In the case of PMSM, low speed energy efficiency is achieved by controlling the stator current vector amplitude at minimum for given torque level. Hence, the same strategy provides maximum torque for given current amplitude, which is helpful when AC drive needs to deliver maximum torque at the current limit. For the mentioned reasons similar strategies are frequently introduced:

- MTPA - Maximum Torque per Ampere. The speed controller demands current amplitude as an output, and MTPA block provides dq current reference that will give maximum torque for that current amplitude, Fig. 5,
- MAPT - Minimum Ampere per Torque. The speed controller demands motor torque as an output, and MAPT block provides dq current reference that will give reference torque, but with minimum stator current amplitude possible, Fig. 5,

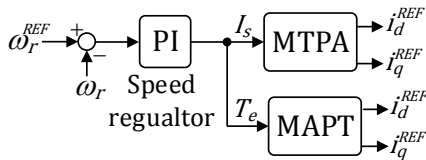


Fig. 5. MTPA and MAPT strategy

MTPA block produces maximum torque for given stator current magnitude:

$$dT_e/dI_s = 0 \quad (23)$$

where stator current magnitude is defined as:

$$I_s = \sqrt{I_{ds}^2 + I_{qs}^2} \quad (24)$$

Analytic solution for MTPA currents exists:

$$i_{ds}^{MTPA} = \frac{\psi_{PM} - \sqrt{\psi_{PM}^2 + 8(L_q - L_d)^2 I_s^2}}{4(L_q - L_d)} \quad (25)$$

$$i_{sq}^{MTPA} = \text{sign}(I_s) \sqrt{I_s^2 - (i_{sd}^{MTPA})^2} \quad (26)$$

On the other hand, MAPT strategy is more suitable for AC drives because it provides linear torque control, and more straightforward torque limiting possibility [10]. However, there is no exact analytic MAPT solution and look-up tables (LUT) are typically used.

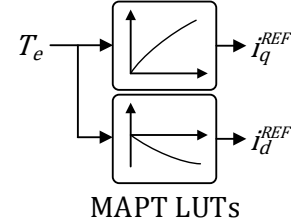


Fig. 6. Two MAPT lookup tables for dq currents

Alternatively, using the reasonable approximation,

$$(L_d - L_q)^x \approx 0, x \in \{3,2\} \quad (27)$$

approximate analytical MAPT solution is found [10]:

$$i_{ds}^{MAPT} = \frac{\psi_{PM} - \sqrt{\psi_{PM}^2 + 12(L_d - L_q)^2 \left(\frac{T_e}{\psi_{PM} K}\right)^2}}{6(L_q - L_d)} \quad (28)$$

$$i_{qs}^{MAPT} = \frac{T_e}{(1.5)P(\psi_{PM} + (L_d - L_q)i_{ds}^{MAPT})} \quad (29)$$

2.1 Optimal control of PMSM at high speeds

At high rotor speeds the iron losses cannot be neglected and energy efficiency algorithm has to minimize the total losses of PMSM:

$$P_{loss} = P_{cu} + P_{Fe} \quad (30)$$

This strategy is called LMC - Loss Minimization Control and it is suitable for high speed operations.

With resistance voltage drop neglected, both types of losses can be represented as function of air-gap vector current components,

$$P_{cu} = R_s \left(i_{do} - \frac{\omega_{dq} L_q i_{qo}}{R_{Fe}} \right)^2 + R_s \left(i_{qo} + \frac{\omega_{dq} (\psi_{PM} + L_d i_{do})}{R_{Fe}} \right)^2 \quad (31)$$

$$P_{Fe} = \frac{\omega_{dq}^2 (L_q i_{qo})^2}{R_{Fe}} + \frac{\omega_{dq}^2 (\psi_{PM} + L_d i_{do})^2}{R_{Fe}} \quad (32)$$

At high rotor speeds, it is necessary to adapt the PMSM current vector to achieve optimal flux level leading to minimum losses at given speed for given (reference) torque. The optimal formula considers the overall controllable losses P_{loss} as a function of the i_{d0} and transforms to:

$$\partial P_{loss} / \partial i_{d0} = 0 \quad (33)$$

Intensive calculations can be omitted if the controller disregards the saliency effects within the interior PMSM (IPMSM) or when surface PMSM (SPMSM) is considered. Letting $L_d = L_q$ (the directional L_d and quadrature inductances L_q are equal) one gets analytic solution for d-axis i_{d0} current which is speed dependent:

$$i_{d0} = -\frac{\omega_{dq}^2 L_d \psi_{PM} (R_s + R_{Fe})}{R_s R_{Fe}^2 + \omega_{dq}^2 L_d^2 (R_s + R_{Fe})} \quad (34)$$

If rotor saliency cannot be neglected ($L_d \approx L_q$), the latter relation can be only used as an initial guess for iterative (i.e. Newton - Raphson -NR) methods of solving much complex power losses model with saliency incorporated. Since (34) represents plausible approximation of the solution (33) based on the physical insight, it can help in reducing the overall number of iteration and save CPU time for real time execution of the advanced control law. As a iteration result, for PMSM with rotor saliency the optimal d-axis current reference becomes the function of both speed ω and the motor torque T . One example of NR solution is given in Fig. 7.

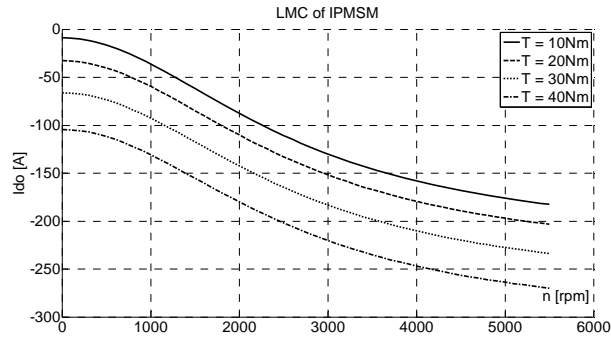


Fig. 7. LMC d-axis current as function of speed and torque

5. SELF-COMMISSIONING OF ENERGY EFFICIENT PMSM DRIVE

In this chapter one particular example of PMSM drive self-commissioning procedure is given. Drive self-commissioning is mainly performed to estimate the unknown motor parameters. These parameters are later used to setup the drive main control algorithms (speed controller, current controllers, FOC, etc...) but

also the advanced model based energy efficient algorithms. Only with automatic self-commissioning the one can get the most of the motor drive capability, more precisely its robust performance and peak efficiency. During the self-commissioning, it is common to setup other hardware parameters, necessary for drive to operate, for example to calibrate the sensors by setting the position and current sensors gains and offset, to check phase connection order, etc...

In this case, target AC drive application is an electrical golf-cart produced by Excar China, with 5kW low voltage (48V) PMSM produced by Nidec motor company IPMSM ACX-3434-12. Motor winding connection is delta, with four pole pairs and designed to run with maximum drive current 400A and maximum mechanical speed 5500 rpm.

The low voltage AC drive self-commissioning procedure is comprised from following phases:

1. First, drive self-check is performed, mostly motor connection, battery status, etc,
2. Second, shaft sensor (in the particular case mechanical resolver) tuning is performed. The motor is slowly rotated and rotor parking was performed to establish resolver analog sine/cosine signals offset, and resolver absolute position offset relatively to drive phase A,
3. Third, with motor at standstill, the stator resistance R_s is measured by injecting of the two level dc current signal,
4. Fourth, with motor maintaining at standstill, L_d and L_q synchronous inductances as 3D function of both d and q currents are measured with HF frequency test signals injected simultaneously in both of the motor axes.
5. Based on L_{dq} and R_s data, current regulator gains
6. Next, motor spins at rated speed, and permanent flux level Ψ_{PM} is calculated based on measured back electro-motive force signal (BEMF),
7. At that point, using L_d , L_q and Ψ_{PM} parameters, model based MAPT (29)- (30) is calculated,
8. If controllable load is available, operator can provide different load steps and start MAPT lookup measurement. This MAPT table is based on minimum current search algorithm which is started for each loading point set by operator. Once all predefined MAPT points are found, MAPT table in full torque range is populated.

All the parameters are stored in control memory (usually EEPROM) and used after the next reset by the advanced motor control algorithm.

In the Fig. 8, the block diagram of self-commissioning drive setup, typical signals, timing and results during and after the parameters autotuning procedure are depicted.

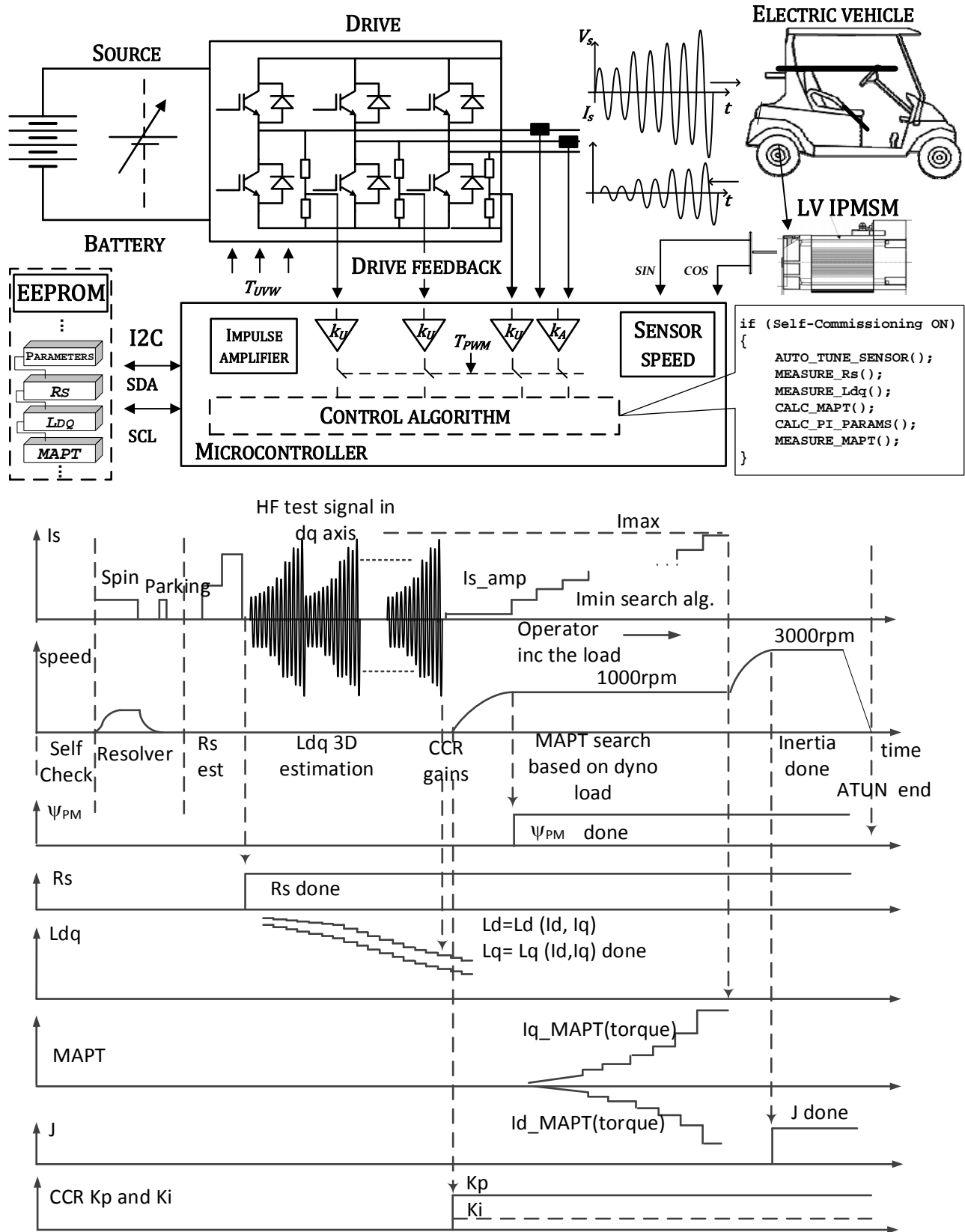


Fig. 8. Self-commissioning of AC drive: block diagram, typical test signals and parameter autotuning results

After the self-commissioning phase is finished, the motor parameters are inspected in detail. First, the algorithm has determined $R_s = 2.95 \text{ m}\Omega$ which is in close agreement with the factory data (factory data $2.84 \text{ m}\Omega$). Second, the dq inductance values are presented as 3D tables on the Fig. 9 and Fig. 10. L_{dq} tables are populated with data from $n \times m$ measurements, where $n=10$ measurement is with HF current amplitude set to proper value in direct axis under the test, and $m=5$ with HF current amplitude set to proper value in its orthogonal axis. Results show the significant saturation (drop of inductance value in one axis with increase of the current in the corresponding axis) but also cross-saturation phenomena (drop of inductance value in one axis with increase of the current in the opposite quadrature axis), especially at high currents. Next, motor is started and while rotating at the speed reference of 1000 rpm parameter $\Psi_{PM} = 0.019 \text{ Wb}$ is measured (factory data 0.01791). Finally, MAPT function is estimated by loading the motor with $n=10$ different loading points in the range from 0 Nm to 42Nm and the MAPT results are places in lookup table and depicted in the Fig 10 as well as presented within the Tab. 1. Similar MAPT is calculated using (29)-(30) with autotuned L_d, L_q and Ψ_{PM} parameters.

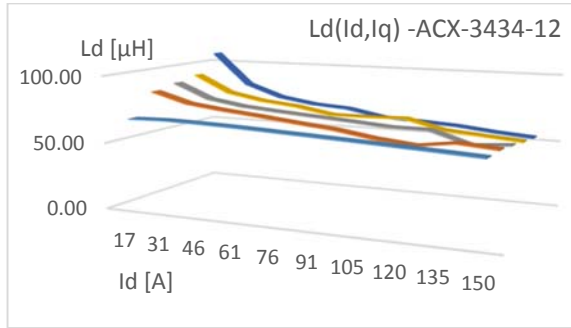


Fig. 9. D-axis synchronous inductance value $L_d(I_d, I_q)$

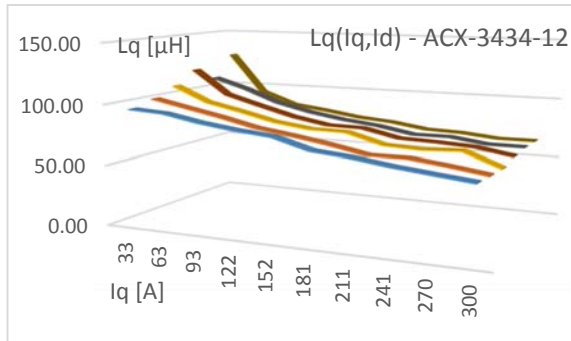


Fig. 10. Q-axis synchronous inductance value $L_q(I_d, I_q)$

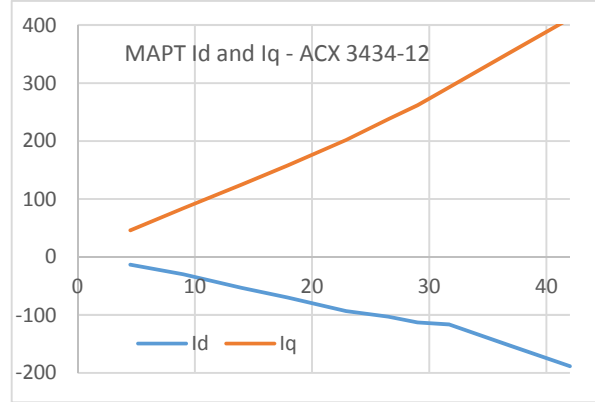


Fig. 11. MAPT functions: $I_q = I_q(T_e)$, $I_d = I_d(T_e)$

Table 1. MAPT table of IPMSM ACX 3434-12 drive

T[Nm]	Id [A]	Iq[A]
4.5	-13.3	46.0
9	-29.9	83.8
14	-53.2	124.9
17.9	-69.8	157.6
22.9	-93.1	201.6
26.5	-103	237.5
29	-113	261.6
31.7	-116.3	292.6
36.9	-152.9	352.5
42.0	-188.3	411.3

CONCLUSION

Most recent trends in the development of energy efficient AC drives were presented in this paper. Two types of motors (IM and PMSM) and two opposite AC drive applications, low-cost appliance drive, and high-performance electrical vehicle drive were considered. It was shown that even with huge difference between the operation principles in motors and AC drives, the energy efficient algorithm for AC motors can be very similar. As an example, more details of energy efficient model based control algorithms for PMSM drive were given. Also, self-commissioning procedure for PMSM drive needed for proper parameterization of used energy efficient algorithms was described. The target application of motor control and self-commissioning algorithms was high performance low voltage PMSM motor drive fed by 48V battery source in the electrical golf-cart. It was found that only after self-commissioning is executed, the golf-cart can run properly with the unknown motor providing the target maximum torque in the low speed region, as well as energy efficiency at higher speeds.

REFERENCES

- [1] E. Levi. (1995). Impact of Iron Loss on Behaviour of Vector Controlled Induction Machines, *IEEE Trans. on Industry Applications*. vol. 31, no. 6, p. 1287-1296. DOI: 10.1109/28.475699.
- [2] B. K. Bose. (2002). Modern power electronics and AC Drives, Upper Saddle River, NJ: Prentice Hall. ISBN 0-13-016743-6.
- [3] W. Sung, J. Shin, Y. Jeong. (2012). Energy-Efficient and Robust Control for High-Performance Induction Motor Drive With an Application in Electric Vehicles, *IEEE Trans. on Vehicular Technology*, vol. 61, no. 8, p. 3394-3405. DOI: 10.1109/TVT.2012.2213283.
- [4] V. Popovic, D. Oros, D. Marcetic (2020). MAPT Strategy of IM Including Iron Loss Phenomena. *Proceeding of 2020 International Symp. on Ind. Electr. and Applications (INDEL)*, Nov. 2020. DOI: 10.1109/INDEL50386.2020.9266260
- [5] Cao-Minh Ta and Y. Hori (2001). Convergence improvement of efficiency optimization control of induction motor drives, *IEEE Trans, Ind Appl.* vol.37, no.6, pp. 1746-1753. DOI: 10.1109/28.968187.
- [6] I. Kioskeridis and N. Margaris (1996). Loss minimization in Induction motor adjustable speed drives. *IEEE Trans, on Ind. Electronics*, vol.43, no. 1, pp. 226-231. DOI: 10.1109/41.481429
- [7] S. Lim and K. Nam (2004). Loss-minimizing control scheme for induction motors. *IEE Proceedings El. Power App.*, vol.151, no.4, pp.385-397. DOI:10.1049/ip-epa:20040384
- [8] D.S. Krischen and D. W. Novotny (1985). On-line efficiency optimization of a variable frequency Induction motor drive. *IEEE Trans, Ind. Appl.*, vol.1A-21, no.4, pp. 610-616. DOI: 10.1109/TIA.1985.349717.
- [9] P. Famouri and J. J. Cathey (1991), Loss minimization control of an induction motor drive," *IEEE Transactions on Industry Applications*, vol. 27, no. 1, pp. 32-37. DOI: 10.1109/28.67529.
- [10] V. Popović, B. Vujkov, M. Vučković, V. Vasić, D. Marčetić and Đ. Oros (2020). MAPT strategy for IPMSM with parameter sensitivity analysis. *Proceeding of 2020 International Symp. on Ind. Electronics and Applications (INDEL)*, DOI: 10.1109/INDEL50386.2020.9266282.
- [11] S. Jung, J. Hong and K. Nam (2013). Current Minimizing Torque Control of the IPMSM Using Ferrari's Method," *IEEE Transactions on Power Electronics*, vol. 28, no. 12, pp. 5603-5617. DOI: 10.1109/TPEL.2013.2245920.
- [12] Jang-Mok Kim and Seung-Ki Sul (1997). Speed control of interior permanent magnet synchronous motor drive for the flux weakening operation. *IEEE Transactions on Ind. Appl.*, vol.33, no.1, pp.43-48. DOI: 10.1109/28.567075.
- [13] Morimoto, S.; Tong, Y.; Takeda, Y.; Hirasa, T. (1994). Loss minimization control of permanent magnet synchronous motor drives. *IEEE Transactions on Industrial Electronics*, vol.41, no.5, pp.511-517. DOI: 10.1109/41.315269.
- [14] Aorith, H.; Wang, J.; Lazari, P. (2013). A new Loss Minimization Algorithm for Interior Permanent Magnet Synchronous Machine drives. *Electric Machines & Drives Conference (IEMDC)* pp.526-533. DOI: 10.1109/IEMDC.2013.6556146.
- [15] Botan, C.; Ratoi, M.; Ostafi, F.; Horga, V.(2010). Minimum energy control of servo drive systems with PMSM. *International Symposium on Power Electronics Electrical Drives Automation and Motion (SPEEDAM)*, vol., no., pp.19-23. DOI: 10.1109/SPEEDAM.2010.5542403.
- [16] Vaez, S.; John, V.I.; Rahman, M.A. (1999). An on-line loss minimization controller for interior permanent magnet motor drives. *IEEE Transactions on Energy Conversion*, vol.14, no.4, pp.1435-1440. DOI: 10.1109/60.815086.
- [17] Chan, C.C.; Chau, K.T. (1996). An advanced permanent magnet motor drive system for battery-powered electric vehicles. *IEEE Transactions on Vehicular Technology*, vol.45, no.1, pp.180-188. DOI: 10.1109/25.481836.
- [18] M. N. Uddin, and Sang Woo Nam (2008). New Online Loss-Minimization- Based Control of an Induction Motor Drive. *IEEE Transactions on Power Electronics*, vol. 23, no. 2, pp. 926-933. DOI: 10.1109/TPEL.2007.915029.
- [19] G. C. D. Sousa, B. K. Bose, and J. G. Cleland (1995), A fuzzy logic based on-line efficiency optimization control of an indirect vector-controlled induction motor drive. *IEEE Trans. Ind. Electron.*, vol. 42, pp. 192-198. DOI: 10.1109/41.370386.
- [20] D. P. Marčetić and E. M. Adžić (2010). Improved Three-Phase Current Reconstruction for Induction Motor Drives With DC-Link Shunt. *IEEE Transactions on Industrial Electronics*, vol. 57, no. 7, pp. 2454-2462. DOI: 10.1109/TIE.2009.2035456.
- [21] D. P. Marcetic, I. R. Krcmar, M. A. Gecic, and P. R. Matic (2014). Discrete rotor flux and speed estimators for high speed shaft-sensorless IM drives. *IEEE Transactions on Industrial Electronics*, vol. 61, no. 6, pp. 3099-3108. DOI: 10.1109/TIE.2013.2258311.



Banja Luka
28–29 May 2021.

DEMI 2021

15th International Conference on
Accomplishments in Mechanical and
Industrial Engineering

www.demi.mf.unibl.org



Comparative Studies on the Microstructure and Corrosion Behaviour of forged and SLM processed 316L Stainless Steel

D. Woelk^a, N. Kazamer^a, G. Marginean^a

^aWestphalian University of Applied Sciences, Neidenburger Str. 43, 45897, Gelsenkirchen, Germany

Abstract *The corrosion behaviour of forged and SLM (Selective Laser Melting) processed 316L samples was investigated in a 3.5% NaCl solution at neutral and light acidic pH. The influence of the oxygen concentration in the testing solution on the corrosion resistance of the alloy was also proved. This made it possible to qualitatively evaluate the influence of the additive manufacturing process on the microstructure of the 316L alloy in comparison to that of the forged steel. Therefore, the logarithmic polarisation curves generated during the electrochemical investigations were compared, especially in respect to the corrosion potential respectively corrosion current density. The results showed that the corrosion resistance of the 3D-printed samples was inferior to that of the forged 316L. Instead of the pitting corrosion that often appears during exposure of the forged material to chloride containing media, the SLM processed material exhibited rather an extensive surface attack. The microscopic examination of the samples revealed large differences in porosity between the microstructures obtained by means of the two manufacturing methods, whereby the 3D-printed samples exhibited a larger number of voids.*

Keywords *selective laser melting, 316L, corrosion behaviour*

1. Introduction

Selective laser melting (SLM) is one of the well-known additive manufacturing processes. This technology can generate complex geometries directly from metallic powders in inert atmospheres. A great advantage is that a CAD model can be read directly into the program of the 3D-printer [1, 2]. Furthermore, the material loss of SLM is considerably lower compared to other classical fabrication –techniques. The process is widely used in aerospace, railroad industry and for small batch production as well as for single part production. However, conventional procedures (such as casting) show advantages concerning lower production time and costs in comparison to SLM in the field of series production [3–6]. During the printing

process, the powder is locally melted by laser beam. The resulting high cooling rate causes dendritic solidification structure with different morphologies, depending on the powder particle diameter, which can show an improvement of the yield strength [7–9]. Furthermore, increased porosity often appears in SLM-produced objects compared to conventionally produced workpieces. The voids allow the medium to penetrate more quickly into deeper regions of the material, which again increases the risk of corrosion [10, 11]. The corrosion resistance can also be influenced by the laser power and scanning speed [12, 13].

There are a variety of materials, which are widely used for industrial applications, for example, 316L stainless steel. This material is

distinguished by various positive properties, especially in respect to a good corrosion resistance in chloride containing solutions [14]. Moreover, this material exhibits good mechanical strength and deformation behaviour [15, 16]. Due to its biocompatibility, 316L is often used for implants, as the material has no negative impact on health or the environment [17]. The corrosion properties of metallic materials are particularly important for their application, as the damage of components in service can often be attributed to corrosion. 316L forms a dense and adherent oxide layer (passive layer) that protects the substrate, hence the wide industrial application [18, 19]. The present susceptibility of chloride induced pitting corrosion is a particular challenge, as it appears more frequently in materials with imperfections and irregularities. The SLM workpieces more often show these unwanted effects, whereby the pitting corrosion finds the access [20–22]. Due to the diverse applications of 316L, research activities are always being carried out to find ways of improving its properties. Other researchers reported about 3D printed samples made of a composite material (316L and glass powder). The glass content led to a reduction in the weight of the whole composite. Moreover, glass powder is a by-product, which is thus being recycled [23].

This experimental work compares the corrosion behaviour of SLM produced 316L samples with that of forged 316L. The electrochemical experiments were done in 3.5% NaCl solution (as produced and deaerated with N₂) at different pH values (neutral and slightly acidic). The results obtained from the polarization curves were associated with the morphology of the 361L material in metallographic cross-section.

Corresponding author

Dr. Norbert Kazamer
 Norbert.kazamer@w-hs.de
 Westphalian University of Applied Sciences
 Neidenburgerstr., 43, 45891
 Gelsenkirchen, Germany

2. Methodology

2.1. Materials and manufacturing

A large technological implementation requires using widely employed materials. The 316L reference forged-material was compared with SLM generated samples, using a powder from the company Flame Spray Technology with a particle size in the range 15 - 45 μm. An SEM micrograph showing the morphology of the material and its chemical composition can be seen in Fig. 1 and Table 1.

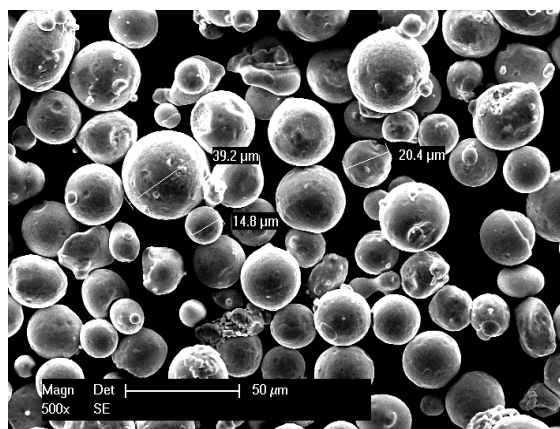


Fig. 1. SEM micrograph of the used 316L powder

Table 1. Chemical composition of the powder according to its data sheet

	Nominal chemical composition (wt.%)					
	Fe	Cr	Ni	Mo	Si	C
316L	Bal.	16.0	10.0	2.0	<1.0	<0.03
Powder		18.0	12.0	3.0		

At least three samples from each batch to ensure reproducibility were manufactured with a metal 3D-printer Orlas Creator under a protective N₂ atmosphere. The most important manufacturing parameters can be found in Table 2.

Table 2: Main printing parameters of the sample

Parameter	Value
Beam expander diameter	40 μm
Mark speed	1750 mm s^{-1}
Angle	45°
Layer thickness	45 μm
Relative beam motion	Translation of the piece
Part build-up strategy	Bottom up

2.2. Characterization

The specimens used for electrochemical characterization were previously ground with a 80 grain size SiC paper to reach a common industrially employed roughness of Ra 1.6 μm . For the metallographic preparation of the samples in cross-section, the embedded specimens were ground up to 1200 grain size SiC paper and polished with 3 μm diamond suspension.

The chemical composition of the forged and the SLM printed samples was determined by means of UV/VIS spectroscopy with a SpectroMAXx equipment.

The microstructural analysis was performed with a FEI EDX equipped Philips XL30 ESEM scanning electron microscope (SEM) at a 10 mm working distance and a cathode voltage of 25 kV. The porosity was calculated from the SEM micrographs with the ImageJ processing software.

The corrosion performance was investigated with a VoltaLab PGP201 Potentiostat/Galvanostat in a conventional respectively deaerated 30 minutes with pure N₂, 3.5 wt.% NaCl solution. Additional measurements were done also at slight acidic pH (3,5), adjusting the NaCl solution with concentrated HCl. The tests were performed at room temperature, using a three electrode-cell, under quasi stationary conditions, applying a scan rate of 0.16 mV s^{-1} . A Pt disc was defined as a counter electrode and a saturated calomel electrode (SCE) with a Luggin capillary as a reference electrode, respectively. The samples were scanned from -600 mV vs. SCE up to 1000 mV vs. SCE and the corresponding corrosion potential (E_{corr}), and current (i_{corr}) were analysed.

3. Results and discussions

The morphology of the SLM processed 316L material is depicted in Fig. 2. For a better three-dimensional presentation of the generated structure, cross-section samples were prepared in respect to planes, which are oriented along the x, y and z direction.

The samples examined in the frame of this research work were not produced with optimal SLM parameters, since a large amount of voids respectively a certain amount of unmelted powder particles is present inside the structure. This observation confirms that the melting pool was unstable. The estimated porosity determined by image processing was in the range 15% up to 18%, depending on the plane orientation. Very important for the corrosion behaviour of such structures, is that the present porosity is just in plane interconnected but not in the whole bulk.



Fig. 2. Three-dimensional representation of the SLM printed 316L material

The chemical composition of the investigated samples was determined in order to obtain information especially concerning the Cr and Mo content, which have a direct influence on the passivation behaviour of the stainless-steel surface. The contents of these elements are similar for both materials (forged and SLM printed, see Table 3). Furthermore, the forged alloy contains a slightly higher amount of Ni, contributing to an improvement of the corrosion resistance.

Table 3: Average value of the chemical composition of the forged and SLM printed material determined by UV spectroscopy.

Nominal chemical composition (wt.%)							
	C	Si	Mn	Cr	Ni	Mo	Fe
Forged	0.086	0.74	1.1	16.25	12.13	2.43	67
SLM Printed	0.039	0.51	1.28	16.21	9.8	2.02	69.2

Figure 3 shows the anodic polarization curves of forged 316L in all the mentioned testing conditions. During the corrosion attack of steel materials in chloride containing aqueous media, the main anodic respectively cathodic electrochemical reactions are the iron oxidation and the oxygen reduction reaction (ORR), respectively.

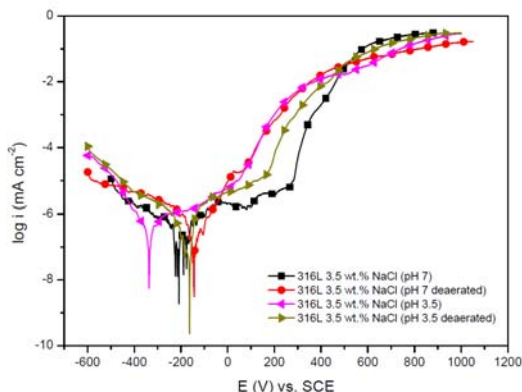
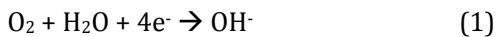
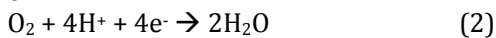


Fig. 3. Half-logarithmic polarisation curves of the forged 316L in different testing solutions

Depending on the pH value of the testing solution, the ORR might generate hydroxyl ions (pH>7) or even just water (pH<7), concerning the following chemical reactions:



or



By comparing the course of the anodic branch, one may observe that the surface of the forged alloy is able to passivate over a wider potential range just in the oxygen containing solutions. Production of hydroxyl ions during the ORR supports the surface passivation process. This observation does not influence very much the E_{corr} respectively the i_{corr} . The sample exposed in the testing NaCl solution with pH 3,5 exhibited

higher values for i_{corr} due to the higher content in dissolved oxygen (DO). The DO has a high solubility in 3,5 wt.% NaCl. Under these conditions, the ORR exhibited the lowest degree of inhibition (see the inclination of the cathodic branch, figure 3) and the E_{corr} was shifted to less nobler potentials. Hence, the DO is an electron acceptor (cathodic reaction), it accelerates the anodic metal dissolution.

Figure 4 displays exemplary a SEM micrograph of the corroded 316L forged material. All the tested samples exhibited local corrosion attack (pitting), which mainly are initiated in regions with nonmetallic inclusions like MnS.

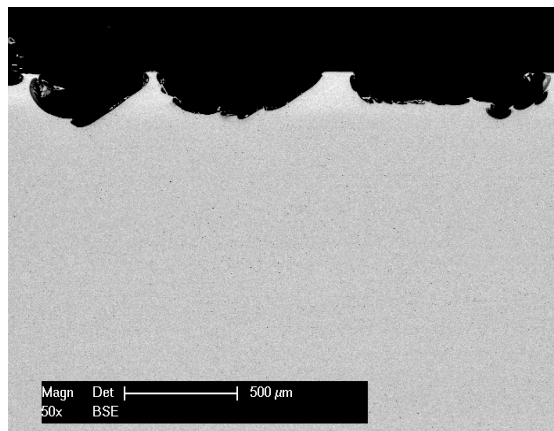


Fig. 4: Example of Cross-section SEM micrograph of the corroded 316L forged material

The polarization curves of the investigated SLM printed 316L material show an additional trend concerning the influence of surface roughness and sample porosity on the corrosion behaviour, depending on pH value respectively on DO concentration.

The anodic branch of the samples tested in neutral chloride solution revealed weak passivation, independently from the DO concentration. These samples exhibit higher values for i_{corr} in comparison with that tested at lower pH values, which confirm a higher kinetic of the corrosion reaction. The presence of numerous voids in the sample structure leads to a higher specific surface which was exposed to corrosion, having a catalytic effect, especially on the oxidation reaction. The kinetics of the cathodic ORR controls not only the rate but also

the extending of localized corrosion under these conditions.

A further aspect which should be considered is that the bottom of the existing voids is covered by a thin oxide layer, which was generated during the SLM processing of the material. A part of this oxide might be reduced during the ORR, especially under neutral conditions. Shifting the solution pH toward lower values will induce supplementary the chemical reaction (2), which will counterbalance the reaction (1). All these aspects produce a better stability of the generated passive film for the samples exposed to media lower pH values.

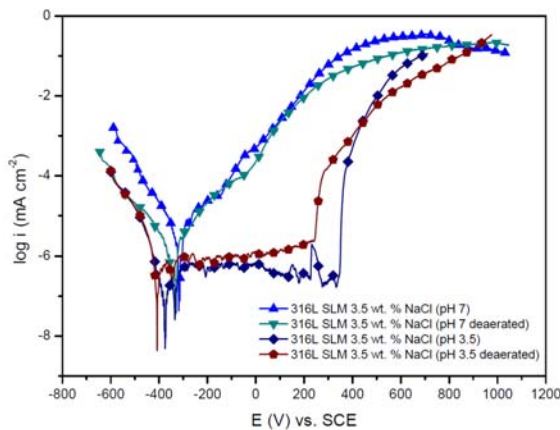


Fig. 5. Half-logarithmic polarisation curves of the SLM printed 316L in different testing solutions

Figure 6 shows exemplary a SEM micrograph of the corroded SLM printed material in cross-section, which clearly reveals a near to homogeneous corrosion attack, with no evidence of pitting corrosion. Based on the nature of the void's interconnection, only after the first layer is completely corroded, the corrosion attack will start in the region of next layer.

The generated corrosion products will assemble in such areas, depending on the surface roughness and will contribute to a partial inhibition of the corrosion reaction for a certain period.

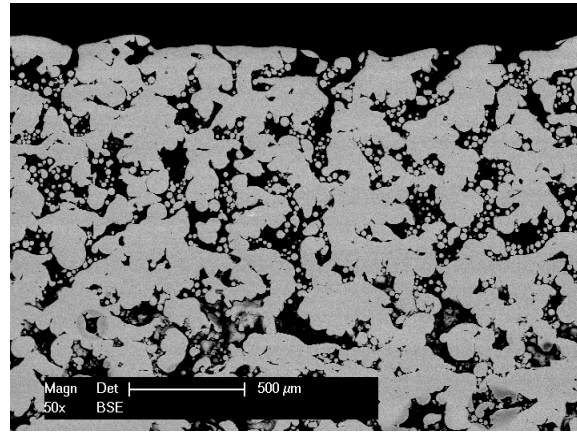


Fig. 6. Example of cross-section SEM micrograph of the corroded 316L SLM printed material

4. Conclusions

In this study, the influence of pH and DO on the corrosion behaviour of forged and SLM printed 316L samples was investigated by testing the alloys in different NaCl solutions at room temperature. The results show that the forged 316L material exhibited local corrosion attack (pitting), initiated in the regions with nonmetallic inclusions, while the 3D printed one displayed rather a generalized surface degradation.

Correlations of the polarisation curves of the tested SLM specimens, showed that the porosity and the presence of some oxides on the surface strongly influence the corrosion resistance. The higher porosity enhanced the degree of corrosion attack in neutral NaCl media. Contradictory observations concerning the corrosion resistance, respectively the stability of the passive film, were made in NaCl solution at pH 3,5.

Supplementary work must be done by further optimization of the printing parameters in order to obtain samples with a reduced amount of small size voids. Moreover, the influence of further pH values on the corrosion mechanism of the printed sample has to be investigated.

5. References

1. Hertlein N, Deshpande S, Venugopal V, et al (2020) Prediction of selective laser melting part quality using hybrid Bayesian network. *Additive Manufacturing* 32:101089. <https://doi.org/10.1016/j.addma.2020.101089>
2. Riemer A, Leuders S, Thöne M, et al (2014) On the fatigue crack growth behavior in 316L stainless steel manufactured by selective laser melting. *Engineering Fracture Mechanics* 120:15–25. <https://doi.org/10.1016/j.engfracmech.2014.03.008>
3. Trosch T, Strößner J, Völkl R, Glatzel U (2016) Microstructure and mechanical properties of selective laser melted Inconel 718 compared to forging and casting. *Materials Letters* 164:428–431. <https://doi.org/10.1016/j.matlet.2015.10.136>
4. Wang D, Yang Y, Liu R, et al (2013) Study on the designing rules and processability of porous structure based on selective laser melting (SLM). *Journal of Materials Processing Technology* 213:1734–1742. <https://doi.org/10.1016/j.jmatprotec.2013.05.011>
5. Yap CY, Chua CK, Dong ZL, et al (2015) Review of selective laser melting: Materials and applications. *Applied Physics Reviews* 2:041101. <https://doi.org/10.1063/1.4935926>
6. Zygula K, Nosek B, Pasiwiec H, Szysiac N (2018) Mechanical properties and microstructure of AlSi10Mg alloy obtained by casting and SLM technique. *World Scientific News* 104:462–472
7. Yin YJ, Sun JQ, Guo J, et al (2019) Mechanism of high yield strength and yield ratio of 316 L stainless steel by additive manufacturing. *Materials Science and Engineering: A* 744:773–777. <https://doi.org/10.1016/j.msea.2018.12.092>
8. Wang X, Carter LN, Pang B, et al (2017) Microstructure and yield strength of SLM-fabricated CM247LC Ni-Superalloy. *Acta Materialia* 128:87–95. <https://doi.org/10.1016/j.actamat.2017.02.007>
9. Montero-Sistiaga M, Nardone S, Hautfenne C, Humbeeck J (2016) Effect of heat treatment of 316L stainless steel produced by Selective Laser Melting (SLM). In: *Proceedings of the 26th Annual International Solid Freeform Fabrication Symposium – An Additive Manufacturing Conference*. Texas, USA
10. Laleh M, Hughes AE, Yang S, et al (2020) Two and three-dimensional characterisation of localised corrosion affected by lack-of-fusion pores in 316L stainless steel produced by selective laser melting. *Corrosion Science* 165:108394. <https://doi.org/10.1016/j.corsci.2019.108394>
11. Kale AB, Kim B-K, Kim D-I, et al (2020) An investigation of the corrosion behavior of 316L stainless steel fabricated by SLM and SPS techniques. *Materials Characterization* 163:110204. <https://doi.org/10.1016/j.matchar.2020.110204>
12. Ni X, Kong D, Wu W, et al (2018) Corrosion Behavior of 316L Stainless Steel Fabricated by Selective Laser Melting Under Different Scanning Speeds. *Journal of Materials Engineering and Performance* 27:3667–3677. <https://doi.org/10.1007/s11665-018-3446-z>
13. Yadroitsev I, Gusarov A, Yadroitsava I, Smurov I (2010) Single track formation in selective laser melting of metal powders. *Journal of Materials Processing Technology* 210:1624–1631. <https://doi.org/10.1016/j.jmatprotec.2010.05.010>
14. Murkute P, Pasebani S, Isgor OB (2019) Production of corrosion-resistant 316L stainless steel clads on carbon steel using powder bed fusion-selective laser melting. *Journal of Materials Processing Technology* 273:116243. <https://doi.org/10.1016/j.jmatprotec.2019.05.024>
15. Sabzi M, Dezfuli SM (2018) Drastic improvement in mechanical properties and weldability of 316L stainless steel weld joints by using electromagnetic vibration during GTAW process. *Journal of Manufacturing Processes* 33:74–85. <https://doi.org/10.1016/j.jmapro.2018.05.002>
16. Zhong Y, Liu L, Wikman S, et al (2016) Intragranular cellular segregation network structure strengthening 316L stainless steel prepared by selective laser melting. *Journal of Nuclear Materials* 470:170–178. <https://doi.org/10.1016/j.jnucmat.2015.12.034>
17. Khalaf MK, Mazhir SN, Mahdi MS, et al (2018) Influence of RF sputtering power on surface properties and biocompatibility of 316L

- stainless steel alloy by deposition of TiO₂ thin films. *Materials Research Express* 6:035401. <https://doi.org/10.1088/2053-1591/aaf2e9>
18. Wang Z, Seyeux A, Zanna S, et al (2020) Chloride-induced alterations of the passive film on 316L stainless steel and blocking effect of pre-passivation. *Electrochimica Acta* 329:135159. <https://doi.org/10.1016/j.electacta.2019.135159>
 19. Wang Z, Di-Franco F, Seyeux A, et al (2019) Passivation-Induced Physicochemical Alterations of the Native Surface Oxide Film on 316L Austenitic Stainless Steel. *Journal of The Electrochemical Society* 166:C3376–C3388. <https://doi.org/10.1149/2.0321911jes>
 20. Zhang Y, Liu F, Chen J, Yuan Y (2017) Effects of surface quality on corrosion resistance of 316L stainless steel parts manufactured via SLM. *Journal of Laser Applications* 29:022306. <https://doi.org/10.2351/1.4983263>
 21. Luo H, Su H, Dong C, Li X (2017) Passivation and electrochemical behavior of 316L stainless steel in chlorinated simulated concrete pore solution. *Applied Surface Science* 400:38–48. <https://doi.org/10.1016/j.apsusc.2016.12.180>
 22. Sun Y, Moroz A, Alrbaey K (2014) Sliding Wear Characteristics and Corrosion Behaviour of Selective Laser Melted 316L Stainless Steel. *Journal of Materials Engineering and Performance* 23:518–526. <https://doi.org/10.1007/s11665-013-0784-8>
 23. Sander G, Jiang D, Wu Y, Birbilis N (2020) Exploring the possibility of a stainless steel and glass composite produced by additive manufacturing. *Materials & Design* 196:109179. <https://doi.org/10.1016/j.matdes.2020.109179>

Production and Computer-Aided Technologies



Banja Luka
28-29 May 2021.

DEMI 2021

15th International Conference on Accomplishments in Mechanical and Industrial Engineering

www.demi.mf.unibl.org



Ironing process in conditions of constant and variable lateral force

S. Djacic^a, S. Aleksandrovic^b, D. Arsic^b, M. Delic^b, V. Lazic^b

^aCoal mine, Pljevlja, Montenegro

^bFaculty of Engineering, University of Kragujevac, Sestre Janjica 6, Kragujevac, Serbia

Abstract Comparison of application of constant and variable lateral force in strip ironing process with double side thinning are presented in the paper. Given are the experimental results for single and multiphase ironing process with constant lateral force during the course of particular process. Mild Steel DC04 material was used. Stripes were 20 mm wide and 2.5 mm thick. Constant lateral force intensities were 5, 10 and 15 kN. Lubrication was with appropriate mineral oil and grease. In other side given is analysis of idea of possibility to apply continuously variable lateral force during the strip ironing process and consequences of this action. Expected is control of strip thickness variation with difficulties because of contact and other appearances influence.

Keywords ironing process, strip sliding test, continuously variable lateral force

1. INTRODUCTION

Ironing forming process has great appliance in modern metal forming industry. It combines characteristics of sheet metal forming and bulk forming processes. Numerous published research papers illustrate one aspect of significance of ironing technology. For this opportunity chosen were selected references [1-16].

Physical modeling has great importance in ironing process research. There are many approaches, but most of them are based on tribological experiments. Different simulative tests have been developed in order to obtain contact parameters, to evaluate the performance of the individual lubricants,

material wear resistance etc. All the tests are simulating real process conditions and allow determination of important parameters. Widely is used so called Schlosser test [1]. One of the first studies about limitations and problems of this test is given in the paper [2]. Different consideration are presented in next papers: friction and lubrication [3-5], manufacturing issues of particular part etc. [6].

In Faculty of Engineering (former well known Faculty of Mechanical Engineering for many years), University of Kragujevac, performed were extensive researches in the past decade based on tribological experimental modelling of ironing process [7-16]. Main physical model is double side thinning strip ironing test, but with new approaches presented in articles [7] and [16]. Different lubrication issues were investigated in papers [8-12]. An attempt with strip ironing test numeric simulation was made in [13]. Extended research with different materials, lubricants, strain rates etc. on classic model presented is in master thesis [14]. Influence of process parameters on the friction

Corresponding author

Dr Srbislav Aleksandrovic, professor
srb.alexand@gmail.com

Faculty of Engineering, University of Kragujevac
Sestre Janjica 6
34000 Kragujevac, SERBIA

coefficient research is given in [15]. In [16] exposed was new method of friction coefficient and contact pressure determination depending on drawing force, lateral force, tool and sample geometry.

In this paper authors have exposed the idea that is possible to realize variable strip thickness by continuously variable lateral force acting in double side thinning ironing test.

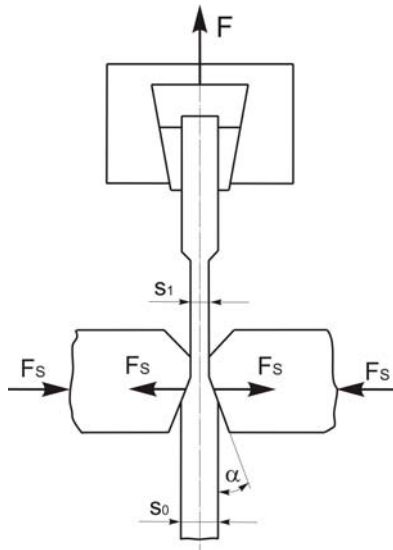


Fig. 1. Acting of test tooling elements

Fig. 1 represents main test tooling elements acting scheme. The thick metal strip is being gripped into holding jaw. The jaw with the sample is moving vertically by drawing force F acting. Lateral forces F_s make thinning of strip sample. Two lateral forces and drawing force F acting simulate the industrial ironing tool work. It is important to notice that in usual situation with constant intensity of lateral force F_s during sliding process, exists the need of initial indentation of lateral tool elements before the start of drawing force F acting. Details of process parameters determination can be seen on [7, 11, 14, 16].

2. THINNING WITH CONSTANT FORCE

Authors have paid attention to deformation of thinning in this and next chapter. It is important to notice that lateral force intensity here is constant in course of single sliding process. Drawing force F dependence on sliding length can be seen in Fig. 2. Strips were made of low carbon steel DC04. Sample width is 20 mm and

initial thickness is 2,5 mm. Applied lubricant is mineral oil and sliding speed is 20 mm/min. With such a speed sliding process lasts about 3 min on 60 mm length. All the experiment details are given in [14]. There are 3 curves in Fig. 2. Each curve corresponds to appropriate lateral constant force F_s , and relate to single strip sample. Constant intensity of F_s make constant thinning deformation. For example, with $F_s=15$ kN percentage thinning is 17% (thickness goes from 2.47 mm to 2.05 mm).

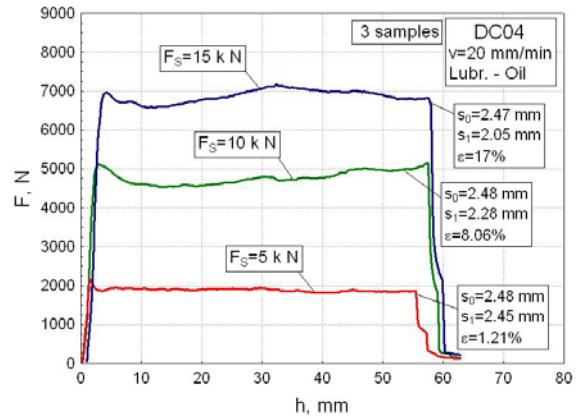


Fig. 2 Drawing force dependence on sliding length, case 1

Fig. 3 shows other situation. Used was one sample and after first 60 mm of sliding pass, performed is second (approximately 45 mm), third (30 mm) and fourth (15 mm) repeatedly over the same surface. Lateral force intensity was 5 kN for all of the four phases each. Realized thinning was relatively small, up to 2,4%.

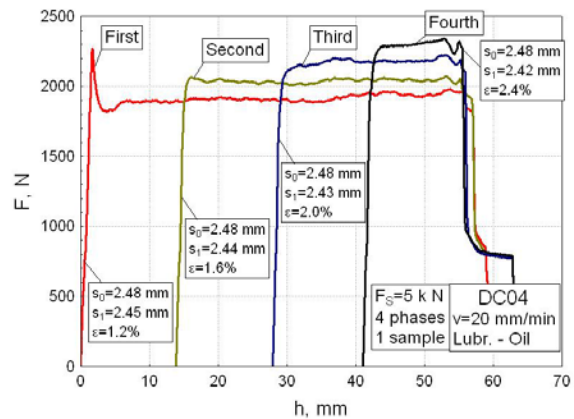


Fig. 3 Drawing force dependence on sliding length, case 2

Fig. 4 presentation is analogous to Fig. 2 with difference in applied lubricant which is, there, special MoS₂ grease [14]. Course of sliding process lasting in condition of smaller friction, and drawing force curves position is lower than in Fig. 2. Thinning deformations are similar to Fig. 2 case.

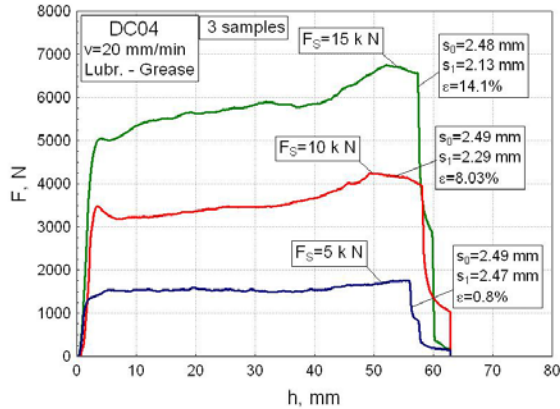


Fig. 4 Drawing force dependence on sliding length, case 3

Fig. 5 correspond to Fig. 3, but grease like lubricant make change in ironing sliding process. There are four passes also, like in Fig. 3 but drawing force is lower and lower in next passes each. This shows different process character in relation to Fig. 3. Thinning deformations are lower also.

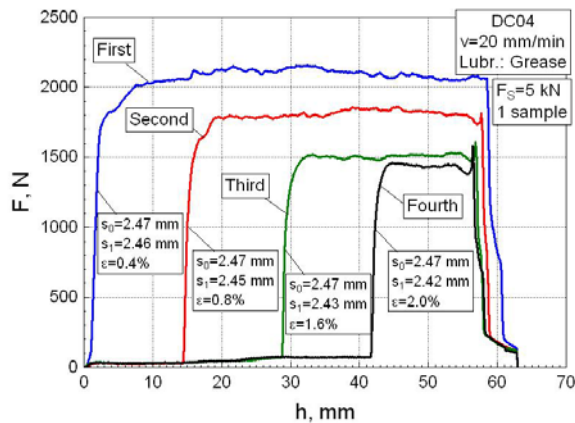


Fig. 5 Drawing force dependence on sliding length, case 4

After previous experimental examples consideration, can be concluded that constant intensity of lateral force F_s simply causes

constant thinning deformation, i.e. constant thickness on corresponding length. Question is, is it possible to realize variable thinning deformation, i.e. variable thickness in course of single sliding, on single sliding length? Authors are trying to make proper answer to previous question in next chapter.

3. THINNING WITH VARIABLE FORCE

After consideration of ironing sliding process in double side thinning model, it seems obvious that crucial role acts lateral force F_s in thinning process. If there is demand for variable thickness on single sliding length, it can be concluded that continuously variable intensity of lateral force F_s can fulfill previous demand. Interaction of lateral force and other influencing factors in ironing process remain open question and subject of further experimental research.

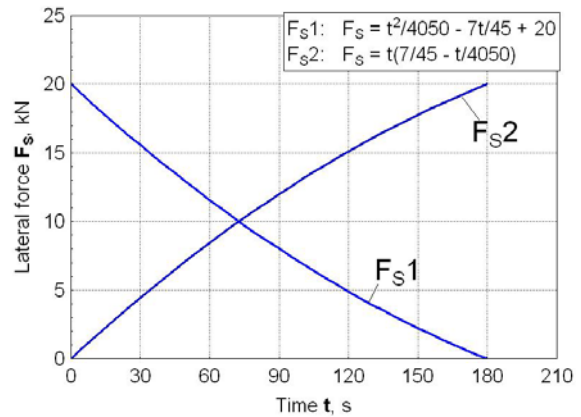


Fig. 6 Theoretic lateral force dependence on time, types 1 and 2

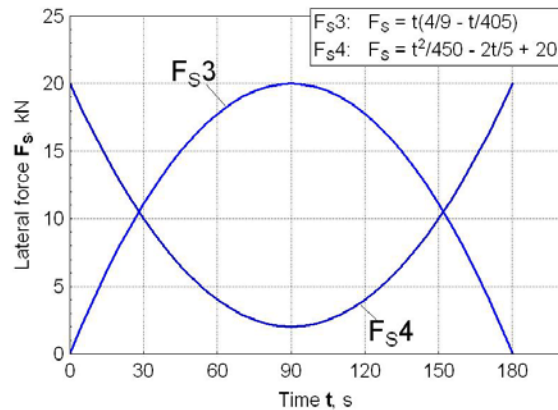


Fig. 7 Theoretic lateral force dependence on time, types 3 and 4

Here, authors have proposed 4 nonlinear functional lateral force F_S dependencies on time (i.e. sliding length), Fig. 6 and Fig. 7, and 2 linear dependencies, Fig. 8.

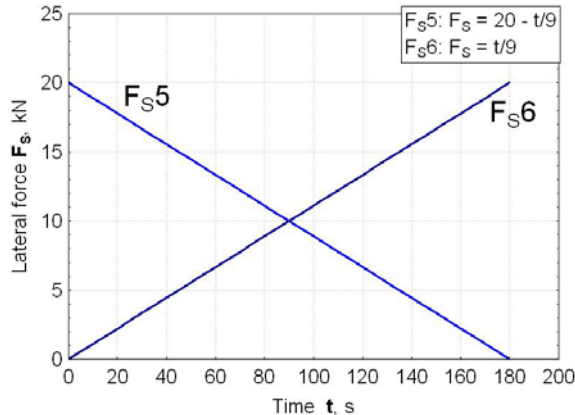


Fig. 8 Theoretic lateral force dependence on time, types 5 and 6

Functions are determined according to experimental frame which makes lateral force F_S intensity and process lasting (see Figures 2, 3, 4 and 5). Expectation is that variable lateral force can cause approximately similar intensity of thinning deformation like constant F_S . Authors are planning further extensive experimental research towards explaining all the interactions in ironing process of this kind.

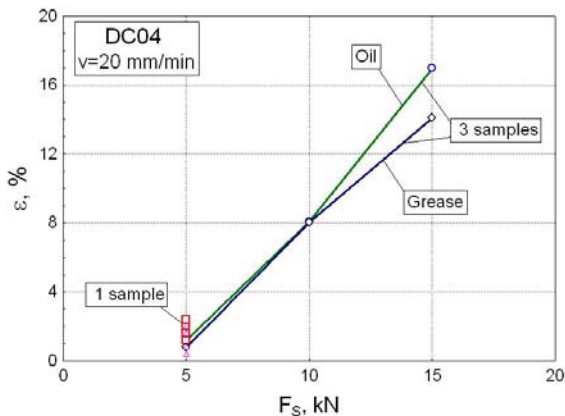


Fig. 9 Thinning deformation dependence on constant lateral force

Although real appropriate experiment is missing, anyway, data from experiments with

constant intensity of lateral force F_S (Figures 2-5) can be used. Concerning to that formed is Fig. 9 which shows all the achieved thinning deformations in examples on Figures 2-5. Useful are cases related to one sample-one lateral force process type. In this cases achieved are higher thinning deformation intensities.

Figures 10, 11 and 12 shows hypothetic situation. Considered are variable lateral force type F_{S2} (Fig. 6) in range 0-15 kN, but used are according thinning deformations from experiment with constant force F_S . It is first rough approximation, but only that data we have at the moment, until the realization of planned extensive experimental research.

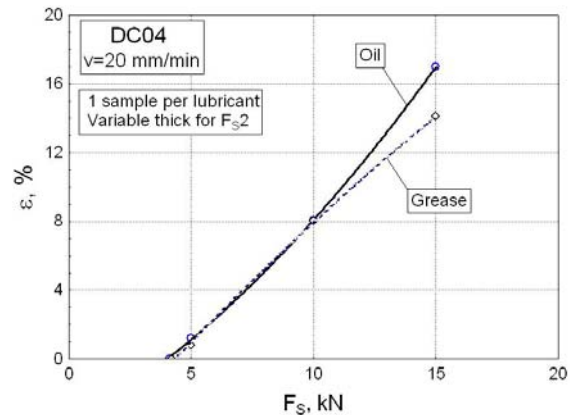


Fig. 10 Thinning deformation dependence on variable lateral force

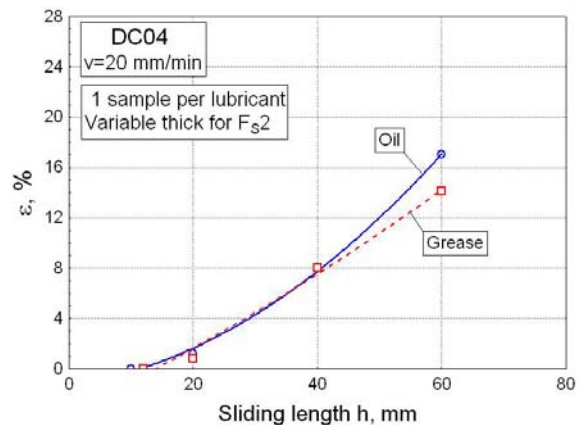


Fig. 11 Thinning deformation dependence on sliding length (variable lateral force)

If the previous premise is true, Figures 10, 11 and 12 show that variable thickness according to lateral force function of continuously variable

intensity during the ironing process can be achieved.

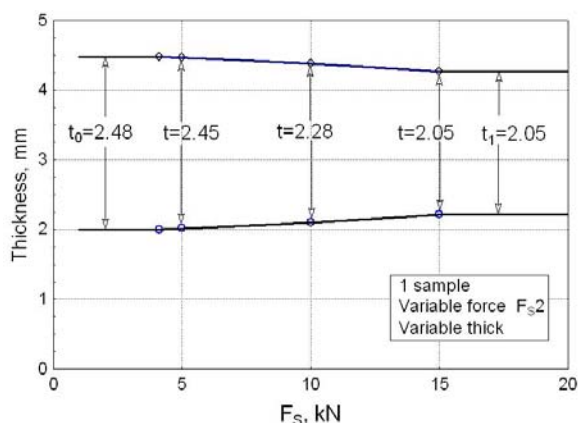


Fig. 12 Thickness dependence on variable lateral force

4. CONCLUSION

Researches of ironing process were conducted mainly on experimental laboratory models in conditions of constant lateral forces intensity. Such forces cause uniform thinning, i.e. constant thickness on related single sliding length.

Here, in this article, authors have made demand to achieve variable thickness on single sliding length. Variable thickness can be achieved with using of proper continuously variable lateral force. Based on experimental results obtained with constant lateral force, can be concluded that exists real possibility of this significant ironing process improvement.

Acknowledgement

The experimental research with results reported in this paper was partially supported by the Ministry of Education, Science and Technological Development, Republic of Serbia through contract TR34002 and authors are very grateful for that.

REFERENCES

[1] Schlosser, D. (1975). Beeinflussung der Reibung beim Streifenziehen von austenitischem Blech: verschiedene Schmierstoffe und Werkzeuge aus gesinterten Hartstoffen. *Bänder Bleche Rohre*, No. 7/8, p. 302-306.(In German).

- [2] Deneuille, P., Lecot, R. (1994).The study of friction in ironing process by physical and numerical modelling. *Journal of Materials Processing Technology*, Vol. 45, No. 1-4, p. 625–630. DOI: [https://doi.org/10.1016/0924-0136\(94\)90409-X](https://doi.org/10.1016/0924-0136(94)90409-X)
- [3] Andreasen, J.L., Bay, N., Andersen, M., Christensen, E., Bjerrum, N. (1997). Screening the performance of lubricants for the ironing of stainless steel with a strip reduction test, *Wear*,Vol. 207, No. 1-2, pp. 1-5.
- [4] Sulaiman, H., Christiansen, P., Bay, N. (2017). Influence of tool texture on friction and lubrication in strip reduction, *Procedia Engineering*, No. 207, p. 2263–2268. DOI: <https://doi.org/10.1016/j.proeng.2017.10.992>
- [5] Ustunyagiz, E., Nielsen, C., Christiansen, P., Martins, P., Bay, N. (2017). Continuous Strip Reduction Test Simulating Tribological Conditions in Ironing, *Procedia Engineering*, No. 207, p. 2286–2291. DOI: <https://doi.org/10.1016/j.proeng.2017.10.996>
- [6] Tatsunori Ozawa et al. (2018). Fabrication of ring groove on inner surface of cylindrical blank by ironing from outer surface, *Procedia Manufacturing*, No. 15, p. 899–906. DOI: <https://doi.org/10.1016/j.promfg.2018.07.407>
- [7] Aleksandrović, S., Đorđević, M., Stefanović, M., Lazić, V., Adamović, D., Arsić, D. (2014). Different Ways of Friction Coefficient Determination in Stripe Ironing Test, *Tribology in industry*, Vol. 36, No. 3, 2014., p. 293-299.(Project TR 34002)
- [8] Djordjević, M., Aleksandrović, S., Lazić, V., Stefanović, M., Nikolić, R., Arsić, D. (2013). Experimental analysis of influence of different lubricants types on the multi-phase ironing process, *Materials Engineering - Materijalov inženierstvo*, Vol. 20, No. 3, p. 147-152.
- [9] Djordjevic, M., Aleksandrovic, S., Lazić, V., Arsic, D., Stefanovic, M., Milosavljevic, D. (2015). Two-phase ironing process in conditions of ecologic and classic lubricants application, *Proceedings of International conference on Tribology SERBIATRIB 2015*, May 13–15, Belgrade, Serbia, p. 407-413.
- [10] Djordjevic, M., Aleksandrovic, S., Arsic, D., Lazić, V., Nikolic, R., Hadzima, B., Kotes, P. (2015). Investigation of the lubricants influence on the ironing process, *Procedia Engineering*, No. 111, p. 149 – 154.
- [11] Đorđević, M., Arsić, D., Aleksandrović, S., Lazić, V., Milosavljević, D., Nikolić, R. (2016). Comparative study of an environmentally friendly single-bath lubricant and conventional lubricants in a strip ironing test, *Journal of*

- Balkan Tribological Association*, Vol.22, No.1A-II, p. 947-958.
- [12] Djordjević, M., Aleksandrović, S., Lazić, V., Arsić, D., Nikolić, R., Hadzima, B. (2016). Investigation of the lubrication influence on single-phase and multi-phase ironing processes, *Procedia Engineering*, No. 149, p. 40 – 47.
- [13] Djordjević, M., Aleksandrović, S., Arsić, D., Lazić, V. (2017). Experimental-numerical analysis of contact conditions influence on the ironing strip drawing process, *Industrial lubrication and tribology*, Vol. 69, Issue 4, p. 464-470. DOI: <https://doi.org/10.1108/ILT-05-2016-0113>
- [14] Djacic, S. (2016). *Metal forming with double sided ironing*, (In Serbian). Master thesis. Faculty of Engineering, University of Kragujevac.
- [15] Aleksandrović, S., Đačić, S., Stefanović, M., Đorđević, M., Lazić, V., Arsić, D. (2017). Influence of process parameters on the friction coefficient in one and multi phase steel strip drawing ironing test, *Proceedings of DEMI 2017 Electrical and Mechanical Engineering and Information Technology*, May 26-29, Banja Luka, p. 77-86.
- [16] Aleksandrović, S., Đačić, S., Đorđević, M., Ratković, N., Arsić, D., Lazić, V. (2020). New method of defining of process parameters in double side thinning strip ironing test, *Tribology in industry*, Vol. 42, No.1, p. 59-69. DOI:<https://doi.org/10.24874/ti.2020.42.01.06> (Project TR 34002)

Porosity distribution in metal injection molded parts

Samir Butković, Emir Šarić, Muhamed Mehmedović

University of Tuzla, Faculty of Mechanical Engineering, Bosnia and Herzegovina

Abstract *Metal injection molding technology is commonly used in production of small and very complex parts. Residual porosity is unavoidable characteristic of P/M parts, affecting their final properties. During injection molding phase powder-binder separation can occur, causing green density variation through cross section of the part. This behaviour is particularly pronounced as complexity of the parts increases. As a consequence, zones with different density and residual porosity can be seen after sintering. In this regard, porosity and hardness distribution of the sintered ring-shaped part is analyzed and presented in the paper.*

Keywords *Metal injection molding, sintering, porosity distribution*

1. INTRODUCTION

Typical and unavoidable characteristic of parts produced by powder metallurgy technologies is residual porosity. Size, shape and distribution of residual porosity are factors that have very high influence on final mechanical and physical properties of the PM parts. Source of residual porosity may be related to compaction (molding) process, as well as sintering process. Ability of green part to shrink evenly during sintering depends on its geometry, condition after compaction (anisotropic oriented microstructure), green density uniformity, etc [1,2].

During die compaction process, powder is pressed in die in order to form shape of the

part. Pressure from the punch is distributed through the compact which causes increasing of contact surfaces between powder particles and their cold welding, Fig. 1. Pressure variation, as well as density, through the cross section of the compact is dependent on friction between particles and friction between powder particles and die wall.

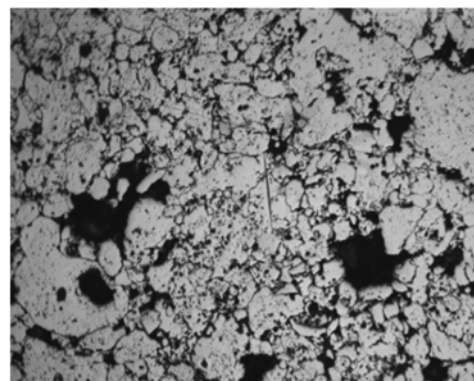


Fig.1. Polished sample of as-compacted copper alloy powder

Corresponding author

Dr. sci Samir Butković
samir.butkovic@untz.ba
Faculty of Mechanical Engineering Tuzla
BiH, Tuzla

This behaviour of powder during compaction leads to formation of zones with different percent of residual porosity, Fig 1. Empty spaces can also be formed under bridges formed by irregular shaped powders, while spherical powder easily flow and fill empty spaces in green part [3].

Metal injection molding technology usually uses spherical powder, mixed with specified binder, which is injected in to die cavity. During injection molding phase, mixture of binder and powder (feedstock) is heated to temperature where binder become liquid. Feedstock is then injected into die cavity, while binder carries the powder to the farthest distances. Using this principle, it is possible to obtain very complex shapes with superior properties compared to other PM technologies.

However, uneven porosity distribution in MIM parts is usually related to separation of binder and metal powder, causing binder rich and powder rich zones in green parts [4,5,6]. Namely, movement of powder particles from high shear rate zones to low shear rate region can result in powder accumulation in the middle of the flow [6].

Flow obstacles, sudden directional changes of feedstock and gravity can cause accumulation of powder in some zones [4,6]. This behavior can be improved through feedstock preparation phase or using favorable molding conditions, but complete avoiding of binder-powder separation can't be achieved.

In this regard, porosity and hardness distribution of the sintered ring-shaped part is analyzed and presented in the paper.

2. EXPERIMENTAL WORK

Analysis of porosity distribution was performed on small, very complex ring-shaped part. Injection molding was done in Arburg 320C molding machine. Feedstock was prepared from spherical heat resistant stainless steel powder mixed with poliactal based binder „Catamold 310N“. Injection molding was done using mold temperature of 125°C, holding pressure of 850 bar and injection speed of 6 cm³/s. After injection molding, most of the binder was removed by catalytic debinding in nitric acid and nitrogen atmosphere. Rest of the binder was removed during first stage of sintering. In this stage initial joining of the particles takes on the function of the residual binder and keeps

the shape of the part. Sintering was done in Elnik furnace, at temperature of 1310°C. Nitrogen atmosphere was used during sintering and cooling of the parts. Spherical powder, with well distributed fine particles between coarse particles, can be observed in the Fig. 2. During debinding stage, gas nitrogen enriched with evaporated nitric acid circulates around the parts, causing degradation of binder from the surface to the part core.

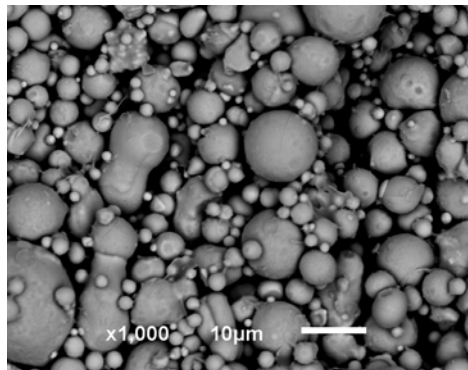


Fig.2. SEM image of metal powder (Catamold 310N) X40CrNiSi 25-20

After removing the most of the binder, empty space and residual binder remain in the parts. Increasing of the parts temperature, at the beginning of the sintering process, initiates diffusion processes which are responsible for neck formation and degradation of residual binder. After 3 h, at sintering temperature, final mechanical and physical properties of parts were achieved, Fig. 3. Then, part was cut, grinded and polished.



Fig.3. Part after sintering

Polishing and etching was done few times in order to reveal pores on the analyzed surface of the part. After preparing the surface, metallographic examination was performed. Mould filling progression and distribution of the porosity on polished part was presented on the Fig. 4 and Fig. 5, respectively.

3. RESULTS AND DISCUSSION

During injection phase of the MIM process, liquid binder carries spherical powder particles from cylinder trough runner system up to the die cavity. Passing through the runner system, mixture of powder and binder changes flow direction encountering various obstacles. Binder rich zones can be recognised in sintered parts as porosity rich zones. Also, these zones have higher capacity for shrinking, compared to powder rich zones, which can result in anisotropic shrinking and defects after injection molding and sintering [7]. For the part presented in the Fig. 4, where four cavities tool was used, feedstock changes its direction four times at angle of 90° , until reaches the gate. Process of filling the die cavity starts at gate position with injection speed of $6 \text{ cm}^3/\text{s}$. High shear rate gradients occur at the gate and separation of powder-binder can occur [6].

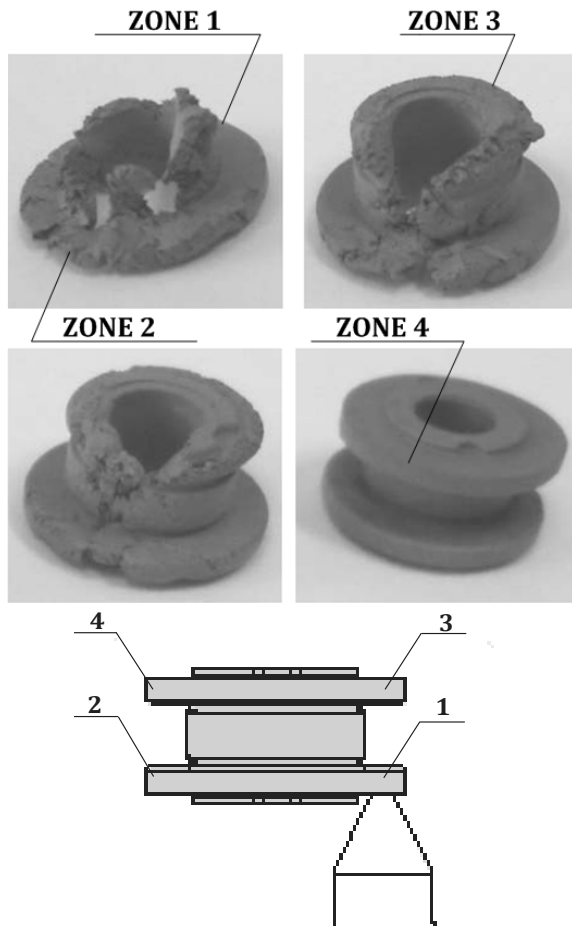


Fig. 4. Mould filling progression and part zones [7]

Gate zone (1) in this case is specific because feedstock impacts opposite wall at very high speed. This zone of the part can be considered as zone with high potential for binder separation, where accumulation of powder takes place. Thus, lower porosity can be observed in zone 1, Fig. 5. From this position feedstock is depleted with powder and the rest of the cavity is filled with reduced powder/binder ratio compared to origin mixture.

After zone 1, feedstock goes to zone 2 and then to the zone 3. These two zones showed similar percent of residual porosity, Fig. 5. Zone 4 is the last filled, with significantly changed feedstock composition compared to zone 1. Feedstock with the lowest powder/binder ratio arrives at position 4, where excessive porosity can be observed.

Experimental results showed that thin zones of the part and zones at the greater distances from the gate, where powder percent in feedstock is reduced, have higher percent of porosity.

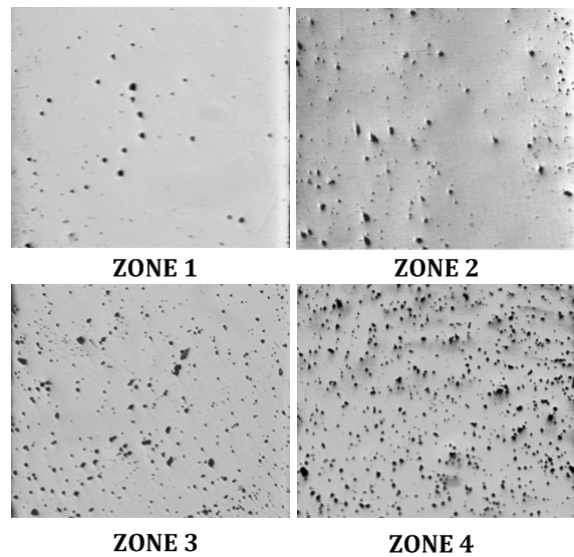


Fig. 5. Sintered and polished sample of ring-shaped Catamold 310N steel part, revealing residual porosity for different zones, 200X

Variation of porosity also affected hardness distribution through the part. Hardness analysis was performed on zones with higher densities (gate position, thicker zones) and zone with the lowest density (zone 4). Average hardness at gate position is 207,3 HV, while average hardness at the zone 4, where the highest porosity was observed, is 188,7 HV, Fig. 6.

The highest hardness was observed at position of gate and zones with higher thickness. Other analysed positions of the part showed significantly lower hardness. Also, results showed that lower porosity caused smaller hardness variation compared to more porous zones.

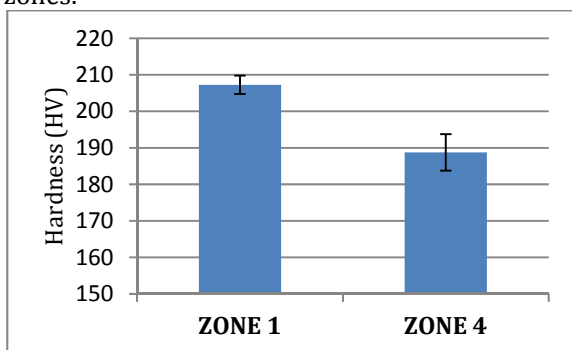


Fig. 6. Hardness of sintered part

4. CONCLUSION

Metallographic examination of ring-shaped part, produced by metal injection molding, showed inhomogeneous properties through the cross section. Residual porosity varied from very low value in powder accumulation zones to very high percent in binder rich zones. Separation of powder and binder during molding is the main reason for density variation in the green part. Gate zone is powder accumulated zone with very low porosity, while the thin walls and remote regions are high porosity zones. Variations of porosity caused significant variations in hardness through the cross section of the part. Hardness varied from 188,7 HV in very porous zones to 229 HV in porosity-free zones. This behaviour leads to density variation in the final part and variation in mechanical properties after sintering, even though the same sintering conditions were applied. Different shrinking capabilities of the different zones of the same part during sintering may cause uneven shrinking and part deformation. Also, it is expected that separation of MIM feedstock intensifies as part complexity increases.

REFERENCES

[1]. Zavaliangos Antonios, Missiaen Jean-Michel, Bouvard Didier. (2006). Anisotropy in Shrinkage During Sintering, Science of Sintering, DOI: [10.2298/SOS0601013Z](https://doi.org/10.2298/SOS0601013Z)

- [2]. Nicolò Corsentino. (2016). Development of a design procedure accounting for the anisotropy of the dimensional change in Powder Metallurgy parts, Doctoral Thesis, University of Trento, Department of Industrial Engineering.
- [3]. John W. Carson, Brian H. Pittenger, Jenike & Johanson, Inc.. (1998) ASM Handbook, Volume 7: Powder Metal Technologies and Applications Bulk Properties of Powders. ASM International
- [4]. Emir Šari, Muhamed Mehmedovi, Samir Butkovi.(2016). Effect of injection parameters and cavity position on MIM green part mass, Journal of Trends in the Development of Machinery and Associated Technology, Vol. 20, No. 1, ISSN 2303-4009 (online), p.p. 29-32
- [5]. Fang Wei, He Xinbo, Zhang Ruijie, Yang Shidi, Qu Xuanhui.(2014). The effects of filling patterns on the powder-binder separation in powder injection molding, Powder Technology Volume 256, Pages 367-376
- [6]. Marco Thornagel, Simulating flow can help avoid mould mistakes, From: <https://www.materialstoday.com/molding-and-pressing/features/simulating-flow-can-help-avoid-mould-mistakes>, 5 October 2010. accessed on: April 02, 2021.
- [7]. Emir Šarić, Muhamed Mehmedović, Samir Butković. (2015). Tehnologija injekcionog presanja metalnih prahova- Faza injektiranje i kalupi, Univerzitet u Tuzli.



Banja Luka
28–29 May 2021.

DEMI 2021

15th International Conference on
Accomplishments in Mechanical and
Industrial Engineering

www.demi.mf.unibl.org



3D printing: technology, materials, and applications in the manufacturing industry

S. Đurović^a, D. Lazarević^b, Ž. Šarkoćević^c, M. Blagojević^d, J. Stanojković^e

^aStrahinja Đurović, Higher Technical Professional School in Zvečan, Serbia (strahinjadjurovic55@gmail.com)

^bPhD, Dragan Lazarević, Fac. of Techn. Sciences Kos. Mitrovica, Univ of Pristina, Serbia, (dragan.lazarevic@pr.ac.rs)

^cPhD, Živče Šarkoćević, Fac. of Techn. Sciences Kos. Mitrovica, Univ of Pristina, Serbia, (zivce.sarkocevic@pr.ac.rs)

^dMilan Blagojević, Fac. of Techn. Sciences Kos. Mitrovica, Univ of Pristina, Serbia, (milan.blagojevic@pr.ac.rs)

^eJelena Stanojković, Fac. of Techn. Sciences Kos. Mitrovica, Univ of Pristina, Serbia, (jelena.stanojkovic@pr.ac.rs)

Abstract *The technology of 3D printing represents the making of three-dimensional (3D) parts layer by layer directly from a computer-aided design (CAD) model file. The technology of 3D printing emerged as a flexible and powerful technique in the advanced manufacturing industry. Besides the previously stated industry, the technology became widespread in a great number of other fields. Even though 3D printing gives engineers and designers a possibility of a clear insight in the process of designing, the emphasis of many parameters, the possibility of easy and early detection of errors and their quick efficient correction, it is increasingly being used for making a variety of products. Besides conventional thermoplastics, the materials being used in 3D printing are ceramics, graphene-based materials as well as metals. This paper presents the overview of available technology types, the application and materials that are used for 3D printing in the machining industry.*

Keywords *3D printing, technology, machining industry, application, STL*

1. INTRODUCTION

3D printing can create physical objects from a geometrical representation by successive addition of material. This 3D process had many experienced a phenomenal expansion in recent years [1]. Charles Hull was a pioneer of the solid imaging process known as stereolithography and the STL (stereolithographic) file format which is still the most widely used format used today in 3D printing. He is also regarded to have started commercial rapid prototyping that was concurrent with his development of 3D printing [2]. This technology can be used to quickly fabricate components with any complex shape by accurately accumulating material using solid modeling according to a computer aided design (CAD) model or computed tomography (CT) scan under computer control [3]. It has the

potential to reduce material waste, decrease labor cost and fast production. Its use in the various fields of manufacturing industries such as automobile, aerospace, medical, etc., has continued to grow for decades [4].

The process is roughly as follows: first build a three-dimensional model through CAD or modeling software, and then scan the cross-section of the built models layer by layer. The printer reads the cross-sectional information in the file and uses liquid, powder or sheet materials to combine them. The cross-sections are printed layer by layer, and then the cross-sections of each layer are glued together in various ways to create a solid body (fig. 1). It can process and manufacture samples of more complicated original embryos, while greatly improving the speed and efficiency of processing and manufacturing, which plays a great

saving effect on reducing related input costs [5]. 3D printer technology can produce products with any complex shape, without having to consider processing problems, and solve the design and manufacturing problems of complex parts. Therefore, 3D printing technology is a very important production method in industrial manufacturing [6].

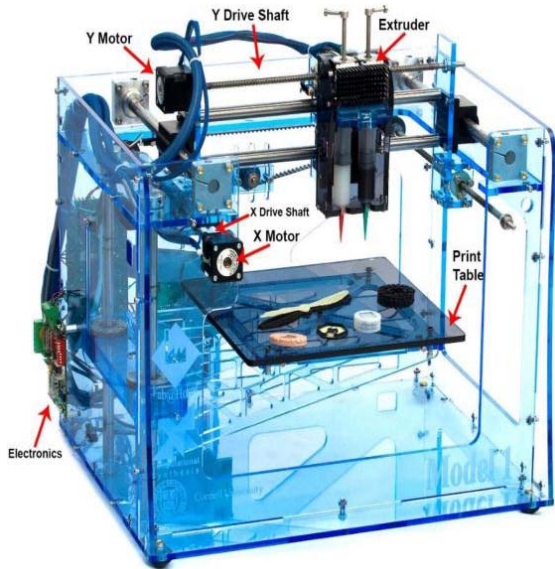


Fig. 1. 3D-printer [2]

Basic advantages and disadvantages of 3D printing:

Advantages

- Less setup costs and less tooling costs
- Lower production costs
- Lower development time and costs (increase the pace of design to product)
- Eco friendly: less influence on CO₂
- Lower cost price for small volumes and complex shaped parts
- Shorter delivery time
- Complex products relatively easy to print
- Flexibility (printing on-demand, customisation)

Disadvantages

- Lower production speed
- Higher investment costs
- Unclear responsibilities regarding intellectual property
- Liability - warranties, certification
- Process variability/ quality
- Not efficient for large series
- Limited choice of material (sometimes)
- Limited dimensions of product

- Complexity of the Supply Chain (3D printing is added to the Supply Chain)[7].

2. TEHNOLOGY

Many different 3D printing processes and technologies have been invented from late 1970. The printers were originally very large and expensive in what they could produce. A large number of Additive manufacturing processes are now available. Some of the methods melt or soften material to produce the layers, e.g. selective laser melting(SLM), selective laser sintering (SLS), fused deposition modeling (FDM), while others cure liquid materials using different other technologies, e.g. stereolithography (SLA) and With laminated object manufacturing (LOM)[2].

2.1 Selective Laser Sintering (SLS)

Selective Laser Sintering is a Layer Manufacturing process that allows generating complex 3D parts by consolidating successive layers of powder material on top of each other. Consolidation is obtained by processing the selected areas using the thermal energy supplied by a focused laser beam (fig. 2.). Using a beam deflection system (galvano mirrors), each layer is scanned according to its corresponding cross section as calculated from the CAD model[8].

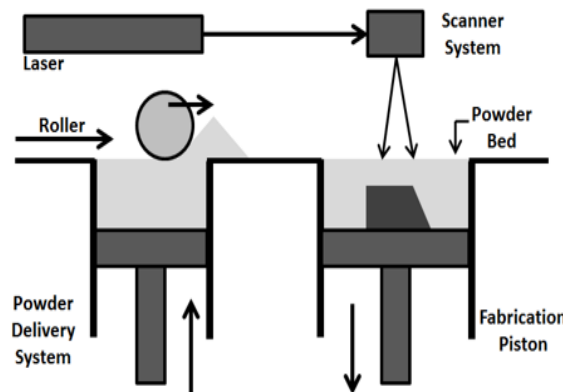


Fig. 2. Selective laser sintering process [16]

2.2 Selective laser melting (SLM)

Another increasingly popular technique of 3D printing is the SLM method—Selective Laser Melting. This technology is protected by several patents. Using this method, elements from

metal powders are produced. However, they exhibit lower strength and durability than parts made with traditional shaping techniques. The SLM method ensures repeatability of mechanical properties, which allows the use of parts produced in this way as elements of machines and devices. The SLM method consists in melting metal powder with a metal beam. The process begins with applying a layer of powder and then levelling it. Selected areas are melted by the laser beam. The next step in the process is to lower the working plate by the layer thickness and apply the powder layer again. The whole process is repeated until the finished model is obtained. (fig. 3.). The produced model should be cleaned of unmelted powder and most often subjected to finishing treatments, which include:

- CNC machining and milling and
- varnishing.

The materials most often used in the SLM method include stainless steels, pure titanium, and its alloys as well as low-melting, zinc, copper, tool steel, silicon carbide, or aluminum oxide alloys. In machines used for SLM printing, it is necessary to use a protective gas in the working chamber and the type depends on the powder that will be used to print the element [14].

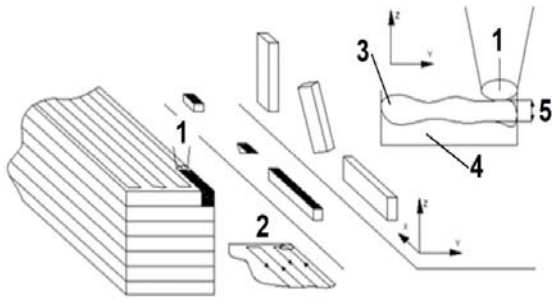


Fig. 3. Schematic principle of SLM technology (scales are not respected), where: (1) laser beam; (2) laser path; (3) melted powder; (4) powdered bed; (5) layer thickness [19]

2.3 Fused deposition modeling (FDM)

Fused Deposition Modeling (FDM) is one of the most popular 3D printing methods [18]. In order to build complex shaped parts, FDM uses support material apart from the build material which supports the overhanging structures during the process and helps in maintaining structural integrity of part until it is

strengthened before the support material is removed by breaking or by dissolving using appropriate solvents. Most of the existing FDM machines use thermoplastic materials which are in a filament form for the extrusion and deposition purpose. Acrylonitrile Butadiene styrene (ABS) and Polylactide (PLA) thermoplastics are predominantly used in the process. [9] Usually 1.75 - 3 mm wire thickness is used. During 3D printing, the material in the form of wire is melted by passing a 0.4 mm diameter mold and the production is carried out by axial movement (fig. 4.). By stacking the layers on top of each other, the object is created [19].

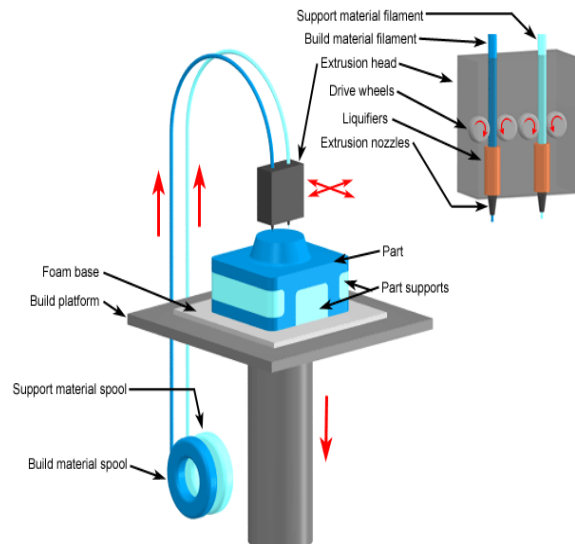


Fig. 4. Schematic Representation of FDM process [9]

2.4 Stereolithography (SLA)

The process of stereolithography starts with a standard tessellation language (STL) file, which now is the standard for every AM process. By slicing the STL file, the 3D model is translated to 2D slices that contain the information of cross-sections. According to these 2D slices, the physical model can be produced layer by layer (fig. 5.). The fundament of stereolithography is the curing reaction of resins, which is an exothermic polymerization process characterized by chemical cross-linking reactions. The reaction is initiated by supplying the energy of UV light and there are two transitions during the curing reaction process: gelation and vitrification [10].

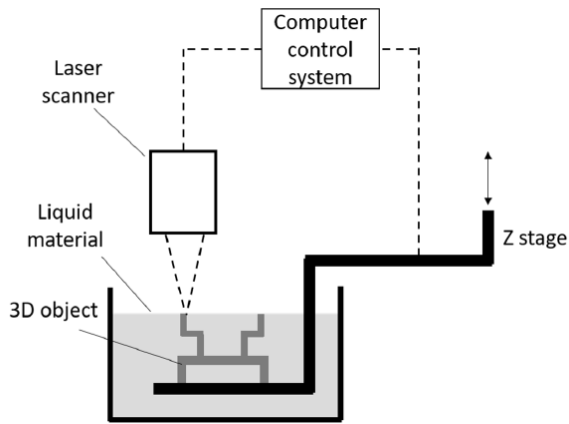


Fig. 5. Hull's stereolithography systems [10].

2.5 Laminated object manufacturing (LOM)

While underrepresented by industrial standards, LOM can offer considerable advantages when compared with the other AM techniques. In contrast to the other AM techniques, which use powdery or liquid raw materials, a versatile range of raw materials, including fiberglass or ceramic fillers, can be processed by SL techniques in general. Within the technique of LOM, a subcategory of SL, nontoxic, relatively inexpensive, and continuous strands of paper or polymer tapes are laminated on top of each other, yielding complex-shaped, 3D multilayers (fig. 6.). Compared with other AM techniques, LOM can accelerate the production of large-scale parts [11].

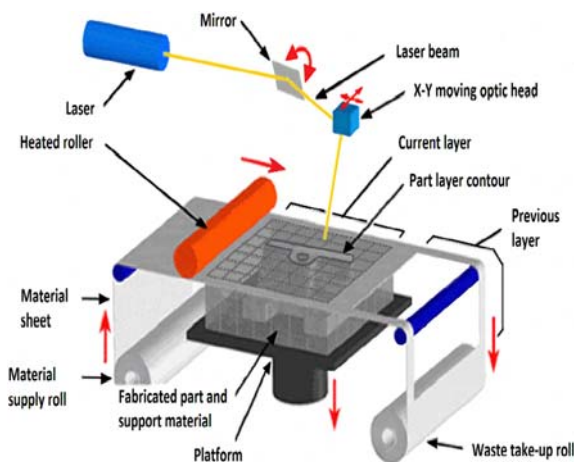


Fig. 6. Basic schematic of the LOM process, to which additional processing steps may be added. The continuous flow of sheet material is marked by red arrows [11]

3. MATERIALS

Metal consumables accounted for 39.4%, lower than plastic 46.5%, mainly because the industrialization of metal printing is in a rapid expansion stage, and the growth of equipment is ahead of the growth of material consumption. Non-metal 3D printing usually uses plastics, resin materials, etc., and metal 3D printing usually uses various alloy powders and wires [5]. Below we will discuss some different type of materials which are suitable for 3D printers:

ABS: Most affordable material for 3D printing, its quite strong, high resolution, flexible and light weighted. This material is used in 3D printer at high temperature in between 220 – 250 degree Celsius. **PLA:** It is also a public demanded product for 3D printing. The specialty of PLA is, it is biodegradable(Environment friendly). It is made from corn, cassava, sugarcane or sugar beet pulp. **Nylon:** It is the choice for premium products from a wide range of applications. Properties like flexibility and strength of nylon make it more valuable PVA: Engineered to be soluble and extensively used for support material because other support materials requires special chemicals to dissolve. **Alumide:** In terms of physical properties it is comparatively similar to nylon. It's a composite material of nylon with aluminum. The difference one can find in shiny and porous surface finish. Alumide is also more durable **Aluminum:** Used in the wide range of applications because of its strength, lightweight, heat resistant, corrosion-resistant, and versatility It is used in different aluminum-based premium alloys. Highly recommended for products with high mechanical stress. **Cobalt chromium:** Well known as superalloy because of high strength, biocompatible, heat resistant, corrosion resistant, hard wearing and low conductivity. Most preferably used in high performance application. **Titanium:** Expensive and the most versatile material to be used for 3D printing. Used in the form of pure powder for metal 3D printing. 3D printing of titanium mostly used in automotive, aerospace and tooling industries. **WAX:** Not used for the final product but uniformly used to make prototypes. Have high resolution and smooth surface easy to make [12].

4. APPLICATIONS

There are many sectors where we can use this technology these are:

Aerospace: In this field many are directly made by using 3D-printer. The aerospace and defence industries contributed 16% of 3D-printing. SLA and material jetting are used to produce high details smooth scale models of aerospace design.

Food: Additives manufacturing of food is being developed by using 3D-printing. NASA also worked on this technology which is making food on 3D-printer in the space. A larger no. of variety of foods are making on 3D-printers such as the chicalotes candies pizza flat food. This technology helps to limit food waste.

Automobile industry: In our automobile industries developed very fast new innovations are comes out from industry. Now a days industries adopted 3D-printing technology for making products.

Medical application: This technology also used in medical application for printing skin bones drug organs medical equipment's tissues pharmaceutical research. 3D-printing also can be used to create human organs.

Art and jewellery: By using this technology also used for printing jewellery. This used for printing many decorative parts [13].

Textile industry: Since 2013, 3D printed cloth production has displayed an impressive increment. Nowadays, it is possible to make 3D Printed clothes, shoes, accessories (sunglasses, watches) and so on [15].

5. CONCLUSION

Three-dimensional (3D) printing is an advanced manufacturing process. This method increase production efficiency, reduce the cost, meet the needs of the population while minimizing the environmental impact. 3D Printing technology could revolutionize the world, and advances in this technology can significantly change and improve the way we manufacture products and produce goods worldwide.

REFERENCES

- [1] Shahrubudina,N., Leea, T.C.,Ramlana,R. An Overview on 3D Printing Technology: Technological, Materials, and Applications *2nd International Conference on Sustainable Materials Processing and Manufacturing (SMPM 2019)*.
- [2] Gokhare,V.G.,Jijabai,J.,Dr.Raut,D.N. A Review paper on 3D-Printing Aspects and Various Processes Used in the 3D-Printing *International Journal of Engineering Research & Technology (IJERT)* Vol. 6 Issue 06, June – 2017. ISSN: 2278-0181 IJERTV6IS060409
- [3] Qian, Y., Hanhua, D., Jin, S., Jianhu, H., Bo, S., Qingsong, W., Yusheng, S. A Review of 3D Printing Technology for Medical Applications. *Engineering*, Vol. 4 (5), August 2018. DOI: 10.1016/j.eng.2018.07.021
- [4] Hossain,A.,Zhumbekova,A.,Chandra Paul,S.,Ryeol Kim,J. A Review of 3D Printing in Construction and its Impact on the Labor Market. *Article in Sustainability* . October 2020. DOI: 10.3390/su12208492.
- [5] Haocheng ,D., Shaoqian, C. Development and Application of 3D Printing and Its Materials. *Insight - Material Science*, Volume 3 Issue 2 | 2020. P.28-31.
- [6] Botao,H.,Guomin,L. 3D Printing Technology and Its Application in Industrial Manufacturing. *IOP Conf. Series: Materials Science and Engineering* 782 (2020) 022065. EMCEME 2019. IOP Publishing doi:10.1088/1757-899X/782/2/022065
- [7] Kubáč, L., Kodym, O. The Impact of 3D Printing Technology on Supply Chain. *MATEC Web of Conferences* 134, 00027 (2017) LOGI 2017 DOI: 10.1051/mateconf/201713400027
- [8] Prof. Dr. Ir. Kruth, J.P.,Ir. Mercelis,P., Prof. Dr. Ir.Froyen,L.Binding Mechanisms in Selective Laser Sintering and Selective Laser Melting. *Rapid Prototyping Journal*. February 2005. DOI: 10.1108/13552540510573365.
- [9] Chennakesava,P.,Shivraj Narayan,Y.Fused Deposition Modeling – Insights. *International Conference on Advances in Design and Manufacturing (ICAD&M'14)*. December 2014,
- [10] Jigang,H.,Qin,Q.,Jie,W .A Review of Stereolithography: Processes and Systems, *Article in Processes*. September 2020. DOI: 10.3390/pr8091138
- [11] Dermeik,B.,Travitzky,N. Laminated Object Manufacturing of Ceramic-Based Materials. *Published by WILEY-VCH Verlag GmbH & Co. KGaA, Weinheim*. 2020. DOI: 10.1002/adem.202000256

- [12] Vikas, K. 3d printers from dimension to technology VIII SEMESTER B. *Tech Students*, Department of Mechanical Engineering Dronacharya College of Engineering, Gurugram, India.
- [13] Shinde, A. A., Patil, R. D., Dandekar, A. R., Dhawale, N. M. 3D Printing Technology, Material Used For Printing and its Applications *International Journal of Scientific & Engineering Research* July-2020 Volume 11, Issue 7, ISSN 2229-5518
- [14] Kowalski, A., Waszkowski, R. Layout Guidelines for 3D Printing Devices. *Article in Applied Sciences*. September 2020. DOI: 10.3390/app10186333.
- [15] Avinc, O., Yildirim, F., Yavas, A., Kalayci, E. 3D printing technology and its influences on the textile industry. *International Journal of Industrial Electronics and Electrical Engineering*, ISSN: 2393-2835. Volume-5, Issue-7, Jul.-2017.
- [16] Serin, G., Kahya, M., Ünver, H. O., Güleç, Y., Durlu, N., Eroğul, O. A review of additive manufacturing technologies. *The 17th International Conference on Machine Design and Production*. July 12 – July 15 2016, Bursa, Turkiye.
- [17] Alvarez, K. L., Lagos, F. R., Aizpun, M. Investigating the influence of infill percentage on the mechanical properties of fused deposition modelled ABS parts, *Ingeniería e Investigación* vol. 36 n.º 3, december – 2016. P (110-116), DOI: 10.15446/ing.investig.v36n3.56610.
- [18] Çabuk, N., Çabuk, S. 3D Printers And Application Fields. 1. *International technological sciences and design symposium*, 27-29 June 2018 - Giresun/TURKEY. P. 349-356.
- [19] Kozior, T., Bochnia, J., Zmarzły, P., Gogolewski, D., Mathia, T. G. Waviness of Freeform Surface Characterizations from Austenitic Stainless Steel (316L) Manufactured by 3D Printing-Selective Laser Melting (SLM) Technology. *Article in Materials*. September 2020. DOI: 10.3390/ma13194372.



Banja Luka
28–29 May 2021.

DEMI 2021

15th International Conference on Accomplishments in Mechanical and Industrial Engineering

www.demi.mf.unibl.org



Effects of shape optimization on the 10 bar truss example

N. Petrovic^a, N. Kostic^a, N. Marjanovic^a

^aUniversity of Kragujevac, Faculty of Engineering, Sestre Janjic 6, 34000 Kragujevac, Serbia

Abstract *This research focuses on determining the effects of structural optimization on 10 bar trusses. Structural optimization is done in Rhino 6, using GA optimization. Shape optimization was done to find savings in used material in relation to total element lengths. The new optimized structure which meets all constraint criteria has different element lengths to the initial design. Optimal values are compared to initial values showing that the total length of elements can be decreased by roughly 28%. By individually observing elements it is possible to see that some elements are now longer and some shorter than in the initial model, but the overall length is decreased. This shows significant savings which are possible through shape optimization, as well as the significance of the entire process.*

Keywords *Truss optimization, shape optimization, mass minimization, element lengths*

1. INTRODUCTION

Optimization is a tool which is being used more and more in planning and designing in order to achieve greater gains and decrease negative effects. This process requires certain time and effort, but compared to the positive effects gained from it, it is cost-effective. The goal is to always balance optimization types (sizing, topology and shape) in order to have the input effort (knowledge, time and resources) at a minimum and to achieve maximal effects (financial, structural, etc.). This is why it is important to see the effects of specific parts of structural optimization, as well as their combinations and determine what the best course of action is for a given problem.

Corresponding author

PhD, Nenad Petrovic
npetrovic@kg.ac.rs

University of Kragujevac, Faculty of Engineering
Sestre Janjic 6
Kragujevac, Serbia

In recent years a lot of research has been done in the field of truss structural optimization. The implementation of realistic variables for sizing optimization showed that using continuous variables like in [1, 2] cannot be created and therefore discrete variables have started becoming the norm. Researchers in [3, 4] showed the differences in using discrete versus continuous variables. Discrete sets of cross-section parameters can be used to represent the possible stock cross-sections which are available for a certain material. Another important factor to consider is the use of constraints. Realistic constraints allow for the design of structures which can be directly implemented in construction. These constraints are still not a standard in research, however they have been used in the past [5-8]. Paper [9] presented the difference in using buckling constraints compared to models optimized without this constraint. Other effects are being researched in this field such as the overall outer surface area [10] and environmental impact. This research covers the use of sizing and shape optimization. All cross-sections in the examples

will have the same area, this is done to minimize the number of different stock used and to show possibilities in savings on material using shape optimization. The motivation is to show the significance of using shape optimization and to determine its efficiency.

2. STRUCTURAL OPTIMIZATION PROBLEM

The problem of structural truss optimization implies optimization of sizing, topological, and shape aspects of an initial model configuration. In practice this is not always possible, and furthermore it is usually more practical to use a single bar cross-section for a structure than to use several due to the possibility of saving in bulk as well as increasing simplicity of construction. The goal of this research is to show the possible improvements of using shape optimization when using a single profile cross-section for constructing a truss.

The objective functions of all structural optimization aim to find the variable combination which would minimize the overall mass, cost or some other factor. In the case of a minimum weight design problem using shape optimization the goal function can be defined as:

$$\left\{ \begin{array}{l} \min W(l) = \sum_{i=1}^{i=n} \rho A l_i \\ \text{subjected to} \left\{ \begin{array}{l} \sigma_{min} \leq \sigma_i \leq \sigma_{max} \text{ for } i=1, \dots, n \\ u_{min} \leq u_j \leq u_{max} \text{ for } j=1, \dots, k \\ |F_{Ai}^{comp}| \leq F_{Ki} \text{ for } i=1, \dots, n \end{array} \right. \end{array} \right. \quad (1)$$

where n is the number of truss elements, k is the number of nodes, l_i is the length of the i th element, A is the cross section area, σ_i is the stress of the i th element, u_j is displacement of the j th node. F_{Aicom} is the axial compression force, F_{Ki} is Euler's critical load (2).

$$F_{Ki} = \frac{\pi^2 \cdot E \cdot I}{l_i^2} \quad (2)$$

E is the modulus of elasticity, and I is the minimum area moment of inertia of the element cross section. Since the buckling constraint changes with each iteration as a result of the change of element lengths with the change in node location, this constraint is considered a dynamic constraints, and its addition drastically increase the complexity of the optimization problem.

3. THE DESIGN PROBLEM

The 10 bar truss is one of the most commonly used examples in truss structural optimization, and presents a good representation for comparing element length changes in shape optimization as it has two points, (1) and (3), which have variable coordinates. The movement of these two points causes a change in the length of 7 bars. The full round cross-sections used are made out of Aluminium 6063-T5 (Young modulus 68947MPa, and density of 2.7g/cm³). Point loads are $F=444.82$ kN in nodes (2) and (4) in the $-y$ direction. The displacement is limited to ± 0.0508 m of all nodes in all directions and axial stress is limited to ± 172.3689 MPa for all bars. Fig. 1 shows the initial configuration of the 10 bar truss problem.

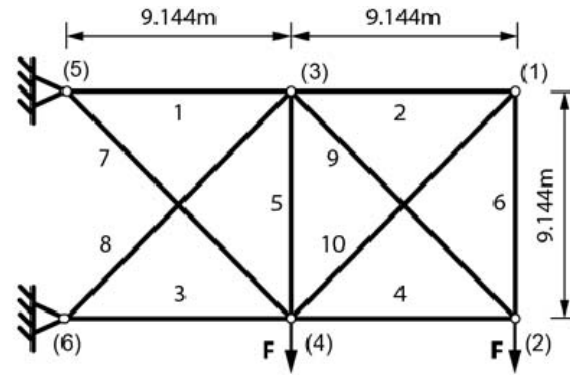


Fig. 1. 10 bar truss problem [4].

Aside from displacement and stress constraints Euler buckling constraints are also used for all elements subjected to compression forces and a minimal element length constraint set at 0.5m for all bars, in order to achieve practically applicable results.

The 10 bar truss used for this research uses the same cross-sections for all elements with a diameter of 240mm. This is determined as the analytical solution to this problem sized according to the most stressed element subjected to buckling and using standard profile diameter values.

The optimization method used is genetic algorithm (GA). An original software was developed for solving this type of problem using Rhino 6 Grasshopper and the Karamba plugin. Shape optimization will be used to compare savings in element lengths and total mass.

4. RESULTS AND DISCUSSION

Using shape optimization the initial configuration is modified to the shape shown in fig. 2. Results shown are the best results out of 10 consecutive optimizations all with the same starting configuration as the initial model shown in fig.1.

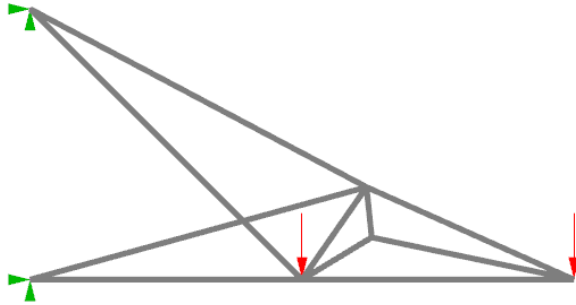


Fig. 2. Optimal shape for the 10 bar truss problem.

The results show that only one bar element has increased in length while all others have been decreased by the optimization process. A comparison of bar element lengths is shown in figure 3.

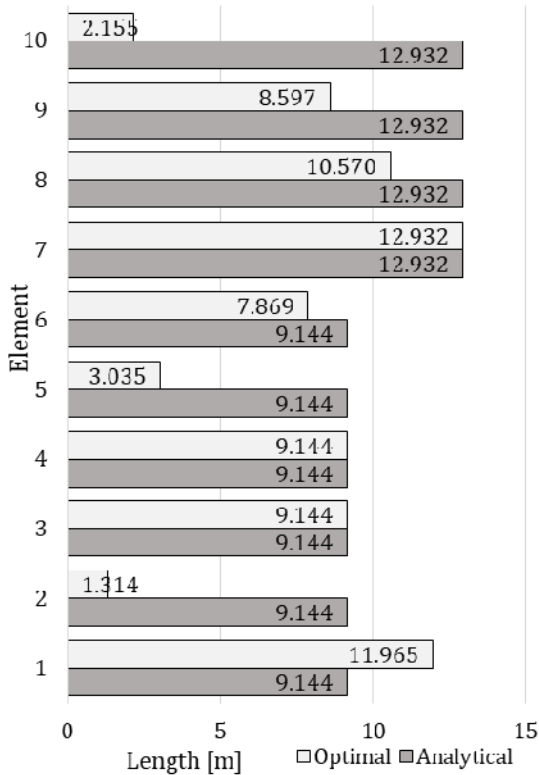


Fig. 3. Bar element length comparison of analytical and optimal models.

Comparing the savings in length by bar element is shown in figure 4. Here the significant difference in savings is much more obvious.

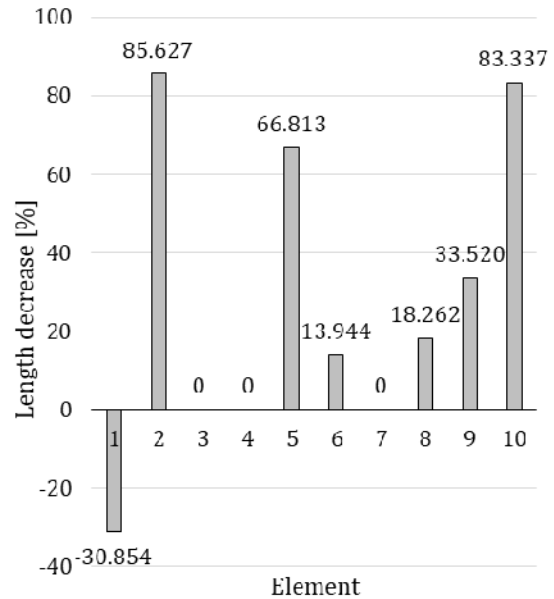


Fig. 3. Savings in element length, by bar, using shape optimization compared to the initial model.

The achieved results, regardless of the individual lengths, show that the total length of elements, and thereby the total material used has significantly decreased. This decrease in length is 28.02% from the initial configuration, which is the exact savings in mass from an initial 13019.482kg to an optimal 9371.591kg.

5. CONCLUSION

Truss optimization can achieve significant improvements in the design process leading to lighter structures which are cheaper to produce while maintaining structural integrity. It is not always cost-effective to conduct all optimization types simultaneously, nor is it always possible due to other influencing factors. Depending on the complexity of the initial design and the constraining problems the use of optimization might be overly complicated, slow or expensive compared to conventional design methods. The future of optimization is in its commercialization and integration into existing CAD software.

Shape optimization can provide significant savings in overall mass, and thereby the same savings in bar lengths if the same cross-section profile is used when optimizing. In this paper a

typical 10 bar truss example was used to demonstrate the effects of shape optimization on element length. The overall savings in length, and mass is 28.02% using the same cross-section diameter which was analytically calculated for the initial solution. This is a substantial difference, especially considering that it was achieved by using only 4 variables (x and y coordinates of two nodes).

The use of other optimization types such as sizing and topology would be able to additionally decrease mass. There is a need to bring optimal solutions closer to practical application. Research in this field needs to strive towards applicable solutions in order to allow further developments.

REFERENCES

- [1] V. Ho-Huu, D. Duong-Gia, T. Vo-Duy, T. Le-Duc, T. Nguyen-Thoi, An efficient combination of multi-objective evolutionary optimization and reliability analysis for reliability-based design optimization of truss structures, *Expert Systems with Applications*, 102 (2018) 262-272.
- [2] N. Petrovic, N. Kostic, N. Marjanovic, COMPARISON OF APPROACHES TO 10 BAR TRUSS STRUCTURAL OPTIMIZATION WITH INCLUDED BUCKLING CONSTRAINTS, *Applied Engineering Letters*, 2 (2017) 98-103.
- [3] N. Petrović, N. Kostić, N. Marjanović, V. Marjanović, Influence of Using Discrete Cross-Section Variables for All Types of Truss Structural Optimization with Dynamic Constraints for Buckling, *Applied Engineering Letters*, 3 (2018) 78-83.
- [4] N. Petrovic, N. Kostic, N. Marjanovic, DISCRETE VARIABLE TRUSS STRUCTURAL OPTIMIZATION USING BUCKLING DYNAMIC CONSTRAINTS, *Machine Design*, 10 (2018) 51-56.
- [5] S. Gholizadeh, Layout optimization of truss structures by hybridizing cellular automata and particle swarm optimization, *Computers & Structures*, 125 (2013) 86-99.
- [6] P.W. Jansen, R.E. Perez, Constrained structural design optimization via a parallel augmented Lagrangian particle swarm optimization approach, *Computers & Structures*, 89 (2011) 1352-1366.
- [7] N. Petrovic, N. Marjanovic, N. Kostic, M. Blagojevic, M. Matejic, S. Troha, Effects of introducing dynamic constraints for buckling to truss sizing optimization problems, *FME Transaction*, 46 (2018) 117-123.
- [8] V.T. Bich Quyen, C.Q. Khanh, T.T. Thuy Van, D.N. Khoa, T.P. Truc, A New Algorithm for Size Optimization of the Truss Structures with Buckling Constraint using Finite Element Method, *IOP Conference Series: Materials Science and Engineering*, 661 (2019) 012041.
- [9] N. Petrović, V. Marjanović, N. Kostić, N. Marjanović, M. Viorel Dragoi, Means and Effects of Constraining the Number of Used Cross-Sections in Truss Sizing Optimization, *Transactions of FAMENA*, 44 (2020).
- [10] J. Brütting, J. Desruelle, G. Senatore, C. Fivet, Design of Truss Structures Through Reuse, *Structures*, (2018).



Banja Luka
28-29 May 2021.

DEMI 2021

15th International Conference on
Accomplishments in Mechanical and
Industrial Engineering

www.demi.mf.unibl.org



Experimental research of surface roughness in powder mixed electric discharge machining

D. Rodic, M. Gostimirovic, M. Sekulic, B. Savkovic, N. Kulundzic, A. Aleksic

University of Novi Sad, Faculty of Technical Sciences, Department for Production Engineering, Trg D. Obradovica 6, 21000 Novi Sad, Serbia.

Abstract *The present application of electric discharge machining is limited by the relatively low surface quality. A possible technological improvement of electric discharge machining can be achieved by innovations of the existing processes. The addition of an electrically conductive powder to the dielectric leads to a modified material removal process called powder-mixed electrical discharge machining. In this paper, a preliminary study is presented to determine the limiting values of input parameters for machining titanium alloys. Based on the available literature sources and preliminary experimental investigations, the suitable conditions for electrical discharge machining of TiAl6V4 are presented. Preliminary investigations with results are presented as well as the influence of input parameters on surface quality. In addition to the basic input parameters such as discharge current and pulse duration, the influence of the graphite powder on the surface quality of the aforementioned machining process is considered in particular.*

Keywords *EDM, graphite powder, titanium alloy, surface roughness*

1. INTRODUCTION

Electrical Discharge Machining (EDM) is an unconventional process whose application is very common in practice. It is a material removal process that can process all electrically conductive materials regardless of their physical and metallurgical properties. This method used in the machining of materials that are difficult to machine and parts with complex geometric shapes that are very difficult or impossible to machine using classical methods. The precondition for carrying out the EDM

process is that the workpiece has at least minimal electrical conductivity [1, 2].

However, the current application of EDM is limited due to the relatively low machining productivity and the low quality of the machined surface. A possible technological improvement of EDM can be achieved by innovations of the existing processes.

The addition of an electrically conductive powder to dielectric creates a modified material removal process called Powder Mixed Electrical Discharge Machining (PMEDM), which significantly affects the EDM process output of difficult-to-machine materials.

Over time, research on EDM intensified and the first scientific papers on this process appeared in the 1960s [3]. Even then, the advantage of this technology was recognized in terms of the possibility of machining difficult-to-machine materials [4]. However, with the development and improvement of other machining processes,

Corresponding author

PhD, Dragan Rodic
rodicdr@uns.ac.rs

University of Novi Sad, Faculty of Technical Sciences,
Department for Production Engineering
Trg D. Obradovica 6
Novi Sad, Serbia

the application of EDM becomes limited in terms of machining productivity and surface quality. Recognizing this fact, author Jeswani published a study in 1980 in which he clearly defined the machining conditions and explained in detail the results obtained [5]. In the experiment, he used graphite powder with a grain size of 10 μm , which he mixed with kerosene at a ratio of 4 g/l. When analyzing the results obtained, the most striking observations are an increase in machining productivity of up to 60 % and a reduction in tool wear of up to 15 %.

The electrically conductive powder added to the liquid dielectric reduces the insulating properties of the dielectric and causes an increase in the working gap between the tool and the workpiece. The increase of the working gap implies the efficiency of the dielectric circulation, i.e. the flushing of the working space between the tool and the workpiece. In this way, EDM becomes stable, which improves the technological characteristics of the process, such as increased machining productivity and reduced roughness of machined surfaces, and also reduces tool wear [6]. Figure 1 shows a comparative view of classical (a) and modified (b) EDM (PMEDM).

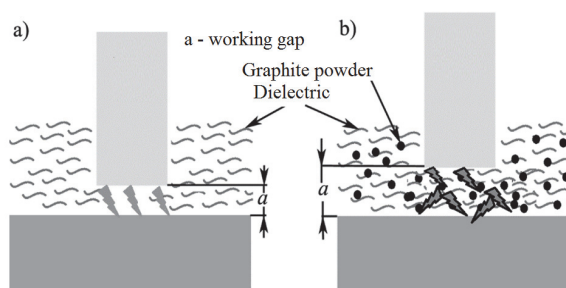


Fig. 1. Comparative view of classical (a) and modified (b) EDM (PMEDM)

The space between the tool and the workpiece, that is, the working gap, is filled with electrically conductive powder particles. Under the influence of DC voltage, a strong electromagnetic field is generated at the smallest local distance between the surface of the tool and the workpiece, i.e. at the point of lowest resistance of the current passage. In the electric field, there is an intense accumulation of dust particles, which create a bridge effect, forming a kind of electrically conductive bridge, that is, the so-called "zigzag" shape. The

increased bridge effect reduces the discharge voltage and the insulation properties of the dielectric [7].

At the same time, the dust particles change the properties of the discharge channel, which equalizes the distribution of sparks on the dust particles and thus reduces the current density. Due to this uniform distribution of discharges, there is uniform removal, i.e. flat craters on the workpiece, which leads to a reduction in surface roughness and thus an increase in machining accuracy [8].

Various kinds of electrically conductive powder may be mixed with liquid dielectric, among which may be pointed out: aluminum, graphite, silicon, copper, silicon carbide, and others. The types of powders that can be used with liquid dielectric, grain size, concentration and their effects on the performance of the PMEDM process have been studied by a smaller number of researchers.

Wong used powders of different electrical conductivities, such as graphite, silicon, aluminum, crushed glass, silicon carbide, and molybdenum sulfate, and studied their influence on surface roughness [9]. In PMEDM, he used a copper tool coated with a high electrical resistance material (silicon) to achieve a constant current during discharge. He concluded that the powders: graphite (grain size 40 μm) and silicon (grain size 45 μm) gave the best results from the surface roughness point of view. A significant reduction of surface roughness was obtained, i.e. $R_a = 0.62 \mu\text{m}$ with silicon powder, while with graphite powder $R_a = 0.75 \mu\text{m}$, i.e. the obtained surface with high gloss (mirror effect), which is the opposite of the classical EDM where mainly dull surfaces are obtained.

Zhao was one of the first to report experimental studies on machining productivity and surface quality during roughing electrical discharge machining in a dielectric with mixed powder [10]. By comparing the obtained results with classical EDM in the same machining regimes, it was found that there was an increase in machining productivity at discharge currents of higher intensity (19 A) and short pulse duration (10 μs). Under the above conditions, the PMEDM obtained an increase in production of about 70%. The improvement in the performance of PMEDM of titanium alloy in kerosene with mixed graphite powder with a size of 37 μm , is shown in [11]. The conducted

experiments showed that the use of graphite powder mixed with kerosene during machining significantly increases the productivity of machining, reduces surface roughness and relative wear of tools.

Despite the considerable advantages offered by the EDM process, its potential has not yet been fully exploited. This is partly due to the fact that this machining is mainly related to the machining of steel materials and less to the machining of advanced structural materials such as titanium alloys. The main objective of this work is to show that electrical discharge machining in a mixed powder dielectric achieves more favorable output performance such as surface roughness compared to classical electrical discharge machining of titanium alloys.

2. MATERIAL AND METHODS

The framework for experimental investigations relates to the choice of machine tool, the medium in which the machining is carried out, and the material of the tool and the workpiece. For the purpose of material machining, a die-sinking EDM machine from the company Agie Charmille called SP1-U, shown in Figure 2, was used.



Fig. 2. EDM machine Agie Charmille SP1-U

Dielectric Ilocut EDM 180 from Castrol was used in the experimental studies. It is a low viscosity mineral oil that ensures successful

flushing of the working chamber. Additives such as graphite powder and surfactants (reagents) are added to the dielectric to better flush the treatment area and avoid the accumulation of particles (shrinkage and accumulation). Asbury PM19 graphite powder was used in titanium alloy machining (PMEDM). The surfactant Tween 20 $C_{58}H_{114}O_{26}$ is a clear liquid with high density. The role of the surfactant is to prevent the accumulation and build-up of graphite powder particles, i.e. to ensure a homogeneous mixture of powder and dielectric during PMEDM.

A typical dielectric circulation system used in PMEDM is shown in Figure 3. This type of specially designed system is built into the work tank of machine SP1-U. A mixer or stirrer assembly is provided to avoid the deposition of powder particles at the bottom of the machining tank. It also helps to prevent stagnation of dust particles on the surface of the workpiece.

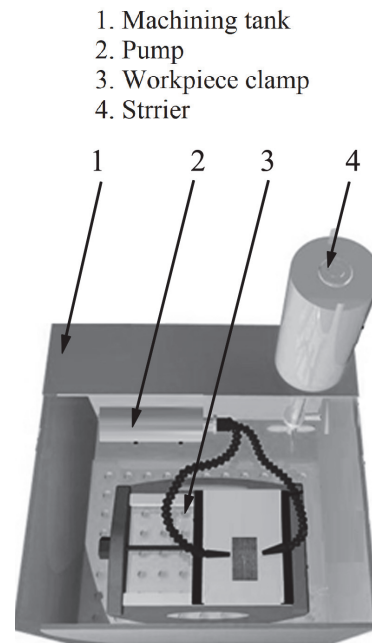


Fig. 3. PMEDM setup

The titanium alloy $TiAl_6V_4$ was selected as a material that is difficult to process. The selected titanium alloy has found application in aerospace, biomedical and many other engineering fields due to its exceptional properties such as high temperature and corrosion resistance. Due to its inherent properties, the machinability of this material is not economically feasible.

A tool made of graphite called Toyo Tanso TTK50 was used for the PMEDM of titanium. Surface roughness measurements were performed using a MarSurf PS1 instrument manufactured by Mahr Metrology. The device can measure various parameters that characterize the surface roughness. For this study, only the arithmetic mean deviation of the profile (Ra) was used. The measurement range of the device is from $-200 \mu\text{m}$ to $+150 \mu\text{m}$. The selected reference length of the measurement, i.e. the movement of the measuring probe on the measuring surface, is 5.6 mm. The device can also be connected to a computer so that the results can be stored and processed via the user interface.

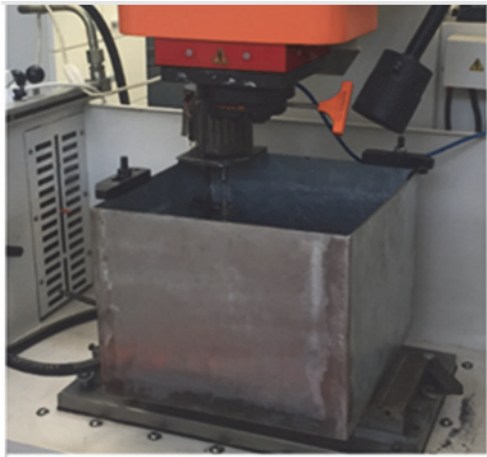


Fig. 4. Installed machining tank of PMEDM

3. EXPERIMENTAL RESULTS AND ANALYSIS

In order to carry out the experiment, it was first necessary to determine the limiting values of the input parameters. This was done for the discharge current, pulse duration and graphite powder concentration. While the other parameters are accepted as per the available literature.

The discharge current is limited by the dimensions of the electrode cross section i.e. current density. Here, the projection in the plane perpendicular to the direction of movement of the tool is taken as the relevant tool area. Therefore, a discharge current in the range of 3.2 and 7.5 A was used in the experimental pilot study on PMEDM titanium alloy, given the variations possible on the machine tool. The assumed discharge current was therefore 4.5 A.

The pulse duration is a time in microseconds for which current flows in each cycle. During this time, a voltage is built up between the tool and the workpiece. According to the research published in [12, 13], when machining titanium alloys, the upper limit of pulse duration was $200 \div 500 \mu\text{s}$. Based on the above, for the purpose of EDM of TiAl_6V_4 , a lower limit of pulse duration of $24 \mu\text{s}$ and an upper limit of $240 \mu\text{s}$ is adopted. For the purpose of this experiment, a pulse duration of $130 \mu\text{s}$ was assumed.

According to the available data from literature, the value of duty cycle above 50% has a negative effect on the surface roughness integrity of titanium alloy [14-16]. During the experiment, the negative polarity of the tool was used during machining in a dielectric with a mixed titanium alloy powder.

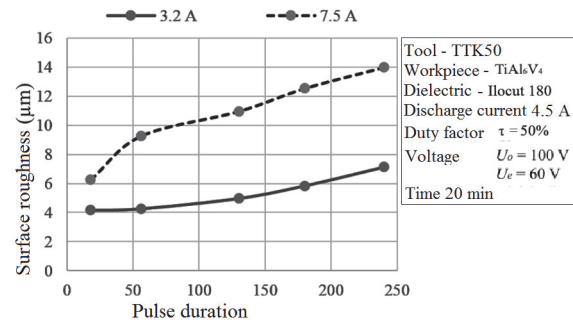


Fig. 5. Trial experiments in order to determine the influence of pulse duration

A review of the literature has shown that the concentration of graphite powder usually ranges from $0 \div 20 \text{ g/l}$ for different tools and workpiece materials [15, 17]. In this study, in order to determine the upper limit of graphite powder concentration, tests were conducted with a powder concentration of 20 g/l . Damage to the surface of the workpiece occurred, Figure 6. Therefore, the tests were carried out with concentrations of 0.6 and 12 g/l .

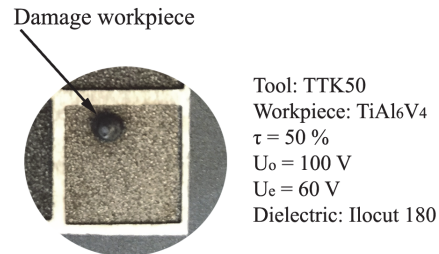


Fig. 6. Damage of workpiece under graphite powder of 20 g/l

The recommended value of surfactant concentration is in the range of 0.5 ÷ 15 g/l. According to studies [14, 15], the addition of surfactants above 10 g/l does not affect the processing effect. Based on the previous findings, a surfactant concentration of 10 g/l was used for these experimental studies, which was assumed to be a constant value during the study.

Based on the above, experimental investigations were carried out. To study the effect of graphite powder concentration, they are used average value of discharge current of 4.5 A, and the degree of the value of pulse duration of 130 µs, Table 1.

Table 1. Table Experimental trials

Exp no.	I [A]	ti [µs]	T [%]	PC [g/l]	Ra [µm]
1	4.5	130	50	0	8.523
2	4.5	130	50	6	7.012
3	4.5	130	50	12	6.254

The results of the experimental studies show that the concentration of graphite powder has a significant effect on surface roughness at 4.5 A discharge current. The percentage decrease in the value of Ra at the given processing conditions was about 27%, Figure 7.

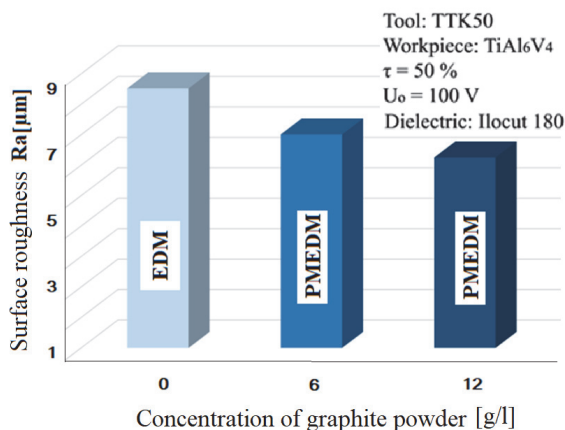


Fig. 7. Influence of concentration of graphite powder

One of the reasons for reducing surface roughness is to increase the working gap between the tool and the workpiece. The addition of graphite powder to a dielectric changes its electrical conductivity, i.e., the overall resistance of the dielectric is reduced.

The improved conductivity of the dielectric helps to generate the spark from a greater distance, thus increasing the discharge gap. This results in an earlier electrical discharge between the tool and the workpiece, leading to a greater working distance. With a larger working distance, the circulation of the dielectric is better, i.e., the flushing of the working space is better.

In addition, the powder particles gain energy after the initial discharge and move rapidly with ions and electrons. Therefore, more electric charges are generated in PMEDM compared to conventional EDM. In addition, the enlarged gap helps to reduce the hydrostatic pressure acting on the plasma channel. These two phenomena provide the enlargement of the through channel [18]. Therefore, the intensity of the discharge energy decreases. The third reason for reducing surface roughness is the occurrence of zigzag shapes of runoff causing multiple runoff paths. This provides an even distribution of energy and the formation of multiple craters in one pulse duration. These craters are shallower than in classical EDM, and surface quality is better.

4. CONCLUSION

Based on the theoretical and experimental research conducted and analyzes performed, conclusions and directions of future research can be reported.

In the present research work, the effect of graphite powder concentration on surface roughness was analyzed. The analysis of the results showed that the process of electrical discharge machining (EDM) in dielectric with mixed powder achieves more favorable performance compared to the classical EDM of titanium alloy. The effect of graphite powder concentration was most pronounced at a discharge current of 4.5 A, where the percentage reduction of the surface roughness was about 27% (at GR = 12 g / l).

The investigations carried out in this work cover only a small part of the field of electrical discharge machining of modern engineering materials.

The future direction would be the study of the PMEDM process for titanium alloys considering a larger number and wider intervals of input factors, as well as studies for different erosion depths.

Acknowledgement

This paper has been supported by the Ministry of Education, Science and Technological Development through the project no. 451-03-68/2020-14/200156: "Innovative scientific and artistic research from the FTS (activity) domain".

REFERENCES

- [1]. Gostimirovic, M., et al. (2018). Inverse electro-thermal analysis of the material removal mechanism in electrical discharge machining. *The International Journal of Advanced Manufacturing Technology*, Vol., no., p. 1-11.
- [2]. Rodic, D., et al. (2020). Fuzzy model-based optimal energy control during the electrical discharge machining. *Neural Computing and Applications*, Vol. 32, no. 22, p. 17011-17026. DOI:10.1007/s00521-020-04909-4
- [3]. Livshits, A.L., *Introduction, in: Electro-erosion Machining of Metals*. Department of Scientific & Industrial Research., 1960, London: Butterworth & Co.,.
- [4]. Pal, M.N., P.K. Mishra, and A. Bhattacharyya. (1970). Optimization of circuit parameters of a relaxation circuit in EDM. *Proc. 4th All-India Machine Tool Design and Research Conf., Madras*, Vol., no., p.
- [5]. Jeswani, M.L. (1980). Effect of the addition of graphite powder to kerosene used as the dielectric fluid in electrical discharge machining. *Wear*, Vol. 70, no. 2, p. 133-139.
- [6]. Klocke, F., et al. (2004). The effects of powder suspended dielectrics on the thermal influenced zone by electrodischarge machining with small discharge energies. *Journal of Materials Processing Technology*, Vol. 149, no. 1-3, p. 191-197. DOI:10.1016/j.jmatprotec.2003.10.036
- [7]. Hu, F.Q., et al. (2013). Surface Properties of SiCp/Al Composite by Powder-Mixed EDM. *Procedia CIRP*, Vol. 6, no., p. 101-106. DOI:10.1016/j.procir.2013.03.036
- [8]. Kansal, H.K., S. Singh, and P. Kumar. (2007). Technology and research developments in powder mixed electric discharge machining (PMEDM). *Journal of Materials Processing Technology*, Vol. 184, no. 1-3, p. 32-41. DOI:10.1016/j.jmatprotec.2006.10.046
- [9]. Wong, Y.S., et al. (1998). Near-mirror-finish phenomenon in EDM using powder-mixed dielectric. *Journal of Materials Processing Technology*, Vol. 79, no., p. 30-40.
- [10]. Zhao, W.S., Q.S. Meng, and Z.L. Wang. (2002). The application of research on powder mixed EDM in rough machining. *Journal of Materials Processing Technology*, Vol. 129, no., p. 30-33.
- [11]. Unses, E. and C. Cogun. (2015). Improvement of Electric Discharge Machining (EDM) Performance of Ti-6Al-4V Alloy with Added Graphite Powder to Dielectric. *Strojniški vestnik – Journal of Mechanical Engineering*, Vol. 61, no. 6, p. 409-418. DOI:10.5545/sv-jme.2015.2460
- [12]. Haşçalık, A. and U. Çaydaş. (2007). Electrical discharge machining of titanium alloy (Ti-6Al-4V). *Applied Surface Science*, Vol. 253, no. 22, p. 9007-9016. DOI:10.1016/j.apsusc.2007.05.031
- [13]. Klocke, F., et al. (2014). Experimental investigations on sinking-EDM of seal slots in gamma-TiAl. *Procedia CIRP*, Vol. 24, no., p. 92-96.
- [14]. Kolli, M. and A. Kumar. (2015). Effect of dielectric fluid with surfactant and graphite powder on Electrical Discharge Machining of titanium alloy using Taguchi method. *Engineering Science and Technology, an International Journal*, Vol. 18, no. 4, p. 524-535. DOI:10.1016/j.jestch.2015.03.009
- [15]. Mohanty, G., et al. (2018). Experimental Investigations on Graphite Mixed Electric discharge Machining of En-19 Alloy Steel. *Materials Today: Proceedings*, Vol. 5, no. 9, p. 19418-19423.
- [16]. Wu, K.L., et al. (2005). Improvement of surface finish on SKD steel using electro-discharge machining with aluminum and surfactant added dielectric. *International Journal of Machine Tools and Manufacture*, Vol. 45, no. 10, p. 1195-1201. DOI:10.1016/j.ijmachtools.2004.12.005
- [17]. Kumar, A., et al. (2012). Machining Efficiency Evaluation of Cryogenically Treated Copper Electrode in Additive Mixed EDM. *Materials and Manufacturing Processes*, Vol. 27, no. 10, p. 1051-1058. DOI:10.1080/10426914.2011.654151
- [18]. Lu, Z., F. Zhao, and Y. Yang. (2008). Research on dielectric breakdown and discharge channel in powder-mixed EDM. *Dalian Ligong Daxue Xuebao/J Dalian Univ Technol*, Vol. 48, no. 3, p. 373-377.



Banja Luka
28-29 May 2021.

DEMI 2021

15th International Conference on
Accomplishments in Mechanical and
Industrial Engineering

www.demi.mf.unibl.org



Analysis of cutting forces in hybrid turning aided by gas combustion heating of workpiece

B. Sredanović^a, Đ. Čiča^a, S. Borojević^a, S. Tešić^a, D. Kramar^b

^aUniversity of Banjaluka, Faculty of Mechanical Engineering, Banja Luka, Republic of Srpska, B&H

^bUniversity of Ljubljana, Faculty of Mechanical Engineering, Aškerčeva 6, 1000 Ljubljana, Slovenia

Abstract

The global industry development is also reflected in the development of special engineering materials. These materials usually have special properties at high temperatures, such as tensile high strength and hardness. Due to these special properties, these materials usually have low machinability. Consequently, it is necessary to develop technologies for machining of mentioned materials, such as hybrid cutting processes. In this paper, the alloy steel X210Cr12 was turned, whereby the workpiece was heated. Heating, as a secondary process, was performed by gas combustion, directly in point next to the point of the cutting tool action. Cutting forces were measured in the two cases: without heating, and by heating of workpiece. Effects analysis and process modeling were performed using Taguchi's experiment design, by combining the cutting parameters of primary process. The analysis showed significant reduction in cutting forces, but also poorer quality of machined surface. Conclusions were made about the possibilities of using this hybrid machining process in material machining.

Keywords hybrid turning, heating, machinability, alloy steel

1. INTRODUCTION

The increasing of using engineering materials with special properties (alloyed structural and tool steels, special titanium and nickel alloys, ceramics, glass, sintered hard metals, composites, and etc.) in industrial, has led to the neediness to develop of the advanced machining methods [1]. Due to chemical content and structure (crystalline or amorphous) of these types of materials, special properties are reflected in increased tensile strength and hardness, durability on high temperatures,

chemical resistance, and etc. Machining of these materials is very difficult regard to mentioned properties. There are difficulties in achieving the machined surface quality and dimensional accuracy, due to high cutting forces, high cutting temperatures, intensive cutting tool wear, unacceptable chip shape, vibrations, and etc. Consequently, there are difficulties to achieve adequate economic, productivity and operate safety, and process sustainability at least.

The development of hybrid processes, as advanced machining processes, is one of the directions to successfully machining of materials with special properties [2, 3]. Hybrid process combines basically processes regard to improved machining efficiency (Fig. 1). CIRP definition of hybrid processes is that hybrid process combines two or more machining process in new one, where advantage of each of them can be used synergistically [2].

Corresponding author

PhD Branislav Sredanović, Assistant Professor
branislav.sredanovic@mf.unibl.org

University of Banjaluka, Faculty of Mechanical Engineering
Vojvode Stepe Stepanovica 75, 78000 Banja Luka,
Republic of Srpska, Bosnia and Herzegovina

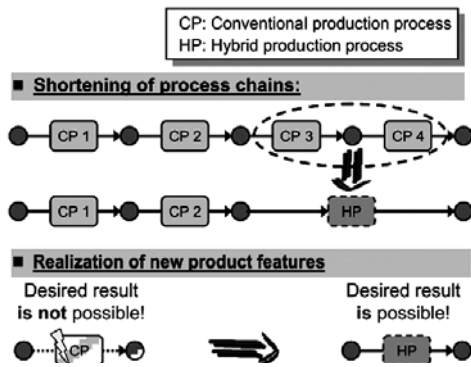


Fig. 1. Principle of hybrid process introduction [2]

There are two types of hybrid processes: aided and mixture. In aided, only one of the combined processes, noted as primary process, directly removes the material, while the other process, noted as secondary, only helps to remove the material by positively affecting the material removal mechanism. In mixture, all involved processes are directly involved in material removal. Hybrid process can involve thermal, mechanical or electrochemical secondary process.

In hybrid cutting processes aided by thermal process, the workpiece material softening due to its heating was used. By increase of temperature, the workpiece material tensile strength and hardness decrease (Fig. 2). It can be utilize with cutting by mechanical cutting tool, turning primarily, with aim to decrease cutting force and cutting tool wear. Other cutting processes (milling and drilling) have constructive limitations, in terms of heat source action point and cutting tool tip relative positioning and orientation.

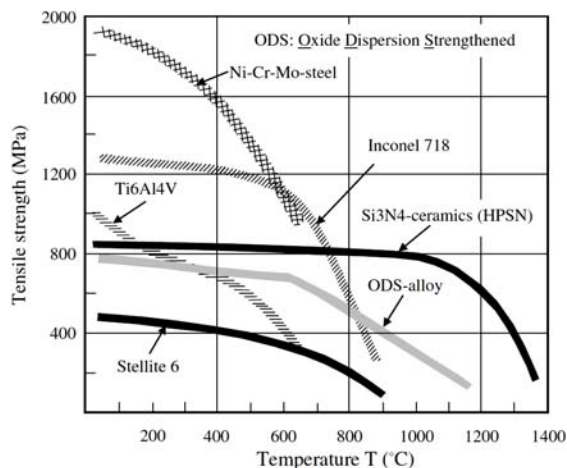


Fig. 2. Tensile strength on different temperatures [3]

As the heat source of secondary process in thermal assisted machining, can be used: laser, plasma, electrical induction, and gas combustion. Laser and plasma are more commonly used due to the ability to focus heat on a small area, and relatively higher temperatures [4-7]. In other hand, laser and plasma devices must be mobile. This types of heat sources often have a high cost, and very high maintenance costs. Devices for electrical induction and gas combustion are much cheaper, and more available in production facilities. Disadvantage of this heating methods are the great heat dissipation and lower temperature [8].

In this study, workpiece was heated by gas combustion. The effect of using this type of heating on the cutting forces was analysed. The standard turning process without heating and the hybrid process were compared, and the machinability indicators were analysed.

2. EXPERIMENTAL SETUP

Experimental research was performed by turning. Machining system was consist lathe Prvomajska assembled with equipment for gas combustion (Fig. 3). In addition, the risk of fire and the possible effect of flame and heat on machine parts, measuring devices and operator were taken into account.

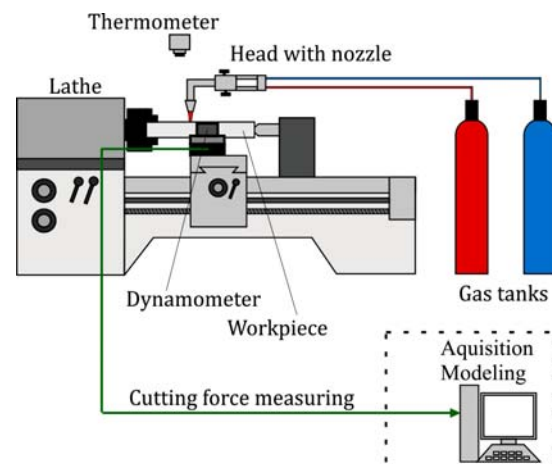


Fig. 3. Schematic of machining system

Equipment for gas combustion was consist operating head, with gas nozzle, and gas flow adjustment valves. Head is connected to the two gas tanks via two hoses. As burning mixture, acetylene and oxygen are stored in the tanks.

Point of heating was placed in front of point of cutting tool, on non-machined surface (Fig. 4). Horizontal distance was between mentioned two point was 15 mm. Gas head was placed above of workpiece surface, on vertical distance of 15 mm. Workpiece materials was tool alloy steels X210Cr12. Its tensile strength on room temperature is $R_m = 600$ MPa. Workpiece was cylinder rod, diameter 50 mm and length 450 mm. This steel contains a relative large percentage of chromium, so it is one of the harder to cutting materials, due to high cutting force, pressures and intensive cutting tool wear. Cutting tool insert was SNMG 12 04 08, grade GC4525, manufactured by Sandvik. Tool holder was PSDNN 2525 M12.

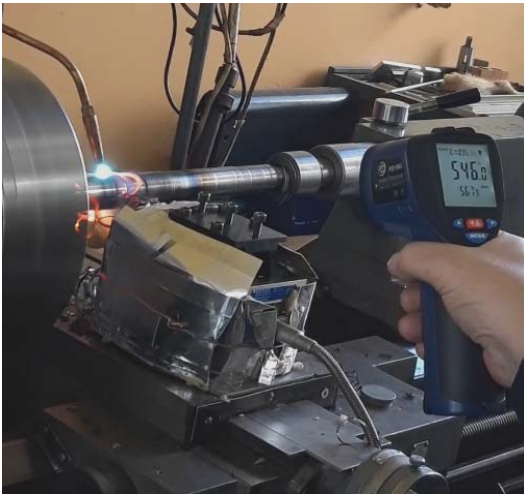


Fig. 4. Experimental measuring

Taguchi L9 plan of experiment was used. In experiment plan was combined primary process parameters, cutting parameters of turning, as follow: depth of cut was a_p of 1, 2 and 3 mm; feed rate f_n was 0.082, 0.164, and 0.330 mm/rev; and cutting speed v_c was 35, 60, and 106 m/min. By Taguchi plan, there was nine combinations made by mentioned tree cutting parameters (Table 1). Same sets of parameter combinations was used in two types turning: turning without heating and turning with heating. Resultant cutting force component: cutting force F_c (N), feed force F_f (N) and passive force F_p (N) was measured for each combination. Kistler measuring chain was used for cutting force measuring. It consisted of Kistler dynamometer Kistler 9259A, amplifier, A/D converter PC card, and analysing PC software.

Table 1. Taguchi plan combinations

Exp no.	Depth of cut a_p (mm)	Cutting speed v_c (m/min)	Feed rate f_n (mm/rev)
1	1.0	35	0.082
2	1.0	60	0.164
3	1.0	106	0.330
4	2.0	35	0.164
5	2.0	60	0.330
6	2.0	106	0.082
7	3.0	35	0.330
8	3.0	60	0.082
9	3.0	106	0.164

Workpiece surface temperatures during research was checked by remote point laser thermometer. Workpiece non machined surface temperature was from 460°C to 560°C. It was depended on feed rate (feed per tooth and cutting speed), because this parameter affects the retention time on the observed workpiece surface area. But, temperatures are not modelled in this part of study.

3. RESULTS AND DISSCUSION

Results of cutting force measuring without and with heating of workpiece are shown on Fig. 5. Can be concluded that cutting forces depends on cutting parameters. The highest value is obtained for $a_p = 3$ mm, $f_n = 0.330$ mm/rev and $v_c = 35$ m/min. Cutting forces in case of workpiece heating showed same tendency, but was lowest compare to forces without heating.

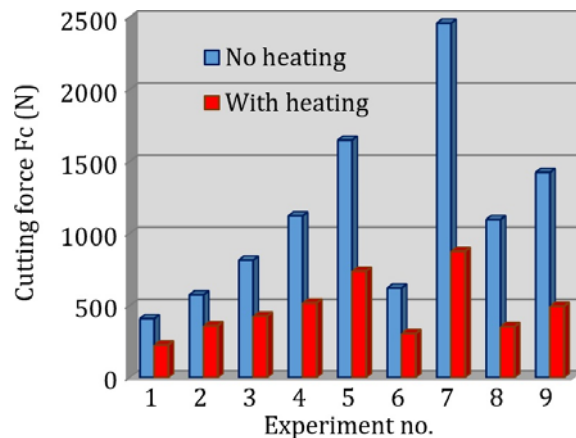


Fig. 5. Cutting forces for two cases of turning

On Fig. 6 and 7 are shown measured feed and passive forces for two cases of turning, without and with heating of workpiece. Based on combination and measured values, can be concluded that feed and passive force increase with increasing of cutting parameters. The higher values was obtained by using of higher values of depth of cut and feed rate, but the lowest value of cutting speed.

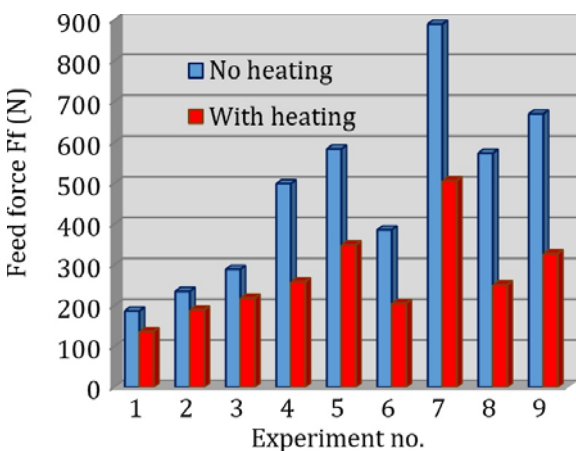


Fig. 6. Feed forces for two cases of turning

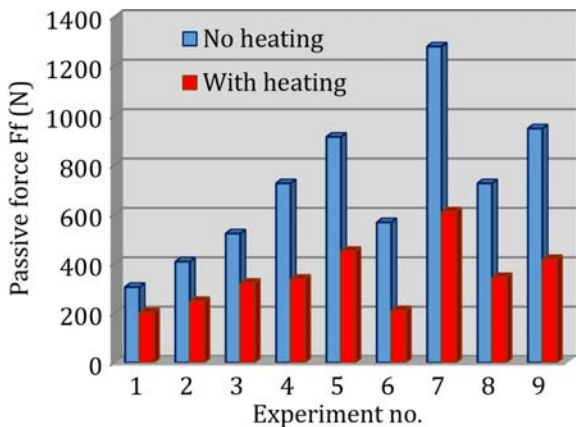


Fig. 7. Passive forces for two cases of turning

Also, values of feed and passive forces in case of heating workpiece were lower in compare to the values obtained by turning without heating. On Fig. 8, the percentage decrease in the value of the forces is shown. Minimum decreasing is obtained for feed forces on turning with cutting parameters $a_p = 1$ mm, $f_n = 0.164$ mm/rev and $v_c = 60$ m/min. Maximum value decreasing is obtained for cutting forces with cutting parameters $a_p = 3$ mm, $f_n = 0.330$ mm/rev and

$v_c = 35$ m/min. However, the highest value of force was measured in this combination in case without heating. Higher percentages of reductions due workpiece heating were obtained in combinations with higher cutting parameter values. Higher percentages of were obtained for cutting forces in comparing with other two resultant cutting force components, also.

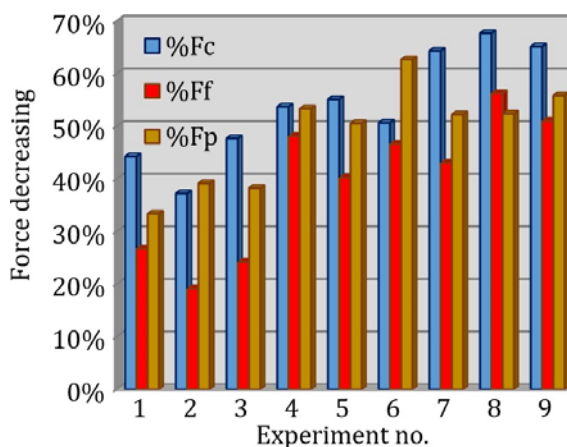


Fig. 8. Percentages decreasing of cutting forces

Modelling and analysing of measured values was performed in DesigExpert 7.1 software. In modelling procedures, each cutting force components were analysed and modelled. Based on initial statistical parameters of F-value and P-value, for: model, each input parameters individually, and combination of input parameters, the software suggested the form of model function. Analyse of variance (ANOVA) was performed on each sets of measured values and adopted models.

In case of turning without workpiece heating, for cutting force model software suggested the linear model with all tree input parameters, but without their interactions:

$$F_c = -309.7 + 528.7 \cdot a_p - 5.0 \cdot v_c + 3751.2 \cdot f_n \quad (1)$$

Based on values and model mean value $\bar{y} = 1131.78$ and standard deviation $SD = 128.03$ was calculated. Signal to noise ratio was $\frac{S}{N} = 23.3$, and regression coefficient was $R^2 = 0.98$.

For feed and passive force, in case of turning without workpiece heating, software suggested the linear models with two input parameters depth of cut and feed rate, and without their interactions, follow as next:

$$F_f = -151 + 237.2 \cdot a_p + 812.4 \cdot f_n \quad (2)$$

$$F_p = -142.8 + 286 \cdot a_p + 1468.1 \cdot f_n \quad (3)$$

For feed force and passive force mean values are $\bar{F}_f = 479.3$ and $\bar{F}_p = 711.1$, respectively. Standard deviation is $SD = 49.5$ for feed force and $SD = 76.8$ for passive force. For feed force signal to noise ratio is $F/N = 23.6$, and regression coefficient $R^2 = 0.96$. For passive force $F/N = 21.1$, and $R^2 = 0.95$.

Based on statistical analyse can be concluded that presented models are adequate. Model response for cutting force components in case of turning without workpiece heating are shown on Fig. 9.

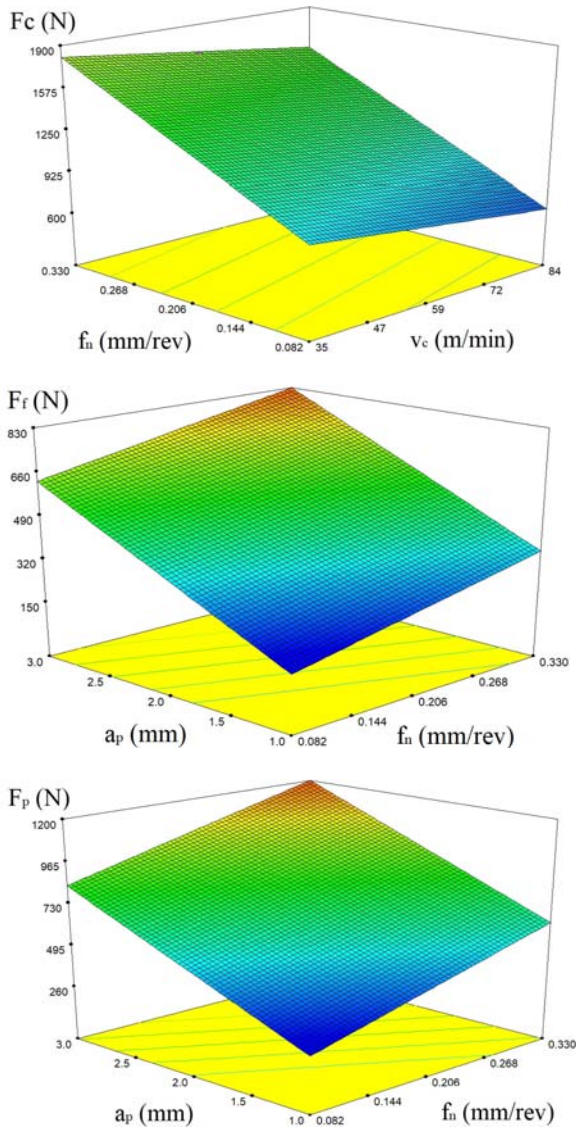


Fig. 9. Model responses for turning without heating

For cutting and feed force in turning with workpiece heating, software suggested linear models with all tree input parameters, and their interactions. For passive force model, there was suggested linear model without parameter interaction. The mentioned models functions are listed below, while their responses are shown in Figure 10.

$$F_c = -72.5 + 78.3 \cdot a_p + 1.5 \cdot v_c + 2696.3 \cdot f_n - 17.6 \cdot v_c \cdot f_n \quad (4)$$

$$F_f = -60.2 + 69.3 \cdot a_p + 1.1 \cdot v_c + 1234.8 \cdot f_n - 8.91 \cdot v_c \cdot f_n \quad (5)$$

$$F_p = -52.3 + 100.2 \cdot a_p - 0.9 \cdot v_c + 828.9 \cdot f_n \quad (6)$$

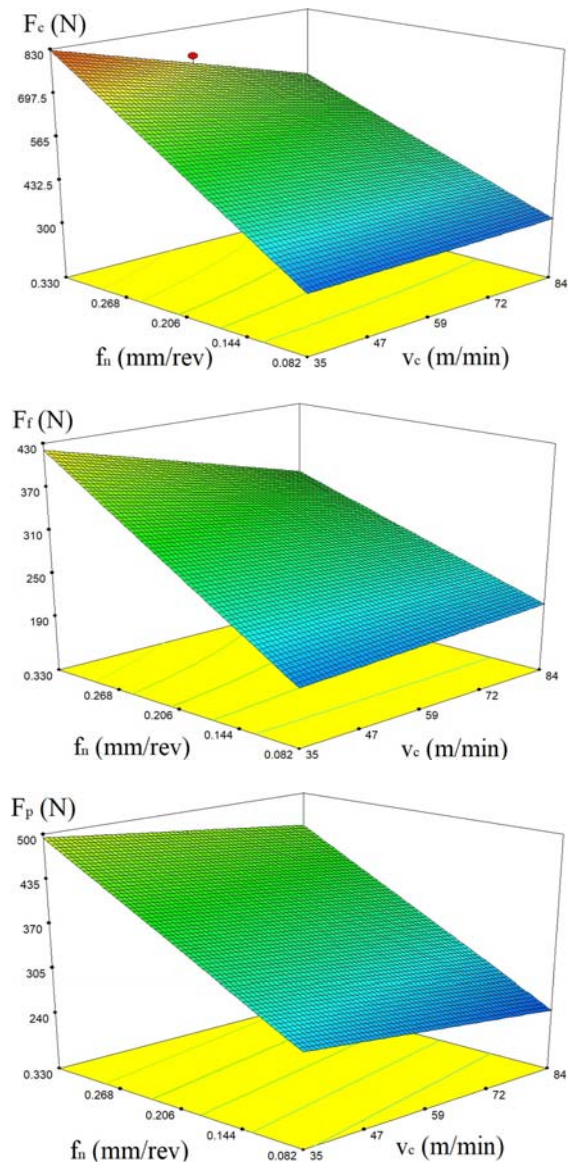


Fig. 10. Model responses for turning with heating

Based on experimental obtained values and model responses, statistical parameters calculation is performed. For cutting force with workpiece heating data, mean value is $\bar{F} = 479.2$, and standard deviation is $SD = 37.8$. Signal to noise ratio was $F/\bar{F} = 23.9$, and regression coefficient was $R^2 = 0.98$. For feed force with workpiece heating data, mean value is $\bar{F} = 271.8$, and standard deviation is $SD = 21.9$. Signal to noise ratio was $F/\bar{F} = 22.5$, and regression coefficient was $R^2 = 0.98$. For passive force with workpiece heating data, mean value is $\bar{F} = 350.7$, standard deviation is $SD = 23.5$, signal to noise ratio is $F/\bar{F} = 25.9$, and regression coefficient is $R^2 = 0.97$. Based on calculated statistical parameters, there was concluded that previous presented linear models are adequate.

Based on analysed data and model responses can be concluded that depth of cut and feed rate have high influence on cutting force components. As the values of these two parameters increase the values of the forces increase. Cutting speed has relative lower influence on cutting force component. Influence of cutting speed is often neglected in cutting force components models. In most cases, with increasing cutting speed, there is a decrease in cutting forces components. In the case of turning assisted by heating the workpiece, the cutting speed has a greater impact, especially in its interaction with the feed rate. The reason for this can be time and position of the heating flame action point. With higher speeds and steps, the workpiece heats up less.

4. CONCLUSION

From other research in this field, can be concluded that hard-to-machining materials are machined by lasers and plasma assisting, but these devices can be expensive and difficult to maintenance. However, laser and plasma have many advantages. In other hand, gas combustion heating devices are much cheaper and available.

Presented research in this paper shows possibility of reducing the cutting forces component in turning, by assisting with gas combustion heating of non-machined workpiece surface. The analysis is showed a significant difference in the values of the cutting forces components. Also, the models have shown that it is possible to adequately describe process and

cutting forces. The value of the cutting forces components is significantly reduced. The reduction averages about 50%.

Additionally, the effect of heat on the machined surface was observed. There was poor machined surface, with visible burnt places. These facts could be investigated in future research, where the penetration of heat through the workpiece would be studied. Future research will directed on optimizing the heater head construction regard flame focusing. Examinations of the influence of its position relative to the cutting edge will be performed. Also, an analysis of the processing of different materials will be carried out, using different methods of workpiece heating.

REFERENCES

- [1] Gresik, W. (2008). *Advanced Machining Processes of Metallic Materials: Theory, Modelling and Application*. Elsevier, Amsterdam.
- [2] Klocke, F., Roderburg, A., Zeppenfeld, C., (2011). Design methodology for hybrid production processes. *Procedia Engineering*, vol. 9, pp. 417-430.
- [3] Virginia, G., et al. (2013). Mechanisms involved in the improvement of Inconel 718 machinability by laser assisted machining (LAM). *International journal of machine tools and manufacture*, vol. 74, pp. 19-28.
- [4] Tian, Yinggang, T., et al. (2008). Laser-assisted milling of silicon nitride ceramics and Inconel 718. *Journal of manufacturing science and engineering*. vol. 130, no. 3, pp. 3 - 10.
- [5] Dumitrescu, P., Koshy, P., Stenekes, J., Elbestawi, M.A. (2006). High-power diode laser assisted hard turning of AISI D2 steel. *Internatiional journal of advance manufacturing technology*, vol. 46, pp. 2009-2016.
- [6] Ding, H., Yung C. Shine, Y. C (2010), Laser-assisted machining of hardened steel parts with surface integrity analysis. *International journal of advance manufacturing technology*, vol. 50, pp. 106-114.
- [7] Masood, S.H., Armitage K., Brandt, M. (2011). An experimental study of laser-assisted machining of hard-to-wear white cast iron. *International journal of advance manufacturing technology*, vol. 51, pp. 450-456.
- [8] Mohammed, K. A., et al. (2020). Experimental Analysis of Hot Machining Parameters in Surface Finishing of Crankshaft. *Journal of Mechanical Engineering Research and Developments*, vol. 43, no. 4, pp. 105-114.



Banja Luka
28–29 May 2021.

DEMI 2021

15th International Conference on Accomplishments in Mechanical and Industrial Engineering

www.demi.mf.unibl.org



Advanced metal forming tools as a main link of digital manufacturing

Ilić Jovica^a, Milutinović Mladomir^b, Kraišnik Milija^c, Marković Milisav^a

^aSenior teaching assistant, M. Sc. Jovica Ilić, Faculty of Mechanical Engineering, University of Banja Luka, (jovica.ilic@mf.unibl.org)

^bAssociate professor, Dr Mladomir Milutinović, Faculty of technical sciences, University of Novi Sad, (mladomil@uns.ac.rs)

^cAssociate professor, Dr Milija Kraišnik, Faculty of Mechanical Engineering, University of East Sarajevo (milija.kraisnik@ues.rs.ba)

^aSenior teaching assistant, M. Sc. Milisav Marković, Faculty of Mechanical Engineering, University of Banja Luka, (milisav.markovic@mf.unibl.org)

Abstract *In metal forming machines, forming tool plays a key role in transforming the initial shape of the material into the final, desired shape. Since the forming machine only provides the necessary movement and force for the deformation process, the tool is the one that is in direct contact with material and defines its final shape, dimensions, accuracy and quality of the treated surface. Modern market is increasingly embracing the concept of Industry 4.0 and global trends related to the implementation of industrial internet, advanced manufacturing, smart factories and interoperability. The role of a advanced metal forming tool is to integrate into the smart metal forming machine and to collect all relevant information in the forming process and perform optimization and corrections during the forming process, according to corrective information obtained from the control unit via feedback. This paper presents a review of modern approaches in the design and development of advanced metal forming tools that can meet the requirements of the concept Industry 4.0 and be integrated into advanced metal forming machines.*

Keywords *smart forming tools, digital manufacturing, metal forming technology*

1. INTRODUCTION

Metal forming technology is one of the most common manufacturing procedures of metal products and components in the industry. Modern products are characterized by increasing complexity, the need for integration into other assemblies, the authenticity of the product and the production batches are in a downward trend. For this reason, modern companies and industry are increasingly oriented towards digital production manufacturing or Industry 4.0. This concept of manufacturing has the potential to meet the increasingly stringent requirements of the

market and legislation. The basic feature of digital manufacturing is reflected in the constant communication and interaction between machines, tools, fixtures and operator [1]. In metal forming technologies, the forming tool plays key role and it is in direct contact with the material and in constant interaction with the forming machine. For that reason, it is expected from modern forming tool to collect all important information from the production process and send it to the control unit and to the forming machine, and through feedback to accept corrective data and optimize the forming process. Collecting such useful information and interactions between the forming machine and

the active forming tool allows optimization of the forming process with a small number of iterations and avoids the occurrence of production scrap and the need for postprocessing.

2. THE CONCEPT OF ACTIVE METAL FORMING TOOL

In order to be able to meet the requirements of digital manufacturing and actively participate in the shaping of the material and its transformation into a finished product, metal forming tool is a complex product. In order to achieve the required level of flexibility and individuality of the tool itself, modern metal forming tools are built from essential elements, according to the Figure 1.

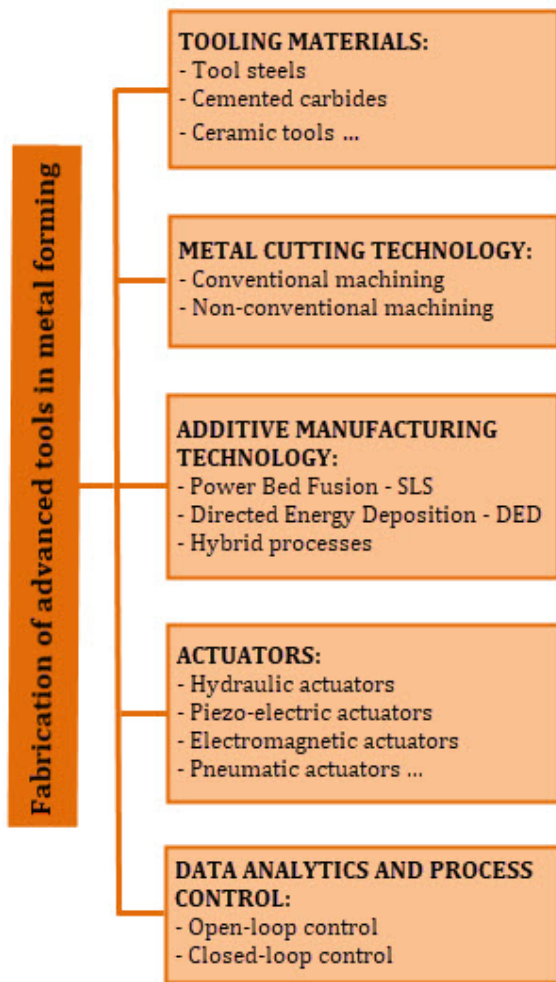


Fig. 1. Fabrication of advanced tools in metal forming [2,4]

2.1 Tooling materials

With the development in the field of materials and their characteristics, tool performance is constantly improved in terms of essential material characteristics for modern forming tools such as toughness, hardness, corrosion resistance, good machinability and good reparability. The tool material must retain its properties in working conditions and at the temperature interval that is achieved in the forming process [2,7]. Commonly used materials for metal forming tools are given in Table 1.

Table 1. Commonly used materials for metal forming tools [7]

Material	Hardness [HRC]	T. range [°C]	Machinability	Weldability
X153CrMoV12	60-62	200-535	Poor	Poor
WC	57-65	37-760	Poor	Fair
X38CrMoV5	31-52	74-650	Good	Good
X165CrMoV12	57-65	37-593	Good	Good
40CrMnMo7	30	>150	Good	Good

2.2 Fabrication methods for metal forming tools

The progress made in the improvement of existing and development of new production technologies, has enabled a significant step forward in the development of modern tools for deformation processing. This is especially true for unconventional metalworking processes. Of the conventional methods of metal processing by cutting, the most commonly used procedures are milling, drilling and grinding, or polishing (Fig. 2). Non-conventional machining processes such as electro-discharge machining and electro-chemical machining have significant applications [9]. Additive manufacturing technologies enabled the optimization of metal forming tools and significant freedom for constructors. They enabled the production of very complex tools with heating and cooling channels and with grips for sensors and actuators [3,10]. In this way was achieved the recording of real parameters during the production process and the possibility of timely influence on the production process. The most commonly used additive manufacturing technologies are Selective Laser Sintering - SLS and Directed Energy Deposition - DED [10]. Since all these technologies have their

advantages and disadvantages, the full potential in terms of production a modern metal forming tools is realized by using hybrid systems, which combine some of these cutting technologies and additive manufacturing technologies (Fig. 2) [3].

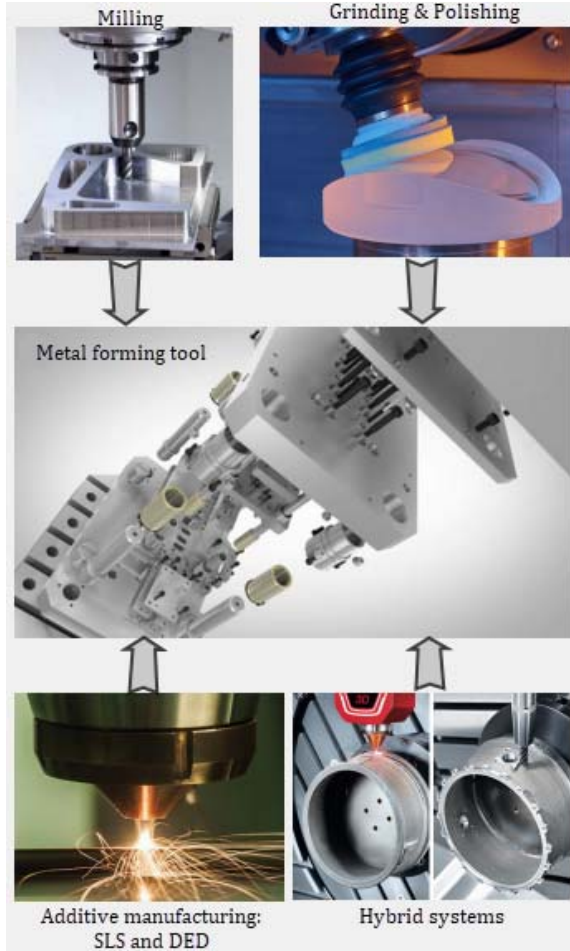


Fig. 2. Commonly used fabrication technologies for advanced metal forming tools

2.3 Sensors

A sensor is a primary sensing element that converts a physical quantity, which is suitable for measurement, into some standard signal. It is often an electrical signal, most often a current or voltage [8]. For the control of complex systems such as metal forming tools, information of high importance about relevant process parameters such as temperature, flow, pressure, time, position, displacement, etc. For this reason, a large number of contact or non-contact sensors are currently used to measure all important quantities during forming process in metal forming tool tool [4,5].

2.4 Actuators

Actuators are very important and common element of modern metal forming tools. They accept commands from the control unit, usually in the form of an electrical signal and then make changes in the tool according to them by generating motion, force, heat and similar [4]. The control signal at the input of the actuator is mostly low energy, which is then transformed in the actuator and amplified into an executive quantity of high energy level. Hydraulic, pneumatic, piezoelectric and electromagnetic actuators are most often used in modern metal forming tools. Important characteristics that these actuators must meet are fast response to the control command, high precision as well as sufficient force [4].

2.5 Control of properties in metal forming tool

Modern metal forming tools, as well as many other modern production systems apply two control systems. These are the open loop control and the closed loop control of product properties. Advanced metal forming tools mainly use a closed loop control system with the ability to monitor tool output and correct deviations from the projected output values (Fig. 3) [5,6].

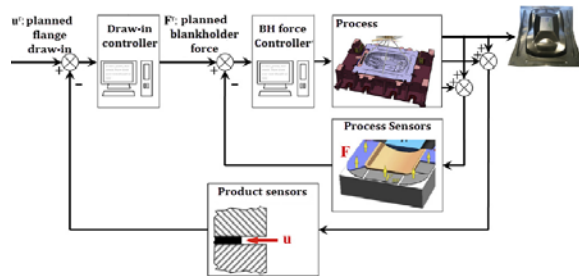


Fig. 3. Typical scheme for closed-loop control of material flow in deep drawing [4]

3. CONCLUSION

Metal forming technologies are increasingly oriented towards the more pronounced application of automation, artificial intelligence and autonomy. This is especially true for modern forming machines and modern forming tools which are, integrated into one system, enable for the transformation of materials into the finished product, while maintaining high

product quality and high repeatability. Since the metal forming tool is in direct contact with the material and only can collect important information directly from the production process, it is required to be equipped with appropriate sensors through which collecting important information about material behavior and process parameters that can be obtained at any time during production process. In addition, from modern metal forming tool is expected to have, if necessary, executive elements - actuators through which it can adequately respond to corrective information. With further development in the fields of modern materials, advanced technologies, measuring devices and smart forming machines, further progress of metal forming tools is expected in terms of complexity, autonomy, sensitivity, flexibility and interoperability.

REFERENCES

Journal papers:

- [1] Yang, D.Y., Bambach, M., Cao, J., Duflou, J.R., Groche, P., Kuboki, T., Sterzing, A., Tekkaya, A.E., Lee, C.W. (2018). Flexibility in metal forming. *CIRP Annals - Manufacturing Technology*, vol. 67, p.p. 743-765.
- [2] Cao, J., Brinksmeier, E., Fu, M., Gao, X.R., Liang, B., Merklein, M., Schmidt, M., Yanagimoto, J. (2019). Manufacturing of advanced smart tooling for metal forming. *CIRP Annals - Manufacturing Technology*, vol. 68, p.p. 605-628.
- [3] Du, W., Bai, Q., Zhang, B. (2016). A novel method for additive/subtractive hybrid manufacturing of metallic parts, *Procedia Manufacturing*, Vol. 5, p.p. 1018-1030, DOI: 10.1016/j.promfg.2016.08.067
- [4] Allwood, J.M., Duncan, R.S., Cao, J., Groche, P., Hirt, G., Kinsey, B., Kuboki, T., Liewald, M., Sterzing, A., Tekkaya, A.E. (2016) Closed-loop control of product properties in metal forming, *CIRP Annals - Manufacturing Technology*, Vol. 65, no. 2, p. 573-596, DOI: 10.1016/j.cirp.2016.06.002
- [5] Doege, E., Seidel, J.H., Griesbach, B., Yun, W.J. (2002) Contactless on-line measurement of material flow for closed loop control of deep drawing, *Journal of Materials Processing Technology*, Vol. 130-131, p.p. 95-99, DOI: 10.1016/S0924-0136(02)00763-X

- [6] Li, M.Z., Cai, Y.Z., Liu, G.C. (2007) Flexible manufacturing of sheet metal parts based on digitized-die, Robotics and Computer-Integrated Manufacturing, Vol. 23, p.p. 107-115, DOI: 10.1016/j.rcim.2005.09.005

Books:

- [7] Roberts, G.A., Kennedy, R., Krauss, G. (1998). *Tool Steels*, ASM International, ISBN: 978-0-87170-599-0
- [8] Popović, M. (2004). *Senzori i merenja* (In Serbian), Zavod za udžbenike i nastavna sredstva, Istočno Sarajevo,

Book chapters:

- [9] Davim, P.J. (2010). Surface Integrity in machining. Grzesik, W., Kruszynski, B., Ruszaj, A. *Surface integrity of machined surfaces*, Springer - Verlag, London, p.p. 143-179, DOI: 10.1007/978-1-84882-874-2
- [10] Brandt, M. (2017). Laser additive manufacturing: materials, design, technologies, and applications. Hölker, J.R., Tekkaya, A.E. *Additive manufacture of tools and dies for metal forming*, Woodhead Publishing, p.p. 439-464, DOI: 10.1016/C2014-0-03891-9



Banja Luka
28-29 May 2021.

DEMI 2021

15th International Conference on
Accomplishments in Mechanical and
Industrial Engineering

www.demi.mf.unibl.org



Improvement of brake triangle through application of reverse engineering and rapid prototyping

P. Đekić^a, B. Milutinović^a, M. Ristić^a, M. Pavlović^a, M. Nikolić^a

^aThe Academy of Applied Technical and Preschool Studies-Niš, Aleksandra Medvedeva 20, Niš, Serbia

Abstract Modern production technologies make it possible to increase productivity, shorten product development time and increase the competitiveness of companies. This paper presents the concept of simultaneous design of an innovated product in order to increase the competitiveness of the company on the example of making a brake triangle. An analysis of the existing production technology and a comparison with world good practice were performed. Also, the application of the software package for the analysis of the virtual 3D model is presented. Based on the conclusions from the stress-strain analysis, the production technology was determined in accordance with modern production technologies. Prototype was made on a 3D printer. The process of simultaneous design using reverse engineering, and rapid prototyping significantly affects the shortening of the production time and facilitates the choice of production technology.

Keywords reverse engineering, rapid prototyping, stress-strain analysis, brake triangle

1. INTRODUCTION

With the introduction of modern production technologies, productivity is increased, product development time is shortened and the competitiveness of companies in both domestic and foreign markets is increased. The combination of modern technologies with computer product development achieves maximum productivity and competitiveness in the global market with optimal engagement of production capacities. [1]

In the product development process, the first step is a product model creation in order to eliminate the shortcomings of the final product. However, the creation of a physical model can

be very complicated and expensive, so in recent times, the creation of a virtual product model is performed, that is, the creation of a product model in a virtual environment. By applying reverse engineering, product improvement starts from the final product and through the process of designing in the opposite direction, an improved product is obtained. Variant solutions are also sought in similar products from competing companies.

Also, due to frequent changes in the model, it is necessary to make more physical models, which requires additional time during product development, but also additional financial costs. By creating a 3D model of the product in the appropriate software package, you get a model in a virtual environment, which can be changed, customized and analyzed without additional financial and time costs. Any change in the model can be done very simply and without the need to create a new prototype, which makes the product development process cheaper and significantly time consuming shorter. The

Corresponding author

PhD, Biljana Milutinović
Biljana.milutinovic@akademijanis.edu.rs

The Academy of Applied Technical and Preschool Studies-Niš
Aleksandra Medvedeva 20
Niš, Serbia

simulation procedure, i.e. stress-strain analysis, gives answers as to whether the product meets the required characteristics, but the main word is its the behaviour in operation. Prototyping is supported by the application of rapid prototyping. Nowadays, in addition to product quality, a significant role is played by the production time, which primarily depends on the choice of production technology, so it is necessary to perform a re-engineering of the production process. [2-6].

This paper presents the process of product innovation on the example of a brake triangle. The second chapter presents an analysis of the shortcomings of the production of the original product, as well as examples of good world practice. The third chapter presents the procedure of stress-strain analysis and the selection of the appropriate variant solution, and the fourth chapter describes the adopted new production technology of brake triangle sleeve.

2. REVERSE ENGINEERING OF BRAKE TRIANGLE

In older generation of rail freight and passenger wagons, brake pads are used, whereby braking is achieved on the principle of traction braking, ie. the creation of friction between the wheels of the wagon and the brake peds. An integral part of such a braking system is the brake triangle shown in Figure 1.



Fig. 1. Brake triangle

Brake pads are mounted at the ends of the brake triangle (marked with red arrows in Figure 2.). The task of the brake triangle is to make contact between the wheels and the brake pads by pulling it, which creates friction and

brakes. The appearance of the braking system is shown in Figure 2.

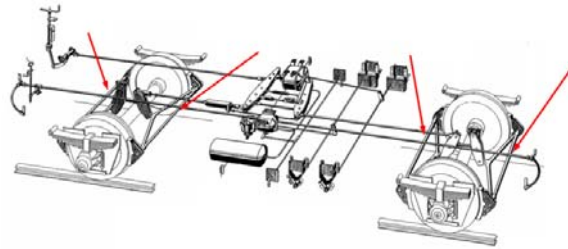


Fig. 2. Wagon braking system

The promotion procedure of brake triangle production technology is based on the following procedure:

- Analysis of possibilities for improvement by applying best world practice
- Analysis of the existing production technology of brake triangle

After analysing the production technology and good examples from practice, the virtual model (3D model) is created and simulated using the appropriate software. Then a physical model is created using rapid prototyping, i.e. by printing a prototype on a 3D printer. Upon completion of the simulation and prototyping using 3D printing, a new production technology is adopted and a new product is developed and tested in real operating conditions.

2.1 Analysis of best world practice examples




The analysis of the shortcomings of the existing production technology of brake triangle from the aspect of technological process, production costs and production time, showed that the current production technology has many disadvantages:

- requires the engagement of more machine tools
- there are many prescribed processing operations of different nominal quality, which increases the possibility of production errors.
- requires the employment of a larger number of employees, which significantly increases the influence of the human factor on the production process.

Therefore, an analysis of the possibilities for improving the technological process was

performed by considering the available world practice. The available solutions for the production of a brake triangle, the production technology and its shortcomings were analyzed, and on the basis of this analysis, the most optimal production technology was adopted. The available solutions are grouped based on similarities in manufacturing technologies are shown in Table 1.

Table 1. Examples of best available practice

A variant solution	Technology
<p>1st variation</p> 	<ul style="list-style-type: none"> • milling • turning • drilling • welding [6]
<p>2nd variation</p> 	<ul style="list-style-type: none"> • forging • turning • drilling • pressing [7-8]
<p>3rd variation</p> 	<ul style="list-style-type: none"> • casting [9]

Based on the performed analysis of the presented variant solutions, it was concluded that those made by forging or casting can be taken into consideration. A solution that has a screw connection is thrown out due to the reliability of the whole assembly. The same applies to the assembly of parts by the lacing process. A more detailed analysis of the load and stress-strain states, as well as the technology of forging and casting, leads to the conclusion that the sleeve of brake triangle should be made by casting. The reason that casting is preferred over forging, although the parts obtained by forging have better mechanical characteristics, lies in the fact that the casting process is cheaper. Namely, in order to make the sleeve and ear of a brake triangle by forging, it is necessary to make a forging tool, which is very expensive and is limited by the number of series it can produce. It is also a problem that a special tool should be made for

each type of brake triangle, which is not economically viable for small series, or if it is necessary to modify, ie. improve the product.

In the case of casting technology, it is very easy and cheap to make a tool (mold) for casting, but the production time per product is longer. If a larger number of products were to be cast at the same time, the production time is significantly faster than with forging, because a larger number of pieces can be cast in one batch. The advantage of the casting process in relation to the forging process is that it is very easy to correct (change) the geometry of product.

2.2 Analysis of the existing production technology

The parts of the brake triangle are made by various machining procedures, whereby the parts are also thermal treated. Their connection into the final product is done by electric arc welding. At the end of the technological process, the surface protection of the product is performed.

Based on the described technological procedure, it can be concluded that the current production technology of a brake triangle, on the one hand, is very complex and demanding, while on the other hand it is poorly cost-effective. When it comes to machining, a number of different machine tools are required (saws; lathe (conventional or CNC lathe/machining centre; milling machines) (conventional/CNC milling machine/machining centre) and CNC plasma/laser.

It should be noted that in case the parts are made on conventional machines, it would be necessary to provide highly qualified employees. In case the parts are made on CNC machines, it is necessary to organize the work with the help of the CNC machine operator, while the G-code would be made by a CNC machine engineer-programmer.



The most demanding part is the sleeve of brake triangle. This part requires high manufacturing accuracy, as well as the brake triangle itself, so it is necessary that each part in the production process is controlled before the joining process. After machining, the parts are thermal treated. After the welding process, it is also necessary to perform a final control of each product. The welding process requires a certified welder and appropriate equipment. At the end of the production process, it is necessary to perform

surface protection of the finished product, so appropriate equipment is needed here as well. In addition to the engagement of a large number of machine tools, the engagement of a large number of employees of various expertise is also necessary: auxiliary workers, toolmakers (turners and mills); CNC machine operator, CNC programmer; welder and shift controller. Also, productivity is very low. A more detailed analysis shows that two procedures are mandatory and cannot be improved or replaced by current technologies, namely thermal treatment and surface protection.

3. TESTING OF THE DEVELOPED MODEL USING COMPUTER SIMULATION

The SolidWorks software package was used to create a 3D virtual model of a sleeve and ear of brake triangle. In order to perform an analysis of product functionality and selection of the optimal solution, two variants were created, which are shown in Table 2.

Table 2. Variant solutions with characteristics

Variant solution	Appearance of the solution
1st variation sleeve 12.2 kg, ear 2.9 kg	
2nd variation sleeve 6.7 kg, ear 2.6 kg	

By comparing the variant solutions, it can be concluded that less material is needed to make the second variant solution, which reduces the time and costs of production. Simulations, i.e. analysis of stress-strain states were performed with 3D models of the sleeve due to a very important role within the brake triangle, for both variant solutions with the same load – torque (160 kN), in order to compare their results. For these simulations, the SolidWorks Simulation module and the finite element method were used. In the first variant solution, the constraints and loads are shown in Figure 3.

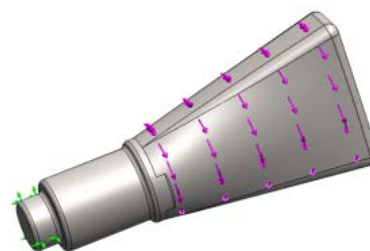


Fig. 3. Constraints and loads – 1st variation

As a basic element in the application of the finite element method, a triangular element was used (Figure 4). Number of nodes was 12036, while number of mesh elements was 7749.

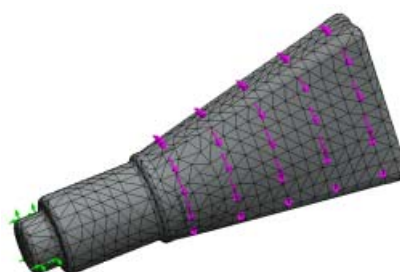


Fig. 4. Meshing – 1st variation

Due to the complex geometry of the work, the correction of the basic elements was performed, i.e. the elements were reduced. The results of the stress-strain analysis are shown in Figure 5.

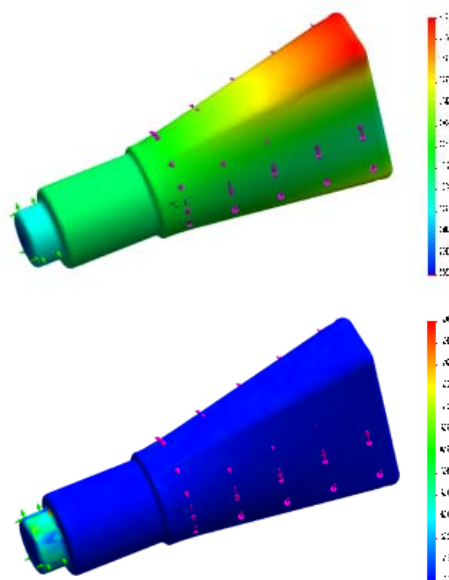


Fig. 5. Stress-strain state of the sleeve under a given load – 1st variation

In the stress diagram, the lower stress are shown in blue, which shows that the stress distribution for a given model is quite satisfactory. In the strain diagram, the largest strain occurs at the end, which is expected according to the given limit and load. The simulation results showed that the product of the presented geometry and material meets the given requirements.

Constraints and loads were set for the second variant solution as well, and meshing was performed (Figure 6). Due to the even more complex geometry in relation to the first variant solution, meshing control was done here as well. Number of nodes was 23315, while number of mesh elements was 14813.

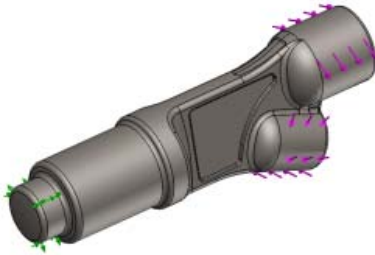


Fig. 6. Constraints and loads – 2nd variation

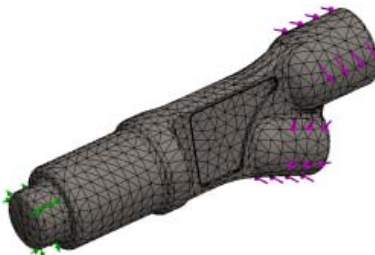


Fig. 7. Meshing – 2nd variation

Then, according to the given parameters, a simulation was done. The simulation results are shown in Figure 7, i.e. stress-strain diagrams.

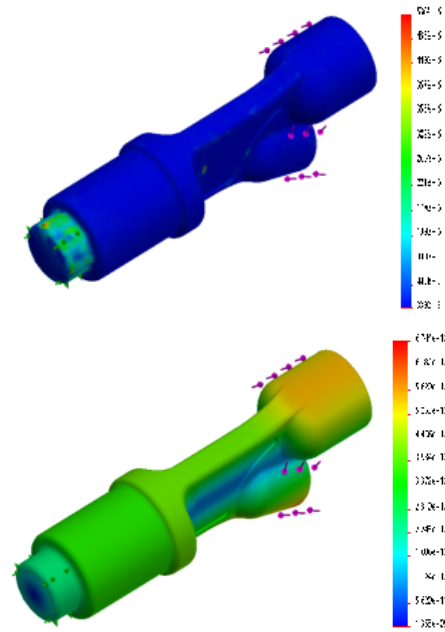


Fig. 8. Stress-strain state of the sleeve under a given load – 2nd variation

Compared to the first variant solution, it can be concluded that in the middle there are places where higher stress values occur, which is quite expected, similar to the reduction of the sleeve wall, which does not affect the functionality of the part in the complete assembly. However, in the strain diagram, the strain differs in relation to the first variant solution, which is a consequence of a partial change in geometry, and the strain is distributed differently along the entire part. The simulation results showed that the second variant solution satisfies the given requirements, whereby the mass of the sleeve is significantly smaller compared to the first variant solution.

4. ANALYSIS OF SELECTED PRODUCTION TECHNOLOGY

The improvement of the production technology was done in the direction of modifying the existing solution so that the parts of the sleeve, profile and pipe are united in assembly 1 (sleeve), and the parts ear and stiffening in assembly 2 (ear of brake triangle) as shown in Figure 9.

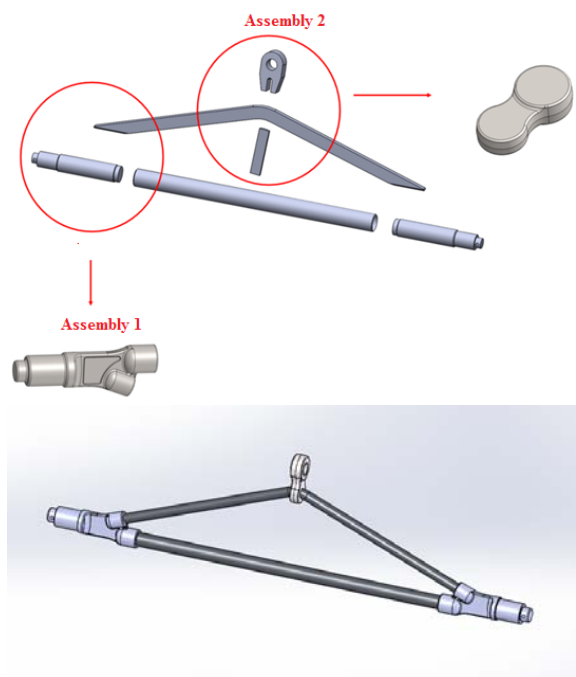


Fig. 9. Improvement of production technology and appearance of the improved product

The production technology a brake triangle consists of six machining processes:

- making a mold for casting
- casting of parts
- machining
- thermal treatment
- assembly
- surface protection.

Based on the conducted analysis, it was concluded that the best production technology is casting. The following production technology of a sleeve and an ear is:

- making molds for casting
- casting in sand based on the made mold.
- thermal treatment by improvement to 260-280 HB.

The mold was made using 3D printing. Molds are composed of functional (cavity, core insert, punch) and support components (guide pins, holder, die plate). Conventional mold making practice that depends on machining operations to generate the desired mold cavity is not found to be competitive any longer. This has led to a significant growth in rapid prototyping-based tooling, referred to as rapid tooling [10,11]. There are a variety of rapid tooling techniques and materials. These processes can be classified as:

- patterns for casting (the fabrication of patterns to produce the sand molds),
- direct rapid tooling (layer-by-layer build-up of mold), in which molds are fabricated in a rapid prototyping system, or
- indirect rapid tooling (shaping of mold from rapid prototyping made master pattern), in which a rapid prototype master is converted into a mold using a secondary process [11, 12].

These processes can also be classified based on their expected mold life (number of parts that sap be produced in the mold), as:

- soft (a few injected parts),
- bridge (several thousand injected parts) and
- hard tooling (above one hundred thousand ejected parts). [11, 12]

The process of making a prototype on a 3D printer was performed in several stages. The first was the optimization of the printing process. The optimization of the printing process includes testing the position of the printing sleeve using the appropriate software, in order to reduce material consumption, surface quality and print speed, as shown in Figure 10.



Fig. 10. Optimization of the printing process of sleeve using software

As an optimal solution, the position of the sleeve marked with Rank 1 was chosen, because it does not require support (minimum material consumption), satisfying the quality of the surface and the shortest printing time. The procedure of 3D printing of a sleeve is shown in Figure 11.

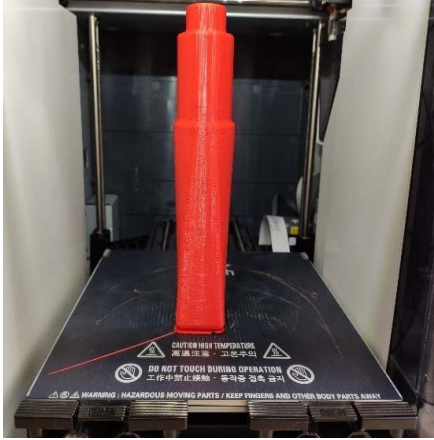


Fig. 11. 3D printing of a sleeve

When it comes to the ear of the brake triangle, based on the software, the position marked Rank 1 in Figure 12 was chosen as the optimal solution.

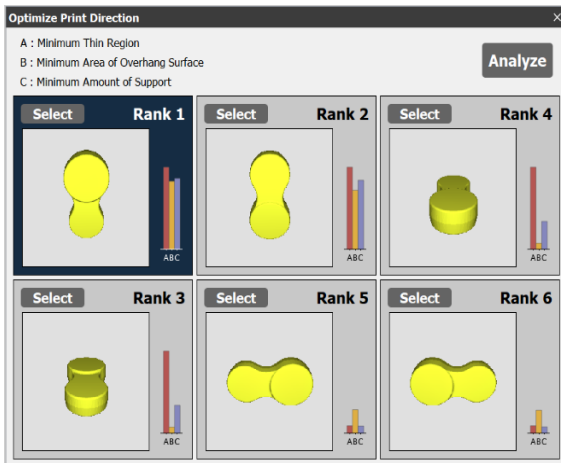


Fig. 12. Optimization of the printing process of ear using software

Also, in this case, it does not require much support when printing, so the lowest material consumption and the fastest time to make the work.

After the optimization procedure, the model was printed with a density of 30% and a wall thickness of 2 mm in order to extend the life of the casting model.

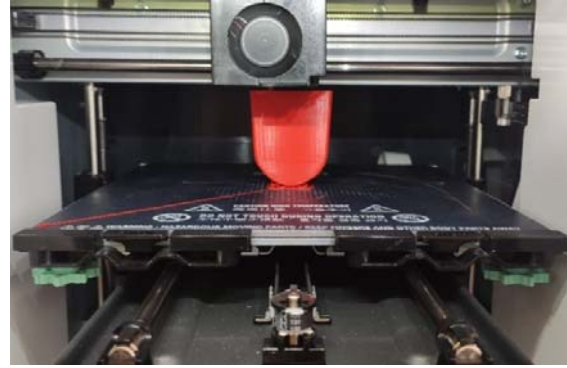


Fig. 13. 3D printing of an ear

The printed parts are shown in Figure 14.



Fig. 14. Foundry models made on a 3D printer

After making the casting mold, the process of casting the product in sand was started. The cast sleeve is shown in Figure 15.



Fig. 15. Casted sleeve of brake triangle

5. CONCLUSION

The process of simultaneous design using reverse engineering, and rapid prototyping significantly affects the shortening of the

production time and facilitates the choice of production technology.

The application of reverse engineering in combination with the appropriate software package for stress-strain analysis significantly shortens the production time, because it is not necessary to create a physical model for testing, but it is done in a virtual environment.

The application of rapid prototyping (3D printing) significantly speeds up the process of making prototypes and ready-made casting stamps, which makes the process of making products competitive.

By combining the appropriate production technology in accordance with the simulation results, productivity is significantly affected, because, on the one hand, the development time is shortened, while, on the other hand, the technological process is optimized. The main result is faster and cheaper production.

Acknowledgement

The research presented in this paper was realized within the project "**Simultaneous design of an innovative product to improve the competitiveness of enterprises**" Support measures for MSMEs, for projects of cooperation with scientific and educational institutions, innovation organizations and associations funded by the Office for Local Economic Development and Niš.

REFERENCES

- [1] Hallem, A., Jovaid. M. (2014). Additive Manufacturing Applications in Industry 4.0. *Journal of Industrial Integration and Management*, vol. 04.
- [2] Boppana F.A., Gonzales, C.L. (2013). An integrated design approach for rapid product development. *Journal of Engineering, Design and Technology*, vol. 11 no 2 pp. 178-189 DOI:10.1108/JEDT-06-2011-0042
- [3] Wego, W. (2011) *Reverse engineering - technology of reinvention*, CRC Press Taylor & Francis Group, Usa
- [4] Zaman, U., Rivvete M. (2018) *Integrated product-process design: Material and manufacturing process selection for additive manufacturing using multi-criteria decision-making* Robotics and Computer-Integrated Manufacturing, vol. 51, pp 169-180
- [5] Douglas, S., Gilbert, T., Gilbert, S. (2014) *Costs and cost effectiveness of additive manufacturing*, U.S. Department of Commerce-National Institute of Standards and Technology
- [6] Metalac PNT d.o.o. From: http://www.metalac-pnt.hr/portal/index.php?option=com_content&view=article&id=71&Itemid=89&lang=hr accessed on: August 15, 2020.
- [7] Ferrum Rail Components. From: <http://www.ferrumwagon.pl> accessed on: August 15, 2020.
- [8] Kuźnia Ostrów Wielkopolski Sp. From: <http://kuzniaostrow.pl/> accessed on: August 15, 2020.
- [9] Jiangsu Newer Train Technology Co. From: www.newertrain.com accessed on: August 15, 2020.
- [10] Nagahanumaiah, K., Subburaj, B. Ravi (2008). *Computer aided rapid tooling process selection and manufacturability evaluation for injection mold development*, Computers in Industry, vol. 59. pp. 262-276.
- [11] Sekulic, M, Gostimirovic, M, Kulundzic. N., Aleksic, A. (2018) *Technological changes in mold making industry*, 13th International Scientific Conference Novi Sad, Serbia
- [12] Altan, T., Lilly, B., Yen, Y.C. (2001) *Manufacturing of Dies and Molds*. CIRP Annals, vol. 50, no 2, pp. 404-422.



Banja Luka
28-29 May 2021.

DEMI 2021

15th International Conference on Accomplishments in Mechanical and Industrial Engineering

www.demi.mf.unibl.org



Energy consumption model of the face milling

S. Tesic^a, Dj. Cica^a, M. Zeljkovic^b, S. Borojevic^a, B. Sredanovic^a, G. Jotic^a

^aUniversity of Banja Luka, Faculty of Mechanical Engineering

^bUniversity of Novi Sad, Faculty of Technical Sciences

Abstract Reducing energy consumption in the metal cutting industry is one of the main challenges of today. To enable reductions in energy consumption, it is of great importance to develop models for monitoring energy consumption. In this paper, the total energy consumption of machine tool during face milling was investigated. The energy consumption model of the face milling operation is analyzed. Experiments were carried out in wet condition as per Taguchi's L9 orthogonal array. The cutting parameters were depth of cut (0.6, 1.0, 1.6 mm), cutting speed (120, 177, 260 m/min) and feed per tooth (0.04, 0.06, 0.10 mm/tooth). In this experiments, the workpieces material was medium carbon steel blanks (C45). Based on nine experiments, the observed model showed great reliability. The largest deviation was 7.5% and the smallest deviation was 0.7%. Based on these deviation values, it was concluded that the observed model can be reliably used to calculate the total energy consumption of the machine tool in face milling.

Keywords Energy consumption, face milling, model

1. INTRODUCTION

Except that it is one of the key branches of the economy in many developed country, the industry is also a major consumer of energy and other resources. The metal processing industry has the largest contribution of the energy consumption in industry and accounts an incredible 37% of total world energy consumption [1, 2]. Consequently, shortage of resources, increasing environmental requirements and increasingly stringent environmental laws pose a major challenge to the metal processing industry. Therefore, the energy consumption in the metal processing industry have received ever increasing

attention nowadays.

The main cause of high energy consumption in metal cutting industry is the low energy efficiency of machine tools, which represent the largest energy consumer in this industry [3 - 6]. Nowadays, a lot of researches are conducted to improve the energy efficiency of machine tools in the metal cutting industry. This researches were mainly focused on optimizing energy consumption and predicting energy consumption. Wang et al. [7] developed multi-objective mathematical model to minimize energy consumption in face milling and furthermore they used evolutionary strategy to identity optimal cutting conditions. Li et al. [8] used genetic algorithm in the optimization of cutting parameters for the purpose energy saving in rough and finish milling. Wang et al. [9] presented an optimization method for energy saving using ant colony optimization solution on the basis of selecting Standard for the Exchange of Product model data-Numerical Control (STEP-NC).

Corresponding author

MSc Sasa Tesic
sasa.tesic@mf.unibl.org

University of Banja Luka, Faculty of Mechanical Engineering
Vojvode Stepe Stepanovica 75, 78000
Banja Luka, Bosnia and Herzegovina

The history of thinking about modeling energy and power consumption dates back to 1992, when Peklenik and Jerela [10] developed a model that indirectly estimates input / output power and energy as a function of cutting force. Gutovski et al. [11] presented a pioneering research in the analysis of machine tool energy according to which the energy consumption of machine tools is not constant during the machining cycle. His model predicted that the total cutting power would consist of the fixed power required to keep the machine running in the inactive phase and of the variable power, which actually represents the cutting power. Researchers [12] developed a model of energy consumption in cutting process which consider influence of spindle speed. This model consists of the energy for standby, the energy required to rotate the spindle, and the energy required to remove the material. Zhao et al. [13] included the influence of the SHP pump in their model in order to make the models for predicting energy consumption more acceptable for all machine tools. However, Lee et al [14] developed a model of energy consumption of the machine tool at the cutting process that includes various influential components. This model takes into account power components: standby power, unload power, cutting related auxiliary power, material removal power and additional load loss. Considering, this model has a high degree of universality for different machine tools and different cutting operations. The aim of this paper is analyze the total energy consumption of the machine tool and the analysis of the model for the consumption of total energy from [14]. This analysis was performed during face milling. The observed model was analyzed for different cutting parameters, namely cutting depth, cutting speed and feed rate. The Taguchi's L9 array was used for conducting the experiments.

2. ENERGY STRUCTURE OF CUTTING PROCESS

The energy structure of the cutting process depends on the power structure that at a given time period varies. From the point of view of energy consumption, the cutting process can be divided into five phases, namely machine startup, standby state, spindle acceleration or deceleration, air cutting and cutting [14]. The air cutting phases implies when there is no load

applied to the cutting tool. Fig. 1 shows the energy profile of a machine tool during a cutting process.

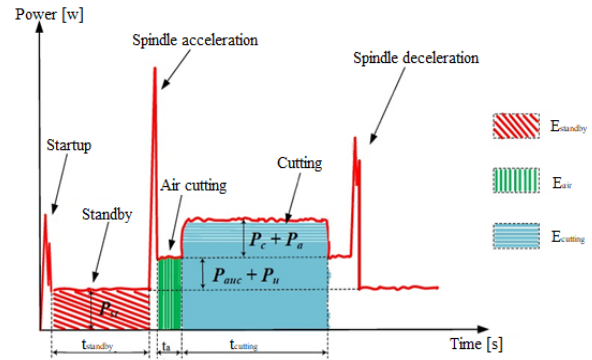


Fig. 1. Energy profile of cutting process [14]

The cutting energy represents the power used over time, as expressed in Eq. 1.

$$E = \int_0^t P(t) dt \quad (1)$$

Since the startup time and the acceleration and deceleration times of the main spindle are very short, as shown in Figure 1, their impact on the total energy consumption in the cutting process is negligible. Based on this, it is concluded that the significant impact on the total energy consumption in the cutting process has the power used in the standby phases (P_{st}), power used in the unload power (P_u), auxiliary power (P_{auc}), cutting power (P_c) and additional load loss (P_a). However, in real production conditions during the standby phase, the machine tool consumes energy during three different periods, namely idle time in waiting for the operations (t_{idle}), setup time (t_{setup}) and tool change time due to tool wear or tool break (t_{tc}). Hence, the total power consumption of the machine tool is the sum of the five components of energy as shown in Equation 2 [14].

$$E_{total} = E_{idle} + E_{setup} + E_{air} + E_{cut} + E_{tc} \quad (2)$$

The models for each energy component of the machine tool in the cutting process are given in Eqs. 3, 4, 5, 6 and 7.

$$E_{idle} = \int_0^{t_{idle}} P_{st}(t) dt = P_{st} \cdot t_{idle} \quad (3)$$

$$E_{setup} = \int_0^{t_{setup}} P_{st}(t) dt = P_{st} \cdot t_{setup} \quad (4)$$

$$E_{air} = \int_0^{t_{air}} P_a(t) dt = (P_{st} + P_{auc} + P_u) \cdot t_{air} \quad (5)$$

$$E_{cut} = \int_0^{t_{cut}} P_{cut}(t) dt = (P_{sp} + P_{awc} + P_u + P_c + P_a) \cdot t_{cut} \quad (6)$$

$$E_{tc} = \int_0^{t_{tc}} P_{sp}(t) dt = P_{sp} \cdot t_{tc} \quad (7)$$

where t_{air} is the air cutting time and t_{cut} is the effective cutting time.

3. EXPERIMENTAL PROCEDURE

The experiments were conducted on a CNC vertical milling center EMCO Concept Mill 450 with 11kW drive motor and maximum spindle speed of 12 000 rpm. A face mill cutter of 50 mm diameter with 5 flutes carbide tool inserts was employed for milling of workpieces with the dimension 50×50×363 mm.

In this experiments, the workpieces material was medium carbon steel blanks (C45). The experimental set-up is shown on Fig. 2. The experiments were performed in wet cutting conditions.

Taguchi orthogonal array L9 has been used for design of experiment (DOE). The experiment was performed using three cutting parameters at three levels. The cutting parameters were depth of cut (0.6, 1.0, 1.6 mm), cutting speed (120, 177, 260 m/min) and feed per tooth (0.04, 0.06, 0.10 mm/tooth).

The energy demand of machining process was measured with device DRANETZ MAVOWAT 30. This measuring chain can to measure different electrical parameters such as current, active power, energy, voltage, etc. Since that aim of this investigation is to analysis the total energy consumption of cutting process, the measuring spot was at the main bus of the electrical cabinet. Fig. 3 shows a power and energy profile of a CNC face milling process.

4. RESULTS AND DATA ANALYSIS

In this part of study, the analysis and verification of the model from equation 2 in face milling was performed. Since the experiment was observed at the level of one operation and with one tool, E_{idle} , E_{tc} i E_{setup} were equal to zero. The air cutting time was during entry and exit from operations. In this case, the model has the form as in Eq. 8:

$$E_{total} = E_{idle} + E_{setup} + E_{air} + E_{cut} + E_{tc} = 0 + 0 + ((P_{sp} + P_{awc} + P_u) \cdot t_{air})_1 + (P_{sp} + P_{awc} + P_u + P_c + P_a) \cdot t_{cut} + ((P_{sp} + P_{awc} + P_u) \cdot t_{air})_2 + 0 \quad (8)$$

Nine experiments were performed to verify the observed model. The reading of the value of total energy consumption for each experiment was performed, as well as the calculation of energy consumption using of the observed model. Experimental values, calculated values and model error are shown in the Table 1.



Fig. 2. The experimental work

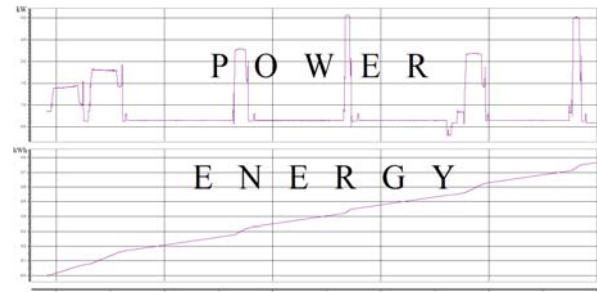
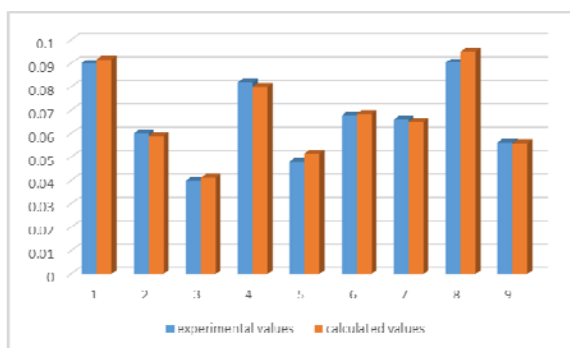


Fig. 3. Power and energy profile of a face milling process

Table 1. Experimental design, experimental and calculated results

Exp no.	Depth of cut (mm)	Cutting speed (m/min)	Feed (mm/z)	Total energy EXP (kWh)	Total energy MODEL (KWH)	Error (%)
1	0.6	120	0.04	0.0901	0.0918	1.89
2	0.6	177	0.04	0.0601	0.0590	1.83
3	0.6	260	0.10	0.0400	0.0412	3
4	1.0	120	0.06	0.0820	0.0802	2.20
5	1.0	177	0.01	0.0480	0.0516	7.5
6	1.0	260	0.04	0.0680	0.0685	0.7
7	1.6	120	0.10	0.0660	0.0651	1.36
8	1.6	177	0.04	0.0904	0.0950	5.09
9	1.6	260	0.06	0.0564	0.0560	0.71

The obtained calculated values of total energy consumption in the milling process, using the observed model, had small deviations from the experimental values, Fig. 4. The largest deviation was 7.5% in Experiment 5, and the smallest deviation was in Experiment 6, which was 0.7%. These deviations are small and based on that, this model gives reliable values of the total energy consumption during face milling. This experiment proved the reliability of this model since different cutting parameters were used for each experiment. A small deviation error can occur due to an error in reading and measuring, but also due to some shortcoming of the model.

**Fig. 4.** Experimental and calculated values of total energy

5. CONCLUSIONS

Reducing energy consumption in the metal cutting industry is one of the main challenges of today. To enable reductions in energy consumption, it is of great importance to

develop models for monitoring energy consumption.

In this paper, a model of total energy consumption during cutting is applied in order to examine its accuracy in face milling. Based on nine experiments, the observed model showed great reliability. The deviations of experimental and calculated values were small for all combinations of different cutting parameters. The largest deviation was 7.5% and the smallest deviation was 0.7%. Based on these deviation values, it was concluded that the observed model can be reliably used to calculate the total energy consumption of the machine tool in face milling.

In the future, this model can be analyzed for other cutting operations.

REFERENCES

- [1] Yi, Q., Ji, Q., Zhu, D., Jin, Y., Li, L. (2020). Design optimization of lathe spindle system for optimum energy efficiency. *J. Clean. Prod.*, vol. 250, DOI: <https://doi.org/10.1016/j.jclepro.2019.119536>
- [2] IEA, 2020, Data and Statistics, International Energy Agency, Paris, France, URL: [https://www.iea.org/data-and-statistics?country=WORLD&fuel=Energy%20consumption&indicator=Total%20final%20consumption%20\(TFC\)%20by%20sector](https://www.iea.org/data-and-statistics?country=WORLD&fuel=Energy%20consumption&indicator=Total%20final%20consumption%20(TFC)%20by%20sector)
- [3] Cai, W., Liu, F., Zhou, X., Xie, J. (2016). Fine energy consumption allowance of workpieces in the mechanical manufacturing industry. *Energy*, vol. 114, pp. 623 – 633, DOI: <https://doi.org/10.1016/j.energy.2016.08.028>

- [4] Hu, L., Peng, C., Evans, S., Peng, T., Liu, Y., Tang R. (2017). Minimizing the machining energy consumption of a machining tool by sequencing the features of a part. *Energy*, vol. 121, pp: 292 – 305, DOI: <https://doi.org/10.1016/j.energy.2017.01.039>
- [5] Xiao, Q., Li, C., Tang, Y., Li, L., Li, L. (2019). A knowledge-driven method of adaptively optimizing process parameters for energy efficient turning. *Energy*, vol. 166, pp. 142-156. DOI: <https://doi.org/10.1016/j.energy.2018.09.191>
- [6] Rajemi, M.F. (2011). Energy analysis in turning and milling. A thesis for the degree of Doctor of Philosophy. The University of Manchester, Manchester
- [7] Wang, Y.C., Kim, D.W., Katayama, H., Hsueh, W.C. (2018). Optimization of machining economics and energy consumption in face milling operations. *Int. J. Adv. Manuf. Technol.*, vol. 99, pp: 2093–2100, DOI: <https://doi.org/10.1007/s00170-018-1848-6>
- [8] Li, J., Lu, Y., Zhao, H., Li, P. and Yao, Y. (2014). Optimization of cutting parameters for energy saving. *The International Journal of Advanced Manufacturing Technology*, vol. 70, pp. 117-124. DOI: [10.1007/s00170-013-5227-z](https://doi.org/10.1007/s00170-013-5227-z)
- [9] Wang, H., Zhong, R.Y., Liu, G., Mu, W.L., Tian, X., Leng, D. (2019). An optimization model for energy-efficient machining for sustainable production. *J. Clean. Prod.*, vol. 232, pp. 1121-1133, DOI: <https://doi.org/10.1016/j.jclepro.2019.05.271>
- [10] Peklenik, J., Jerele, A. (1992). Some Basic Relationship for Identification of the Machining Processes. *CIRP Annals – Manufacturing Technology*, vol. 41, pp: 155 – 159, DOI: [https://doi.org/10.1016/S0007-8506\(07\)61174-3](https://doi.org/10.1016/S0007-8506(07)61174-3)
- [11] Gutovski, T., Dahmus, J., Thiriez, A. (2006). Electrical energy requirements for manufacturing processes. 13th CIRP International Conference on Life Cycle Engineering, Leuven, Belgium, pp. 623-627.
- [12] Li, L., Yan, J., Xing, Z. (2013). Energy requirements evaluation of milling machines based on thermal equilibrium and empirical modelling. *J. Clean. Prod.*, vol. 52, pp: 113–121, DOI: <https://doi.org/10.1016/j.jclepro.2013.02.039>
- [13] Zhao, G., Hou, C., Qiao, J., Cheng, X. (2016). Energy consumption characteristics evaluation method in turning. *Adv. Mech. Eng.*, vol. 8, pp: 1–8, DOI: <https://doi.org/10.1177/1687814016680737>
- [14] Li, L., Li, C., Tang, Y., Yi, Q. (2017). Influence factors and operational strategies for energy efficiency improvement of CNC machining. *J. Clean. Prod.*, vol. 275, pp. 220 – 238, DOI: <https://doi.org/10.1016/j.jclepro.2017.05.084>



Banja Luka
28–29 May 2021.

DEMI 2021

15th International Conference on Accomplishments in Mechanical and Industrial Engineering

www.demi.mf.unibl.org



Modern approach in process planning and optimization of the product manufacturing

D. Lukić^a, M. Milošević^a, R. Čep^b, I. Kuric^c, M. Kljunović^a, M. Zagoričnik^a

^aUniversity of Novi Sad, Faculty of Technical Sciences, Trg Dositeja Obradovica 6, Novi Sad, Serbia

^bTechnical University of Ostrava, Faculty of Mechanical Engineering, 17. listopadu 15, Ostrava, Czech Republic

^cUniversity of Žilina, Faculty of Mechanical Engineering, Univerzitna 1, Žilina, Slovakia

Abstract Manufacturing processes planning as objects of optimization are characterized by a variety of solutions in all phases, from the selection of raw materials, production technologies, machining processes and operations, manufacturing resources, machining parameters, etc. In order to achieve productivity and economy as the most important criteria for optimization in the production, it is necessary to optimize the manufacturing process plans.

The subject of research in this paper relates to the design and optimization of the manufacturing process, based on the application of the rules of priority of the machining operation of selected machining features and simulation techniques in the CAD/CAM system. For the case study, a product was selected—a lever, on which machining features are defined, possible machining operations, appropriate cutting tools and machining parameters, tool approach directions, and then variants of manufacturing processes are defined by applying the precedence relationship of machining operations. The second level of optimization is performed through the selection of optimal cutting tools and machining parameters. The machining simulation was realized in SolidCAM software, and as an output the best solution of the manufacturing process was obtained from the aspect of processing time, i.e. productivity.

Keywords Process planning, Optimization, Precedence relationship, CAM Simulation, Productivity

1. INTRODUCTION

The production system will work well only if it meets the requirements of customers, ie if a usable, well-designed, economical, environmentally friendly, economical, competitive and market-acceptable product is produced at the right time. [1].

The most important role in meeting market demands is played by the processes of design, planning, management and production.

Corresponding author

Assoc. Prof. Dejan Lukić
lukicd@uns.ac.rs

University of Novi Sad, Faculty of Technical Sciences,
Department of Production Engineering
Trg Dositeja Obradovica 6, 21000 Novi Sad,

Therefore, the function of technological preparation of production is very important, because it represents the integration function of these processes. [2].

Two basic tasks within the technological preparation of production are the process planning and optimization of the product manufacturing, whose automation is solved through the development of CAPP (Computer Aided Process Planning) system and its integration with other CAX systems. CAPP systems represent a "bridge" between product design -CAD (Computer Aided Design), production planning and management -PPC (Production Planning System), quality management-CAQ (Computer Aided Quality) and the production process itself -CAM (Computer

Aided Manufacturing), so it can be said that it is the key integration component in the CIM system [3-5].

Manufacturing process planning includes the transformation of raw materials through the implementation of manufacturing operations into the finished part, and then the assembly of parts into final product. The basic tasks that are solved within the manufacturing process planning are: Manufacturability analysis, Selection and definition of raw materials, Selection of machining features, Definition of a process plan (Selection of machining processes, Selection of machining operations, Selection manufacturing resources, Selection cutting parameters and strategies), Generating NC programs, Determination of machining time and cost, Generating technological documentation (routing and operation sheets, NC programs) [2]. Considering that it consists of a large number of activities, process planning carries a large level of solution variability, from the choice of raw materials, choice of manufacturing technologies, processes, operations, elements of the manufacturing systems (machines, tools, fixtures...), machining parameters, etc.

Optimization of manufacturing processes is finding the best solutions for certain conditions that are based on technological and economic criteria of optimization with the application of certain optimization methods. In order to achieve productivity and economy as the most important criteria for optimization in the production, it is necessary to optimize the manufacturing processes [6, 7].

The main goal of this research is process planning and optimization of the selected part-lever, by applying the relationship of priority among machining operations, as well as the simulation technique within the CAM system.

The precedence relationships of machining operations are defined on the basis of dimensional, geometric, technological and economical precedence constraints. Based on these rules, precedence matrices for determining operation sequence for the given part are formed, and afterwards, machining operations are grouped into appropriate process plans. For the given rational variants of process plans, a simulation of machining process is performed within the SolidCAM software. The obtained output is the best variant of process plan for the lever on the basis of manufacturing time as the adopted objective function.

2. THEORETICAL BASIS

In real production conditions, two approaches are mainly applied in the manufacturing process planning [2, 8].

1. The **first** or traditional approach comes down to the fact that based on the analysis of product characteristics machining surfaces are defined, then on the basis of experience, types and sequence of machining processes are determined first, and types and sequences of machining operations with all the necessary information, such as manufacturing resources, machining parameters, manufacturing time....

2. The **second** approach is based on the recognition and extraction of features for which the possible machining operations with the necessary manufacturing resources and manufacturing parameters are defined, then the sequence of machining operations is defined and later grouped into appropriate manufacturing process (Figure 1).

The first approach is based on the individual process planning which greatly emphasizes the influence of a designer, and is a significantly faster approach but does not offer great possibilities for optimization. The second approach provides considerably better possibilities for optimization and development of modern CAPP systems that are based on the application of feature technologies, methods of artificial intelligence, etc.

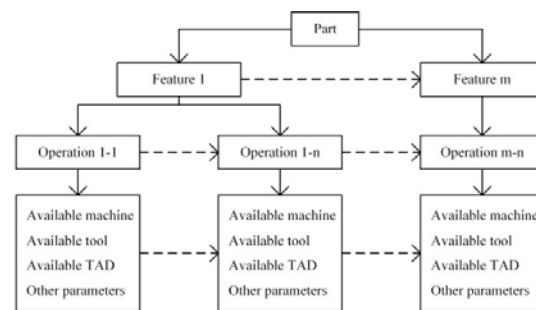


Fig. 1. Represented structure of a process plan [8, 9]

The problem of optimizing process plans belongs to the class of combinatorial optimization problems and it includes the recognition of appropriate machining features and the definition of sequences of machining operations and processes with the determination of appropriate machines, fixtures, measuring instruments, tools, cutting parameters and machining strategies. Solving these tasks also includes necessary constraints which are called

the precedence constraints or relationships and whose consideration makes this problem even more complex. Objective function for the evaluation of process plans is usually defined by machining cost, machining time, surface roughness and quality [10, 11].

Precedence relationships among machining operations can be grouped on the basis of technical and economical constraints. According to that fact, the following groups of this constraints are defined [11-15]: dimensional, geometric, technological and economical precedence.

Dimensional precedence: Determining precedence among machining operations due to dimensional reasons is related to surface dimensioning and can be defined in the form of the following rule: „Before machining a desired surface a surface related to whom the considered surface is dimensioned is machined first, and priorities have surfaces dimensioned in relation to a datum“.

Geometric precedence: Determining priorities among machining operations due to geometric reasons is related to the requirements in terms of interaction between surfaces and axes, or so-called position tolerances. In this case, precedence can be defined in the following form: „Surface related to whom the position tolerance of other surface is defined has the priority in machining“.

Technological precedence: This group of constraints is mostly related to the precedence relationships among operations for machining a feature that do not require more machining operations (e.g., drilling before counter boring, counter boring before reaming, turning before grinding, etc.).

Economical precedence: These constraints are, above all, related to reduction in manufacturing cost which is achieved by applying more productive or more economical method or a tool instead of less productive or less economical method or a tool.

CAD/CAM systems enable the simulation of machining processes and are of special importance for the manufacturing process planning that is realized on CNC machining systems. By simulating machining processes, ie. tool paths, the possibility of collision of tools with fixtures, machine parts, workpieces, etc. is provided and excluded. Within the simulations of machining processes, it is possible to determine the optimal type and order of

machining operations and appropriate machining tools and parameters based on the time obtained by simulating the machining process.

3. PROCESS PLANNING AND OPTIMIZATION OF LEVER MANUFACTURING

This chapter presents the process planning and optimization of lever manufacturing (Fig. 2), which is produced in serial production. The adopted raw material is a prismatic section 240x80x50mm from steel -C45.

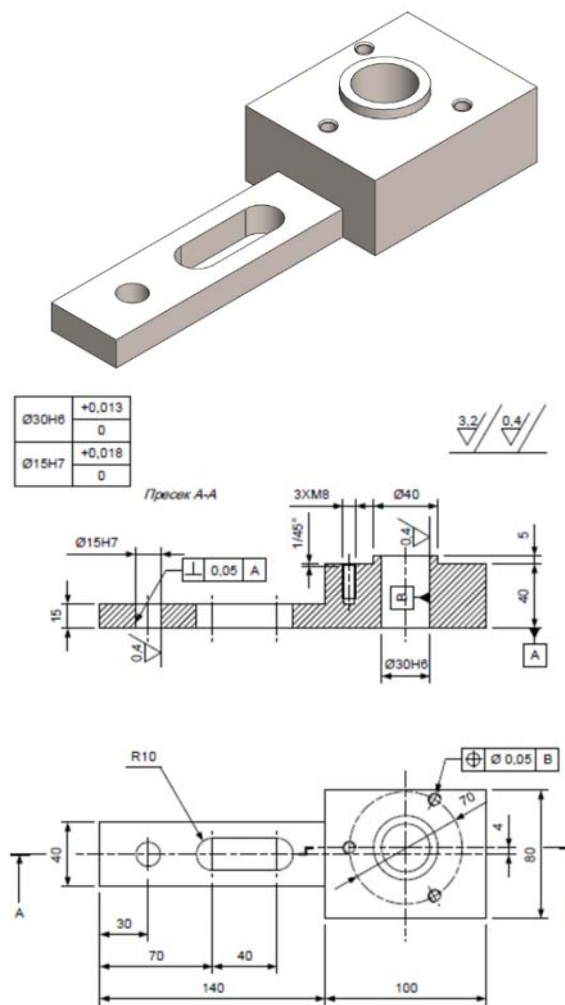


Fig. 2. 3D model/2D drawing of lever part

3.1. Defining machining features and variants of operation and tools

As the first step in the application of this method, the recognition and extraction of machining features was performed. The designations of the selected machining features are presented in

Figure 3, while their specifications are presented in Tables 1. Based on the extracted machining features, possible operation and tools for their machining are defined, which are presented in Tables 2.

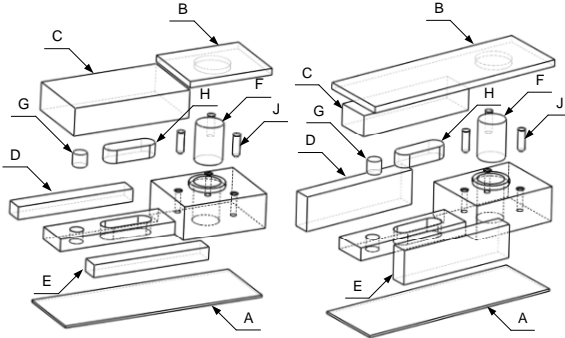


Fig. 3. Designations of extracted machining features for two variants manufacturing processes

Table 1. Specification of machining features

Mach. feature	Name	Dimension [mm]	Surf. quality	Geometric tolerance
A	Flat plane	240x80x2,5	N8	Base A
B	Step	100x80x7,5 or 240x80x7,5	N8	-
C	Step	140x80x32,5 or 140x40x25	N8	-
D	Step	140x20x15 or 140x40x20	N8	-
E	Step	140x20x15 or 140x40x20	N8	-
F	Hole	Ø30H6 x 45	N5	Base B
G	Hole	Ø15H7 x 15	N5	\perp 0,05 A
H	Slot	60 x 20 x 15	N8	-
J	3x thread	3x M8 x 20 bore 1/45°	N8	\oplus 0,05 B

Finally, the machining operations and tool approach directions (TAD) are given in Tables 3, and the corresponding cutting tools in Tables 4. Analyzing, it was observed that four characteristic tool approach directions (TAD) corresponding to the four sides of the prismatic part. Based on that, it can be concluded that four clamping are required during the machining of the lever. Features A, F, G and H share the same tool approach direction as features B, C, F, G, H and J. Feature A can be processed together with features whose direction of tool approach is in the + Z direction, while features B, C and J are processed with features whose direction of tool approach is in the -Z. Two clamping are reserved for these two groups of machining features. This

means that features F, G and H can be processed in either of these two clamping. Features D and E are processed separately because they do not share the same tool approach direction with each other. Two clamping are provided for them.

Table 2. Operations and tools for machining features

Mach. feature	Rough machining	Semi-finish machining	Finish machining
A	OP: Rough face milling Cutting tool: Face mill cutter Ø100; End mill cutter Ø20	OP: Semi-finish face milling Cutting tool: Face mill cutter Ø100; End mill cutter Ø20	
B	OP: Rough face/step milling Cutting tool: Face mill cutter Ø100; End mill cutter Ø20	OP: Semi-finish face/step milling Cutting tool: Face mill cutter Ø100; End mill cutter Ø20	
C	OP: Rough face/step milling Cutting tool: Face mill cutter Ø100; End mill cutter Ø20	OP: Semi-finish face/step milling Cutting tool: Face mill cutter Ø100; End mill cutter Ø20	
D	OP: Rough step milling Cutting tool: End mill cutter Ø20	OP: Semi-finish step milling Cutting tool: End mill cutter Ø20	
E	OP: Rough step milling Cutting tool: End mill cutter Ø20	OP: Semi-finish step milling Cutting tool: End mill cutter Ø20	
F	OP: Drilling hole Cutting tool: Drill Ø28	OP: Core drilling hole Cutting tool: Core drill Ø29,8	OP: Rough reaming; Finish reaming Cutting tool: Reamer Ø29,95; Reamer Ø30H6
G	OP: Drilling hole Cutting tool: Drill Ø12,5	OP: Core drilling hole Cutting tool: Core drill Ø14,8	OP: Rough reaming; Finish reaming Cutting tool: Reamer Ø14,95; Reamer Ø15H7
H	OP: Drilling hole Rough slot milling Cutting tool: Drill Ø19; End mill cutter Ø18		
J	OP: Drilling hole Cutting tool: Drill Ø6,8	OP: Counterboring; Tapering thread. Cutting tool: Counterbore drill 45°, Taper M8	

Table 3. Defined cutting operation, tool ID and TAD

Mach. feature	Machining operation	Tools ID	TAD
A	Rough face milling (OP1)	T01, T02	+Z
	Semi-finish face milling (OP2)	T02	+Z
B	Rough face/step milling (OP3)	T01, T02	-Z
	Semi-finish face/step milling (OP4)	T02	-Z
C	Rough step milling (OP5)	T01, T02	-Z
	Semi-finish step milling (OP6)	T02	-Z
D	Rough step milling (OP7)	T02	-Y
	Semi-finish step milling (OP8)	T02	-Y
E	Rough step milling (OP9)	T02	+Y
	Semi-finish step milling (OP10)	T02	+Y
F	Drilling hole (OP11)	T03	+Z, -Z
	Core drilling hole (OP12)	T04	+Z, -Z
	Rough reaming hole (OP13)	T05	+Z, -Z
	Finish reaming hole (OP14)	T06	+Z, -Z
G	Drilling hole (OP15)	T07	+Z, -Z
	Core drilling hole (OP16)	T08	+Z, -Z
	Rough reaming hole (OP17)	T09	+Z, -Z
	Finish reaming hole (OP18)	T10	+Z, -Z
H	Drilling hole (OP19)	T11	+Z, -Z
	Rough slot milling (OP20)	T12	+Z, -Z
J	Drilling hole (OP21)	T13	-Z
	Counterboring (OP22)	T14	-Z
	Tapering thread (OP23)	T15	-Z

Table 4. Defined cutting tools

Tools ID	Cutting tools name	Tool specification (Sandvik Coromant)
T01	Facemill cutter Ø100mm	345-100C8-13M
T02	End mill cutter Ø20mm	1P330-2000-XA 1620
T03	Drill Ø28 mm	880-D2800L32-02
T04	Core drill Ø29,8 mm	BR20-36CC06F-EH25
T05	Fine boring Ø29,95 mm	825-36TC06-EH25
T06	Fine boring Ø30H6 mm	825-36TC06-EH25
T07	Drill Ø13 mm	460.1-1300-039A1-XM GC34
T08	Drill Ø14,8 mm	460.1-1480-044A1-XM GC34
T09	Reamer Ø14,95 mm	435.T-1500-A1-XF H10F
T10	Reamer Ø15H7 mm	435.T-1500-A1-XF H10F
T11	Drill Ø19 mm	460.1-1900-057A1-XM GC34
T12	End mill cutter Ø18 mm	1P330-1800-XA 1620
T13	Drill Ø6,8 mm	460.1-0680-034A1-XM GC34
T14	Counterbore drill 1/45°	1C050-0150-045-XA 1620
T15	Thread taper M8	E207M8

3.2. Defining the order of machining operation and variants of process plans

The rules of dimensional, geometric, technological and economic constraints for the execution of the machining operations are shown in Table 5. Based on these relations, a precedence matrix for machining operations was formed, which is shown in Figure 4.

On the basis of the precedence matrix for machining operations, four main variants of the process plans have been developed. Figure 5 shows one of the variants of manufacturing process plan.

Table 5. Precedence relationships among operations

Machining operation	Precedence machining operation			
	Dimens.	Geom.	Technol.	Econom.
OP1				
OP2			OP1	
OP3				
OP4			OP3	
OP5				
OP6			OP5	
OP7				
OP8			OP7	
OP9				
OP10			OP9	
OP11				
OP12			OP11	
OP13			OP12	
OP14			OP13	
OP15		OP2		OP5
OP16		OP2	OP15	
OP17		OP2	OP16	
OP18		OP2	OP17	
OP19				OP5
OP20			OP19	
OP21	OP11	OP14		
OP22		OP14	OP21	
OP23		OP14	OP22	

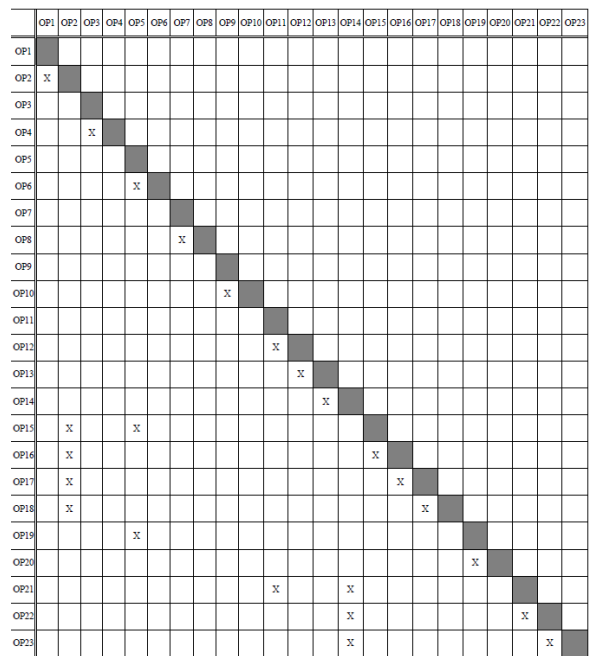


Fig. 4. The precedence matrix for machining operations

For all four variants of process plans, it is characteristic that they have four clamping, ie four sub-operations.

Tables 6-9 show the order of machining operations and sub-operation of processing for all four variants of manufacturing process plans.

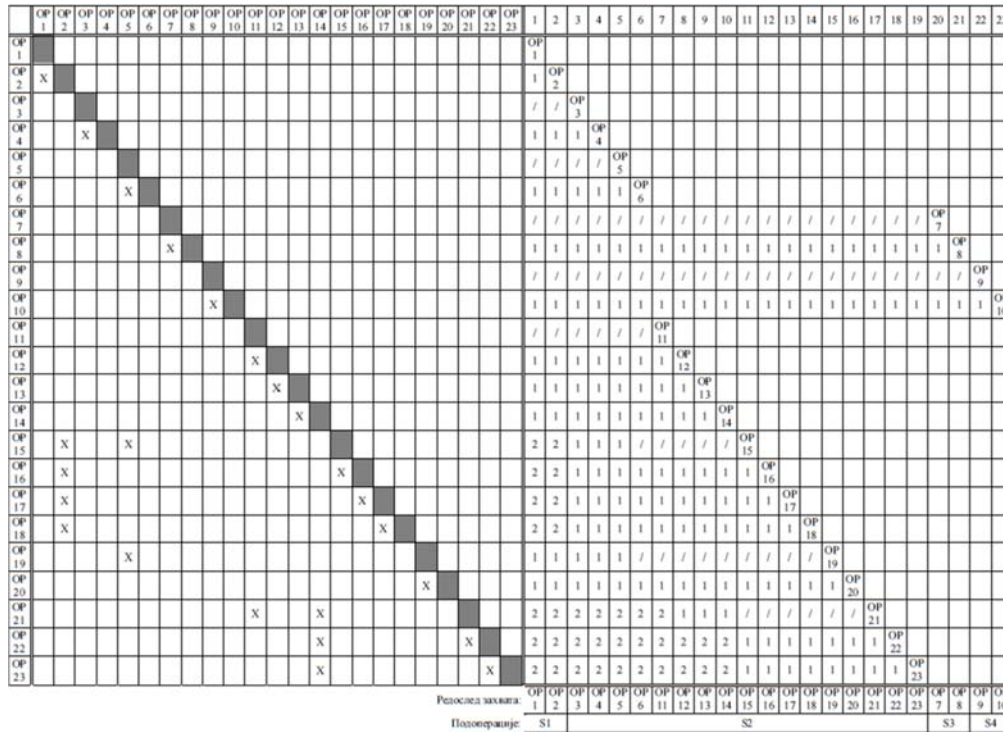


Fig. 5. The generated operation sequence and their grouping into process- variant 1

Table 6. Manufacturing process plan - variant 1

Sub operation	ID machining operation	TAD
S1	OP1, OP2	+Z
S2	OP3, OP4, OP5, OP6, OP11, OP12, OP13, OP14, OP15, OP16, OP17, OP18, OP19, OP20, OP21, OP22, OP23	-Z
S3	OP7, OP8	-Y
S4	OP9, OP10	+Y

Table 7. Manufacturing process plan - variant 2

Sub operation	ID machining operation	TAD
S1	OP1, OP2	+Z
S2	OP7, OP8	-Y
S3	OP9, OP10	+Y
S4	OP3, OP4, OP5, OP6, OP11, OP12, OP13, OP14, OP15, OP16, OP17, OP18, OP19, OP20, OP21, OP22, OP23	-Z

Table 8. Manufacturing process plan - variant 3

Sub operation	ID machining operation	TAD
S1	OP1, OP2	+Z
S2	OP3, OP5, OP4, OP6, OP11, OP12, OP13, OP14, OP15, OP16, OP17, OP18, OP19, OP20, OP21, OP22, OP23	-Z
S3	OP7, OP8	-Y
S4	OP9, OP10	+Y

Table 9. Manufacturing process plan - variant 4

Sub operation	ID machining operation	TAD
S1	OP1, OP2	+Z
S2	OP7, OP8	-Y
S3	OP9, OP10	+Y
S4	OP3, OP5, OP4, OP6, OP11, OP12, OP13, OP14, OP15, OP16, OP17, OP18, OP19, OP20, OP21, OP22, OP23	-Z

The technological graph in Figure 6, shows the variance of the realization machining operations for all 4 set variants of process plans. These four basic variants can be expanded with two subvariants, considering the order of realization of the machining operation and the volume of material that is removed during the processing of machining features B and C, D and E (Figures 7 and 8).

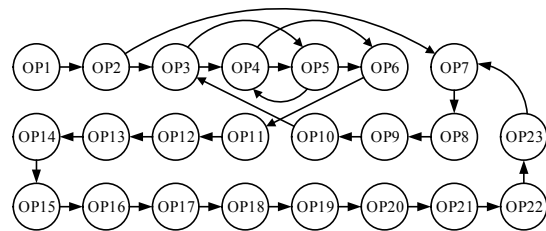


Fig. 6. Technological graph of variants for realization machining operation in process plans

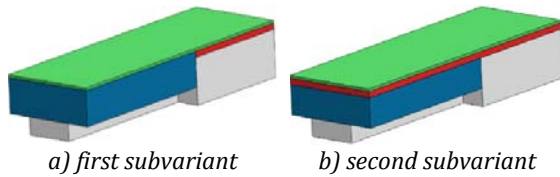


Fig. 7. Two subvariants for variants 1 and 2

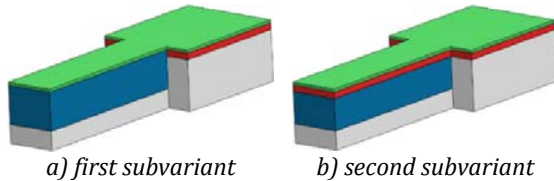


Fig. 8. Two subvariants for variants 3 and 4

Finally, there are a total of eight variants of the process plans for lever manufacturing, which are simulated using SolidCAM software. For each variant, during the simulation of the machining process, the realization times were performed, both for individual operations and machining features, sub-operations and, finally, the total manufacturing time for all variants. In this way, it is possible to compare the processing time for the same machining feature or operation among the variants of the processing operation.

3.3 Results of CAM simulation of variants of lever manufacturing process plans

Table 10 shows the obtained results of the simulation of the manufacturing process plans for all eight variants. In these results, variant with the shortest processing time was singled out, namely variant 3.1.

Table 10. Results of CAM simulations

Variant	Var. 1.1	Var. 1.2	Var. 2.1	Var. 2.2	Var. 3.1	Var. 3.2	Var. 4.1	Var. 4.2
	[m:s]	[m:s]	[m:s]	[m:s]	[m:s]	[m:s]	[m:s]	[m:s]
Total time	18:43	21:39	19:52	21:43	18:36	20:18	19:52	20:55

Variation of the manufacturing process plans was realized at the level of variation of cutting tools and parameters. End mill cutter Ø20 mm, in position T02, is the most represented tool in the processing of this part. It is involved in the processing of eight of the twenty-three operations, which represents of about 74% of the total processing time. Ten milling cutters with a diameter range from Ø25 mm to Ø40 mm were selected, with the manufacturer's recommended processing parameters. With

these tools, the processing simulation was performed on variant 3.1, at position T02. The obtained results are shown in Tables 11.

The milling cutter that proved to be optimal is R216.38-25045ICC45K 1640, with a diameter of Ø25 mm, a maximum machining depth of 45 mm and eight cutting edges. The total processing time has been reduced from 18:36 to 10:56 minutes, which is the optimal solution for the process plan of lever manufacturing.

Table 11. Simulation results of cutting tool variants T02 [16]

Tool specification	Diameter [mm]	Cutting depth [mm]	Num. of cutting edges	Total time [m:s]
1P330-2000-XA 1620*	20	32	3	18:36
316-25SM550C25010P 1730	25	15	5	17:20
316-25SL442-25005P 1730	25	30	4	21:18
R216.38-25045ICC45K 1640	25	45	8	10:56
R216.25-25050GCK54P 1620	25	54	5	15:13
1P240-2500-XA 1630	25	45,5	4	16:48
1P222-2500-XA 1630	25	32,5	4	16:11
RA390-025EH25-17L	25,4	15,7	2	25:00
R390-032EH25-17M	32	15,7	3	21:25
RA390-038M32-17L	38,1	15,7	2	35:16
R390-040B32-17H	40	15,7	4	20:21

* the cutting tool that was originally selected

4. CONCLUSION

This paper presents the principle of application of the rules of precedence relationships of machining operations as a method for obtaining possible variants and optimization of process plans for product manufacturing. In determining the order of machining operations, four constraints were taken into account: dimensional, geometric, technological and economic precedence.

Based on the 2D drawing/3D model of the lever, machining features are defined and cutting tools are selected. The determination of the variants of the order of machining operations was performed on the basis of the matrix of relations of machining operations, which contains four stated limitations. Eight variants of the procedure were derived from this matrix. Using SolidCAM software, a simulation of the adopted variants of manufacturing processes was performed, where the optimal output was adopted on the basis of the minimum processing time, i.e., maximum productivity.

The defined matrix of precedence among operations with machining times represent the fundamental basis for the optimization of process planning by applying one of the numerous metaheuristic algorithms that exist today. These methods are faster and more capable for solving complex optimization tasks, and hereby this would represent the proper continuation of this research.

Acknowledgement

This paper is part of a research on the project “Application of smart manufacturing methods in Industry 4.0”, No.142-451-3173/2020, Provincial Secretariat for Higher Education and Scientific Research of the Autonomous Province of Vojvodina and on the project “Innovative scientific and artistic research from the FTS (activity) domain”, No. 451-03-68/2020-14/200156, Ministry of Education, Science and Technological Development of the Republic of Serbia.

REFERENCES

- [1] Unger, D., Eppinger, S. (2010). Improving product development process design: a method for managing information flows, risks, and iterations, *Journal of Engineering Design*, vol. 22, no. 10, p. 689-699. DOI:[10.1080/09544828.2010.524886](https://doi.org/10.1080/09544828.2010.524886)
- [2] Lukic, D. (2012). *Razvoj opšteg modela tehnološke pripreme proizvodnje*. (In Serbian), DrSC Dissertation, Faculty of Technical Sciences, University of Novi Sad.
- [3] Xu, X., Wang, L., Newman, S.T. (2011). Computer-aided process planning – A critical review of recent developments and future trends. *International Journal of Computer Integrated Manufacturing* vol. 24, no. 1-3, p.1-31, DOI: [10.1080/0951192X.2010.518632](https://doi.org/10.1080/0951192X.2010.518632).
- [4] Milosevic, M., Lukic, D., Antic, A., Lalic, B., Ficko, M., Simunovic, G. (2017). e-CAPP: A distributed collaborative system for internet-based process planning, *Journal of Manufacturing Systems*, vol. 42, p. 210-223, DOI: [10.1016/j.jmsy.2016.12.010](https://doi.org/10.1016/j.jmsy.2016.12.010)
- [5] Álvares A., Ferreira J.C., Lorenzo R. (2008). An integrated web-based CAD/CAPP/CAM system for the remote design and manufacture of feature-based cylindrical parts, *Journal of Intelligent Manufacturing*, vol. 19, no. 643, p.643-659, DOI: [10.1007/s10845-008-0117-1](https://doi.org/10.1007/s10845-008-0117-1)
- [6] Lukic, D., Milosevic, M., Antic, A., Borojevic, S., Ficko, M. (2017). Multi-criteria selection of manufacturing processes in the conceptual process planning, *Advances in Production Engineering & Management*, vol. 12, no. 2, p. 151-162. DOI: [10.14743/apem2017.2.247](https://doi.org/10.14743/apem2017.2.247)
- [7] Borojevic, S., Lukic, D., Milosevic, M., Vukman, J., Kramar, D. (2018). Optimization of process parameters for machining of Al 7075 thin-walled structures, *Advances in Production Engineering & Management*, vol. 13, no. 2, p. 125-135, DOI: [10.14743/apem2018.2.278](https://doi.org/10.14743/apem2018.2.278)
- [8] Lukic, D., Milosevic, M., Eric, M., Đurđev, M., Vukman, J., Antić, A. (2017). Improving manufacturing process planning through the optimization of operation sequencing, *Machine Design*, vol. 9, no.4, p. 123-132. DOI: [10.24867/MD.9.2017.4.123-132](https://doi.org/10.24867/MD.9.2017.4.123-132).
- [9] Salehi, M., Tavakkoli-Moghaddam, R. (2009). Application of genetic algorithm to computer-aided process planning in preliminary and detailed planning, *Engineering Applications of Artificial Intelligence*, vol. 22, no. 8, p. 1179-1187. DOI: [10.1016/j.engappai.2009.04.005](https://doi.org/10.1016/j.engappai.2009.04.005)
- [10] Wang, J.F., Kang, W.L., Zhao, J.L., Chu, K.Y. (2016). A simulation approach to the process planning problem using a modified particle swarm optimization, *Advances in Production Engineering & Management*, vol. 11, no. 2, p. 77-92. DOI: [10.14743/apem2016.2.211](https://doi.org/10.14743/apem2016.2.211)
- [11] Đurđev, M., Cep, R., Lukic, D., Antic, A., Popovic, B., Milosevic, M. (2021). A genetic crow search algorithm for optimization of operation sequencing in CAPP, *Applied Sciences*, vol. 11, no. 5, p. 1-22, DOI: [10.3390/app11051981](https://doi.org/10.3390/app11051981)
- [12] Lian, K., Zhang, C., Shao, X. (2011). Optimization of process planning with various flexibilities using an imperialist competitive algorithm, *International Journal of Advanced Manufacturing Technology*, Vol. 59, No. 5-8, pp. 815-828. DOI: [10.1007/s00170-011-3527-8](https://doi.org/10.1007/s00170-011-3527-8)
- [13] Lukic, D., Milosevic, M., Vukman, J., Đurđev, M., Antic, A. (2017). Applying precedence relationships and CAD/CAM simulation in time-based optimization of process planning, *Applied Engineering Letters*, vol 2, no. 4, p. 130-138, <https://www.aeletters.com/wp-content/uploads/2017/12/AEL00054.pdf>
- [14] Petrovic, M., Mitic, M., Vukovic, N, Miljkovic, Z. (2016). Chaotic particle swarm optimization algorithm for flexible process planning, *International Journal Advanced Manufacturing Technology*, vol. 95, no. 9-12, p. 2535-2555. DOI: [10.1007/s00170-015-7991-4](https://doi.org/10.1007/s00170-015-7991-4)
- [15] Halevi, G., Weill, R.D. (1995). *Principles of Process Planning – A Logical Approach*, Chapman & Hall, Inc.
- [16] Sandvik Coromant. Digital machining. From: <https://www.sandvik.coromant.com/en-gb/products/pages/digital-machining.aspx>, accessed on: March 20, 2021.



Banja Luka
28–29 May 2021.

DEMI 2021

15th International Conference on
Accomplishments in Mechanical and
Industrial Engineering

www.demi.mf.unibl.org



Effect of various fluid flow on temperature of an angular contact ball bearings in motorized spindle

M. Knežev^a, M. Zeljković^a, C. Mladenović^a, H. Smajić^b, A. Stekolschik^b, A. Živković^a

^aFaculty of technical science, Department of production engineering, Vladimira Perića Valtera 2, 21000 Novi Sad.

^bFaculty of Vehicle Systems and Production, Institute for production, Betzdorfer Strasse 2, 50697 Cologne

Abstract *Newer generations of machine tools are challenged with drastically increasing productivity and reducing production costs. It have caused development of High speed machining technology and high speed spindles i.e. motorized spindles, for drastically increasing productivity and reducing production costs. High speed cause high generated temperature and sudden failure, so prediction of temperature behavior is of great significance. The main sources of heat on the motorized spindle occurs due to electric losses in motor and friction torque on bearings with angular contact. Those temperatures must be discharged out, and it is solved by cooling jacket around the stator, compressed oil mist, and forced air convection. This paper considers effect of cooling jacket around stator and various of fluid flow on front and rear bearings temperature. This paper presents a 2D Finite element model thermal model of the motorized spindle with angular contact ball bearings,*

Keywords *Motorized spindle, finite element method, angular ball bearing, cooling*

1. INTRODUCTION

Machining, in general, remains a major manufacturing process in various industries. Almost all metal parts go through machining at some stage of their production. Therefore, any progress in machining techniques would have a significant effect on the cost and timing of manufacturing. [1] High speed machining drastically increases productivity and reduces manufacturing cost, and has attracted the interest of engineers for many years.

However, an increase of the spindle speed also generates adverse effects such as noise, chattering, and heat generation in the spindle systems. [2] In high speed machining, the excessive heat generation in the spindle induces uneven thermal expansion within different machine elements, which not only causes friction and wear on the spindle, but also results in large machining tolerances. [3] While the high speed spindles are still relatively new. Many studies on the various point of views of spindle systems have been carried out through different kind analysis and experiments.

The dimensional accuracy and surface quality of machined workpiece depend upon thermal, dynamic, etc. characteristic of machine tool spindle system.

High speed spindles are known to suffer from lack of reliability and sudden failure, which originate, mostly, from thermal loads. [4]

Corresponding author

MSc, Miloš Knežev
knezev@uns.ac.rs

Faculty of technical Science, Department of production engineering
Vladimira Perića Valtera 2,
Novi Sad, Serbia

According to statistics, the responsibility of thermal error on the total geometrical error of workpiece is as high as 70%. [5] In [6] and [7], has been shown that the thermal error of numerical control lathe can be as high as 80 μm when n = 2000 rpm and CNC machining center can be as high as 50 μm when n = 8000 rpm, which is obviously unacceptable for NC machining. According to mentioned above, it is very significant to study the thermal characteristics of spindle in order to reduce its influence on the machining accuracy of machine tools.

2. HIGH SPEED SPINDLE

Compared with conventional spindles, motorized spindles are equipped with a built-in motor, so that power transmission devices such as gears and belts are eliminated. This design also reduces vibrations, achieves high rotational balance, and enables precise control of rotational accelerations and decelerations. It soon became obvious that the high speed operation and the very high heat dissipation of built-in motors push other spindle components to their limits. [8] Scheme of high speed spindle has been presented on Fig. 1.

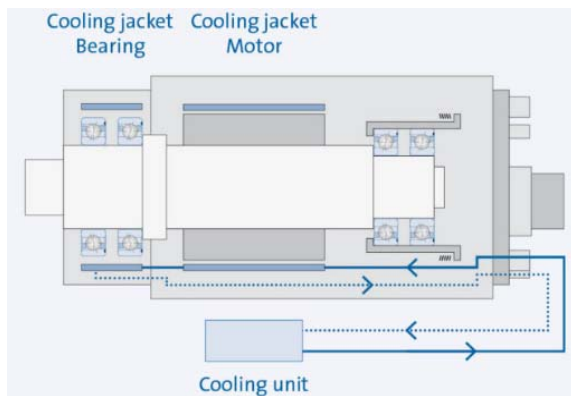


Fig. 1. Scheme of high speed spindle, and cooling system installation. [9]

According to producers, high speed spindles are equipped with an effective liquid cooling system. Cooling jackets are located in the area of the front bearings as well as around the spindle/motor/stator, in order to minimize increases in operating temperature, which can be caused by bearing friction as well as motor losses. The reduction in operation related to heat development increases the spindle performance

and provides high productivity as well as high machining quality.

The maximum detachable performance of the spindle is achieved in a specified coolant temperature range of 20 °C to 25 °C. The actually available performance depends upon coolant temperature and from the medium used. [9]

3. THERMO-MECHANICAL FEM MODEL OF THE COLLING JACKET

This paper presents Finite element model analysis of motorized spindle, with focus on cooling jacket, i.e. how cooling fluid flow effects on spindle temperature behavior. The geometry of the spiral cooling jacket around the stator surface of the motorized spindle has been shown on Fig. 2.

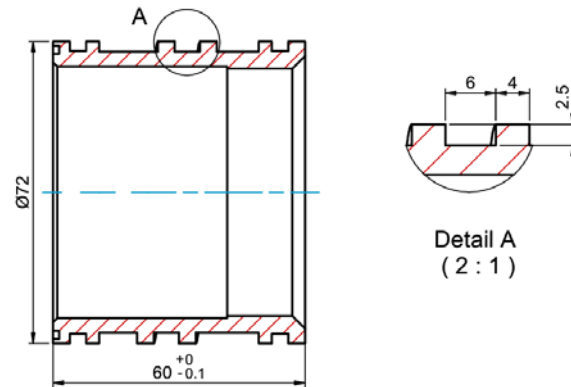


Fig. 2. Geometric model of the cooling jacket around the stator of the motorized spindle.

Commercial softwares were used for modeling and analyzing. The surface i.e. 2D model of motorized spindle been modeled in Siemens NX software, than the whole analysis has been carried out in Ansys Workbench.

The electrical motor of a motorized spindle is a significant source of heat. Motorized spindles typically use AC induction motors, and the effective input power of the motor is given as:

$$P = \sqrt{3} \cdot U \cdot I \cdot \cos \varphi$$

Where U is input voltage and I is the current through each lead. The phase angle φ between voltage and current determines the relative amount of effective power versus the measured apparent power. The effective electric input power is converted into mechanical output

power and losses. The major portion of the losses is converted into heat.

The motor heat generation is estimated with the knowledge of speed and torque and is given by:

$$Q_{motor} = 2 \cdot \pi \cdot f_{motor} \cdot M_{motor} \cdot \frac{1 - \eta_{motor}}{\eta_{motor}}$$

Where the f_{motor} is the motor frequency, while torque M_{motor} is determined from the sum of torques related to actual bearings moments, and η_{motor} is the motor efficiency.

In table 1 has been given motor input parameters.

Table 1. Motor input parameters

Exp no.	Voltage [V]	Freqency [Hz]	Current [A]	Power [kW]	efficiency
1	220	1500	12.3	3	0.88

The heat generated by the spindle bearings and spindle motor are the dominant heat sources causing thermal deformation. The heat dissipation is governed by the forced convective heat transfer of coolant in coolant channel and the flow of air around the spindle. This analysis consider heat generated by motor, and how changing the fluid flow effect on temperature of cooling jacket.

Forced convection through stator cooling channels. The convection coefficient is estimated based on the equation:

$$h_v = \frac{Nu \cdot k}{l_t}$$

where Nu is Nusselt number, k is the thermal conductivity of the fluid, l_t channel length.

$$Nu = 0,012(R_e^{0,87} - 280)Pr^{0,4} \left[1 + \left(\frac{D}{L} \right)^{\frac{2}{3}} \right] \left(\frac{Pr}{Pr_w} \right)^{0,11}$$

$$Re = \frac{V \cdot D}{\nu}$$

$$V = \frac{Q}{A} = \frac{Q}{h \cdot b}$$

Re is Reynolds number, and Pr is Prandtl number ($0.7 < Pr < 100$) of the coolant, D is hydraulic

diameter, ν is the kinematic viscosity of the fluid, and $Pr/Pr_w \approx 1$ for water.

Conduction between stator, cooling jacket and housing has been calculated and modelled according to resistance network to the motorized spindle. This network specifies the resistances in conduction and convection from stator, cooling jacket, and housing. In order to have simplified equations, resistances at each contact are calculated

$$R = \frac{\ln \left(\frac{R_o}{R_i} \right)}{2 \cdot \pi \cdot l \cdot k}$$

Where R_o is outer radius, R_i is inner radius of considered element, l is element length, and k is the thermal conductivity of material. On the figure 3 conduction network has been presented and R_{kkh} is conduction resistance between cooling jacket and housing, where cooling jacket have been considered as cylinder, while R_{skh} is conduction resistance among cooling jacket and stator.

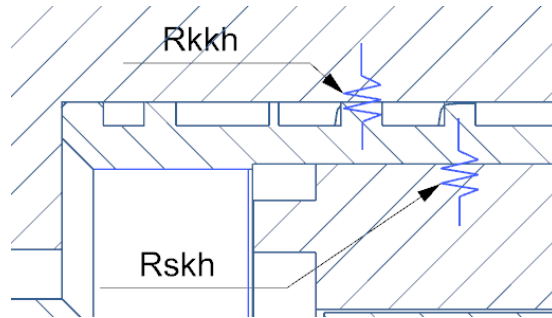


Fig. 3. Radial conduction between stator/cooling and jacket/housing

A free convection coefficient can be assumed for ambient air around a stationary surfaces like the spindle housing, and can be adopted as 12 W/mK. Aim of this analysis is mathematical model development of stator cooling jacket, and how fluid flow effect on motorized spindle. Therefore, all other heat sources, convections, radiation are constant. Thus the analysis were performed for three flows 14 l/min, 20 l/min and 28 l/min. While bearings are the most responsible for spindle operation, results will be focused on them. On the figure 4, have been showed overall temperature field, according to heat sources: front bearing $H_f=0,6188$ W, rear bearing $H_r=0,5813$ W, and motor $H_m=29,466$ W,

as well as the heat sinks in cooling jacket $H_{cj}=3523$ W.

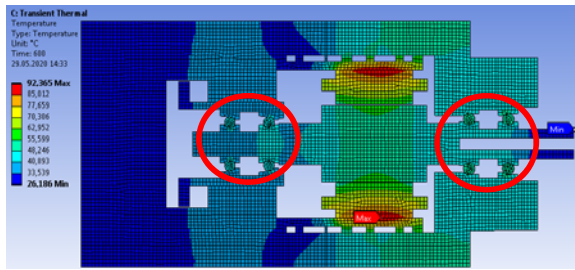


Fig. 4. Overall temperature of motorized spindle with considered zones

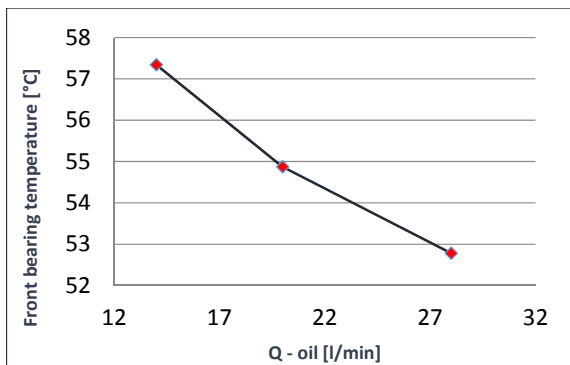


Fig. 5. Maximum temperature at front bearing varies as the fluid flow changes

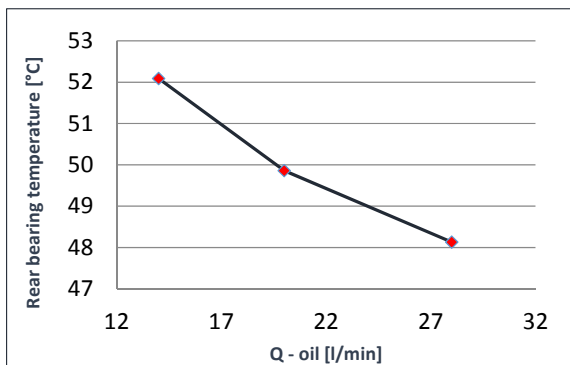


Fig. 6. Maximum temperature at rear bearing varies as the fluid flow changes

Figures 5 and 6, shows how reducing fluid flow increase temperature on bearing. Here can be seen that double reduced fluid flow increase temperature for around 4°. So there is an opportunity for optimization and find adequate fluid flow.

4. CONCLUSION

This paper discussed the mathematical model for predicting the bearings temperatures, affected by temperature generated in motor as a consequence of electric losses. Thermal model of the spindle has been created by using the finite element approach. This approach was chosen because of its major advantage, which is that heat conduction can be easily integrated with complex geometries and physical conditions, especially for any further analyses of the temperature influence on static and dynamic behaviour. On the other hand this method presents an analytic method for calculating the heat generated on the motor, based on the current parameters as well as the forced convection in cooling jacket based of fluid flow. Study showed how reducing fluid flow would increase bearing temperatures.

Acknowledgement

This research (paper) has been supported by the Ministry of Education, Science and Technological Development through the project no. 451-03-68/2020-14/200156: "Innovative scientific and artistic research from the FTS (activity) domain".

This research (paper) has been supported by the DBU – Deutsche Bundesstiftung Umwelt, An der Bornau 2, 49090 Osnabrück, Germany

REFERENCES

- [1] A. Zahedi and M. R. Movahhedy, "Thermo-mechanical modeling of high speed spindles," *Sci. Iran.*, vol. 19, no. 2, pp. 282–293, Apr. 2012, doi: 10.1016/j.scient.2012.01.004.
- [2] K. J. H. Al-Shareef and J. A. Brandon, "On the effects of variations in the design parameters on the dynamic performance of machine tool spindle-bearing systems," *Int. J. Mach. Tools Manuf.*, vol. 30, no. 3, pp. 431–445, Jan. 1990, doi: 10.1016/0890-6955(90)90187-N.
- [3] C. H. Chien and J. Y. Jang, "3-D numerical and experimental analysis of a built-in motorized high-speed spindle with helical water cooling channel," *Appl. Therm. Eng.*, vol. 28, no. 17–18, pp. 2327–2336, Dec. 2008, doi: 10.1016/j.applthermaleng.2008.01.015.
- [4] H. Li and Y. C. Shin, "Integrated Dynamic Thermo-Mechanical Modeling of High Speed Spindles, Part 1: Model Development," *J. Manuf. Sci. Eng.*, vol. 126, no. 1, pp. 148–158, Feb. 2004, doi: 10.1115/1.1644545.
- [5] L. Zhang, J. Xuan, and T. Shi, "Obtaining More Accurate Thermal Boundary Conditions of Machine Tool Spindle Using Response Surface

- Model Hybrid Artificial Bee Colony Algorithm,” *Symmetry (Basel)*, vol. 12, no. 3, p. 361, Mar. 2020, doi: 10.3390/sym12030361.
- [6] Q. Li and H. Li, “A general method for thermal error measurement and modeling in CNC machine tools’ spindle,” *Int. J. Adv. Manuf. Technol.*, vol. 103, no. 5–8, pp. 2739–2749, 2019, doi: 10.1007/s00170-019-03665-7.
- [7] K. Liu, Y. Liu, M. Sun, X. Li, and Y. Wu, “Spindle axial thermal growth modeling and compensation on CNC turning machines,” *Int. J. Adv. Manuf. Technol.*, vol. 87, no. 5–8, pp. 2285–2292, Nov. 2016, doi: 10.1007/s00170-016-8593-5.
- [8] B. Bossmanns and J. F. Tu, “A thermal model for high speed motorized spindles,” *Int. J. Mach. Tools Manuf.*, vol. 39, no. 9, pp. 1345–1366, Sep. 1999, doi: 10.1016/S0890-6955(99)00005-X.
- [9] “GMN.”
<https://www.gmn.de/en/spindles/know-how/motor-cooling/>.



Banja Luka
28-29 May 2021.

DEMI 2021

15th International Conference on Accomplishments in Mechanical and Industrial Engineering

www.demi.mf.unibl.org



Knee Prosthesis Biomaterial Selection by Using MCDM Solver

D. Petković^a, M. Madić^a, G. Radenković^a

^aFaculty of Mechanical Engineering University of Niš, A. Medvedeva 14, Niš

Abstract *Biomaterials are a special class of contemporary materials used to make prostheses, parts of organs or to replace entire organs. They are used to replace soft and hard tissues. Metal biomaterials are mostly used to replace hard bone tissues and joints. There is no ideal substitution for natural biological material, but each of the biomaterials has a number of advantages and disadvantages. The problem of choosing the most favorable biomaterial is a complex process of multi-criteria decision-making, which requires a lot of knowledge and experience. In order to help decision makers in solving this complex task, a decision support system named MCDM Solver is proposed. MCDM Solver is used in decision-making process to rank the biomaterials with respect to several criteria. In this paper, MCDM Solver was used to select knee prosthesis material.*

Keywords *Biomaterial selection, multi-criteria decision making (MCDM), MCDM Solver, decision support system, knee prosthesis*

1. INTRODUCTION

Material selection process is a complex task which needs knowledge of materials engineering, technologies, operational research and design. To select the suitable material for an application necessitates the simultaneous consideration of many conflicting and diverse criteria.

Biomaterials are commonly characterized as materials used to construct artificial organs, rehabilitation devices, or implants to replace natural body tissues [1]. Selection of an appropriate material for a given biomedical application is important from more points of view – medical, technological, and economic.

Nowadays, there is a large number of biomedical materials and manufacturing processes, each having its own properties, applications, advantages and limitations. Therefore, many difficult decisions need to be made while selecting a material for a specific biomedical implant. In order to select the most

suitable biomedical material, the decision maker should have a complete understanding of the functional requirements of the product and a detailed knowledge of the considered criteria for a specific biomedical application [2]. Unsuitable choice of a biomedical material may lead to a premature failure of the product, a need for repeated surgery, a cell death, chronic inflammation or other impairment of tissue functions as well as an extension of healing period and overall increasing of the costs [3].

Only with a systematic and structured mathematical approach the best alternative for a specific engineering product can be selected. The material selection problems with multiple non-commensurable and conflicting criteria can be efficiently solved using multi-criteria decision making (MCDM) methods. The MCDM methods have the capabilities to generate decision rules while considering relative significance of considered criteria upon which the complete ranking of alternatives is determined [4].

Decision support system (DSS) is a special class of information system oriented to the decision-making process and aims to support, mainly business decision-doing processes. DSS is a symbiosis of information systems, application of functional knowledge and ongoing decision-making process [5]. Their main goal, as the goal of other information systems, is to improve the efficiency and effectiveness of an organization. This paper is focused on the application of developed DSS named MCDM Solver for solving biomaterial selection problem. The most suitable biomaterial for femoral component of knee-joint replacement was selected by applying MCDM Solver.

2. MCDM SOLVER

MCDM Solver is an “on-line” DSS which was developed within the doctoral dissertation of Dušan Petković. The developed DSS is located on the “Virtuode” Company web site (<https://virtuodeportalapp.azurewebsites.net/>) and it is available to everyone who registers by creating an account (Fig. 1). This DSS offers the possibility of working with maximization, minimization and target criteria [6].

The input data for MCDM Solver:

- Initial matrix of decision-making with target value of criteria (**Step 1**);
- η - Confidence level of decision maker in significance of the selected criteria (where $\eta=1$ corresponds to 100% confidence level, while $\eta=0$ corresponds to a confidence level of 0);
- Pairwise significance evaluation of the selected criteria.

Based on the input data, MCDM Solver can determine the values of the criteria weights (Step 2) and ranking alternatives (Step 3) with the corresponding values by means of Extended TOPSIS [7], Comprehensive VIKOR [8] and Comprehensive WASPAS [6, 9] methods.

Developed DSS architecture is flexible and easy to upgrade, so it enables the inclusion of new models that will come in the future. *MCDM*

Corresponding author

PhD, Dušan Petković
dusan.petkovic@masfak.ni.ac.rs

Faculty of Mechanical Engineering of Niš
 Aleksandra Medvedeva 14
 Niš, Serbia

Solver has a user-friendly interface, which enables a simple and efficient way of entering the necessary data [10]. Its use simplifies the solution of the MCDM problems, especially material selection problems, because it does not require expert knowledge from the decision making theory from the user.



Fig. 1. MCDM Solver – initial layout

3. BIOMATERIAL SELECTION FOR TOTAL KNEE REPLACEMENT

Knee prostheses are implanted in the human body to relieve pain and restore form and function. A total knee replacement is shown in Fig. 2. In order to match the performance of a natural knee, the materials of prosthesis are required to have several specific properties with values approaching those of natural biological materials (bone and tissue).

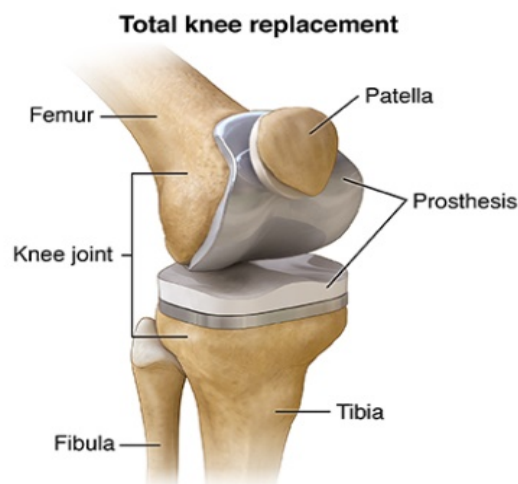


Fig. 2. Main components of a total knee replacement

In this study, 15 metallic biomaterials (biologically comparative materials) that are currently used and could be used for the femoral component of knee-joint implants are

considered as candidate materials [4, 11, 12]. Biomaterials which considered as alternatives include stainless steels (SS), Co-Cr alloys, titanium and titanium alloys as listed in Table 1 [6, 13]. It shows commercial names, state and standards which define quality of these materials.

For any knee implant to be successful it needs to have high strength, biocompatibility, wear and corrosion resistance, durability, and machinability. In addition, elastic modulus and density should be near to the bone values in order to minimize stress-shielding effect. Finally, material cost is criterion of the smallest, but not negligible significance for knee replacement biomaterial selection.

Table 1. List of potential biomaterials for knee replacement

Material	Commercial name	State
M1	BioDur® 316LS Stainless	Annealed
M2	Carpenter 22Cr-13Ni-5Mn	Annealed
M3	BioDur® 108 Alloy	Annealed
M4	BioDur® 734 Stainless	Annealed
M5	BioDur® Carpenter CCM® Alloy	Annealed
M6	BioDur® CCM Plus® Alloy	Annealed at 1093 °C/1 h
M7	Micro-Melt® BioDur® Carpenter CCM® alloy	Annealed at 1093 °C/30 minutes
M8	Carpenter MP35N Alloy	35 % deformed and aged at 538 °C/4 h
M9	Carpenter L-605 Alloy	Annealed at 1204 °C
M10	CP Titanium Grade 4	Annealed
M11	Titanium Alloy Ti 6Al-4V ELI	Recrystallized Annealed
M12	Protasul 100, (Ti-6Al-7Nb)	Annealed 700 °C/1 h
M13	Ti-5Al-2.5Fe	Centrifugal casted
M14	ATI Allvac® Titanium alloy	Annealed na 704 °C
M15	Ti-15Mo-5Zr	Quenched

The considered material property criteria are:

- Yield strength (C1);

- Tensile strength (C2);
- Elongation (C3);
- Elastic modulus (C4);
- Density (C5);
- Corrosion resistance (C6);
- Biocompatibility (C7);
- Machinability (C8);
- Hardness (C9);
- Cost (C10).

The criteria such as corrosion resistance, biocompatibility and machinability initially are defined by using linguistic terms. An 11-point scale is used for better understanding and representation of the qualitative attributes and converting linguistic terms into corresponding dimensionless numbers [6], as shown in Table 2.

Table 2. Qualitative criteria and conversion values in format of 11-point scale

Qualitative measure of material selection factor assigned	Value
Exceptionally low	0.045
Extremely low	0.135
Very low	0.255
Low	0.335
Below average	0.410
Average	0.500
Above average	0.590
High	0.665
Very high	0.745
Extremely high	0.865
Exceptionally high	0.955

4. RESULTS AND DISCUSSION

Based on the input data, i.e. initial decision matrix, confidence level $\eta=1$ and pairwise significance evaluation of the criteria, weights of the criteria are determined (shown in Fig 3).

Calculate weights

The screenshot shows a software interface for calculating weights. At the top left, there is a text input field for $\eta = 1$ and a label $\eta \in [0.0 - 1.0]$. Below this is a grid of criteria comparison options. The criteria listed are C1 (MPa), C2 (MPa), C3 (%), C4 (GPa), C5 (g/cm³), C6, C7, C8, C9 (HV), and C10 (€/kg). Each criterion is paired with a comparison operator: '=', '>', '<', '>=', '<=', or '<'. A blue 'Calculate' button is located to the right of the comparison grid.

MCDM Solver calculation of the subjective weights (confidence level $\eta=1$) of criteria were carried out based on modified digital logic (MDL) method [14]. This is a pair-wise comparison method, where participants/criteria are presented with a worksheet and asked to compare the importance of two criteria at a time (Fig 3). Thereby hardness (C9) biocompatibility (C7) and corrosion resistance (C6), are considered as the most influential criteria with weights of 0.144, 0.139 and 0.133, respectively. Criteria such as elongation (C3), elastic modulus (C4) and density (C5) are equally influential with weights of 0.094. The cost and machinability are the least influential criteria with weights of 0.055 and 0.061, respectively.

Fig. 3. Pairwise significance evaluation of the criteria

Table 3. Initial decision matrix for for knee replacement biomaterial selection

Biomaterial	C1 (MPa)	C2 (MPa)	C3 (%)	C4 (GPa)	C5 (g/cm ³)	C6	C7	C8	C9 (HV)	C10 (€/kg)
M1	250	585	57	193	7.95	0.41	0.59	0.865	174	3.8
M2	450	825	45	193	7.86	0.5	0.59	0.865	225	5
M3	580	930	52	200	7.64	0.5	0.745	0.865	304	1.6
M4	450	840	39	195	7.75	0.5	0.59	0.865	270	4.2
M5	585	1.035	25	241	8.28	0.745	0.745	0.335	304	35
M6	880	1.35	22	241	8.28	0.745	0.745	0.41	410	37
M7	1.115	1.42	28	241	8.29	0.745	0.745	0.335	455	140
M8	1.34	1.4	21	235	8.43	0.665	0.59	0.255	425	60
M9	415	1.035	60	243	9.22	0.665	0.665	0.335	155	58
M10	550	670	22	103	4.51	0.955	0.955	0.5	280	21
M11	710	880	12	105	4.43	0.865	0.865	0.41	304	29
M12	850	950	12	105	4.52	0.955	0.955	0.41	318	25
M13	820	900	6	112	4.45	0.865	0.955	0.41	260	26
M14	570	690	15	103	4.48	0.865	0.865	0.5	278	26.5
M15	920	960	25	78	5.06	0.865	0.865	0.41	280	31
Target value	1340	1420	60	16	1.3	0.955	0.955	0.865	455	1.6
Criteria weights	0.1	0.089	0.094	0.094	0.094	0.133	0.139	0.061	0.144	0.055

The Step 3 is the ranking of the biomaterials by means of MCDM Solver. Ranking orders of biomaterials for femoral component of the hip prosthesis using different MCDM methods (TOPSIS, WASPAS and VIKOR) are shown in Fig.

4. In order to make ranking results clearer and more readable, they are also shown in Table 4. As could be seen, the best ranked biomaterial is M12, while the M10 is the second ranked biomaterial.

The ranking results also show that Ti-alloys are the most suitable materials for this biomedical application, while stainless steels and Co-Cr alloys are less preferable alternative.



Fig. 4. Ranking results

Ranked results indicate unambiguously that Ti-6Al-7Nb (Commercial name Protasul 100) is the most preferable material for the total knee replacement. The second ranked biomaterial is pure Ti which seems to be excellent biomaterial, but not to be suitable for this application due to its poor tribological properties.

Table 4. Ranking results obtained by using MCDM Solver

Biomaterial	Class	TOPSIS	WASPAS	VIKOR
M1	SS	15	13	13
M2	SS	14	11	12
M3	SS	9	4	10
M4	SS	13	10	11
M5	Co-Cr alloys	10	12	9
M6	Co-Cr alloys	8	9	6
M7	Co-Cr alloys	6	8	5
M8	Co-Cr alloys	11	15	15
M9	Co-Cr alloys	12	14	14
M10	Ti	2	3	2
M11	Ti-alloy	4	5	3
M12	Ti-alloy	1	2	1
M13	Ti-alloy	5	7	7
M14	Ti-alloy	7	6	8
M15	Ti-alloy	3	1	4

It is also interesting that there is total matching of the TOPSIS and VIKOR results for the first and second ranked biomaterials (M12 and

M10). On the other hand, WASPAS and VIKOR the last three ranking results are totally matched (M1, M9 and M8).

5. CONCLUSION

In this paper, the application of developed DSS named MCDM Solver for solving biomaterial selection problem is considered. Thanks to MCDM Solver, the material selection process is carried out much faster and easier, because it comes down to selection of potential materials and pairwise significance evaluation of the selected criteria. Hence a complex mathematical apparatus is avoided and ranking process is faster, comfortable to work and reliable.

Ranked results showed that Ti-6Al-7Nb alloy is the most preferable biomaterials for the femoral component of knee prosthesis. The results also proved that stainless steels and Co-Cr alloys are not good biomaterial selection for knee prosthesis.

Acknowledgement

This research was financially supported by the Ministry of Education, Science and Technological Development of the Republic of Serbia.

REFERENCES

- [1] Petković D., Radenković G., Mitković M. (2012). Fractographic investigation of failure in stainless steel orthopedic plates. *Facta Universitatis: Series Mechanical engineering*, vol. 10 pp. 7–14.
- [2] Chatterjee P. et al. (2009) "Selection of materials using compromise ranking and outranking methods. *Materials and Design*, vol. 30, pp. 4043–4053.
- [3] D. Petković et al. Decision Support System for Selection of the Most Suitable Biomedical Material. *Proceeding of 5th International Conference on Information Society and Technology ICIST 2015*, March 2015, Kopaonik, p. 28-31.
- [4] Jahan A., Edwards K. L., Multi-criteria Decision Analysis for Supporting the Selection of Engineering Materials in Product Design, Butterworth-Heinemann, 2013.
- [5] Čupić M., Tummala R., Suknović M. (2001). *Odlučivanje - formalni pristup*. Fakultet organizacionih nauka, Beograd.

- [6] Petković D. (2017). Selection of biomaterials - Multi-criteria decision analysis and development of decision support system. (In Serbian). PhD dissertation. University of Niš, Faculty of Mechanical Engineering.
- [7] Jahan A., Bahraminasab M., Edwards K.L. (2012). A target-based normalization technique for materials selection. *Materials and Design*, vol. 35, pp. 647-654.
- [8] Jahan A., Mustapha F., Ismail M.Y., Sapuan S.M., Bahraminasab M. (2011). A comprehensive VIKOR method for material selection. *Materials and Design*, vol. 32, pp. 1215-1221.
- [9] Petković D., Madić M., Radenković G. (2015). Ranking of Biomedical Materials by Using Comprehensive WASPAS Method. *Proceedings of MASING 2015*, September 2015, Faculty of Mechanical Engineering of Niš, p. 339-344, Niš.
- [10] Petković D., Madić M., Radenković G. (2020). Decision Support System for Biomaterial Selection, *Proceedings of MASING 2020*. December 2020, Faculty of Mechanical Engineering of Niš, p. 283-286.
- [11] Bahraminasab M., Jahan A. (2011). Material selection for femoral component of total knee replacement using comprehensive VIKOR. *Materials & Design*, vol. 32, pp. 4471-4478.
- [12] Jahan A. et al. (2013). VIKOR method for material selection problems with interval numbers and target-based criteria. *Materials & Design*, vol. 47, pp. 759-765.
- [13] Chen Q., Thouas G.A. (2015). Metallic implant biomaterials. *Materials Science and Engineering R*, vol. 87, pp. 1-57.
- [14] Dehghan-Manshadi B., Mahmudi H., Abedian A., Mahmudi R. (2007). A novel method for materials selection in mechanical design: combination of non-linear normalization and a modified digital logic method. *Materials & Design*, vol. 28, pp. 8-15.



Banja Luka
28–29 May 2021.

DEMI 2021

15th International Conference on Accomplishments in Mechanical and Industrial Engineering

www.demi.mf.unibl.org



An open architecture control system for multi-axis wood CNC machining center

S. Živanović^a, Z. Dimić^b, A. Rakić^b, M. Knežević^c, S. Mitrović^b

^aUniversity of Belgrade, Faculty of Mechanical Engineering, Serbia

^bLOLA Institute, Belgrade, Serbia

^cTechnical School, Gradiska, Serb Republic

Abstract This paper presents an open architecture control system for multi-axis wood computer numerical control (CNC) milling machining centre, based on LinuxCNC. The wood CNC machining system is supported by an equivalent virtual machine in a CAD/CAM environment, as well as in the control system. Simulation within virtual environment is essential for multi-axis machining, and the developed virtual machines are used for program verification and monitoring of the machining process. The virtual machine in the programming system allows the verification of the program before it's sent to the actual machine, while the virtual machine in the control system represents the final verification of the program, as well as the process monitoring system. Configuration of the control system and implementation of virtual machines will be shown, along with the conducted machining experiments that ensued after the successful simulation on developed virtual machines.

Keywords virtual machine, programming, wood CNC machine tool, CAD/CAM

1. INTRODUCTION

Modern CNC systems are developed with the end-user in mind, where implemented designs emphasize the ease of use, customizability and extensibility. However, CNC machine tools' expensive hardware (base structure, linear and rotary guides, servo drives, servos, hydraulics, etc.) frequently outlives the provided software that is essential for the proper machine utilization. The end result leads to machines that are physically in working condition, but are rendered useless by the outdated software. New, commercially available CNC units end up costing more than the actual machine tool's worth and/or do not facilitate the necessary

functions that are specific for the machine tool at hand. To overcome these issues, a solution may be found in the open-architecture domain, where one of the most commonly applied ones is LinuxCNC [1].

As the authors have plenty of experience in configuring, modifying, and implementing LinuxCNC on various machine tools and robots [2-8], the development and implementation of a control system for a multi-axis wood machining centre was just a sequel.

This paper presents sequences in the development and configuration of a control system for a multi-axis wood machine tool, utilizing virtual commissioning. In order to cover all aspects of using open-architecture software tools, the paper is organised into six sections, including the Introduction. Section 2 shows the details of the multi-axis wood CNC machining centre, with an emphasis on machine structure and its kinematic complexity as the main drivers behind our open-architecture

Corresponding author

Dr Zoran Dimic, zoran.dimic@li.rs
corresponding author's e-mail

Lola Institute, Kneza Viseslava 70A, 11030 Belgrade, Serbia

approach. As the most important part of control system development by virtual commissioning methodology, section 3 covers the development of the virtual multi-axis wood CNC machining centre. Configuration of virtual machines in the CAD/CAM system is shown together with corresponding control and programming systems. Structure of LinuxCNC as a software tool for control system development is briefly presented in section 4. Necessary steps in development and configuration of control systems based on LinuxCNC are given in the same chapter. Proof of machine tool functionalities with the newly developed control system is presented in section 5. Concluding remarks are given in section 6.

2. MULTI AXIS WOOD CNC MACHINING CENTER

The multi-axis wood CNC machining centre considered in this paper is a vertical milling machine tool with complex kinematics in Y'(V)OXZBA spindle-tilting arrangement, Fig. 1a.

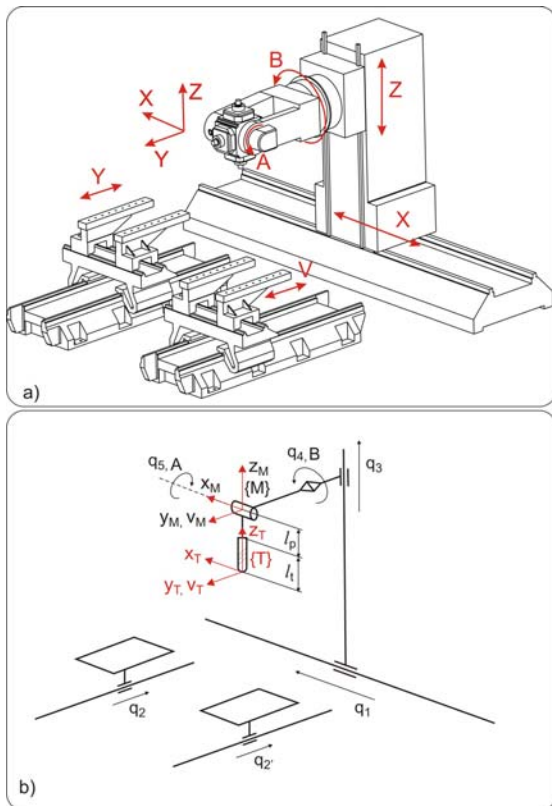


Fig. 1. Multi-axis wood CNC machining center Bacci MX6

The machine is equipped with two work tables which enable setting up the workpiece on one, while the other is used in operation. Alternatively, the two tables can be connected kinematically in order to better utilize the available workspace. Aforementioned table strategies are implemented as user-switchable through the open-architecture software extension. The existence of two work tables is “omitted” in order to solve the kinematic equations for machine tool from the previous figure [2].

The kinematic model of the machine’s mechanism is shown in Fig. 1b. Coordinate reference frame (M) and the coordinate tool frame (T) are attached to the pivot, and the tooltip, as well as joint coordinates $q = [q_1, q_2, q_2', q_3, q_4, q_5]$ and the world coordinates ${}^M = [x_T, y_T, z_T, A_T, B_T]$. The inverse kinematic solutions for both worktables are:

$$\begin{aligned} x_T &= q_1 - (l_p + l_t) \sin q_4 \cos q_5 \\ y_T &= q_2 + (l_p + l_t) \sin q_5 \\ y_T &= q_2' + (l_p + l_t) \sin q_5 \\ z_T &= q_3 - (l_p + l_t) \cos q_4 \cos q_5 \\ A_T &= q_5 \\ B_T &= q_4 \end{aligned} \quad (1)$$

where coordinates x_T, y_T, z_T and angles A_T, B_T determine tool position and orientation in the Cartesian coordinate system. Pivot length and tool length are designated as l_p and l_t , respectively.

The direct kinematic solutions were derived as shown in the next equations:

$$\begin{aligned} q_1 &= x_T - (l_p + l_t) \sin B_T \cos A_T \\ q_2 &= y_T + (l_p + l_t) \sin A_T \\ q_2' &= y_T + (l_p + l_t) \sin A_T \\ q_3 &= z_T - (l_p + l_t) \cos B_T \cos A_T \\ q_4 &= B_T \\ q_5 &= A_T \end{aligned} \quad (2)$$

where $q_i, i=1,2,\dots,5$ and q_2' are scalar joint variables controlled by the actuators.

3. VIRTUAL MACHINE CONFIGURATION

Programming of wood CNC machining is conventional, similar to any other milling or drilling CNC operation. Originally, specialized CAD/CAM software PITAGORA [1] was used for programming of the considered Bacci machine tool. This approach required the adoption of

non-standard axes directions and kinematics. Implementation of a new control system enabled the adoption of a standard kinematic model, making it possible to utilize widely available CAD/CAM systems.

One of the established systems for programming and verification of NC programs for wood CNC machining centre is shown in section 4. The CAD model of a workpiece is the basis for tool path generation, stored in CLF (Cutter Location File) format. The CAD/CAM system PTC Creo is used as a programming system.

Generated tool path can be checked in three ways:

- tool path simulation,
- material removal simulation (NC Check),
- machine simulation, according to CLF.

After successful verification of the tool path, the program is postprocessed and the resulting G code is sent to the machine for the execution.

3.1 Virtual machine in programming system

The configured virtual wood CNC machining centre is used to simulate the tool path generated in the CAD/CAM system.

Virtual machine simulation is crucial for the following reasons [1]: (i) programming environment configuration, including virtual machine; (ii) NC program verification prior to machining, and (iii) collision detection, essential for 5 axis machining.

CLF-based machine simulation is enabled through specifying kinematics that are utilized on the virtual model of the machine within the CAD/CAM environment. This allows a virtual machine model to function like a system of rigid bodies [4,5,7,8].

The kinematic model generation required applying slider type links for all translational axes (X, Y, and Z) and cylinder links for two rotational axes (B and A). The corresponding movement limits are defined for each axis [1].

To start the machine simulation, it is necessary to define the coordinate system of the workpiece (MACH_ZERO) and the coordinate system of the tool (TOOL_POINT). These coordinate systems connect the coordinate systems of the workpiece and the tool with corresponding coordinate systems on the virtual machine.

Matching these coordinate systems enables the setting of the workpiece on the configured

virtual machine and setting the tool at the head of the main spindle on the virtual machine during simulation.

A single chair machining strategy (Fig. 2a) is given as an example in order to demonstrate the programming and simulation capabilities of our developed system.

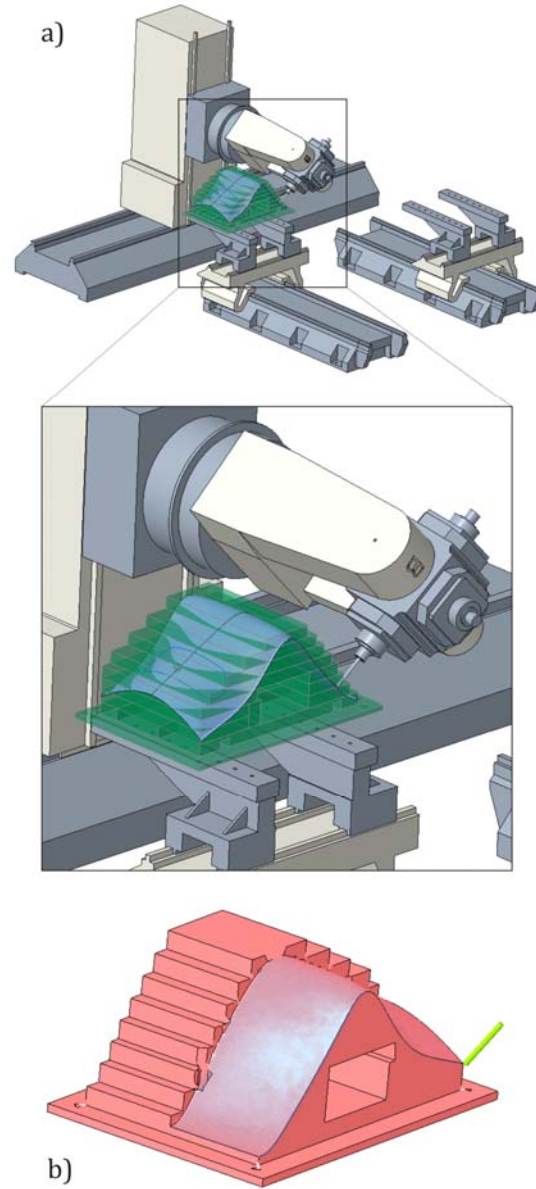


Fig. 2. Programme verification through virtual machining

A surface milling strategy was applied for the machining of the chair's shape. After generating the tool path for five-axis machining, material removal simulation was performed in order to verify the tool path. An example of a material removal simulation is shown in Fig.2b. Result of

the simulation (the virtual workpiece) helps determine the accuracy of future machining by comparison with the standard CAD model of the workpiece. The tool path verification was followed by post-processing and obtaining the G code ready for transfer to the control unit. The obtained G code is finally verified on a virtual machine integrated with the real machine control system, shown in Chapter 4.2.

4.2 Virtual machine in the control system

The virtual machine has a significant role when developing a control system for a machine with complex kinematics. Considering all safety precautions necessary for testing of the kinematic functions intended for real machine, virtual commissioning [9,10] proves priceless during development. Our approach implies error-driven development without safety issues. Virtual machines are also significant during machine tool exploitation. Machining program verification by virtual machining is a crucial task on multi-axis machine tools which allows:

- visual detection of collisions between the moving parts of the machine and between the tool, workpieces and fixtures;
- checking if the machine can execute the specified tool path within the limited motions, ranges, and speeds.

Virtual machine development under the LinuxCNC software environment relies on OpenGL and several interface classes written in Python programming language [6]. Python is an interpreted programming language, with a gentle learning curve, suitable for scripting tasks, such as development and configuration of virtual environments. The basic concept of a virtual machine configuration is shown in Fig. 3. Here, models of machine components were imported in ASCII STL format and connected according to the established kinematic model via rotational or translational joints. The ASCII STL files of the machine components were obtained from the CAD environment of the PTC Creo.

After the virtual machine is configured, it is integrated within the control system. During the execution of the machining program, the virtual machine components are moving in real-time, fully synchronized with the moving parts of the real machine [2], which was confirmed by machining experiments.

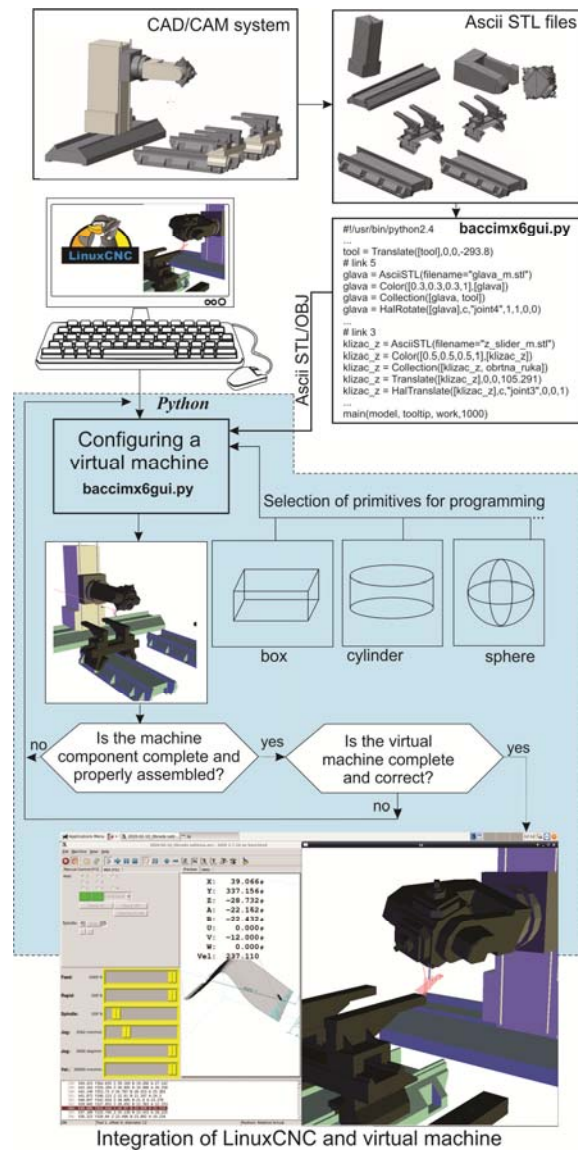


Fig. 3. Configuring virtual machine in control system

4. PROGRAMMING AND CONTROL SYSTEM BASED ON LINUXCNC

During the development of the control and programming system for the multi-axis machining centre, the main objective was to enable the use of standard CAD/CAM systems to generate a machining program.

Using expensive postprocessors for this machine was not an option. Thus, all non-standard and complex functionalities of the machine had to be encapsulated in term of object-oriented programming.

The solution lies in complex switchable kinematic functions, developed machine cycles and intuitive graphical interfaces. After all development effort, end-user can generate a machining program using standard CAD/CAM system such as PTC Creo, CATIA or similar, choosing one among multiple generic postprocessors, Fig. 4.

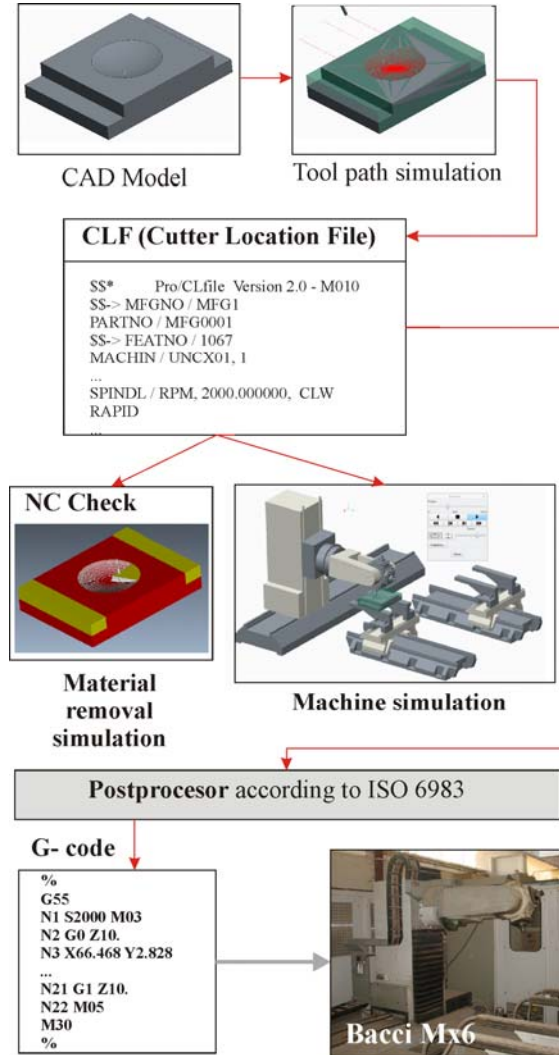


Fig. 4. Programming system

The CAD model of a workpiece is the base for tool path generation. In this study, CAD/CAM system PTC Creo is used to generate a cutter location file (CLF). Generated tool path is tested through the NC Check (material removal simulation) software module, followed by the G-code generation. Postprocessing for the vertical 5-axis milling machines, configured for AB spindle-tilting type, is used to obtain the

machining program. The CAD/CAM system PTC Creo can perform a verification of the obtained programs through virtual simulation. In order to configure LinuxCNC for motion control of the machining centre, as well as control of all the sequential processes that enable axis initialisation, tool change, etc., some development steps had to be made. The key part was coding and testing switchable kinematic functions. Using remappable M functions, M200, M201 and M202, kinematics switchability [2] is achieved as shown in Fig. 5.

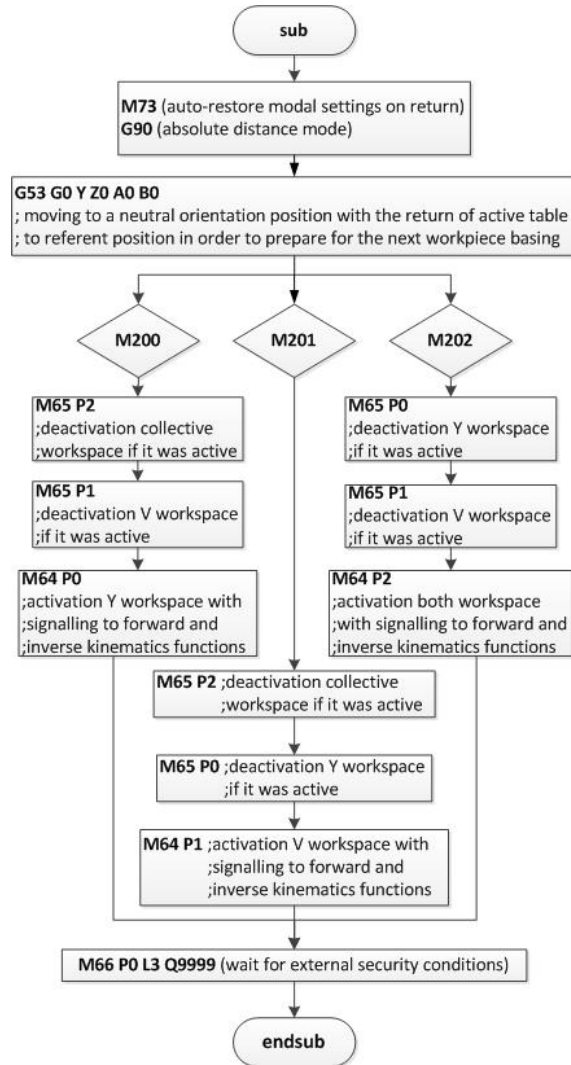


Fig. 5. Customized M functions

After getting a virtual machine environment, which is depicted in the next section in detail, kinematic functions are implemented in the control system. During the test procedure, control signals intended for real machine tool are connected to the virtual machine. That way,

test procedures are carried out safely without real machine involvement and the possibility of collisions and damages.

5. MACHINING EXPERIMENTS

Machining experiments were conducted on wood, with respect to production demands of the corresponding industry. Before machining, the programs' tool paths were simulated in LinuxCNC and the virtual machine that's integrated with the control system.

The first test was a 5-axis machining of a concave calotte (Fig. 6), for which an example of programming and simulation in a CAD/CAM environment is shown in Fig. 4.



Fig. 6. 5-axis machining of a concave calotte

The second test was a 5-axis machining of a mould for chair production, with significant immediate finishing-pass surface machining, Fig.7. In this case, virtual machine simulation is essential, providing the collision avoidance mechanism, which detects errors in the workpiece set up and possible collisions of

machine parts with the workpiece during machining.

The realized examples have shown that the established kinematic model of the machine and the developed control system, including an adequate environment for programming and program verification, are well-based and ready for industrial applications.

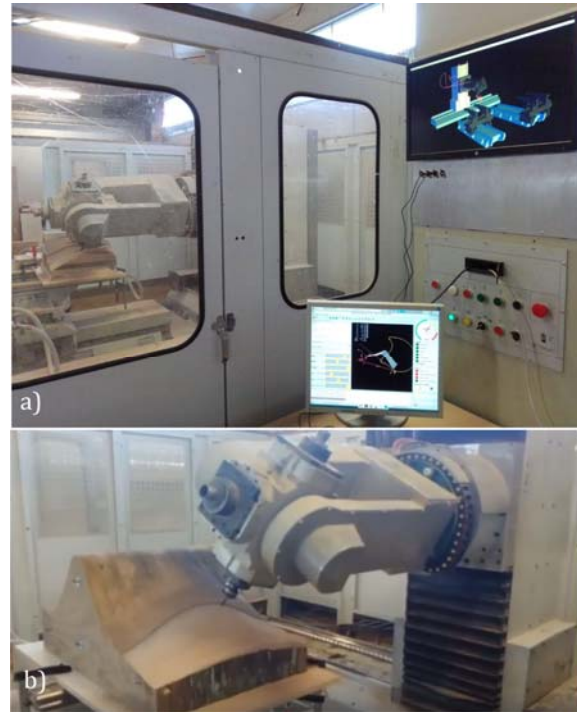


Fig. 7. 5-axis machining a mould for chair production

6. CONCLUSION

This paper presented a methodology for development and configuration of a control system for a multi-axis wood machine tool through virtual commissioning. During the development of the physical machine tool's control system, virtual machines were used for algorithms' testing, an important step for the validation of the new controller's functions.

The developed control system is low-cost and easy to setup, which is especially suitable for retrofit and modernization of older machine tools. The open architecture software is suitable for the development of complex kinematics functions for multi-axis machine tools. Due to the modularity, flexibility, openness, and availability, the proposed system is convenient for machine tools with specific reconfigurable kinematic structures and unique functionalities.

Directions for further research may relate to increasing the functionality of the control system in the field of monitoring and diagnostics, as well as further improving the methods of programming and verification of machining programs.

Acknowledgement

The presented research was supported by the Ministry of Education, Science and Technological Development of the Republic of Serbia by contract no. 451-03-9/2021-14/200105 dated 5 February 2021 and by contract 451-03-9/2021-14/200066 dated 28 January 2021.

REFERENCES

- [1] Linux CNC. From: <http://linuxcnc.org/>, accessed on: February 08, 2021.
- [2] Rakic, A., Zivanovic, S., Dimic, Z., Knezevic, M., (2021). Digital twin control of multi-axis wood CNC machining center based on LinuxCNC. *BioResources*, vol. 16, no. 1, p.1115-1130. DOI: 10.15376/biores.16.1.1115-1130
- [3] Zivanovic, S., Glavonjic, M., Milutinovic, D. (2015). Configuring A Mini-Laboratory and Desktop 3-Axis Parallel Kinematic Milling Machine. *Strojniški vestnik - Journal of Mechanical Engineering*, vol.61, no.1, p. 33-42, DOI:10.5545/sv-jme.2013.1619.
- [4] Zivanovic, S., Tabakovic, S., Zeljkovic, M., Milojevic, Z. (2016). Configuring a machine tool based on hybrid O-X glide mechanism, *Machine Design* vol.8, no.4, p.141-148.
- [5] Glavonjic, M., Milutinovic, D., Zivanovic, S., Dimic, Z., Kvirgic, V. (2010). Desktop 3-axis parallel kinematic milling machine, *International Journal of Advanced Manufacturing Technology*, vol.46, p. 51-60 DOI: 10.1007/s00170-009-2070-3.
- [6] Dimic Z., Milutinovic, D., Zivanovic, S., Kvirgic, V. (2016). Virtual environment in control and programming system for reconfigurable machining robot, *Technical Gazette*, vol. 23, no. 6, p. 1821-1829, DOI: 10.17559/TV-20150210133556.
- [7] Zivanovic, S., Dimic, Z., Vorkapic, N., Mitrovic, S. (2019). Configuring of 3 axis mini CNC machine tool with control system based on LINUXCNC, 14th International Conference on Accomplishments in Mechanical and Industrial Engineering DEMI 2019 Conference Proceedings, p. 15-28.
- [8] Živanović, S., Glavonjić, M., Milutinović, D. (2015). Configuring a mini laboratory and desktop 3-axis parallel kinematic milling machine. *Strojniški Vestnik*, vol.61, no. 1, p. 33-42. DOI: 10.5545/sv-jme.2013.1619
- [9] Hoffmann, P., Schumann, R., Maksoud, T. M. A., and Premier, G. C. Virtual commissioning of manufacturing systems: a review and new approaches for simplification. *Proceedings of the 24th European Conference on Modelling and Simulation*, June 2010, Kuala Lumpur, Malaysia, p. 175-181.
- [10] Lee, C. G., and Park, S. C. (2014). Survey on the virtual commissioning of manufacturing systems. *Journal of Computational Design and Engineerin*, vol. 1, no. 3, p.213-222. DOI: 10.7315/JCED.2014.021

Energetics and Thermal Engineering



Banja Luka
28–29 May 2021.

DEMI 2021

15th International Conference on
Accomplishments in Mechanical and
Industrial Engineering

www.demi.mf.unibl.org



Monitoring of Thermal Stresses of Hot Water Boiler Tube Plate in regime of starting up

Dragoljub Živković^a, Milena Rajić^a, Milan Banić^a, Marko Mančić^a

^a Faculty of Mechanical Engineering, University of Niš, Address: Aleksandra Medvedeva 14, Niš, Serbia

Abstract Hot water boiler structure is exposed to high pressure and temperature during its operational life. Safe and reliable operation of hot water boiler is limited by thermal constraints of its structure. High thermal stresses occur during the regular operation, especially in boiler elements with thick walls. The highest stress field is present during the non-stationary operating regimes such as starting-up, changing operating load or sudden shutdown, when it may be caused due to protection system when permitted parameters are exceeded. These conditions lead to uneven heating or cooling of the boiler structure, with high temperature gradients causing high thermal stresses. This paper presents the results of experimental analysis of the hot water boiler during the process of start-up. The aim was to verify the numerical model of hot water boiler and to monitor the state of the highest thermal stresses of the boiler structure. The analysis focused on the tube plate, the element with the thickest wall and where the major breakdowns occur. Paper presents the experimental and numerical results of the analysis of hot water boiler in regime of starting-up.

Keywords hot water boiler, start up, thermal stresses

1. INTRODUCTION

The operating characteristics of hot water boilers are clearly defined by standards and norms [1]. The hot water boiler elements are designed and built in accordance with the requirements of the Standard for pressure vessels [2] and these elements are subjected to subsequent control. The boiler elements are exposed to high pressures and temperatures of the working medium (water and/or steam) so that the manoeuvring characteristics are limited by thermal stresses in certain parts of the boiler structure. The highest thermal stresses occur in

non-stationary operating modes.

It is important to emphasize that the process of starting up the boiler represents one of the most critical transient modes of the boiler plant. Cwynar specifically presented in [3] this operational mode for steam boilers and the method of determining the critical parameters that characterize the boiler operation in the transient modes. Taler [4] presented an optimized procedure of starting up the steam boiler, but with taking into account the thermal stresses in the critical elements of the boiler. Analysis [4-9] are done according to the limitations and recommendations defined by the Standard [2]. However, the structural numerical analysis, which was done using the finite element method, showed that there are certain deviations of stress-strain values from the recommended ones defined by [2], especially in boiler elements with openings

Corresponding author

dr Milena Rajić
milena.rajic@masfak.ni.ac.rs

Faculty of Mechanical Engineering, University of Niš,
Address: Aleksandra Medvedeva 14, Niš, Serbia

[10]. These results indicate the existence of certain limitation in the current standards and possibility to check different stress-strain states. In this way, it is possible to influence to the revision of current standards in order to make safer and more reliable operation of such plants.

In [10], Dzierwa specifically analysed the stress state of critical elements of the steam boiler in the regime of starting up. Results showed that there is stress concentration in those parts of the boiler structure where there is a sudden change in the geometry of the element, such as openings, holes, curves. Having that in mind, Taler and Dzierwa analysed [11,12] the stress-strain state of the steam boiler plant elements with complex geometry in the regimes of starting up and sudden abrupt stop of the boiler, as two critical regimes.

The boilers' experience during operation indicates the failures as a consequence of breakdowns in certain parts of the boiler elements. Such failures may be caused by corrosion process, as well as inadequate handling of the plant, but also by the occurrence of material fatigue of those boiler elements that are exposed to high pressures and temperatures [13]. An overview of emergency conditions and their classification is given in [13] in both steam and hot water boilers plants. Based on the presented analysis, critical elements of hot water boilers can be observed, which need to be analyzed separately and the conditions under which accidents occur can be determined.

Transient operational regimes are considered to be non-stationary. They have not only the load change, but also the stress state change of the structure. This is especially evident when there is sudden load change, change of operational modes, start of the boiler or sudden abrupt stoppage due to accidents or necessary interventions. In such cases, the large temperature gradients exist in the boiler elements, which cause the appearance of thermal stresses that are dominant and much higher than the stresses caused by high pressures of the working fluid [14-15]. These transient regimes are specifically analysed in this paper.

One of the most critical transient operational regime is considered to be the process of starting-up the boiler, when there are high thermal stresses in the boiler elements. Thermal stresses represent a consequence of

the resulting temperature differences in the boiler structure, due to the high temperature gradients of the combustion products during the process of starting-up the boiler and low temperatures of the structure itself. Thermal stresses are especially high in boiler elements with a large wall thickness [5-7]. The thermal stresses of the tube plate of the first reversing chamber are considered to be of the great importance, where the major failures had been occurring [8-23] and where the largest temperatures differences appear.

In this paper the numerical and experimental results of hot water boiler in the regime of starting-up is presented. Thermal stresses of boiler's structure were monitored in the transient regime of starting up.

2. DYNAMIC PROBLEM OF THERMOELASTICITY

The regime of starting up the boiler presents the complex dynamic problem of thermoelasticity of its structure. When setting up a mathematical model for thermoelasticity problems, it is necessary to define the constitutive equations of thermoelasticity [24-25]:

$$\{\epsilon\} = [D]^{-1}\{\sigma\} + \{\alpha\}\Delta T \quad (1)$$

$$S = \{\alpha\}^T \{\sigma\} + \frac{\rho Q_0}{T_0} \Delta T \quad (2)$$

Where: $\{\epsilon\}$ - total strain tensor (Cauchy strain tensor); $[D]^{-1}$ - elasticity matrix; $\{\sigma\}$ - tensor determined by Hooke's law for an ideal elastic body as $\{\sigma\} = [D]\{\epsilon^e\}$; $\{\epsilon^e\}$ - elastic strain tensor; $\{\alpha\}$ - tensor of the coefficient of the linear thermal expansion; $\Delta T = T - T_{ref}$ where T - temperature for which the value of relative deformation is required and T_{ref} - reference temperature at which the relative deformation in all directions is equal to 0; S - entropy, where $Q = T_0 S$ and T_0 - absolute reference temperature.

Using the total strain tensor $\{\epsilon\} = [\epsilon_{11} \epsilon_{22} \epsilon_{33} \epsilon_{12} \epsilon_{13} \epsilon_{23}]^T$ and temperature change ΔT as independently variables and replacing entropy S with the amount of heat Q according to the second law of thermodynamics for return processes in the eq.(2) is obtained:

$$\{\sigma\} = [D]\{\epsilon\} - \{\theta\}\Delta T \quad (3)$$

$$Q = T_0 \{\theta\}^T \{\epsilon\} + \rho C_v \Delta T \quad (4)$$

Where: $\{\theta\}$ - thermoelastic coefficient vector $\{\theta\} = [D] \cdot \{\alpha\}$; C_v - specific heat capacity at

constant deformation or volume

$$C_p = C_p - \frac{E}{\rho} (\alpha)^T \cdot (\theta)$$

Substituting Q from eq.(4) into the equation of conservation of thermal energy according to the first law of thermodynamics, where it refers to the differential control volume given in eq. (5) it is obtain eq.(6):

$$\rho c \left(\frac{\partial T}{\partial t} + (v)^T (\nabla) T \right) + (\nabla)^T (q) = \dot{q} \quad (5)$$

$$\frac{\partial Q}{\partial t} = T_0 (\theta)^T \frac{\partial (\alpha)}{\partial t} + \rho C_p \frac{\partial (T)}{\partial t} - [K] \nabla^2 T \quad (6)$$

Where: (∇) - vector operator; (v) - heat transfer velocity vector; (q) - heat flux vector; \dot{q} - rate of thermal energy generation per unit volume; $[K]$ - thermal conductivity matrix.

In static and transient thermoelasticity analyses, the instantaneous total stress energy of an element (for FEA-finite element analysis) is calculated as:

$$U_T = \frac{1}{2} \int_V (\sigma)^T (\epsilon) dV \quad (7)$$

The most general case of the thermoelasticity equations, expressed in vector form representing the coupled dynamic thermoelasticity problem [23-25], is given as:

$$\mu \nabla^2 (u) + (\lambda + \mu) \text{grad div } (u) - (3\lambda + 2\mu) \alpha_T \text{grad } \theta + [F] - \rho [a] = 0 \quad (8)$$

$$\nabla^2 \theta - \frac{1}{\alpha} \theta + \frac{W}{\lambda \alpha} - \frac{(3\lambda + 2\mu) \alpha_T}{\lambda \alpha} \text{div } (u) = 0 \quad (9)$$

Where the coupling of the equations is achieved by the fourth term of the eq.(9). In eq.(8) and eq.(9) are given: (u) - displacement vector; μ and λ - Lamé constants given as $\lambda = \frac{E\nu}{(1+\nu)(1-2\nu)}$ and $\mu = \frac{E}{2(1+\nu)}$; α_T - coefficient of linear thermal expansion.

The coupled quasi-stationary thermoelasticity problem is obtained with a slow thermal process, when the acceleration of displacement can be neglected ($[a] = 0$) and in the absence of volume forces ($[F] = 0$), then the equations (8) and (9) are reduced to:

$$\mu \nabla^2 (u) + (\lambda + \mu) \text{grad div } (u) - (3\lambda + 2\mu) \alpha_T \text{grad } \theta = 0 \quad (10)$$

$$\nabla^2 \theta - \frac{1}{\alpha} (1 + \alpha_T) \theta + \frac{W}{\lambda \alpha} = 0 \quad (11)$$

Where ϵ_s represents the coupled coefficient of temperature field and displacement field and is defined according to [24,25] as $\epsilon_s = \frac{(3\lambda + 2\mu) \alpha_T}{(2 + \nu) \rho c}$.

The uncoupled quasi-stationary problem of thermoelasticity is obtained by neglecting the coupling and acceleration of displacement:

$$\mu \nabla^2 (u) + (\lambda + \mu) \text{grad div } (u) - (3\lambda + 2\mu) \alpha_T \text{grad } \theta = 0 \quad (12)$$

$$\nabla^2 \theta - \frac{1}{\alpha} \theta + \frac{W}{\lambda \alpha} = 0 \quad (13)$$

The stationary thermoelasticity problem is obtained when there is no change in size over time. The basic equations are further simplified and take the form:

$$\mu \nabla^2 (u) + (\lambda + \mu) \text{grad div } (u) - (3\lambda + 2\mu) \alpha_T \text{grad } \theta = 0 \quad (14)$$

$$\nabla^2 \theta + \frac{W}{\lambda \alpha} = 0 \quad (15)$$

With these relations given in the previous steps, the stiffness matrix is obtained which is used for numerical analysis.

3. EXPERIMENTAL PROCEDURE

Experimental procedure was done in order to identify the influence of the transient regime of the starting up the hot water boiler on its structure. Temperature measurements were performed. The experimental measurement procedure included obtaining the temperatures of the boiler walls. Due to the lack of adequate literature data on the temperature value of the boiler construction, as well as on the change of temperature field over time, the obtained data are of exceptional importance. The data were used to form a numerical model for the analysis of boiler start up.

The experimental procedure had the aim to determine the temperatures of the tube plates of the first and second reversing chambers, at defined points and at certain boiler loads. In this way, knowing the temperature field of the structure, the analysis of thermal stresses that are presented would be more accurate and reliable comparing the real data.

The experimental method of temperature measurement was performed by using temperature probes. The measurement procedure required the determination of exact locations for the installation of measuring probes. The measurement is planned to be on the tube plates on the gas side, where unobstructed access is enabled as well as installation of probes. There were adopted 6

measuring points, with 4 on the tube plate of the first reversing chamber and 2 on the tube plate of the second reversing chamber. As the temperature of the flue gases at the nominal operating mode of the boiler is around 1200 °C at the outlet of the fire tube, a mantle probe, 3.5 m long, was adopted. On the same tube plate of the second draft, 2 measuring points were selected at defined places located in the zone of flue gases that leave the third draft, go in the shielded reversing chamber from the back and go to the chimney. The flue gas temperature to which the thermocouples would be exposed in this zone is around 230 °C. There are 2 more measuring points on the tube plate of the second reversing chamber, in the zone of flue gases that leave the second and enter the third draft, the temperature of the gases in this zone is around 450 °C (Fig.1). The aim of this experiment was to determine the change in temperature at certain points of the tube plate during the starting up the boiler, i.e. in the range of 0% to 100% load change.



Fig. 1 Installation of temperature probes

All output signals were connected to the computer and the system made it possible to monitor the change in temperature in real time, in different load conditions, during the operation of the hot water boiler.

The temperature of the structure was monitored and recorded in different operating modes of the boiler. According to the boiler load, with the experimental results, temperature gradients were monitored, which lead to thermal stresses.

The obtained measured temperature values were used to define the boundary conditions and more closely determine the numerical

model. In this way, a more precise temperature field of the structure was used and the numerical model approached the exact thermal state of the real structure. The measured values were also used for the validation of the numerical model, not only in the nominal mode of operation, but also in the mode of starting up the boiler.

4. NUMERICAL ANALYSIS – FINITE ELEMENT METHOD

Numerical analysis of stress-strain field of the hot water boiler structure was performed using FEM in ANSYS program package, while a CAD model was created using SOLIDWORKS software package according to technical documentation of the boiler manufacturer [16,26]. Since the geometric model is symmetrical in relation to the plane that passes through its longitudinal axis and is normal to the plane of the substrate, considering the assumed heat load symmetry, half of the geometric model is neglected – the right side of the symmetry plane. The influence of the neglected part of the model is defined by the limitation of the number of degrees of movement freedom of nodes in the symmetry plane applied by a software package symmetry relation. The geometric model analysis results have determined that some elements of the model have a function of connecting the hot water boiler to the water supply network. These elements are also excluded from the analysis since they have no significant effect on the stress-strain state of the model. In addition to these elements, the boiler connection elements that have safety features are also neglected. The geometric model was transformed into the discretized FEM with the application of advanced meshing tool capable of creating adaptive discrete model. The discretized model consisted of 1661038 nodes, forming 310620 finite elements. The discretized model is presented in Fig.2 and Fig.3. In the analysis, the materials that are used (which correspond to the real state of boiler construction) have the characteristics given in [16,28,29].

By analyzing the structural load of the boiler, it can be determined that boiler loads are: loads resulting from the weight of the boiler elements themselves, loads resulting from the thermal expansion on higher temperatures and boiler

operating loads (that is changed during the observed time period).

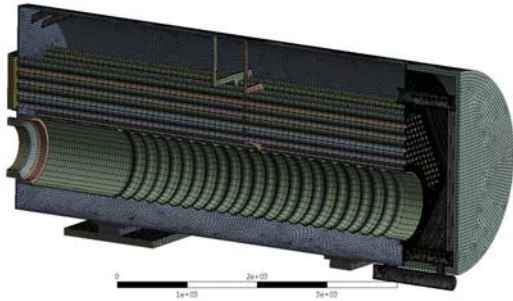


Fig. 2 Discretized structure of hot water boiler

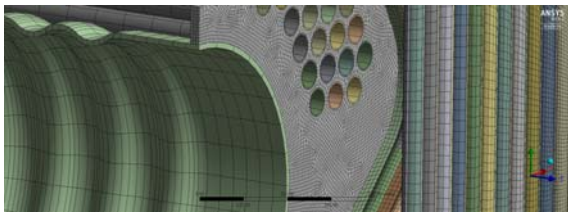


Fig. 3 Part of a numerical model of a discretized structure of a hot water boiler – Tube Plate

Numerical analysis model is analysed in the time domain. The presented model is considered to be of great importance while it is based on the variable operating mode from 0% to 100% of the load in a given time. In the case of the real hot water boiler, based on the experimental results, there is load reduced after 100s when the boiler starts. In numerical model, this period of reducing load is not considered. The numerical model is defined so that the load is not reduced as on a real boiler, but that the boiler load increases linearly, as is the case up to 100s. The aim of this analysis is to see what would happen to the structure if there were no changes in the character of the temperature rise curve of the structure, i.e. if the safety protection on the boiler did not work.

The analysis included the heat load that changes over time. The predicted heat load to which the boiler structure is exposed, which originates from the combustion of fuel in the fire tube is set from 0 to 100s based on the data obtained experimentally by measurements on a hot water boiler. An increase in boiler load up to 120s by extrapolating the curve was then considered to analyse the case without changing

the character of the structure temperature curve (Fig. 4).

The change of the boiler temperature in time period was simulated by applying thermal analysis in the transient mode during 3600s, i.e. one hour from the starting up the boiler, i.e. from the starting the heating of the boiler elements.

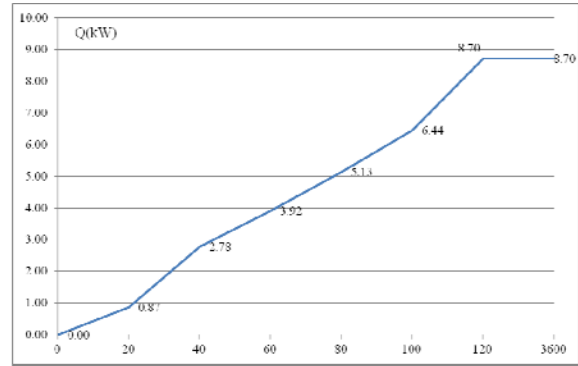


Fig. 4 Heat load change of fire tube Q as a function of time t (s)

It is noticed that a relatively short period of time is needed until the approximately stationary state is obtained, in which the temperature field of the boiler does not change over time. The results show that after an hour, steady state is established. The temperature fields of the boiler structure, observed at time period 50s, 100s and an hour, are shown in Fig. 5, 6 and 7. The changes in the temperature field of individual parts of the structure, such as the tube plate of the first reversing chamber are shown in Fig. 8, 9 and 10, after 50s, 100s and 3600s from the moment of starting up the boiler.

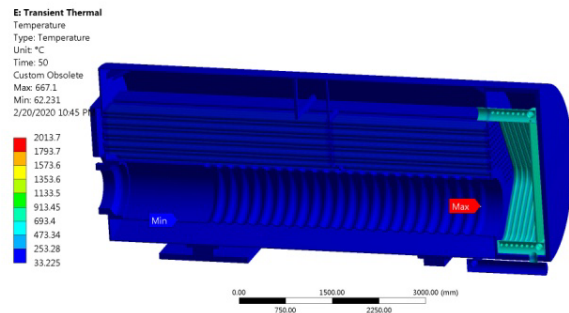


Fig. 5 Temperature distribution of boiler elements after 50s from the moment of starting up the boiler

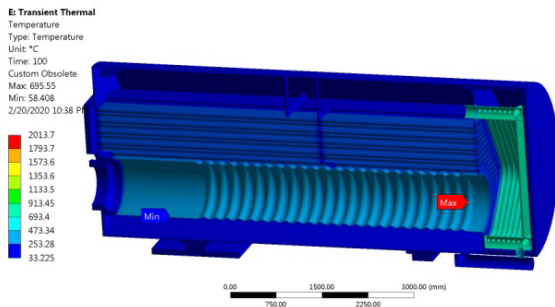


Fig. 6 Temperature distribution of boiler elements after 100s from the moment of starting up the boiler

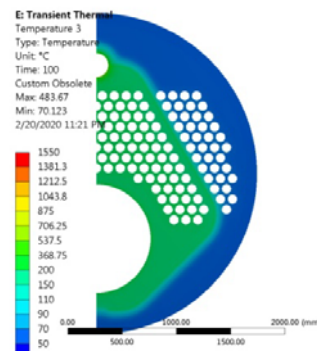


Fig. 9 Temperature distribution of the tube plate of the first reversing chamber after 100s from the moment of starting up the boiler

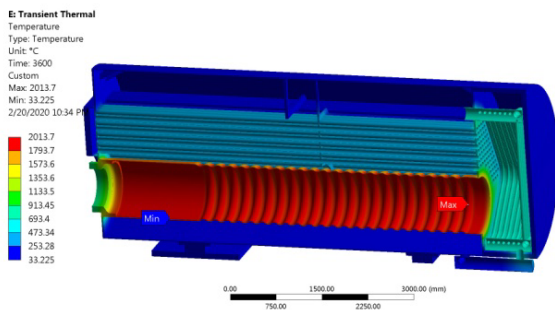


Fig. 7 Temperature distribution of boiler elements after 3600s from the moment of starting up the boiler

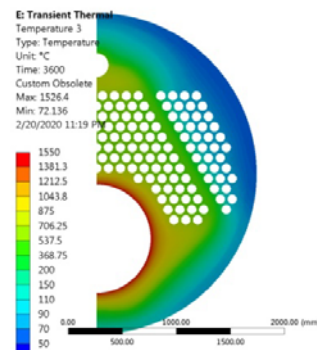


Fig. 10 Temperature distribution of the tube plate of the first reversing chamber after 3600s from the moment of starting up the boiler

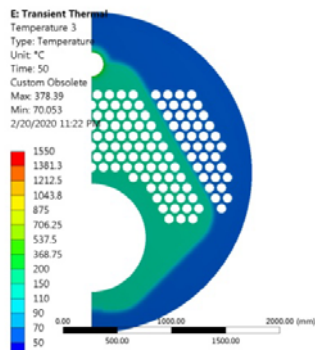


Fig. 8 Temperature distribution of the tube plate of the first reversing chamber after 50s from the moment of starting up the boiler

The presented results of the change of the temperature field of the boiler structure (Fig. 6 and 9) are compared with the measured values on the real object. Based on the measured temperature values by the experimental procedure, the numerical model can be verified. This was the reason to install thermocouples on the pipe plates. By verifying the temperature field on these elements, the resulting temperature field of the structure can be adopted with certainty. In the previous chapter, 6 measuring points on the boiler were defined, where the values of the construction temperature are experimentally determined. The locations of these measured points were also identified on the numerical model, in order to compare the values. The comparative values of the temperatures on the pipe plate of the first turning chamber are shown in the Table 1. The results indicate a significant match between the measured values of temperatures and the values obtained numerically. Especially of the

measuring points on the tube plate of the second reversing chamber and on the tube plate of the first turning chamber, but towards the outer circle (third flue). A relative difference of 26% refers to the measured temperatures of the tube plate of the first reversing chamber, closer to the fire tube. The measured temperature values, which are higher than those obtained by numerical analysis, can be explained by the high sensitivity of the probes and the positioning of the probe tips. Also, in this part, the measurement was difficult due to the high flue gas flow rates.

Table 1. Comparative analysis of temperatures obtained by experimental and numerical analysis

No.	Position	Experimental result [°C]	Numerical result [°C]
1	Tube plate 1 – t1	805.5	595.7
2	Tube plate 1 – t2	727	577.9
3	Tube plate 2 – t1	133.6	133.6
4	Tube plate 2 – t2	136.6	133.4
5	Tube plate 1 – t3	83.1	96.1
6	Tube plate 1 – t4	80.7	94.4

Comparative analysis of the results also allows verifying the numerical model. It is very important to emphasize that in the process of starting-up the boiler, the accumulation of thermal energy is done first in the walls of the structure, and only later, when stable operation is achieved, the water is heated.

5. RESULTS AND DISCUSSION

In order to analyse the stress state of the hot water boiler structure, the critical moment was chosen to present the results. At the considered moment, i.e. at time $t = 100s$ from the beginning of boiler start up, the stress-strain state of the structure was analysed. As the temperature differences between the construction and the heating medium are large at this moment, it is expected that the stresses are the highest. Fig. 11 and 12 show the state of stress and strain (respectively) at a given moment of time.

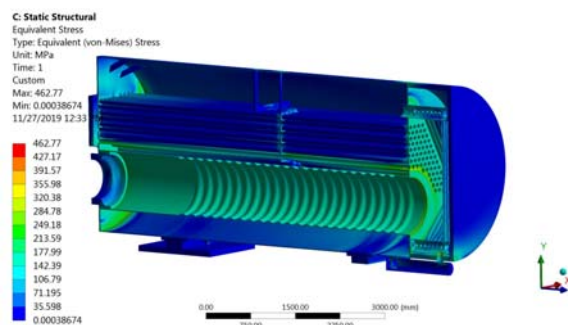


Fig. 11 Equivalent stresses of hot water boiler structural elements at 100s from the moment of starting up the boiler

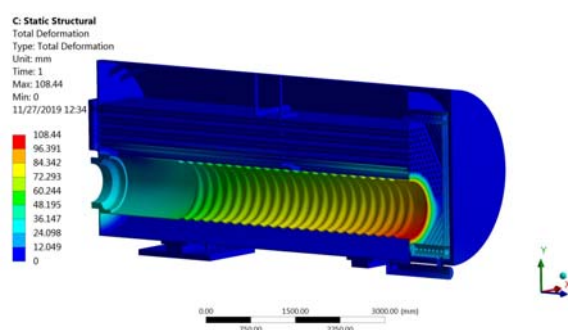


Fig. 12 Total deformation of hot water boiler structure at 100s from the moment of starting up the boiler

As can be seen from the Fig.13, the maximum stress values are about 410 MPa, while the tensile strength of the material itself (P265GH according to DIN EN 10028-2 [16,28,29]) of which the pipe wall is made $R_m = 410-530 \text{ N/mm}^2$, and yield strength $R_p = 255 \text{ N/mm}^2$. At high temperatures of the tube wall, the yield strength is even significantly lower. The maximum stress values are exactly on the tube plate, in the zone of the first line flue gas pipes of the second draft (Fig.11). This also indicates that these are the critical values. The stresses state in the tube plate is shown in Fig. 13 where these critical stresses can be observed. Under these conditions, the results of direct deformation in the axis normal to the tube plate are given in Fig. 14. The installed protection system, which reduces the heat load at that time $t = 100s$, leads to a reduction of the stress state from the critical obtained values. Without exposing the boiler construction to elevated stress, the boiler operation is then safe and secure.

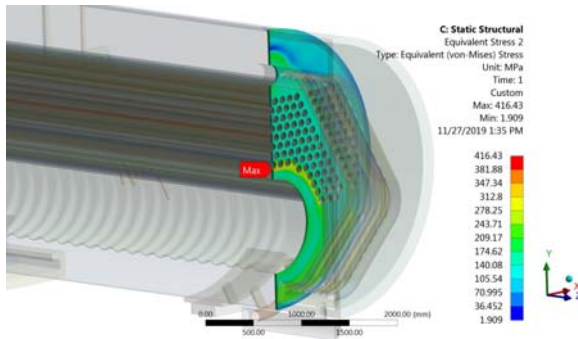


Fig. 13 Equivalent stresses of tube plate of the first reversing chamber at 100s from the moment of starting up the boiler

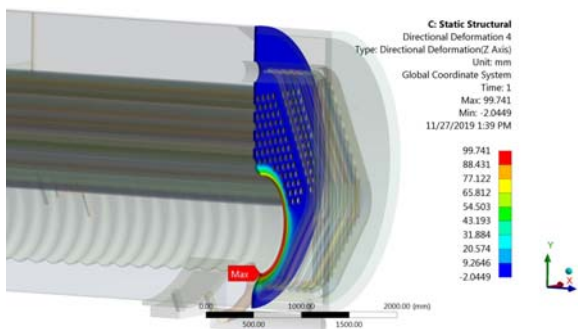


Fig. 14 Total deformation (directional Z Axis) of the tube plate of the first reversing chamber at 100s from the moment of starting up the boiler

The most critical transient operating regime is starting up the boiler and it was analyzed as a quasi-stationary state. The results of the experimental procedure showed that at the time point, exactly 100s after the boiler was started and put in operation, the system of safety protection reduced the boiler power from 75% to 58% of the load. This is done precisely in order to change the character of the temperature rise curve of the boiler structure, i.e. as the critical element. When the boiler starts, the largest amount of heat is received by the boiler structure, and then over time it begins to heat the working fluid. Due to this phenomenon, which can lead to critical stresses, the analysis of the stress-strain field of the boiler structure was performed at that very moment, just before the reduction of the boiler power. The results of the analysis show the appearance of high stress-strain state, but still in the zone that is allowed, on the tube plate of the first reflecting chamber, in the zone of the first row of flue pipes of the second draft. This is exactly the location where accidents occur in

boilers during its operation. Due to the existence of these critical stresses, a dynamic analysis was performed that was programmed to monitor the change in heat load in real time. With a real boiler, the power increases to 75% and then lowers, only to increase again to 100%. However, in the dynamic model, the boiler load increase curve was extrapolated to show the condition if no load drop occurred. Namely, already in 120s, the boiler would work with 100% load and that condition would be maintained for up to an hour. The results of the dynamic model show that in that case high temperatures and critical thermal stresses would occur, especially on the tube plates of the first and second reflecting chambers. The results of the dynamic model were verified with experimental values in the time interval when the heat load increases up to 100 s from the moment the boiler is put into operation.

6. CONCLUSIONS

The performed analysis showed that the tube plate of the first reversing chamber, the boiler element with the thickest wall, is exposed to the highest thermal stresses. This part of the boiler is exposed to temperatures $300\text{ }^{\circ}\text{C}$, which means it is exposed to yield stress. In this condition, continuous accumulation of plastic deformations occurs at a rate that depends on the level of stress, temperature and material characteristics. Intermittent cycles of drying, operation in stationary mode and cooling process, which are difficult to describe analytically, affect the fields of residual deformations and stresses before the considered n-th cycle of boiler operation. In strain-stress analysis in function of constructive parameters and load history of an element, the zero initial state of the previous stress is usually taken. However, it should be taken into account that such initial conditions lead to higher calculated values of the allowed rate of drying. Experimental research of hot water boilers shows that the heating of the tube plate during the process of starting-up the can be presented as an approximate quasi-static temperature change. Under these conditions, the temperature field in the tube plate is quasi-stationary, i.e. only its level changes until the character of the change remains the same. At the beginning of the process of boiler start-up, when temperature of the tube plate is the

lowest, maximal temperature differences occur. Due to the high temperature differences, the equivalent stresses are also the highest. Having that in mind, it can be concluded that the stresses are highest at the lowest temperatures of the tube plate, when the creep strain rate has the highest values. This means that the material is the strongest at the highest load.

Acknowledgement

This research was financially supported by the Ministry of Education, Science and Technological Development of the Republic of Serbia (Contract No. 451-03-9/2021-14/200109).

REFERENCES

- [1] Standard EN 12953-1. (2012). *Shell boilers - Part 1: General*. CEN/TC 269 - Shell and water tube boilers. European Committee for Standardization. Brussels.
- [2] Standard EN 12953-3. (2016). *Shell boilers. Design and calculation for pressure parts*. CEN/TC 269 - Shell and water tube boilers. European Committee for Standardization. Brussels.
- [3] Cwynar, L. (1981). *Pusk parowych kotlow*. (in Russian). Energoizdat, Moscow.
- [4] Taler, J., Dzierwa, P., Taler, D., Harchut, P. (2015). Optimization of the boiler start-up taking into account thermal stresses, *Energy*, vol. 92, part 1, p.160-170. DOI: [10.1016/j.energy.2015.03.095](https://doi.org/10.1016/j.energy.2015.03.095)
- [5] Alobaid, F., Karner, K., Belz, J., Epple, B., Kim, H.G. (2014). Numerical and experimental study of a heat recovery steam generator during start-up procedure. *Energy*, vol. 64, p.1057-1070. DOI: [10.1016/j.energy.2013.11.007](https://doi.org/10.1016/j.energy.2013.11.007)
- [6] Kim, T.S., Lee, D.K., Ro, S.T. (2000). Analysis of thermal stress evolution in the steam drum during start-up of a heat recovery steam generator. *Applied Thermal Engineering*, vol. 20, no. 11, p.977-992. DOI: [10.1016/S1359-4311\(99\)00081-2](https://doi.org/10.1016/S1359-4311(99)00081-2)
- [7] Krüger, K., Franke, R., Rode, M. (2004). Optimization of boiler start-up using a nonlinear boiler model and hard constraints. *Energy*, vol. 29 no.12-15, p. 2239-2251. DOI: [10.1016/j.energy.2004.03.022](https://doi.org/10.1016/j.energy.2004.03.022)
- [8] Dzierwa, P. (2016). Optimum heating of pressure components of steam boilers with regard to thermal stresses. *Journal of Thermal Stresses*, vol. 39, no. 7, p.874-886. DOI: [10.1080/01495739.2016.1189773](https://doi.org/10.1080/01495739.2016.1189773)
- [9] Dzierwa, P., Taler, D., Taler, J., Trojan, M. Optimum Heating of Thick Wall Pressure Components of Steam Boilers. *Proceedings of the ASME 2014 Power Conference POWER2014*, July 28-31, 2014, Baltimore, Maryland, USA, American Society of Mechanical Engineers, Power Division (Publication) POWER, 2014. DOI:10.1115/POWER2014-32080
- [10] Dzierwa, P., Taler, J. (2014). Optimum Heating of Pressure Vessels With Holes. *Journal of Pressure Vessel Technology*, vol. 137. DOI: [10.1115/1.4027584](https://doi.org/10.1115/1.4027584)
- [11] Dzierwa, P. (2014). Optimum Heating of Pressure Components of Complex Shape, In book: *Encyclopedia of Thermal Stresses*. DOI:10.1007/978-94-007-2739-7402.
- [12] Taler, J., Dzierwa, P. A new procedure for optimum heating of pressure components with complex shape, *Proceedings of the 2nd International Conference on Engineering Optimization 2010*, September 6 - 9, 2010, Lisbon, Portugal.
- [13] Todorović, M., Živković, D., Mančić, M. Breakdowns of hot water boilers, *Proceedings of the 17th International Symposium on Thermal Science and Engineering of Serbia SIMTERM 2015*, Sokobanja, Serbia, 2015, p. 761-769.
- [14] Todorović, M., Živković, D., Mančić, M. Starting up hot water fire-tubes boilers. *International Scientific Conference UNITECH' 14 Gabrovo*, Gabrovo, Bulgaria, ISSN: 1313-230X, p.192-197.
- [15] Todorović, M., Živković, D., Mančić, M., Milčić, D. (2014). Dynamic behaviour of hot water boilers during start up, *Facta Universitatis, Series: Mechanical Engineering*, vol. 12, no. 1, p. 85-94.
- [16] Rajić, M., Banić, M., Živković, D., Tomić, M., Mančić, M. (2018). Construction Optimization of Hot Water Fire-Tube Boiler Using Thermomechanical Finite Element Analysis. *Thermal Science*, vol. 22, Suppl. 5, S1511-S1523. DOI: [10.2298/TSC18S5511R](https://doi.org/10.2298/TSC18S5511R)
- [17] Rajić, M., Jovanović, D., Živković, D. Stress and deformation state in furnace tube, smoke tubes and tube plate of the hot water boiler, *Proceedings of the 7th International Congress of Serbian Society of Mechanics*, Sremski Karlovci, June 24-26, 2019, p. 1-9.
- [18] Dzierwa, P. (2018). New start-up curves for a 200 MW steam boiler with natural circulation. *Proceedings of the MATEC Web of Conferences 240*, 05007 (2018), ICCHMT 2018. DOI:10.1051/mateccconf/201824005007
- [19] Taler, J., Węglowski, B., Zima, W., Grądziel, S., Zborowski, M. (1999). Analysis of Thermal

- Stresses in a Boiler Drum During Start-Up. *ASME. J. Pressure Vessel Technol.* vol. 121, no. 1, p. 84-93. DOI: [10.1115/1.2883672](https://doi.org/10.1115/1.2883672)
- [20] Taler, J., Węglowski, B., Taler, D., Trojan, M., Sobota, T., Dzierwa, P., Pilarczyk, M., Madejski, P., Nabagło, D. (2015). Method of determination of thermo-flow parameters for steam boiler. *Journal of Power Technologies*, vol. 95, no. 4, p. 309-316.
- [21] Taler, J., Taler, D., Kowal, A. (2011). Measurements of absorbed heat flux and water-side heat transfer coefficient in water wall tubes. *Archives of thermodynamics*, vol. 32, no. 1, p. 77-88. DOI: 10.2478/v10173-011-0004-6
- [22] Sanaye, S., Rezazadeh, M. (2007). Transient thermal modelling of heat recovery steam generators in combined cycle power plants. *Int. J. Energy Res.* vol. 31, p. 1047-1063. DOI:10.1002/er.1297
- [23] Duda, P., Rzaša, D. (2015). A method for optimum heating and cooling boiler components of a complex shape. *J Therm. Sci.* vol. 24, no. 4, p. 364-369. DOI:10.1007/s11630-015-0796-9
- [24] Damjanović, S. (1995). *Thermal stresses of the steam turbine rotor during stationary and non-stationary modes of operation*, Master's thesis, University of Belgrade, Faculty of Mechanical Engineering, Belgrade.
- [25] Živković, D., Rajić, M., Banić, M., Mančić, M. Thermal Stresses of Hot Water Boiler Structure during the process of Start-up, *Proceedings of the 5th International Conference Mechanical Engineering in XXI Century MASING 2020*, Niš, Serbia, December 09-10, 2020, p.71-76.
- [26] Živković, D., Rajić, M., Banić, M., Mančić, M., Popović, B. The Analysis of Thermo-Mechanical State of Steam Turbine Rotor in Non-Stationary Modes of Operation, *Proceedings of the 4th International Conference Mechanical Engineering in XXI Century*, Faculty of Mechanical Engineering, 2018, Niš, Serbia, p. 33-36.
- [27] Technical Documentation of Hot Water Boiler Minel kotlogradnja – TE110V, (in Serbian), Minel kotlogradnja, Belgrade, 1992.
- [28] ThyssenKrupp Materials International, Seamless Carbon Steel Pipe for High-Temperature Service, www.s-k-h.com
- [29] Lucefin Group, Tehnical Card – P235GH, 2011, www.lucefin.com



Banja Luka
28-29 May 2021.

DEMI 2021

15th International Conference on Accomplishments in Mechanical and Industrial Engineering

www.demi.mf.unibl.org



Perspectives of Hydropower Potentials in Republika Srpska

O. Kašiković^a, D. Golubović^b, D. Milić^b

^aBSc, MH "Elektroprivreda Republike Srpske"-Matično preduzeće a.d. Trebinje, okasikovic@ers.ba

^bPhD, University of East Sarajevo, Faculty of Mechanical Engineering, dusan.golubovic@ues.rs.ba

^bMSc, University of East Sarajevo, Faculty of Mechanical Engineering, davor.milic@ues.rs.ba

Abstract Along with the development of technique and technology, the demand for electricity also increases. Combustion of fossil fuels continues to be the main way of obtaining electricity, both in our country and in the region. There is a need to use renewable energy sources as much as possible. Water energy appears to be a source of renewable energy that could be used to a large extent. This energy source is used much more than other renewable energy sources. In Republika Srpska, facilities that enable the use of water energy are put into operation to a certain extent and the construction of new plants is also planned.

Keywords hydropower, hydropower plants, renewable energy sources

1. INTRODUCTION

Renewable energy sources are energy sources that have unlimited reserves, which means that they renew themselves in a relatively short period of time. There are different forms of energy that belong to this group, but the most commonly used are: water energy (hydropower), wind energy, solar energy, geothermal energy and biomass energy.

Hydropower is one of the most important renewable sources of energy. This form of energy can be used in technical conversion plants. The water energy is converted into mechanical energy in the turbines, and then the generators convert mechanical energy into electrical energy.

Corresponding author

BSc, Oksana Kašiković
okasikovic@ers.ba

MH "Elektroprivreda Republike Srpske"
Stepe Stepanovića bb
Trebinje, Bosnia and Herzegovina

2. HYDROPOWER CAPACITIES IN THE WORLD

During 2019, the utilization of hydropower potentials in the world reached a record high of 4,305 TWh, which is an increase of 105 TWh compared to 2018. Over 50 countries have increased their installed hydropower capacity, particularly [1]:

- Brazil - 4.92 GW
- China - 4.17 GW
- Laos - 1.89 GW.

With a total installed hydropower capacity of 50.07 GW, India overtook Japan to become the fifth largest capacity.

The biggest project in 2019 was "Belo Monte" in Brazil with 18 turbines and 11.23 GW of installed capacity.

Other important projects completed during the previous year are "Xayaburi" in Laos with 1.285 GW of installed capacity, and "Mangdech" in Bhutan with a capacity of 720 MW.

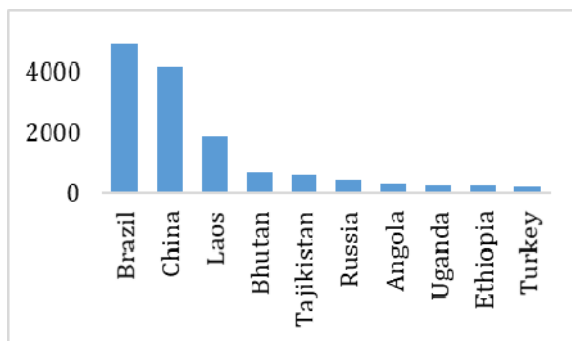


Fig. 1 Countries with the highest increases in installed hydropower potentials

The total installed hydropower potentials worldwide reached 1,403 GW in 2019. This data indicates an increase of 111 GW compared to 2018 [2]. In the period 2015-2019, the average growth rate of installed capacities was 2.1%. In the previous year, the growth rate was 1.2% [1]. Fig. 2 shows the total installed hydropower potentials in the world.

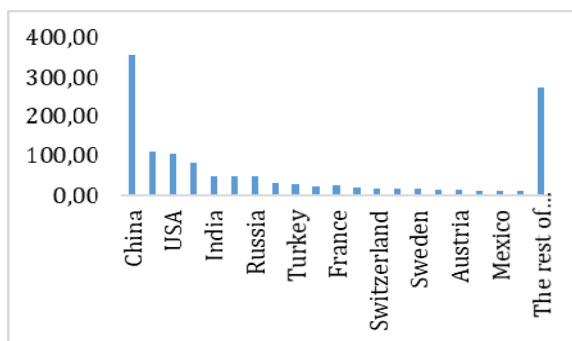


Fig. 2 Hydropower potentials in the world

In the report "Transforming Energy Scenario", IRENA proposes the increase in the installed hydropower capacities worldwide by 25% until 2035, i.e. by 60% until 2050. This would prevent the global temperature from rising 2° above pre-industrial period [1].

The annual increase in installed capacities depends on many factors, including the fact when the projects in the development phase will become operational. Therefore, it is necessary to increase investments in hydropower capacities in the coming period.

3. HYDROPOWER CAPACITIES IN RS

Republika Srpska is an area with abundant hydropower potentials. The basins of the rivers

Drina, Trebišnjica and Vrbas have great hydropower potentials. The basins of the rivers Bosna, Una, Sana and Neretva have somewhat less potentials. A graphical representation of the hydropower potentials in the RS is shown in Fig. 3 [3].

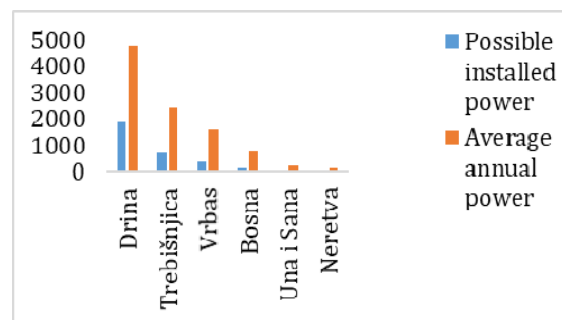


Fig. 3 Hydropower potentials in Republika Srpska

3.1 Trebišnjica Basin

The river Trebišnjica basin has a large hydropower potential that can be used very efficiently.

The construction of the hydropower system Trebišnjica (HES Trebišnjica) took place in several phases. In the first phase, two hydropower plants were built, namely HPP Dubrovnik and HPP Trebinje 1. In the second phase, PS HPP Čapljinica and HPP Trebinje 2 were built [3].

- a) HPP Trebinje 1 (Fig. 4) is a hydropower plant with a powerhouse at the toe of the dam that works with three generators and an installed capacity of 2x54 + 1x60 MW. It works with an installed flow of 3x70 m³/s and an average annual production of 370 - 420 GWh. The type of generator used in this hydropower plant is a Francis turbine [4].



Fig. 4 HPP Trebinje 1 [4]

- b) HPP Trebinje 2 (Fig. 5) is a hydropower plant operating with a Kaplan turbine and an installed capacity of 8 MW and an installed flow of 45 m³ / s. The average annual production of HPP Trebinje 2 is 14.5 GWh [5].

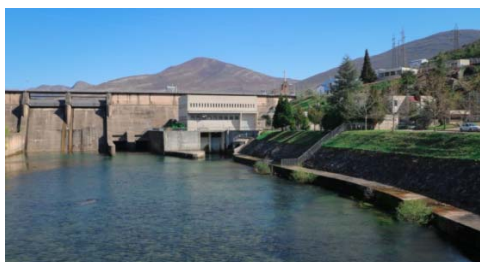


Fig. 5 HPP Trebinje 2 [5]

- c) HPP Dubrovnik (Fig. 6) is a derivation hydropower plant with an accumulation that operates with two generators which have got the installed capacities of 126 MW and 117.5 MW if both generators are active. The type of generator used is a Francis turbine with an installed flow of 48 m³/s [6].



Fig. 6 HPP Dubrovnik [6]

- d) PS HPP Čapljina (Fig. 7) is a pumped storage hydropower plant that works with two generators, an installed capacity of 420 MW and an installed flow of 225 m³ / s. The type of generator used in this hydropower plant is a Francis turbine [7].



Fig. 7 PS HPP Čapljina [7]

3.2 Drina Basin

The river Drina is formed by the confluence of the rivers Piva and Tara and is the largest tributary of the Sava River. The length of the river Drina is 341 km. Together with the river Tara, it is about 500 km long [3].

The hydropower potential of the river Drina basin is the least used potential in the Balkans and as such needs special attention.

The installed hydropower capacities in the river Drina basin are: HPP Uvac, HPP Kokin Brod, HPP Bistrica, HPP Potpeć, HPP Piva, HPP Višegrad, HPP Bajina Bašta and HPP Zvornik with a total installed capacity of 1,932 MW and an average annual production of 6,350 GWh [3]. Among the previously mentioned hydropower plants, only HPP Višegrad is located in Republika Srpska. HPP Višegrad (Fig. 8) operates with three generators which have an installed capacity of 105 MW each. Therefore, the total installed capacity of HPP is 315 MW.



Fig. 8 HPP Višegrad [8]

The river Drina basin is divided into three hydropower systems: "Gornja Drina", "Srednja Drina" and "Donja Drina".

3.3 Vrbas Basin

The river Vrbas empties into the river Sava, creating three characteristic units [3]:

- In the upper stream, from the source to Jajce, it is a mountain river,
- In the middle stream, from Jajce to Banja Luka, with a pronounced slope of the riverbed, it breaks through a deep limestone canyon, and
- In the lower stream, from Banja Luka to its mouth, it is a typical lowland river.

The plants that enable the exploitation of the hydropower potential of the river Vrbas are HPP Jajce 1, HPP Jajce 2, HPP Bočac and HPP Bočac 2. In this way, 22.5% of the total potential of the river Vrbas is used.

- a) HPP Bočac (Fig. 9) is a hydropower plant in the river Vrbas basin that uses 16.2% of the total hydropower potential. It works with two generators of 55 MW each, so the total installed capacity of HPP is 110 MW [9].



Fig. 9 HPP Bočac [9]

- b) HPP Bočac 2 (Fig. 10) is a hydropower plant with a powerhouse at the toe of the dam built on the existing dam of the compensation basin of HPP "Bočac". It works with two generators with an installed capacity of 4,995 MW each, so the total installed capacity of the HPP is 9.99 MW [10].



Fig. 10 HPP Bočac 2 [10]

HPP Bočac 2 was put into operation in August 2018.

4. PLANNED CONSTRUCTION OF NEW HYDROPOWER PLANTS IN RS

Since Republika Srpska has great potentials, it is planned to build several hydropower plants as follows:

- Hydropower system "Gornji Horizonti",
- Hydropower system "Gornja Drina",
- Hydropower system on the rivers Bistrica and Janjina,
- HPP Cijevna 3,
- Hydroelectric power plant Dubrovnik Phase II.

4.3 Hydropower system "Gornji Horizonti"

Within the hydropower system "Gornji Horizonti", the construction of three plants is planned as follows:

- HPP Dabar,
- HPP Bileća
- HPP Nevesinje.

4.3.1 HPP Dabar

HPP Dabar is a derivation plant that belongs to the planned hydropower system of hydroelectric power plants on the river Trebišnjica and is the most important hydroelectric power plant in the system "Gornji Horizonti" and it consists of [11]:

- Accumulation Nevesinje,
- Dam Pošćenje,
- Derivation tunnel with an intake house,
- Surge tank,
- Pressure penstock,
- Powerhouse,
- Channel through Dabarsko polje,
- Embankments Grebak and Vranjača.

The animation of the HPP Dabar's powerhouse is given in Fig. 11.

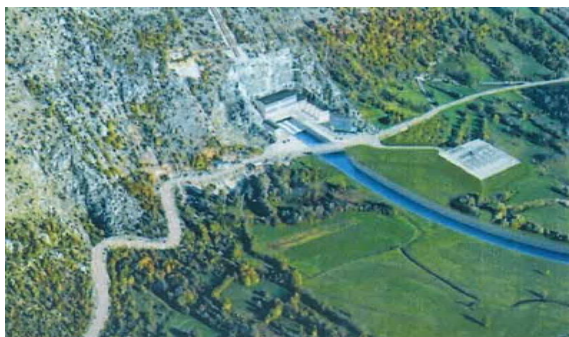


Fig. 11 Animation of the HPP Dabar's powerhouse [11]

The installed capacity of HPP Dabar is 159 MW, and the planned annual production is 252 GWh.

4.3.2 HPP Bileća

HPP Bileća is a derivation plant that belongs to the hydropower system of hydroelectric power plants on the river Trebišnjica and it consists of the following elements [11]:

- Reservoir in front of the intake house,
- Intake house,
- Penstock, outlet with chute,
- Surge tank,
- Control gate,
- Penstock to the powerhouse,
- Powerhouse,
- Tailrace tunnels.

The location of the powerhouse of HPP Bileća is shown in Fig. 12.



Fig. 12 Location of the powerhouse of HPP Bileća [11]

The installed capacity of HPP Bileća is 33 MW, and the planned annual production is 122 GWh.

4.3.3 HPP Nevesinje

HPP Nevesinje also belongs to the planned hydropower system of hydroelectric power plants on the river Trebišnjica in the system "Gornji Horizonti". The construction in two phases is planned. In the first phase, a dam with an accumulation with a normal water surface of 946 m above sea level would be built, while in the second phase the dam would be raised to form a lake with a 24 m higher normal water surface [11].



Fig. 13 Disposition of water management and hydroelectric system plants within HPP Nevesinje [11]

The installed capacity of HPP Nevesinje is 35 MW, and the planned installed capacity is 65 GWh.

4.4 Hydropower system "Gornja Drina"

Within HPS "Gornja Drina", the construction of the following plants is planned:

- HPP Buk Bijela,
- HPP Foča,
- HPP Paunci.

4.4.1 HPP Buk Bijela

HPP Buk Bijela is an accumulation plant with a powerhouse at the toe of the dam and belongs to the planned system of hydroelectric power plants in the upper stream of the river Drina. It consists of [11]:

- Gravity concrete dams with a powerhouse,
- Reservoir.

Fig. 14 shows the planned HPP Buk Bijela.



Fig. 14 Animation of the planned HPP Buk Bijela [11]

The installed capacity of HPP Buk Bijela is 94 MW, and the planned annual production is 332 GWh.

4.4.2 HPP Foča

HPP Foča is an accumulation plant with a powerhouse at the toe of the dam which, like HPP Buk Bijela, belongs to the planned system of hydroelectric power plants in the upper stream of the river Drina. This plant consists of [11]:

- Gravity concrete dam with spillways,
- Powerhouse,
- Reservoir.

The animation of the planned HPP Foča is shown in Figure 15.



Fig. 15 Animation of planned HPP Foča [11]

The installed capacity of HPP Foča is 44 MW, and the planned annual production is 176 GWh.

4.4.3 HPP Paunci

HPP Paunci is an accumulation plant with a powerhouse at the toe of the dam and also one of the planned production plants within the project in the upper stream of the river Drina.

Like HPP Foča, HPP Paunci consists of the following elements [11]:

- Concrete gravity dam with spillways,
- Powerhouse,
- Reservoir.

The animation of the planned HPP Paunci is shown in Figure 16.



Fig. 16 Animation of the planned HPP Paunci [11]

The installed capacity of HPP Paunci is 43 MW and the planned annual production is 167 GWh.

4.5 Hydropower system on the rivers Bistrica and Janjina

4.5.1 River Bistrica

The construction of three hydroelectric power plants on the river Bistrica is planned as follows:

- HPP Bistrica B-1,
- HPP Bistrica B-2a,
- HPP Bistrica B-3.

The above mentioned plants are derivative and consist of the following elements [11]:

- Concrete gravity dam and intake on the partition profile,
- Derivation tunnel,
- Surge tank,
- High-pressure penstock,
- Powerhouse.

A graphic presentation of hydropower plants on the river Bistrica with the installed capacity and planned annual production is shown below.

Table 1 HPP on the river Bistrica [11]

Plant	Installed capacity	Planned annual production
HE Bistrica B-1	10,70	42,96
HE Bistrica B-2a	7,24	29,08
HE Bistrica B-3	16,16	62,44

4.5.2 Janjina River

The river Janjina represents a catchment area of the river Drina located in the eastern part of Bosnia and Herzegovina. It is planned that one production plant will be built in order to use the hydropower potential of the river Janjina.

HPP Janjina J-1 is a derivation plant and consists of [11]:

- Gravity concrete dam and an intake on the partition profile,
- Derivation tunnel,
- Surge tank,
- Pressure penstock,
- Powerhouse.

The installed capacity of HPP Janjina J-1 is 4.47 MW, while the planned annual production is 16 GWh.

4.6 HPP Cijevna 3

HPP Cijevna 3 is a hydropower plant with a powerhouse at the toe of the dam with a gravity concrete dam consisting of [11]:

- Gravity blocks that connect the dam to the left or right bank of the river,
- Evacuation part located in the central part of the dam,
- Powerhouse as a part of the dam in the riverbed closer to the left bank.

The installed capacity of HPP Cijevna 3 is 14 MW, and the planned annual production is 69 GWh.

4.7 HPP Dubrovnik Phase II

HPP Dubrovnik II is a derivation plant with an accumulation. It represents the last phase in the construction of the system. It consists of the following elements [11]:

- Reservoir Gorica,
- Concrete gravity dam Gorica,

- Derivation systems,
- Powerhouse,
- Tailrace systems.

The installed capacity of HPP Dubrovnik II is 304 MW, and the planned annual production is 318 GWh.

5. CONCLUSION

From the above, it can be concluded that Republika Srpska has an extremely large hydropower potential. This potential is particularly noticeable in the river Drina basin, because it is the least used in that part of Republika Srpska. Significant hydropower capacities are in operation. However, these capacities can be greatly expanded if new plants are constructed.

The construction of certain plants is planned with the PE "Elektroprivreda Srbije" (HPP Paunci, HPP Buk Bijela, HPP Foča), i.e. with the company "Hrvatska elektroprivreda" d.d. (HPP Dubrovnik II). In both cases, the share of MH "Elektroprivreda RS" would be at least 50%. In this way, Republika Srpska would get additional 520.72 MW from new hydropower plants, i.e. the annual production of electricity from hydroelectric power would increase by 1429.72 GWh.

The construction of the previously mentioned plants would increase the use of water and hydropower energy. This would, to some extent, reduce the need for fossil fuels, which is also the ultimate global goal.

REFERENCES

[1] 2020 Hydropower Status Report – Sector Trends and Insights, IHA – International Hydropower Association. From: https://www.hydropower.org/sites/default/files/publications-docs/2020_hydropower_status_report.pdf, accessed on: October 22, 2020.

[2] 2019 Hydropower Status Report – Sector Trends and Insights, IHA – International Hydropower Association. From: https://www.hydropower.org/sites/default/files/publications-docs/2019_hydropower_status_report.pdf, accessed on: October 24, 2020.

[3] Hidroenergetski potencijal RS. From: <https://ers.ba/hidroenergetski-potencijal/>, accessed on: October 25, 2020.

[4] HE Trebinje I. From: <https://henatrebisnjici.com/het-1>, accessed on: October 25, 2020.

[5] HE Trebinje II. From: <https://henatrebisnjici.com/het-2/>, accessed on: October 25, 2020.

[6] HE Dubrovnik. From: <https://www.hep.hr/proizvodnja/hidroelektrane-1528/he-dubrovnik/he-dubrovnik-1735/1735>, accessed on: October 25, 2020.

[7] PHE Čapljina. From: <https://henatrebisnjici.com/phecapljina/>, accessed on: October 26, 2020.

[8] HE na Drini. From: <https://www.henadrini.com/fotografije/he-na-drini/>, accessed on: October 29, 2020.

[9] HE „Bočac“. From: <http://www.henavrbasu.com/hevNovi/DocNovi.aspx?cat=219&subcat=220&id=1163&lang=cir>, accessed on: October 29, 2020.

[10] HE „Bočac 2“. From: <http://www.henavrbasu.com/hevNovi/DocNovi.aspx?cat=219&subcat=221&id=1164&lang=cir>, accessed on: October 29, 2020.

[11] Plan razvoja MH Elektroprivrede Republike Srpske (2019.-2029.)



Banja Luka
28-29 May 2021.

DEMI 2021

15th International Conference on
Accomplishments in Mechanical and
Industrial Engineering

www.demi.mf.unibl.org



Computational investigation of hot air generation system using pellets for driving an absorption process

M. Ilić^a, V. Stefanović^a, S. Pavlović^a, M. Grozdanović^a, G. Ilić^a

^aUniversity of Niš, Faculty of Mechanical Engineering, 14 Aleksandra Medvedeva Street

Abstract Environmental problems are forcing humanity to find alternative methods of generating energy and to use that energy efficiently without much loss and ecofriendly. Biomass-pellets are one form of primary renewable energy source which has potential for more effective utilization in residential and industrial processes in the Balkans. This paper shows a numerical study of the hot air generating system of a driving component of an absorption heat pump, obtaining the temperature and velocity field inside its computational domain, case includes a defined geometrical model of hot air generator, boundary conditions and all governing partial differential equations for continuity, species, energy, and pressure. The calculation approach of all the equations that are highly coupled are solved using a finite volume, central difference scheme. The time-based procedure implemented in work is a fully implicit scheme in software Fluent. Initial discussion about the obtained parameters and their effects on this case is presented.

Keywords absorption heat pump, generator, hot air, CFD

1. INTRODUCTION

In this paper, a numerical temperature and velocity field simulation of a new hot air generator on biomass was performed to comprehend the potential for coupling with absorption heat pump, for the separation of ammonia and water. Electric compression heat pump systems are under public scrutiny due to the negative impact on the environment, the use of synthetic refrigerants and the increase in the load on the power system due to peak periods of electricity consumption. One of the alternatives to compressor cooling and heating systems is an absorption heat pump that uses environmentally friendly working fluids and can be run from various heat sources (gas, biomass, etc.), including waste heat and energy from solar systems. Direct connection between AHP Generator and hot air heat source which is investigated in this work from renewable heat source e.g., biomass can increase the efficiency

of the absorption system, reduce the consumption of funds and the size, complexity of the system, but the problems of compatibility of materials with ammonia-water and poor heat transfer properties of air are a challenge. Heat and mass transfer modelling was used to predict the performance of spiral rib generators and compact tube bundles forming powers up to 15 kW. A test plant for testing hot air generator with heat pump absorption (ammonia - water) was formed, which was used for cooling and heating. Hot air - generator performance was recorded in the range of air temperature (from 5 to 30 ° C inlet, outlet from 80-140 ° C), at air flow rate 6500 m³/h. The results of this investigation can be used to guide the development of air-connected heat and mass exchangers for compact absorption heat pumps. Further research will be conducted based on presented work.

2. CONTEMPORARY STATE OF THE ART OF ABSORPTION SYSTEMS

With the growing demand for environmentally safe and economic heat pumps that are independent of the electrical infrastructure required for compression systems, researchers De Francisco et al., 2002; Velazquez and Best, 2002; Kim and Ferreira, 2009 have developed solar-powered absorption systems [1,2,3], Lazzarin et al., 1996; Chua et al., 2002; Horuz and Callander, 2004; Wang et al., 2007, powered on natural gas [4,5,6,7], Moia et al., 2011 on micro gas turbines [8] and Keinath et al., 2012 on diesel engine exhaust gas [9]. The reviewed works here by Chua et al., 2002; Izquierdo et al., 2008; Moia et al., 2011; Keinath et al., 2012 include also indirect absorber/condenser cooling through a hydraulic loop and direct air cooling by Chua et al., 2002.



Fig. 1. Absorption Heat Pump made by Italian manufacturer

Indirectly cooled systems usually show lower efficiency compared to an equivalent direct cooling system due to the additional temperature difference it introduces between the working fluid and the medium fluid, and due to the parasitic power required by the hydraulic fluid pump. All system-level absorption studies studied in presented literature here used conventional coils with round tubes and flat fins to dissipate heat into the environment. In many cases, conventional air-connected heat exchangers make up a large part of the overall size of the system. Investigations are needed to develop new compact air-connected heat exchangers for use as an absorber and

condenser. The reduced size and weight of the system because of the innovative design of the components could improve the sustainability of the absorption heat pumps..

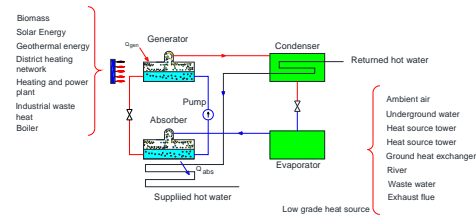


Fig. 2. Basic scheme of Absorption heat pump system

3. PHYSICAL AND MATHEMATICAL MODEL OF PELLET HOT AIR GENERATOR FOR AHP

A previous review of contemporary AHP technology and its investigations shows that mainly driving heat come from gas or waste heat, but very little or no from direct use of biomass - pellets in the generator. As an initial part of the investigation, the hot air generator on pellet was numerically simulated by burning the pellets to get a temperature and velocity field inside the combustion chamber, as an initial part in its modification to a AHP generator, Fig. 3. The hot-air generator was manufactured by the company "Megal ad" Bujanovac, and the maximum heating capacity tested in work was 15 kW.

The hot air generator will first be tested to acquire working parameters and in further investigations connected to absorption heat pump [1], mentioned in the previous chapters, Fig. 1. The shape and dimensions of the hot air generator are shown in Figures 3, 4. The evaporation temperature of the solution in the Italian GAHP generator is about 130 °C at 30 bar for the efficiency of gas utilization G.U.E. of 1.3 for a water outlet temperature of 50 °C, and for a weight ratio of refrigerant solution (NH₃-H₂O) of 0.45. The task of the further development of the biomass driven absorption heat pump will be to achieve as efficiently as it can presented parameters above.



Fig. 3. Hot Air Generator for driving the AHT

Firstly, several physical assumptions had to be reported and after the mathematical approach:

- the hot air generator model is three-dimensional and stationary, and combustion in a fixed layer is assumed inside the burner chamber.

- the real case of fuel supply to the combustion zone is replaced by the introduction of a piece of solid fuel (wood pellets from biomass) in the form of a dispersed phase in the domain of mathematical model (using "discrete phase" model within FLUENT software) [1];

- with regard to the adopted concept of mass consumption in the FLUENT, the mass flow of the dispersed phase is defined on the basis of fuel consumption for the tested CFD mode for 15 kW;

- It is assumed that the piece of fuel (dispersed phase) is spherical in shape, uniform density in all directions, where the size of the piece to be inserted is defined by the actual dimensions of the pellet (length and diameter) and fragmentation model is considered through Rosin-Rammler distribution.

- resistance to heat transfer and mass of pieces of pellets from biomass that are introduced into the fireplace are neglected due to relatively small pieces and small Biot number lower than 1 (one), while the temperature of introduced objects currently reaches the fuel temperature in the combustion zone [3];

- the interaction of fuel pieces (dispersed phase) is neglected, but they react only in the continuous phase;

- a two-stage combustion process is assumed which is described in the combined final reaction rate model / vortex dissipation model in the FLUENT software;

- volatile constituents for the tested fuel used in the model are presented in the form of a fictitious formula based on the elemental composition and technical analysis.

The conservation equations solved by FLUENT are shown below as a RANS model in the Cartesian coordinate system.

- The mass conservation equation:

$$\frac{\partial \rho}{\partial t} + \nabla(\rho \vec{u}) = S_m \quad (1)$$

As it is assumed that $\frac{\partial \rho}{\partial t}$ is equal to zero we get the final form of equation 1:

$$\nabla(\rho \vec{u}) = S_m \quad (2)$$

ρ is the density of the fluid stream, \vec{u} is the velocity vector, $\vec{u} = (u_x \vec{i} + u_y \vec{j} + u_z \vec{k})$,

t is time and the S_m is the mass source term inside the firebox.

- Momentum conservation equation:

$$\frac{\partial(\rho \vec{u})}{\partial t} + \nabla(\rho \vec{u} \vec{u}) = -\nabla p + \nabla \cdot \overline{\overline{\tau}} + \rho \vec{g} + \vec{F} \quad (3)$$

where p is the static pressure, $\overline{\overline{\tau}}$ - the Reynolds turbulent stress tensor, and $\rho \vec{g}$, are the gravitational body force and the external body forces and can be neglected, $\frac{\partial(\rho \vec{u})}{\partial t}$ is equal zero. According to given assumptions the momentum equation has the following form:

$$\nabla(\rho \vec{u} \vec{u}) = -\nabla p + \nabla \cdot \overline{\overline{\tau}} \quad (4)$$

while $\overline{\overline{\tau}} = \mu_{eff} (\nabla \vec{u} + \nabla \vec{u}^T)$ and $\mu_{eff} = \mu_k + \mu_t$ [Pas] is the effective viscosity as the sum of μ_k molecular and μ_t turbulent viscosity. Molecular viscosity depends on temperature while turbulent on k - ϵ turbulent parameters.

- Energy conservation equation:

$$\frac{\partial(\rho H)}{\partial t} + \nabla(\rho \vec{u} H) = \nabla \cdot \left(\frac{\lambda_t}{c_p} \nabla H \right) + S_h \quad (5)$$

Under the assumption that Lewis no. $Le = \frac{\lambda}{\rho c_p Dm} = 1$ where λ is conduction coefficient, λ_t turbulent conduction coefficient, Dm - mass diffusion rate, c_p - specific heat

capacity under constant pressure, S_h – source term of heat production, and that the $\frac{\partial(\rho H)}{\partial t}$ is equal to zero and the total enthalpy is calculated by equation:

$$H = \sum_j H_j Y_j \quad (6)$$

Where Y_j is the mass of the particle j , and its enthalpy is defined as:

$$H_j = \int_{T_{ref,j}}^T c_{p,j} dT + h_j^0(T_{ref,j}) \quad (7)$$

here $h_j^0(T_{ref,j})$ the enthalpy of formation of species j at referent absolute temperature $T_{ref,j}$.

- Conservation equation of chemical species:

$$\frac{\partial(\rho Y_j)}{\partial t} + \nabla \cdot (\rho \vec{u} Y_j) = -\nabla \cdot \vec{J}_i + R_i + S_i \quad (8)$$

Here R_i is the formation speed of species i during the chemical reaction and S_i is the speed of species formation because of the disperse phase. Mass transport for the turbulent model of combustion is represented as:

$$\vec{J}_i = -\left(\rho D_{i,m} + \frac{\mu_t}{Sc_i}\right) \nabla Y_i - D_{T,j} \frac{\nabla T}{T} \quad (9)$$

$Sc_i = \frac{\mu_t}{\rho D_i}$ is the Schmidt's number for turbulent flow, and is the coefficient of turbulent diffusion. Other important equations for sub models of the dispersed phase for solid parts of pellets during combustion and chemical kinetics can be found in combustion literature.

Computational domain and Boundary conditions

The calculation domain of this case is the part on the side of the combustion products and on the side of the air because the combustion takes place inside the chamber and it is important to achieve the temperature field. For this geometry, three types of surfaces are identified as boundary conditions, one air inlet, pressure outlet (on the side of flue gases and hot air), and opaque wall shown below in Figure 4. The fuel mass inlet is 3.3 kg/h equivalent to 15 kW of simulated furnace capacity. The outlet is defined at the top of the domain where hot air leaves the domain, while the flue gases pass through the pipe heat exchanger leaving the domain at the top. Numerical calculations and graphics values were obtained on a workstation HP Z620, CPU: Xeon E5-2695 v2 (2

processors) 2.4 GHz, RAM: 32 GB, GPU: Radeon RX580 8GB, OS: Windows 10 pro x64, 24 cores. The finite volume method is applied to the case and discretization of domains, as an integral part of the FLUENT software package. The number of finite volumes of the tetrahedron within the domain is 403802.

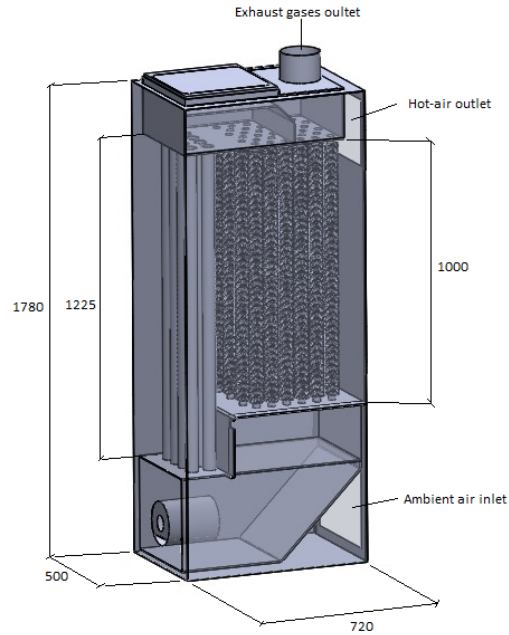


Fig. 4. Dimensions of computational domain of hot air generator

The discretization of partial differential equations is done by the 'Second Order-Upwind' scheme, and the SIMPLE algorithm was used for pressure and velocity field. The criterion for the convergence of the iterative process was that the last two values do not differ by more than 10^{-5} . Convergence was achieved after 10,000 to 12,000 iterations.

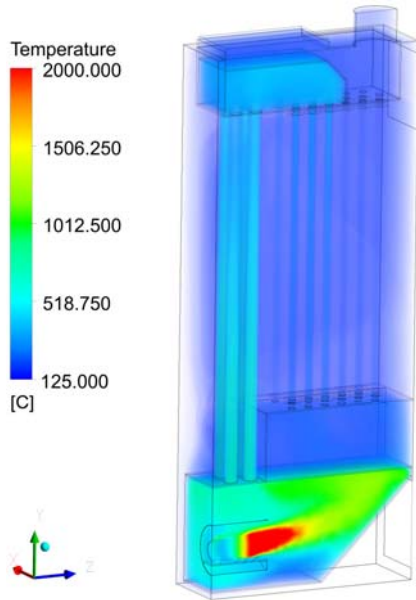


Fig. 5. Flue gas temperature at 15 kW of burner power through gaseous side

After converged solution achieved results in form of temperature field are shown on Fig. 5, and 6. In flue outlet part of the generator we have temperatures of around 130 °C, and on hot air side outlet we have temperatures of 80 - 140°C this temperature level could be appropriate for initiating the absorption process in generator of absorption heat pump for heat gains and triggering the absorption process, as the products of propane butane combustion are in that range.

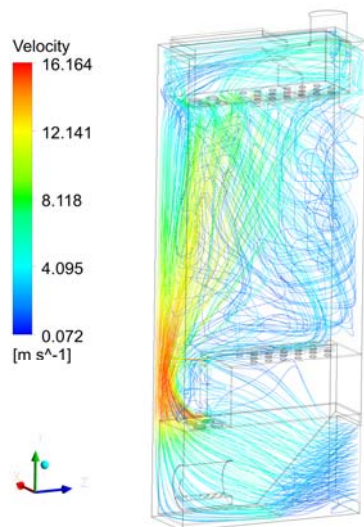


Fig. 6. Velocity of hot air inside the generator 15 kW of burner power

For simulated flow of 700 m³/h velocities inside the machine and the outlet varies between 0.5 and 17 m/s.

This velocity range is appropriate for downward flow stream of AHP generator as pressure drops could be significant inside due to construction.

4. CONCLUSION

Essence of the work presented is a numerical simulation of pellet hot air generator and its combustion. It gave us the temperature field within the domain, as shown on Figure 5 and velocity on Figure 6. This is of high importance for estimating possible working parameters of AHP system and its cooling and heating capacities. It is predictable from the Figure 5 which level of absorption heating capacity it will achieve. The operating temperatures of the ammonia / water solution in the generator range from 80 to 160 °C for a pressure range of 30-35 bar, when the ammonia evaporates from the solution; there are possibilities of creating different shapes and sizes of generators, which can be placed in the upper positions of the furnace, depending on the temperature and heat flux. It can be seen from Figure 5 that the average volumetric temperature of the furnace for the required heat loads is above 400 °C, which is sufficient to start the absorption process within the AHP. With these results, further research will continue with the production of a surface generator and connection to an AHP ammonia / water furnace and heat pump for actual performance tests.

Acknowledgement

This research was financially supported by the Ministry of Education, Science and Technological Development of the Republic of Serbia (Contract No. 451-03-9/2021-14/200109).

REFERENCES

- [1] De Francisco, A., Illanes, R., Torres, J., Castillo, M., (2002). Development and Testing of a Prototype of Low-Power Water–Ammonia Absorption Equipment for Solar Energy Applications. *Renewable Energy*, vol. 25 no 4 p. 537-544.
- [2] Velázquez, N., Best, R., (2002). Methodology for the Energy Analysis of an Air Cooled Gax Absorption Heat Pump Operated by Natural Gas and Solar Energy. *Applied Thermal Engineering*, vol. 22 no. 10, p. 1089-1103
- [3] Kim, D., Ferreira, I., (2009). Air-Cooled Libr–Water Absorption Chillers for Solar Air Conditioning in Extremely Hot Weathers. *Energy Conversion and Management*, vol. 50 no. 4, p. 1018-1025
- [4] Lazzarin, R., Gasparella A., Romagnoni P., (1996), Experimental Report on the Reliability of Ammonia-Water Absorption Chillers, *International Journal of Refrigeration*, vol. 19 no. 4 p. 247-256
- [5] Chua, H., Toh, H., Ng, K. (2002), Thermodynamic Modeling of an Ammonia–Water Absorption Chiller, *International Journal of Refrigeration*, vol. 25 no. 7, p. 896-906
- [6] Horuz, I., Callander, T., (2004). Experimental Investigation of a Vapor Absorption Refrigeration System. *International journal of refrigeration*, vol. 27 no 1, p. 10-16.
- [7] Wang, L., Chen, Q., (2007). Thermodynamic Performance Analysis of Gas-Fired Air-Cooled Adiabatic Absorption Refrigeration Systems. *Applied thermal engineering*, vol. 27 no. 8, p. 1642-1652.
- [8] Moya, M., Bruno, P., et al. (2011). Performance Analysis of a Trigeneration System Based on a Micro Gas Turbine and an Air-Cooled, Indirect Fired, Ammonia–Water Absorption Chiller, *Applied Energy*, vol. 88 no. 12 p. 4424-4440.
- [9] Keinath, C., Delahanty, C., Garimella, S., (2012). Diesel Engine Waste-Heat Driven Ammonia-Water Absorption System for Space-Conditioning Applications



Banja Luka
28-29 May 2021.

DEMI 2021

15th International Conference on Accomplishments in Mechanical and Industrial Engineering

www.demi.mf.unibl.org



Review of Solar Dish Stirling Engines for Micro-Cogeneration

M. Grozdanović^a, V. Stefanović^a, S. Pavlović^a, M. Laković-Paunović^a, M. Ilić^a,
N. Tomić^a

^aUniversity of Niš, Faculty of Mechanical Engineering, 14 Aleksandra Medvedeva Street, Niš, Serbia

Abstract *The exploitation of renewable energy sources is the future of energy systems. The utilization of solar energy is a promising way to reduce using fossil fuels for electricity generation. Solar dish Stirling engine is one of most efficient ways to produce electricity with relatively high efficiency. The objective of the present paper is to review and discuss the studies about solar dishes coupled with Stirling engines for heat and electricity generation (cogeneration). The solar dish concentrator is a type of solar collector with the highest concentration ratio and it can be utilized in many ways, but one of the most popular is with the Stirling engine. Stirling engine is type of external combustion engine and it has average efficiency of up to 30 %. The overall system efficiency can be increased with the utilization of useful heat. This idea is also called solar micro-cogeneration. In this work, the most important and the most recent studies are included. The most important results are clearly summarized and the future trends in the field are highlighted.*

Keywords *solar energy, solar dish concentrator, Stirling engine, micro-cogeneration*

1. INTRODUCTION

The exploitation of fossil fuels for electricity generation brought problems with carbon emissions. [1, 2] Utilization of renewable energy sources (RES) can be the way to reduce bad impact to the environment, [3] and they are accounted as promising way to produce energy for the community. RES are solar energy, wind power, geothermal energy, etc. But solar energy can be efficient source for heat and power production. [4] Solar energy can be utilized as non concentrated and concentrated solar power. [5]

Concentrated solar power (CSP) systems are one of most modern systems for RES utilization. CSP systems use a number of mirrors to concentrate the sun's rays on a relatively small receiver. The produced heat can be used to generate power or for industrial processes. [1,6] There are four CSP technologies already being used globally in the heat and power industry: parabolic trough concentrators (PTC), linear Fresnel reflectors, solar towers, and parabolic dish concentrators. [1, 7, 8]

Parabolic solar dish concentrators (solar dish collectors) can be used for operation in medium and high temperature levels. [9] Compared to PTC, parabolic dish concentrators have better performance because of the higher concentration ratio, lower thermal losses and higher thermal efficiency. [10] Solar dish collectors can be used in many applications for heat and electricity generation. [9, 11]

Corresponding author

Master in Mechanical Engineering, Milan Grozdanović
milan.grozdanovic@masfak.ni.ac.rs
University of Niš, Faculty of Mechanical Engineering
14 Aleksandra Medvedeva Street
Niš, Serbia

Solar dish is usually coupled with Stirling engine. Solar dish – Stirling systems (SDSS) are promising technology for heat and power generation. [12, 13] The SDSS have high solar=electricity efficiency, scalable power generation and high modularity. SDSS consists of a parabolic dish concentrator and a Stirling engine system. [14] Stirling engine is type of external combustion engine and it has average efficiency of up to 30 %. The overall system efficiency can be increased with the utilization of useful heat. This idea is also called solar micro-cogeneration. [14, 15]

Cogeneration or combined heat and power production (CHP) is simultaneous production of electricity and usable thermal energy. The exhaust heat from any thermal power plant can be used for CHP applications. The micro-cogeneration or mCHP can be defined as the simultaneous production of heat/cooling, energy and power based on small energy conversion units below 15 kWel. [16]

In this paper, the most recent real mCHP solar dish Stirling systems will be presented. In the next heading the review of mCHP systems will be given.

2. REVIEW OF SIMULATED PLANTS

Guarino *et al.* worked on dish-stirling solar concentrator coupled to a seasonal thermal energy storage system in the southern Mediterranean basin. They introduced heat and electric power cogeneration plant which consists of a field of dish-Stirling collectors, a seasonal geothermal storage and a system of water-to-water heat pumps (Figure 1). The CHP plant is designed to produce heat and electricity to supply one building of the Department of Engineering in Palermo. This system is combination of CSP and a Borehole Thermal Energy Storage (BTES). They used TRNSYS software for operation numerical simulations, and the plant is simulated on hourly base. They didn't have real plant, except a pilot dish-Stirling collector located at Department, which is used for experimental data. They also used energy and economic performance indicators to select the best configurations among 1440 analysed cases. Results showed that it is possible to cover 97 % of thermal loads and 64 % of electricity loads. [17]

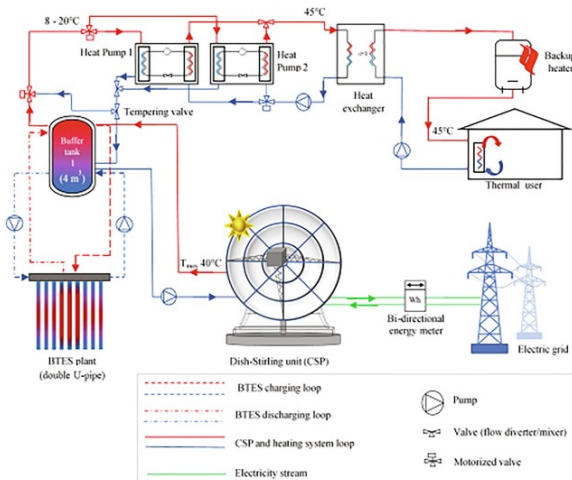


Fig. 1. Schematic representation of the proposed CHP plant [17]

Ferreira *et al.* developed a methodology for the thermal-economic optimization of solar Stirling mCHP system, at the design stage (Figure 2). With this methodology, the authors defined a methodology for the thermal-economic optimization and accounted both heating and hot water needs. The design of this system required solving a mathematical model that take into account the geometric, optical and thermal behaviour of all components. They formulated thermal-economic model as a non-linear optimization problem with non-linear constraints, and modelled each component using first law balance. The objective were the minimization of the total investment cost and the maximization of the efficiency of the system. The authors used MatLab programming language. The thermal efficiencies were between 66.3% and 76.1%. [18]

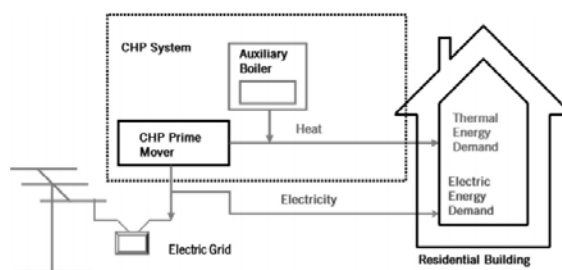


Fig. 2. Schematics of a layout of the cogeneration-integrated system for a residential building, considering the integration of the CHP prime mover with the electric grid, a backup boiler, both interconnected to the residential building. [18, 19]

Al-Dafaie et al. proposed utilizing rejected heat from Stirling engine to produce potable water. Their idea was to evaporate water and then to condense it on a cold surface continuously cooled by the ambient (Figure 3). In the proposed system the conventional heat exchanger is replaced by a heat exchanger with an evaporator that evaporates water. They put mathematical model and then simulated the system with real weather data for six days. An economic analysis for four different scenarios is also done. The results showed that water production varies during the day, it can improve efficiency of Stirling engine. [20]

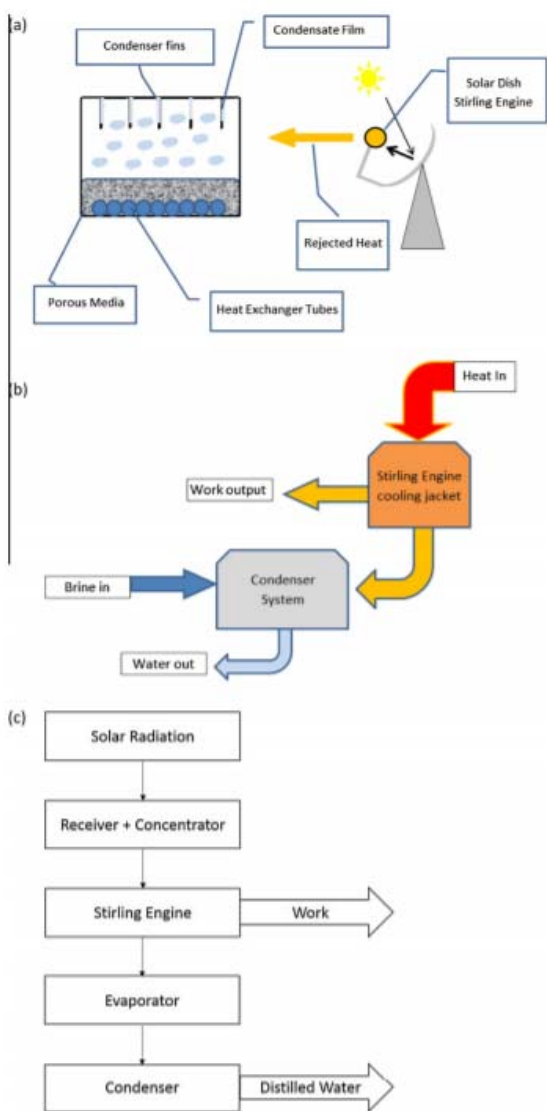


Fig. 3. (a) Schematic diagram showing the basic idea of the proposed study. (b) How the system is connected. (c) Energy flow diagram and system output [20]

Prinsloo et al. worked on a novel Stirling solar mCHP for rural African village locations. They proposed system which can help to enable solar energy utilization within the physical and socio-economic reality of isolated rural areas in South Africa. It will be a stand-alone 100% renewable energy solar powerpack in rural microgrid energy distribution network applications. The system will deliver around 3 kW of heat and 1 kW of electricity. They used TRNSYS software for modeling the main components of the proposed mCHP system. Statistical weather data are used for performance exploring. The main goal is to reduce fuel wood consumption for hot water and electricity generation. [21]

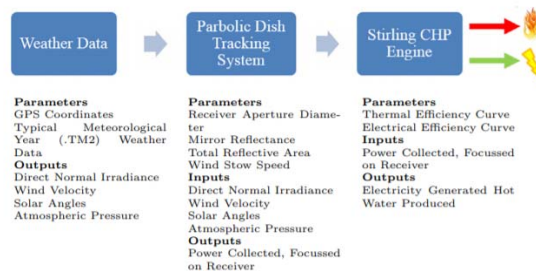


Fig. 4. TRNSYS sequential model flow diagram for solar micro-CHP powerpack [21]

Moghadam et al. worked on sizing a solar dish Stirling mCHP system for residential application. They used 3E analysis for analysing proposed system. They also used five different locations in Iran with diverse climatic and solar irradiation conditions because energy demands of the building and output power of the engine depends on of weather condition and solar irradiation flux. The system had to produce electricity, and energy for heating and cooling (Figure 5). There were three scenarios for solar dish Stirling system. The first scenario: solar dish Stirling engine is sized for the lowest annual electric power demand; the second scenario: solar dish Stirling engine is sized for the highest annual electric power demand; the third scenario: a solar dish Stirling engine with constant output capacity was considered for the five locations. Results showed that this system can help to decrease carbon emissions and also to save primary energy. The payback period is acceptable in all scenarios. [22]

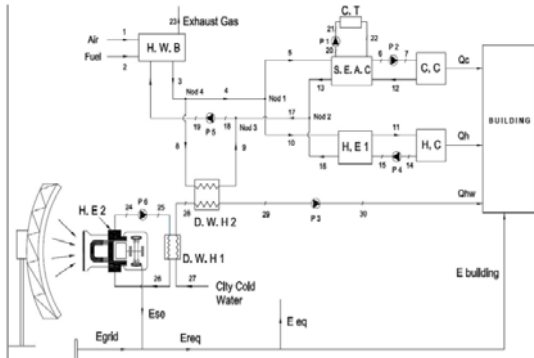


Fig. 5. Schematic of the solar dish Stirling micro-CHP system [22]

Romage et al. proposed hybrid compression/absorption chiller driven by Stirling engine and low-capacity solar dish concentrator (Figure 6). The whole system consists of 5 subsystems: space conditioning system (SCS), compression refrigeration system (CRS), thermal engine system (TES), absorption refrigeration system (ARS) and solar energy system (SES). They worked on energy and mass balance of each subsystem. The hybrid compression/absorption chiller is powered by solar dish Stirling engine, compression is powered by Stirling work output, and absorption is powered by rejected heat of Stirling engine. They used many variables for modeling and simulation. Results showed that this new system can be sustainable supplier for heat and cold energy in SCS. This is for climate conditions in Mexico City. [23]

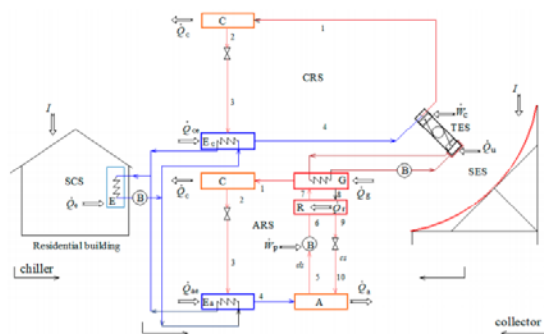


Fig. 6. Schematic diagram of the hybrid compression/absorption chiller fed by Stirling engine and solar energy [23]

Guarino et al. worked on integrating a dish-Stirling concentrator into energy systems used for meeting the air conditioning demand of an office building. They assumed a natural gas boiler for heating purposes and air-cooled

chillers for the cooling periods, and a reversible heat pump for both heating and cooling. Dish-Stirling concentrator had two operating modes - electric-mode and a cogenerative-mode. The TRNSYS software is used for system simulations. Results showed that the cogenerative-mode can achieve better performance than electric-mode. Results also showed that dish-Stirling system allows promising energy-saving and reduction in CO₂ emissions. [24]

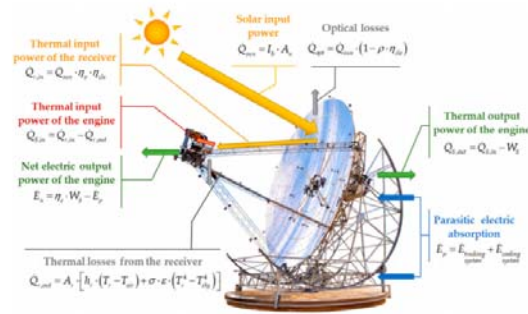


Fig. 7. Scheme of the energy balance of a dish-Stirling concentrator [24]

Ferreira et al. worked on methodology for the thermal-economic optimization of mCHP solar dish Stirling engine system. They considered the maximization of the annual worth from the system operation, subjected to the nonlinear thermodynamic and economic constraints. MatLab was used for numerical simulations and the Generalized Pattern Search optimization algorithm with MADSPositiveBasis2N was used in the determination of the optimal solution. Thermal-economic methodology and the use of optimization algorithms enabled the best combination of geometrical and operational parameters of the system which allowed the best economic output. [25]

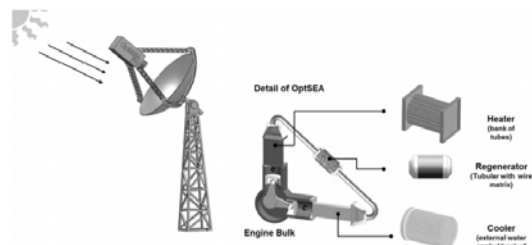


Fig. 8. Schematic layout of solar-powered Stirling engine for micro-generation [25]

Authors didn't find any real plant with solar dish Stirling engine for micro-cogeneration.

3. CONCLUSIONS

Solar dish Stirling engine is a promising way to utilize solar thermal energy for electricity generation. The efficiency can be increased if rejected heat is utilized for heating, cooling, etc. Solar dish Stirling engine micro-cogeneration plant is promising technology for sustainable energy supply, both for on-grid and off-grid systems.

In this paper, several mCHP systems are presented. It can be seen that this systems can be feasible.

This paper is the introduction in research of solar dish micro-cogeneration for PhD thesis of first author.

Acknowledgement

This research was financially supported by the Ministry of Education, Science and Technological Development of the Republic of Serbia (Contract No. 451- 03-9/2021-14/200109)

REFERENCES

- [1] Busceni, A., Lo Brano, V., Chiaruzzi, C., Ciulla, G., Kalogeri, C. (2020). A validated energy model of a solar dish-Stirling system considering the cleanliness of mirrors. *Applied Energy*, vol. 260, DOI: <https://doi.org/10.1016/j.apenergy.2019.114378>
- [2] Bilgili, M., Ozbek, A., Sahin, B., Kahraman, A. An overview of renewable electric power capacity and progress in new technologies in the world. *Renew Sustain Energy Rev* 2015;49:323–34. <https://doi.org/10.1016/j.rser.2015.04.148>.
- [3] Murugan, S., Horak, B. (2016). Tri and polygeneration systems - A review. *Renewable and Sustainable Energy Reviews*, vol. 60, p. 1032-1051. DOI: <http://dx.doi.org/10.1016/j.rser.2016.01.127>
- [4] Rafiei, A., Loni, R., Mahadzir, S. B., Najafi, G., Pavlovic, S., Bellos, E. (2020). Solar desalination system with afocal point concentrator using different nanofluids. *Applied Thermal Engineering*, vol. 174, DOI: <https://doi.org/10.1016/j.applthermaleng.2020.115058>
- [5] Kasaeian, A., Bellos, E., Shamaeizadeh, A., Tzivanidis, C. (2020). Solar-driven polygeneration systems: Recent progress and outlook. *Applied Energy*, vol. 264, DOI: <https://doi.org/10.1016/j.apenergy.2020.114764>
- [6] Buscemi, A., Panno, D., Ciulla, G., Beccali, M., Brano, V.L. (2018). Concrete thermal energy storage for linear Fresnel collectors: Exploiting the South Mediterranean's solar potential for agri-food processes. *Energy Convers Manag* 2018;166. <https://doi.org/10.1016/j.enconman.2018.04.075>.
- [7] Zhang, H. L., Baeyens, J., Degreève, J., Cacères, G. (2013). Concentrated solar power plants: review and design methodology. *Renew Sustainable Energy Review* ;22:466–81. DOI: <https://doi.org/10.1016/j.rser.2013.01.032>.
- [8] Ogunmodimu, O., Okoroigwe, E. C. (2018). Concentrating solar power technologies for solar thermal grid electricity in Nigeria: A review. *Renewable Sustain Energy Review*, vol. 90, p. 104-119. DOI: <https://doi.org/10.1016/j.rser.2018.03.029>
- [9] Pavlovic, S., Daabo, A. M., Bellos, E., Stefanovic, V., Mahmoud, S., Al-Dadah, R. K. (2017). Experimental and numerical investigation on the optical and thermal performance of solar parabolic dish and corrugated spiral cavity receiver. *Journals of Cleaner Production*, vol 150, p. 75-92. DOI: <http://dx.doi.org/10.1016/j.jclepro.2017.02.201>
- [10] Abid, M., Ratlamwala, T., Atikol, U., (2015). Performance assessment of parabolic dish and parabolic trough solar thermal power plant using nanofluids and molten salts. *Int. J. Energy Res.* 40, 550e563. <http://dx.doi.org/10.1002/er.3479>
- [11] Pavlovic, S. (2017). *Istraživanje optimalnih parametara solarinih paraboličnih koncentrišućih prijemnika toplote sa aspekta primene u sistemima poligeneracije*. (In Serbian). PhD thesis. Mašinski fakultet Univerziteta u Nišu.
- [12] Zayed, M.E., Zhao, J., Elsheikh, A. H., Zhao, Z., Zhong, S., Kabeel, A. E. (2021). Comprehensive parametric analysis, design and performance assessment of a solar dish/Stirling system. *Process Safety and Environmental Protection*, vol. 146, p. 276-291. DOI: <https://doi.org/10.1016/j.psep.2020.09.007>
- [13] Zayed, M.E., Zhao, J., Li, W., Elsheikh, A.H., Zhao, Z., Khalil, A., Li, H., (2020). Performance prediction and techno-economic analysis of solar dish/Stirling system for electricity generation. *Appl. Therm. Eng.* Vol. 164, 114427. DOI:

- <https://doi.org/10.1016/j.applthermaleng.2019.114427>
- [14] Yan, J., Peng, Y. D., Cheng, Z. R., Liu, F. M., Tang, X. H. (2017). Design and implementation of a dish-Stirling concentrated solar power system. Proceedings of 2017 International Conference on New Energy and Future Energy System (NEFES 2017), vol. 93 012052 DOI: :10.1088/1755-1315/93/1/012052
- [15] Singh, U. R., Kumar, A. (2018). Review on solar Stirling engine: Development and performance. *Thermal Science and Engineering Progress*, vol. 8, p.244-256. DOI: <https://doi.org/10.1016/j.tsep.2018.08.016>
- [16] Pehnt, M., Cames, M., Fischer, C., Praetorius, B., Schneider, L., Schumacher, K., Voß, J.-P. (2006). *Micro Cogeneration - Towards Decentralized Energy Systems*. Springer, Berlin
- [17] Guarino, S., Buscemi, A., Ciulla, G., Bonomolo, M., Lo Brano, V. (2020). A dish-stirling solar concentrator coupled to a seasonal thermal energy storage system in the southern mediterranean basin: A cogenerative layout hypothesis. *Energy Conversion and Management*, vol. 222, 113222. DOI: <https://doi.org/10.1016/j.enconman.2020.113228>
- [18] Ferreira, A. C., Nunes, M. L., Teixeira, J. C. F., Martins, L. A. S. B., Teixeira, S. C. F. C., Nebra, S. A. (2017). Design of a solar dish Stirling cogeneration system: Application of a multi-objective optimization approach. *Applied Thermal Engineering*, vol. 123, p. 646-657. DOI: <http://dx.doi.org/10.1016/j.applthermaleng.2017.05.127>
- [19] Maghanki, M. M., Ghobadian, B., Najafi, G., Galogah, R. J. (2013). Micro combined heat and power (MCHP) technologies and applications. *Renewable and Sustainable Energy Review*, vol. 28, p. 510-524. DOI: <http://dx.doi.org/10.1016/j.rser.2013.07.053>
- [20] Al-Dafaie, A. M. A., Dandolan, M.-E., Al-Nimr, M. A. (2016). Utilizing the heat rejected from a solar dish Stirling engine in potable water production. *Solar Energy*, vol. 136, p. 317-326. DOI: <http://dx.doi.org/10.1016/j.solener.2016.07.007>
- [21] Prinsloo, G., Dobson, R., Mammoli, A. (2016). Model based design of a novel Stirling solar micro-cogeneration system with performance and fuel transition analysis for rural African village locations. *Solar Energy*, vol. 133, p. 315-330. DOI: <http://dx.doi.org/10.1016/j.solener.2016.04.014>
- [22] Moghadam, R. S., Sayyaadi, H., Hosseinzade, H. (2013). Sizing a solar dish Stirling micro-CHP system for residential application in diverse climatic conditions based on 3E analysis. *Energy Conversion and Management*, vol. 75, p. 348-365. DOI: <http://dx.doi.org/10.1016/j.enconman.2013.06.008>
- [23] Romage, G., Jimenez, C., Reyes, J. de J., Zacarias, A., Carvajal, I., Jimenez, J. A., Pineda, J., Venegas, M. (2020). Modeling and Simulation of a Hybrid Compression/Absorption Chiller Driven by Stirling Engine and Solar Dish Collector. *Applied sciences*, vol. 10 (24), 9018. DOI: <https://doi.org/10.3390/app10249018>
- [24] Guarino, S., Catrini, P., Buscemi, A., Lo Brano, V., Piacentino, A. (2021). Assessing the Energy-Saving Potential of a Dish-Stirling Concentrator Integrated Into Energy Plants in the Tertiary Sector. *Energies*, vol. 14 (4), 1163. DOI: <https://doi.org/10.3390/en14041163>
- [25] Ferreira, A. C., Nunes, M. L., Teixeira, J. C. F., Martins, L. A. S. B., Teixeira, S. C. F. C., Nebra, S. A. (2016). Thermodynamic and economic optimization of a solar-powered Stirling engine for micro-cogeneration purposes. *Energy*, vol. 111, p. 1-17. DOI: <http://dx.doi.org/10.1016/j.energy.2016.05.091>



Banja Luka
28–29 May 2021.

DEMI 2021

15th International Conference on Accomplishments in Mechanical and Industrial Engineering

www.demi.mf.unibl.org



Influence of building envelope on building energy consumption

J. Skerlić^a, D. Nikolić^b, J. Radulović^b, A. Radojević^b, M. Djordjević^a, A. Mišković^c

^aUniversity of Pristina in Kosovska Mitrovica; Faculty of Technical Sciences, Knjaza Milosa 7, 38220 Kosovska Mitrovica, Serbia

^bUniversity of Kragujevac, Faculty of engineering; Sestre Janjic 6, 34000 Kragujevac, Serbia

^cAcademy of professional studies Šumadija; Trg topolivaca 4, 34000 Kragujevac, Serbia

Abstract *The query of energy stability has become the key query of the world economic and social system in the last few years. In addition to its high development and evolution of its relationship to energy security, the EU also faces with the problem of environmental pollution, global warming and climate changes. For several decades, it has been recognized that renewable energy sources are the main support of the energy independence of the world in the future.*

Extensive efforts have been made to reduce CO₂ emissions generated by the intensive combustion of fossil fuels, to meet the growing energy needs of humanity. Continuous adoption of numerous directives in EU countries leads to the reduction of existing environmental imbalances on Earth, as well as greater energy efficiency.

The building envelope is a critical component for energy losses and heating energy consumption. So it is very important to design energy efficient buildings or implement the principles for improvement energy efficiency of already existing buildings. Paper shows the real consumption of primary and final energy in Serbian building, with variable thermal insulation thickness and different windows. A comparative analysis has showed that the improvement of the building envelope can greatly contribute to the improvement of building energy efficiency and reduction of energy consumption. The investigated building was located in Kragujevac, Serbia. The building is simulated in software EnergyPlus, while Open Studio plug-in Google SketchUp was used for building design. The paper also shows the building energy rate, depending on the thermal insulation thickness.

Keywords *building, thermal insulation, window, simulation, energy efficiency*

1. INTRODUCTION

Energy resources and their utilization relate to sustainable development. In attaining sustainable development, increasing the energy efficiencies of processes utilizing sustainable energy resources plays an important role. Humanity is in constant researching of new energy sources that would cover the growing energy needs. Many sources indicate that the construction sector has a high level of energy consumption, which is 20-40% of total energy

consumption, which means that we have a high level of CO₂ emissions of about 36%. Therefore, we should strive to improve the energy efficiency of the building. The EU obliges its members to continuously increase energy efficiency by adopting numerous directives in order to achieve greater energy efficiency and reduce existing environmental imbalances on Earth.

In Serbia, the building sector consumes more than 50% of the total energy consumption [1]. Heating systems in Serbia consume 60% of total

energy consumption [2]. The main reason for this is a large number of energy inefficient buildings in Serbia. For this reason, it is necessary to explore all aspects of energy consumption. The building envelope is one of the critical components for energy losses and heating energy consumption. So it is very important to design energy efficient buildings or implement the principles for improvement energy efficiency of already existing buildings.

The paper represents an energy analysis of a single - family residential building for three cases, with a small thickness of the insulation layer and ordinary single glazed windows, with a larger thickness of the insulation layer and with the use of higher quality windows (double and triple glazing) on facades with greater insulation thickness and their impact on heating energy consumption in typical residential buildings in Serbia. Heating system operated from October 15th to April 14th next year. The investigated building is located in the city of Kragujevac, Serbia. The building is simulated in software EnergyPlus, while Open Studio plug-in Google SketchUp was used for building design[3-6]. Obtained results show the real consumption of final and primary energy for heating. The paper also shows the building energy rate depending on the thermal insulation thickness, according to the Serbian standards. This very useful knowledge is also needed for identifying energy efficiency and energy conservation opportunities, as well as for dictating the right energy management strategies of a country.

2. MODEL OF ANALYZED BUILDING

The modeled residential building is shown in Figure 1. It is one-store building and it contains from 6 conditioned zones (living room, kitchen, hall, bathroom and two bedrooms). The total floor area of the building is 81 m². The windows are double glazed. The concrete building envelope, roof, and the floor were thermally insulated by polystyrene. In this investigation, the polystyrene thickness varied (0.05 m, 0.1 m and 0.15 m).

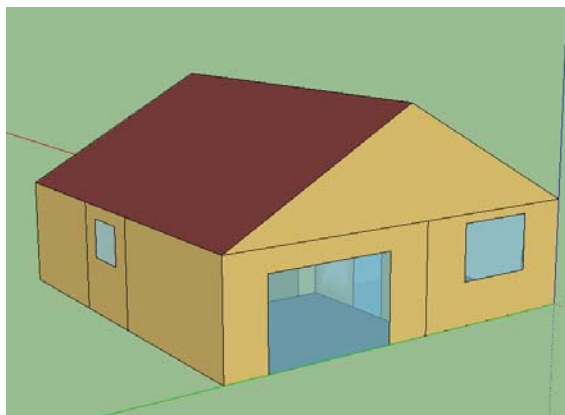


Figure. 1. Modeled building in EnergyPlus - south facade

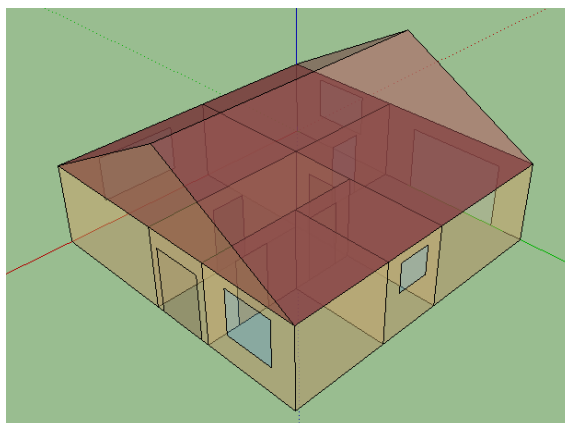


Figure. 2. Modelled building in EnergyPlus - X ray view

Generally, electricity in building is consumed for lighting, domestic hot water (DHW) and appliances. It is analyzed real heating energy consumption (final and primary energy) in the residential building. First, it will be given the required heating energy for the modeled building (obtained with simulation in EnergyPlus software), for different thermal insulation thickness, then real energy consumption and building energy rate.

3. REQUIRED HEATING ENERGY

The amount of required heating energy Q_h in the analyzed residential building is obtained by simulations in software package EnergyPlus (Table 1). The heating energy is independent of the heating system. The results below show the amount of heating

energy Q_{hr} , as well as the total final energy consumption Q_f (annually), in the case of different thermal insulation thickness: 0.05 m, 0.1 m and 0.15 m.

Table 1. Building final energy consumption for different thermal insulation thickness

Energy consumption, GJ	Case 1
Heating (Q _h)	32.73
Lighting	0.5
Electric equipment	8.91
Total energy consumption	42.14
Energy consumption, GJ	Case 2
Heating (Q _h)	23.66
Lighting	0.5
Electric equipment	8.91
Total energy consumption	33.07
Energy consumption, GJ	Case 3
Heating (Q _h)	22.29
Lighting	0.5
Electric equipment	8.91
Total energy consumption	31.7

Based on Table 1 it can be concluded that the consumption of heating energy depends on the thickness of the thermal insulation. Heating energy consumption is the lowest in case of maximum thermal insulation thickness. Figure 2 shows a comparison of the energy consumption in the building, depending on the insulation thickness.

In the further investigations, it will be discuss the case of building with 0.15 m thermal insulation thickness, because it is the most favorable case from the aspect of energy efficiency. In this case, the required heating energy has the lowest value; heating losses are the smallest, as the U value through the building envelope. By implementation of some other principles of energy efficiency, building energy consumption could be reduce even more. Also, incorporation of renewable energy sources has

a significant role in the reduction of total building energy consumption.

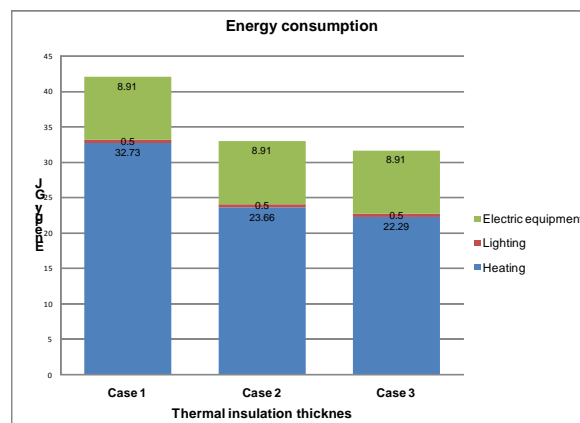


Figure 2. Structure of energy consumption in modeled building

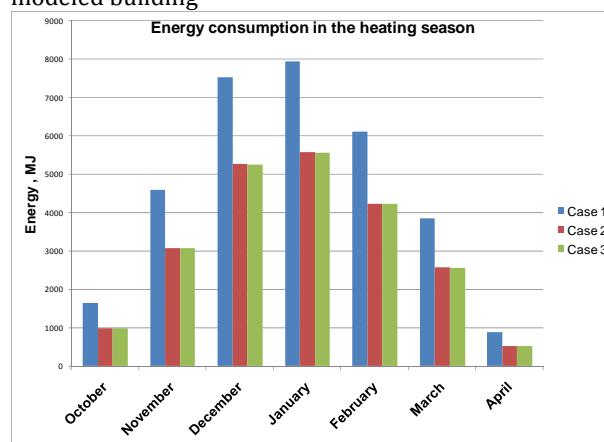


Figure 3. Energy consumption in the heating season for case 1,2,3

Table 2 shows a comparison of the U values for exterior wall, interior wall and roof in the buildings with different thermal insulation thickness. With increasing of thermal insulation thickness (which is placed at exterior walls), U values decreasing through the building envelope. By implementation of some other principles of energy efficiency, building heating energy consumption could be reduce even more.

Table 2. U values for exterior walls, interior walls and roof, in the cases of the building with different thermal insulation thickness

U [W/m ² -K]	Case 1
Exterior wall	0.429
Interior wall	0.490
Roof	1.138

U [W/m ² -K]	Case 2
Exterior wall	0.250
Interior wall	0.490
Roof	1.138
U [W/m ² -K]	Case 3
Exterior wall	0.177
Interior wall	0.490
Roof	1.138

4. REAL HEATING ENERGY CONSUMPTION

The amount of real heating energy consumption (Q_{fin}) depends of different values of some efficiency coefficients. These coefficients are related to base board efficiency, boiler efficiency, pump efficiency and heat exchanger efficiency. Some of these coefficients figure in terms of real energy consumption calculating, and they are different for different space heating system, like equation for real energy consumption [7, 8].

4.1 Real final heating energy for analyzed building and electric space heating

Real energy consumption for electric space heating in building is given in equation (1):

$$Q_{fin} = \frac{Q_h}{\eta_{er}} \quad (1)$$

where η_{er} stands for efficiency of convective electric baseboard ($\eta_{er}=0.95$, [9]).

4.2 Real consumption of final and primary heating energy

According to the above coefficients and equation 1, real consumption of final heating energy consumption (Q_{fin}) for analyzed electric space heating system in modelled building can be calculated. Primary heating energy consumption (Q_{prim}) is calculated by multiplying the real final heating energy consumption with the corresponding primary conversion multiplier. For Serbia, primary conversion multiplier for for electricity is 3.04 [1].

Next table (Table 3) shows results for real consumption of final and primary heating energy, for analyzed heating system in the modelled building. It is also presented the specific heating energy consumption in analyzed buildings (real final heating energy per conditioned area).

Table 3. Building real final and primary heating energy consumption (kWh)

Insulation thickness	Case 1
Required heating energy (Q_h)	9091.65
Real final heating energy (Q_{fin})	9570.157
Heating energy/area (Q_{fin}/A)	112.25
Primary heating energy (Q_{prim})	35586.011
Insulation thickness	Case 2
Required heating energy (Q_h)	6572.222
Real final heating energy (Q_{fin})	6918.128
Heating energy/area (Q_{fin}/A)	81.14
Primary heating energy (Q_{prim})	27925
Insulation thickness	Case 3
Required heating energy (Q_h)	6191.666
Real final heating energy (Q_{fin})	6517.543
Heating energy/area (Q_{fin}/A)	76.45
Primary heating energy (Q_{prim})	26769.444

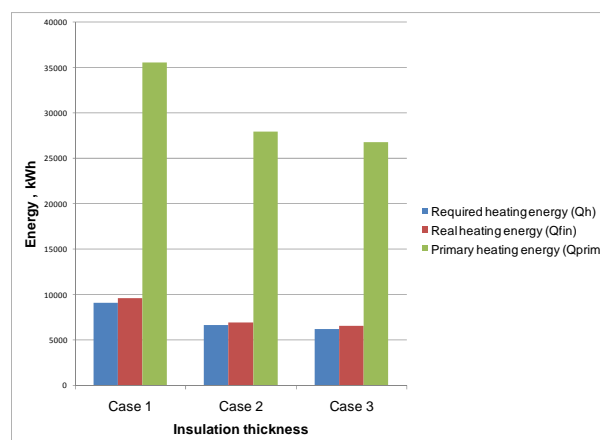


Figure 4. Required heating energy, final and primary heating energy consumption in modeled building for different thermal insulation thickness

Figure 4 shows the graphical presentation of obtained results for required, real final and primary heating energy for three different cases – thermal insulation of 0.05 m, 0.1 m and 0.15 m. It can be concluded that real annual final heating energy consumption in the building with the 0.1 m of thermal insulation is lower by 22%, compared to the building with smallest insulation of 0.05m. In the case of thermal insulation of 0.15 m - real annual final heating energy consumption is lower by 25%, compared to the building with smallest insulation of 0.05 m. The percentage of the annual primary energy saving is the same as in case of real final energy saving.

5. BUILDING ENERGY RATE

A Building Energy Rating or BER is an energy label with accompanying advisory report for buildings. The building rating is a simple A to G scale. A-rated buildings are the most energy-efficient and will tend to have the lowest energy bills. The Advisory Report identifies potential energy performance improvements that could lead to better comfort levels, reduced energy use and costs. A BER is valid for up to 10 years provided that there is no material change to the home that could affect the energy performance.

A BER in the EU is based on the calculated energy performance and associated carbon dioxide emissions for the provision of space heating, ventilation, water heating and lighting under standardised operating conditions. The characteristics of the major components of the home including dimensions, orientation, insulation, and space and hot water system efficiencies are used in the calculation. The energy performance is expressed as:

(a) Annual primary energy use per unit floor area (kWh/m²) represented on an A to G scale; and

(b) Associated annual Carbon Dioxide (CO₂) emissions in kgCO₂/m².

A BER is only an indication of the energy performance of a home, it does not include electricity used for purposes other than heating, lighting, pumps and fans. Therefore the energy used for electrical appliances such as cookers, fridges, washing machines and TVs is excluded. The standards and rules for building energy rating are different in different countries. In Serbia, building energy rate is determined only on the basis of annual building energy

consumption for heating per m² of heated space [11]. Analyzed building belongs to the group of typical Serbian buildings which are built in 1970 i 1980s. These buildings are energy-inefficient buildings, so that is the main reason for the great values of energy consumption for heating and specific heating energy consumption (per m² of heating area). This building is classified at D-rate, because in modeled cases 2 and 3, the specific energy consumption was in range of 70 -105 kWh/m² (Table 4).

Table 4. Building energy rate in Serbia

		<i>New building</i>	<i>Old building</i>
Building Energy Rate	QH,nd,rel [%]	QH,nd [kWh/(m ² a)]	QH,nd [kWh/(m ² a)]
A+	≤ 15	≤ 9	≤ 10
A	≤ 25	≤ 15	≤ 18
B	≤ 50	≤ 30	≤ 35
C	≤ 100	≤ 60	≤ 70
D	≤ 150	≤ 90	≤ 105
E	≤ 200	≤ 120	≤ 140
F	≤ 250	≤ 150	≤ 175
G	> 250	> 150	> 175

6. CONCLUSION

The paper represents an energy analysis of a single - family residential building for three cases, with a small thickness of the insulation layer and ordinary single glazed windows, with a larger thickness of the insulation layer and with the use of higher quality windows (double and triple glazing) on facades with greater insulation thickness and their impact on heating energy consumption in typical residential buildings in Serbia.

Software EnergyPlus was used for simulating of building energy behaviour, while building design was conducted in Open Studio plug-in for Google SketchUp software.

Three cases of the thermal insulation thickness at the same building, with electric space heating system are investigated – 0.05 m, 0.1 m and 0.15 m. It was calculated required heating energy consumption, real final and primary heating energy consumption and specific energy consumption.

Obtained results showed that real annual final heating energy consumption in the building with the 0.15 m of thermal insulation and with

the use of higher quality windows is lower by 25%, compared to the building with smallest insulation of 0.05 m and ordinary single glazed windows.

In accordance with Building Energy Rating in Serbia, this building is classified at D-rate, because in modeled cases 2 and 3, the specific energy consumption was in range of 70-105 kWh/m².

This fact means that the energy efficiency of the analyzed building can be significantly improved by thermal insulation on the external walls and by installing high quality windows as an integral part of the facade. By taking further measures to improve energy efficiency, financial savings can be increased at a very high level.

Acknowledgement

This paper presents results obtained within realization of two projects TR 33015 and III 42006, funded by Ministry of Education, Science and Technological Development of the Republic of Serbia. The authors would like to thank to the Ministry for their support during these investigations.

REFERENCES

- [1] Bojić M., Nikolić N., Nikolić D., Skerlić J., Miletić I., (2011). A simulation appraisal of performance of different hvac systems in an office building, *Energy and Buildings*, 43/6, p. p. 2407-241.
- [2] Nikolic D., Skerlic J., Radulovic J., (2017). Energy efficient buildings – legislation and design, 2nd International Conference on Quality of Life, Kragujevac, Conference Proceedings, p. 55-60.
- [3] Anonymous, (2009). ENERGYPLUS, Input Output Reference - The Encyclopedic Reference to EnergyPlus Input and Output, University of Illinois & Ernest Orlando Lawrence Berkeley National Laboratory
- [4] R.H. Henninger, M.J. Witte, D.B. Crawley, Analytical and comparative testing of EnergyPlus using IEA HVAC BESTEST E100-E200 test suite, *Energy and Buildings* 36 (8) (2004) 855-863.
- [5] The board of trustees of the University Of Illinois and the regents of the University Of California through the Ernest Orlando Lawrence Berkeley, National Laboratory, ENERGYPLUS, EnergyPlus Engineering Document, The Reference to EnergyPlus Calculations (in case you want to need to know), March 29, 2004.
- [6] Milorad Bojić, Jasmina Skerlić, Dragan Cvetković, Danijela Nikolić, Marko Miletić, Positive net buildings: simulations and optimization, Conferinta nationala de instalatii – Instalatii pentru inceputul mileniului trei, Romania, Sinaia, 17-19. Oktobar 2012., Proceedings, ISBN 978-973-755-857-2, pp. 79-86.
- [7] Zrnić, S., Čulum, Ž., (1966). *Grejanje i klimatizacija sa primenom solarne energije*, Naučna knjiga, Beograd
- [8] Todorović, B. (2005). *Projektovanje postrojenja za centralno grejanje*, Mašinski fakultet Univerziteta u Beogradu, Beograd
- [9] *Pravilnik o energetskej efikasnosti zgrada*, Beograd, 2011., <https://www.mgsi.gov.rs/lat/dokumenti/pravilnik-o-energetskej-efikasnosti-zgrada>, (accessed 10.02.2021.)



Banja Luka
28–29 May 2021.

DEMI 2021

15th International Conference on
Accomplishments in Mechanical and
Industrial Engineering

www.demi.mf.unibl.org



Experimental investigation of hydrogen engine working cycle with a lean mixture

I. Grujić^a, N. Stojanović^a, A. Davinić^a, R. Pešić^a

^aUniversity of Kragujevac, Faculty of Engineering, Department for Motor Vehicles and Motors, 6 Sestre Janjić STR., 34000 Kragujevac, Serbia

Abstract *The hydrogen is known as promising fuel in the future. The main advantage of the hydrogen is chemical composition which is responsible for low emission of carbon components. In the paper experimental work with hydrogen is presented, which was performed on a test engine specially modified for work with gaseous fuels. The injection and ignition parameters providing regular engine work are shown, at presented regime. The engine work was achieved with lean mixture, in order to reduce the combustion speed of the hydrogen, which should lead to the reduction of temperatures that occur during the working process, in order to avoid creation of high concentration of nitrogen oxides, which are characteristic when hydrogen is used. The working cycle as well as the combustion process and exhaust emissions were analyzed. It was concluded that with adequate injection and ignition parameters the regular engine work can be achieved, with satisfying performances.*

Keywords *hydrogen, experiment, injection and ignition parameters, performance*

1. INTRODUCTION

The mobility and transportation are important activity of human life. However, the vehicles as the main part of transportation systems have and downside. The increased number of vehicles is followed by the increased number of active IC engines. IC engines are considered as one of greatest polluters, and because of this, the tendency in past few years is to find the alternative for IC engines. In most cases, as the alternative electric motors are considered – electric drive train. Electric drive train is promoted as something new, and as the

perfection of technology. However, nobody takes into the consideration that the electric drive train do not remove the emission, but only dislocates it. Not many takes into consideration the necessary materials and infrastructure for vehicles electrification. This means that many points were not taken into the consideration when electric drive train is promoted. All of this shift the best perspective toward the hybrid vehicles. In the future one can expect the hybrid drive train to become the most common type of drive train used at vehicles. The most used IC engine will be spark ignition engine, while diesel engines will probably be used only where is necessary (at trucks, boats...).

The option that should be taken into consideration is usage of alternative fuels. One of the fuels that is considered as possible alternative fuel for conventional spark ignition engine is hydrogen [1]. The early research shows that the hydrogen is very adequate fuel for using in the spark ignition engines. The main

Corresponding author

M.Sc., Nadica Stojanović
nadica.stojanovic@kg.ac.rs

University of Kragujevac, Faculty of Engineering,
Department for Motor Vehicles and Motors
6 Sestre Janjić STR.
Kragujevac, Serbia

reason for this is the high auto ignition temperature, which is around 848 K [2]. The main reason why hydrogen is taken into the consideration as fuel ecological, as its chemical composition doesn't include carbon so, in theory, shouldn't have carbon components in the exhaust [3]. However, the hydrogen has and bad sides. The great combustion speed and great energy are causing higher combustion temperatures which causes the increment of nitrogen oxides [4]. Because of this, hydrogen is commonly considered only as an additive for conventional fuels [5].

In this paper, experimental investigation of the prechamber IC engine performance with hydrogen is presented. The aim of the paper is to show that the engine work with lean mixture can provide regular engine performance with hydrogen as fuel, as well as to reduce the concentration of nitrogen oxides which are the greatest problem in the exhaust when hydrogen is used.

2. EXPERIMENTAL INVESTIGATION

The experimental investigation of an IC engine with hydrogen as fuel was conducted at the Faculty of Engineering, University of Kragujevac in the Laboratory for IC engines and fuels.

Gas installation was developed and implemented on the existing IC engine testing rig. The scheme of gas installation can be seen on the Figure 1.

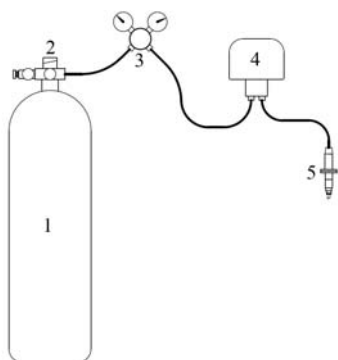


Fig. 1. The scheme of gas installation

The main parts of gas installation are the fuel tank (1), valve (2), pressure regulator (3), flow meter (4) and prechamber (5). The gas pressure in the tank is 200 bar. Regulated injection pressure is 100 bar. The GDI injector and spark plug mounted in the prechamber. The main use

of the prechamber is to provide the stratified mixture, where the mixture in the prechamber will be always rich and in the cylinder will be always lean. The rich and lean mixture should reduce the hydrogen combustion speed and to decrease the combustion temperatures, which should led to regular engine work with low nitrogen oxides emission. The experiment was conducted on a single cylinder engine. The use of a single cylinder engine, which basically was diesel engine, gives several advantages. In the earlier research ignition system was developed for this engine, which can allows it, to work as a spark ignition engine. The prechamber was made as to have external dimensions as diesel engine injector, so the mounting was easy. The main characteristics of the modified engine are given in the Table 1.

Tab. 1. Test engine characteristics

Name	Value	Unit
Bore	8.5	cm
Stroke	8	cm
Cylinder volume	454	cm ³
Prechamber volume	9.32	cm ³
Compression ratio	10.4:1	-

In order to achieve the aim of the paper, two sets of measurements will be presented and explained. In the first case, engine worked with globally stoichiometric mixture, while in the second case the mixture was globally lean. The both measurements were performed for the same engine speed and load.

This was achieved thanks to the prechamber. With the added prechamber, the test engine can work with fully opened throttling valve in the entire work range. By opening the throttling valve, engine takes more air during the intake stroke and provides globally lean mixture. In the second case, the engine worked with the closed throttling valve, reducing the amount of intake air, thus providing the stoichiometric mixture.

The hydrogen injection was performed in the prechamber, as well as the mixture ignition.

3. RESULTS AND DISCUSSION

It should be noted that the pressure measurement was done in the cylinder, so all results will be shown for the cylinder, and not for the prechamber. However, the pressure in the prechamber is not too important as all of the

engine characteristics depend on the cylinder indicating parameters. The prechamber pressure measurement is too complicated, it requires special spark plugs with pipe pressure sensors. Also, the gas in the pipe can enter the resonating area and cause incorrect results. The cylinder pressure for both regimes is presented on the Figure 2.

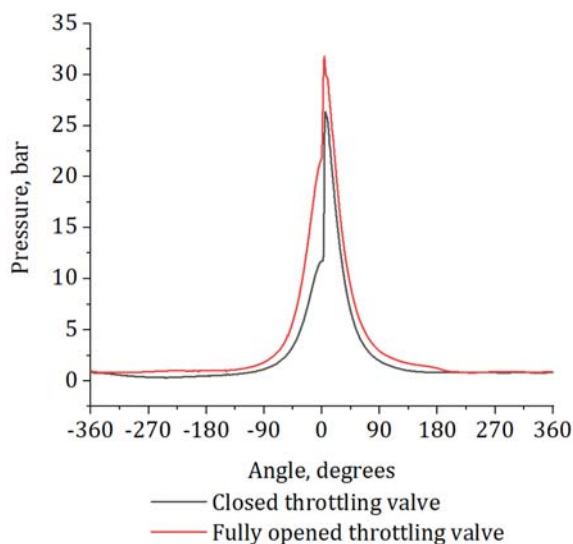


Fig. 2. Cylinder pressure

As presented on the Figure 2, in the case with the closed throttling valve, the maximal pressure, as well as the pressure at the end of the compression stroke, is lower than in the case with fully opened throttling valve. This is because of the lower mixture mass that has entered the cylinder. The mixture mass in the case of the closed throttling valve was 4.3 times lower than the mixture mass in the case of the fully opened throttling valve. However, the pressure increment is much higher, which is caused by the air/fuel ratio. In the case of the closed throttling valve, the mixture was stoichiometric. The combustion speed of hydrogen is biggest for stoichiometric mixture, which can be seen and from heat release rate diagram (Figure 3).

The interesting period in the heat release rate is the period before ignition. The enlarged view of the period is given on the Figure 4.

In both cases heat release exists in the period where ignition is not initiated by spark plug. That's means that the combustion starts during the compression. According to the research of other authors the hydrogen autoignition

temperature is around 848 K [2]. However, by investigating the previous research it was found that the hydrogen combustion is specific, with a period of slow combustion, after which main combustion starts, which is characterized with high combustion speed [6]. This means that despite the high autoignition temperature possibility of autoignition exists during the compression. This can be caused by the hot spots or because of the HHO gas forming in the engine cylinder, and which can be easily autoignited. However, the main combustion is still caused by the spark plug ignition and can be successfully controlled. In the case of the closed throttling valve this is less dominant, because of worse combustion conditions. This can probably be avoided reducing the compression ratio.

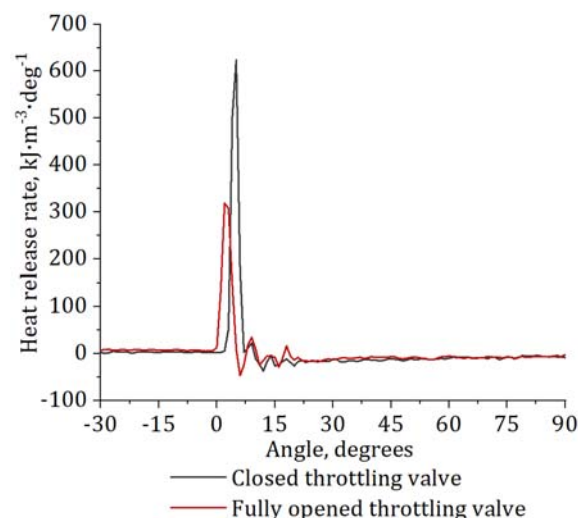


Fig. 3. Heat release rate

As for the closed throttling valve, heat release is less intensive during the compression, less fuel was combusted in this period, so the majority of the fuel was combusted during the main combustion, which causes higher pressure increment. In the case of the fully opened throttling valve, more intensive heat release during the compression have caused higher pressures during the compression stroke with greater compressed mixture mass, respectively. However smaller the initial mass, it has caused higher starting temperatures as well as the stoichiometric mixture which has caused higher combustion temperatures, which is shown on the Figure 5.

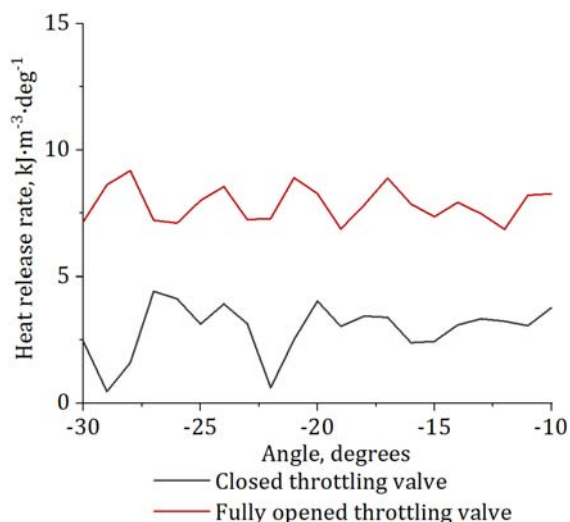


Fig. 4. Heat release rate during the compression

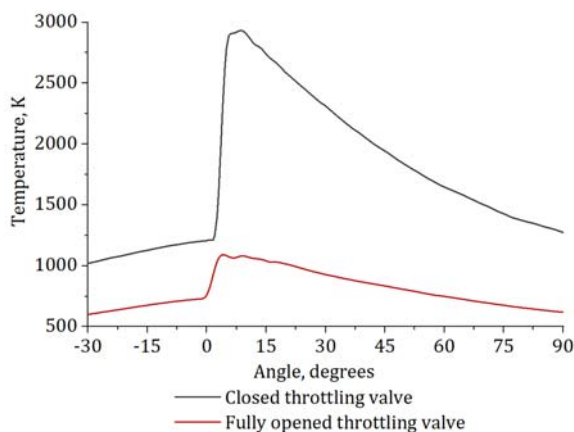


Fig. 5. Combustion temperature

The higher temperature has caused higher concentration of nitrogen oxides. In the case of the closed throttling valve the value of nitrogen oxides was 2191 ppm, while in the case of the fully opened throttling valve the value of nitrogen oxides was 86 ppm. The lean mixture caused the lower combustion temperatures and this have reduced the nitrogen oxides significantly, which means that the aim of the paper was accomplished.

CONCLUSION

The hydrogen can be successfully used as only fuel for IC engine. Its combustion is very specific, which was shown in the paper. The prechamber provided the mixture stratification and by that even work at small loads with fully

opened throttling valve. This have led to the possibility to work with globally lean mixture and to reduce the concentration of nitrogen oxides. This means that mixture stratification can be a good direction in the future researches with hydrogen. The prechamber can be a good direction. The future research should give attention to the prechamber shape optimization, in order to obtain even better results.

ACKNOWLEDGEMENT

This paper was realized within the framework of the project "The research of vehicle safety as part of a cybernetic system: Driver-Vehicle-Environment", ref. no. TR35041, funded by the Ministry of Education, Science and Technological Development of the Republic of Serbia.

REFERENCES

- [1] Rievaj, V., Gaňa, J., Synák, F. (2019). Is hydrogen the fuel of the future? *Transportation Research Procedia*, vol. 40, p. 469-474. DOI: [10.1016/j.trpro.2019.07.068](https://doi.org/10.1016/j.trpro.2019.07.068)
- [2] Das, L.M. (1996). Hydrogen-oxygen reaction mechanism and its implication to hydrogen engine combustion. *International Journal of Hydrogen Energy*, vol. 21, iss. 8, p. 703-715. DOI: [10.1016/0360-3199\(95\)00138-7](https://doi.org/10.1016/0360-3199(95)00138-7)
- [3] Srinivasana, C.B., Subramanian R. (2014), Hydrogen as a spark ignition engine fuel technical review. *International Journal of Mechanical & Mechatronics Engineering IJMME-IJENS*, vol. 14, no. 5, p. 111-117.
- [4] Firmansyah, A.R.A., Aziz, M.R., Heikal, E. Zainal (2017). Diesel/CNG mixture autoignition control using fuel composition and injection gap. *Energies*, vol. 10, no. 10, p. 1639. [10.3390/en10101639](https://doi.org/10.3390/en10101639)
- [5] Pana, C., Negurescu, N., Cernat, A., Nutu, C., Mirica, I., Fuiorescu D. (2017). Experimental aspects of the hydrogen use at diesel engine. *Procedia Engineering*, vol. 181, p. 649-657. DOI: [10.1016/j.proeng.2017.02.446](https://doi.org/10.1016/j.proeng.2017.02.446)
- [6] Lawton, J., Weinberg, F.J. (1969). *Electrical aspects of combustion*, University of London, London.



Banja Luka
28-29 May 2021.

DEMI 2021

15th International Conference on
Accomplishments in Mechanical and
Industrial Engineering

www.demi.mf.unibl.org



Integration of large-scale heat pumps in the district heating system of Skopje

Igor Shesho*, Done Tashevski*, Risto Filkoski*, Monika Uler-Zefikj*

* Faculty of Mechanical Engineering, University "Ss Cyril and Methodius", Skopje, R. Macedonia

Abstract *In the residential sector in EU countries space heating and domestic hot water system participate with more the 80% in the final energy consumption. Cost-effective and energy efficient option for residential and commercial buildings is DHC which is currently dominated by fossil fuels, such as coal and gas. Upgrading existing systems with integrating renewable technologies can lead to significant benefits regarding climate change mitigation, energy security and human health. The main aim of this paper is analyzing the possibilities for integrating heat pump together with thermal storage in the district heating system in Skopje, R. North Macedonia, considering current network system, growing population, climate conditions and pollution issue. Different scenarios will be analyzed by changing the COP of the heat pump in order to get an overview of the most feasible option taking into consideration the heat production, electricity consumption and payback period. The energy model is developed and analyzed for the part operated by Balkan Energy Group. It tends to provide insight of the benefits provided by the system upgrade and cost analysis for installation, operation and maintenance of the equipment.*

Keywords *heating, heat pump, thermal storage*

INTRODUCTION

In the final energy consumption 50% attributes to heat used in the residential and industrial sector [1]. Space heating and domestic hot water system in the residential sector in EU countries participate with more than 80% in the final energy consumption [2]. The renewable sector provides still modest 16% of the total energy consumption in the EU because it is still based on fossil fuels [3].

Heating and cooling are required throughout

the year, but demand depends on climate conditions. In cold climates, home heating in winter accounts for the majority of energy use in buildings, whereas in hot climates, cooling is needed in the summer months. In every region, hot water is needed throughout the year. In most countries, these needs are met by decentralized heating or cooling systems, such as boilers or air conditioners, installed in buildings [4]. Individual heating solutions only allow one specific type of fuel, e.g. coal, oil or natural gas and mean that the heating bill is fully financially exposed to price increases of a specific fuel.

Corresponding author

PhD, Associate professor, Igor Shesho
igor.seso@mf.edu.mk
Faculty of Mechanical Engineering, University "Ss Cyril and Methodius"
Karpos II, P.B 464
Skopje, R. Macedonia

Deaistrict heating (DH) is a cost-effective and energy efficient solution which can provide at least half of the total heat demand in the 14 countriros [5]. With DH, it is possible to achieve independence from fuel import and

CO₂ targets, as well as take advantage of the free-market forces driving price changes on different types of fuel [6]. However, DH supply in general is currently dominated by fossil fuels and needs time to become decarbonized. Several studies have shown that the potential to make it more efficient and renewable is very high achieving significant benefits for energy security, human health and climate change mitigation.

According to the Heat Roadmap Europe 2050 scenario, DH is supplied mostly by decarbonized energy sources and 25% of the total DH demand is met by large-scale heat pumps (HPs). Based on the project results (HRE4) it is suggested that large - scale HPs could have a big role in future DH systems, providing flexible and supply safe systems making DH systems meet rising urban energy needs, improve efficiency, reduce emissions and provide cost-effective temperature control [5].

Cogeneration and large-scale HP are the main sources for DH supplying around 38% and 25% respectively considered data from over 14 countries [7]. They possess their own set of low-carbon benefits offering supply of both low-carbon electricity and low-carbon heat. Combined heat and power and renewable energy sources (RES) represent a series of proven, reliable and cost-effective technologies that are already making an important contribution to meeting global heat and electricity demand and are fully technically capable for implementing in other systems in Europe [8-10]. HPs have the potential of establishing connections between different energy systems such as the electrical grid, the gas grid and the DH grid providing increase of the flexibility of the CHP and the profitability of existing heating networks [5]. Also, they can be the link between the need for cooling and the need for heating. By adding thermal energy storage (TES) tank to the system the excess heat produced during summer months by the HP can be used during winter periods when the heat demand is greater [11].

The potential of HPs in meeting the cooling needs is given in study [10] which shows that 49 units out of 143 supply cold water in district cooling networks. The cooling sector is

developing and growing fast and is expected to double until 2050 mainly in the service sector, such as hospitals, schools, offices and commercial buildings. This means that the connection between cogeneration heating plant (CHP) and large-scale HPs for 'cold storage' can have future prospects [10].

Studies suggest that DH, together with thermal storage and large-scale HPs, is more feasible, fuel-efficient, and cheaper than individual solutions in areas with high urban density. Together with cogeneration they can respond to both high and low electricity availability hours and both high and low heat demand hours [5].

BACKGROUND

DH systems provide hot water to commercial, residential, service buildings as well as to industrial users, and heat for space heating. Heat is generated centrally by a CHP and distributed to the consumers by network of pipelines. CHP can use different types of fuels, both fossil and renewable-based fuels and can operate at high level of fuel utilization. CHP technology can be distributed quickly, almost without geographic limitations, can provide highly efficient process heat and electricity. The heating network pipelines are usually made of polyurethane and are designed for a maximum supply temperature of 130 °C because it is the highest temperature that the material can withstand in continuous operation [12].

The classification of DH system may be done based on many parameters, as: size of the DH system depending on the length of the piping system, number of substations or number of connected consumers; historical developments in geographical regions; technology generations (1st, 2nd, 3rd and latest 4th generation); technical issues as: heat generation (centralized, decentralized), heat distribution (steam, water), heat consumption (direct/ indirect system), operational temperature level etc. [13].

According to the temperature levels the DH systems can be divided into several categories: High Temperature DH Systems, abbreviated as HT, with supply and return temperature of

100/50 °C accordingly; Low Temperature DH Systems, abbreviated as LT, 80/40 °C; Very Low Temperature DH Systems, abbreviated as VLT, 60/30 °C; Ultra Low Temperature DH System, abbreviated as ULT, 45/30 °C; Thermal Grids, abbreviated as TG, 28/8 °C; and District cooling systems, abbreviated as DCS, 10/15 °C [14].

HP projects in connection to DH can be complex and very different. There are a lot of different types and possibilities in relation to heat sources and temperature levels as well as in which part of the DH grid they are implemented. According to the latter there are two main ways of integrating HPs into the thermal networks, centralized and decentralized integration. Centralized integration is when the main large capacity feed-in points are few or one. On the opposite, the decentralized integration is composed of smaller generation technologies on many locations in the network. If the integration is centralized the mitigating circumstance is that the required infrastructure is available and needs small adjustments [14].

According to historical data the first case where large HPs embedded and were used to supply district heating systems was in Switzerland in 1942. The installation was composed of three units providing total heat capacity output of 5.9 MW. Afterwards, in the beginning of 1980s the interest in use of large HPs in DH systems was growing, while the peak in the use of power-to-heat plants occurred in 1990 when it supplied more than 30% of the heat demand. Nowadays, this share is around ten percent represented only by the large-scale HPs. Countries with highest HPs capacities installed in DH are Sweden, Denmark, Norway, Italy, Finland, and China [15]. Historically, HPs with greater capacities as of 16 MW were installed in the period 1980-2000, whereas HPs with capacities of approximately 5 MW were popular until 2016 which according to the study is due to the refrigerant used. In the case study for this paper are predicted several HP units with total capacity of 20MW [10].

The main types of HPs are compression and absorption HPs. A compression HP is used to supply to energy sink with higher temperature

heat than those provided by heat source, usually using a compressor to perform the additional work [16]. Additionally, HPs differ according to the heat source and can use internal or external heat source. External sources bring energy into the system from outside, while internal sources do not bring additional energy to the system [14]. Whereas, the three general types of heat sources of HPs are water, air and ground sources, whereas there is huge variety in terms of their deviation inside these divisions, as sewage water, ambient water, geothermal heat, flue gas, industrial excess heat or solar heat storage etc. [10,17]. Industrial excess heat is a low temperature heat recovery deriving from the industrial processes and its temperature range is 15–40 °C. Lake, river, sea water and groundwater belong to the category of ambient water and their temperatures usually depend on the seasons and vary between 2 to 14 °C. Sewage water is generated by human activity and is treated before being used in the system. The temperature range of sewage water is from 12 up to 20 °C [15]. HPs vary based on the refrigerants used where the global split is to synthetic and natural refrigerants, and as expected in the later years HPs using natural refrigerants are encouraged due to different EU regulations [18].

The way to evaluate the HP performance is using the coefficient of performance (COP) which is a quotient between the heating or cooling energy provided to electrical energy consumed and usually is in the range between 3 and 4 [16, 19]. Current world research is implemented in order to improve the HPs efficiency because several percent increase of COP gives considerable savings in the operation of the HPs and increases the environmental impact [20]. The COP of the HPs is dependent from the source of energy, technological solution, temperature levels and other parameters. The capacity of the HP depends on the DH system characteristics and is usually selected based on the heat load demand ranging between 50–70% ($k=0.5-0.7$) of the max heat load demand [21].

MODEL DEVELOPMENT

Based on the Survey conducted by the State Statistical Office on energy consumption in

Households in R. Macedonia, it was obtained that the average specific consumption in 2014 in the Households was around 160 kWh/m², and it is projected that with the implementation of the obligations from the EE Law it will converge to the EU level in 2018 – 112 kWh/m². For comparison, the highest energy consumption in 2014 for heating in Households in the EU was 188.8 kWh/m² consumed by Luxembourg and the average consumption was around 115.5 kWh/m². Until 2018 the average heating consumption in Households decreased by 3 kWh/m², amounting 112 kWh/m² and the highest heating consumption was realized by Latvia with 178.6 kWh/m². The overview of the average heating energy consumption of Households per heating area in the EU in a time period from 2000 until 2018 and in Macedonia for 2014 and 2018 is given in Figure 1 below [22].

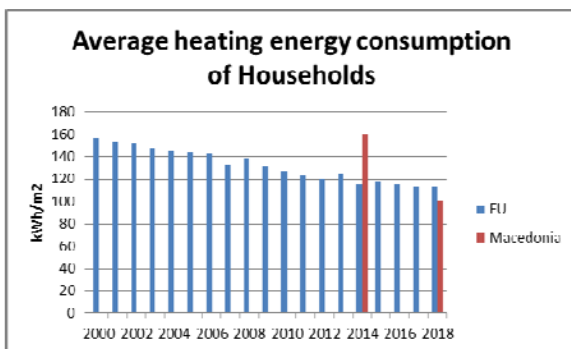


Fig. 1: Overview of the average heating energy consumption of Households from 2000 till 2018

Figure 2 shows the annual demand for heating energy for Skopje divided by months, as well as the electricity produced by the CHP „TE-TO“ AD Skopje for 2019. As expected, the heat demand is highest during the winter periods especially January and December, whereas from May till August the heat demand equals zero.

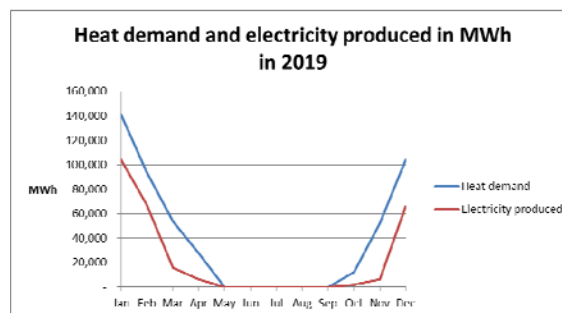


Fig. 2: Energy balance by BEG for 2019

The DH system of the city of Skopje meets the heating needs of about 40% of the city, with a total connected heat capacity of 630 MW, which consists of three independent heating systems operated by: Balkan Energy Group, ESM Energetika and Toplifikacija Skopje North.

The main aim of this study is analyzing the possibilities for integrating HPs in the DH system of the capital city Skopje, considering climate conditions in R. Macedonia. Therefore, energy model for the DH system in Skopje was developed and analyzed for the part operated by Balkan Energy Group (BEG).

Namely, the largest central heating system is the one operated by BEG, which connects active consumers with a total capacity of 450 MW and disconnected customers (possible quick connection to the system only by opening the valves) with a capacity of 100 MW. The BEG system actively operates two heating plants with hot water boilers and one combined thermal power plant (TPP).

Heat generation in DH system operated by BEG is provided by three heating plants and one CHP, as follows: HP „Toplana Istok“ is located in the eastern industrial zone of the city, with installed hot water capacity of 279.12 MW and HP „Toplana Zapad“, located in the western zone of the city, with installed hot water capacity of 162.82 MW. The HP “11 Oktomvri” has installed hot water capacity of 28.25 MW and it is preserved - not in function since 2015. The total available installed hot water capacity of the heat plants is 470.19 MW. The CHP „TE-TO“ AD Skopje has combined cycle gas turbine (CCGT) with installed heat thermal capacity of 160 MW for district heating and electrical power of 220 MW. It is located in the

immediate vicinity of „Toplana Istok“. It should be noted that the „TE-TO“ AD Skopje is an unregulated producer of thermal energy and its participation in the system primarily depends on the market conditions of profitability of the plant. As average the yearly heat production of the system is around 500 GWh_{th} whereas the share between the heat from CHP plant and heating plants in total heat production is variable, considering yearly variations in the factors influencing the operational feasibility of the CHP.

The production of thermal energy in the heating plants is realized through hot water boilers that work on natural gas as primary fuel, while as a reserve fuel in case of lack of natural gas they can also operate on fuel oil. The produced heat energy in the heating plants is distributed through the distribution network with a length of about 200 km to the end users, through 2700 heating substations. [12].

In the DH system, two distribution pipelines are directly connected, which creates a connection between the two heating plants, as follows: Pipeline B from heating plant „Toplana Istok“ is connected to the pipeline „Partizanska“ from heating plant „Toplana Zapad“, where the connection is provided by a pumping station, ie a pump placed on the bypass of the pressure line B in the direction of flow towards heating plant „Toplana Zapad“. Pipeline A from heating plant „Toplana Istok“ is connected with the pipeline Kozle from heating plant „Toplana Zapad“.

This study considers the possibility for coupling DH system and CHP with RES by adding HPs and TES as complementary solution to the system, as well as analyses the cost-effectiveness of the existing heating system upgrade for Skopje city with four scenarios containing different technical characteristics. The benefit of integrating HPs in the DH system which is connected to CHP is that the process can be adjusted in order to optimize the efficiency, according to the use of RES as well as to the electricity/ fuel prices.

In this case the HP would be supplied with electricity needs from the CHP, whereas the excess heat produced would be stored in the heat storage tank and used in case of necessity.

The idea for the HPs is to cover the peak demands of heat energy and use them as addition to the base heat energy produced by the boilers and CHP. The planned HPs would be electric large-scale HPs with total electrical capacity of 20 MW. Depending on the considered scenario the COP of the HPs would be variable in the range between 3 and 4. That is an average practical COP of a HP according to [10]. The output temperatures of the HP are defined by the DH system and vary between < 70 °C and > 80 °C, which should be taken into consideration when defining the HPs technical characteristics.

As a modeling software for the dynamic simulations is used TRNSYS (Transient System Simulation). The general scheme of the model development is presented on Figure 3.

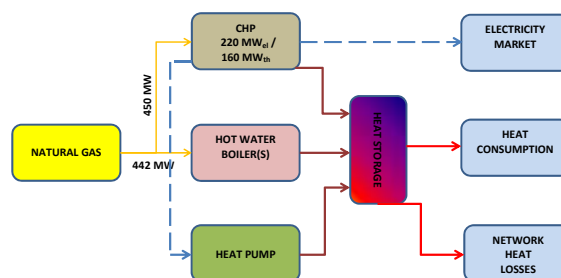


Fig. 3: Scheme of the system including heat pump and heat storage tank

The main application of tank storages is for buffering daily peaks. The DH network pressure level and the main source temperature are most relevant for pressure and temperature levels of the TES. Generally, the tanks for hot water storage can be separated into 3 major types: unpressurized storages with maximal temperature of 98 °C; 2-zone storages with highest temperature up to 120 °C; and pressurized storages with temperature no more than 150 °C. Empirical formula used for dimensioning a heat storage given in [12] is 50 m³/MW peak load of thermal output. Generally, the storage capacity of heat storage tanks is designed to cover from 5 to 12 h [12].

The control strategy of the system is choosing the heat sources that can provide heating energy with the lowest production price at the considered moment. Therefore it is analyzed

the influence of the TES integration, as a potential measure to increase the flexibility of the CHP and HP in providing heat energy. The planned TES in the analyzed scenarios is foreseen to have 10,000 m³ water storage capacity, with operating temperatures of 90 °C at the top and 50 °C at the bottom. The water would be heated using HPs and used to charge the heat energy store. In the work process of the thermal storage it is important to follow the thermodynamic properties of the tank, to check the yearly energy balances and the interaction of the tank with the environment [11].

Nevertheless, TES embedded in the DH systems are conventional and cost-efficient technology that provide flexibility in power systems [24, 25].

As previously mentioned, four different scenarios will be analyzed as follows:

- scenario 1 – DH system with HPs of 20 MW with COP 4 and storage tank of 10,000 m³;
- scenario 2 – DH system with HPs of 20 MW with COP 3 and storage tank of 10,000 m³;
- scenario 3 – DH system with HPs of 20 MW with COP 4 without storage tank; and
- scenario 4 – DH system with HPs of 30 MW with COP 3 and storage tank of 10,000 m³.

In the presented scenarios hourly values for heating power and the temperature regime of the heating system are given as measured values i.e. the HP maximal outlet temperature is set at 75°C. Also, the hourly market prices for electrical energy from HUPEX exchange are used for the same year for which the data for the heating system is given. The CHP is optimized depending on the electricity price if it will deliver heat to the network when the electricity price is acceptable, or it will supply the HPs and thermal energy to the heat network. In the case if there is no need for heating energy to the DH system the heat is accumulated in the TES which is the main idea behind the integration in the system.

In order to calculate the gained net cash from the operation the following financial parameters were taken into consideration:

- price for purchase of natural gas 0.32 €/nm³,
- price for maintenance of boilers 10 €/MWh,
- price for maintenance of CHP 6 €/MWh,
- price for maintenance of HP 15 €/MWh,
- price for heat energy sold 53 €/MWh,
- electricity price for HP operation 53 €/MWh
- price for electricity on spot market – HUPEX 2019

The model intends to provide insight of the benefits provided by the system upgrade and cost analysis for installation, operation and maintenance of the equipment [7].

RESULTS AND DISCUSSIONS

In general, the parametrical analysis is directed toward estimation of the influence of the HP efficiency (COP) and implementation of TES on the overall system performance and cost-effectiveness. On Figure 5 are presented the results gained from the model simulation regarding heating energy share by heat source for each of the previously defined three Scenarios.

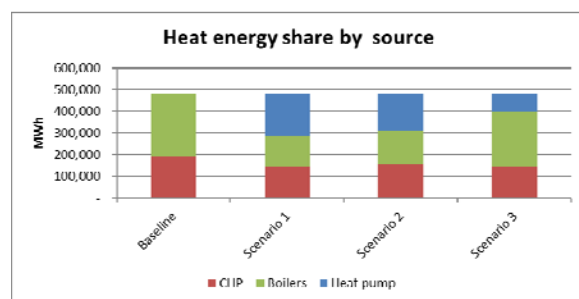


Fig 4: Heat share in total heating energy by heat source as function of a Scenario

According the presented data on Figure 4 can be drawn conclusion that the Scenario 1 has larger heat energy share from the HP as a result of higher COP=4 compared with COP=3 of Scenario 2, considering that all other system elements are the same in those two scenarios.

Regarding the Scenario 3, can be noticed that has significantly lower HP share and higher boilers share in the total required heating energy. The main reason for the significant differences is that in Scenario 3, the system is without TES. The heat share from the HP in the Scenarios with thermal energy storage tank is between 30%-40% and without TES is less than 20% which confirms the significance of TES in providing flexibility and increase utilization of HP and CHP.

On the next Figure 5 are presented data for the fuel consumption (electricity for HP) by heat source for each of the Scenarios. The fuel consumption (natural gas) is presented in energy terms in order to be comparable with the electrical energy consumption for the HP.

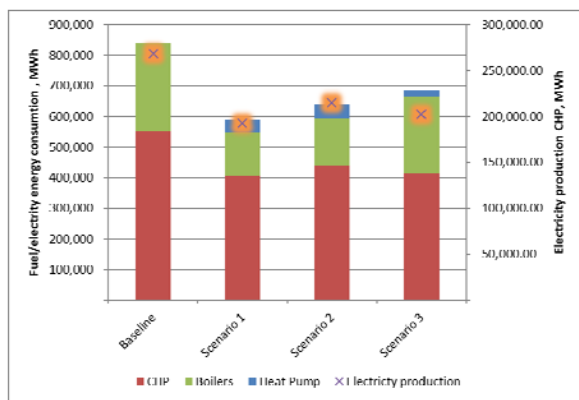


Fig. 5: Fuel consumption by heat source for each scenario and CHP electricity production

According the presented data on Figure 5, can be concluded that the least total fuel/electricity consumption has the system in Scenario 1 (the fuel consumption of the CHP considers the total consumption for heat and electricity production). It is noticeable that within the Scenario 1 and Scenario 2 the dominating fuel consumption is by CHP which is positively affecting the cons-effectiveness of the system, since it has highest energy efficiency coefficient (considering that is operating in combined regime). Also Scenario 1 and 2 have considerably less total fuel/electricity consumption compared to the Scenario 3 and the electricity production has nearly same values for all three scenarios.. On Figure 6 is presented cash flow overview for the baseline and the Scenarios. On the Figure 8 is given overview for the payback period for installing

HP into the DH system as a function from the investment costs and heat energy price.

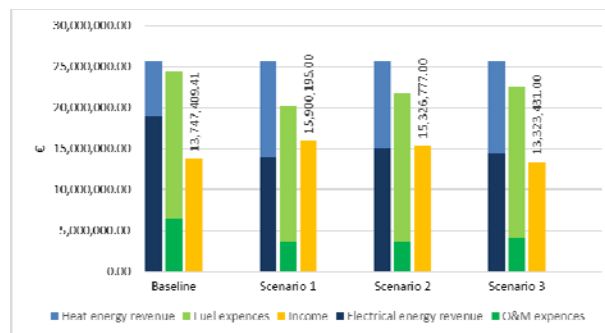


Fig. 6: Cash flow overview

Analyzing Figure 6, a difference can be made between the total revenues and total operating expenditures that arise from the systems' operability. It can be notice that the income for the Scenario 3 is lower compared to baseline case which indicates that this DH systems settings are not feasible. The reason can be located that in this Scenario it is not foreseen TES and the system lacks flexibility causing lack of utilization of the HP and CHP potentials. It is obvious that TES in DH has significant contribution toward increasing the operational flexibility of CHP and HP. It should be noted that within the payback period calculations, in the total investment costs are considered equipment costs, electrical grid connection costs, construction costs and costs for heat source. The investment costs of HPs are described in detail by [18] and emphasize the importance of the choosing the heat source, size, components and configuration of the HP when calculating the budget needed. The investment costs for HPs vary largely but have a linear correlation with the thermal capacity of the HPs [12]. So, this gives us the possibility to form an approximate value of the expenditures for HPs with total capacity of 20 MW to cost of around 8 M€. The construction costs of the HPs depend mainly of the thermal capacity of the HP and by using the graph presented in the analysis done by [18] it can be noted that the construction costs have also a linear dependence from the capacity of the HP, so the total construction costs for HPs with capacity of 20 MW would be 2 M€. The electricity related investment costs would be around 2.6 M€ whereas the heat source investment costs would be 2.4 M€. In the results from the detailed analysis done by [18]

where the total investment costs for HPs using different heat sources are calculated for the largest capacity of 10 MW, and the linear dependence which shows that the costs double with doubling the capacity of the HP, it can be concluded that the total investment cost for HP with capacity of 20 MW will be 15 M€ where half of the investment costs correspond to the price of the HP and the others are almost equally split between the costs for heat source, electricity and construction. According to [11] the construction costs of thermal energy store depend from its size and type. For 10,000 m³ storage tank the price will be 1.2 M€. Giving all the above mentioned, the total investment costs for heat pump and thermal store amount 16.2 M€ and this value is taken as reference in the following calculations. Considering this data, the simple payback period for the Scenario 1 is 7,5 years, for the system in Scenario 2 is 10 years and Scenario 3 has negative value i.e. it is not feasible. Main difference between Scenario 1 and Scenario 2 is in the HP efficiency, where it is considered COP = 4 and COP = 3 accordingly. It is performed analysis regarding the influence of the technology cost (HP specific investment costs) on the system cost-effectiveness i.e. payback period, presented on the next Figure 7. On the diagram on Figure 7, the results for Scenario 3 are not presented since in all cases the payback periods have negative values i.e. the income is lower than the compared baseline scenario.

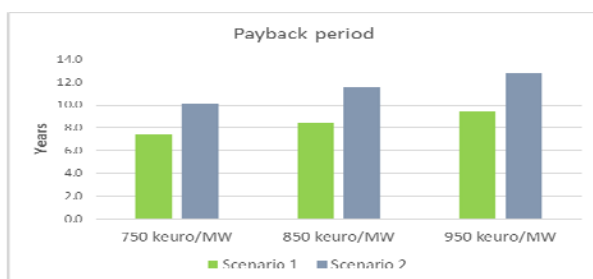


Fig.7: Payback period vs. investment costs

It is important to note that the payback period has high sensitivity to the changes in the electricity prices and those changes affect also the supply of the DH system. These are the results

mainly of the revenue from the CHP electricity (by HPs) to being based on fuel combustion. Visual representation of the payback periods is given in Figure 7 as well as the variations of the payback time when the investment costs for the HPs and the electricity price are different. Whereas, the sensitivity analysis brought insight that the technology cost and discount rates does not affect the heat pump technology and that the system coupled with the large-scale HPs sensitivity is lower compared to the system without large-scale heat pumps implemented.

CONCLUSION

The cash flow and payback period times were analyzed for four different scenarios including HPs and thermal energy storage with different capacities, taking into consideration the heat production, energy consumption and investment costs. For all categories were done cost correlations on the real values with assumptions for integration RES in the DH system. Also, payback period variations were done with variable input parameters regarding HPs' investment costs and sold heating energy price. The results showed that it's a must integrating TES in the systems with renewable energy sources in order the system to be feasible and same time it improves system cost effectiveness. Also it must be noted that Scenario 3 which is without TES it is not feasible even with 30% decreased investment cost.

HPs have the potential of establishing connections between the electricity and heating sector providing increase of the flexibility of the CHP and the profitability of existing heating networks. Implementing large-scale HPs to the existing energy system enables more operating hours of CHP and reduces the number of boilers operating hours in DH system. Additionally, with coupling large-scale HPs with CHP and their implementation in the DH system the CO₂ emissions reduce, the possible critical excess in electrical energy decreases and higher fuel savings can be achieved.

LITERATURE

- [1] International Energy Agency. Key world energy statistics. Paris: International Energy Agency; 2018.

- [2] Eurostat. Share of fuels in the final energy consumption in the residential sector, 2016 (nrg_110a). Updated 31 May 2018. Eurostat; 2016.
- [3] Tian Z, Zhang S, Deng J, Fan J, Huang J, Kong W, et al. Large-scale solar district heating plants in Danish smart thermal grid: Developments and recent trends. *Energy Convers Manage* 2019;189:67–80. <https://doi.org/10.1016/j.enconman.2019.03.071>.
- [4] IRENA (2017), Renewable Energy in District Heating and Cooling: A Sector Roadmap for REmap, International Renewable Energy Agency, Abu Dhabi. www.irena.org/remap
- [5] Paardekooper, S., Lund, R. S., Mathiesen, B. V., Chang, M., Petersen, U. R., Grundahl, L., David, A., Dahlbæk, J., Kapetanakis, I. A., Lund, H., Bertelsen, N., Hansen, K., Drysdale, D. W., & Persson, U. (2018). Heat Roadmap Europe 4: Quantifying the Impact of Low-Carbon Heating and Cooling Roadmaps. Aalborg Universitetsforlag.
- [6] State of Green, 2016, District energy Energy Efficiency for Urban Areas.
- [7] Buoro, D., Pinamonti, P., Reini, M. (2014). Optimization of a Distributed Cogeneration System with solar district heating. *Applied Energy*. vol. 124, p. 298 – 308. DOI: <https://doi.org/10.1016/j.apenergy.2014.02.062>.
- [8] Rutz, D., Doczekal, C., Zweiler, R., Hofmeister, M., Laurberg Jensen, L. (2017). *Small modular renewable heating and cooling grids A Handbook*. WIP Renewable Energies, Munich, Germany.
- [9] Lund, H., Werner, S., Wiltshire, R. (2014). 4th generation district heating (4GDH): Integrating smart thermal grids into future sustainable energy systems. *Energy*. vol. 68, p.1 – 11. DOI: <https://doi.org/10.1016/j.energy.2014.02.089>
- [10] Andrei, D., Vad Mathiesen, B., Averfalk, H., Werner, S., Lund, H. (2017). Heat Roadmap Europe: Large-Scale Electric Heat Pumps in District Heating Systems. *Energies*. vol. 10, p. 2 – 18. DOI: 10.3390/en10040578
- [11] Mangold, D., Schmidt, T., Dohna, A., Spah, D., (2016). *Guideline for Seasonal Thermal Energy Storage Systems in the Built Environment*. Solites, Stuttgart, Germany.
- [12] ILF Consulting Engineers Austria GmbH, AIT Austrian Institute of Technology GmbH, Joint Research Centre. (2017). *Long term (2050) projections of techno-economic performance of large-scale heating and cooling in the EU*. EU Publications
- [13] Rutz, D., Winterscheid, C., Pauschinger, T., Grimm, S., Roth, T., Doračić, B., Dyer, G., Østergaard, T.A., Hummelshøj, R. (2019). *Upgrading the performance of district heating networks Technical and non-technical approaches*. WIP Renewable Energies, Munich, Germany.
- [14] Marguerite, C., Geyer, R., Hangarthner, D., Lindahl, M., Pedersen, S. V. (2019). *IEA Heat Pumping Technologies Annex 47 Heat Pumps in District Heating and Cooling Systems Task 3: Review of concepts and solutions of heat pump integration*.
- [15] Averfalk, H., Ingvarsson, P., Persson, U., Gong, M., Werner, S. (2017). Large heat pumps in Swedish district heating systems. *Renewable and Sustainable Energy Reviews*. vol. 79, p. 1275 -1284. DOI: <http://dx.doi.org/10.1016/j.rser.2017.05.135>.
- [16] Dominković, D. F. (2015). *The Role of Large Scale Heat Pumps in Future Energy Systems*. MSc. University of Zagreb Faculty of Mechanical Engineering and Naval Architecture.
- [17] PV Heating & Air. These Are the 3 Heat Pump Heat Sources. From: <https://www.pvhvac.com/blog/these-are-the-3-heat-pump-heat-sources>, accessed on: 22.01.2021.
- [18] Pieper, H., Ommen, T., Buhler, F., Lava Paaske, B., Elmegaard, B., Brix Markussen, W. (2018). Allocation of investment costs for large-scale heat pumps supplying district heating. *Energy Procedia*. vol. 147, p. 358 – 367. DOI: <https://doi.org/10.1016/j.egypro.2018.07.104>.
- [19] Members of Annex 35/13. (2014). *Application of Industrial Heat Pumps IEA*. IEA Industrial Energy-related Systems and Technologies. Final Report part 1.
- [20] Kurtz-Orecka, K., Tuchowski, W. (2018). Combined heat pump-district heating network energy source. *E3S Web of Conferences*. vol. 49. DOI: <https://doi.org/10.1051/e3sconf/20184900063>.
- [21] Lauka, D., Gusca, J., Blumberga, D. (2015). Heat Pumps Integration Trends in District Heating Networks of the Baltic States. *Procedia Computer Science*. vol. 52. p. 835 – 875. DOI: 10.1016/j.procs.2015.05.140.

- [22] Odyssee-Mure. KEY INDICATORS. From: <https://www.indicators.odyssee-mure.eu/online-indicators.html>, accessed on: 02.02.2021.
- [23] Ochs, F., Heidemann, W., Muller-Steinhagen, H. (2009). Performance of Large-Scale Seasonal Thermal Energy Stores. *Journal of Solar Energy Engineering*. vol. 131. DOI: 10.1115/1.3197842.
- [24] Gadd, H., Werner, S. (2015). Thermal energy storage systems for district heating and cooling. *Advances in Thermal Energy Storage Systems*. p. 467 – 478. DOI: 10.1115/1.3197842.
- [25] Connolly, D. (2009). *A review of energy storage technologies*. PhD. University of Limerick.
- [26] Kazagic, A., Merzic, A., Redzic, E., Tresnjo, D. (2019). Optimization of modular district heating solution based on CHP and RES - Demonstration case of the Municipality of Visoko. *Energy*. vol. 181. p. 56 - 65



Banja Luka
28-29 May 2021.

DEMI 2021

15th International Conference on Accomplishments in Mechanical and Industrial Engineering

www.demi.mf.unibl.org



Possibility for energy saving in Serbian building with photovoltaic-thermal collectors

D. Nikolić^a, J. Skerlić^b, J. Radulović^a, V. Šušteršič^a, A. Radojević^a, I. Terzić^a

^aFaculty of engineering, University of Kragujevac; Sestre Janjic 6, 34000 Kragujevac, Serbia

^bFaculty of Technical Sciences, University of Pristina temporarily settled in Kosovska Mitrovica; Knjaza Milosa 7, 38220 Kosovska Mitrovica, Serbia

Abstract *In the last few decades, buildings have been recognized as large energy consumers, so it is necessary continuously implementation of different measures for improving energy efficiency of existing and construction of energy efficient new buildings. The use of renewable energy sources is essential, and solar energy represents the most promising and most reliable source of energy. This paper analyzes the energy consumption in a single-family residential building with photovoltaic/thermal (PV/t) collectors. Electricity in the building is used for space heating, lighting, DHW system and electrical appliances. The system with photovoltaic/thermal collectors generates heating energy, which is used to prepare hot water in the buildings DHW system, as well as electricity which is used for other needs. The rest of the energy needs are compensated by purchasing energy from the electricity distribution system. Energy consumption and energy generation data were obtained based on simulations performed in the EnergyPlus software, while building, i.e. a house for a family of four, was designed in Open Studio plug-in for Google Sketch Up. The considered facility is positioned in the city of Kragujevac. This analyzes show the possibility for energy saving in heating energy and electricity from by photovoltaic thermal collector in residential Serbian building.*

Keywords *building, photovoltaic/thermal collector, simulation, generated energy, energy saving*

1. INTRODUCTION

Serbia is one of the countries with extremely low energy efficiency. The reasons for this are the use of outdated, energy inefficient technologies in industry, construction and infrastructure, inadequate legislation and insufficiently developed environmental awareness of the population.

Building sector in a world is a large energy consumer with amount of even 40 % of total energy consumption. Serbia has about 300-400000 energy inefficient buildings, without thermal insulation - energy inefficient homes, with an annual energy consumption of 220 kWh/m², while the European average energy consumption is 60 kWh/m², so energy consumption in buildings in Serbia is at the

level of even 50 % [1, 2]. That is why it is very important to build energy efficient buildings that involve renewable energy technology. Systems of renewable energy can generate the energy (electricity, thermal energy) to partially or completely satisfying building energy needs. These buildings have reduced energy consumption, a longer life cycle and contribute to environmental protection through lower greenhouse gas emission [3, 4].

Solar energy is the most promising renewable energy source because it does not bring pollution, which is disproportionately large compared to the use of fossil fuels. In conventional solar systems, solar energy is converted into electricity or heat. A special type of solar technology is the joint use of photovoltaic modules and solar collectors in

photovoltaic-thermal or PV/t collectors (hybrid systems). It is expected that PV/t technology, as renewable energy technology, become competitive with conventional energy production and has a significant potential for domestic use in the future [5].

This paper analyzes the energy consumption and possibilities for energy saving in a single-family residential building with a PV/t collector. Electricity in the building is used for space heating, lighting, electrical appliances and for the domestic water heating. The PV/t system generates thermal energy, which is used for water heating, as well as the electricity for space heating, lighting, electrical appliances, etc. The rest of the energy needs are compensated by purchasing energy from the electricity distribution system. Energy consumption data were obtained by simulations performed in the EnergyPlus software [6]. Previously, a building model was designed in Open Studio plug-in for Google SketchUp software. The considered facility is positioned in the city of Kragujevac.

The analyzes show various parameters such as total energy consumption, energy consumption in DHW system, heating energy consumption, and generated energy by PV/t collector.

2. MATERIALS AND METHODS

2.1 Model of analyzed building

The modelled single-family residential building is shown in Figures 1 and 2. It is one-store building and it has 6 conditioned zones (living room, kitchen, hall, bathroom and two bedrooms).

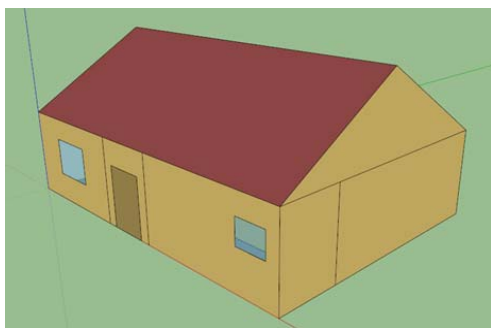


Fig. 1. Modeled building in EnergyPlus - south facade

The total floor area of the building is 88 m². The windows are double glazed with the air gap of 15 mm, with total area of 5.85 m², and the U-

value of 2.72 W/(m²K). Inward opening side-hung windows are implemented in modelled buildings.

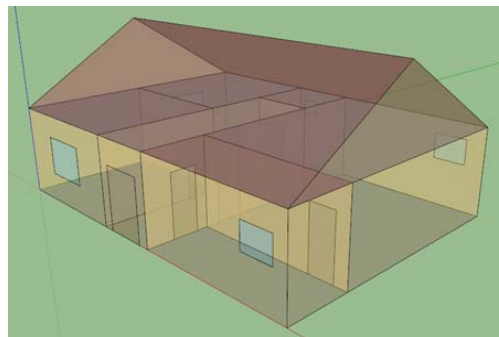


Fig. 2. Modelled building in EnergyPlus - X ray view

The building envelope and roof are thermally insulated by polystyrene (thermal insulation thickness - 0.15 m). The building has the south-north oriented roof with a slope of 32°. The external wall consists of brick, heavy concrete, insulation, air space and gypsum board, with U value 0.177 W/(m²K). The inner wall consists of two layers of gypsum boards between which there is air space. The floor construction consists of lightweight concrete, air layer and acoustic plate, with U value 0.517 W/(m²K). The ceiling consists of lightweight concrete, air space and an acoustic plate. Above the ceiling is the attic zone (non-conditioned zone).

The building was simulated through a year, when heating system operates from October 15 to April 15, which is a common practice in Serbia. Every conditioned zone in the building is equipped with an electric baseboard heater. Air temperatures in the heated rooms are set to 20°C from 07:00-09:00 and from 16:00-21:00, and to 15°C from 09:00-16:00. The simulation time step is 15 min.

2.2 Location and Climate

The investigated building is located in the city of Kragujevac, in Sumadija region which is in the central part of the Republic of Serbia. Its average height above sea level is 209 m. Its latitude is 44°10' N and longitude 20°55' E. The time zone for Kragujevac is GMT+1 h. Kragujevac has a moderate climate, with warm and humid summers (with temperatures as high as 37°C). The winters are cool, and snowy, with temperatures as low as -12 °C [7].

The EnergyPlus uses weather data from its own database file. Input file in EnergyPlus contains a large variety of parameters for solar radiation calculating for every day in the year. Daily average solar radiation for Serbia is different in different parts of country – it is about 1,1 kWh/m² at the north of Serbia and 1,7 kWh/m² at the south of Serbia in January; in July it is about 5,9 kWh/m² at the north and 6,6 kWh/m² at the south of Serbia. Annually average solar radiation in Serbia is from 1 200 kWh/m² for north-west to 1 800 kWh/m² at the south of Serbia, while in Central Serbia, where the analyzed house is located, this value is 1550 kWh/m² [8].

2.3 Model of PV/t collectors

Four photovoltaic/thermal collectors are installed on the south-oriented part of the roof (slope angle of 32°). Thermal efficiency of PV/t collectors is 30 % and cell efficiency of PV panel is 15 %.

The input object in EnergyPlus software SolarCollector:FlatPlate:PhotovoltaicThermal provides a simple PV/t model that is provided for quick use during design or different studies. The user can set up values for a thermal efficiency and the incident solar heats the working fluid. This model of PV/t collector is water-based model and it is a part of plant loop with nodes connected to a plant loop and the plant operating scheme determines flows. No other details of the PVT collector's construction are required as input data [6].

In these investigations, temperature of the water heating in solar loop is limited to 65°C. Main tank has volume of 250 l while instantaneous tank has volume of 80 l. Monthly hot water consumption is 14 m³, and total monthly water consumption is 25 m³.

3. BUILDING ENERGY CONSUMPTION

Total finally energy consumption E_F in a building is related to the electricity. Electricity in a building is consumed for heating (eh), lighting (el), domestic hot water (DHW) and appliances (eq).

$$E_F = E_{eh} + E_{el} + E_{DHW} + E_{eq}$$

where:

- E_{eh} - electricity consumption of the electric heating,
- E_{el} - electricity consumption for lighting,

- E_{DHW} - electricity consumption for DHW system and
- E_{eq} - electricity consumption for the appliances (electric equipment).

Generated energy E_{GEN} in a building, by PV/t collectors is equal to sum of generated electricity $E_{GEN, PV}$ and generated thermal energy $E_{GEN, THERMAL}$, i.e.

$$E_{GEN} = E_{GEN, PV} + E_{GEN, THERMAL}$$

Net-energy consumption in building with PV/t collectors is:

$$E_{NET} = E_F - E_{GEN}$$

4. RESULTS AND DISCUSSION

The aim of presented investigation is to show the possible energy saving in building with photovoltaic/thermal collector. Comparisons of two identical single-family residential buildings were made, one without and the other with a PV/t collector on the roof. At the end, there is provided a comparison of the obtained results.

4.1 Case 1 – Building without PV/t collector

The results of the energy consumption in the building without PV/t collector are given in the Table 1.

The largest part of energy consumption is related to the electrical heating system (29.188 GJ), then to the domestic hot water heating (20.93 GJ). Electrical appliances consume 4.37 GJ of electricity, while lighting consumes 0.23 GJ. All data are obtained for building energy simulation through one year, so total yearly building energy consumption is 54.718 GJ.

Table 1. Energy consumption in building without PV/t collector (Case 1)

Energy consumption (GJ)	Case 1
Heating	29.188
Lighting	0.23
Electric equipment	4.37
DHW system	20.93
Total energy consumption	54.718

Figure 3 shows the distribution of annual building energy (electricity) consumption, in GJ and %, in the building without PV/t collector. As it can be seen, the largest share of energy, 53%,

is spent on heating, then 38% on DHW system. Electrical equipment and lighting spent 8 % and 1 % of total energy consumption, respectively.

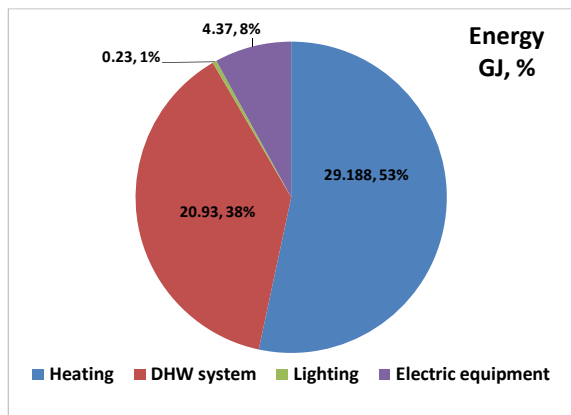


Fig. 3. Schematic presentation of energy consumption for building without PV/t collector

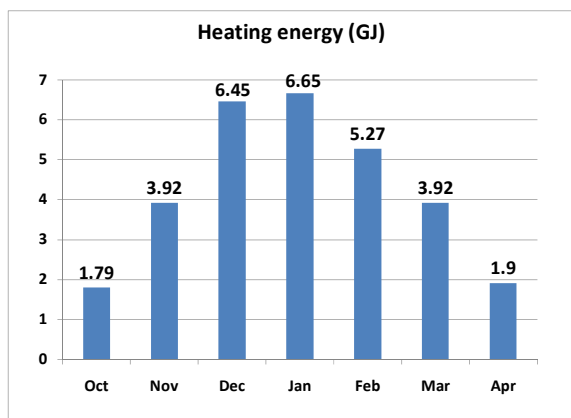


Fig. 4. Monthly heating energy consumption for building without PV/t collector

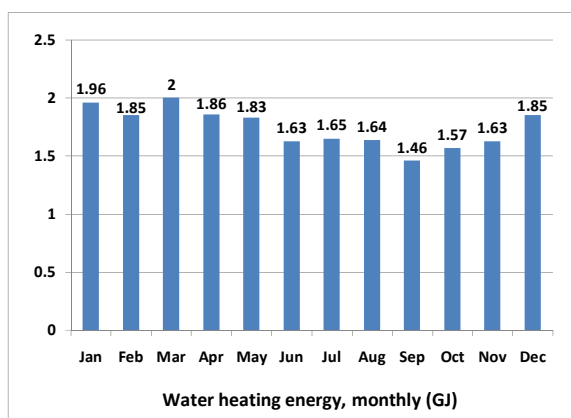


Fig. 5. Monthly energy consumption for DHW system, in building without PV/t collectors

Figure 4 shows monthly heating energy consumption in GJ, for building without PV/t collectors. Heating energy consumption for January has the greatest value – 6.65 GJ.

Fig. 5 shows monthly energy consumption in DHW system in the case without PV/t collectors, and the greatest value is for March – 2 GJ.

4.2 Case 2 – Building with PV/t collectors

The results of the energy consumption in the building with PV/t collectors, and generated energy are given in the Table 2.

Table 2. Energy consumption and generated energy in building with PV/t collector (Case 2)

Energy consumption (GJ)	Case 2
Heating	24.42
Lighting	0.23
Electric equipment	4.37
DHW system	10.34
Total energy consumption	39.36
Generated electricity	4.768
Generated thermal energy	10.59
Total generated energy	15.358

The largest rate of energy consumption is related to the heating system (24.42 GJ), then to the DHW (10.34 GJ). Appliances and lighting consume same energy amount. Total yearly building energy consumption is 39.36 GJ.

Figure 6 shows the distribution of building energy consumption, in GJ and %, in the building with PV/t collectors. Heating system has share of 62% in total building energy consumption, and DHW has share of 26% in total building energy consumption. Electrical equipment and lighting spent 11% and 1% of total energy consumption, respectively.

Yearly generated thermal energy with PV/t collectors is 10.59 GJ and generated electricity is 4,768 GJ, i.e. their sum is 15.358 GJ. This value represents energy saving in building, achieved by PV/t collectors. Total generated energy by PV/t is 15.892 GJ - 10.595 GJ of energy related to thermal energy and 5,297 GJ is electricity

(4,768 GJ of electricity is directly used, while 0.529 GJ is sold to the utilities).

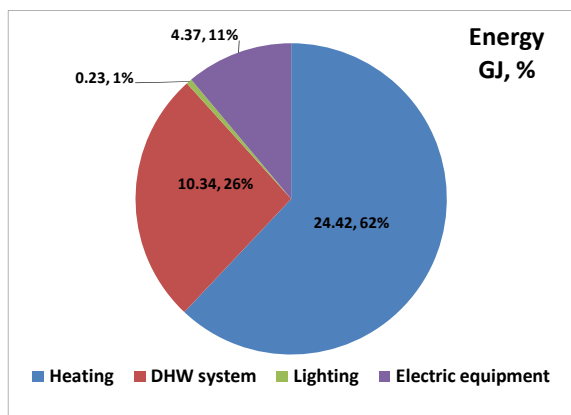


Fig. 6. Schematic presentation of energy consumption for building with PV/t collectors

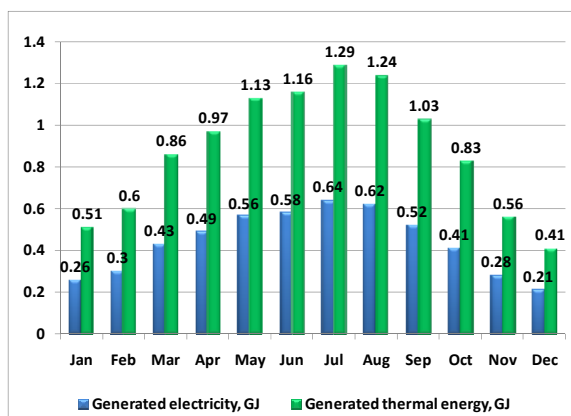


Fig. 7. Generated energy (electricity and thermal) with PV/t collectors

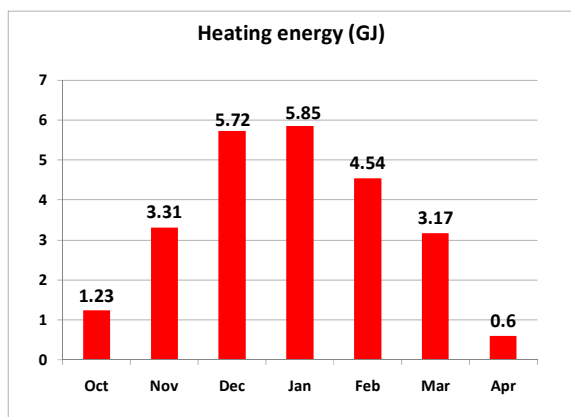


Fig. 8. Monthly heating energy consumption for building with PV/t collector

Figure 7 shows monthly generated energy by PV/t collectors, which generate a larger amount of energy during the summer period. The highest generated amount of both, electricity and heat is in July and amounts 1.29 GJ of thermal energy and 0.64 GJ of electricity.

Figure 8 represents monthly heating energy consumption in GJ, for building with photovoltaic/thermal collectors. It can be concluded that heating energy consumption for January has the greatest value – 5.85 GJ.

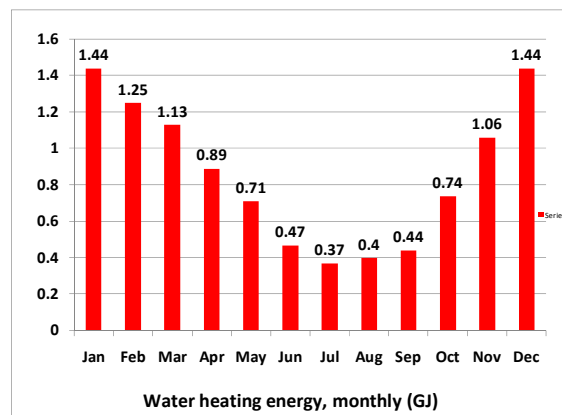


Fig. 9. Monthly energy consumption for DHW system, in building with PV/t collectors

Figure 9 shows monthly energy consumption in DHW system, for building with PV/t collectors. It can be concluded that it has the greatest value for January and December, 1.44 GJ, and the smallest value in July, 0.37 GJ. Smaller values of energy consumption for DHW system are in summer months, when PV/t collectors generate a significant amount of electrical and thermal energy.

4.3 Comparison of the obtained results

Based on the obtained research results, it can be concluded that installation of PV/t collectors can significantly improve building energy efficiency. If the total annual energy consumption in building is compared for two analyzed buildings, Case 1 and Case 2, it can be achieved energy saving of 15.358 GJ in building with installed photovoltaic/thermal collectors. Expressed as a percentage, that is the amount of even 28 %. This fact clearly shows the importance of implementation PV/t collectors in buildings.

Zondag, in his review paper [9], gave the analysis of PV/t collectors and their applications in different climate, and concluded that possible energy saving with this solar systems can be 23-38 %, depending on climate conditions.

Next figure (Figure 10) shows comparison of monthly energy consumption for Case 1 and 2.

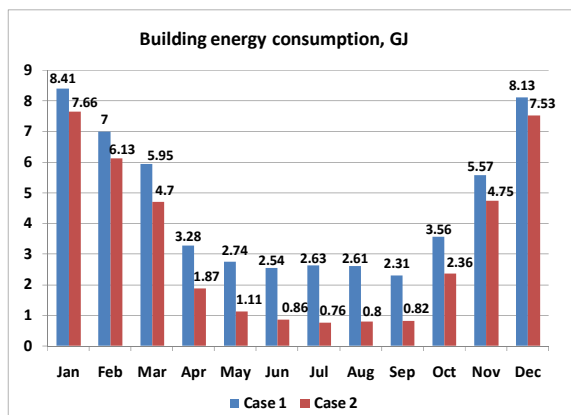


Fig. 10. Monthly building energy consumption for building without and with PV/t collectors

Building with PV/t collectors on the roof has lower energy consumption through whole year, especially in summer months. In those months, a great amount of solar energy is available, and PV/t collectors generate significant amount of electricity and thermal energy. This fact is according to the Figure 7.

Due to the large amount of generated thermal energy in the summer months, the energy consumption in the DHV system is lower in the building with PV/t collectors (Figure 11).

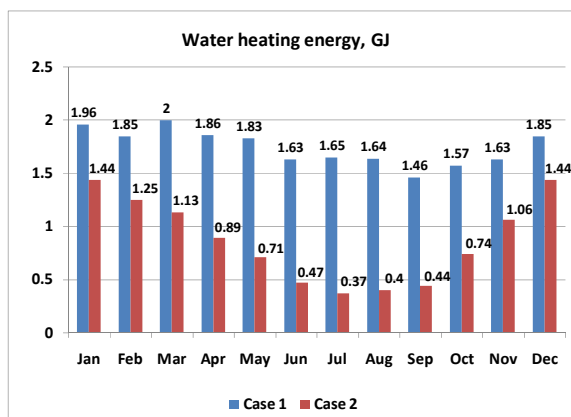


Fig. 11. Monthly building energy consumption for water heating in DHW system, for building without and with PV/t collectors

During the winter months, there is a possibility of electricity generation by PV/t collectors during the sunny days. The amount of generated electricity is not huge but it certainly presents energy saving (Figure 12).

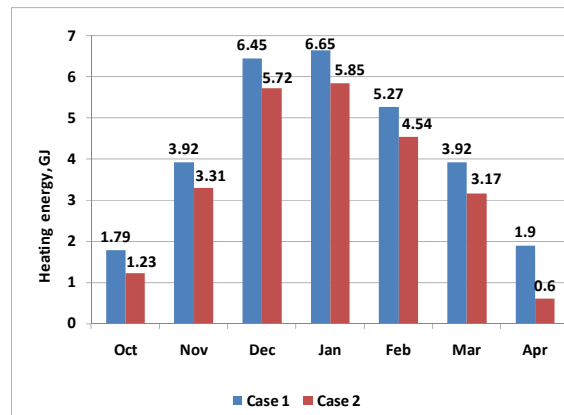


Fig. 12. Monthly consumption of heating energy, for building without and with PV/t collectors

5. CONCLUSION

In buildings, solar energy can be directly used by installation of photovoltaic/thermal collectors. PV/t collectors can improve building energy efficiency and they are representing renewable energy technology with high potential for great energy savings, due to simultaneous generation of electricity and thermal energy.

Single-family residential building, located in the city of Kragujevac, Republic of Serbia, is analyzed in this paper. Simulations were conducted for the same building – with and without installed PV/t collectors.

Annual energy consumption in building without PV/t collectors is 54.718 GJ, while in building with PV/t collectors, it is 39.36 GJ. Results obtained by simulation in EnergyPlus software show annual energy saving of 15.358 GJ, i.e. 28 %. Generated energy by PV/t is 15.892 GJ - 10.595 GJ of energy related to thermal energy and 5,297 GJ is electricity.

In addition to high energy savings, i.e. economic saving, that can be achieved by various solar systems, we should not neglect their very small detrimental impact on the environment.

Acknowledgement

This paper presents results obtained within realization of two projects TR 33015 and III 42006, funded by Ministry of Education, Science and Technological Development of the Republic of Serbia. The authors would like to thank to the Ministry for their support during these investigations.

REFERENCES

- [1] Bojić M., Nikolić N., Nikolić D., Skerlić J., Miletić I., (2011). A simulation appraisal of performance of different HVAC systems in an office building, *Energy and Buildings*, vol.43, no. 6, p. 2407-2415
- [2] Nikolic D., Skerlic J., Radulovic J., Energy efficient buildings – legislation and design, *Proceeding of 2nd International Conference on Quality of Life*, 2017, Kragujevac, p. 55-60
- [3] Nikolić D., Skerlić J., Šušteršič V., Radojević A., Aleksić N., Variances in building energy consumption – influence of domestic hot water system parameters, *Proceeding of 5th International Scientific Conference "Conference on Mechanical Engineering, Technologies and Applications" COMETA 2020*, 2020, Jahorina, Republika Srpska, p. 436-443
- [4] Nikolic D., Lukić N., Radulovic J., Skerlic J., Energy optimization of Serbian buildings using the Hooke-Jeeves algorithm, *Proceeding of 4th International Conference on Renewable Electrical Power Sources ICREPS 2016*, 2016, Belgrade, p. 443-452
- [5] Charalambous P.G., Maidment G.G., Kalogirou S.A., Yiakoumetti K., (2007). Photovoltaic thermal (PV/T) collectors: A review, *Applied Thermal Engineering*, vol 27, no. 2-3, p. 275-286
- [6] Anonymous, *ENERGYPLUS, Input Output Reference - The Encyclopedic Reference to EnergyPlus Input and Output*, University of Illinois & Ernest Orlando Lawrence Berkeley National Laboratory, 2009.
- [7] Nikolic D., Skerlic J., Šušteršič V., Radulović J., Mišković A., INFLUENCE OF HOT WATER TEMPERATURE IN DHW SYSTEM ON BUILDING EXERGY OPTIMIZATION, *Proceeding of 13th International Conference on Accomplishments in Electrical and Mechanical Engineering and Information Technology DEMI 2017*, 2017, Banja Luka, Republika Srpska, p. 177-184
- [8] Lukic N., Babic M. (2008)., *Solarna energija*, Masinski fakultet u Kragujevcu, Centar za RGE, Kragujevac
- [9] Zondag H.A., (2008). Flat-plate PV-Thermal collectors and systems : a review, *Renewable and Sustainable Energy Reviews*, vol 12, no. 4, p. 891-959



Banja Luka
28–29 May 2021.

DEMI 2021

15th International Conference on Accomplishments in Mechanical and Industrial Engineering

www.demi.mf.unibl.org



Experimental investigations of FSI mechanisms in pipeline systems

R. Brđanin^a, U. Karadžić^b, A. Bergant^c, J. Ilić^d

^aUniversity of East Sarajevo, Faculty of Production and Management Trebinje, Stepe Stepanovića bb, Trebinje 89101, Bosnia and Herzegovina

^bUniversity of Montenegro, Faculty of Mechanical Engineering, Džordža Vašingtona bb, Podgorica 81000, Montenegro

^cLitostroj Power d.o.o. (Full-Time) and University of Ljubljana, Faculty of Mechanical Engineering (Part-Time), Ljubljana 1000, Slovenia

^dUniversity of Belgrade, Faculty of Mechanical Engineering, Belgrade, Kraljice Marije 16, Belgrade 11000, Serbia

Abstract This paper deals with experimental investigations of fluid-structure interaction (FSI) mechanisms in pipeline systems. The experimental setup for investigation of water hammer and its side effects, unsteady friction, transient cavitation, column separation and FSI is installed at Faculty of Mechanical Engineering, Podgorica, Montenegro. Experimental runs have been performed with different initial values of pressure in the upstream end high-pressurized tank and with pipeline, valve and elbow, restrained and released. Some of the obtained results are presented and the pressure histories for different system conditions, as well as differences between pressure transducers readings, are discussed.

Keywords water hammer, experimental setup, FSI, pressure transducers

1. INTRODUCTION

Water hammer analysis is a fundamental part of the design process of piping systems for hydro power plants or water distribution networks. Knowing and describing the phenomena that accompany water hammer (fluid-structure interaction - FSI, column separation, unsteady friction and visco-elasticity) is essential for reliable and safe operation of the plant [1, 2]. The influence of FSI effect can be significant,

especially for non-anchored pipelines. A better understanding of the FSI effect leads to improved pipeline design and reduced possibilities for hydraulic system breakdown [3]. Physical experiments are a prerequisite for demonstrating the importance of FSI, and at the same time are essential for the validation of theory [4].

Transient pressures in straight pipelines generate axial stresses and strains in the pipe wall by means of different mechanical processes: the circumferential strain produced by the inner pressure generates an axial strain related with the Poisson effect (Poisson coupling); the shear stress between the fluid and the pipe wall directly loads the conduit in the axial direction (friction coupling); and finally, unbalanced forces at the points where there is a singularity in the piping system (e.g.

Corresponding author

MSc, Radislav Brđanin
radislav.brdjanin@fpm.ues.rs.ba

University of East Sarajevo, Faculty of Production and Management Trebinje
Stepe Stepanovića bb, 89101
Trebinje, Bosnia and Herzegovina

at the valve section) load the conduit as well (junction coupling) [5]. When these mechanisms are large enough to excite and to move the pipe, their effects on the transient pressure wave can be considerable and FSI occurs [6]. In this paper, two FSI mechanisms are experimentally investigated, Poisson coupling and junction coupling mechanism.

2. EXPERIMENTAL SETUP

Experimental setup for investigation of water hammer and its side effects (unsteady friction,

cavitation, column separation, trapped air, FSI), as well as pipeline filling and emptying (Fig. 1), is installed at the University of Montenegro, Faculty of Mechanical Engineering [7]. It consists of a horizontal pipeline (steel pipe of total length $L = 55.37$ m; internal diameter $D = 18$ mm; pipe wall thickness $e = 2$ mm; maximum allowable pressure in the pipeline $p_{\max,all} = 25$ MPa) that connects the upstream end high-pressurized tank (HPT) to the outflow tank.

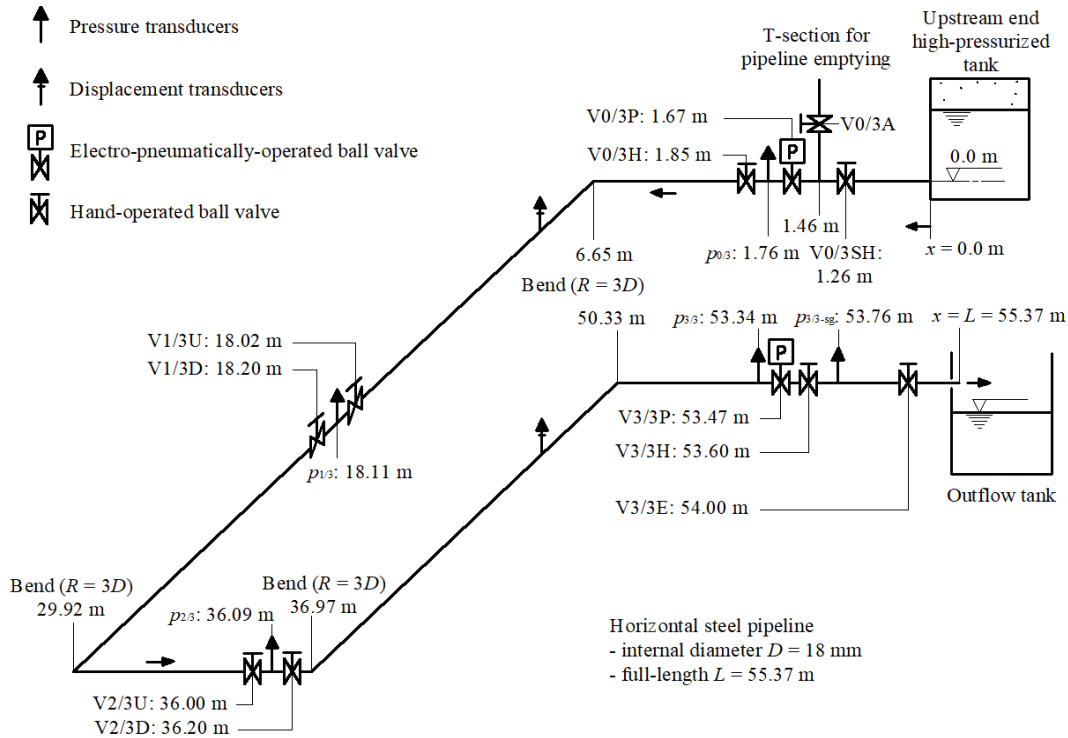


Fig. 1. Layout of the experimental setup

Four valve units are positioned along the pipeline including the end points. The valve units at the two tanks (positions 0/3 and 3/3) consist of an electro-pneumatically operated ball valve and a hand-operated ball valve. Valve units at the two equidistant positions along the pipeline (positions 1/3 and 2/3) consist of two hand-operated ball valves. All units are connected to the intermediate pressure transducer blocks. A T-section with two valves placed at the upstream valve unit serves for pipeline filling and emptying experiments. There are four bends (90°) along the pipeline with radius $R = 3D$. The pipeline is restrained

against axial displacement in 37 points (near the valve units and bends). The supports are released when performing FSI effect experiments. The air pressure in the upstream end tank can be adjusted up to 800 kPa. The pressure in the tank is kept constant during each experimental run by using a high-precision fast-acting air pressure regulator (precision class: 0.2 %) in the compressed air supply line. Four piezoelectric and four piezoresistive high-frequency pressure transducers are positioned within the valve units along the pipeline including the end points (Fig. 1). Absolute dynamic pressures at positions $p_{0/3}$, $p_{1/3}$, $p_{2/3}$ and $p_{3/3}$ are measured by high-frequency piezoelectric absolute pressure transducers (pressure range: from 0 MPa to 6.9 MPa;

resonant frequency: 500 kHz; acceleration compensated; discharge time constant: 10 seconds (fixed)), and in addition absolute dynamic and static pressures are measured by piezoresistive pressure transducers (pressure range: 0 MPa to 3 MPa, sensitivity: 10 mV/3kPa, precision $\pm 0.1\%$). The datum level for all pressures measured in the pipeline and at the tank is at the top of the horizontal steel pipe (elevation 0 m in Fig. 1.). Two displacement transducers for measuring the pipeline movement (measuring range: 0 mm to 10 mm, precision $\pm 0.2\%$) are placed on their own supports, so they can be moved to different positions along the pipeline. The water temperature is continuously monitored by the thermometer installed in the outflow tank. The fast closing electro-pneumatically operated ball valves (V3/3P and V0/3P) are controlled with filtered compressed air which is supplied through a plastic pipeline from the pressure regulator, in which the pressure is independent from the rest of the system. The transient event can be triggered by fast closing or opening of the downstream end valve, using either the V3/3P or the V3/3H or by upstream end valve V0/3P. Valves V3/3P and V3/3H are equipped with a fast-response displacement sensor (measurement range: from 0° to 90° , frequency response: > 10 kHz) which measures the change of the valve angle (α) during its closing or opening. In addition, transients can be induced by closing or opening the hand-operated valves along the pipeline (valves V0/3H; Vi/3U and Vi/3D; $i = 1, 2$). Two strain-gauge pressure transducers ($p_{0/3\text{-sg}}$ and $p_{3/3\text{-sg}}$; pressure range: from 0 MPa to 1 MPa, uncertainty: $\pm 0.5\%$) are installed at the upstream end high-pressurized tank and at the downstream end of the pipeline. These transducers are used for the evaluation of the initial conditions in the system. The hand operated ball valve (V3/3E) is used for adjustment of the initial pipe velocity. The initial velocity (velocities larger than 0.3 m/s) is measured by the electromagnetic flow meter (uncertainty: $\pm 0.2\%$). All measured data are collected by the programmable logic controller (PLC) connected to a PC, with the software that is also used to control the electro-pneumatically operated ball valves.

3. RESULTS AND DISCUSSION

Experimental runs have been performed with different initial values of pressure in the upstream end high-pressurized tank, different velocities in the pipe system and with pipeline, valve and elbow, restrained and released. In the paper, three different experimental tests results are presented; test with restrained system – water column separation case WCS (Figure 2.), test with the straight section released – WCS-FSI-PC case (Poisson coupling - Figure 3.) and test with the straight section and downstream-end EPV released – WCS-FSI-PCJC case (Poisson coupling and junction coupling - Figure 4.). Initial velocity and HPT pressure for all tests are $V_0 = 2.0$ m/s and $H_{\text{HPT}} = 21.5$ m, respectively. In Figures 2.a), 3.a) and 4.a) measured head at the downstream end of the pipeline is shown, and in Figures 2.b), 3.b) and 4.b) first pressure pulse is enlarged. Red line represents measurements of the piezoelectric, and blue line readings of the piezoresistive high-frequency pressure transducer.

Figure 2. shows measured head at the downstream end of the pipeline after downstream end EPV is closed (water column separation case). The closure of the EPV causes water hammer with transient cavitation and column separation. For this test, as it may be noticed in the Figure 2.b), readings of both transducers show very good agreement.

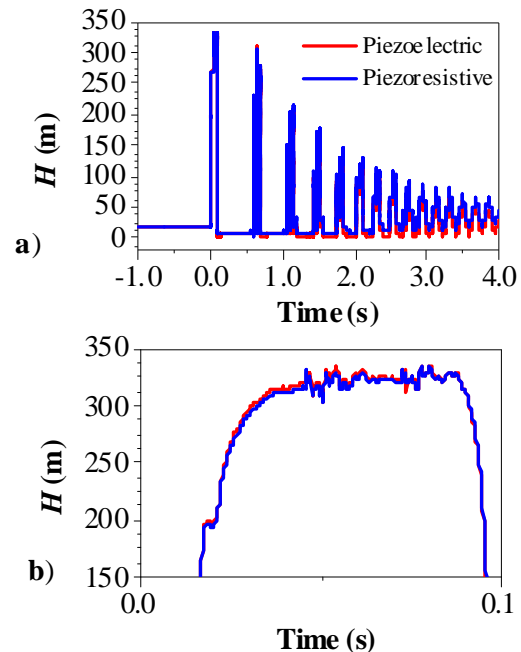


Fig. 2. Measured head at downstream pipeline end – WCS case

In Figure 3. the case with Poisson coupling included is shown. Releasing the straight pipe section causes FSI effect to occur at the valve position, which leads to a smaller pressure rise ($\Delta H_{WCS-FSI-PC} = 272$ m) than for the case of the restrained system ($\Delta H_{WCS} = 313$ m). Occurrence of the FSI effect is evident in Figure 3.b) where pressure fluctuations caused by the moving pipe section are present. For the first part of the pressure pulse piezoelectric transducer shows different response, while the second part is quite similar as for the WCS case. It seems that the readings of the piezoresistive transducer (quite different compared to the piezoelectric one) better indicate the occurrence of the FSI effect (energy transfer between water and the pipeline).

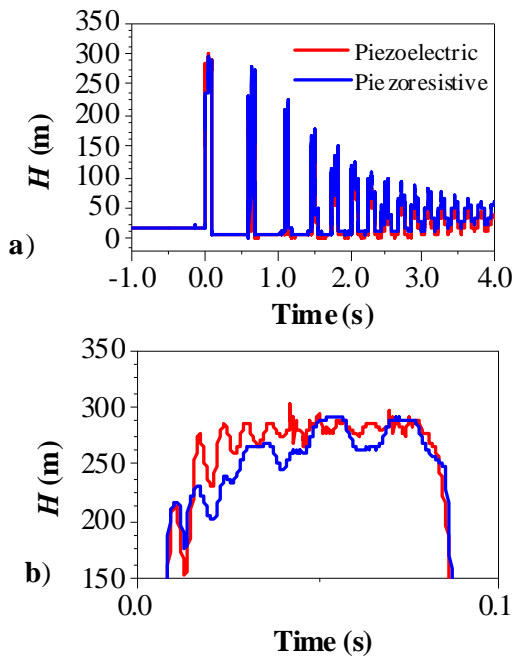


Fig. 3. Measured head at downstream pipeline end – WCS-FSI-PC case (Poisson coupling)

Figure 4. depicts the case with Poisson and junction coupling included. In this case pressure rise is $\Delta H_{WCS-FSI-PCJC} = 274$ m and it is also less than $\Delta H_{WCS} = 313$ m, but close to $\Delta H_{WCS-FSI-PC} = 272$ m. Now, the straight pipe section and the downstream end EPV are released. In this test the system behaves similar like for the Poisson coupling (PC) case, although there are couple of differences. If we look in Figures 3.b) and 4.b) - piezoelectric transducer, energy transfer is a bit smaller than for the PC case, but the pressure rise is almost the same. In Figure 4.b) there is a

peak at the very right side, obviously as a consequence of junction coupling.

When compared to the case of the restrained system, the FSI effect, caused by releasing the straight section of the pipe and the EPV valve, leads to an attenuation of the pressure pulse.

For the both cases the influence of the FSI is strong at the beginning of the transient event (first pressure peak), while later the system behaves similarly as if it was restrained.

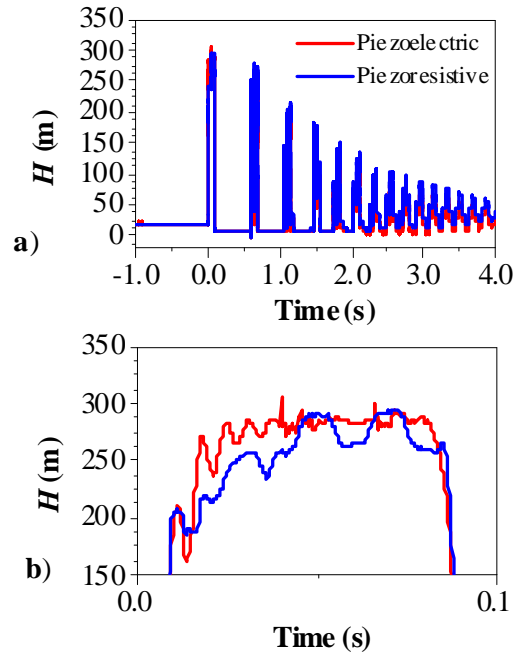


Fig. 4. Measured head at downstream pipeline end – WCS-FSI-PCJC case (Poisson and junction coupling)

4. CONCLUSION

Fluid-structure interaction may have important effect, especially in non-anchored pipeline systems. In this paper FSI mechanisms have been experimentally investigated. Tests conducted on laboratory experimental setup have shown that releasing the pipeline system elements causes FSI effect, due to Poisson and junction coupling mechanism. In the presented cases, the FSI effect, caused by releasing the straight section of the pipe and the EPV valve, leads to an attenuation of the pressure pulse. For the both cases the influence of the FSI is strong at the beginning of the transient event (first pressure peak), while later the system behaves similarly as if it was restrained. Also, there was a conclusion that the readings of the piezoresistive transducer, when compared to

the piezoelectric, would better indicate the occurrence of the FSI effect.

in *Mechanical and Industrial Engineering – DEMI 2019*, May 2019, Banja Luka, p. 195-200.

Acknowledgement

The authors gratefully acknowledge the support of the Ministry of Science of Montenegro and of the Ministry of Education, Science and Technological Development of Republic of Serbia through the project „Research and development of improved measures for protection of hydropower plants during hydraulic transients in order to increase their reliability and energy efficiency“. In addition, the support from Slovenian Research Agency (ARRS) conducted through the project L2-1825 and the programme P2-0126 is gratefully acknowledged as well.

REFERENCES

- [1] Bergant, A., Tijsseling, A.S., Vítkovský, J.P., Covas, D.I.C., Simpson, A.R., Lambert, M.F. (2008). Parameters affecting water wave attenuation, shape and timing. Part 1: Mathematical tools. *Journal of Hydraulic Research*, vol. 46, no. 3, p. 373-381.
- [2] Bergant, A., Tijsseling, A.S., Vítkovský, J.P., Covas, D.I.C., Simpson, A.R., Lambert, M.F. (2008). Parameters affecting water wave attenuation, shape and timing. Part 2: Case studies. *Journal of Hydraulic Research*, vol. 46, no. 3, p. 382-391.
- [3] Ferras, D., Manso, P.A., Schleiss, A.J. and Covas, D.I.C. (2018). One-Dimensional Fluid–Structure Interaction Models in Pressurized Fluid-Filled Pipes: A Review, *Applied Science*, 8, 1844.
- [4] Tijsseling, A. (2019). An overview of fluid-structure interaction experiments in single-elbow pipe systems. *J Zhejiang Univ-Sci A (Appl Phys & Eng)*, 20 (4), p. 233-242.
- [5] Ferras, D., Manso, P.A., Schleiss, A.J. and Covas, D.I.C. (2017). Fluid–structure interaction in straight pipelines with different anchoring conditions. *Journal of Sound and Vibration*, 394, pp. 348-365.
- [6] Tijsseling, A. (2007). Water hammer with fluid-structure interaction in thick-walled pipes. *Computers and Structures*, 85 (11), p. 844–851.
- [7] Brđanin, R., Ilić, J., Karadžić, U., Božić, I. Experimental water hammer setup at University of Montenegro – description and possibilities. *Proceedings of the 14th International conference on Accomplishments*



Banja Luka
28-29 May 2021.

DEMI 2021

15th International Conference on Accomplishments in Mechanical and Industrial Engineering

www.demi.mf.unibl.org



The use of passive techniques to improve heat transfer in pellet stove

M. Jovčevski^a, M. Laković^a, F. Stojkovski^b, M. Jovčevski^b, M. Mančić^a, S. Pavlović^a

^aFaculty of Mechanical Engineering, University of Nis, Nis, Serbia

^b“Ss. Cyril and Methodius” University, Faculty of Mechanical Engineering, Skopje, Republic of North Macedonia

Abstract *The purpose of this paper is to analyze and evaluate the potential opportunities for improving heat transfer and the impact on the efficiency of the pellet stove, as well as the environmental benefits. The possibilities for improving the heat transfer in the heat exchange surfaces between the combustion products and the working fluid (water) will be researched. The basis of the research lies in the possibilities for reducing the temperature of the products of combustion. Based on the results of the analysis, the optimal mechanism/device for improving the heat transfer should be selected. Improving the energy efficiency of the pellet boiler was tested using turbulators. Turbulators are specific elements made of twisted metal plates, installed in the heat exchanger vents in the stove, which turn the airflow from straight to spinning, increasing the heat transfer rate in the exchanger. A mathematical model will prove the potential and justification for the use of devices to improve the heat transfer coefficient i.e., increase the efficiency coefficient.*

Keywords *biomass, pellet stove, turbulators, heat transfer, energy efficiency*

1. INTRODUCTION

Pellet stoves are heat exchangers which burn compressed fuel and create a heat source for residential or industrial buildings. By constantly feeding fuel from a pellet storage tank, the stove produces a constant flame that requires little physical adjustment. In recent years biomass has become the most important renewable source for heat generation. Today's central heating systems operate with wood pellets since renewable energy can reach an efficiency coefficient of over 90% [1].

The need to increase the thermal performance

as well as the energy efficiency of pellet stoves to save costs leads to the development and use of many techniques to improve heat transfer. The goal of increased heat transfer is to encourage or accommodate high heat fluxes [2]. This leads to a reduction of the warmth money handler size, which usually ends up in less opportunity cost. Another advantage is that the reduction of the temperature drive, which reduces the entropy generation and will increase the second law potency [3].

Techniques for improving heat transfer in a heat exchanger are classified into three different categories [4]: passive techniques, active techniques, complex techniques. In this Turbulators cause rotational flow or secondary fluid flow. Various devices can be used to induce this effect, which includes the insertion of strips, arrangements to change the flow through the pipes, and modifications to the geometry of the channels. Dimensions, ribs, spirally twisted

Corresponding author

Milica Jovčevski
milica.jovic@masfak.ni.ac.rs

Faculty of Mechanical Engineering, University of Nis,
Aleksandra Medvedeva 14,
Nis, Serbia

strips are examples of modification of their geometry. Turbulator inserts include tapered parts, spiral strips, or inserts such as nuts and wire coils [5].

Turbulators as elements to improve heat transfer in heat exchangers have been studied a long time ago. In 1959, a group of authors found that the use of turbulator increased in heat transfer [6]. This claim was confirmed by [7-13]. In these studies, were used either water or air as the working fluid. The application of the turbulator affects the pressure drop. Monis Abdulmamon et al [14] proved by experimental research that pressure drop increase by 10%. Using twisted tape turbulators the group of authors proved that pressure drop [15]. The influence of turbulators on pressure drop was investigated in both laminar and turbulent flow [16]. Twister tape turbulators were used in this paper. Studies have shown that with this type of turbulator, a half pitch of turbulator gives greater efficiency of heat transfer than when it is used a full pitch of the turbulator [17, 18]. When it comes to Nusselt's number by applying these inserts, analyzes have shown that it increases [19, 20].

2. MATHEMATICAL MODEL AND MEASUREMENTS

A schematic representation of the operation and connection of the boiler is given in Fig.1.

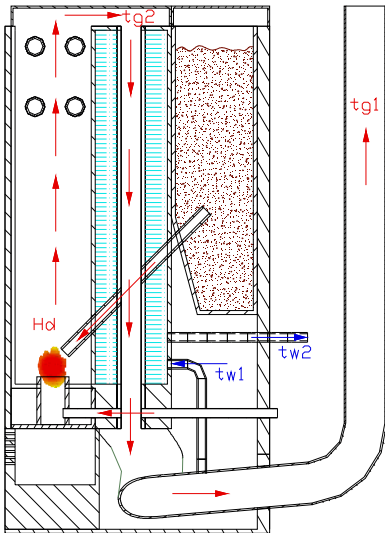


Fig.1 Hot water boiler operating scheme

To obtain the performance of a hot water boiler, measurements were made. Measurements were

made on the boiler without any modifications and the latter on the boiler with built-in tin turbulators in the space of the heat exchanger. The measurements were performed on certain current and thermodynamic parameters to obtain the difference in efficiency obtained on the boiler without and with turbulators.

The efficiency of the boiler can be determined according to the expression [21]:

$$\eta_{\text{boiler}} = 1 - \sum \eta_i$$

η_i is the partial degree of the energy conversion.

The main interest of these measurements is to define the heat exchange of gases in the heat exchanger towards the working medium, where the heat and time required for heating the working medium (water) is not taken into account, considering the case is stationary. Certain concessions have been made regarding the definition of the partial degrees of beneficial effect, i.e., are adopted for constants with a value of 1. Hence, a ratio of the energy obtained from the exhaust gases of the boiler with the energy obtained from the fuel is expressed through the equation [7]:

$$\frac{Q_g}{Q_d} = \eta_{PF}$$

where the energy of the gases can be written through the expression:

$$Q_g = m_g C_{pg} (T_{g2} - T_{g1})$$

and the energy obtained from the fuel:

$$Q_d = B \cdot H_f$$

to see the relative difference obtained when installing turbulators.

According to the temperature of the exhaust gases in some modes, the density is calculated:

$$\rho_g = \frac{P_{\text{atm}}}{RT}$$

The mass flow is:

$$m_g = \rho_g \cdot Q_{\text{tor}} \text{ [kg/h]}$$

2.1 Defining fuel flow

Fuel flow is directly dependent on the rotation of the worm mechanism which has the role of bringing pellets to the firebox. In each different operating mode of the boiler, the mechanism doses differently. Data on the percentage of dosing capacity of the mechanism are read directly from the computer unit that is installed on the boiler, wherewith a calibration coefficient with the operating modes, an approximate calculation is made for the mass flow of fuel.

2.2 Temperature of gases

The temperature of the exhaust gases is read directly from the computer built into the furnace, where it registers it through local sensors in the boiler. The ambient temperature of the air entering the boiler is read by a local sensor that is placed in the room. In Figure 2 is presented the thermometer which was used in this research.



Fig.2. Thermometer for determining the ambient temperature

2.3 Gas flow

For each different operating mode, the boiler fan operates at a different speed to achieve the required air/combustion gas flow. The values of the fan speed in the individual operating modes are read on the built-in computer of the boiler. The air/gas flow is obtained by measuring the velocity of the flow in the exhaust branch of the boiler by measuring the difference between the total and current pressure with the help of the Prandtl-Pit probe (figure 3 and figure 4).



Fig 3. Prandtl-Pit probe

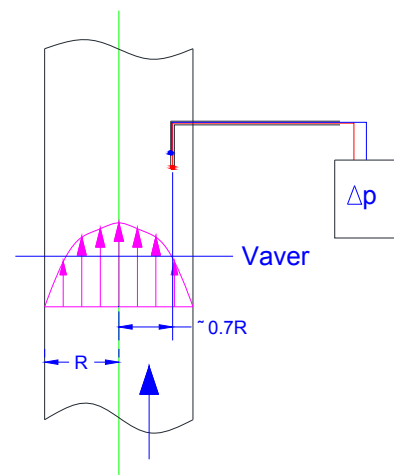


Fig 4. Probe layout scheme

The probe is placed in the exhaust branch of the boiler in the vertical part, opposite to the direction of flow. The top of the probe is set at 0.7R - 70% of the length of the radius seen from the axis of the branch to measure the velocity in the zone of the velocity profile where the mean velocity vector is located, through which the volumetric flow of gases is defined. Through the already registered temperature of the exhaust gases, a calculation of the correction of the air density was made, which obtained the mass flow.

Through the relation

$$v = \sqrt{\frac{2\Delta p}{\rho}}$$

the average flow velocity in the measurement zone was calculated. According to the read values for the number of the fan speed in the

individual operating modes, static pressures or velocities of airflow were measured. According to the continuity equation, the volumetric airflow values are obtained for the cross-section of the exhaust branch [22]. On the Table 1 is presented measured values for the flow rate of the gases. In the Figure 5 can be seen volume flow diagram depending on the number of fan speeds.

Table 1. Measured values for the flow rate of the gases

n [rpm]	pt-pst [Pa]	v [m/s]	A [m ²]	Q [m ³ /h]
1590	4,5	2,254	0,005	40,79
1740	4,1	2,617		47,35
1890	3,625	2,85		51,57
2060	6	3,16		57,18
2230	5,85	3,27		59,17
2650	9,5	4,06		73,47

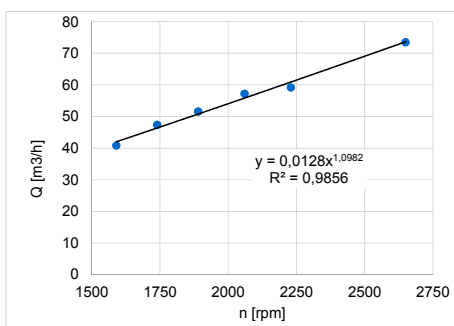


Fig 5. Volume flow diagram depending on the number of fan speeds

According to the trend of the volume flow curve about the number of the fan speed, it can be noticed that it is linear, so concerning the exponent, a correction of the calculated values for airflow is made, which is taken into account in the following calculations and presented in the Table 2.

Table.2. Aspirator(ventilator) speed and the flow of air through the boiler

n [rpm]	Q_corr. [m ³ /h]
1590	41,974
1740	46,343
1890	50,748
2060	55,783
2230	60,858
2650	73,556

3. RESULTS AND DISCUSSION

In this paper, the analysis was made for a pellet stove model Alba by the producer Eco Shpar Ohrid. The stove has a maximum power of 18 [kW]. Two measurements of the stove parameters were performed. The first measurement is completed without any modification of the stove, while the second measurement is performed for a stove with installed metal twisted plates -turbulators in the air heat exchanger, which were hand-made and are non-standard.

The boiler, which is controlled via an electronic unit, has 6 operating modes, and in each operating mode, it has a different option. In this analysis, all modes of operation are covered. As for fuel, pellets, its main feature, heat can be adopted by the manufacturer. The pellets have the EN Plus A2 standard. The lower thermal power of the fuel given by the manufacturer is 16560kJ / kg [23]. In Table 3. the values taken as standard values during the measurements in both cases with and without turbulators are shown.

Table 3. Pellet Stove Operating Parameters

operating mode	fan operating speed	auger dosing percentage	pellet mass flow
mode	n [min-1]	auger [%]	m_pel [kg/h]
1	1590	25	1,2
2	1740	33	1,6
3	1890	43	2,09
4	2060	53	2,57
5	2230	63	3,06
6	2650	73	3,54

*Auger is mechanism for pellets dosing.

In each mode of operation of the stove, the temperature difference of water is constant and is 20 [°C], room air temperature is 21[°C], water flow 0,16 [l/s]. The pellet flow is standard and is provided by the manufacturer for each stove operating mode. This is in stationery condition. The same applies to the fan speed used to control the exhaust gas flow from combustion. In Table 4 the supplied thermal power from the fuel for each mode of operation of the boiler at a constant temperature difference of 20[°C] is shown.

Table 4. Brought thermal energy from the fuel

Hd min [kWh/kg]	m_pel [kg/h]	Qd [kW]
4,6	1,2	5,52
	1,6	7,36
	2,09	9,614
	2,57	11,822
	3,06	14,076
	3,54	16,284

There is a big difference in the energy supplied by the fuel and it is in the range from 5.52 kW to 16.28 kW. It can be noticed that the least energy is needed in the first mode of operation, and the most in the sixth mode. However, a very important factor that must not be neglected is the time for which the required amount of energy of 18 kW of the water is achieved. Thus, in the first mode of operation, it would take a much longer time with the sixth mode of operation to achieve the required amount of energy. Therefore, the electronic unit with which the boiler is equipped has a function to control in which operating mode the boiler will operate to achieve the required amount of energy in the shortest time. In this case of analysis, the heating time of the working medium is neglected, as it is considered as stationary.

On the next Fig. is presented resultants of energy efficiency of pellet boiler with and without turbulators.

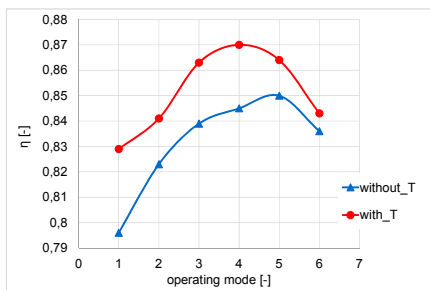


Fig.6. Diagram. Comparison of efficiencies without and with turbulators in absolute values

To analyse the efficiency as presented in the diagram in absolute values, it is easy to draw a primary conclusion that with the use of turbulators, the zone of maximum efficiency is

moved to the left for the lower operating mode of the boiler, and the same is improved efficiency. approx. 2%. As mentioned above, due to the compromise made and the exclusion of additional degrees of beneficial effects inside the boiler, the efficiency in further exposure is not analysed in absolute terms, but in a relative relationship to show the overall picture of the boiler. The efficiencies compared on a relative basis are given in Figure 7.

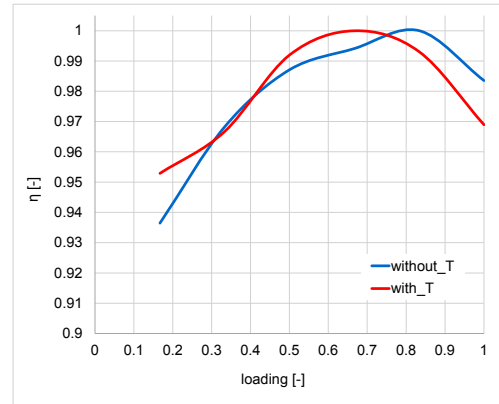


Fig.7. Diagram of relative comparison of boiler efficiencies without and with turbulators in relation to the relative load (operating mode) of the boiler

In the diagram, the efficiencies are presented on a relative basis 1 in relation to the relative operating mode (percentage of load) of the boiler 1. According to the derived results, it can be seen when installing turbulators in the heat exchanger, the zone of the optimal operating range of the boiler is moved to the left, i.e., it is obtained for a lower operating mode, concerning when the boiler operates without built-in turbulators. Also, the shape of the efficiency curve has changed, where for the boiler without built-in turbulators a scale shift can be observed in front of the zone of optimal operation from low to high efficiency, with the boiler without turbulators having a wider operating characteristic. On the other hand, when using turbulators, the operating efficiency curve changes its shape and becomes narrower, with a tendency of concentrated work around the optimal zone, with the curve itself being more symmetrical.

The efficiency on the other hand is also analysed on a relative basis through the relative flow of pellets in the system, where the shape of the curves is identical. Through a simplified analysis of the curves, using interpolation

polynomial functions of the 3rd and 4th order, the functional dependences of the relative efficiency concerning the operating mode are derived, i.e., the flow of pellets in the system (Figure 8 and Figure 9).

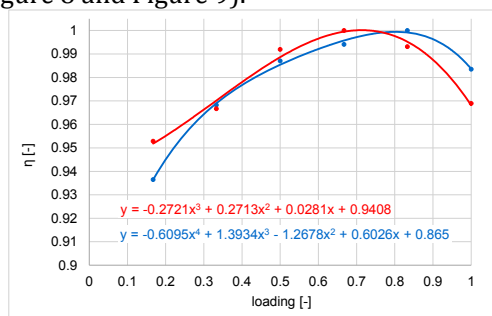


Fig.8. Interpolation functions for the efficiencies concerning the operating mode of the boiler

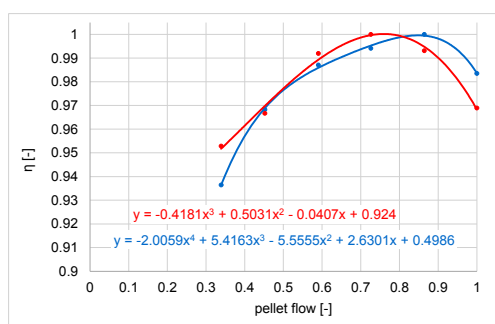


Fig.9. Interpolation functions for efficiency concerning the flow of pellets

4. CONCLUSION

In this analysis, an attempt is made to improve the efficiency of the pellet stove without modifying the stove body, but only by inserting turbulators therein. Turbulators are used inside tubes of pellet stove to improve the turbulent convective heat transfer coefficient in the gas side since the heat transfer coefficient on the outside is very high. The overall objective of this application is to improve the boiler efficiency, although other factors such as pressure drop, changes in the waterside heat transfer coefficient, fouling, and manufacturing cost are also important. As the exhaust gases in pellet stoves are high, the task of the turbulator is to enable a larger contact area, the transition of flow from laminar to turbulent flow and thus reduce the temperature of the exhaust gases and increase the efficiency of the boiler.

In this paper, a test was delivered on a pellet stove with a power output of 18 [kW], where two configurations were examined: the stove as

it is and the stove with installed turbulator strips. The tests were guided accordingly to the operating modes of the stove. The parameters such as fan speed, pellet mass flow and air temperatures were obtained from the data acquisition system of the stove. Water temperature and flow were measured, and most importantly, the air velocity in the exhaust pipe was measured with a Prandtl-Pitot tube, for later determining the airflow rate. The turbulator strips were hand made without controlled dimensions of the thickness, twist angle and pitch.

The results show that the turbulator installments do increase the amount of heat exchanged with swirling the airflow in the exchanger. By observing the exhaust gas temperatures and amount of wasted heat, using the indirect method, the efficiency was simply calculated and compared for the two configurations on a relative scale. Better efficiency has been achieved in all modes of operation and significant in the fourth mode, i.e., around 66,7 % of stove's load.

Acknowledgement

This research was financially supported by the Ministry of Education, Science and Technological Development of the Republic of Serbia (Contract No. 451-03-9/2021-14/200109)"

REFERENCES

- [1] M. Jovčevski, M. Jovčevski, F. Stojkovski, M. Laković, "Performance Analysis of a Pellet Stove with Turbulator Installments", 19th Conference on Thermal Science and Engineering of Serbia, Sokobanja, pp.253-259, 2019
- [2] Kiran K, Asalammaraja, Manoj, Umesh, "A Review on Effect of Various Types of Tube Inserts on Performance Parameters of Heat Exchanger, International Journal of Research in Advent Technology, Vol.2, No.6, E-ISSN: 2321-9637, June 2014
- [3] Bejan A., "Entropy Generation Minimization", CRC Press, Boca Raton, FL, 1996
- [4] D. Shriwas, J. Saini, "Heat Transfer Enhancement Technique in Heat Exchanger: An Overview", IJRTI, Volume 3, Issue 9 | ISSN: 2456-3315, 2018
- [5] Quality Certification Scheme, ENplus Handbook For countries not managed by any national licensor/supporter, Part 3: Pellet Quality, Brussels: European Pellet Council (EPC), 2015.
- [6] Kreith, F and Margolis, D, "Heat transfer and friction in turbulent vortex flow" Appl. Sci. Res.Vpl. 8 PP457-473, 1959.

- [7] Thorsen, R. and Landis, F. "Friction and heat transfer characteristic in tubular swirl flow subject to large transverse temperature gradient" Trans. ASME J. heat transfer, Vol. 90. PP 87-97, 1968.
- [8] Oliver, D, R, and Shoji, Y, "Heat transfer enhancement in a round tube using different tube inserts" non-Newtonian fluid J. Cham. Engng. Res. And Det. Vol. 70, PP 558-564, 1992.
- [9] Yakoya, S., Takagi, S., Lguchi, M., Murkawa, K., Yasugaira, W. and Hara, S. "Development of swirling flow generator in immersing nozzle" ISIJ. Int. Vol. 40, P.P 584-588, 2000.
- [10] Chang, S. W. "Forced heat convection in a reciprocating duct fifying with 45 degree crossed ribs" Int. J. thermal Sci. Vol. 41, P.P 229-240, 2002.
- [11] Chang S. W., JYih Jena and Jin Shuen Liou, "Turbulent heat transfers and pressure drop in tube fitted with serrated twisted tape" International journal of thermal science Vol. 46, PP. 506-518, 2007.
- [12] Mr. Krishna S. Borade, Prof. M. Khanwalkar and Prof. V. N. Kapatrar, "Experimental investigation of heat transfer enhancement with different square jagged twisted tape and Cuo/water nanofluid". Internationl Journal of innovative studies in science and engineering technology, Vol. 2, Issue. 2 P.P 34-39, 2016
- [13] Pragnesh Kumar Prajrpati, Umang Soni and Ashvin Suthar, "Increase the heat transfer rate of double pipe heat exchanger with quadratic tubular (Baffle) Attached twisted tape insert". International journal of advance engineering and research development, Vol. 3 Issue. 5 P.P 204-212, 2016.
- [14] Monis Abdulmamon, V. N. Kapatkar, " Enhancement of heat transfers with conical hole filament insert in flow through circular tube" international journal of research in mechanical engineering and technology. Vol.3, Issue 2, PP 270-273, 2013.
- [15] A. H. Dhumal, G. M. Kerkal and K. T. Pawale, "Heat transfer enhancement for tube in tube heat exchanger using twisted tape inserts" IJAERS Vol. 4, Issue. 5 P.P 89-92, 2017.
- [16] Nimish Dubey and Mr. Morrish Kumar, "Design modification in heat exchanger twisted tape for heat transfer enhancement: A review "international journal of engineering sciences and research technology Vol. 6 No. 7 PP 1-5, 2017.
- [17] Klaczak, A. " Heat transfer and pressure drop in tube with short tabulators" Wsrme and Stoffebetrugung, Vol. 31, PP 399-401, 1996.
- [18] [68] Lokanath, M. S. " Performance evaluation of full length and half-length twisted tape inserts on laminar flow heat transfer in tube in proceeding og 3rd" ISHNT-ASME heat and mass transfer conference India, PP 319-324, 1997.
- [19] Gawander A. V., Dange M.M. and Nalawade D. B. "Heat transfer enhancement with different square jagged twisted tapes" IJERA ISSN2248-9622, 2014.
- [20] D. R. Hase, N. K. Sane, and D. V. Ghewade. "Heat augmentation with using non-matallic flow divider type insert in force convection" 6th National conference RDME P.P 62-67, 2017
- [21] Slave Armenski, "Termotehnicki masini i uredi" (in Macedonian), University "Ss. Cyril and Methodius", 1995, ISBN 9989430403.
- [22] Aleksandar Nospal,"Strujnotehnicki merenja i instrumenti", University "Ss. Cyril and Methodius", 2004, ISBN 9989-704-02-3
- [23] <https://www.enplus-pellets.eu/en-in/>



Banja Luka
28–29 May 2021.

DEMI 2021

15th International Conference on Accomplishments in Mechanical and Industrial Engineering

www.demi.mf.unibl.org



The impact of thermal power plants on river thermal pollution -A case study

M. Laković^a, M. Jovčevski^a, F. Stojkovski^b, V. Stefanović^a, M. Mančić^a, M. Rajić^a

^a Faculty of Mechanical Engineering, University of Nis, Nis, Serbia

^b University "Ss. Cyril and Methodius" Faculty of Mechanical Engineering Skopje, North Macedonia

Abstract A reliable and safe working of a thermal power plant is connected with available natural water streams. Ecological problems connected to the reliable and safe workings of a thermal power plant are directly connected with the availability of natural waterflows. Ecological problems related to waste water which appear while the power plant is working represent a great challenge of its workings. They use water from available streams as a coolant. The cooled water leaves the thermal power plants premises under high heat, under which is then returned back to the stream where it came from. This way, the streams are caused thermal pollution. In this study, it is measured the influence of Kostolac B (a working thermal power plant) on the habitat of Danube river when it flows through Serbia. A mathematical model of thermal pollution was made based on EDF model and an initial numerical simulation in ANSYS FLUENT to achieve the results. During the formation of both models, meteorological and hydrological data was used as well as the working parameters of the considered thermal power plant. The results which were given thanks to these two methods overlap and give approximately the same solutions and confirm the existence of thermal pollution in the Danube river around thermal power plant Kostolac B.

Keywords thermal power plant ; environmental impact; thermal pollution ; waste water, numerical simulation

1. INTRODUCTION

Thermal power plants which use coal, are great pollutants and are hazardous towards the environment. Usually, when there is such kind of pollution, everybody think of air pollution. However, thermal power plants also pollute natural watercourses. In order for a thermal power plant to work, a great deal of cooling water is needed. That water is supplied through natural watercourses. After the water is being used in the power plant to cool off the

condenser, it's being brought back as waste water with a temperature increase. This type of pollution is called thermal pollution.

Thermal pollution is discerning the quality of the water using any action which changes the ambient waters temperature [1]. This type of pollution is categorized in the physical characteristics of waste water. Waste waters temperature shows the quantity of heat which is held inside it [2]. The increase of water temperature has a negative effect on the ecosystem of the stream itself (rivers, lakes, seas, oceans). With the temperature increase, oxygen in the water is reduced thus directly affecting the ecosystem of the water source itself [3]. Fish and other organisms adjusted towards a certain temperature range can die if the waters temperature is drastically changed (either increase or decrease which is known as

Corresponding author

Mirjana Laković
lmirjana@masfak.ni.ac.rs

Faculty of Mechanical Engineering, University of Nis,
Aleksandra Medvedeva 14,
Nis, Serbia

thermal shock) [4]. With the increase in water temperature, the waters ecosystem uses a higher amount of oxygen and organic materials. To build a thermal power plant, we are looking at the distance of the adjacent watercourses. So depending of the location of the thermal power plant itself, steam power plants basically use two types of cooling systems – closed (recirculation) and open (once-through) system [5]. Which system will be implemented is directly connected to the distance of the power plant to the cooling water stream. In the once-through system, the water which is taken from the source flows thorough a condenser, gets heated using steam, then is put back in the stream in a chosen location.

The closed system however, the heated cooling water is cooled again and afterwards is being returned to the condenser. Cooling the cooling water is done in accumulated lakes, cooling towers or by spraying.

2. THERMAL POLLUTION

Thermal pollution wasn't considered as a big pollutant of ecosystems at first. Research in this particular area start in 1960 and precisely the thermal pollution which comes from thermal power plants was taken in consideration because it turned out that they are the biggest polluters of the water [6]. Once the problem was exposed, a group of authors started to research the area based on meteorological data for a specific area [7]. Water temperature through sensitive analysis is given a closer look [8]. This analysis is based on confirming the dependency of certain parameters such as water currents, water temperature as well as the characteristics of the canal itself.

Some studies are focused on the connection between the increase of demand for electricity and waste water [9,10]. Other connect climate change and the workings of the thermal power plants pointing that in order for the plant to work, it depends on the water temperature, increasing the temperature the production and efficiency of the power plant itself is reduced [11]. Similar studies but for different localities were lead by [12, 13].

Some of the studies only dealt with the influence of only one thermal power plant [14] whilst there are analysis and effects of more thermal power plants connected on one power source [15].

In recent years, numerical tools to predict and calculate thermal pollution are used. A lot of the studies show how big the similarities are between the results measuring heat overload on water sources and the creation of numerical simulations [16, 17, 18].

3. THERMAL POWER PLANT KOSTOLAC

In Serbia, thermal power plants are usually based by the Danube, Sava and Morava rivers. Serbia cooperates with the countries from the region when it comes to controlling the effects of cross-border pollution. The Danube River has a significant importance for Serbia. The pollution levels of the Danube River also reflect on the water quality of Djerdap Lake. The development of regional cooperation in the area of water resource management is of great importance. Within that regard, the ratification of the international convention of cooperation for protecting and sustaining the Danube River as well as signing the Memorandum of the confluence of Sava River, a sustainable water management is being put in place as well as regulating the usage, protection of the water and the active ecosystem from thermal and malicious influences [19]. In that regard, in this paper is considered the thermal pollution of the water which is caused by Kostolac B.

TPP Kostolac is located near the City of Pozarevac. The total power of the thermal power plant is 1.010 MW. It contains four units grouped as Kostolac A and Kostolac B. Kostolac A is comprised from 2 units – 1 with power of 100MW the other of 210MW. Kostolac B is comprised from 2 unties 350MW each [20]. On fig 1, the location of the power plant is shown.



Fig.1 Location of TPP Kostolac

From the fig 2 it can be see the distance between the Danube River as well as the canal of the Mlave River which connects this thermal power plant with the Danube.



Fig.2. Connection of the Kostolac thermal power plant with the Danube

In the Republic of Serbia there are measuring stations on natural water flows which feed us information regarding water temperature, level as well as water streams. On fig 3, part of those stations locations are shown and are directly located on the Danube.



Fig.3. Part of the reporting surface water stations network in Serbia [21]

Near PP Kostolac, measurement station Smederevo is located which gathers data on Danube's characteristics before arriving to the thermal power plant, as well as measurement station Veliko Gradiste, located downstream of the power plant. On fig 4 it can be seen the data shown of the water temperature of the Danube River which are read from these stations [22].

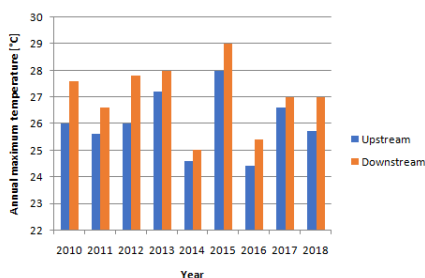


Fig.4. Annual maximum temperatures of the Danube River near the Kostolac thermal power plant

What can be seen from the diagrams is that the water temperature of the Danube is higher

downstream from Kostolac which can be used as an indication that there is thermal pollution from this power plant towards the river. In the next table, the values of minimal water flow rate of measurement station Smederevo are presented. The values shown are from the summer as that is when the water flow is lower because of the high temperatures. These measurements are used later to form the numerical model.

Table 1. Minimal water flow rate for July, August and September from 2010-2019

Year	Minimal water flow rate [m ³ /s]		
	July	August	September
2010	4110	3770	4120
2011	3200	2600	2140
2012	3250	2050	2350
2013	3050	2150	2250
2014	3600	4440	4750
2015	2950	2600	2520
2016	3610	3600	2650
2017	3150	3350	3290
2018	3420	2250	2150
2019	2710	2730	2370

4. EDF METHOD FOR ASSESSING THE IMPACT OF THERMAL POLLUTION ON THE RIVER

In this paper, the working of the condenser of the Kostolac B power plant is analyzed. The mathematical model of the condenser workings of this construction is developed in previous studies [23]. The design conditions predicted that the temperature of the cooling water at the inlet to the power plant is 12°C and the pressure of the condenser is 0.44bar. By applying the mathematical model, taking in consideration a constant flow of cooling water 13000kg/s, is obtained that the temperature of the water increases by 7°C (fig.5).

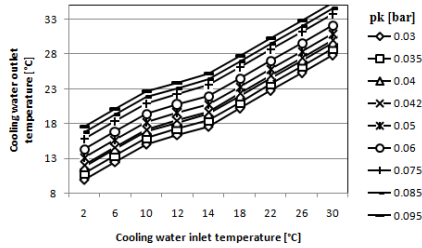


Fig.5.Temperature of the cooling water outlet depending on condensing pressure and temperature of cooling water inlet

Electricity of France (EDF) Group developed the mathematical model of water temperature fluctuation within rivers [24]. This model is comprised by formulas with an exponential factor and as:

$$\Delta t = \Delta t_{max} e^{-kx} \quad (1)$$

Where:

- Δt - temperature of the river downstream from the exhaust of heated water from the thermal power plant
- Δt_{max} - maximum heating of the river caused by the exhaust of the outlet hot water
- k- climate factors
- x- distance

Factor k has value 0.001-0.01.

If we analyze fig 4 it can be seen that in 2015, water temperature was the highest. Just by that reason alone, the EDF model was built for 2015 furthermore the numerical simulation for the same period.

On the next diagram, the EDF curve model is shown.

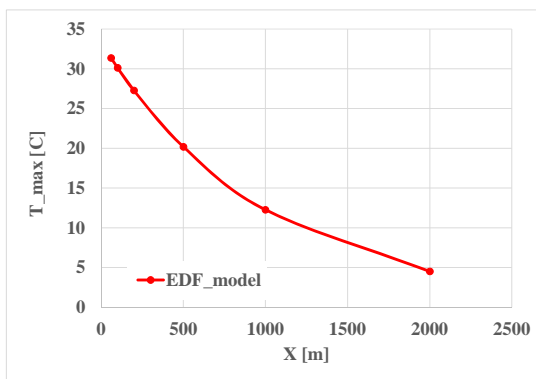


Fig.6. EDF model temperature

What can be seen from the diagram is that with the increase of distance, the dependency curve of temperature and distance falls. That is why this method is more suitable to use in greater distances – 20km and more. But it is also a good solution when there is a small canal. The diagram is drawn out for the period of the max temperature period – summer of 2015. For the coefficient K is used value of 0.001. This value refers to climate area. The group of authors [25] uses the same value of this coefficient and because of similar characteristics of the areas in this paper is used that value.

5. NUMERICAL ANALYSIS OF THE INFLUENCE OF COOLING WATER FROM THE KOSTOLAC B THERMAL POWER PLANT ON THE DANUBE RIVER

Numerical simulation at the junction of the river Danube and the effluent cooling water channel was made using the program ANSYS FLUENT. Simulation of flow is presented with a 3D model, where the flow is treated as a forced flow. The boundary conditions used in this model are the input of the mass flow and temperature of the water in the Danube, mass flow and temperature at the entrance to the effluent channel (Mlava river channel).The geometrical characteristics of the channel are given on the figure 7.

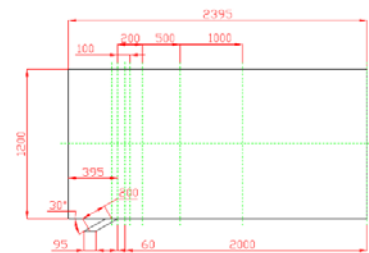


Fig.7. The geometrical characteristics of the channel

In the simulation, the gravitational acceleration is taken into account. The upper plate represents the water free surface with the adopted boundary condition "Symmetry" in order not to get a refund of flow or an undefined flow direction. The outlet flow of the effluent channel is taken as the "outflow" with 100% outflow conditions. Mesh model is a 3-dimensional, composed of 87,912 volumetric hexagonal cells, connected with 104,884 nodes. The convergence of the results is obtained up to

10-8. The boundary conditions of the model and solution convergence are shown in Figure 8.

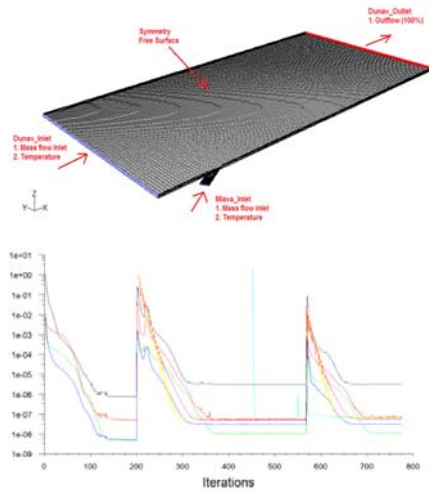


Fig. 8. The boundary conditions of the 3D flow model and solution convergence

The obtained temperature change on the water surface due to effluent water intake into the Danube is presented in Figure 9. Presented results are obtained for atmospheric parameters and power plant operating conditions for August 2015.

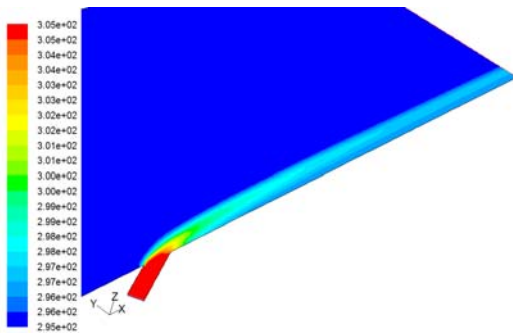


Fig.9. Temperature change on the water surface, August 2015

Table 2 shows numerically obtained results for the maximum temperature of mixed water in different cross-sections downstream the junction area, for August 2015. Danube flow rate was 2,880m³/s, while the effluent flow rate was 29.5m³/s. The average Danube temperature before mixing with effluent water was 27°C. The average temperature change in the whole cross-section of the Danube is noticeable, although temperature does not rise dramatically. The Large flow rate of the Danube compared to effluent flow rate gives a low

sensitivity of the river to temperature changes due to local inflow.

Table 2. Maximum temperature of the mixed water in different cross-sections downstream of junction area, for August 2015

Section Temperature	
[m]	[°C]
60	33.29
100	32.29
200	31.10
500	29.86
1000	29.10
2000	28.68

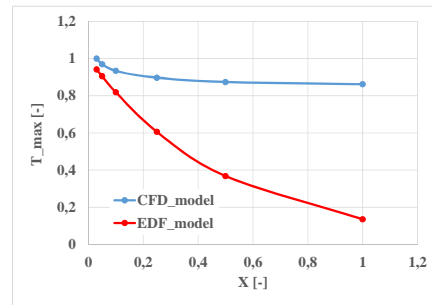


Fig.10. Presentation of CFD results compared to EDF model based on relative temperature 'T' and relative length behind inlet of channel 'X'

According to the diagrams, it can be seen that the simplified initial CFD model and the gathered results, give a similar trend of flattening the temperature curve as the river is elongated, same as the EDF model. The percentile difference in temperature which shows between these two models is the result that in the CFD model, it is not take in consideration the environment and climate change, but rather taken and looked as a theoretical model of flow – mixing two waters sources with different hydraulic and temperature states.

The temperature change in different cross-sections along the Danube flow, downstream of the river junction is shown in Figure 11. The influence of effluent water stretches along hundreds of meters, or even a few kilometres downstream, by the right riverbank.

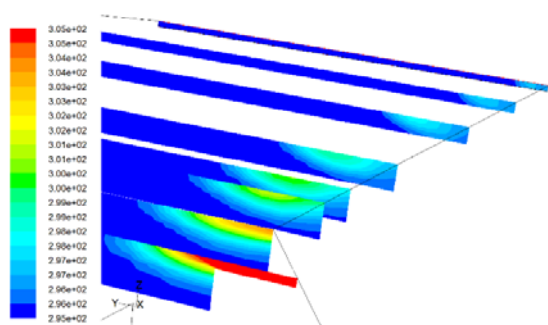


Fig.11. Water temperature in different cross-section along the Danube flow (downstream the river junction August 2015)

According to presented simulation results, it is obvious that the right riverbank area downstream the power plant is directly exposed to the risk of change in the ecosystem due to thermal effluent from the plant. The main stream of the river still is not at risk, due to the small flow rate of the effluent water (only 1% of the river flow in the worst hydrology conditions). The change in the surface water temperature is noticeable in 30m towards the centre of the river stream.

6. CONCLUSION

In this paper, the thermal pollution of the river that occurs due to the operation of the thermal power plant is considered. Thermal power plants use large amounts of water to perform various processes. The water is used in the process of cooling the condensers. After cooling the condenser, the water returns to the river with higher temperature, thus creating thermal pollution of the river.

The thermal pollution of the Danube River due to the operation of the Kostolac B thermal power plant was analyzed. The numerical CFD model and mathematical EDF model were done. It can be noticed that the temperature changes in the same sense and by the same rules when was used the mathematical EDF model and when was used the numerical simulation.

The temperature of the Danube River and in the area of TPP Kostolac is increased by 1°C. But, seeing as the Danube is a river with a very big water flow, it can be seen that these fluctuations do not cause any great harmful effects on ecosystem. The Danube remains in the second water category as described by law in the waters of the Republic of Serbia.

Further research plans on the thermal pollution caused by thermal power plants will deduct towards the analysis of the cause of this type of pollution on the Sava River. Seeing as Sava is smaller in capacity when compared to the Danube and TPP Nikola Tesla use water from Sava River, which has a higher capacity than TPP Kostolac. Thermal pollution is expected to be more pronounced on the smaller river.

Acknowledgement

This research was financially supported by the Ministry of Education, Science and Technological Development of the Republic of Serbia (Contract No. 451-03-9/2021-14/200109)"

REFERENCES

- [1] Precht H, Christophersen J, Hensel H, Larcher W.(1973), *Heat Exchange with the Environment*. Berlin, Heidelberg: Springer; pp. 545-564
- [2] Markov Z., Georgievska M. (2016), *Wastewater treatment*, Konard-Adenauer-Stiftung e. V. Wilfried Martens Centre for European Studies, Skopje
- [3] Povrenovic D., Knezevic M., (2013), *Fundamentals of waste treatment technology water* (in Serbian), Faculty of technology and metallurgy Belgrade
- [4] Chapter 10 - *Water Quality and Catchments*, MarcLos Huertos, *Ecology and Management of Inland Waters A Californian Perspective with Global Applications 2020*, Pages 315-358
- [5] Mihajlov J., (1965), *Thermal power plants, design and building*, (in Serbian), Tehnicka knjiga, Zagreb
- [6] Edinger, J.E.; Geyer, J.C (1965), *Heat Exchange in the Environment*; Edison Electric Institute:New York, NY, USA
- [7] Hogan, M.; Patmore, L.C.; Seidman, H., (1973) *Statistical Prediction of Dynamic Thermal Equilibrium Temperatures Using Standard Meteorological Data Bases*; Report EPA-660/2-73-003; U.S. Environmental Protection Agency (EPA), Office of Research and Development: Washington, DC, USA
- [8] Bartholow J., (1989), *Stream temperature investigations: field and analytic methods instream flow information paper no. 13*, U.S. Fish Wildl. Serv. Biol. Rep. 89 (17). 139 pp.

- [9] Feeley, T.J., T.J. Skone, G.J. Stiegel, A. McNemar, M. Nemeth, B. Schimmoller, J.T. Murphy, and L. Manfredo. (2008), *Water: a critical resource in the thermoelectric power industry*. Energy 33, 1–11.
- [10] USDOE/NETL (USDOE / National Energy Technology Laboratory). 2009a (revised). *Water Requirements for Existing and Emerging Thermoelectric Plant Technologies*. DOE/NETL-402/080108
- [11] IPCC (Intergovernmental Panel on Climate Change). (2007), *Climate Change 2007: Impacts, Adaptation and Vulnerability. Contribution of Working Group II to the Fourth Assessment Report of the Intergovernmental Panel on Climate Change* [Parry, M.L., Canziani, O.F., Palutikof, J.P., Van der Linden, P.J., and Hanson, C.E. (eds.)]. Cambridge University Press, Cambridge, United Kingdom and New York, NY, USA
- [12] Hurd, B. and M. Harrod. (2001), *Water Resources: economic analysis. In: Global Warming and the American Economy*, Edward Elgar Publishing Ltd, Cheltenham, pp. 106–131.
- [13] Arnell, N., Tompkins, E., Adger, N., and Delaney, K., (2005). *Vulnerability to Abrupt Climate Change in Europe*, ESRC/ Tyndall Centre Technical Report No 20, Tyndall Centre for Climate Change Research, University of East Anglia, Norwich.
- [14] Contador L.(2005), *Adaptive management, monitoring, and the ecological sustainability of a thermal-polluted water ecosystem: a case in SW Spain*, Environmental Monitoring and Assessment, Springer, 104:19–35, DOI: 10.1007/s10661-005-6399-2
- [15] Stewart R J, Wollheim W M, Miara A, Vörösmarty C J, Fekete B, Lammers R B and Rosenzweig B (2013), *Horizontal cooling towers: riverine ecosystem services and the fate of thermoelectric heat in the contemporary Northeast US Environ. Res. Lett.* 8 025010
- [16] Monica Fossati et al. (2011), *Numerical Study of the effect of a power plant cooling water discharge in the Montevideo Bay*, Journal of Applied Mathematics, vol.2011, Article ID 970467, 23 pages
- [17] Y. Yunli, W. Deguan, W. Zhigang, and L. Xijun, *Numerical simulation of thermal discharge based on FVM method*, Journal of Ocean University of China, vol. 5, no. 1, 2006.
- [18] Hongyun Xie et al.(2020), *Online simulation of nuclear power plant primary systems*, Science and Technology of Nuclear Installations, vol. 2020, Article ID 8819239, 9 pages.
- [19] Izveštaj o strateškoj proceni uticajastrategije razvoja energetike republike Srbije do 2025. sa projekcijama do 2030. Na životnu sredinu
- [20] www.eps.rs, accessed on: April 2, 2021
- [21] Laković, M. Banjac M., Bogdanovic-Jovanovic J., Jovic M., Milovanovic Z., *Risk of Thermal Pollution of the Danube Passing through Serbia due to thermal power plant*, THERMAL SCIENCE, Vol. 22, Suppl. 5, pp. S1323-S1336
- [22] www.hidmet.gov.rs, accessed on: Mart 25, 2021
- [23] Laković, M., et al. (2012), *Coal-Fired Power Plant Power Output Variation due to Local Weather Conditions*, Energy Sources, Part A: Recovery, Utilization, and Environmental Effects, 34 , 23, pp. 2164-2177
- [24] Penney, S.; Bell, J.; Balbus, J. (2009) *Estimating the Health Impacts of Coal-Fired Power Plants Receiving International Financing*. Report of Environmental Defence Fund.
- [25] Marc A. Rosen et al (2015). *Evaluating the Thermal Pollution Caused by Wastewaters Discharged from a Chain of Coal-Fired Power Plants along a River*, Sustainability, 7, 5920-5943; doi:10.3390/su7055920
- [26] Alibek Issakhov & Yeldos Zhandaulet (2019) *Numerical simulation of thermal pollution zones' formations in the water environment from the activities of the power plant*, Engineering Applications of Computational Fluid Mechanics, 13:1,279-299, DOI:10.1080/19942060.2019.1584126



Banja Luka
28–29 May 2021.

DEMI 2021

15th International Conference on Accomplishments in Mechanical and Industrial Engineering

www.demi.mf.unibl.org



Numerical investigation of centrifugal pump with cylindrical blades and different blade wrap angle

J. Bogdanović Jovanović^a, Ž. Stamenković^a, M. Kocić^a, J. Petrović^a

^aUniversity of Niš, Faculty of Mechanical Engineering, Aleksandra Medvedeva 14, 18000 Niš, Serbia

Abstract Centrifugal pumps are type of turbomachines that are widely used in practice for various purposes. Therefore it is very important that they work in optimal operation mode. When designing centrifugal pumps, many recommendation are used from the literature, but the real operating parameters are determined afterwards, testing the pump prototype. One of the methods used today, during the pump impeller design and before the prototype testing, are numerical simulations (ie. cfd). The flow characteristics of the centrifugal pump, also the pump head, power and efficiency curves are numerically determined and analysed, with respect to the change in the impeller blade geometry. Only wrap angle of the impeller blades has changed ($\Delta\varphi=50, 55, 60, 65, 70$ and 75 degrees), while the other geometric parameters remain the same.

Keywords Centrifugal pump, performance characteristics, wrap angle, numerical simulations

1. INTRODUCTION

Centrifugal water pumps are one of the most widely used turbomachines and machines in general, which is utilized in the industry, water supply, agriculture etc. The energy efficiency of pumps greatly increases the energy efficiency of the systems in which the pump operates. Therefore, it is very important that the pump achieves the design operating parameters and achieves high levels of efficiency.

Different theories are used in the pump design process, one-dimensional, two-dimensional and (quasi) three-dimensional theory, and each of them has its advantages and disadvantages [1,2].

Over the decades, many researchers have

tried to develop appropriate algorithms for optimizing the design of a centrifugal pump, according to the parameters that change during that optimization. It mostly affects the change of blade angles as well as the wrap angle. Numerical and experimental investigations how changes in blade angles and other geometric parameters affect pump operating curves have been discussed in many published papers [3-6].

The study of plastic centrifugal pumps with semi-open impeller design with large wrap angles from 100° to 150° , but also changing the inlet and outlet blade angles, show increasing of pump head and efficiency with increasing the wrap angle values [6]. The experimental results show that the pump with the largest wrap angle has wide area for high efficiency and stable operation [4].

On the other hand, the study of high-speed centrifugal pump ($n_q=185$) shows that with the wrap angle increasing from 110° to 130° pump head decreases, while efficiency increase when operates with smaller flow rates, but decreases for higher flow rates [5].

Corresponding author

Professor Jasmina Bogdanović Jovanović
bminja@masfak.ni.ac.rs

University of Niš, Faculty of Mechanical Engineering
Aleksandra Medvedeva 14
Niš, Serbia

According to one experimental study [7], when the optimization parameter of the pump operation is the number of blades, it was concluded that the performance of centrifugal pump tends to be more sensitive against the change in rotational speed rather than the change in the number of blade.

Therefore, solutions for optimizing the operation of the centrifugal pump are sought in profiling the impeller blade, where the inlet and outlet angle of the blade and, also, the wrap angle play the important role. The aim of this study is to analyze the influence of different blade wrap angle values on the operating characteristics of a low-speed centrifugal pump, which have simple cylindrical blades.

2. CENTRIFUGAL PUMP DESIGNS

Centrifugal pumps with cylindrical blades are usually used, due to the simplicity of construction and easy and low-cost production. Self-priming pumps are with cylindrical blades, since such a blade design allows for better pump performance. Comparing with pumps with twisted blades, pumps with cylindrical blades obtained lower efficiency. Therefore, improving the efficiency aspect can be a challenge in the designing process of centrifugal pumps with cylindrical blades.

A centrifugal pump with 9 blades, shown in Fig.1, is investigated in the paper. One of the cases we analysed was tested experimentally and its measured performance curves, for rotational speed 3000 rpm, are published [8].

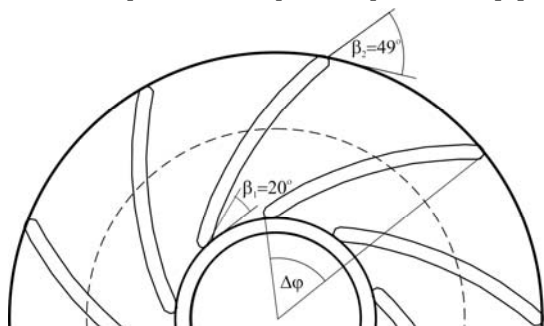


Fig. 1. Centrifugal pump impeller

The blades are designed as circular arcs, rounded on the leading and trailing edge of the profile. The impeller dimensions are: suction tube $D_s=60$ mm, inlet diameter $D_1=70$ mm, outlet diameter $D_2=190$ mm, exit width $b_2=9$ mm, hub diameter $D_h=80$ mm. Blade inlet angle $\beta_1=20^\circ$ and outlet angle $\beta_2=49^\circ$, and these angles

are fixed at a later change of wrap angle, as well as all impeller diameters [9].

Best efficiency point (BEP) is obtained for $Q^+=65$ m³/h (18 l/s), $H^+\approx 48$ m and $\eta^+=72\%$. Specific speed of the pump is $n_s=22$.

The wrap angle of this experimentally tested centrifugal pump is $\Delta\phi=60^\circ$. The numerical investigations were conducted for wrap angle values: 50, 55, 65 and 70 degrees. Fig. 2 shows blade profiles in all investigated cases. As previously stated, the inlet and outlet blade angles are not changes, just the wrap angles. Numerous numerical simulations were performed for the operating flow range, to determine the operating curves of all impeller models.

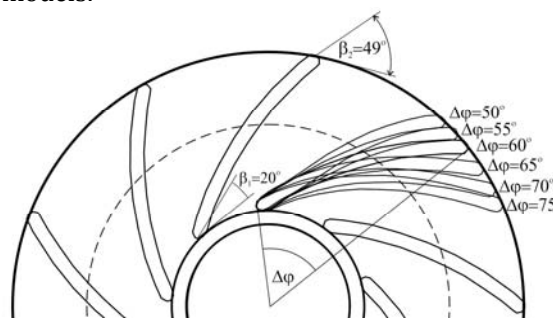


Fig. 2. Blade profiles for different wrap angles

All geometric models of pumps are made using Cfturbo software, and they are consists of inlet stator, impeller and spiral casing.

3. NUMERICAL SIMULATIONS

The geometry of the centrifugal pump impeller, as well as the inlet part and the spiral casing were discretized as follows: the impeller using TurboGrid and stator elements using ICFM CFD software, shown in fig.3.

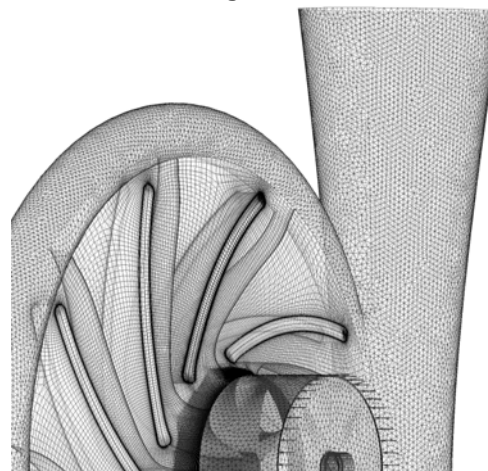


Fig. 3. Mesh of the centrifugal pump

Obtained numerical mesh is consists of around $2,4 \cdot 10^6$. The number of mesh elements slightly differs from one impeller model to another, while the meshes of the inlet part and the spiral casing remain the same in all cases.

The computational domain of centrifugal pump impeller is extended radially, as it is a regular practice in cfd, to prevent any influence of the backward flow at the impeller outlet.

Mesh of the pump impeller is hexaedral, consists of more than $1,6 \cdot 10^6$, while the inlet part and the spiral casing is tetrahedral.

For numerical interpolation was used a high-resolution scheme. The chosen turbulence model is standard SST, since this turbulence model is recommended for numerical simulation of flow in centrifugal pumps [10].

The convergence criteria were that the root mean square values of the equation residuals are 10^{-5} . Note that this criterion is not fulfill for all flow rates, due to very complex geometry of the domain, which is consists of three mutually connected geometric parts.

3.1 Validation of numerical results

In order to confirm numerical simulation results, the numerical values of pump head and efficiency were compared with results obtained by measurements, given in the paper [8]. Due to simple 2D pump geometry, results are in an excellent agreement, as it can be seen in Fig.4.

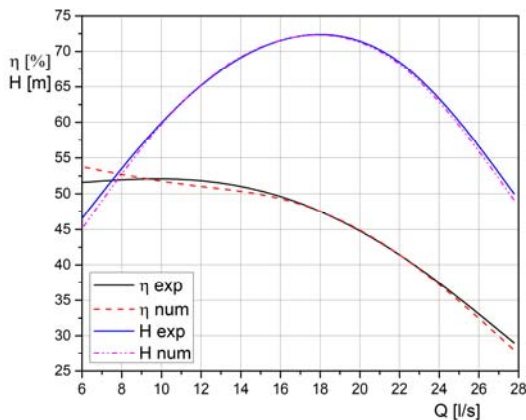


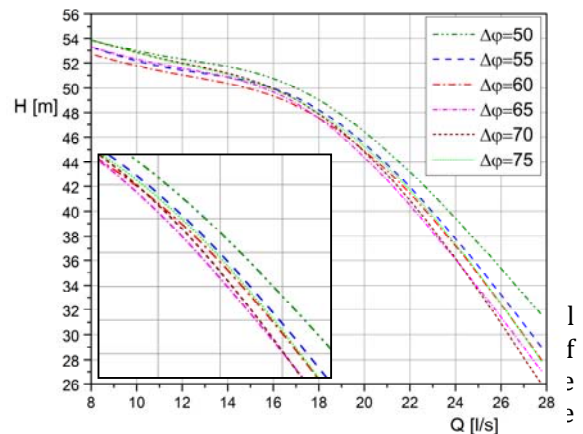
Fig. 4. Validation of experimental results

4. CFD RESULTS

After a numerous numerical simulations have been conducted for the centrifugal pumps with radial blades and different wrap angles, for a range of flow rates and, the pump performance curves are compared and analysed.

The centrifugal pump head curves are given in fig.5. The head curves are obtained for centrifugal pumps with different warp angles, but the same other geometric characteristics (fig.2). Wrap angles varies from 50 to 75 degrees, ie. $\Delta\phi=50, 55, 60, 65, 70$ and 75 . The impeller blade geometry used for validation of numerical results has a wrap angle $\Delta\phi=60^\circ$.

For the flow rates right of BEP (ie. for higher flow rates), as the wrap angle increases, the pump head decreases, up to the wrap angle $\Delta\phi=75^\circ$, when pump head has a slightly higher values. For the lower flow rates, no rule can be drawn regarding the influence of the wrap angles on the pump head value.



efficiency curves, but the efficiency increases with the increasing the wrap angle.

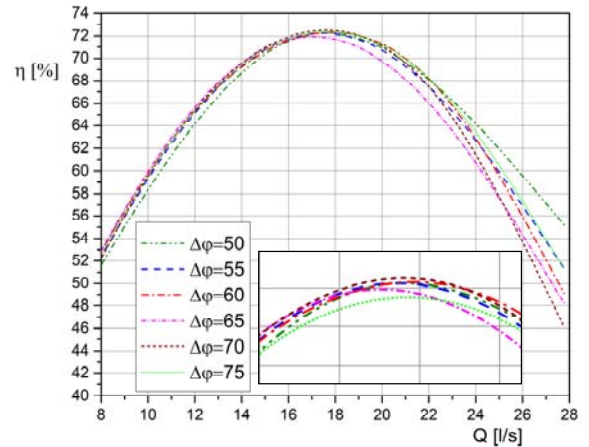


Fig. 6. Efficiency of centrifugal pumps with different warp angles.

In optimal flow regimes, $\pm 20\%$ of the BEF, the efficiency is almost the same for all cases, but precisely the higher efficiencies are provided for a larger wrap angles.

Power curves, shown in fig.7, change in a way that the shaft power decreases when the wrap angle increases.

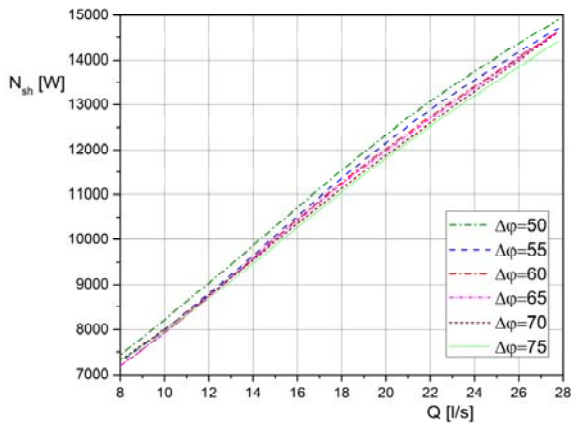


Fig. 7. Shaft power for different warp angles.

For the higher flow rates of the best efficiency point it is noticeable a larger change in efficiency curves. In this area, as the wrap angle increases, the efficiency of the pump decreases. In the area of lower volume flow rates, the pump head increasing the wrap angle. But this trend goes to a certain wrap angle, for $\Delta\varphi=75^\circ$ and smaller flow rates the pump efficiency slightly decreases.

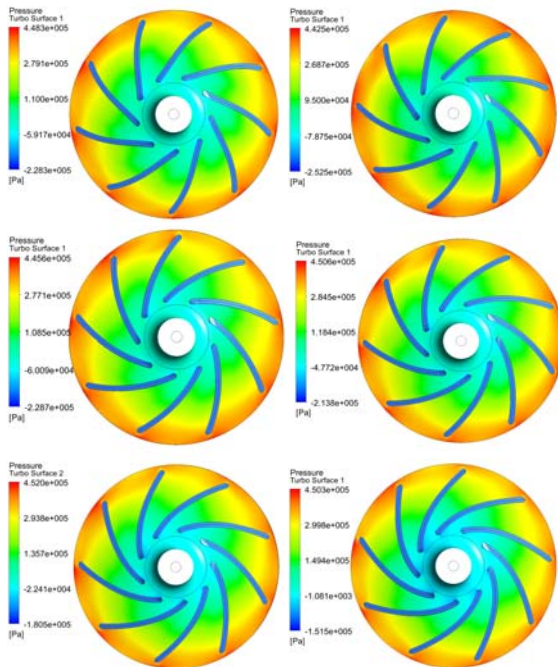


Fig. 8. Pressure field in centrifugal pump impellers for BEP, for $\Delta\varphi=50, 55, 60, 65, 70$ and 75 degrees.

The visualisation of pressure field in pump impellers is given in fig.8. It can be noticed a negligibly small pressure change in the centrifugal pump impeller for different wrap angles operating in the same flow regime.

Velocity streamline presented in fig.9 for BEP, show backflow regions in impellers with

smaller wrap angles. With increasing the wrap angle, the flow in the impeller becomes more smoother and with less or no backflow regions, which causes the hydraulic loss in the pump impeller.

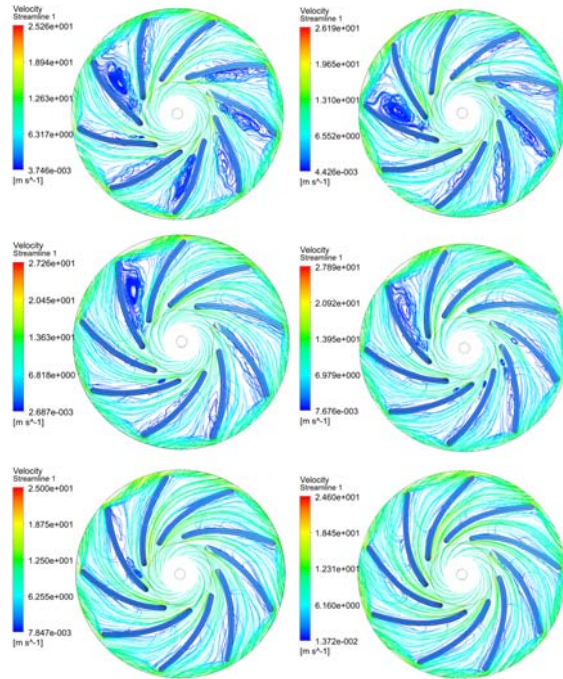


Fig. 9. Velocity streamlines in centrifugal pump impellers for BEP, for $\Delta\varphi=50, 55, 60, 65, 70$ and 75 degrees, respectively.

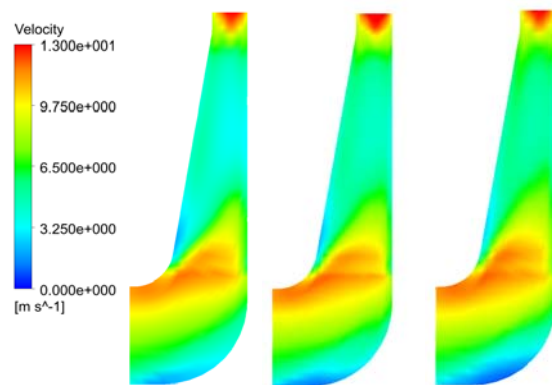


Fig. 9. Pressure field in meridional cross-sections of centrifugal pump impellers operating in BEP, for $\Delta\varphi=50, 60,$ and 70 degrees

For the higher values of $\Delta\varphi$ the more uniform distribution of velocity field is present, around BEP.

As expected, the velocity streamline (fig 10, 11 and 12) are more unevenly distributed in the pump impeller for the lower flow rates, with

several area of backward flow, while there is more uniform distribution of the velocity streamline for the higher volume flow rates.

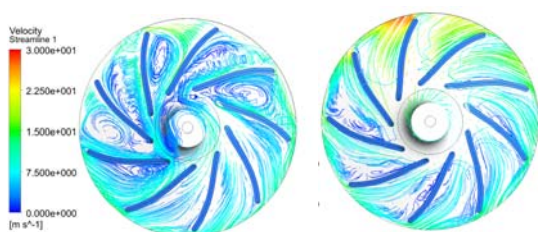


Fig. 10. Velocity streamlines in centrifugal pump impellers ($\Delta\varphi=50^\circ$), for $0,3\cdot Q^+$ and $1,5\cdot Q^+$

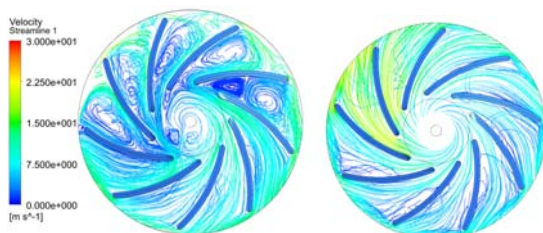


Fig. 11. Velocity streamlines in centrifugal pump impellers ($\Delta\varphi=60^\circ$), for $0,3\cdot Q^+$ and $1,5\cdot Q^+$

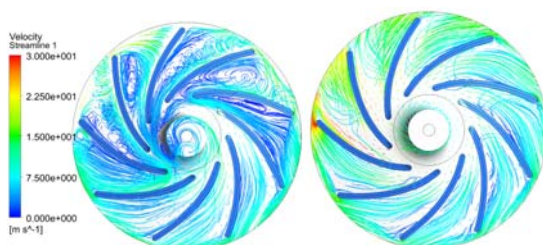


Fig. 12. Velocity streamlines in centrifugal pump impellers ($\Delta\varphi=70^\circ$), for $0,3\cdot Q^+$ and $1,5\cdot Q^+$, respectively

Total pressure distribution in the pump impeller for the wrap angle $\Delta\varphi=60^\circ$ and for the different velocity flow rates is shown in fig,13.

The optimal pump regime shows the most even distribution of the total pressure in the pump impeller.

The cases for lower and higher velocity flow rates shows uneven distribution of the total pressure, especially in the lower volume flow rates, as expected.

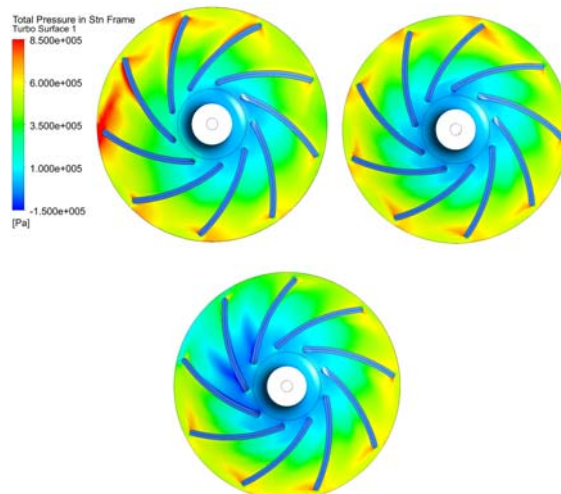


Fig. 13. Total pressure in centrifugal pump impellers ($\Delta\varphi=60^\circ$), for $0,3\cdot Q^+$, Q^+ and $1,5\cdot Q^+$, respectively

5. CONCLUSIONS

Numerical simulations of flow in turbomachines are a very useful way to numerically test them during the designing process. The obtained results can be analysed in detail, and model correction can be made during the design phase, production of the machine model.

Regarding the change of wrap angles, it has been considered the range of angles: $\Delta\varphi=50, 55, 60, 65, 70$ and 75 .

Analyzing the pump head curve, one can conclude: for the higher flow rates the pump head decreases as the wrap angle increases, and the pump head values differ up to 18%. For the lower flow rates, no rule can be established, and the difference in pump head for all wrap angles are up to 2 m, which is up to 4%.

The pump efficiency changes in a way that for the higher flow rates, the efficiency decreases as the wrap angle increases. The efficiency values differ up to 16%. In the area of lower flow rates, the pump head curves do not differ significantly for the different wrap angles (up to 2%), but as increasing the wrap angle the efficiency increases too.

The shaft power curves differs up to 5% in the whole range of pump flow rates. Also, it is noticeable that the shaft power decreases when the wrap angle increases.

The velocity fields and velocity streamline in the centrifugal pump impellers are very different for different cases of wrap angles and

the the values of velocity flow rate. Depending how much flow rate deviates from the BEP, the velocity distributions are showing more or less area of backward flow. For smaller flow rates the vortex backflow is much more present, while for the larger flow rate the streamline are more evenly distributed.

Acknowledgement

This research was financially supported by the Ministry of Education, Science and Technological Development of the Republic of Serbia.

REFERENCES

- [1] Gulich, J. F., (2008). *Centrifugal Pumps*. Springer, Berlin. ISBN 978-3-540-73694-3
- [2] Karassik I., Messina J., Cooper P., Heald C., (2001). *Pump handbook*. McGRAW-HILL. ISBN 0-07-034032-3
- [3] Han, X., Kang, Y., Li, D., Zhao, W. (2018). Impeller Optimized Design of Centrifugal Pump: A Numerical and Experimental Investigation. *Energies* 2018, 11(6), 1444; <https://doi.org/10.3390/en11061444>.
- [4] Tan, L., Zhu, B., Cao, S., Bing, H., Wang, Y. (2014). Influence of Blade Wrap Angle on Centrifugal Pump Performance by Numerical and Experimental Study. *Chinese Journal of Mechanical Engineering*, vol. 27, no. 1, p. 171-177. DOI: 10.3901/CJME.2014.01.171
- [5] Huang, X., Yuan, S., Zhang, J., Zhang, X. (2016). Effects of blade wrap angle on performance of high specific speed centrifugal pump. *Journal of drainage and irrigation machinery engineering (JDIME)*, 34 (9) p. 742-747. DOI: 10.3969/j.issn 1674-8530.16.0087 (in chinese)
- [6] Li, J., Tang, L., Zhang, Y., Zhang, (2020). The Influence of Blade Angle on the Performance of Plastic Centrifugal Pump. *Hindawi-Advances in Materials Science and Engineering*, vol. 2020, 20 p. <https://doi.org/10.1155/2020/7205717>
- [7] Effendy, S., Effendy, M., (2019). Micro-engineering. *Proceeding of AIP Conference 2019*, paper 2114, 020016. <https://doi.org/10.1063/1.5112400>
- [8] Grapsas V., Anagnostopoulos J., Papanotis E., Experimental and numerical study of a radial flow pump impeller with 2D-curved blades, *Proceedings of the 5th IASME / WSEAS International Conference on Fluid Mechanics and Aerodynamics*, August 25-27, 2007, Athens, Greece, p. 175 – 180.
- [9] J., Papanotis E., (2006). CFD Analysis and Design Effects in a Radial Pump Impeller, *WSEAS Transactions on fluid mechanics*, Issue 7, Vol. 1, p. 763 – 770, July 2006 ISSN: 1790-5087.
- [10] Al-Obaidi, A. R., (2019), Effects of Different Turbulence Models on Three-Dimensional Unsteady Cavitating Flows in the Centrifugal Pump and Performance Prediction, *International Journal of Nonlinear Sciences and Numerical Simulation (IJNSNS)*, 20(3-4), p. 487 – 509. DOI:10.1515/ijnsns-2018-0336



Banja Luka
28-29 May 2021.

DEMI 2021

15th International Conference on
Accomplishments in Mechanical and
Industrial Engineering

www.demi.mf.unibl.org



DESIGN OF THE AIR CONDITIONING SYSTEM IN THE DATA CENTER

S. Stavreva^a, M. Serafimov^b, C. Dimitrieska^a, K. Popovski^a

^aUniversity "St. Kliment Ohridski", Faculty of Technical Sciences- Bitola M. Falanga 37, 7000 Bitola Republic of North Macedonia

^bUniversity "St. Cyril and Methodius", Faculty of Mechanical engineering – Skopje Karpos II bb 1000, Skopje, Republic of North Macedonia

Abstract Heating, ventilation and air conditioning systems in data centers should provide ventilation, filtration, cooling and dehumidification, humidification and heating of the air, to operate continuously throughout the year and to be flexible if expansion or reconstruction is required, without interrupting the operation of the data center. If the necessary operating conditions of the data processing and telecommunications equipment are taken into account, their achievement and maintenance is a major challenge for heating, ventilation and air conditioning systems (HVAC). This paper analyzes the air conditioning and ventilation system of an existing data center, which needs to be reconstructed due to the changes that occurred during the period of its operation and offers suggestions by integrating proven best solutions in designing the air conditioning system and ventilation. The relevant load for cooling and heating has been calculated and the air conditioning and ventilation system has been designed to improve its energy efficiency.

Keywords data center, conditioning and ventilation, datacom equipment, load, HVAC systems

1. HVAC SYSTEM FEATURES

The data center has three rooms, in two of them the data processing and telecommunications equipment (datacom equipment) is located, while the third is a room for telecommunications equipment. In the period when the data center building was built, all the previously mentioned rooms were a single space. At that time this unique space was air conditioned with an air conditioning system with an air-conditioning cabinet and duct air

distribution. This system is still in operation today, but a change has been made in the duct air distribution compared to the original performance. Due to the changes that took place in the building in terms of space and installed datacom equipment, changes were made in the air conditioning system.

The rooms in which the datacom equipment is located are identical. Before the reconstruction, for conditioned of these rooms, in each room there is one air-conditioning cabinet which supply conditioned air into the raised-floor air space. The air exits this air space through perforated floor tiles located near the inlets of datacom equipment. The hot exhaust air from the datacom equipment then migrates back to the inlet of the air conditioning cabinet.

A common split channel system has been constructed for both rooms. The cooled air from

Corresponding author

Associate professor PhD., Sevde Stavreva
sevde.stavreva@uklo.edu.mk

Faculty of Technical Sciences- Bitola
M. Falanga 37, 7000 Bitola
Bitola, Republic of North Macedonia

this duct system is brought to the raised-access floor of one of the data center rooms. The two rooms of the data center have a common raised-access floor, due to which the air from the split system is distributed in the raised-access floor of both rooms. To extract the recirculating air, anemostats are placed in both rooms of the dropped ceiling, which are connected with flexible hoses to the horizontal return channel placed in the dropped ceiling. This channel connects to the indoor unit of the split system. In front of this unit a mixing box is connected for mixing the recirculating air with the outside air. In both rooms of the data center on the dropped ceilings anemostats are placed, which with flexible hoses, are connected to the existing air supply duct.

The room for telecommunication equipment does not actually have air conditioning. From this room only air is extracted through the central return horizontal duct system. The room is made with a raised-access floor.

2. PROPOSAL FOR NEW TECHNICAL SOLUTIONS

The need for reconstruction of the HVAC system is due to the changes that have occurred in the data center, in terms of change and upgrade of data com equipment during its operation. At the time of the initial construction of the air conditioning system, the heat load was quite small compared to today's load on the rooms.

During the design of the new air conditioning solution, care was taken to reconstruct the old air conditioning system and to use the existing equipment and to upgrade it with a new one, due to the heat loads in the center.

Additional reasons why the existing HVAC system needs to be reconstructed is that it should be independent of the other systems in the building and separate for each room and in the premises of the data centers a certain overpressure should be maintained [2].

The data center has regulated air parameters, it works 24 hours a day, seven days a week, all year round, and every interruption in work results in loss of work continuity and high costs. For these reasons, it is recommended that the air conditioning equipment has an independent power supply (aggregate power supply) [7].

2.1 Rooms for datacom equipment

The air conditioning parameters of the rooms intended for operation of datacom equipment are stricter and they mainly depend on the requirements set by the equipment manufacturers, and depending on the type of installed equipment, four standardized conditions are complied [1] with (class 1 to 4) and the fifth class NEBS which determines the operating conditions of the telecommunication equipment. In particular, the considered rooms with datacom equipment belong to class 1 and the parameters that should be maintained in such rooms are in the range of temperatures of (18-27)°C and relative humidity of (20-75)%. An internal temperature of 20°C is required for this data center.

Currently, for air conditioning of these rooms in each of the rooms, there is one air-conditioning cabinet, identical in both rooms. The air-conditioning cabinets have a filter, air cooler with water and a fan. The air cooler with piping is connected to the central cold water system for the whole building. Due to this one of the main conditions for air conditioning of this type of rooms, an independent system from other systems in the building, is not met. In addition, the old air conditioning system should be reconstructed, because it is not recommended to place the air-conditioning cabinet in the room where the data equipment is located, when water is used as a heating and cooling fluid, due to the risk of splashing on a pipe with water, which would lead to flooding of the equipment placed in the room.

The new solution predicts the dismantling of these two air-conditioning cabinets and their transfer to the newly planned machine room and to be used for air conditioning of the room for telecommunication equipment. For air conditioning of the rooms with datacom equipment, a new air-conditioning cabinets is provided for each room. Because the new air-conditioning cabinets for energy saving are designed to work with free cooling option (natural cooling), ie they will work with glycol, they can not be installed on the rooms, so they will be installed in the newly designed machine room. The new air-conditioning cabinets are planned to be equipped with direct evaporative air cooler, glycol cooler, glycol condenser, electric heater and steam humidifier. The electric heater is intended for space heating in case of overhaul of the center. A steam humidifier is needed to regulate the relative

humidity. Because with the new technical solution the amount of air that is introduced on the rooms is greater than before, additional perforated floor tiles are provided.

For both rooms with datacom equipment there is already a common channel split system. With this system it will be possible to completely cool one of the rooms, due to which it will be a reserve, which can be used in case of air-conditioning cabinets failure, which is of particular importance for safe operation of the data center [3]. In order for this system to be able to perform air conditioning separately in one of the rooms, it is necessary to make a partition in the raised-access floor with which the air can be completely directed in one room. In addition, this system can be used for natural cooling (free cooling). For that purpose, a mixing box for mixing the external and recirculating air is provided at the entrance of the indoor unit of the split system, whereby the mixing ratio of the two air currents is performed automatically.

2.2 Room for telecommunications equipment

The room for telecommunications equipment is not air conditioned at the moment before the reconstruction.

For air conditioning of this room it is proposed to use the two air-conditioning cabinets that are installed in the rooms for datacom equipment. Air-conditioning cabinets for air conditioning of rooms for working with datacom equipment should be professional with precise temperature control of 0.5°C and relative humidity of 5% [1]. The installed air-conditioning cabinets do not meet these requirements and therefore it is suggested that the air-conditioning cabinets from the rooms with data be used for air conditioning of the room for telecommunication equipment for which other criteria for its work are prescribed. These air-conditioning cabinets are complete with an air cooler with water and fan. They are without humidifiers and air heaters, but for this type of room it is not a problem, because the equipment can work in a wide range of relative humidity (10-80) % [1]. A problem with the heating of the room can occur only if the telecommunication center is not fully operational. In most of the year, only one air conditioner is enough for air conditioning of

this room, due to which practically one will be a reserve that is recommended for this type of rooms [3]. Since the provided air-conditioning cabinets are with air coolers with water, they cannot be installed in this rooms they will be installed in the new machine room. The extraction of air from this room and its supply to the air-conditioning cabinet is done through suction grilles which are connected with a duct to the plenum which is placed above the air-conditioning cabinet. For the supply of a certain amount of outside air, ducts are connected to the plenums that supply the outside air. Because the cooling of the equipment in the telecommunication center is done through the equipment, it is not necessary to install perforated floor tiles for air intake. The air conditioners are connected by air to the room of the telecommunication center and they are connected to the central cold water system.

3. HVAC LOAD, MECHANICAL EQUIPMENT AND SYSTEM

The mechanical systems provide for environmental criteria in a data center are significant user of energy. HVAC systems account for about 31% of the total energy consumption of the data center [6]. Great care should be taken when selecting the typical components that make up the HVAC system in the data center. Therefore, the components of the HVAC system need to be considered as a part of it to optimize energy efficiency.

3.1 HVAC load and systems for rooms with datacom equipment

As mentioned, the rooms in which the datacom equipment is located are identical and therefore a calculation is made for one room, but the same applies to the other. The area of one room is 72.4 m². The heat dissipation from the datacom equipment that is placed on the raised-access floor in the center is 16.3 kW. The cooling load from external sources is 3.6 kW [4], the lighting load is 1.1 kW and the cooling load from the operation of the fan is 1.5 kW, so the total cooling load is 22.5kW.

The relevant cooling load for the selection of equipment for indoor temperature of 20°C is 27 kW (22.5 x 1.2 = 27 kW), given that in the catalogs for air-conditioning cabinets the data given refers to an indoor temperature of 24°C.

To air-condition each room for datacom equipment, one air-conditioning cabinet with lower air intake has been selected. The air flow for each air conditioner cabinet is 10000 m³/h. The injection of air-conditioned air with a temperature of 13°C is done in the raised-access floor of the room.

Based on the measurements of the velocities at the exit from the perforated floor tiles [1], in order to inject the required amount of air, it is necessary to install another 10 new perforated floor tiles with dimensions of 500 x 400 mm.

There may be a need for heating in the room only if the equipment in the room does not work (repairs or replacement of existing equipment with another). In such cases for room heating built-in electric heaters are used in air-conditioning cabinets. The total installed heating capacity in both air conditioners is 10 kW. For a room area of 72.4 m², the specific heating load is 138 W/m². Specific heating load for such rooms can not be greater than 120 W/m² [4], which means that the installed heating capacity in the air-conditioning cabinets is sufficient, ie no additional heating is required.

3.2 HVAC load and systems for room with telecommunication equipment

Due to the changes made in the air conditioning and ventilation system, the room for telecommunication equipment is not air conditioned.

According to the data of the manufacturer of the telecommunication equipment, the indoor air quality conditions that should be maintained in the room where the equipment works are not very rigorous and the temperature in normal working conditions should be in the interval (10-35)°C and the relative humidity (10-80)% [1]. 25 °C is recommended as the optimal temperature, but it is good to provide a temperature of 23 °C.

The air conditioning of this room will be done with the air-conditioning cabinets that are planned to be removed from the rooms for datacom equipment. To select air conditioners, it is first necessary to determine the cooling load from external and internal sources.

The load from internal sources arises from heat dissipation from the operation of the equipment and from the lighting. The heat dissipation from the equipment is 29.3kW, the cooling load from external sources is 8.8 kW [4] and from the

lighting is 2.2 kW. To determine the total cooling setting, the heat from the fan operation must be added. For air conditioners planned to be installed, this heat is 2.5 kW, with a total cooling load of 42.8 kW.

For equipment selection, this load is increased by 10%. Accordingly, the relevant cooling load is 47.08 kW (1.1 x 42.8 = 47.08).

According to the relevant cooling load, the provided existing air-conditioning cabinets with their characteristics are appropriate. The air flow for each air-conditioning cabinet is 10,000 m³/h.

There may be a need for heating in the room only if the equipment in the room does not work (repairs or replacement of existing equipment with another). In such cases, the built-in electric heaters in the air-conditioning chambers are used for heating the room. The total installed heating capacity in both air-conditioning cabinets is 20 kW. For a room area of 146.2 m², the specific heating load is 137 W/m². The specific heating load for such rooms can not be greater than 120 W/m² [4], which means that the installed heating capacity in the air conditioners is sufficient, ie no additional heating is required.

Natural cooling mode (free cooling) is included for the air conditioning of this room.

4. FREE COOLING OF THE DATA CENTER

The data center operates continuously 24/7 and has great potential to reduce the energy required for cooling by applying "free cooling" (natural cooling). In the HVAC system is the utilization of outside air under certain conditions to allow chillers to be off or operated at reduced capacity. The mentioned rooms should be cooled even in winter during low outdoor temperatures. During this period, natural cooling with outside air can be used, which saves cooling energy. In this process it is important to determine at what outside air temperature the cooling in the rooms will be done completely without the use of electricity for cooling [6].

From the point of view of energy saving, it is best to adopt this temperature to be the same as the temperature of the air in the room (for example 13°C). However, in this case, the system operates exclusively with outside air, which in this case is 40,000 m³/h, which is technically more difficult to do in this case. This

temperature can be optimally determined by techno-economic analysis, or can be oriented between (0 and 5)°C, which corresponds to the climatic conditions where the building is located.

For the given conditions, with an adopted temperature of 2.5°C, the calculated required amount of outdoor air for natural cooling is 16,000 m³/h. For this amount of outside air, two external fixed grilles with approximate dimensions of 800x800 mm should be installed. For the needs of the rooms with datacom equipment, a duct split system with air flow of 10,700 m³/h has been installed. This split system can be used as a backup for both rooms with datacom equipment, with a small modification in the air distribution it will be able to provide complete air conditioning for one of the rooms. The system can be used for natural cooling at low outdoor temperatures, but due to the small air flow relative to the refrigeration load it can cover 50% of the cooling needs.

5. CONCLUSION

The observed facility in which the heating, ventilation and air conditioning system was reconstructed has two rooms for data equipment and one for telecommunication equipment. The rooms are air-conditioned with air-conditioning system with air-conditioning cabinets and duct air distribution, during which changes are made during the operation of the data center. The reconstruction needs to be done for several reasons, such as: increased heat load in the data center due to changes in the data equipment, independence of the air conditioning system from other systems in the building, fulfillment of the conditions for safe operation of the data center. The total cooling load of each room of the data center has been calculated and the equipment of the HVAC system has been selected. When designing the new solution of the HVAC system, the existing equipment was used and upgraded with a new one. Also, when designing the system and selecting its components, the standards for designing systems used in data centers [8] and energy saving measures are respected, as well as the best integrated solutions [5]. Considering that the data center operates 24 hours a day, 365 days a year, the introduction of energy saving measures is of particular importance and

therefore the HVAC system includes a natural cooling mode, which increases the energy efficiency of the data the center.

REFERENCES

Books:

- [1] ASHRAE Technical Committee 9.9. (2011). *Thermal Guidelines for Data Processing Environments*. W. Stephen Comstock, Atlanta.

Book chapters:

- [2] ASHRAE Technical Committee 9.9. (2005). Best Practices. Helms, C., Michaels, C., Walker, J. *High Density Data Centers*. W. Stephen Comstock, Atlanta, p. 157-173.
- [3] ASHRAE Technical Committee 9.9. (2005). Availability and Redundancy. Geshwiler, M., Helms, C., Michaels, C. *Design Considerations for Datacom Equipment Centers*. W. Stephen Comstock, Atlanta, p. 131-137.
- [4] ASHRAE Technical Committee 9.9. (2005). HVAC Load Considerations. Geshwiler, M., Helms, C., Michaels, C. *Design Considerations for Datacom Equipment Centers*. W. Stephen Comstock, Atlanta, p. 17-23.
- [5] ASHRAE Technical Committee 9.9. (2008). Best Practices. Helms, C., Michaels, C., Walker, J. *Best Practices for Datacom Facility Energy Efficiency*. W. Stephen Comstock, Atlanta, p. 157-175.
- [6] ASHRAE Technical Committee 9.9. (2008). Mechanical Equipment and Systems. Helms, C., Michaels, C., Walker, J. *Best Practices for Datacom Facility Energy Efficiency*. W. Stephen Comstock, Atlanta, p. 157-175.
- [7] ASHRAE Technical Committee 9.9. (2008). Electrical Distribution Equipment. Helms, C., Michaels, C., Walker, J. *Best Practices for Datacom Facility Energy Efficiency*. W. Stephen Comstock, Atlanta, p. 97-108.

Standards:

- [8] ANSI/ASHRAE Standard 62.1 (2004): *Ventilation for Acceptable Indoor Air Quality*. American Society of Heating, Refrigeration and Air-Conditioning Engineers. Atlanta.



Banja Luka
28–29 May 2021.

DEMI 2021

15th International Conference on Accomplishments in Mechanical and Industrial Engineering

www.demi.mf.unibl.org



The use flat plate collectors in a pumped thermal energy storage latent system

S. Pavlović^a, E. Bellos^b, V. Stefanović^a, M. Ilić^a, M. Grozdanović^a, C. Tzivanidis^b

^a Faculty of Mechanical Engineering, Department of Thermal Engineering, Thermoenergetics and Process Engineering, University in Niš, Niš, Serbia

^b Thermal Department, School of Mechanical Engineering, National Technical University of Athens, Zografou, Heron Polytechniou 9, 15780 Athens, Greece

Abstract

The use of renewable energy sources for electricity is one of the most promising techniques in order to face environmental problems and high CO₂ emissions. However, the power production from photovoltaics and wind energy is not stable and this fact creates issues between the production profile and the demand profile. Therefore, an effective storage technique is needed, except for the idea of batteries. The objective of the present investigation is the investigation of a novel pumped thermal energy storage system. This system uses the volatile electricity from renewables in order to feed a heat pump that produces heating at a medium temperatures level (e.g. 150°C) and stores it in a latent storage unit. The stored thermal energy can be used later in an organic Rankine cycle for power production when there is the proper demand. The novelty of this work is the incorporation of flat plate collectors for assisting the heat pump in order to increase the overall performance of the examined storage system. According to the results, the ambient source system leads to maximum power to power ratio of 38.5% and this value is lower than the respective values of the solar-assisted system. The maximum system efficiency was found for storage tank temperature at 220°C and evaporator temperature at 30°C, and in this case, the system energy efficiency is 19.1%, while the system exergy efficiency is 19.7%. For the typical case of ($T_{st}=150^{\circ}\text{C}$ and $T_{evap}=70^{\circ}\text{C}$) the solar-assisted system presents a 61.1% power to power ratio which is 58.7% higher than the ambient source case.

Keywords Solar energy, Flat plate collector, latent storage, volatile electricity, renewables

1. INTRODUCTION

The use of renewable energy sources for electricity production becomes more and more

famous in the last year because it is an effective way to face the numerous environmental problems of our society [1-3]. The use of photovoltaics and wind energy are common ways to produce electricity from clean energy at a reasonable cost [4]. However, there is a problem with the need for a storage system for overcoming the difference between the electric production and the demand profiles. Therefore a lot of research has been performed in the last years in order to determine the proper ways which can lead to suitable and viable storage of

Corresponding author

PhD, Saša Pavlović
sasa.pavlovic@masfak.ni.ac.rs

Faculty of Mechanical Engineering, Department of Thermal Engineering, Thermoenergetics and Process Engineering, University in Niš, Niš, Serbia

electricity. The recent research has been focused on alternative techniques and not on the usual choice of batteries which is associated with some disadvantages as the reduced life [5]. An interesting idea for the storage of volatile electricity from renewables is the use of pumped thermal energy storage. In this idea, the produced electricity from the renewables that cannot be used directly in the grid feeds a heat pump (HP) in order to produce heating at a high temperature (e.g. at 150°C) by absorbing heat by the ambient heat sink. This produced heating is stored with a sensible or latent storage tank and it will be used later when there is demand for electricity. More specifically, this stored heat can be used in a thermodynamic cycle, usually an organic Rankine cycle (ORC) for producing electricity when there is demand. In this direction, there are literature studies that have studied this idea. Frate et al. [6] studied this idea and they found a power to power ratio of 55% after a detailed investigation. They found that the use of cyclopentane on both thermodynamic cycles is a proper choice when there are regenerators in the cycles. Roskosch et al. [7] studied the idea of HP-ORC and calculated the power to power ratio to be ranged from 37% to 56%.

Moreover, another choice is to feed the heat pump with a heat source in order to insert heat in the heat pump at a higher temperature. Solar energy or geothermal energy can be used in order to feed the heat pump and so finally the power to power efficiency can be increased. The use of a geothermal heat sink for feeding the heat pump has been examined by Scharrer et al. [8] and the power to power ratio is found at 50%. The investigation of a solar energy heat sink for feeding the heat pump has been examined by Sonsaree et al. [9] by using a low-temperature heat input up to 70°C. The combination of solar energy and ambient source for feeding the heat pump has been examined by Henchoz et al. [10]. In this case, the power to power ratio has been found in the range of 56% to 65%, while the availability of the system is about the 84% of the year period. A theoretical study about the variable heat source temperature that feeds the heat pump has been examined by Eppinger et al. [11] where the maximum power to power ratio has been found at 80%.

The objective of the present study is the investigation of an HP-ORC system that exploits

the solar thermal energy from flat plate collectors (FPC) in order to achieve high power to power ratio. This design is examined in detail and it is compared to the ambient source heat pump case. Moreover, the examined storage system is a latent one in order to have higher performance compared to the sensible [11]. The analysis is conducted by a developed model in Engineering Equation Solver (EES) [12].

2. MATERIALS AND METHODS

2.1 The examined system

Figure 1 depicts the examined configuration which includes a solar field with flat plate collectors, a heat pump, a latent storage system and an organic Rankine cycle. The working fluid in both cycles (HP and ORC) is cyclopentane because it is a proper choice according to the literature [6, 11]. In all the cases, the electricity input is selected to be $P_{el,in}=20$ kW. Table 1 includes all the data that have been used in the proper analysis. The storage temperature of the latent system is ranged from 120°C to 220°C, while the evaporator temperature from 20°C to 80°C. The case with $T_{evap}=20$ °C is the ambient source case. Moreover, the storage efficiency is selected to be 95 %.

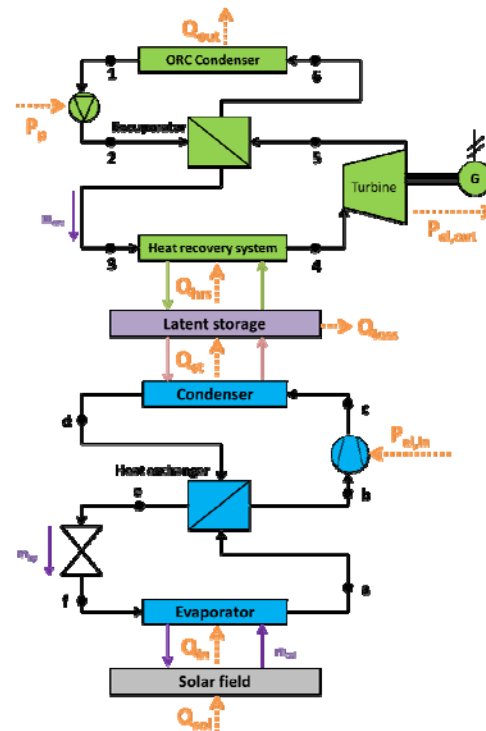


Fig. 1. The examined HP-ORC configuration

Table 1. Inputs parameters in the present investigation

Parameter	Symbol	Value
Electricity input in the HP	$P_{el,in}$	20 kW
Turbine isentropic efficiency	$\eta_{is,tur}$	80%
Compressor ssentropic efficiency	$\eta_{is,com}$	80%
Pump isentropic efficiency	$\eta_{is,p}$	80%
Electromechanical efficiency in the ORC generator	η_{mg}	97%
Compressor motor efficiency	$\eta_{mot,com}$	97%
Pump motor efficiency	$\eta_{mot,p}$	97%
Storage tank efficiency	η_{st}	95%
HP evaporator temperature	T_{evap}	20 °C - 80°C
Storage temperature	T_{st}	120 °C - 220°C
Temperature difference in the heat exchanger	ΔT_{min}	5°C
ORC cindenser temperature	T_{reject}	30°C
Ambient temperature level	T_{am}	25°C
Solar irradiation level	G_T	800 W/m ²

2.2 Basic mathematical formulation

The collector solar thermal efficiency (η_{col}) is given as below [13]:

$$\eta_{col} = \frac{Q_u}{Q_{sol}} = 0.77 - 3.75 \frac{T_{f,in} - T_{am}}{G_T} - 0.015 \frac{(T_{f,in} - T_{am})^2}{G_T} \quad (1)$$

The solar irradiation on the solar field (Q_{sol}) is found by the product of the collecting area (A_{col}) and of the solar irradiation (G_T):

$$Q_{sol} = A_{col} \cdot G_T \quad (2)$$

The useful heat product is calculated as:

$$Q_u = m_{col} \cdot c_p \cdot (T_{f,out} - T_{f,in}) \quad (3)$$

The fluid input temperature in the collector ($T_{f,in}$), the fluid outlet temperature ($T_{f,out}$), the ambient temperature (T_{am}), the solar irradiation (G_T), the mass flow rate on the collector (m_{col}) and the specific heat capacity (c_p) are used in the previous equations.

The HP coefficient of performance (COP) is defined as below:

$$COP = \frac{Q_{cond}}{P_{el,in}} \quad (4)$$

The latent storage tank efficiency of the storage system (η_{st}) is given as below:

$$\eta_{st} = \frac{Q_{hrs}}{Q_{st}} \quad (5)$$

The ORC electrical efficiency of the ORC is defined as below:

$$\eta_{orc} = \frac{P_{el,out}}{Q_{hrs}} \quad (6)$$

The system energy efficiency ($\eta_{en,sys}$) is calculated as below:

$$\eta_{en,sys} = \frac{P_{el,out}}{P_{el,in} + Q_{sol}} \quad (7)$$

The system exergy efficiency ($\eta_{ex,sys}$) is calculated as below by using the Petela model for the solar irradiation exergy factor [14]:

$$\eta_{ex,sys} = \frac{P_{el,out}}{P_{el,in} + Q_{sol} \cdot \left[1 - \frac{4}{3} \cdot \frac{T_0}{T_{sum}} + \frac{1}{3} \cdot \left(\frac{T_0}{T_{sum}} \right)^4 \right]} \quad (8)$$

The sun temperature is selected at $T_{sun}=5770$ K and the reference temperature at $T_0=298.15$ K. Moreover, figure 1 can be used for the definition of the various heat and power rates.

3. RESULTS AND DISCUSSION

The first step in the results section is the investigation of the heat pump performance and of the ORC efficiency. Figure 2 shows that higher storage temperature leads to higher ORC efficiency and also to lower COP in the heat pump. The higher evaporator temperature leads to higher COP in the heat. These are reasonable results and in accordance with the thermodynamics and the behavior of the equivalent Carnot cycle in the same conditions (both work and refrigeration Carnot cycles respectively). The next step is the investigation of the ambient source system which is the reference one. Figure 3 shows that the

electricity production is maximized for the storage tank temperature at 150°C and in this case, the power production is 7.7 kW and the respective power to power ratio is 38.5%. So, it is obvious that there is a need for optimizing the storage tank temperature level in the ambient source system.

The next step is the investigation of the system that is assisted by the flat plate collectors. The results are given in figures 4 to 7. Figure 4 illustrates the power to power ratio for different combinations of the evaporator temperature and the storage temperature. It is obvious that a higher evaporating temperature increases the power to power ratio, while a higher storage temperature has a negative impact on this parameter. However, after the limit of 200°C, the reduction is not so intense. Moreover, a critical issue is that in all the cases, there is an enhancement compared to the case of the ambient source heat pump. Figure 5 depicts the demanded collecting area for the operation of the solar-assisted HP-ORC system. It can be said that higher power to power efficiency is associated with a higher collecting area; a reasonable result because the higher performance requires higher heat inputs in the evaporator. So, it can be said that it is not possible to design a system of maximum power to power ratio at 90.7%, the demanded collecting area is 320 m² ($T_{st}=120^{\circ}\text{C}$ and $T_{evap}=80^{\circ}\text{C}$).

Figures 6 and 7 depict the energy and the exergy efficiencies of the examined system. Both figures show that higher storage temperature leads to higher system efficiency and lower evaporator temperature leads to higher system efficiency (both energetic and exergetic). The curves of these figures have similar trends and it is an interesting result. The maximum system efficiency was found for storage tank temperature at 220°C and evaporator temperature at 30°C, and in this case, the system energy efficiency is 19.1%, while the system exergy efficiency is 19.7%.

The previous analysis indicates that the solar-assisted system is more efficient than the ambient source system. For the case of $T_{st}=150^{\circ}\text{C}$ which maximizes the efficiency of the

ambient source system, the power to power ratio of it is 38.5%. On the other hand, for this storage temperature and for a typical evaporator temperature of 70°C for FPC, the power to power ratio is 61.1%, which means a 58.7% increase with the FPC assistance. In this case, the collecting area that is demanded is 129 m² which is a reasonable value.

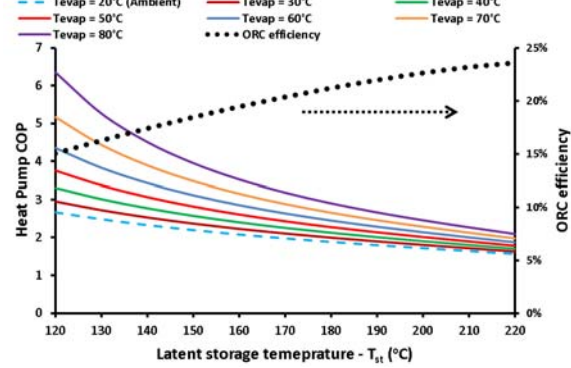


Fig. 2. Performance of the heat pump and of the ORC for different values of the evaporator temperature and the storage temperature

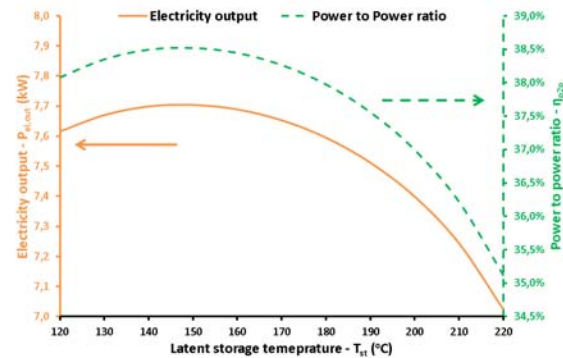


Fig. 3. Performance of the ambient source HP-ORC system

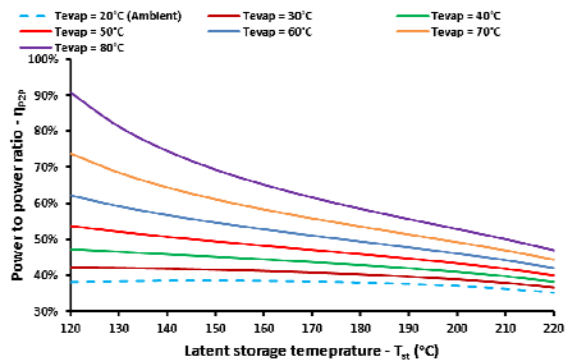


Fig. 4. Power to power efficiency for different values of the evaporator temperature and the storage temperature

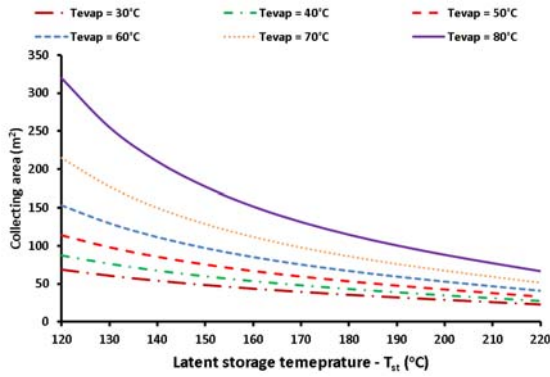


Fig. 5. Demanded collecting area for different values of the evaporator temperature and the storage temperature

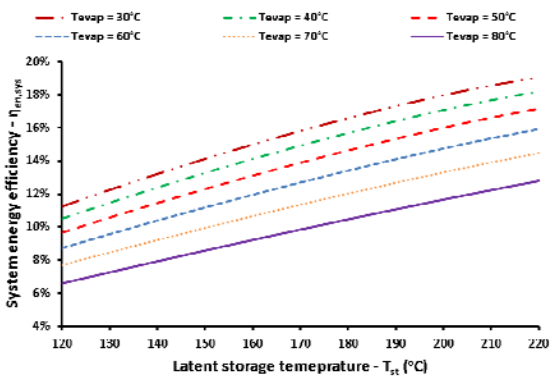


Fig. 6. System energy efficiency for different values of the evaporator temperature and the storage temperature

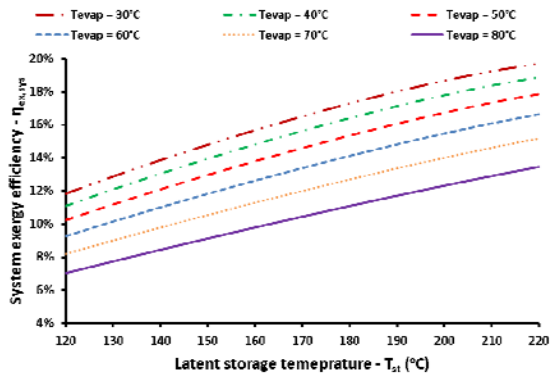


Fig. 7. System exergy efficiency for different values of the evaporator temperature and the storage temperature

4. CONCLUSIONS

The objective of the present study is the investigation of a pumped thermal energy storage latent system that uses flat plate collectors in order to feed a heat pump – ORC

configuration. The analysis is parametric with a developed model in Engineering Equation Solver. The most important conclusions of this work are given below:

- The higher storage temperature leads to higher ORC efficiency and also to lower COP in the heat pump. The higher evaporator temperature leads to higher COP in the heat.

- In the ambient source system, the electricity production is maximized for the storage tank at 150°C and in this case, the power production is 7.7 kW.

- It is found that higher power to power efficiency is associated with higher collecting area; a reasonable result because the higher performance requires higher heat inputs in the evaporator.

- The maximum system efficiency found for storage tank temperature at 220°C and evaporator temperature at 30°C, and in this case, the system energy efficiency is 19.1%, while the system exergy efficiency is 19.7%.

- For the typical case of ($T_{st}=150^{\circ}\text{C}$ and $T_{evap}=70^{\circ}\text{C}$) the solar-assisted system presents a 61.1% power to power ratio which is 58.7% higher than the ambient source case of 38.5% and the demanded collecting area for this case is 129 m².

In the future, there is a need for dynamic analysis of an HP-ORC system coupled to FPC in order to examine the daily enhancement by the use of the solar collectors. Also, the dual system can be studied by the use of both ambient and solar as heat sinks, especially for days with low solar potential.

Acknowledgment

"This research was financially supported by the Ministry of Education, Science and Technological Development of the Republic of Serbia (Contract No. 451- 03-9/2021-14/200109)"

REFERENCES

- [1] Pavlovic, S., Bellos, E., Le Roux, W.G., Stefanovic, V., Tzivanidis, C. (2017). Experimental investigation and parametric analysis of a solar thermal dish collector with spiral absorber. *Applied Thermal Engineering*, vol.121, p.126-

135. DOI:
<https://doi.org/10.1016/j.applthermaleng.2017.04.068>
- [2] Fang, Y., Wei, Y. (2013). Climate change adaptation on the Qinghai–Tibetan Plateau: The importance of solar energy utilization for rural household. *Renewable and Sustainable Energy Reviews*; vol. 18, p.508-518. DOI: <https://doi.org/10.1016/j.rser.2012.10.037>
- [3] Stefanovic, V.P., Pavlovic, S.R., Bellos, E., Tzivanidis, C. (2018). A detailed parametric analysis of a solar dish collector. *Sustainable Energy Technologies and Assessments*, vol. 25, p.99-110. DOI: <https://doi.org/10.1016/j.seta.2017.12.005>
- [4] Khan, M.J., Yadav, A.K., Mathew, L. (2017). Techno economic feasibility analysis of different combinations of PV-Wind-Diesel-Battery hybrid system for telecommunication applications in different cities of Punjab, India. *Renewable and Sustainable Energy Reviews*, vol. 76, p. 577-607. DOI: <https://doi.org/10.1016/j.rser.2017.03.076>
- [5] Barbosa, V., Nogueira, T., Carati, E., Felgueiras, C. (2018). Supercapacitor in battery charges of photovoltaic panel: analysis of the technical feasibility. *Energy Procedia*, vol. 153, p. 0-85. DOI: <https://doi.org/10.1016/j.egypro.2018.10.019>
- [6] Frate, G.F., Ferrari, L., Desideri, U. (2020). Multi-criteria investigation of a pumped thermal electricity storage (PTES) system with thermal integration and sensible heat storage. *Energy Conversion and Management*, vol. 208:112530. DOI: <https://doi.org/10.1016/j.enconman.2020.112530>
- [7] Roskosch, D., Venzik, V., Atakan, B. (2020) Potential analysis of pumped heat electricity storages regarding thermodynamic efficiency. *Renewable Energy*, vol.147(3), p.2865-2873. DOI: <https://doi.org/10.1016/j.renene.2018.09.023>
- [8] Scharer, D., Eppinger, B., Schmitt, P., Zenk, J., Bazan, P., Karl, J., Will, S., Pruckner, M., German, R. (2020). Life Cycle Assessment of a Reversible Heat Pump–Organic Rankine Cycle–Heat Storage System with Geothermal Heat Supply. *Energies*, vol. 13, p. 32-53. DOI: <http://dx.doi.org/10.3390/en13123253>
- [9] Sonsaree, S., Jiajitsawat, S., Asaoka, T., Aguirre, H., Tanaka, .K. Organic Rankine Cycle Power Generation from Industrial Waste Heat Recovery Integrated with Solar Hot Water System by using Vapor Compression Heat Pump as Heating Booster in Thailand, International Conference on Cogeneration, Small Power Plants and District Energy (ICUE 2016) BITEC, Bang-Na, Thailand, September 2016, p.14-16. DOI: <https://doi.org/10.1109/COGEN.2016.7728939>
- [10] Henchoz, S., Buchter, F., Favrat, D., Morandin, M., Mercangöz, M. (2012). Thermoeconomic analysis of a solar enhanced energy storage concept based on thermodynamic cycles. *Energy*, vol. 45(1), p. 358-365. DOI: <https://doi.org/10.1016/j.energy.2012.02.010>
- [11] Eppinger, B., Zigan, L., Karl, J., Will, S. (2020). Pumped thermal energy storage with heat pump-ORC-systems: Comparison of latent and sensible thermal storages for various fluids. *Applied Energy*, vol.280, p.115940. DOI: <https://doi.org/10.1016/j.apenergy.2020.115940>
- [12] F-Chart Software, Engineering Equation Solver (EES), 2015. Available at: (<http://www.fchart.com/ees>) accessed on: March 25, 2021
- [13] Technical Guidelines, Technical Chamber of Greece, TOTEE 20701-1/2017, 1st Edition, Athens, 2017
- [14] Petela, R. (2003). Exergy of undiluted thermal radiation. *Solar Energy*, vol.74(6), p.469-488. DOI: [https://doi.org/10.1016/S0038-092X\(03\)00226-3](https://doi.org/10.1016/S0038-092X(03)00226-3)



Banja Luka
28–29 May 2021.

DEMI 2021

15th International Conference on
Accomplishments in Mechanical and
Industrial Engineering

www.demi.mf.unibl.org



Energy Management To Low-Carbon Cities: the Example of the City of Kragujevac

A. Radojević^a, D. Nikolić^a, J. Skerlić^b, J. Radulović^a

^aFaculty of engineering, University of Kragujevac; Sestre Janjic 6, 34000 Kragujevac, Serbia

^bFaculty of Technical Sciences, University of Pristina temporarily settled in Kosovska Mitrovica; Knjaza Milosa 7, 38220 Kosovska Mitrovica, Serbia

Abstract Serbia first ratified the United Nations Framework Convention on Climate Change (UNFCCC) in 2001, and then the Paris Agreement in 2017. By ratifying the Paris Agreement, Serbia has committed to reduce greenhouse gas emissions by 9.8% by 2030, compared to 1990 level of emissions. As cities are responsible for over 70% of all GHG emissions, they are becoming a main place to act and combat climate change and reduce GHG emissions. In Serbia, there is a legal obligation of cities and municipalities to establish a system of energy management (SEM). The city of Kragujevac established the SEM in 2015. The paper gives an overview of energy efficiency measures implemented in this period and how the measures have affected the reduction of CO₂ emissions, and thus the decarbonization of the city.

Keywords Energy management, Energy planning, Low-Carbon Cities, energy efficiency measures

1. INTRODUCTION

Today, approximately 72% of the total population of the European Union lives in larger and smaller cities and suburbs. Although the rate of change is slowing, the share of the population living in cities continues to grow and is likely to reach more than 80% by 2050 [1]. Cities consume over two-thirds of the total amount of energy consumed worldwide. Over 70% of all greenhouse gases (hereinafter: GHG) emissions originate from cities [2].

There are a number of plans and strategies in the European Union related to reducing CO₂ emissions. Some of these plans until 2050 are presented in two strategic documents: Energy Roadmap 2050 and A Roadmap for moving to a competitive low carbon economy in 2050, and they foresee targets for reducing greenhouse gases by 80-95% compared to the baseline year of 1990 [3].

The Covenant of Mayors (CoM) is a successful European initiative which encourages local

authorities to be proactive in fighting climate change. The methodology is applied to over 1600 signatories in Europe, representing over 80 million inhabitants

Signatory cities pledge actions to support the implementation of the 40% greenhouse gas-reduction target by 2030. For a baseline year of their choice, summarising energy consumption and CO₂ emissions for different sectors and fuels (referred to as energy carriers).

The EU Covenant of Mayors (CoM) is an international initiative, part of the Global Covenant of Mayors, that directly engages local governments to adopt climate and energy targets at least matching the EU targets. By voluntarily adhering to the CoM, local authorities committed to decarbonise and increase resilience in their territory and share their emission inventories and climate action plans [4].

In the case of the city of Kragujevac, the highest emissions are the result of the energy consumption in public buildings - 49%, public

lighting - 36% and public transport - 15% [5]. The last document adopted in the Republic of Serbia that deals with GHG emissions is the Law on Climate Change [6], adopted in March 2021. This law regulates, among other things, the system for limiting the GHG and for adapting to changed climatic conditions, monitoring and reporting on the low-carbon development strategy and its improvement. GHGs are carbon dioxide (CO₂), methane (CH₄), nitrogen suboxide (N₂O), fluorocarbons (HFCs), perfluorocarbons (PFCs), and sulfur hexafluoride (SF₆) and nitrogen trifluoride (NF₃).

The aim of this law is to establish a system to reduce GHG emissions in a cost-effective and economically efficient manner, thus contributing to the achievement of scientifically necessary levels of GHG emissions, to avoid dangerous global climate change and adverse impacts of climate change, reducing GHG emissions and adapting to changed climate conditions through the adoption and implementation of public policy documents, the establishment of mechanisms for timely, transparent, accurate, consistent, comparable and complete reporting and verification of information on compliance with the Law on Ratification of the UN Framework Convention on Climate Change (with annexes), the Law on Ratification of the Kyoto Protocol, the Law on Ratification of the Doha Amendments to the Kyoto Protocol with the United Nations Framework Convention on Climate Change and the Law on Ratification of the Paris Agreement, as well as the Monitoring and Reporting of GHG Emissions from Human Sources and removed by sinks and adapted climate change activities conditions undertaken in a cost-effective and economically efficient manner. In order to achieve the objectives of this law, state bodies and organizations should adopt appropriate sectoral policies and measures within the scope of their competence.

In the forthcoming period, the Low Carbon Development Strategy will be adopted in order to determine strategic directions of action and public policy related to the limits of GHG emissions from sources, as well as transparent and accurate monitoring of the achievement of these emission limits.

The law further addresses vehicle fuel consumption and CO₂ emissions, GHG emissions from installations and aeronautical activities,

the system for monitoring and reporting on national GHG emissions, projections of GHG emissions from sources and removals by sinks, the system for reporting on GHG policies, measures and projections, administrative fees, supervision and penal provisions.

Until bylaws dealing with various sectors, including buildings, which are one of the biggest causes of CO₂ emissions, are adopted, local self-governments in Serbia are left to implement energy policy, the introduction of energy management systems and energy planning as one of the ways to reduce GHG emissions, primarily CO₂ emissions.

The paper further analyzes how the introduction of an energy management system can lead to a reduction of CO₂ emissions.

2. ORGANIZATION OF CITIES IN SERBIA IN THE FIELD OF ENERGY MANAGEMENT

Starting in 2006, when the local government units were supposed to submit energy balance sheets to the Ministry of Mining and Energy for the first time, cities and municipalities appointed persons who started dealing with energy efficiency issues in some way. In these first reports, in addition to energy consumption in public buildings, CO₂ emissions were also shown.

2.1 Legal framework for the energy management system in RS

According to the Law on Efficient Use of Energy [7], all local government units with more than 20,000 inhabitants have an obligation to appoint an energy manager.

2.2 Organization of Cities in Serbia in the Field of Energy Management

In the cities and municipalities in Serbia, organization of the energy management system is different from place to place, as is a number of employees in these jobs and appointed energy managers. Thus, in Novi Sad, there is the Energy Agency, which employs an energy manager, while in Belgrade it's the Energy Secretariat, and in Niš, the City Assembly appoints an energy manager, and there is a department that deals with these issues. In other cities and municipalities mainly only one person - energy manager - deals with activities related to energy

efficiency, greater use of renewable energy sources, and thus reduction of GHG emissions.

2.3 Organization of the City of Kragujevac in the Field of Energy Management

In accordance with the Law on Efficient Use of Energy, the city of Kragujevac appointed an energy manager in 2016.

According to the Law on Efficient Use of Energy, the energy manager:

1. Collects and analyzes data on the energy use by the SEM payers
2. Drafts the energy efficiency program and plan to be adopted by the City of Kragujevac
3. Submits annual reports on the achievement of the objectives contained in the energy efficiency program and plan to the relevant Ministry
4. Proposes measures that contribute to the efficient use of energy and participates in their implementation

During 2015, the Department for Energy Efficiency was formed, and after the reorganization of the city administration in 2020, there is a Department for project management and energy efficiency. The main task of the Department is also to monitor and analyze energy consumption and propose energy efficiency measures.

2.4 Results of the Established Energy Management System in Kragujevac

2.4.1 Measures Implemented on the Primary and Secondary Schools' Facilities

The paper analyzes measures in primary and secondary schools.

In the period from 2015 to 2020, the following measures were implemented at school facilities:

1. Installation of thermoregulatory equipment
2. Replacement of carpentry
3. Combined measures: replacement of carpentry and installation of thermoregulation equipment
4. Combined measures: replacement of carpentry, insulation of building walls and installation of thermoregulation equipment

Combined measures: replacement of carpentry, insulation of building walls, replacement of LED lighting, measures on the district heating system (the reference year is 2015).

Table 1. Energy efficiency measures implemented in schools

	Name of School	Implemented energy efficiency measures
Primary schools		
1.	PS "21. Oktobar"	Installation of thermoregulatory equipment
2.	PS "Sveti Sava"	Installation of thermoregulatory equipment
3.	PS "Svetozar Marković"	Installation of thermoregulatory equipment
4.	PS "Mirko Jovanović"	Installation of thermoregulatory equipment
5.	PS "Radoje Domanović"	Installation of thermoregulatory equipment
6.	PS "Milutin i Draginja Todorović"	Replacement of carpentry and installation of thermoregulatory equipment
7.	PS "19.oktobar"	Heating system change, insulation of building walls, replacement of carpentry
8.	PS "Treći kragujevački bataljon"	Replacement of carpentry, insulation of building walls and installation of thermoregulatory equipment
9.	PS "Dositej Obradović"	Replacement of carpentry
10.	PS "Natalija Nana Nedoljković"	Replacement of carpentry
11.	PS "Živadinka Divac"	Replacement of carpentry
12.	PS "Vuk Stefanović Karadžić"	Replacement of carpentry
13.	PS "Natalija Nana Nedeljković"	Replacement of carpentry
14.	PS "Sveti Sava"	Replacement of carpentry
15.	PS "Moma Stanojlović"	Replacement of carpentry, insulation of building walls, replacement of LED lighting, measures on the district heating system
16.	PS "Stanislav Sremčević"	Replacement of carpentry, insulation of building walls, replacement of LED lighting, measures on the district heating system
Secondary schools		
1.	Second Kragujevac High School	Replacement of carpentry
2.	Secondary Vocational School	Replacement of carpentry
3.	First Technical School	Replacement of carpentry
4.	"Toza Dragović"	Replacement of carpentry

2.4.2 CO₂ emission in the baseline year

The base year was 2015, after which energy efficiency measures were implemented at the listed primary and secondary school facilities. Consumption data have been taken from the Energy Efficiency Program for the City of Kragujevac for the period 2018-2020 [8]. To calculate CO₂ emissions, the conversion factors given in Table 2 were used.

Table 2. Conversion factors for calculating CO₂ emission

Fuel	Unit	kWh/jm	Emission kg/kWh
Raw lignite	t	3.600,0000	0,35
Dried lignite	t	4.500,0000	0,35
Brown coal	t	5.000,0000	0,35
Stone coal	t	6.000,0000	0,35
Coal – coke	t	7.000,0000	0,35
Wood	m3	1.680,0000	0,30
Wood waste	t	4.500,0000	0,30
Biomass	t	3.600,0000	0,35
Heating oil	t	4.500,0000	0,35
Crude heating oil	t	5.000,0000	0,35
Propane-Butane	t	6.000,0000	0,35
Natural gas	t	7.000,0000	0,35
Biogas	m ³	1.680,0000	0,30
Electricity	t	4.500,0000	0,30
Solar energy	t	3.500,0000	0,30
Geothermal water	m3	11.390,0000	0,25
Wind energy	t	11.000,0000	0,28

Tables 3, 4 and 5 provide an overview of CO₂ emissions [t] in primary and secondary schools for the baseline year 2015, before energy efficiency measures were implemented.

Table 3: CO₂ emission in primary schools for 2015

Primary schools - Year 2015	Total CO ₂ emission [t]	7037
	Heating-generated CO ₂ emission [t]	5368
	Electricity-generated CO ₂ emission [t]	1669

Table 4: CO₂ emission in secondary schools for 2015

Secondary schools - Year 2015	Total CO ₂ emission [t]	4159
	Heating-generated CO ₂ emission [t]	3174
	Electricity-generated CO ₂ emission [t]	985

Table 5: CO₂ emission in primary and secondary schools for 2015

Total primary and secondary schools - Year 2015	Total CO ₂ emission [t]	11196
	Heating-generated CO ₂ emission [t]	8542
	Electricity-generated CO ₂ emission [t]	2654

Figure 1 shows the distribution of total CO₂ emissions in [%] in primary and secondary

schools in 2015. It can be seen that the largest part of the emission comes from heating (76%).

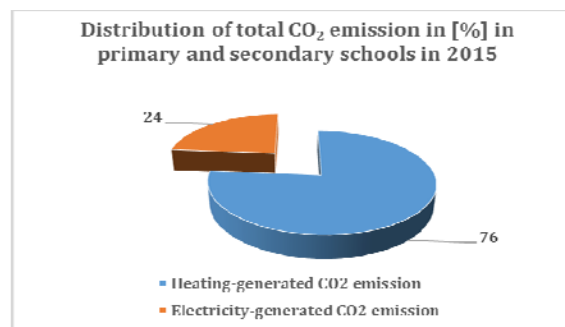


Fig. 1. Distribution of total CO₂ emissions [%] in primary and secondary schools in 2015

2.4.3 CO₂ emission in 2020

Tables 6, 7 and 8 show the emission in 2020, after the implemented measures.

Table 6. CO₂ emission in primary schools for 2020

Primary schools - Year 2020	Total CO ₂ emission [t]	3294
	Heating-generated CO ₂ emission [t]	2098
	Electricity-generated CO ₂ emission [t]	1196

Table 7: CO₂ emission in secondary schools for 2020

Secondary schools - Year 2020	Total CO ₂ emission [t]	1841
	Heating-generated CO ₂ emission [t]	1306
	Electricity-generated CO ₂ emission [t]	535

Table 8: CO₂ emission in primary and secondary schools for 2020

Total primary and secondary schools - Year 2020	Total CO ₂ emission [t]	5135
	Heating-generated CO ₂ emission [t]	3404
	Electricity-generated CO ₂ emission [t]	1731

Figure 2 shows the distribution of total CO₂ emissions in [%] among primary and secondary schools in 2020. It can be seen that most of the emission still comes from heating (66%). As the largest part of the implemented measures referred to the measures on the district heating system, the ratio of emissions originating from heating and electricity was changed. It is now closer, which means that the following measures need to be implemented in order to save electricity. This can be the replacement of interior lighting with LED lighting or the installation of PV panels on the roofs of these buildings.

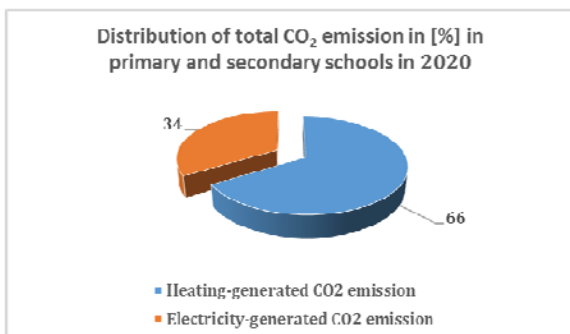


Fig. 2. Distribution of total CO₂ emissions in [%] among primary and secondary schools in 2020.

2.4.4 Reduction of CO₂ emissions caused by the implementation of measures in primary and secondary school buildings

Tables 9, 10 and 11 show the reduction of CO₂ emissions in primary and secondary schools in [t].

Table 9. Reduction of CO₂ emissions [t] in primary schools in the period 2015-2020

Reduction of CO ₂ emission [t] in primary schools	Reduction of the total CO ₂ emissions [t]	3743
	Reduction of the heating-generated CO ₂ emissions [t]	3270
	Reduction of the electricity-generated CO ₂ emissions [t]	473

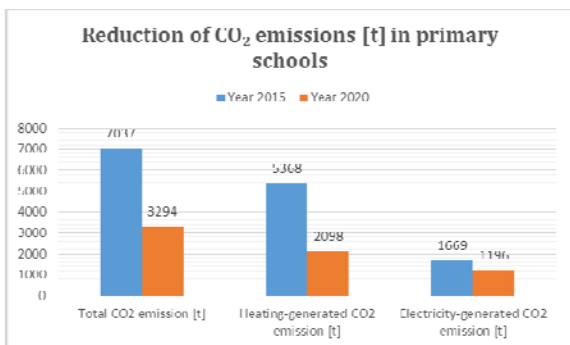


Fig.3 Reduction of CO₂ emissions [t] in primary schools

Table 10: Reduction of CO₂ emissions [t] in secondary schools in the period 2015-2020

Reduction of CO ₂ emissions [t] in secondary schools	Reduction of the total CO ₂ emissions [t]	2318
	Reduction of the heating-generated CO ₂ emissions [t]	1868
	Reduction of the electricity-generated CO ₂ emissions [t]	450

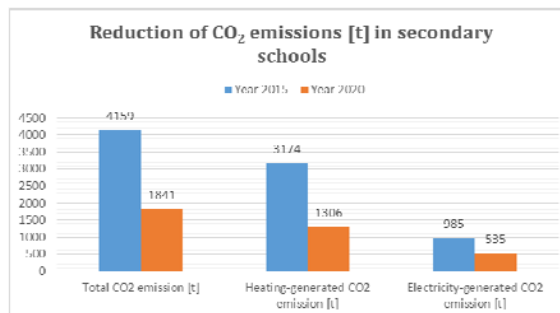


Fig. 4. Reduction of CO₂ emissions [t] in secondary schools

Table 11: Reduction of CO₂ emissions [t] in primary and secondary schools in the period 2015-2020

Total reduction of CO ₂ emissions [t] in primary and secondary schools	Reduction of the total CO ₂ emissions [t]	6061
	Reduction of the heating-generated CO ₂ emissions [t]	5138
	Reduction of the electricity-generated CO ₂ emissions [t]	923

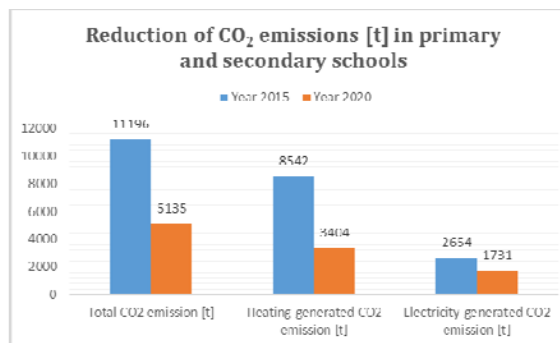


Fig.5 Reduction of CO₂ emissions [t] in primary and secondary schools

Table 12 shows the percentage reduction of CO₂ emissions in primary and secondary schools in the period 2015-2020. The decrease was 53% in primary schools, 56% in secondary schools and 54% in total in primary and secondary schools.

Table 12: Reduction of CO₂ emissions in [%] in primary and secondary schools in the period 2015-2020

Reduction of CO ₂ emissions [%] in primary schools	53
Reduction of CO ₂ emissions [%] in secondary schools	56
Total reduction of CO ₂ emissions [%] in primary and secondary schools	54

3. CONCLUSION

By ratifying the Paris Agreement, Serbia has committed itself to reducing greenhouse gas emissions by 9.8% by 2030 compared to 1990 levels. As cities are responsible for over 70% of all GHG emissions, they are becoming a major place to act and combat climate change and reduce GHG emissions. The implementation of energy efficiency measures in cities can significantly contribute to the reduction of CO₂ emissions. The introduction of energy management systems and the planning of energy efficiency measures in buildings lead to a reduction of CO₂ emissions by 53-56%.

Acknowledgement

This paper presents results obtained within realization of two projects TR 33015 and III 42006, funded by Ministry of Education, Science and Technological Development of the Republic of Serbia. The authors would like to thank to the Ministry for their support during these investigations.

REFERENCES

- [1] European Commission (Joint Research Center, European Forum for Geography and Statistics, Directorate-General for Regional Policy)
- [2] https://www.c40.org/why_cities, accessed on Feb. 01, 2021
- [3] Radojević, A., Nikolić, D., Janjušević, M., Skerlić, J., Gordić, D., POSSIBILITIES FOR REDUCING CO₂ EMISSIONS IN PUBLIC BUILDINGS USING BIOMASS, Tractors and power machines, Novi Sad, Dec. 2020., Vol.25, No.5, p.21-28
- [4] Radojević A., Nikolić D., Skerlić J., Analysis of CO₂ emissions in the public sector - the example of the city of Kragujevac, *Proceeding of IX International Conference on social and technological development*, 2020, Trebinje, Republika Srpska, p. 28-38
- [5] Radojević A., Nikolić D., Skerlić S., Gordić D., The impact of energy efficiency measures on reducing CO₂ of public buildings in the city of Kragujevac, *Proceeding of 5th International Scientific Conference "Conference on Mechanical Engineering Technologies and Applications" - COMETA 2020*, 2020, Jahorina, Republika Srpska, p. 471-478
- [6] Law on Climate Change (Official Bulletin of the RS, no. 26/2021)
- [7] Law on Efficient Use of Energy (Official Bulletin of the RS, no. 25/13)
- [8] Official Bulletin of the City of Kragujevac (2018); Energy Efficiency Program of the City of Kragujevac for period 2018-2020. Official Bulletin of the City of Kragujevac, No.13/2018



Banja Luka
28–29 May 2021.

DEMI 2021

15th International Conference on
Accomplishments in Mechanical and
Industrial Engineering

www.demi.mf.unibl.org



Analysis of seasonal deviations influence on air-cooled condenser performances

J. Škundrić^a, P. Živković^b, D. Mitrović^b, M. Vukić^b, D. Đurica^c, B. Bačić^c

^aFaculty of Mechanical Engineering, University of Banja Luka, Republika Srpska, Bosnia and Herzegovina

^bFaculty of Mechanical Engineering, University of Niš, Serbia

^cThermal Power Plant "Stanari", Republika Srpska, Bosnia and Herzegovina

Abstract

As technology of materials in use for building of boiler and turbine plants becomes more and more developed, the air-cooled condensers become increasingly popular to use in thermal power plants. The link between the technology of materials improvement and air-cooled condensers usage is in the fact that such type of a condenser significantly raises the condensation temperature and consequently the condensation pressure, so the temperature and the pressure of the fresh steam must also be raised. Since the widespread usage of the air-cooled condensers in thermal power plants started recently, there is still a number of unknown variables regarding their steady functioning and the most of them are related to the stochastic nature of the seasonal atmospheric deviations during the year. The most dominant quantities responsible for those atmospheric deviations are, of course, the ambient temperature, the wind speed and the insolation, followed by the humidity and the air pressure. This paper presents an insight into some of those quantities, with an accent on the wind data and the air temperature. As an example, thermal power plant in Stanari was analyzed. The goal of this paper was to find the best starting point for some possible further improvements of condensers of this type.

Keywords thermal power plant, air-cooled condenser, condensation, wind speed, air temperature

1. INTRODUCTION

In its basics, a thermal power plants function according to the Clausius-Rankine thermodynamic cycle with superheated water steam. In the cycle, the wet steam, after being discharged from the turbine, has to be condensed to the entirely liquid state so the cycle could go on. The very process of the condensation is nothing more than the process of heat transfer from the discharged steam to

the environment of the thermodynamic system considered.

In order to achieve considered demands, an appropriate heat exchanger is needed, and the most common devices of that type are either water-cooled or air-cooled heat exchangers. Until recently, air-cooled condensers were not used in thermal power plants because the technology of materials used in steam boilers and turbine plants was on the level which had been limiting by both the fresh steam temperature and pressure. This consequently had been limiting the overall efficiency of the plant and not leaving enough room for further

Corresponding author

MSc, Jovan Škundrić
jovan.skundric@mf.unibl.org

Faculty of Mechanical Engineering, University of Banja Luka
Bulevar vojvode Stepe Stepanovića 71
Banja Luka, Republika Srpska, Bosnia and Herzegovina

decreasing the efficiency by using the air-cooled condenser.

Condensing processes in the thermal power plants were, almost as a rule of a thumb, organized in water cooled condensers, which would use either water from a nearby river, or recirculated water from dedicated wet cooling towers. Such a design has a major advantage compared to the air-cooled condensers by means of significantly higher efficiency considering the heat transfer and consequently almost steady condensing pressure and the heat drop in thermodynamic cycle of the plant, but it also demands having enough water on the site where the thermal power plant is about to be built. Recently, the technology of materials was significantly improved, which also led to the improvement of thermal power plants overall efficiency, which finally left enough room for using air-cooled condensers when necessary.

Given all this, nowadays in scenarios when we have a coal mine, and appropriate nearby site for a thermal power plant, but we do not have a river or enough water for the wet cooling towers, the air-cooled condenser can be, and usually is an appropriate alternative. In this paper, an example of air-cooled condenser application will be examined as a part of the coal mine and thermal power plant "Stanari", Republic of Srpska, with its advantages and disadvantages and also with some possibilities for further improvement of its function.

2. SOME SPECIFICITIES OF AIR-COOLED CONDENSERS IN THE THERMAL POWER PLANT

On the Figure 1. the simplified scheme of an air-cooled condenser is given in order to make the analysis regarding the issues of its operation, presented below, easier for the reader to follow. One must have in mind that the element which represent the condenser in the scheme is, really, just one of a dozen or more cells within the condenser. Often, condensers of this type are designed in a way that suction side of cells are not protected from the side wind,

and such a design is also present in the thermal power plant Stanari condenser.

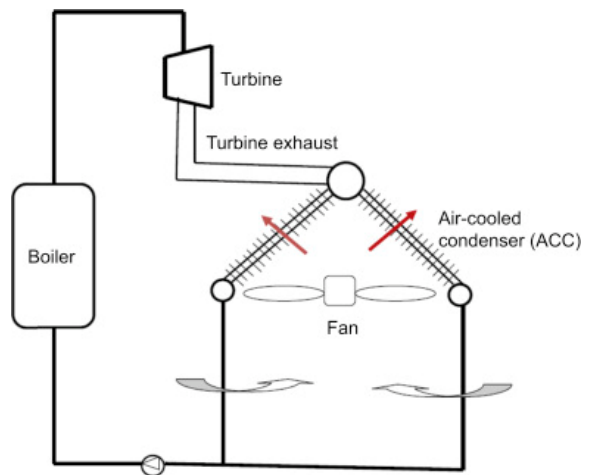


Fig. 1. Air-cooled condenser simplified scheme, [3]

Above mentioned air-cooled condensers disadvantages can be easily understood if we consider the heat flux to the surrounding air and the amount of heat being taken from the steam in the unit of time, [1, 2]:

$$Q = A \alpha_a (t_w - t_a) \quad (1)$$

$$Q_s = \dot{m}_s r x \quad (2)$$

where, in the equation (1), Q is the convective heat flux from the condenser outer wall to the surrounding air, A is the surface of the condenser, α_a the convective heat transfer coefficient on the air side, and t_w , t_a are temperatures of the condenser outer wall and of the surrounding air, respectively. In the equation (2), Q_s is the amount of heat (for the unit of time) being taken from the wet steam during condensation, \dot{m}_s is the mass flow of the condensing steam, r is the latent heat of the steam at the condensing pressure and x is the dryness factor of the steam.

In the steady state, heat flux (1) must be equal to the heat content (2) per unit time, with addition of the overall heat due to radiation from the Sun (Q_r):

$$Q = Q_s + Q_r = A \alpha_a (t_w - t_a) = \dot{m}_s r x + Q_r \quad (3)$$

Detailed consideration of the quantities influencing the convective heat transfer coefficient can be presented as follows [1, 2]

$$\alpha = f(\vec{v}, c_p, \rho, \lambda, \nu, L) \quad (4)$$

where \vec{v} stands for velocity of the fluid, c_p for its heat capacity, ρ for density, λ for thermal conductivity, ν for kinematic viscosity and L for characteristic length. It becomes obvious which quantities we must maintain if we want to keep constant heat content being taken from the steam as atmospheric conditions change. Characteristic length in the equation (4) is a constant value and is practically part of the condensers design. The heat capacity, density, thermal conductivity and kinematic viscosity can vary in some amount with changing humidity and temperature of the air, but the dominant influence is the air velocity. Air velocity is directly proportional to the convective heat transfer coefficient, so it is very important to have its magnitude as high as possible and its direction as close to the optimal as possible, especially in conditions of high ambient temperatures.

To let aside the radiation from the Sun, now it is clear that quantities which impact condensers operation the most are temperature and the air velocity. When, ambient air temperature rises, for constant α_a , the heat flux from equation (1) will decrease, which further leads to decreasing of the heat content being extracted from the steam. In such a case, if the mass flow of the steam in equation (2) remains constant, latent heat must decrease, which then leads to the increasing of the condensing pressure, consequently lowering the heat drop of the cycle. Also, if the velocity of air streaming across the convective surface of the condenser decreases, α_a will also decrease, again lowering the heat flux from equation (1) leading to the same problem explained in previously.

Considering all above mentioned, the fairly low air temperature, combined with proper mass

flow of the air are the desirable conditions, meaning that atmospheric conditions in which either the air temperature is raised or the air mass flow is disturbed are the least convenient ones.

3. THE REVIEW OF AIR-COOLED CONDENSER ISSUES IN THERMAL POWER PLANT STANARI

It is certainly clear that the major issues with the air-cooled condenser exist in hot summer days when ambient air temperatures rise high enough. In such a case, the temperature difference between the ambient and the temperature of condensation at the desirable pressure becomes too small for efficient heat transfer. In addition to the high radiation from the Sun in those times of the year, it is more than obvious that condensing pressure will inevitably rise. Increase in condensing pressure to some extent leads to decreasing efficiency of the plant, meaning higher fuel consumption, but not rarely the increase can be of such extent that the mass flow of fresh steam has to be decreased and the demanded power of the plant simply cannot be reached. Moreover, as with higher condensing pressure, the condensing temperature also rises, less steam is being extracted for regenerative heating of the condensate. This for a consequence has even higher mass flow of the steam streaming into the condenser for the same power, worsening the plant operation.

Unfortunately, this is just the temperature part of the operational issues. Obviously, the air mass flow must be carefully considered. As mentioned before, the air mass flow strongly depends on its velocity, which is being maintained with 30 axial fans, each of nearly 10 meters in diameter. The fans used can achieve very air high flow rates, but, being designed as axial, the pressure gains are rather small and consequently rather easy to be disturbed. One of the main factor which disturbs the air flow is a side wind on the suction side of

the fans. Side wind, if its speed is high, provokes sub-pressure on the suction side which increases the pressure head the fan must overcome, which lowers the flow of the air being forced across the condenser. In order to achieve a proper insight in the most critical periods for the condensers operation it is very important to determine months with strong winds, beside the months with high temperatures. Wind gusts from the directions the condenser casings are open to must be treated with additional care. In thermal power plant Stanari, the air-cooled condenser is positioned in a way that its north-west side is the most critical regarding the side wind negative impact, so the data for winds from that direction are of the highest importance.

4. DATA AND DISCUSSION

The data from the local meteorological station within the plant are presented in the Table 1. The average outdoor temperature, average wind speeds, their extreme values as well as the percentages of days on a monthly level for maximum wind speeds exceeding 5 m/s and outdoor temperatures exceeding 30°C are presented. Those values were chosen as a critical considering the project conditions of the condenser and considering that such parameters were confirmed as critical in the operational practice of the plant. The average solar irradiations, presented in the Table 1., were obtained from the global solar atlas [6].

As it can be seen on Figure 5, area around the power plant is a region with relatively slow winds comparing to other nearby regions. According to the wind map, mean wind speed at 50 meters height on the site the power plant is built on is always below 3 m/s, which is in perfect compliance with the data from the Table 1. Regarding magnitudes of mean monthly wind speeds annually, obviously the highest values are in the winter season, while during the summer, those values are the lowest.

On the other hand, if we consider the extreme values of the wind speed presented in the Table 1., it appears that standard deviation of the wind speed is pretty high for this region which is also clear from the shape of the distribution graph given on the Figure 4. The magnitude of the wind speed deviation from its mean value is probably the most visible in column 7 in Table 1., where percentage of days on a monthly level with appearance of the wind speed higher than 5 m/s are presented. Also, the deviations from the mean value appears to be the largest from winter to midsummer and somewhat smaller in autumn, while number of days with the wind speed higher than 5 m/s is the largest in winter and from late spring till early summer.

Analyzing the specific wind directions on the wind frequency rose (Figure 2.) it can easily be seen that the wind from north-west is the most frequent. Furthermore, the wind speed rose and mean wind speed distribution diagram (Figures 3. and 4.) clearly show that exactly the wind from north-west direction is also the slowest one on this area. The strongest winds blow from south and south-west directions, but as it can be seen on the Figure 2., their frequencies are not high.

Regarding the air temperature, the situation is pretty much as we could expect. The highest average temperatures are present during the summer with somewhat balanced values, while the most frequent appearance of temperatures higher than 30°C is from mid to late summer with significant peak in August.

Finally, considering the solar irradiations on a monthly level, the situation is also as expected, with the highest values during the summer, with certain peaks in July and August, while spring and autumn are characterized with significantly lower values. In winter, as it can be seen in Table 1. solar irradiations are approximately three times lower than the ones during the summer, so their influence is practically negligible.

Table 1. Data from power plant local meteorological station for year 2020 [4]

Date	Max Outdoor Temp (°C)	Average Outdoor Temp (°C)	Average wind speed (m/s)	Max Wind speed (m/s)	Min Outdoor Temp (°C)	Wind speed greater than 5 m/s (%)	Max temperature greater than 30°C (%)	*Average solar irradiance (kWh/m ²)
12/2019	18.9	5.4	2.3	8.6	-2.0	35.5	0	48
01/2020	19.0	1.1	2.0	7.5	-8.5	45.2	0	56
02/2020	21.9	6.3	0.8	9.9	-5.1	37.9	0	66
03/2020	26.5	7.5	1.1	9.2	-5.7	35.5	0	99
04/2020	29.6	12.7	0.7	7.1	-5.3	30.0	0	105
05/2020	30.0	15.8	1.3	10.9	1.0	48.4	0	132
06/2020	36.5	20.5	1.3	9.9	7.8	43.3	23.3	145
07/2020	36.1	22.0	0.9	10.9	7.6	25.8	51.6	165
08/2020	42.0	23.8	0.9	5.8	12.3	16.1	64.5	153
09/2020	36.2	19.4	1.8	7.3	7.5	33.3	46.7	106
10/2020	31.5	12.8	0.9	6.9	1.9	12.9	6.5	87
11/2020	25.7	7.7	1.8	6.3	-2.1	16.7	0.0	56

* Average solar irradiances for the power plant site were taken from Global Solar Atlas [6]

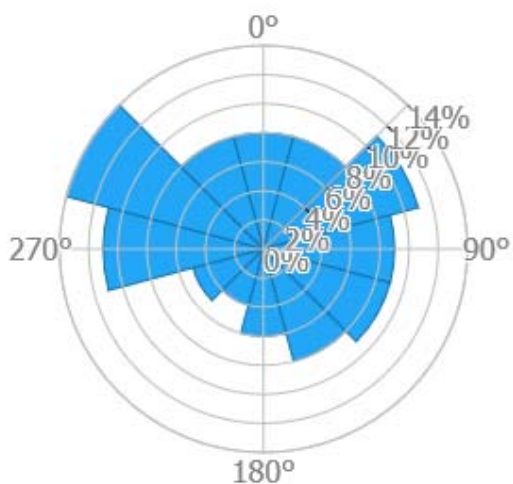


Fig. 2. Wind frequency rose, [5]

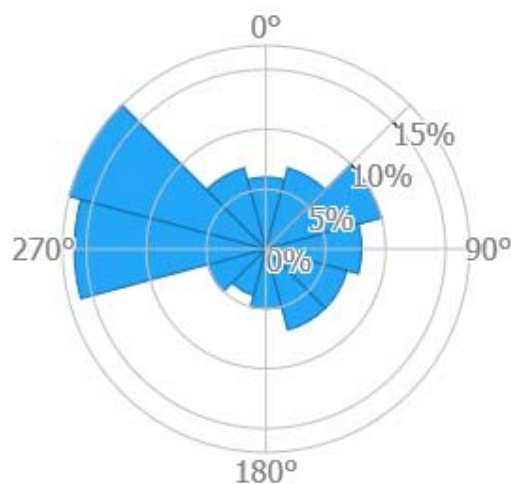


Fig. 3. Wind speed rose, [5]

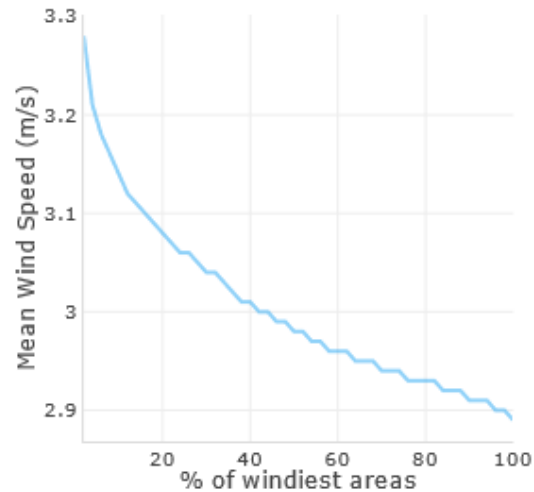


Fig. 4. Mean wind speed distribution, [5]



Fig. 5. Wind map for Stanari region, [5]

5. CONCLUSION

The wind speed of 5 m/s appears to be a borderline for problems in condensers performances and the site the plant is built on is obviously not a windy one with mean speed not exceeding 3 m/s on a monthly level. It is obvious that we can hardly

consider the wind as a major and persistent problem regarding the condensers functioning. As was noted in the discussion, deviations of the wind speed from the mean value are significant and frequencies of those deviations are not negligible, so the wind can still be the problem when combined with high ambient temperatures.

In the winter season the influence of the side wind is not very limiting due to low air temperatures and practically negligible solar irradiations. In such conditions the magnitudes of the heat flux achieved are high even with a low speed of the air streaming across the condenser. In spring, as it can be seen in the Table 1. the air temperatures over 30°C either do not appear at all or their appearance is near to negligible. Although the wind gusts are rather frequent in that time of the year, it is very unlikely that it can decrease the demanded power and can, in the worst-case scenario, increase the fuel consumption to some extent. As the operational practice of the plant confirms, the real problems obviously appear in the summer. During summer, we have practically all the negative atmospheric influences present at the same time. As previously stated, during the summer season we have the strongest solar irradiations, very high ambient temperatures with a very pronounced temperature peaks combined with the occurrence of the wind gusts of certain frequencies. The operational practice of the plant highlights the August as the most problematic month regarding the condenser performance. In August, as it can be seen in the Table 1., the frequencies of wind gusts are rather low, but temperatures are in their peak values. It becomes obvious that the wind is more of a worsening factor rather than an isolated problem in this case. Obviously that the major problem remains the high outdoor temperature, and that the air temperature should be the starting point for improving the condensers performance in this thermal power plant.

Acknowledgement

I would especially like to thank my esteemed colleagues from thermal power plant "Stanari" for all the precious help they gave me in writing this paper.

REFERENCES

- [1] Ilić, G., Vukić, M., Radojković, N., Živković, P., Stojanović, I. (2014). *Termodinamika 2 – osnove prostiranja toplote i materije (in Serbian)*. Faculty of Mechanical Engineering, University of Niš, Niš.
- [2] Kozić, Đ. (2019). *Termodinamika, inženjerski aspekti (in Serbian)*. Faculty of Mechanical Engineering, University of Belgrade, Belgrade.
- [3] Blanco, M., Santigosa, L. R. (2017). *Advances in Concentrating Solar Thermal Research and Technology*. Elsevier.
- [4] Data from meteorological station in thermal power plant "Stanari".
- [5] Global Wind Atlas. From: <https://globalwindatlas.info/>, accessed on: February 25, 2021.
- [6] Global Solar Atlas. From: <https://globalsolaratlas.info/>, accessed on: February 25, 2021.



Banja Luka
28–29 May 2021.

DEMI 2021

15th International Conference on Accomplishments in Mechanical and Industrial Engineering

www.demi.mf.unibl.org



Domestic wastewater treatment in the rural areas of the Republic of Serbia

N. Aleksić^a, V. Šušteršič^a, J. Nikolić^a, N. Rakić^a, D. Gordić^a

^aUniversity of Kragujevac, Faculty of Engineering, Sestre Janjić 6, 34000 Kragujevac

Abstract Wastewater collection and treatment have a wide range of impacts on the environment and the economy, both locally and globally. The lack of a sewage system outside of central urban areas and the insufficient number of constructed and operative wastewater treatment plants are leading problems concerning the management and treatment of municipal, domestic, and industrial wastewater in the Republic of Serbia. In the Republic of Serbia, about 418 million m³ of wastewater was discharged in 2019, from which 308 million m³ was wastewater from municipalities with a public sewage system. Currently, only about 64 % of the population has a connection to the public sewage system and Serbia treats approximately 48 million m³ of wastewater. The highest number of people, about 44% of the population, lives in rural settlements and discharges wastewater from their households into septic tanks. For small communities in the rural settlements, on-site treatment technologies using natural systems are a highly efficient, adequate, and inexpensive treatment. This paper provides an overview of the situation in the wastewater sector in the Republic of Serbia and discusses on-site treatment technologies and/or the possibility of reuse of household wastewater in rural settlements that aren't connected to the sewage system in the Republic of Serbia.

Keywords Domestic wastewater, rural settlements, decentralized treatment, Republic of Serbia

1. INTRODUCTION

According to the Our World in Data, in 2017, 4.1 billion people were living in urban areas, and 3.40 were living in rural areas [1]. That means that globally, more people live in urban areas than in rural areas, with 55 % of the world's population was living in urban areas in 2018 [2]. The percentage of people living in rural areas will steadily decrease as people migrate from rural areas into cities, but currently, the percentage of people living in rural areas is still huge. The way of life in rural

areas is quite different than in urban areas. Rural areas are not densely populated nor developed as urban areas. In rural areas usually, there are no sewers, no system for the collection of wastewater nor wastewater treatment systems [3]. Today, the large amounts of untreated wastewater from rural areas are discharged into the ground, and rural lakes, rivers and groundwater are becoming major sources of environmental pollution and potential health hazards for the local population [4]. Domestic wastewaters have a significant impact on sources of environmental pollution. Domestic wastewater characteristics in rural areas are different from the characteristics of wastewater from urban cities. The content of organic matter and nutrients is higher, and the content of heavy metals and other inorganic pollutants is lower [3]. Affordable and effective

Corresponding author

Junior researcher, Natalija Aleksić, natalija94u@gmail.com

University of Kragujevac, Faculty of Engineering
Sestre Janjić 6
34000 Kragujevac, Republic of Serbia

domestic wastewater treatment is a critical issue in public health and disease prevention around the world, particularly so in developing countries that often lack the financial and technical resources necessary for proper treatment facilities [5]. Also, in many countries, it is required from small communities to treat wastewater discharges to increasing standards of lesser environmental impacts but must achieve that goal at locally sustainable costs [6]. For the treatment of domestic wastewater in rural areas in many countries, decentralized system is used. Decentralized wastewater treatment systems are designed to operate at a small scale. Decentralized wastewater treatment systems can reduce the effects of wastewater disposal on the environment and public health, but may also increase the ultimate reuse of wastewater, depending on community type, technical options, and local settings [7]. According to available data, in 2019, in the Republic of Serbia approximately 44 % of the population reside in rural areas [8], and over 35 % of them are not served by sewage systems, including the wastewater treatment plants [9]. The percentage of the rural population connected to the public sewage system is about 9% [10] and they mainly discharge their wastewater into septic tanks, threatening groundwater, which accounts for 73% of Serbia's drinking water supply [11].

2. RURAL SETTLEMENTS IN THE REPUBLIC OF SERBIA

The Republic of Serbia covers an area of 88,361 km², and it is populated by 7 186 862 inhabitants, according to the latest data [12]. Administratively, the territory of the country consists of two autonomous provinces Kosovo and Metohija and Vojvodina and 174 local self-government units-[13].

The classification of urban and rural areas presents an essential topic in scientific research. In the Republic of Serbia, official national statistics use legal criteria to determine the type of settlement [12]. Following these criteria, settlements are defined as urban according to the decision of the local authorities. Settlements that are not covered by this criterion are classified in the category of "other", and automatically considered rural [14]. Fig. 1 presents statistical classification at the settlement level in the Republic of Serbia.

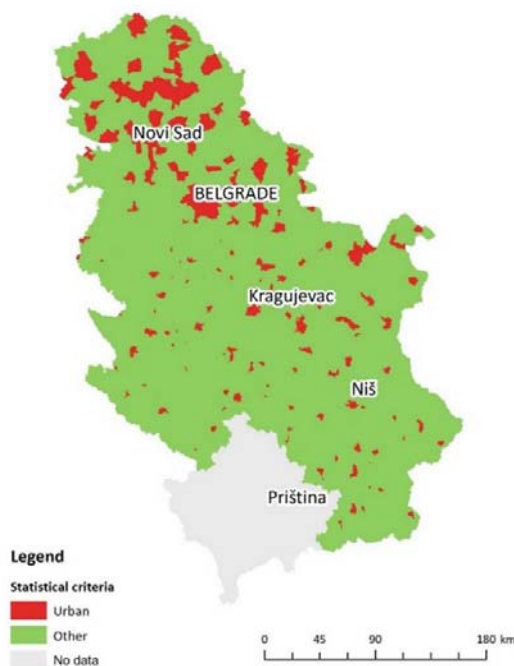


Fig. 1. Statistical classification at the settlement level [12]

The total population in the Republic of Serbia was 6 944 975 in 2019. About 3 907 243 (56.26 %) was classified as an urban population, and 3 037 732 (43.74 %) as a rural population [15]. According to the latest census, in 2011, there were 167 urban settlements in Serbia, and 4542 settlements were classified as "other". In 2011 about 59.44 % of inhabitants lived in urban settlements, while 40.6 % lived in other settlements. Also, 90.69% of settlements in Serbia have fewer than 2000 inhabitants, and 25% of the population of Serbia lives in these settlements [13]. According to the size, settlements with less than 500 inhabitants dominate, followed by settlements with 500-999 inhabitants, Table 1 [16].

Table 1. Number of settlements according to population size [16]

	Urban settlements		Rural settlements	
	Total	%	Total	%
> 500	5	2.99	2950	64.95
500 - 999	3	1.80	845	18.60
1000 - 1999	8	4.79	460	10.11

Depending on the level of urbanization, the connection to the public sewerage network is diverse in different parts of Serbia. Fig. 2 shows the number of households connected to the public sewage system.

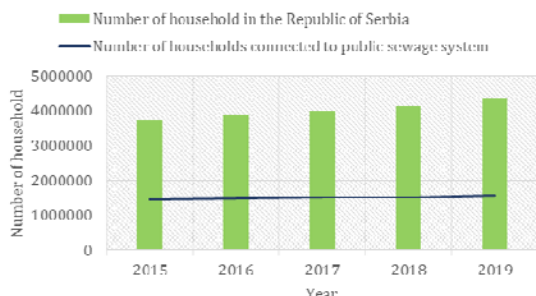


Fig. 2. Number of households connected to public sewage system [12]

Of the total number of inhabitants in Serbia, a relatively large number of both urban and rural inhabitants are not connected to the public sewage system, and mostly they use septic tanks for the discharge of wastewater from the households [17]. The urban/rural coverage with a sewage system is 87.5 and 22.2%, respectively [17]. Fig. 3 shows wastewater discharged from the municipality with/without public sewage systems.

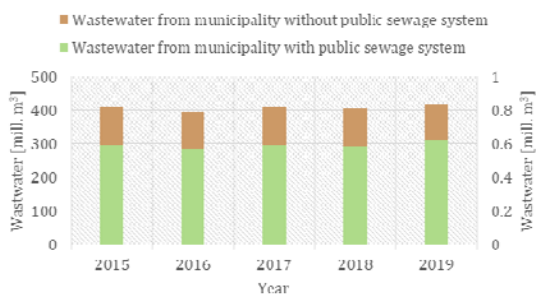


Fig. 3. Wastewater discharged from the municipality with/without public sewage systems [12]

In 2019, the total amount of wastewater from settlements was higher by 3.5% than in the reference period in 2018. The amount of wastewater discharged into the public sewer was increased by 5.3% compared to the same period in 2018. The amount of discharged wastewater into septic tanks is lower by 1.2% compared to 2018 [18]. When it comes to the discharge of wastewater into the sewage system

in 2019 compared to 2018, households recorded an increase of 5.5%, the industrial sector increase of 5.4%, and other users an increase of 3.9 %, Fig. 4.



Fig. 4. Discharged wastewater from settlements according to type [18]

The previous figure shows that a large amount of discharged wastewater comes from households as domestic wastewater. Currently, there are no data for domestic wastewater of small settlements (rural areas). With a large proportion of Serbia's population remaining in small settlements (communities of < 2000 inhabitants), it can be estimated that the amount of domestic wastewater is significant. Also, rural coverage with a sewage system is only 22.2%, which means that there are possibilities for planning and constructing different domestic wastewater treatment plants for small settlements that are not connected to the sewerage network. Solving these problems would have a significant impact on wastewater management in the Republic of Serbia. Pressure on surface and ground waters from non-point sources of pollution remains relatively low, but it is noted that septic tanks in small communities do represent an issue of concern for Local government units [19]. Also, to align with EU environmental standards, 320 wastewater treatment facilities should be constructed in Serbia [10] and solving the wastewater treatment in rural areas could contribute to wastewater management goals.

3. DECENTRALIZED SYSTEMS

Decentralized wastewater treatment consists of a variety of approaches for collection, treatment, and dispersal/reuse of wastewater for individual households, institutional or industrial facilities, entire communities, etc.

Nowadays, decentralized systems can be designed for a specific site, thus overcoming the problems associated with site conditions [20]. Therefore, these systems can easily be applied and used in rural areas. Treatment options range from simple and cost-effective, passive treatments with soil dispersion, usually referred to as septic or on-site systems, to complex and mechanized or biological approaches providing advanced treatment by collecting and treating waste from buildings and discharging to either

soil or surface waters [21]. Fig. 5 presents the operational diagram of a typical decentralized wastewater treatment system with methods of treatment.

The concept of decentralized wastewater treatment has been implemented in various developed and developing countries of the world.

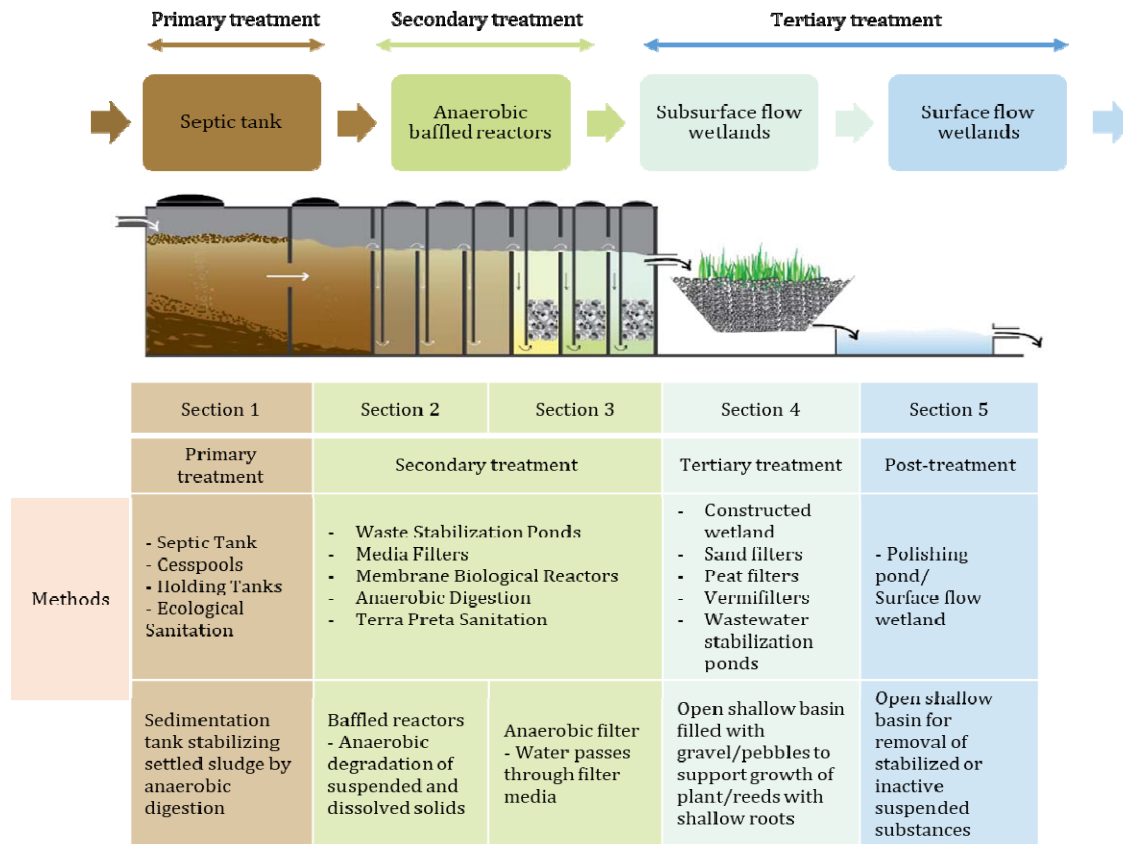


Fig. 5. Operational diagram of a typical decentralized wastewater treatment system [21-24]

Many authors described the application of decentralized systems in small communities /rural areas in different countries.

Guo et al. [25] carried out the study between 2009 and 2011 in rural areas in China. Aim of the study was to assess problems involved with decentralized treatment in villages. They found out that decentralized treatment is the most popular wastewater treatment method in villages, and that the most common primary treatment technology used in rural areas is the septic tank. The use of septic tanks in rural

areas of the Republic of Serbia is the primary technology for the treatment of domestic wastewater. There are no available data about decentralized systems in the Republic of Serbia. Istenic et al. [26] provided the first international survey data from Central and East European countries focused on small, decentralized rural treatment systems including nature-based systems (such as treatment wetlands). There are some countries with long-term good experience with this type of process, Table 2.

Table 2. Statistics data of nature-based wastewater treatment plants (WWTP) in some countries [26]

Country	Inhabitants connected to nature-based WWTPs (10 ³)	Total numbers of nature-based WWTPs (-)	Total number of treatment wetlands (-)
Bulgaria	0	5	5
Czech. Rep.	120	740	690
Estonia	9	197	14
Hungary	5	32	10
Latvia	55	10	10
Lithuania	No data	No data	No data
Poland	50	1000	500
Romania	0	6	6
Slovakia	0	10	5
Slovenia	5	80	80
Ukraine	343	1570	65
Total	537	3650	1385

Brunner et al. [27] examined the affordability of decentralized wastewater treatment systems for future users in rural areas, based on their experience in planning the decentralized wastewater treatment systems for slums of two rural towns in India. Planning on these decentralized wastewater treatment systems may generalize and apply to other developing countries seeking socially acceptable low-cost solutions with reasonable pollution reduction for resolving the sanitation crisis. Datta et al. [28] analysed constructed wetlands for the treatment of rural wastewater in semi-arid tropic villages. Constructed wetlands provide improved wastewater management and increased water efficiency. This study was conducted in Telangana in Kothapally village. The treated wastewater was stored in a farm pond and was utilized for irrigation in the nearby agricultural fields, and this perennial source of water helped nearby farmers to cultivate two additional crops. The study demonstrated that villagers manage to use a constructed wetland to treat the wastewater generated from their households. They reused water for irrigation. Also, many authors proposed applying multi-criteria decision analysis for selecting appropriate decentralized treatment technology. Younes [29] used the Median Ranked Set sample and

Analytic Hierarchy Process to improve the decision-making process in choosing the proper decentralized system for wastewater treatment in rural areas. According to the study, the best-decentralized option for wastewater treatment in rural areas, based on a cluster level, is using activated sludge as a wastewater treatment technology. The modified septic tank is the best treatment option for wastewater treatment on a household level. The introduced integrated model may offer a promising tool to improve the decision-making process. Also, it would help the environmental planners in terms of uncertainty reduction and subjectivity of human judgments.

Decentralized systems allow flexibility in wastewater treatment management. Also, it is possible to combine processes to meet treatment goals and address environmental requirements. Decentralized systems provide an opportunity to reuse wastewater in agriculture without contaminating surface water bodies and groundwater.

4. DISCUSSION

Decentralized systems are applied in areas where centralized systems do not exist, and the individual houses are scattered over a large area. There is a high level of knowledge regarding the implementation and performance of decentralized wastewater systems at the expert and scientific levels. However, the transfer into practice is insufficient, and there are low awareness and recognition of these systems at the institutional and administrative levels. Moreover, there is also a lack of good examples of decentralized systems in the Republic of Serbia. Domestic wastewater treatment technology in rural areas changes according to social conditions and takes the most suitable form for a society (inhabitants) that uses the technology. When the technology of treatment used in one country is conveyed to another country, it is necessary to examine its adaptability from various aspects. Choosing the most appropriate option for the domestic wastewater treatment in rural areas requires a thorough analysis of all factors such as simplicity of design and construction, operation and maintenance, cost, environmental impact, cultural acceptability, simplicity of design and construction, operation and maintenance, local conditions. Septic tanks are usually wastewater

treatment solutions in the rural areas of the Republic of Serbia. This solution allowed domestic wastewater to be used for obtaining agricultural fertilizer, but now this solution is not enough because of stricter environmental standards.

When choosing the decentralized systems in rural areas, the following aspects must be assessed:

- Location of rural settlements or households.
- The number of inhabitants.
- The flow and the amount of the domestic wastewater for chosen rural settlements or households - usually is estimated based on well-known formulas. The flow and the amount of the wastewater are comparable to results of the Statistical Office of the Republic of Serbia for wastewater of urban inhabitants and industry. That results could indicate the significance of wastewater pollution in those rural settlements or households.
- Characteristics of domestic wastewater.
- Type of decentralized system for wastewater treatment - conducting environmental impact assessment studies.
- Treatment efficiency.
- Reuse of treated domestic wastewater.
- Financial demands for construction of decentralized wastewater treatment.
- The operation process, maintenance, health, hygiene, and other aspects.

Choosing the proper decentralized system is a multi-criteria decision-making problem that requires extensive operational, financial, environmental, social, and technical evaluations. The environmental decision-making process is complex and has a high uncertainty degree. Objective determination and constructing an appropriate hierarchical structure are essential for the process because of conflict of interests among local units and inhabitants of small settlements. Rural residents generally have limited finances, so it is difficult to raise the capital required to invest in and construct decentralized systems. In addition to increasing government investment, to secure enough social funds to address this problem it is significant to establish a long-term financial security system.

5. CONCLUSION

Currently, emission-quality standards for the urban wastewater treatment plant also are applied for rural wastewater. Achieving these standards is challenging, and unrealistic because of the typical economic situation in rural areas. Therefore, characteristics of rural areas must be taken into account when new sewage, drainage, and water quality standards are developed.

Applying of decentralized wastewater treatment system is considered a powerful solution for the domestic wastewater problem of rural areas. Decentralized systems help communities achieve the goals of sustainability: good for the environment, good for the economy and the people. Treated wastewater could be reused in agriculture, into households for toilet flushing, for landscaping, and surface storage ponds, environmental and recreation, groundwater recharge. In Serbia, about 44% of the population lives in rural settlements and discharges wastewater from their households into septic tanks. Further research is needed to study and gather information for the selection of appropriate sites and the installation of decentralized systems in rural areas in the Republic of Serbia.

Acknowledgement

This research has been supported by the Ministry of Education, Science and Technological Development, Republic of Serbia (Project III 42013).

REFERENCES

- [1] Ritchie, H., Roser, H. (2018). Urbanization. Published online at OurWorldInData.org. From: <https://ourworldindata.org/urbanization>, accessed on: March 02, 2021.
- [2] United Nations. (2019). *World Urbanization Prospects: The 2018 Revision*. Methodology, Department of Economic and Social Affairs, Population Division, United Nations publication, Sales no. E19.XIII.7.
- [3] Chen, F., Yao, Q. (2014). The Development of Rural Domestic Wastewater Treatment in China. *Advanced Materials Research*, vol. 1073-1076, p. 829-832. DOI: [10.4028/www.scientific.net/amr.1073-1076.829](https://doi.org/10.4028/www.scientific.net/amr.1073-1076.829)

- [4] Mateo-Sagasta, J., Marjani Zadeh, S., Turrall, H. (2017). *Water pollution from agriculture: a global review*. The Food and Agriculture Organization of the United Nations, Rome, and the International Water Management Institute on behalf of the Water Land, and Ecosystems research program, Colombo.
- [5] Mara, D. (2013). *Domestic Wastewater Treatment in Developing Countries*. Routledge.
- [6] Capodaglio, A., Callegari, A., Ceconet, D., Molognoni, D. (2017). Sustainability of decentralized wastewater treatment technologies. *Water Practice and Technology*, vol. 12, no 2, p. 463-477. DOI: [10.2166/wpt.2017.055](https://doi.org/10.2166/wpt.2017.055)
- [7] Boguniewicz-Zabłocka, J., Capodaglio, A. (2017). Sustainable Wastewater Treatment Solutions for Rural Communities': Public (Centralized) or Individual (On-Site) – Case Study. *Economic and Environmental Studies*, vol. 17, p. 1103-1119. DOI: [10.25167/ees.2017.44.29](https://doi.org/10.25167/ees.2017.44.29)
- [8] The World Bank. Rural population - Serbia. From: <https://data.worldbank.org/indicator/SP.RUR.TOTL?locations=RS>, accessed on: March 03, 2021.
- [9] Gavrilović, D. (2020). *Municipalities and regions in the Republic of Serbia, 2020*. Statistical Office of the Republic of Serbia, Belgrade. ISSN: [2217-798](https://doi.org/10.2217-798)
- [10] Flanders Investment & Trade. (2017). *Water Sector in Serbia*. Economic and Trade, Office Embassy of Belgium, Belgrade.
- [11] World Bank. (2015). *Water and wastewater services in the Danube region: Serbia country note*. Washington.
- [12] Gavrilović, D. (2020). *Statistical Yearbook of the Republic of Serbia, 2020*. Statistical Office of the Republic of Serbia, Belgrade. ISSN: 0354-4206
- [13] Gajić, A., Krunić, N., Protić, B. (2021). Classification of Rural Areas in Serbia: Framework and Implications for Spatial Planning. *Sustainability*, vol. 13, no. 4:1596. DOI: [10.3390/su13041596](https://doi.org/10.3390/su13041596)
- [14] Bogdanov, N. (2007). *Small rural households in Serbia and rural non-agricultural economy*. DIS PUBLIC d.o.o., Beograd.
- [15] The World Bank. Urban population - Serbia. From: <https://data.worldbank.org/indicator/SP.URB.TOTL?locations=RS>, accessed on: March 05, 2021.
- [16] Mitrović, M. (2015). *Villages in Serbia - Changes in structure and problems of sustainable development*. Statistical Office of the Republic of Serbia, Belgrade.
- [17] Arcadis Ecolas & Institute for European Environmental Policy (2007). 06/11347 - Task 2 - Benefits for fYRoM and other countries of SEE of compliance with the environmental acquis, Final Report– Part II: Country-specific report Serbia.
- [18] Statistical Office of the Republic of Serbia, Urban wastewater, 2019. From: <https://www.stat.gov.rs/en-US/vesti/20200522-otpadne-vode-iz-naselja-2019/?a=25&s=0>, accessed on: March 10, 2021.
- [19] The International Commission for the Protection of the Danube River, Serbia. From: <https://www.icpdr.org/main/danube-basin/serbia>, accessed on: March 10, 2021.
- [20] Massoud, M., Tarhini, A., Nasr, A. (2009). Decentralized approaches to wastewater treatment and management: Applicability in developing countries. *Journal of Environmental Management*, vol. 90, no. 1, p. 652-659. DOI: [10.1016/j.jenvman.2008.07.001](https://doi.org/10.1016/j.jenvman.2008.07.001)
- [21] Khalid, U., Orozco Garcia, C. (2019). Integrated Decentralised Wastewater Treatment for Rural Areas with a Focus on Resource Recovery. RUVIVAL Publication Series, vol. 4, -, p. 39-64. DOI: [10.15480/882.1740](https://doi.org/10.15480/882.1740)
- [22] Gutterer, B., Sasse, L., Panzerbieter, T., Reckerzügel, T. (2009). *Decentralised Wastewater Treatment Systems (DEWATS) and Sanitation in Developing Countries*. Water, Engineering and Development Centre, UK.
- [23] Al-Muyeed, A. (2017). Technical guidelines for designing a decentralised waste water treatment system. Water Aid, From: https://www.pseau.org/outils/ouvrages/wateraid/technical_guidelines_for_designing_a_decentralised_waste_water_treatment_system_2017.pdf, accessed on: March 14, 2021.
- [24] Lourenço, N., Nunes, L.M. (2020). Review of Dry and Wet Decentralized Sanitation Technologies for Rural Areas: Applicability, Challenges and Opportunities. *Environmental Management*, vol. 65, no. 5, p. 642–664. DOI: [10.1007/s00267-020-01268-7](https://doi.org/10.1007/s00267-020-01268-7)
- [25] Guo, X., Liu, Z., Chen, M., Liu, J., Yang, M. (2014). Decentralized wastewater treatment technologies and management in Chinese villages. *Frontiers of Environmental Science & Engineering*, vol. 8, no. 6, p. 929–936. DOI: [10.1007/s11783-013-0623-z](https://doi.org/10.1007/s11783-013-0623-z)
- [26] Istenic, D., Bodík, I., Bulc, T. (2014). Status of decentralised wastewater treatment systems and barriers for implementation of nature-based systems in central and eastern Europe. *Environmental Science and Pollution Research*, vol. 22, no. 17, p. 12879–12884. DOI: [10.1007/s11356-014-3747-1](https://doi.org/10.1007/s11356-014-3747-1)
- [27] Brunner, N., Starkl, M., Kazmi, A.A., Real, A., Jain, N., Mishra, V. (2018). Affordability of

- Decentralized Wastewater Systems: A Case Study in Integrated Planning from INDIA. *Water*, vol. 10, no. 11:1644. DOI: [10.3390/w10111644](https://doi.org/10.3390/w10111644)
- [28] Datta, A., Singh, H., Raja, S., Dixit, S. (2021). Constructed wetland for improved wastewater management and increased water use efficiency in resource scarce SAT villages: a case study from Kothapally village, in India. *International Journal of Phytoremediation*, p. 1-10. DOI: [10.1080/15226514.2021.1876627](https://doi.org/10.1080/15226514.2021.1876627)
- [29] Younes, M.K. (2020). Integration of Mathematical Median Ranked Set Sample and Decision Making AHP Tools to Enhance Decentralized Wastewater Treatment System *Journal of Water Chemistry and Technology*, vol. 42, p. 472-479. DOI: [10.3103/S1063455X20060132](https://doi.org/10.3103/S1063455X20060132)



Banja Luka
28–29 May 2021.

DEMI 2021

15th International Conference on
Accomplishments in Mechanical and
Industrial Engineering

www.demi.mf.unibl.org



Optimization of the cooling system of the refrigerated display case in the supermarket

Ivan Rajič^a, Diana Bogdan^b, Petar Gvero^c

^a*Energoing d.o.o., Medjugorje, BiH*

^b*Faculty of Mining Prijedor, University of Banja Luka, BiH*

^c*Faculty of Mechanical Engineering Banja Luka, University of Banja Luka, BiH*

Abstract Supermarkets are places where modern man mainly procures basic foodstuffs. A large number of food products that are stored in the refrigerated display cases of supermarkets also require large refrigeration space, which directly affects the increase in electricity consumption. One of the ways to achieve an energy efficient cooling system in refrigerated display. One of the ways to achieve an energy efficient cooling system in refrigerated display cases is the use of electronic expansion valve (EEV) controlled by a PID controller (Proportional – Integral – Derivative). PID enables process control with lower compressor pressure and lower condensing temperature as well as better adaptation of the cooling system variation of external temperature compared to cooling system with a conventional thermal expansion valve. In this paper are analyzed two scenarios of the cooling cycle of electricity consumption of a refrigerated display case in a supermarket located in Mostar with the aim of obtaining a solution on possible electricity savings. The first scenario is a thermostatic expansion valve (TEV), and the second scenario is a refrigerated display case in which a cooling process using a electronic expansion valve (EEV). The Software package Solkane 8 was used for the technical analysis of the system [1] Considering the price of equipment and the difference in annual electricity consumption, the comparison of the results of technical-economic analysis of the cooling system according to condensing temperature achieves a return on investment in the second year of operation, but after a period of operation of 3 years, 11% energy savings are achieved in relation to cooling systems for the same purpose equipped with TEV.

Keywords refrigerated display, TEV, EEV, electricity, PID controller

1. INTRODUCTION

Corresponding author

PhD Petar Gvero, Banja Luka, Faculty of Mechanical Engineering University of Banja Luka
petar.gvero@mf.unibl.org

MSc Diana Bogdan, Prijedor, Faculty of Mining University of Banja Luka, rtrs.diana@gmail.com

BSc Ivan Rajič, Medjugorje, Energoing d.o.o Leopolda Mandića 3, energoing@tel.net.ba

Energy efficiency is an intelligent way to improve and secure energy supply, to increase competitiveness and standards, as well as to reduce negative impacts of energy systems on the environment. There are numerous advantages to applying energy efficiency improvement measures in final consumption, services and energy distribution. One of these measures is the installation of electronic equipment to control refrigeration systems to reduce electricity wastage.

For this purpose, an analysis of the operation of the refrigerated display cases of supermarkets in city Mostar is performed for two scenario:

- TEV Scenario; a refrigerated display case in which the cooling process is controlled by TEV, and
- EEV Scenario; a refrigerated display case in which the cooling process is controlled by EEV and a condensing temperature controller.

Refrigerated display cases and chambers are used to store food products in supermarkets and are significant consumers of electricity [7]. Most often, the cooling process in such refrigerated cabinets is controlled by means of a TEV. The cooling process controlled by TEV is characterized by:

- adjustment of the bending temperature is done by means of a TEV spring,
- classic way of process control; there is no possibility to regulate the operation of the condenser at lower temperatures and pressures during cold days and
- high costs for electricity that are a direct consequence of the application of this method of controlling the cooling process.

The cooling process controlled by EEV is characterized by:

- process control using controllers and probes,
- the cooling system operates at lower condensing pressure and temperatures compared to TEV process control and
- automatic condenser control better coordinates the operation of the system during the changes in ambient temperatures, which significantly reduces the required compressor power compared to a TEV controlled system.

Numerous practical examples [3] have shown that the application of electronic application in food cooling system achieves significant energy savings.

1.1 Refrigeration system analysis TEV Scenario

Refrigerated display cases in supermarkets are energy consumers operating in medium temperature (MT), and low temperature mode (LT). The temperature of the refrigerated space

of cold cabinets in MT mode is (0 - 8) °C, while for LT mode is ((-25) - (-18)) °C. Cooling system energy conversion process according TEV Scenario take place between operating pressures $p_1 = 3 \text{ bar}$ and $p_2 = 18 \text{ bar}$. Water or air cooled condensers are most commonly used in such systems. The process of transformations the pressure of the condensed working medium to the evaporating pressure is performed in a TEV. In addition to meeting the requirements of the cooling system, when designing adequate cooling capacity it is necessary to take into account heat losses to the environment. Cold air that goes outside the frame of a vertically placed refrigerated display case is the cause of heat loss to the environment about 64% [3].

The basic components of the cooling system to the TEV Scenario shown in Fig. 1 are:

- 4 refrigerated cabinets operating in “plus temperature mode” ((+2)-(+4))°C. The cooling capacity of each cabinet $Q_c = 4 \text{ kW}$,
- refrigeration power of compressor $P_{comp.} = 19 \text{ kW}$, operates at evaporation temperature $T_{evap.} = -10^\circ\text{C}$, and condensation temperature $T_{cond.} = 45^\circ\text{C}$,
- pipeline with safety and controlled armature and
- valve TEV [3].

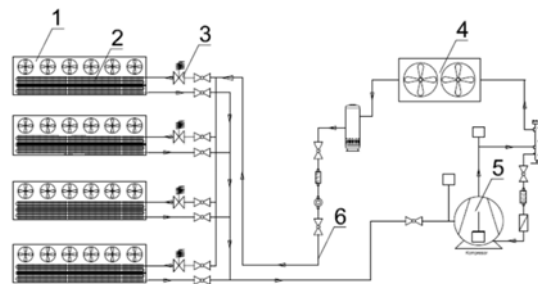


Fig. 1 Shema of cooling system – TEV Scenario
Legend: 1 - refrigerated display case; 2 – exchanger; 3 – TEV; 4 - controller refrigerated display case; 5- capacitor; 5 - compressor; 6 – pipeline with armature.

Ambient temperature values presented in “Table 1 Electricity consumption TEV Scenario” represent the average values of air temperatures for the area of city Mostar in the period of years (2015 – 2019)[2]. The calculation also takes into account the reserve of the compressor as well as the defrost time.

Based on this, the daily operation of the compressor of 18 hour adopted. Throughout the year, the refrigeration system operates in the mode 18/24 hours. The working substance is freon R404, which is the most common fluid in supermarkets systems (large consumers).

Table 1. Electricity consumption TEV Scenario

Den u godini	Sat	2015.god.	2016.god.	2017.god.	2018.god.	2019.god.	2015-2019	Temperatura deležanja (°C)	Temperatura isparivača (°C)	Ušatak isparivača (kW)	Ušatak kondenzera (kW)	Snaga komp. (kW)	COP [1]	Protok (g/s)	Poroznja eten (kWh)
1.1.	00:00	-2.8	0.6	3.4	4.1	7.4	2.5	45	-10	0	0	0	0	0	0
1.1.	01:00	-3	0.1	2.6	4.1	7.4	2.2	45	-10	16	22.5	6.49	2.46	155.47	6.49
1.1.	02:00	-3	-0.4	2.3	4.2	7.3	2.1	45	-10	0	0	0	0	0	0
1.1.	03:00	-2.9	-0.6	1.8	4.2	7.4	2.0	45	-10	16	22.5	6.49	2.46	155.47	6.49
1.1.	04:00	-2.8	-0.7	1.5	4.4	7.4	2.0	45	-10	0	0	0	0	0	0
1.1.	05:00	-3	-0.7	1.3	4.5	7.3	1.9	45	-10	16	22.5	6.49	2.46	155.47	6.49
22.7.	11:00	39.7	316	371	331	35	39.7	45	-10	0	0	0	0	0	0
22.7.	12:00	40.8	342	374	337	35.2	36.9	45	-10	16	22.5	6.49	2.46	155.47	6.49
22.7.	13:00	41.9	356	378	338	36.1	37.1	45	-10	16	22.5	6.49	2.46	155.47	6.49
22.7.	14:00	39.8	355	376	334	35.2	36.3	45	-10	16	22.5	6.49	2.46	155.47	6.49
22.7.	15:00	39.7	352	365	326	32.2	35.2	45	-10	16	22.5	6.49	2.46	155.47	6.49
31.12.	16:00	5.7	7	5.6	8.2	6.9	6.7	45	-10	16	22.5	6.49	2.46	155.47	6.49
31.12.	17:00	4.9	6.4	4.2	8	6.7	6.0	45	-10	0	0	0	0	0	0
31.12.	18:00	4.4	5.5	2.9	7.9	6.8	5.7	45	-10	16	22.5	6.49	2.46	155.47	6.49
31.12.	19:00	3.4	5.4	3.9	7.5	6.7	5.4	45	-10	16	22.5	6.49	2.46	155.47	6.49
31.12.	20:00	2.8	4.4	3.9	7.7	6.8	5.1	45	-10	16	22.5	6.49	2.46	155.47	6.49
31.12.	21:00	2	4.8	3.9	7.3	6.3	4.9	45	-10	16	22.5	6.49	2.46	155.47	6.49
31.12.	22:00	1	4.3	3.6	7.4	5.7	4.4	45	-10	16	22.5	6.49	2.46	155.47	6.49
31.12.	23:00	0.7	4	3.6	7.4	5.9	4.3	45	-10	0	0	0	0	0	0

Cooling system analyses TEV Scenario is performed by entering the set values of condensation and evaporation temperature for each operating hour of the year in the Solkane 8 software package. The condensing temperature taken into account is the most unfavorable design value of the temperature characteristic of the environment in which the cooling system is located. Based on the inlet temperatures, the values of the mass flow of the refrigerant, the required power of the condenser, evaporator and compressor as well as the values of the cooling coefficient of the process necessary for the calculation of electricity consumption are obtained. According to the results of the analysis of the cooling system according to the TEV Scenario shown in "Table 1 Electricity consumption TEV Scenario" it can be concluded that every operating hour, regardless of external conditions, the power of the compressor and evaporator is constant.

The system consumes 6,9 kWh of electricity, ie constantly the same amount of energy is taken from the city network and reserved for these types of consumers. Also, in "Table 1 Electricity consumption TEV Scenario" it is noticed that the classic cooling system with TEV does not have the possibility to adapt to variations in outdoor temperature, i.e. at ambient temperatures $T_{amb.} < 10^{\circ}\text{C}$ system works according to the design inlet temperatures and consumes the same amount of energy. Total electricity consumption of the cooling system TEV Scenario for a period of one year $E_{el.e} = 42639 \text{ kWh}$.

1.2 Refrigeration system analysis EEV Scenario

Cooling system EEV Scenario has shown in Fig.2 contains the same component and their parameters as the cooling system TEV Scenario other than TEV, which has been replaced by an EEV and a controller that controls the condensing temperature. Built-in probes measure the inlet and outlet air temperature in the exchanger and the gas temperature at the evaporator outlet and control the EEV. Also, the probes are placed before and after the compressor and condenser controlled by the controller, so that the condensing temperature depends on the outside temperature. In conditions of lower outdoor temperature, the condensing temperature is reduced, and thus the value of the operating pressure of the condenser of cooling system is lower.

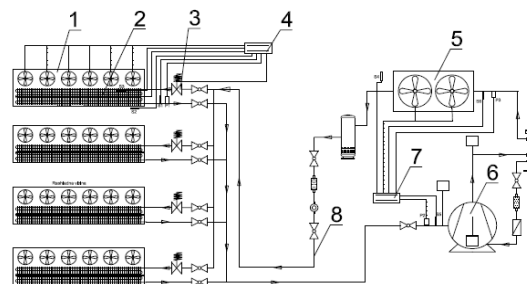


Fig. 2 Shema of cooling system EEV Scenario
 Legend: 1 - refrigerated display case; 2 – exchanger; 3 – EEV; 4 - controller refrigerated display case; 5- capacitor; 6 – compressor; 7 – compressor controller; 8 – pipeline with armature

The cooling system analysis procedure EEV Scenario is performed in the same way as the cooling system analysis TEV Scenario. According to the results of the analysis shown in Table 1.2. it can be concluded that in relation to the classical cooling system with TEV, the working process of the cooling system with EEV for the same $T_{evap} = -10^{\circ}\text{C}$ takes place at lower condensation temperatures. Also, the power consumption changes in relation to the outside temperature T_v for the following conditions:

- for conditions when $T_{v+10} \leq 20^{\circ}\text{C}$ (T_{v+10} is outdoor temperature increased by 10°C , the minimum electricity consumption ($E_{el.e} = 2.93 \text{ kWh}$),

- for conditions when ambient temperatures are significantly higher than 10°C, which is often the case for southern areas, electricity consumption is adjusted to the temperature conditions and
- for the conditions when $T_{v+10} \geq 45^\circ\text{C}$ electricity consumption $E_{el.e} = 6.49 \text{ kWh}$, according to the design temperature, is the consumption of systems with TEV.

- cooling system energy consumption EEV Scenario is lower by about 41% compared to TEV Scenario for the coldest day of the year 08.01.

Table 2 Electricity consumption EEV Scenario

Den u godini	Set	2015.god.	2016.god.	2017.god.	2018.god.	2019.god.	2015-2019	Temp.komp.denzacije (°C)	Temp.isparavanja (°C)	Učinek isparavanja (kW)	Učinek kondenzacije (kW)	Snaga komp. (kW)	COP [-]	Protok (t/s)	Potrošnja elen (kWh)
1.1.	00:00	-2.8	0.6	3.4	4.1	7.4	2.5	20	-10	0	0	0	0	0	0
1.1.	01:00	-3	0.1	2.6	4.1	7.4	2.2	20	-10	16	18.9	2.93	5.47	112.79	2.93
1.1.	02:00	-3	-0.4	2.3	4.2	7.3	2.1	20	-10	0	0	0	0	0	0
1.1.	03:00	-2.8	-0.6	1.8	4.2	7.4	2.0	20	-10	16	18.9	2.93	5.47	112.79	2.93
1.1.	04:00	-2.8	-0.7	1.5	4.4	7.4	2.0	20	-10	0	0	0	0	0	0
1.1.	05:00	-3	-0.7	1.3	4.5	7.3	1.9	20	-10	16	18.9	2.93	5.47	112.79	2.93
22.7.	11:00	39.7	33.6	37.1	33.1	35	35.7	-10	0	0	0	0	0	0	0
22.7.	12:00	40.8	34.2	37.8	33.7	35.2	36.3	46.3	-10	16	22.8	6.77	2.36	158.95	6.77
22.7.	13:00	41.9	35.6	37.8	33.8	36.3	37.1	47.1	-10	16	23	6.95	2.3	161.2	6.95
22.7.	14:00	39.8	35.5	37.6	33.4	35.2	36.3	46.3	-10	16	22.8	6.77	2.36	158.95	6.77
22.7.	15:00	39.7	35.2	36.5	32.6	32.2	35.2	45.2	-10	16	22.5	6.53	2.45	156	6.53
31.12.	16:00	5.7	7	5.6	8.2	6.9	6.7	20	-10	16	18.9	2.93	5.47	112.79	2.93
31.12.	17:00	4.9	6.4	4.2	8	6.7	6.0	-10	0	0	0	0	0	0	0
31.12.	18:00	4.4	5.5	3.9	7.9	6.8	5.7	20	-10	16	18.9	2.93	5.47	112.79	2.93
31.12.	19:00	3.4	5.4	3.9	7.5	6.7	5.4	20	-10	16	18.9	2.93	5.47	112.79	2.93
31.12.	20:00	2.8	4.4	3.9	7.7	6.8	5.1	20	-10	16	18.9	2.93	5.47	112.79	2.93
31.12.	21:00	2	4.8	3.9	7.3	6.3	4.9	20	-10	16	18.9	2.93	5.47	112.79	2.93
31.12.	22:00	1	4.3	3.6	7.4	5.7	4.4	20	-10	16	18.9	2.93	5.47	112.79	2.93
31.12.	23:00	0.7	4	3.6	7.4	5.9	4.3	-10	0	0	0	0	0	0	0

Total electricity consumption of the cooling system EEV Scenario for a period of one year $E_{el.e} = 25107.73 \text{ kWh}$.

2. ECONOMIC ANALYSIS

The electricity consumption of the cooling systems is a function of the ambient temperature. Economic analysis of refrigeration systems TEV and EEV Scenarios refer to:

- electricity consumption of cooling systems as a function of temperature on day 08.01. when the lowest ambient temperature in the year $T_{amb} = -0,1^\circ\text{C}$ was recorded,
- electricity consumption of cooling systems as a function of temperature on day 22.07. when the highest ambient temperature in the year $T_{amb} = 37,1^\circ\text{C}$ and
- recorded monthly energy consumption of cooling systems over a period of one year.

By comparing the diagrams of electricity consumption as a function of temperature shown in Fig. 3 and Fig. 4 cooling systems according to the proposed scenarios can be concluded:

- cooling system energy consumption EEV Scenario ($E_{el.e} = 2.93 \text{ kWh}$) is significantly lower compared to TEV Scenario ($E_{el.e} = 6.49 \text{ kWh}$) for the coldest recorded day in the year 08.01. and

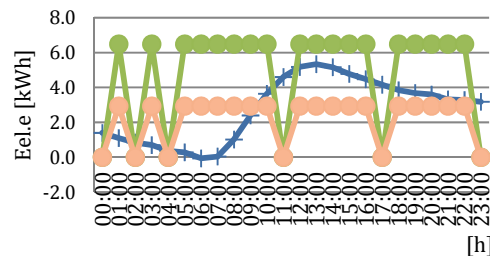


Fig. 3 Electricity consumption diagram of cooling systems TEV Scenario and EEV Scenario on day 08.01.-the coldest day of the year

Legend: — temperatura;
 ■ energy consumption TEV Scenario;
 ■ energy consumption EEV Scenario.

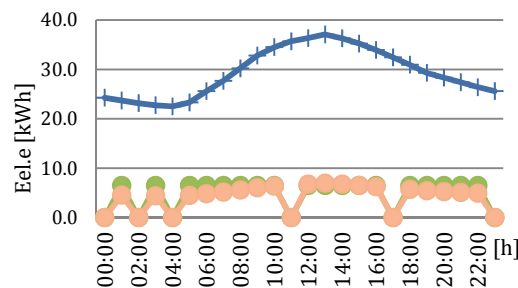


Fig. 4 Electricity consumption diagram of cooling systems TEV Scenario and EEV Scenario on 22.07. the warmest day of the year

Legend: — temperatura;
 ■ energy consumption TEV Scenario;
 ■ energy consumption EEV Scenario.

According to the electricity consumption diagram shown in Fig. 4 it can be seen that the cooling system with EEV consumes less electricity for its operation throughout the year compared to the cooling system with TEV. Namely, by installing EEV in cooling system electricity consumption was reduced from $E_{el.TEV} = 42639.30 \text{ kWh}$ on $E_{el.EEV} = 25107 \text{ kWh}$ that is $E_{el.EEV} = 0.698 \cdot E_{el.TEV}$ in 12 months.

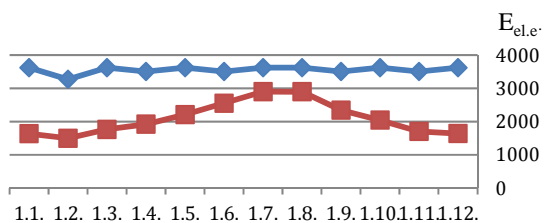


Fig. 5 Monthly diagram of electricity consumption of cooling systems TEV Scenario and EEV Scenario
 Legend: ■ electricity consumption TEV Scenario;
 ■ electricity consumption EEV Scenario.

Table 3 Annual energy consumption

Cooling system	$E_{el,e}$ [kWh]	Price $E_{el,e}$ [KM]
TEV Scenario	42639	10659.75
EEV Scenario	25107	6276.75
Saving	17532	4383.00

Therefore, for the cooling system EEV Scenario energy consumption is reduced by 41,12% (for the Mediterranean climate on annual basis). According to current prices [5] the cost of installation and conversion of the system from TEV Scenario to EEV Scenario is 9580 KM. The diagram shown in Fig. 5, i.e. if the amount of costs of changing the cooling system TEV Scenario to cooling system EEV Scenario is observed over a period of 15 years, it can be concluded that the investment would pay off after 2.5 year

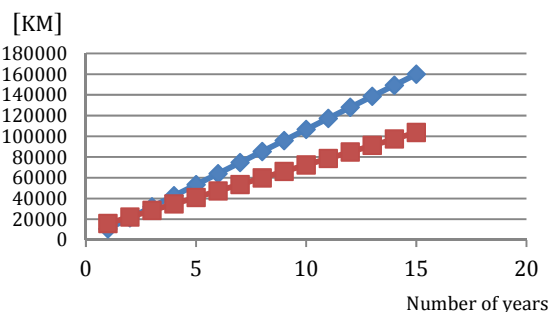


Fig. 5 Cost-effectiveness diagram of cooling system conversion TEV Scenario to cooling system EEV Scenario
 Legend: ■ cost-effectiveness TEV Scenario;
 ■ cost effectiveness EEV Scenario.

3. CONCLUSION

In this paper, a technical and economic analysis of a cooling system with 4 refrigerated cabinets with total capacity of $Q_c = 16 kW$ was performed. For each hour during the year in relation to the outside temperature, the basic parameters of the system components

(temperature and pressure) are determined. Based on the technical analysis of the systems according to two scenarios, it can be concluded that by introducing EEV control with condensing controllers, the cooling process is conducted with lower pressure and lower condensing temperature, which results in reduced electricity consumption compared to the outdoor temperature. The payback period of the cooling system installation investment EEV Scenario with condensing temperature controller is 2.5 years.

REFERENCES

- [1] <https://solkane-refrigerants.software.informer.com/download/>
- [2] Energoing d.o.o Medjugorje, energoing@tel.net.ba
- [3] Federalni Hidrometeorološki zavod, Sarajevo (2020), fhmzbih@fhmzbih.gov.ba
- [4] www.danfoss.com
- [5] JP Elektroprivreda HZ HB d.d., Mostar. (2020). ured.gen.dir@ephzhh.ba
- [6] Arias, J. (2015). *Energy usage in Supermarkets Modeling and Field Measurements, PhD Thesis*
- [7] www.google.com



Banja Luka
28–29 May 2021.

DEMI 2021

15th International Conference on
Accomplishments in Mechanical and
Industrial Engineering

www.demi.mf.unibl.org



Influences on Urban Air Quality in the City of Niš

P. Živković^a, M. Tomić^b, J. Janevski^a, M. Vukić^a, B. Radovanović^a

^aUniversity of Niš, Faculty of Mechanical Engineering, Aleksandra Medvedeva 14, Niš, Serbia

^bUniversity of Novi Sad, Faculty of Technical Sciences), Dositeja Obradovića Square 6, Novi Sad, Serbia

Abstract Air quality in urban areas is being influenced by many factors, mostly anthropogenic. Proper estimation of pollutant distribution is very important for making decisions for air quality improvement. Application of CFD techniques is giving the most detailed information about pollutant dispersion. If we consider pollution a problem, application of CFD techniques is not a solution for the problem, but an estimation tool, which gives the data needed to the environment protection experts. In this paper, influence of a large point source of pollution is being investigated, as well as the simultaneous traffic influence. As being well known that wind characteristics have the largest influence on pollutant dispersion, they were carefully treated. There are two main wind directions on the City of Niš area, so two groups of simulations were done, for each main wind direction separately. For pollutant dispersion estimation PHOENICS software package was used. The results of the numerical simulation show good agreement with the measured wind data and CO₂ concentrations.

Keywords pollution, point source; traffic, PHOENICS, COPERT, CO₂ concentration

1. INTRODUCTION

Energy, especially electrical, is of vital importance in the world today. Many assessments of the fuel resources, mostly fossil, clearly marks the fact that such resources, especially for oil, are close to the end. The need for energy constantly rises, so introduction of new resources is inevitable. All these facts points to the necessity of transition to the sustainable development, especially to the usage of renewable energy sources. Wind energy clearly takes its place, considering its large potentials, purity and availability. The present constrains are mostly of financial nature. The most important task is the *siting* of

wind turbines (obtaining the best possible locations for installing of the turbines, considering the possibility for energy production and minimization of losses). For that purpose, the wind atlas method is developed, which became easy for use with the fast development of computers. Position of wind turbine is in strong correlation with energy production. According to the previous research [1,4,5], linear models can not estimate correctly the wind energy potentials in the terrain where the ruggedness index (index that represents the terrain slope value) exceeds 0.3. In such a case, using full CFD models, followed by experimental validation is necessary. Even if all of the above mentioned is satisfied, there is possibility that the wind warm is not going to have the predicted outpun during the project lifetime, which is 25-30 years, which is about the same as the climatic periode, which lasts for 32 years.

Corresponding author

PhD, Predrag Živković
pzivkovic@masfak.ni.ac.rs

University of Niš, Faculty of Mechanical Engineering
Aleksandra Medvedeva 14
Niš, Serbia

2. MEASUREMENT

In order to make as precise estimation of the point source impact on the air quality in the City of Niš, both measurements on the District heating plant in Niš and the traffic emissions were performed simultaneously. The measurements in the District heating plant were performed over the entire heating season, when there are emissions, on the exhaust collector after the 4 existing boiler units. Traffic intensity estimation was estimated via traffic counting on six major crossroads in the City of Niš (Jagodin Mala, 7. Juli, Theater, Marger, Clinical Center and Nemanjić Blvd.). The data were collected from 5AM until 1AM the next day for each location, from the end of October to the beginning of December. For the location Jagodin Mala (red circle above the river, others are counterclockwise, as mentioned above) measurements were performed for about 10 days, for each working day and weekend in this period, as well as for 4 days in the summer [4,5].



Fig. 1. Location of the pollutant immission measuring sites

As can be seen on the Fig. 1, the measuring locations are carefully chosen and fairly represents the crossroads with highest traffic intensity in the City of Niš. This data were used to estimate the traffic intensity for each direction for all major streets in the City of Niš. It is assumed that traffic intensity for other locations and streets can be estimated on the basis of the data collected.

Simultaneously with the traffic counting, CO₂ imission measurement was performed using the TESTO 454 gas analyzer with ambient CO₂ probe 0632 1240. Measurements were performed on distances 1, 3 and 5m from the street, on height of 1m. Wind measurements were performed on 3 locations in the city, for the two years period. On

those locations, wind speed and direction, temperature and CO₂ concentration were measured on the height of 10m. Wind measurements were performed with second generation cup anemometer produced by the firm Vetrotipalnik – Ljubljana, CO₂ concentration with probe TGS4161 produced by company Figaro Engineering Inc., Japan, and temperature measurements by PT100 element with precision of 0.5^oC.

2.1 Sensor characteristics

The sensors were chosen by the specific temperature, humidity and concentration levels in the City of Niš free atmosphere. The measuring period was about two years.

2.1.1 Cup anemometer technical data

The anemometer used was manufactured by Vetrotipalnik Ljubljana. It is second generation cup anemometer, with direction sensor mounted on the same shaft with the speed sensor. During the measurement period, considering the city of Niš climate, there was no frosting of the sensor (during the winter period).

The measuring range of the anemometer is 0.5÷50m/s, with precision of 0.1m/s. Wind speed lower than 0.5m/s is measurable, but with lower accuracy. Wind direction is being measured with precision of 22.5^o, which should be improved in the following period, by applying new sensor, mounted on another shaft. Sampling rate was 0.5sec, while the measuring results are being shown as average over the 10sec period. All sensors are mounted on the 10m high mast.

Table 1. Cup anemometer technical data

Wind speed measurement	
Measuring range	0.5÷50m/s
Accuracy	±0.1m/s
Temperature range	-40÷80 ^o C
Rel. humidity range	0÷100%RH
Acquisition speed	2samples/sec
Wind direction measurement	
Measuring range	0÷360 ^o
Accuracy	±0.1 ^o
Temperature range	-40÷80 ^o C
Rel. humidity range	0÷100%RH
Acquisition speed	2samples/sec

2.1.2 CO₂ sensor technical data

The main goal of this measurement technique was developed following the need to understand the CO₂ distribution in the atmosphere, mostly performed by the wind. For this purpose, the specific measuring device was developed by the firm IMD-Niš. The sensor used as the hart od the device is TGS4161, CO₂ measurement sensor, product of the Figaro Engineering Inc., Japan. The characteristics of the sensor used are shown in the following table. From this data one can notice that the sensor can operate normally in the entire measuring range, since the lowest measured value of CO₂ concentration was just under 400ppm, and the higher about 1000ppm. For measurement on the exhaust gasses collector in the District heating plant, TESTO 454 gas analyser was used.

Table 2. CO₂ sensor technical data

Model number		TGS 4161		
Sensing element type		Solid electrolyte		
Target gases		Carbon dioxide		
Typical detection range		350 ~ 10,000 ppm		
Electrical characteristics	Heater resistance	RH	70 ± 7Ω at room temp.	
	Heater current	IH	approx. 50mA	
	Heater power consumption	PH	approx. 250mW	
	Electromotive force	EMF	220~490mV in 350ppm CO ₂	
	Sensitivity	ΔEMF	44~72mV	EMF(350ppm CO ₂)- EMF(3500ppm CO ₂)
	Heater voltage	VH	5.0 ± 0.2V (DC)	
Sensor characteristics	Response time	approx. 1.5 min. (to 90% of final ΔEMF value)		
	Measurement accuracy	approx. ±20% at 1,000ppm CO ₂		
Operating conditions		-10~50°C, 5~95%RH		
Storage conditions		-20~60°C, 5~90%RH (store in moisture proof bag with silica gel)		
Standard test conditions	Test gas condition	CO ₂ in air at 20±2°C, 65±5%RH		
	Circuit condition	VH = 5.0±0.06V DC		
	Conditioning period before test	12 hours or longer		

2.1.3 Temperature sensor technical data

The temperature sensor used is PT100 element, with precision of ±0.1°C. This measurement was added in order to ensure the comparison of the measured data with standard ones.

2.2 Results and discussion

2.2.1 Traffic measurement

From the data obtained by the IT Sector of MUP R. Serbia, there are 60880 vehicles registered in the City of Niš. According to the composition of this fleet of vehicles, using Copert [4,5,6] software, CO₂ emission estimation was performed. In the Figure 2, comparison between estimated CO₂ emission and measured CO₂ concentration for one of the measured locations is presented:

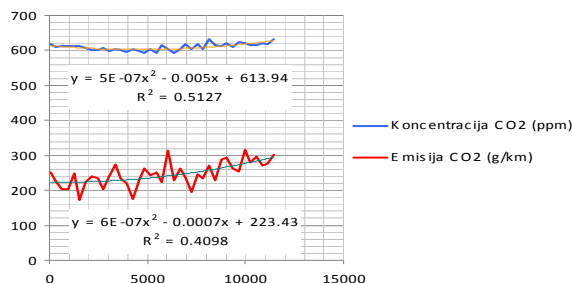


Fig. 2. Comparison of estimated CO₂ emission and measured CO₂ concentration

In the Figure 3.a. measured traffic frequency for the chosen location and date is presented. Data have been averaged over 5 min intervals. Two extremes can be noticed, one in the morning, between 9 and 10 AM (morning rush-hour) and between 3 and 4 PM (afternoon rush-hour). Number of vehicles in the period from 1 to 5 AM is <50 per hour, which is negligible, comparing to ~3000 per hour during rush hours:

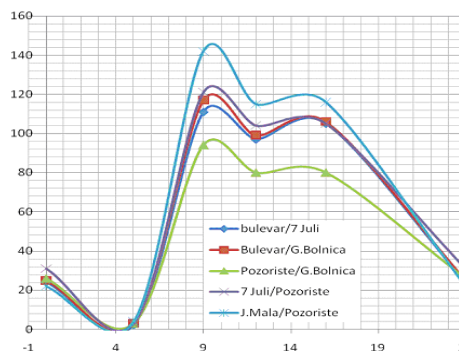
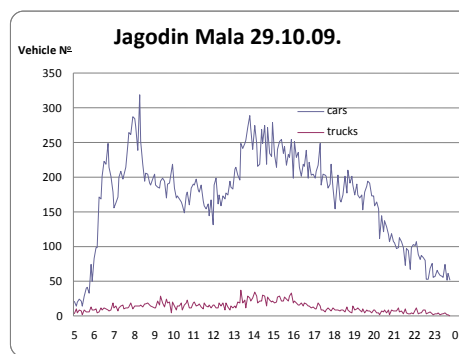


Fig. 3. Measured frequency of vehicles on the location (up) and distribution approximation for all measured locations used for COPERT(down)

2.2.2 Wind measurement

Wind measurements were performed on 3 different locations – near the street (to measure the influence of traffic), in the City Fortress (to indicate the influence of green and forested areas) and in the suburbia (to indicate the influence of individual households on the outdoor air quality).

The results from all measuring sites shows the dominant wind direction same as the Nišava river (sector 60°), which flows through the chosen domain and the influence of the larger Morava river (sector 330°), which is about 7km to the west from Niš. The results are very similar to the ones from the main meteorological station Niš.

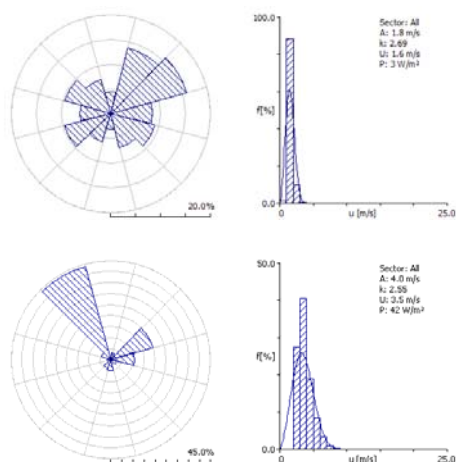


Fig. 4. Wind roses and Weibull distribution histogram on the measuring site 1 (up) and the Main meteorological station Niš (down)

2.2.3 CO₂ measurement

The data comparison for the first half of April is presented. This measurements on both measuring locations shows the significant decrease of CO₂ concentration on the end of the heating season (marked with circle on both diagrams). This shows that the start predictions are correct, and that these measurements, after thorough analysis, can take us closer to understanding of the CO₂ distribution into the atmosphere.

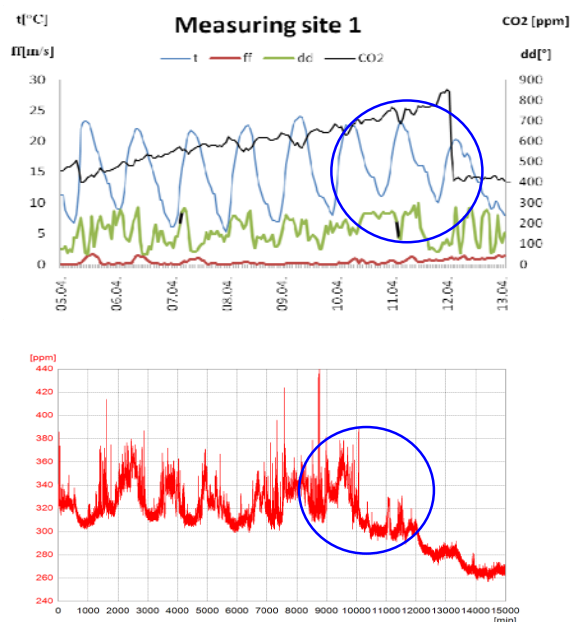


Fig. 5. Data collected on the Measuring site 1 (suburban, up) and the CO₂ concentration measurement on the Measuring site 3 (park area, down)

One can notice that traffic frequency increase leads to an adequate CO₂ concentration level increase on the measuring location. Such measuring results were compared with the long-term wind, temperature and CO₂ concentration measurements on 3 different measuring locations in the City of Niš. The results obtained show the potential of proper estimation of air quality in urban areas, using available, precise and inexpensive instruments. Knowing the exhaust gasses composition, other pollutant concentrations can be estimated.

Besides the traffic, which is mostly with constant frequency annually, the emission source of a similar size is the District heating plant Niš. It possesses 14 heat sources with the installed capacity of 254MW, located on three locations, as follows: Krivi Vir – 128MW, Jug – 60MW and Majakovski – 14.3MW. The rest of potentials is located on 11 locations in local boiler houses for heating the residential building blocks. The fuel used is natural gas – 90% and heavy oil – 10%.

Within the area of interest, District heating plant Krivi Vir is located. Usual fuel is natural gas. The conversion from heavy oil to natural gas was very important, as this plant is surrounded by the most dense populated area in the City of Niš, with over 50.000 inhabitants,

and its potentials are just over the half of the entire capacities in the City, which led to the significant improvement of the air quality in the City, especially in the surroundings. Measurements on the exhaust gasses collector in the District heating plant Krivi Vir showed the expected 8.8% of CO₂, and about 58ppm of NO_x, 52ppm of NO₂ and virtually nonexistent amount of CO (in the range -1 to 1ppm) which corresponds to the reversible nature of carbon based products of the natural gas combustion, which was confirmed by repetitive measurements. This shows that by monitoring the natural gas consumption the emission is easily predictable. The diagram of the natural gas consumption for an entire season is presented on the following Figure 6.

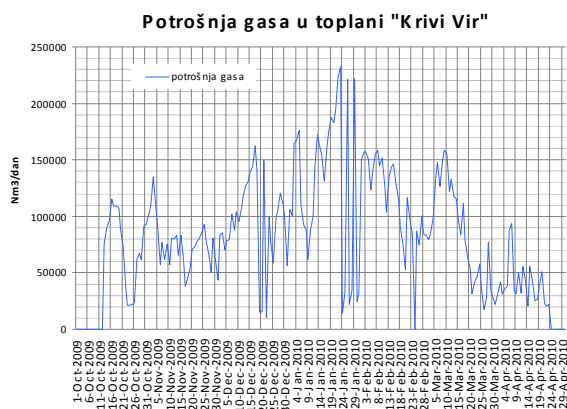


Fig. 6. Natural gas consumption diagram for an entire season in the District heating plant Krivi Vir

3. NUMERICAL ANALYSIS

Estimation of the pollution dispersion is relatively difficult for modeling. From the other hand, as the size of the model was relatively large, namely 5×3.2×1km (or 16km³), and the available computers have limited power, the model could not be too complex. As the physics of the street canyons is relatively well described in available literature, the aim of the investigation in this paper was to estimate the influence of a point source of pollution over the urban core of the City of Niš. Mathematical model used is expressed by the following transport equations:

Continuity equation

$$\frac{\partial(\rho)}{\partial t} + \frac{\partial}{\partial x_i}(\rho u_i) = 0 \quad (1)$$

Momentum (Navier-Stokes) equations:

$$\frac{\partial(\rho u_i)}{\partial t} + \frac{\partial}{\partial x_j}(\rho u_i u_j) = \frac{\partial}{\partial x_j}(\tau_{ij}) - \frac{\partial p}{\partial x_i} + f_i \quad (2)$$

Energy equation:

$$\frac{\partial(\rho h)}{\partial t} + \frac{\partial}{\partial x_i}(\rho u_i h) = \frac{\partial}{\partial x_i}(j_{ih}) + S_h \quad (3)$$

Passive scalar (CO₂) transport equation:

$$\frac{\partial(\rho c)}{\partial t} + \frac{\partial}{\partial x_i}(\rho u_i c) = \frac{\partial}{\partial x_i}(j_{ic}) + S_c \quad (4)$$

Where ρ is the density, u_i are the three main velocity components, p is the pressure, f_i are the body forces and any additional momentum sources, h is the enthalpy, c is a scalar contaminant and S_h and S_c represent the generation/destruction rate of energy and species respectively. The τ_{ij} is the momentum shear stress tensor, the j_{ih} is the diffusion flux of energy transport and j_{ic} is the diffusion flux of species transport.

3.1 Numerical model

As the former equations represent the system of averaged equations, it was needed to implement a turbulent model in order to close the system and to convert the given set of differential equations into algebraic, which were solved using the PHOENICS software. This paper uses the previously adjusted model to estimate the air velocity, pressure and CO₂ concentrations for the complex configuration of the central urban area of the City of Niš. The available turbulent models can be find in the literature [2,7,8]. Standard k-ε turbulent model was adopted, with special treatment of the passive scalar equations. The details are given in the following table:

Table 3. CO₂ Standard k-ε turbulent model transport equations and constants [3]

Transport equation	Φ	Γ_Φ	S_Φ
Turbulent kinetic energy	k	ν_t/σ_k	$\rho (G - \varepsilon)$
Turbulent kinetic energy dissipation	ε	ν_t/σ_ε	$\rho (\varepsilon / k)(C_{\varepsilon 1}G - C_{\varepsilon 2}\varepsilon)$
$G = \nu_t (\partial_k U_i + \partial_i U_k) \partial_k U_i$			$\nu_t = C_\mu k^2 / \varepsilon$
$(\sigma_k, \sigma_\varepsilon, C_{\varepsilon 1}, C_{\varepsilon 2}, C_\mu) = (1.0, 1.314, 1.44, 1.92, 0.09)$			

4. RESULTS AND DISCUSSION

4.1 Wind fields

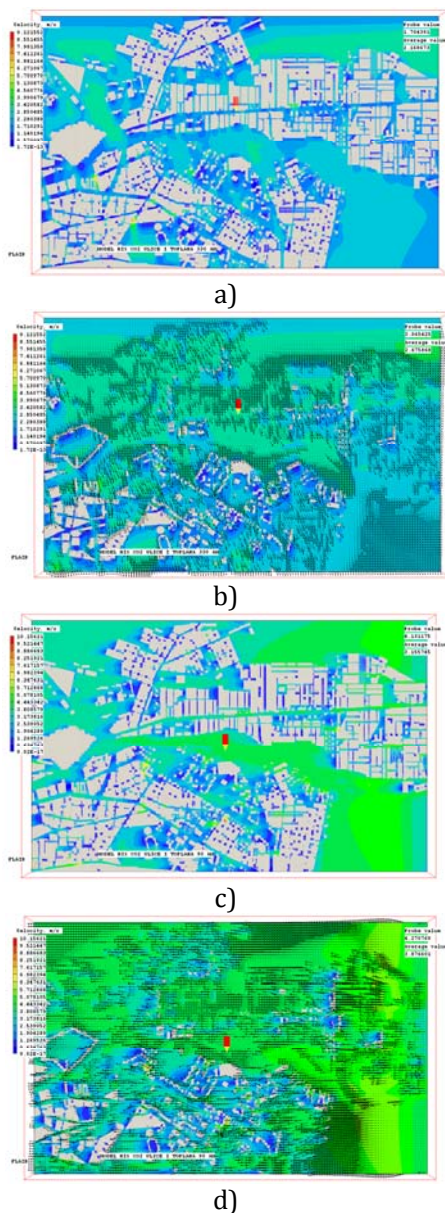


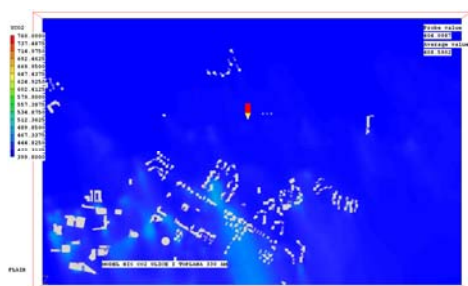
Fig. 7. Wind speed fields for North-Western wind on pedestrian head level – 1.75m (a) and above houses – 12m (b), and for Eastern wind on 1.75m (c) and 12m (d)

As can be seen on the Figure 7, the maximum wind speed is slightly over 9m/s for the NW wind, and slightly over 10m/s for the E wind, which is in good agreement with the expectations. Average wind speeds are 2.2m/s and 2.7m/s for NW and 3.2m/s and 3.9m/s for E wind on 1.75m and 12m height, respectively. This again show good agreement with the lower influence of the buildings on larger heights from the ground.

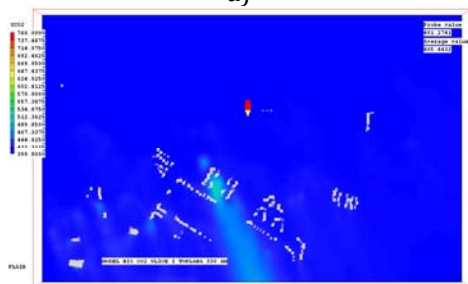
It is obvious that the Eastern wind has deeper penetration into the domain, as the river Nišava flows through the middle of the chosen domain in the general East-West direction. Such data have been expected, considering the street canyon physics. It can be noticed that the lowest wind speeds are on the bottom of the streets, which is expected, as the objects act as the wind shields. Finally, one can conclude that software package COPERT is efficient tool for traffic induced pollution estimation. As can be seen in the Table 4, traffic is the most influential emission factor in the City of Niš. With almost 88000 tCO₂ per annum, it covers over 38% of all emissions. This confirms that the traffic is the largest single air pollution source.

4.1 CO₂ concentration fields

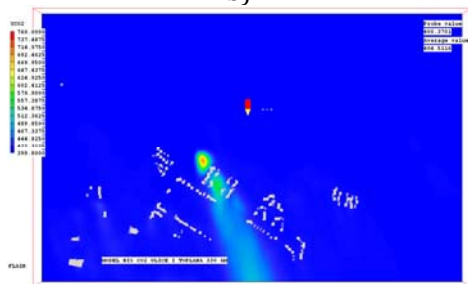
The previous study [8] showed that there is a negligible amount of traffic until 6AM, and the District heating plant Niš starts working at 5AM (or even non-stop, with reduced capacity, when temperatures are subzero), the emission of the District heating plant Niš can be separated in this period from the traffic emissions. As the height of the traffic sources is on the height of about 0.5m, and the District heating plant Krivi Vir main chimney is of 56m height, it is obvious that the vertical distribution becomes more important than for the traffic. On the following Figures 8 and 9 the horizontal fields at the height of 22m, 32m, 42m and 50m are shown for the case of a NW and E wind, respectfully.



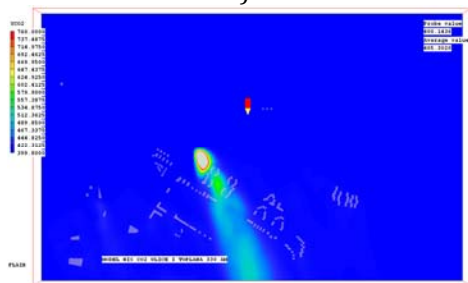
a)



b)



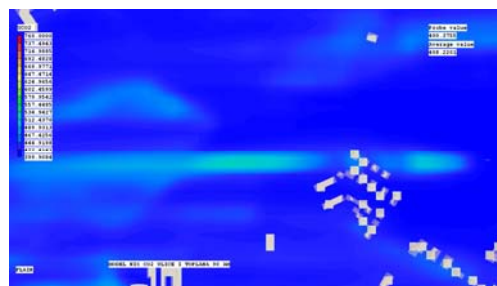
c)



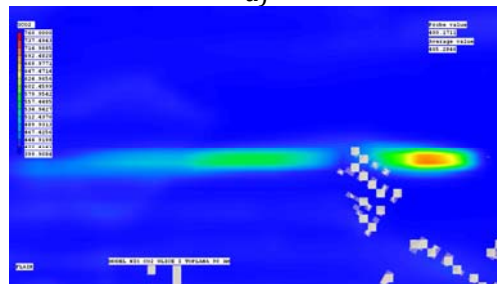
d)

Fig. 8. CO₂ concentration fields for the NW wind, minimal traffic, plant in full power, in the horizontal planes at 22m (a), 32m (b), 42m (c) and 50m above ground (d)

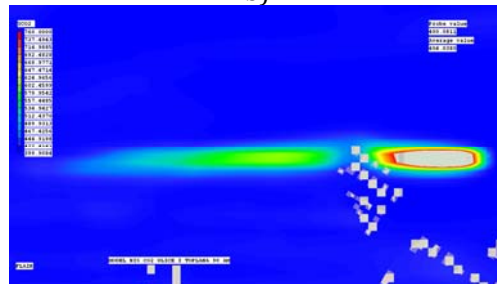
From both Figures 8 and 9 one can notice diminishing influence of the traffic and increasing influence of the exhaust gasses plume from the District heating plant Krivi Vir main chimney, as we approach its height. The influence was examined up to the tallest building height. One can notice that maximum CO₂ concentrations are about 550ppm for the NW and 670ppm for the E wind at 50m, on the highest floors level.



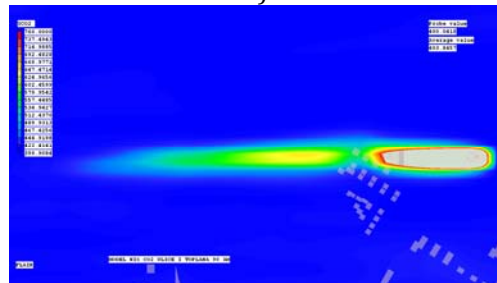
a)



b)



c)



d)

Fig. 9. CO₂ concentration fields for the E wind, minimal traffic, plant in full power, in the horizontal planes at 22m (a), 32m (b), 42m (c) and 50m above ground (d)

Further investigation shows that the initial concentration drops to about 1% at the distance of 350m, which is acceptable for the existing urbanization levels. The CO₂ concentration changes for about 1ppm at the distance of 2km at the downwind direction.

As there are residential buildings at about 300m from the chimney, the transition from heavy oil to natural gas has led to substantial decrease of the pollution levels, especially for the particle pollution, which does not exist for the natural gas. Higher wind speeds between the buildings in the downwind direction leads to the faster dissipation of the pollutants, as well as the lowering the plum. However, the pollution is increased on the upwind sides of the buildings. On the Figure 10 vertical distribution of pollutant concentration is shown. One can notice the obviously increased concentrations for the combined sources, as shown on the Figure 10.b.

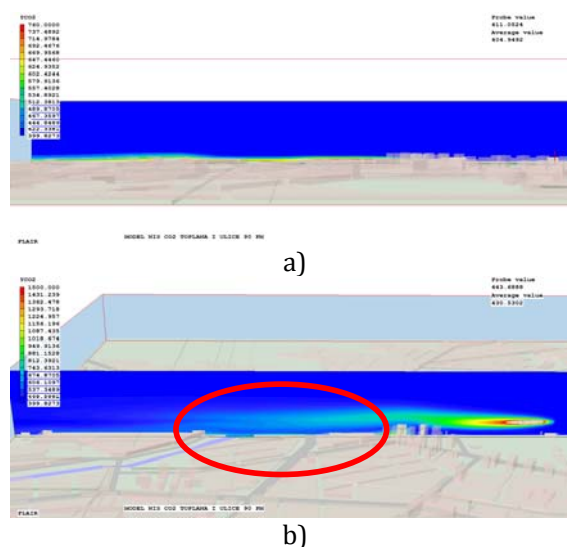


Fig. 10. CO₂ concentration fields for the E wind, for only traffic (a) and both traffic and District heating plant (b)

5. CONCLUSION

As the mankind needs for transportation causes dramatic increase of number of vehicles with IC engines used, the air pollution in urban areas also increases. The need for precise definition of the pollution levels in such areas becomes vital for the well-being of the people, in order to prevent further increase of pollution or to decrease it.

Also, the precise definition of the point sources of pollution is very important, as they are usually in the same level of magnitude. One of the easiest solutions for concentration decreasing could be using of combined heat and power plants, where it is applicable. This study has shown that for the current levels of urbanizations in the City of Niš, the residential buildings should be removed at least 300m from the larger point sources in order to avoid reaching the maximum allowed concentrations.

One can conclude that software package COPERT is efficient tool for traffic induced pollution estimation. As can be seen in the Table 4, traffic is the most influential emission factor in the City of Niš. With almost 88000 tCO₂ per annum, it covers over 38% of all emissions. This confirms that the traffic is the largest single air pollution source.

The use of CFD software is one of the possible solutions for improving our diagnostic abilities. Comparing the current practice of one or couple samplings per day with the possibility of continuous measurement and acquiring actual concentration fields, clearly marks the improvements achieved. There is possibility of defining the vertical distributions of a pollutant, as shown on Figure 10. This enables defining the influence not only on pedestrians, but also to the people living on the higher levels in buildings.

Table 4. Category ratio in the CO₂ balance in the City of Niš [9]

Heat source	Power [TJ]	IPCC emiss.fac.[kgCO ₂ /TJ]	CO ₂ emission [t]	Ratio
District heating plant	1284,96	56100	72086.26	31.30%
Heating with wood	315,44	112000	35329.28	15.34%
Heating with coal	356,73	198500	35156.55	15.26%
Traffic			87699.38	38.09%
Sum			230271.47	100.00%

Acknowledgement

This paper is part of the work on the Project 451-03-68/2020-14200109 with the Government of Republic of Serbia.

REFERENCES

- [1] Fenger J., Hertel O., Palmgren F. (1998). *Urban Air Pollution – European Aspects*, Kluwer Academic Publishers, Dordrecht, Netherlands.
- [2] European Environment Agency (2008). *Report bulletin No. 171*.
- [3] Živković P. (2010). *Istraživanje uticaja karakteristika tehnološkog procesa u referentnom postrojenju na kvalitet vazduha u neposrednom okruženju*, (In Serbian), PhD thesis, Faculty of Mechanical Engineering Niš.
- [4] Ntziachristos L., Samaras Z. (2000). *COPERT 3–Computer Programme to calculate Emissions from Road Transport, Methodology and emission factor (version 2.1)*, European Environment Agency; Copenhagen, Denmark.
- [5] Živković P., Tomić M., Ilić G., Vukić M., Stevanović Ž. (2012), *Specific approach for continuous air quality monitoring*, Chemical Industry, Vol 66., Is. 1, pp 85-93.
- [6] Živković P., Tomić M., Ilić G. (2011). *Measurements of traffic induced pollution in the city of Niš*, SDEWES 2011, Dubrovnik, Croatia, (CD Proceedings).
- [7] Živković P., Tomić M., Ilić G. (2011). *Traffic intensity influence on the city of Niš air quality* SDEWES 2011, Dubrovnik, Croatia, (CD Proceedings).
- [8] Živković P., Ilić G., Tomić M., Vukić M., Stevanović M. Ž., Stevanović Ž.Ž., Ogrizović M. (2010). *Air pollution estimation on the city of Niš territory*, International Symposium Power Plants 2010, Vrnjačka Banja, Serbia, (CD Proceedings).
- [9] Republički zavod za statistiku (2009). *Bilans uglja i Bilans za ogrevno drvo 2009*, R. Srbija.

Mechanics and Design



Banja Luka
28–29 May 2021.

DEMI 2021

15th International Conference on
Accomplishments in Mechanical and
Industrial Engineering

www.demi.mf.unibl.org



Comparative free vibration analysis of FG plate and FG plate resting on an elastic foundation

D. Čukanović^a, D. Milosavljević^b, G. Bogdanović^b, A. Radaković^c, N. Velimirović^c

^aUniversity of Priština, Faculty of Technical Sciences, Knjaza Miloša 7, 38220 Kosovska Mitrovica, Serbia

^bUniversity of Kragujevac, Faculty of Engineering, Sestre Janjić 6, 34000 Kragujevac, Serbia

^cState University of Novi Pazar, Vuka Karadžića bb, 36300 Novi Pazar, Serbia

Abstract

The introductory part of the paper gives basic considerations about materials as an always current field of research, pointing out the importance and impact that materials have in different branches of industry and the human environment. Special emphasis is placed on functionally graded materials as modern materials in the group of engineering composites. The basic relations that define the interaction of the functionally graded plate and the elastic foundation are presented. One-parameter (Winkler model) and two-parameter mathematical model (Winkler-Pasternak model) of elastic foundation are described in detail. The equations of motion for the case of a FG plate as well as FG plate resting on an elastic foundation are derived by applying the Hamilton's principle. The theoretical procedure for analytical solution of equations of motion is described by applying Navier's assumed forms of displacement which define contour conditions for a freely supported rectangular plate. Finally, the results of free vibration analysis of FG plates and FG plates resting on an elastic foundation are presented. The influence of the elastic foundation, described by one-parameter and two-parameter mathematical models, on free vibrations of the FGM plate was considered and appropriate conclusions were made.

Keywords functionally graded materials, Winkler model, Winkler-Pasternak model, free vibrations

1. INTRODUCTION

Materials science is one of the oldest branches of engineering and applied science. In modern society materials appear as one of the most important areas of research at the global level through various disciplines. The increasing use of new materials in medicine, dentistry, aircraft industry, automotive industry enables a more comfortable, reliable and safer living environment. On the one hand, materials can be

classified into a group characterized by a wide field of application, a large volume of continuous production, unlimited resources and thus a very competitive price and market availability. On the other hand, there is a group of new materials, characterized by special properties and applications, limited resources, high demands in terms of production, characteristics and quality which causes a high price. Such materials have an application limited only to expensive and responsible constructions. Functionally graded materials (FGM) are a group of new materials in the family of engineering composites. FGM is a composite material formed of two or more constituents with a continuous change of properties in a certain direction. In this way,

Corresponding author

PhD, Assistant professor, Dragan Čukanović
dragan.cukanovic@pr.ac.rs

University of Priština, Faculty of Technical Sciences
Knjaza Miloša 7
38220 Kosovska Mitrovica, Serbia

plane and transverse stresses are reduced, in general, stress concentration is prevented and thermo-mechanical properties are improved [1, 2].

2. MATHEMATICAL MODEL OF PLATE-ELASTIC FOUNDATION INTERACTION

In addition to the analysis of simply supported or rigid fixed plate, a very commonly analysed problem is the interaction of the plate and the elastic foundation [3, 4]. Mathematical models of the plate on an elastic foundation are often used to describe a large number of engineering problems in civil engineering, road and railway industry, biomechanics and other fields of engineering. Figure 1 shows a plate of dimension $a \times b$ supported on an elastic foundation and loaded with an arbitrary load $q(x, y)$.

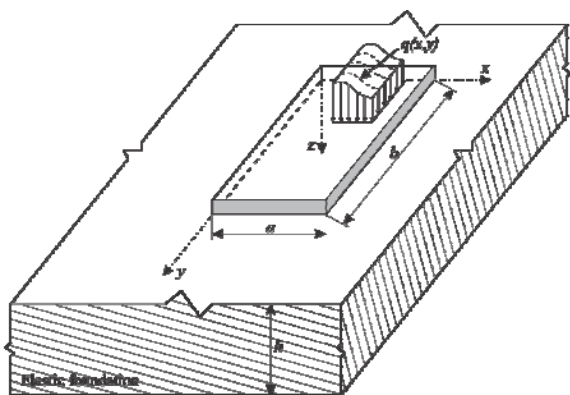


Fig. 1. Plate resting on an elastic foundation

2.1 One-parameter model (Winkler's model)

The simplest mathematical model of an elastic foundation is based on the concept of the modulus of reaction of the foundation. Winkler was the first to introduce this model into applied mechanics. In this model, the basic assumption is that the vertical displacement of a point on an elastic foundation is proportional to the pressure at that point and does not depend on the pressure on adjacent points. Winkler's model is represented by a system of vertical, linearly elastic springs which is mutually independent.

Since the elastic foundation is described by a single parameter, this model is also called a one-

parameter foundation model, where the effective contact load:

$$q_e(x, y) = kw(x, y) \quad (1)$$

k - spring stiffness coefficient (foundation reaction modulus),
 $w(x, y)$ - vertical displacement (subsidence of the foundation).

The strain energy of the elastic foundation is:

$$U_e = \int_A \frac{1}{2} kw^2 dA \quad (2)$$

The assumption of an elastic foundation as a system of independent springs in most cases represents a large approximation. For example, when solving problems in civil engineering the construction elements are supported on the ground, so that the ground is in that case an elastic foundation. The ground is a continuum in which the influence from one point is transferred to the surrounding points. This fact clearly indicates the approximation introduced by Winkler where he assumed that the springs do not affect each other. However, due to its simplicity, Winkler's model has remained in use until today and a large number of authors have in the meantime been engaged in its improvement with the introduction of two-parameter models.

2.2 Two-parameter model (Winkler-Pasternak's model)

Pasternak proposed an improvement on Winkler's model by introducing a shear interaction between springs, by connecting them with a layer of fictitious, incompressible sliding elements that are deformed only by shear.

The effective contact load in the Winkler-Pasternak's model of a plate on an elastic foundation is given by the expression:

$$q_e(x, y) = kw(x, y) - G\nabla^2 w(x, y) \quad (3)$$

where:

G - shear modulus and
 $\nabla^2 = \frac{\partial^2}{\partial x^2} + \frac{\partial^2}{\partial y^2}$ - Laplace operator.

The strain energy of the elastic foundation for the case of the two-parameter model is:

$$U_e = \int_A \frac{1}{2} k w^2 dA + \int_A \frac{1}{2} G \left[\left(\frac{\partial w}{\partial x} \right)^2 + \left(\frac{\partial w}{\partial y} \right)^2 \right] dA \quad (4)$$

3. DISPLACEMENT-STRAIN RELATIONS AND CONSTITUTIVE EQUATION OF ELASTICITY FOR FGM

The subject of the free vibration analysis in this paper are FGM plate and FGM plate on elastic foundation (Fig. 2.). The plate (length a , width b and height h) is made of functionally graded material consisting of the two constituents, namely, metal and ceramics.

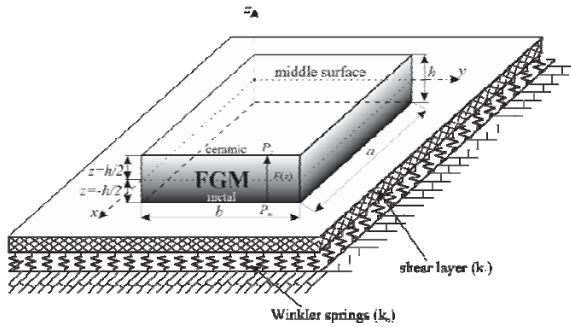


Fig. 2. Geometry of the FGM plate on an elastic foundation

Based on the higher order shear deformation theory (HSDT) the starting point for defining the kinematic displacement-strain relations will be the assumed forms of the displacement components in the form [5]:

$$\begin{aligned} u &= u_0(x, y, t) - z w_{0,x} + f(z) \theta_x \\ v &= v_0(x, y, t) - z w_{0,y} + f(z) \theta_y \\ w &= w_0(x, y, t) \end{aligned} \quad (5)$$

where $f(z)$ is shape function [6]:

$$f(z) = z \left(\cosh \left(\frac{z}{h} \right) - 1.388 \right) \quad (6)$$

In case of small strains, normal and shear strain components are obtained by well-know relations in linear elasticity:

$$\boldsymbol{\varepsilon} = \boldsymbol{\varepsilon}^{(0)} + z \mathbf{k}^{(0)} + f(z) \mathbf{k}^{(1)}; \quad \boldsymbol{\gamma} = f'(z) \mathbf{k}^{(2)} \quad (7)$$

The elastic constitutive relations for FGM are given as follows:

$$\begin{Bmatrix} \sigma_{xx} \\ \sigma_{yy} \\ \tau_{xz} \\ \tau_{yz} \\ \tau_{xy} \end{Bmatrix} = \begin{bmatrix} C_{11}(z) & C_{12}(z) & 0 & 0 & 0 \\ C_{12}(z) & C_{22}(z) & 0 & 0 & 0 \\ 0 & 0 & C_{44}(z) & 0 & 0 \\ 0 & 0 & 0 & C_{55}(z) & 0 \\ 0 & 0 & 0 & 0 & C_{66}(z) \end{bmatrix} \begin{Bmatrix} \varepsilon_{xx} \\ \varepsilon_{yy} \\ \gamma_{xz} \\ \gamma_{yz} \\ \gamma_{xy} \end{Bmatrix} \quad (8)$$

where the coefficients of the constitutive elasticity tensor could be defined through engineering constants:

$$\begin{aligned} C_{11}(z) &= C_{22}(z) = \frac{E(z)}{1-\nu^2} \\ C_{44}(z) &= C_{55}(z) = C_{66}(z) = \frac{E(z)}{2(1+\nu)} \\ C_{12}(z) &= \frac{\nu E(z)}{1-\nu^2}. \end{aligned} \quad (9)$$

Due to the gradient change of the plate structure in the direction of the z coordinate the modulus of elasticity could be defined in accordance to the power-law distribution as:

$$E(z) = E_m + E_{cm} \left(\frac{1}{2} + \frac{z}{h} \right)^p, \quad E_{cm} = E_c - E_m \quad (10)$$

4. EQUATIONS OF MOTION OF FGM PLATE RESTING ON ELASTING FOUNDATION

In order to obtain the equations of motion, by applying Hamilton's principle, it is necessary to define the strain energy of the plate and the elastic foundation as well as the kinetic energy:

$$U = \int_A \int_{h^-}^{h^+} \left(\sigma_{xx} \varepsilon_{xx} + \sigma_{yy} \varepsilon_{yy} + \sigma_{zz} \varepsilon_{zz} + \tau_{xy} \gamma_{xy} + \tau_{xz} \gamma_{xz} + \tau_{yz} \gamma_{yz} \right) dA dz \quad (11)$$

$$U_e = \frac{1}{2} \int_A \left\{ k_0 w^2 + k_1 \left[\left(\frac{\partial w}{\partial x} \right)^2 + \left(\frac{\partial w}{\partial y} \right)^2 \right] \right\} dA \quad (12)$$

$$K = \frac{1}{2} \int_{-h/2}^{h/2} \int_A \rho(z) \left[\left(\frac{\partial u}{\partial t} \right)^2 + \left(\frac{\partial v}{\partial t} \right)^2 + \left(\frac{\partial w}{\partial t} \right)^2 \right] dA dz \quad (13)$$

where material density in an arbitrary cross-section z is defined in accordance to the power-law distribution as:

$$\rho(z) = \rho_m + \rho_{cm} \left(\frac{1}{2} + \frac{z}{h} \right)^p \quad \rho_{cm} = \rho_c - \rho_m \quad (14)$$

By applying Hamilton's principle:

$$\delta \int_{t_1}^{t_2} [K - (U + U_e)] dt = 0 \quad (15)$$

the equations of motion for FGM plates resting on an elastic foundation (described by the Winkler-Pasternak mathematical model) are obtained in the form:

$$\begin{aligned} \delta u_0: N_{xx,x} + N_{xy,y} &= I_1 \ddot{u} - I_2 \dot{w}_{,x} + I_4 \ddot{\theta}_x \\ \delta v_0: N_{yy,y} + N_{yx,x} &= I_1 \ddot{v} - I_2 \dot{w}_{,y} + I_4 \ddot{\theta}_y \\ \delta w_0: M_{xx,xx} + 2M_{xy,xy} + M_{yy,yy} - k_0 w + k_1 (w_{,xx} + w_{,yy}) &= \\ &= I_1 \ddot{w} + I_2 (\ddot{u}_{,x} + \ddot{v}_{,y}) - I_3 (\dot{w}_{,xx} + \dot{w}_{,yy}) + I_5 (\ddot{\theta}_{x,x} + \ddot{\theta}_{y,y}) \quad (16) \\ \delta \theta_x: P_{xx,x} + P_{xy,y} - R_x &= I_4 \ddot{u} - I_5 \dot{w}_{,x} + I_6 \ddot{\theta}_x \\ \delta \theta_y: P_{xy,x} + P_{yy,y} - R_y &= I_4 \ddot{v} - I_5 \dot{w}_{,y} + I_6 \ddot{\theta}_y \end{aligned}$$

where I_i ($i=1,2,3,4,5$ and 6) are terms due to inertia.

In the case of FGM plates without elastic foundation, the equations of motion are:

$$\begin{aligned} \delta u_0: N_{xx,x} + N_{xy,y} &= I_1 \ddot{u} - I_2 \dot{w}_{,x} + I_4 \ddot{\theta}_x \\ \delta v_0: N_{yy,y} + N_{yx,x} &= I_1 \ddot{v} - I_2 \dot{w}_{,y} + I_4 \ddot{\theta}_y \\ \delta w_0: M_{xx,xx} + 2M_{xy,xy} + M_{yy,yy} &= \\ &= I_1 \ddot{w} + I_2 (\ddot{u}_{,x} + \ddot{v}_{,y}) - I_3 (\dot{w}_{,xx} + \dot{w}_{,yy}) + I_5 (\ddot{\theta}_{x,x} + \ddot{\theta}_{y,y}) \quad (17) \\ \delta \theta_x: P_{xx,x} + P_{xy,y} - R_x &= I_4 \ddot{u} - I_5 \dot{w}_{,x} + I_6 \ddot{\theta}_x \\ \delta \theta_y: P_{xy,x} + P_{yy,y} - R_y &= I_4 \ddot{v} - I_5 \dot{w}_{,y} + I_6 \ddot{\theta}_y \end{aligned}$$

Analytical solutions will be derived for the simply supported rectangular FGM plate. In order to satisfy the previously boundary conditions, the following Navier's solution is assumed [5]:

$$\begin{aligned} u_0(x, y, t) &= \sum_{m=1}^{\infty} \sum_{n=1}^{\infty} U_{mn} \cos \frac{m\pi x}{a} \sin \frac{n\pi y}{b} e^{i\omega t} \\ v_0(x, y, t) &= \sum_{m=1}^{\infty} \sum_{n=1}^{\infty} V_{mn} \sin \frac{m\pi x}{a} \cos \frac{n\pi y}{b} e^{i\omega t} \end{aligned}$$

$$\begin{aligned} w_0(x, y, t) &= \sum_{m=1}^{\infty} \sum_{n=1}^{\infty} W_{mn} \sin \frac{m\pi x}{a} \sin \frac{n\pi y}{b} e^{i\omega t} \\ \theta_x(x, y, t) &= \sum_{m=1}^{\infty} \sum_{n=1}^{\infty} T_{xmn} \cos \frac{m\pi x}{a} \sin \frac{n\pi y}{b} e^{i\omega t} \quad (18) \\ \theta_y(x, y, t) &= \sum_{m=1}^{\infty} \sum_{n=1}^{\infty} T_{ymn} \sin \frac{m\pi x}{a} \cos \frac{n\pi y}{b} e^{i\omega t} \end{aligned}$$

By substituting (18) into (16) the following equation is obtained:

$$[\mathbf{K} - \omega^2 \mathbf{I}] \bar{\mathbf{U}} = \mathbf{0} \quad (19)$$

The determinant in (19) must be equal to zero value in order to get nontrivial solutions

$$|\mathbf{K} - \omega^2 \mathbf{I}| = 0 \quad (20)$$

5. NUMERICAL EXAMPLES AND RESULTS

Previously obtained theoretical results were applied to simulate specific engineering problems. Numerical examples of free vibration of FGM plates and FGM plates on an elastic foundation were made and the obtained results were analyzed. The analysis was done for the case of FGM plates of metal and ceramic constituents (*Al-Aluminum*, $E_m=0.7 \cdot 10^5$ [MPa], $\nu=0.3$, $\rho_m=2702$ [kg/m³]) and ceramic (*Al₂O₃-Alumina*, $E_c=3.8 \cdot 10^5$ [MPa], $\nu=0.3$, $\rho_m=3800$ [kg/m³]).

To display the numerous values of natural frequencies of FGM plate it is necessary to normalize the obtained values according to:

$$\tilde{\omega} = \omega h \sqrt{\frac{\rho_m}{E_m}} \quad (21)$$

Table 1 shows the non-dimensional natural frequencies of a rectangular FGM plate for the first mode of vibration and different values of the power law index p . The results obtained in this paper are compared with the results based on 3D theory of elasticity given in [7]. Based on the comparative analysis, it can be concluded that the results obtained in this paper are good matched with the results obtained by the mentioned 3D theory of elasticity.

Table 1. Non-dimensional natural frequencies of a rectangular FGM plate

a/b	a/h	Theory	$\tilde{\omega}$		
			p=0	p=1	p=5
0.5	5	3D [7]	0.2713	0.2088	0.1754
		HSDT	0.2705	0.2081	0.1753

Table 2 shows the non-dimensional natural frequencies of a rectangular (a/b=0.5) FGM plate resting on an elastic foundation for different values of the Winkler's coefficient (k_0), Pasternak's coefficient (k_1) and power law index p . First, only one coefficient was introduced, then the second, in order to determine which of the mentioned two coefficients has the greater impact. The analysis of the results shows that the influence of the Pasternak's coefficient (k_1) on the natural frequency value is far greater than the influence of the Winkler's coefficient (k_0).

Table 2. Non-dimensional natural frequencies of a rectangular FGM plate resting on an elastic foundation

k ₀	k ₁	Theory	$\tilde{\omega}$		
			a/h=5; a/b=0.5		
			p=0	p=1	p=5
100	0	HSDT	7.2125	5.8654	5.2358
0	100	HSDT	11.1150	10.8450	10.9920
100	100	HSDT	11.3950	11.1780	11.3593

6. CONCLUSION

The paper points out the importance and topicality of the research of modern composite materials with special emphasis to the functionally graded material. In addition to FGM plates, the interaction of FGM plates with an elastic foundation was also analyzed. The basic relations that define the mentioned interaction are shown. The Winkler's and Winkler-Pasternak's mathematical model are presented. Under the assumption of small strains the kinematic relations between displacement and strain has been established based on the HSDT theory which includes the shape function. Based on the strain energy of the plate and the elastic foundation as well as kinetic energy, the equations of motion were derived using the Hamilton principle. By applying Navier's assumed forms of displacement for the simply

supported rectangular FGM plate, a procedure for analytically solving the equations of motion was developed. The previously described theoretical results were used to obtain numerical results. The results of free vibration of FGM plates and FGM plates resting on an elastic foundation were analyzed, on the basis of which the following conclusions were made:

- results obtained in this paper based on HSDT theory are good matched with the results obtained by the 3D theory of elasticity.
- the influence of the Pasternak's coefficient (k_1) on the natural frequencies value is far greater than the influence of the Winkler's coefficient (k_0).

REFERENCES

- [1] Jha, D.K., Kant, T., Singh, R.K. (2013). A critical review of recent research on functionally graded plates. *Composite Structures*, vol. 96, p. 833-849. DOI: 10.1016/j.compstruct.2012.09.001
- [2] Udupa, G., Shrikantha, S. R., Gangadharan, K. V. (2014). Functionally graded composite materials: An overview. *Procedia Materials Science*, vol. 5, p. 1291-1299. DOI:0.1016/J.MSPRO.2014.07.442
- [3] William, S. T. (1990). *Analysis of plate on elastic foundations*. Texas Tech University, Texas, USA. Phd thesis.
- [4] Wang, Y. H., Tham, L. G., Cheung, Y. K. (2005). Beams and plates on elastic foundations: a review. *Progress in Structural Engineering and Materials*, vol. 7, no. 4, p. 174-182. DOI: 10.1002/pse.202
- [5] Reddy, J. N., (2004). *Mechanics of Laminated Composite Plates and Shells: Theory and Analysis*. CRC Press LLC, New York, United State of America.
- [6] Čukanović. D., Radaković. A., Bogdanović. G., Milanović. M., Redžović. H., Dragović. D. (2018). New Shape Function for the Bending Analysis of Functionally Graded Plate. *Materials*, vol. 11, no. 12, 2381. DOI: 10.3390/ma11122381
- [7] Guoyong, J., Zhu, S., Shuangxia, S., Tiangui, Y., Siyang, G. (2014). Three-dimensional exact solution for the free vibration of arbitrarily thick functionally graded rectangular plates with general boundary conditions. *Composite Structures*, vol. 108. p. 565-577. DOI: 10.1016/j.compstruct.2013.09.051



Banja Luka
28–29 May 2021.

DEMI 2021

15th International Conference on
Accomplishments in Mechanical and
Industrial Engineering

www.demi.mf.unibl.org



Propagation of elastic waves in isotropic and anisotropic media

A. Radaković^a, D. Milosavljević^b, G. Bogdanović^b, D. Čukanović^c, N. Velimirović^a

^aState University of Novi Pazar, Vuka Karadžića bb, 36300 Novi Pazar, Serbia

^bUniversity of Kragujevac, Faculty of Engineering, Sestre Janjić 6, 34000 Kragujevac, Serbia

^cUniversity of Priština, Faculty of Technical Sciences, Knjaza Miloša 7, 38220 Kosovska Mitrovica, Serbia

Abstract

The paper observes the propagation of elastic waves through isotropic and anisotropic media. The emphasis is on the propagation of Lamb waves. The constitutive matrix of anisotropic composite materials is defined using the field of privileged directions. The separation into pure and quasi wave modes is shown. The technology of obtaining dispersion curves and phase velocity diagrams has been developed and implemented. The phase velocity dispersion relations are shown as a function of the product of frequency and laminate thickness at a fixed value of the ration propagation angle. On the other side, phase velocity diagrams are shown at a fixed value of the ratio of the product of frequency and laminate thickness and longitudinal velocity. Coupling of quasimodes in anisotropic materials has been shown. To obtain the results, analytical methods based on the higher order shear deformation theory were used. The dispersion curves show the switching points from one quasimode to another, as well as the values of the frequency at which the switching occurs.

Keywords elastic waves, high-order deformation theories, composite laminates, wave modes

1. INTRODUCTION

Wave propagation in composite materials is complex problem due to the heterogeneity and anisotropy of the constituents. In that case, the velocity of the wave mode depends on the direction of wave propagation in relation to the privileged directions, frequencies, wavelengths, etc. According to [1], when elastic waves propagate in isotropic constructions such as plate, there is an alternating repetition of reflection on the upper and lower surface of the laminate. The resulting propagation of the

waves that occurs as a result of their mutual action is guided parallel to the contour surfaces of the plate. Such a wave can be modeled by introducing surface contour conditions into the equations of motion. In this way, the notion of dispersion is introduced, which means that the velocity of propagation of a guided wave along the plate is a function of frequency or wavelength. Dispersion relations can be obtained based on two theoretical approaches. An approach based on the use of 3D elastic theory is given in [2-5], while an approach based on the application of shear deformation theories is given in [1, 6]. Dispersion relations for an elastic isotropic plate with infinite dimensions with respect to thickness were first developed by Lamb. For this reason, guided waves that propagate in the plane of an elastic plate with stress-free surfaces are also known Lamb waves. Since the guided waves remain

Corresponding author

PhD, Assistant professor, Aleksandar Radaković
aradakovic@np.ac.rs

State University of Novi Pazar
Vuka Karadžića bb
36300 Novi Pazar, Serbia

limited within the structure, they can cover large distances and thus enable the examination of large areas. This test is performed using a limited number of sensors. This property makes them suitable for monitoring the integrity of structures such as high pressure vessels, fuel tanks, pipelines, etc. In isotropic plates, guided waves can be classified into three types according to their polarizations. Waves that are polarized in a plane perpendicular to the plate are **symmetric** (S) or extensional waves and **antisymmetric** (A) or bending waves. Waves that are polarized in the plane of the plate are shear horizontal (SH) waves. SH waves can also be symmetrical or antisymmetrical with respect to the middle plane of the plate. S and A waves are affected by the strain state of the plane xz (displacements u and w), while SH waves are affected by out-of-plane strains (displacement v only). S_n and A_n with index $n=0,1,2,3,\dots$, represent symmetric and antisymmetric Lamb wave modes, respectively. SH_n with even and odd index n denote symmetric and antisymmetric SH waves, respectively.

2. CONSTITUTIVE MATRIX

If the material is reinforced by one family of fibers then the composite material has one privileged direction so the material is transversely isotropic with respect to that direction. The constitutive matrix of a fiber-reinforced composite material can be expressed in two ways:

- Through engineering constants or
- Through the elastic constants defined in Spencer's papers [7, 8].

The first one is a much more common way, especially in engineering practice. The second one has a greater theoretical application due to its invariance in relation to the rotation of the coordinate system. Therefore, it is not necessary to use transformations of the elasticity matrix, but this matrix will have the same shape in any coordinate system.

The direction of the fiber can be defined using a unit vector that can vary from point to point. Since the direction of the fiber depends on the position, the formulation of constitutive equations independent of the coordinate system was adopted in the paper [7 - 10].

The procedure for deriving the constitutive matrix for materials reinforced with one family of fibres was described first in [9] and later in

detail for the volume wave propagation in [10]. In these papers, the authors assumed a specific strain energy as a function of the strain and the direction vector of the fibres for the case of a material reinforced by a single family of fibres. Then, using the tensor calculus, they defined the constitutive matrix coefficients for this material in the form:

$$\begin{aligned}
 C_{11} &= \lambda + 2\mu_T + (4\mu_L - 4\mu_T + 2\alpha + \beta a_1^2) a_1^2 \\
 C_{12} &= \lambda + \alpha (a_1^2 + a_2^2) + \beta (a_1^2 a_2^2) \\
 C_{13} &= \lambda + \alpha (a_1^2 + a_3^2) + \beta (a_1^2 a_3^2) \\
 C_{14} &= \alpha a_2 a_3 + \beta a_1^2 a_2 a_3 \\
 C_{15} &= 2(\mu_L - \mu_T) a_1 a_3 + \alpha a_1 a_3 + \beta a_1^3 a_3 \\
 C_{16} &= 2(\mu_L - \mu_T) a_1 a_2 + \alpha a_1 a_2 + \beta a_1^3 a_2 \\
 C_{22} &= \lambda + 2\mu_T + (4\mu_L - 4\mu_T + 2\alpha + \beta a_2^2) a_2^2 \\
 C_{23} &= \lambda + \alpha (a_2^2 + a_3^2) + \beta (a_2^2 a_3^2) \\
 C_{24} &= 2(\mu_L - \mu_T) a_2 a_3 + \alpha a_2 a_3 + \beta a_2^3 a_3 \\
 C_{25} &= \alpha a_1 a_3 + \beta a_1 a_2^2 a_3 \\
 C_{26} &= 2(\mu_L - \mu_T) a_1 a_2 + \alpha a_1 a_2 + \beta a_1 a_2^3 \quad (1) \\
 C_{33} &= \lambda + 2\mu_T + (4\mu_L - 4\mu_T + 2\alpha + \beta a_3^2) a_3^2 \\
 C_{34} &= 2(\mu_L - \mu_T) a_2 a_3 + \alpha a_2 a_3 + \beta a_2^3 a_3 \\
 C_{35} &= 2(\mu_L - \mu_T) a_1 a_3 + \alpha a_1 a_3 + \beta a_1^3 a_3 \\
 C_{36} &= \alpha a_1 a_2 + \beta a_1 a_2 a_3^2 \\
 C_{44} &= \mu_T + (\mu_L - \mu_T) (a_2^2 + a_3^2) + \beta a_2^2 a_3^2 \\
 C_{45} &= (\mu_L - \mu_T) a_1 a_2 + \beta a_1 a_2 a_3^2 \\
 C_{46} &= (\mu_L - \mu_T) a_1 a_3 + \beta a_1 a_2^2 a_3 \\
 C_{55} &= \mu_T + (\mu_L - \mu_T) (a_1^2 + a_3^2) + \beta a_1^2 a_3^2 \\
 C_{56} &= (\mu_L - \mu_T) a_2 a_3 + \beta a_1^2 a_2 a_3 \\
 C_{66} &= \mu_T + (\mu_L - \mu_T) (a_1^2 + a_2^2) + \beta a_1^2 a_2^2
 \end{aligned}$$

where $\mathbf{a}=(a_1, a_2, a_3)$ is vector defining a privileged direction and $\mu_L, \mu_T, \lambda, \alpha, \beta$ are material constants which according to [99] can also be expressed through other value that are much more suitable for direct measurement, such as engineering constants. The material constant μ_L represents the shear modulus along the privileged direction \mathbf{a} , while μ_T represents the shear modulus perpendicular to the privileged direction \mathbf{a} . Other constants λ, α, β

can be expressed through value such as Young module and Poisson number.

The stress-strain relation for isotropic behavior would be obtained if it were adopted to be $\mu_T = \mu_L$ and $\alpha = \beta = 0$.

3. ANALYSIS OF ELASTIC WAVE PROPAGATION BASED ON HSDT THEORY

From the two mentioned approaches in the analysis of elastic wave propagation, in this paper a method based on shear deformation theories was chosen. The application of this method is more applicable to numerical methods, but represents an approximation in relation to 3D theories of elasticity. Dynamic equations of motion based on the second order shear deformation theory for the linearly elastic material reinforced by two families of fibers were performed in detail in [6].

In the area of linear elasticity, the displacement field is assumed in the form:

$$\begin{aligned} u(x, y, z, t) &= u_0(x, y, t) + z\psi_x(x, y, t) + \frac{z^2}{2}\phi_x(x, y, t) \\ v(x, y, z, t) &= v_0(x, y, t) + z\psi_y(x, y, t) + \frac{z^2}{2}\phi_y(x, y, t) \\ w(x, y, z, t) &= w_0(x, y, t) + z\psi_z(x, y, t) \end{aligned} \quad (2)$$

To obtain dynamic equations of motion, it is necessary to use the relationship between stress and strain in the area of linear elasticity and introduce correction factors in the form:

$$\begin{aligned} \gamma_{0xz} &\rightarrow \kappa_1 \gamma_{0xz}; \quad \gamma_{0yz} \rightarrow \kappa_2 \gamma_{0yz}; \quad \epsilon_{0z} \rightarrow \kappa_3 \epsilon_{0z} \\ \phi_x + \frac{\partial \psi_z}{\partial x} &\rightarrow \kappa_4 \left(\phi_x + \frac{\partial \psi_z}{\partial x} \right) \\ \left(\phi_y + \frac{\partial \psi_z}{\partial y} \right) &\rightarrow \kappa_5 \left(\phi_y + \frac{\partial \psi_z}{\partial y} \right) \end{aligned} \quad (3)$$

Using Hamilton's principle, the dynamic equations of motion are defined in the form:

$$\begin{aligned} \delta u_0 : \frac{\partial N_x}{\partial x} + \frac{\partial N_{xy}}{\partial y} &= I_1 \frac{\partial^2 u_0}{\partial t^2} + \frac{I_3}{2} \frac{\partial^2 \phi_x}{\partial t^2} \\ \delta v_0 : \frac{\partial N_y}{\partial y} + \frac{\partial N_{xy}}{\partial x} &= I_1 \frac{\partial^2 v_0}{\partial t^2} + \frac{I_3}{2} \frac{\partial^2 \phi_y}{\partial t^2} \\ \delta w_0 : \frac{\partial Q_x}{\partial x} + \frac{\partial Q_y}{\partial y} &= I_1 \frac{\partial^2 w_0}{\partial t^2} \end{aligned} \quad (4)$$

$$\begin{aligned} \delta \psi_x : \frac{\partial M_x}{\partial x} + \frac{\partial M_{xy}}{\partial y} - Q_x &= \frac{I_3}{2} \frac{\partial^2 \psi_x}{\partial t^2} \\ \delta \psi_y : \frac{\partial M_y}{\partial y} + \frac{\partial M_{xy}}{\partial x} - Q_y &= \frac{I_3}{2} \frac{\partial^2 \psi_y}{\partial t^2} \\ \delta \psi_z : \frac{\partial R_x}{\partial x} + \frac{\partial R_y}{\partial y} - N_z &= I_3 \frac{\partial^2 \psi_z}{\partial t^2} \\ \delta \phi_x : \frac{\partial S_x}{\partial x} + \frac{\partial S_{xy}}{\partial y} - R_x &= \frac{I_1}{2} \frac{\partial^2 u_0}{\partial t^2} + \frac{I_5}{4} \frac{\partial^2 \phi_x}{\partial t^2} \\ \delta \phi_y : \frac{\partial S_y}{\partial y} + \frac{\partial S_{xy}}{\partial x} - R_y &= \frac{I_1}{2} \frac{\partial^2 v_0}{\partial t^2} + \frac{I_5}{4} \frac{\partial^2 \phi_y}{\partial t^2} \end{aligned}$$

where $\bar{\mathbf{F}} = [N_{xx}, N_{yy}, N_z, N_{xy}, M_{xx}, M_{yy}, M_{xy}, S_{xx}, S_{yy}, S_{xy}]^T$

and $\bar{\mathbf{F}}_s = [Q_{xz}, Q_{yz}, R_x, R_y]^T$ are components of load vectors per unit width corresponding to plane or shear stresses.

Assumed forms of analytical solutions for this type of problem are given in [1] as:

$$\begin{aligned} u_0 &= U_0 e^{i[(k_x x + k_y y) - \omega t]}; \quad v_0 = V_0 e^{i[(k_x x + k_y y) - \omega t]} \\ w_0 &= W_0 e^{i[(k_x x + k_y y) - \omega t]}; \quad \psi_z = \Psi_z e^{i[(k_x x + k_y y) - \omega t]} \\ \phi_x &= \Phi_0 e^{i[(k_x x + k_y y) - \omega t]}; \quad \phi_y = \Phi_y e^{i[(k_x x + k_y y) - \omega t]} \\ \psi_x &= \Psi_x e^{i[(k_x x + k_y y) - \omega t]}; \quad \psi_y = \Psi_y e^{i[(k_x x + k_y y) - \omega t]} \end{aligned} \quad (5)$$

where is ω angular frequency.

If the assumed forms of the solution substitute in (4), the equations of motion is transformed into the matrix form by using of elementary algebraic transformation of matrices:

$$\mathbf{L}\mathbf{U} = \mathbf{0} \quad (6)$$

where is \mathbf{L} matrix of significant coefficients

while $\mathbf{U} = [U_0 \ V_0 \ W_0 \ \Psi_x \ \Psi_y \ \Psi_z \ \Phi_x \ \Phi_y]^T$

is displacement amplitudes vecor.

According to [6], it is possible to separate into an antisymmetric part corresponding to the bending waves:

$$\underbrace{\begin{bmatrix} L_{33} & L_{34} & L_{35} \\ L_{34} & L_{44} & L_{45} \\ L_{35} & L_{45} & L_{55} \end{bmatrix}}_{\mathbf{L}_{as}} \begin{Bmatrix} W_0 \\ \Psi_x \\ \Psi_y \end{Bmatrix} = 0 \quad (7)$$

and symmetric mode corresponding to extension waves:

$$\underbrace{\begin{pmatrix} L_{11} & L_{12} & L_{16} & L_{17} & L_{18} \\ L_{12} & L_{22} & L_{26} & L_{18} & L_{28} \\ L_{16} & L_{26} & L_{66} & L_{67} & L_{68} \\ L_{17} & L_{18} & L_{67} & L_{77} & L_{78} \\ L_{18} & L_{28} & L_{68} & L_{78} & L_{88} \end{pmatrix}}_{\mathbf{L}_s} \begin{pmatrix} U_0 \\ V_0 \\ \Psi_z \\ \Phi_x \\ \Phi_y \end{pmatrix} = 0 \quad (8)$$

Detailed coefficients can be found in [11]. For the existence of non-trivial solutions of equations (7) and (8) it is necessary to be:

$$\det(\mathbf{L}_s) = 0 \text{ and } \det(\mathbf{L}_{as}) = 0. \quad (9)$$

By substituting the expression for the phase velocity $c_p = \omega/k$ and wave number projections $k_x = k \cos(\alpha)$ and $k_y = k \sin(\alpha)$ polynomial equations are obtained by k . Polynomial equations are solved by fixing the product fh and using relation $\omega = 2\pi f$. The solutions of the equation for k^2 are obtained by a numerical procedure. When the values of these solutions are sorted, 5 different curves corresponding to the symmetric or three different curves corresponding to the antisymmetric mode are obtained by using the symbolic and numerical programming in Matlab. By forming ordered pairs of phase velocity and propagation angle for fixed value of fh , phase velocity diagrams in the polar coordinate system are obtained.

4. NUMERICAL RESULTS

Based on the previously described theoretical assumptions numerical results are given. For numerical examples, material with the following characteristics was used [10]:

$$\begin{aligned} \lambda &= 5.65 \cdot 10^9 \text{ Nm}^{-2}; \quad \mu_r = 2.46 \cdot 10^9 \text{ Nm}^{-2} \\ \mu_L &= 5.66 \cdot 10^9 \text{ Nm}^{-2}; \\ \alpha &= -1.28 \cdot 10^9 \text{ Nm}^{-2}; \quad \beta = 220.9 \cdot 10^9 \text{ Nm}^{-2} \end{aligned} \quad (10)$$

By fixing the value of fh , it is possible to obtain a diagram of the phase velocity c_p in function of the propagation angle change of the plane wave in the polar coordinate system.

The Figures 1a and 1b are obtained by varying the angle of wave propagation from 0° to 360° .

Due to the simplicity of the display, it is necessary to normalize the results. Normalization is performed using a longitudinal wave velocity in the direction of the fibers:

$$c_L = \sqrt{\frac{C_{11}}{\rho}} \quad (11)$$

where C_{11} is the elasticity constant in the direction of the fibers and ρ is the density of the material. In the pictures, it is possible to notice a clear separation of the modes obtained by sorting the solutions of the polynomial equation by k^2 . Five curves correspond to the symmetric propagation mode and three curves correspond to the antisymmetric propagation mode. When the direction of propagation does not coincide with the material direction of the layer, then there is no appearance of pure modes but quasi modes appear. For a layer reinforced by one family of fibers, the coefficients of the constitutive matrix are given by the equation (1).

It should be emphasized that Figures 1 and 2 show the results for a material in which the fibers are significantly stronger than the matrix so that the anisotropic properties are very pronounced.

The dimensionless values phase velocity of wave propagation in one layer at different values of the propagation angle and fixed value of ratio $fh/cL = 0.25$ are given in Figure 1:

a) Antisymmetric mode:

- **light blue color** - phase velocity diagram corresponding to the lowest value k^2 . This phase velocity represents a quasi-shear horizontal antisymmetric mode qSH_1 when the shear mode is dominant
- **purple color** - phase velocity diagram corresponding to the largest value of the solution of the polynomial by k^2 . This phase velocity corresponds to the antisymmetric quasi-bending mode A_0
- **red color** - phase velocity diagrams obtained for the value of the solution of the polynomial by k^2 which is between the maximum and minimum value of the solution, and is denoted by qA_1 , which clearly indicates the dominant antisymmetric mode, ie. bending mode

b) Symmetric mode:

- **light blue and black color** - phase velocity diagrams corresponding to the lowest and

highest values k^2 , and represent quasi-shear horizontal modes qSH_2 and qSH_0 respectively.

- **red, purple and blue color** - phase velocity diagrams obtained for sorted values of polynomial solutions by k^2 (sorted from a smaller solution to a larger one) and correspond to the quasi-extension modes that are denoted qS_2, qS_1, qS_0 .

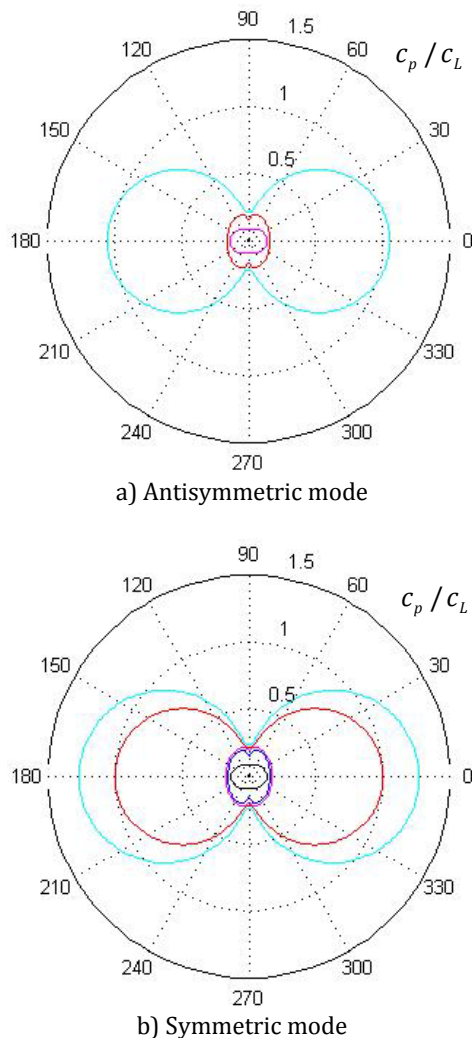


Fig. 1. Phase velocity diagrams of wave propagation in one layer at different values of the propagation angle and fixed value of ratio $fh/c_L=0.25$

It can be seen in Figure 1 that the maximum and minimum values of the phase velocities occur when the direction of propagation coincides with the material direction or is perpendicular to the material direction. In this case, the absence of completely clean modes is noticeable, quasi-modes are already appearing.

The fundamental mode is closest to the pure mode, ie the phase velocity diagram of this mode is elliptical.

Figure 2 shows the dispersion curves of wave propagation in one layer of material reinforced by one family of fibers. It is not difficult to notice that in the antisymmetric mode there is a coupling of quasi-modes, namely quasi-bending (qA_n) and quasi-horizontally shear (qSH_{2n-1}).

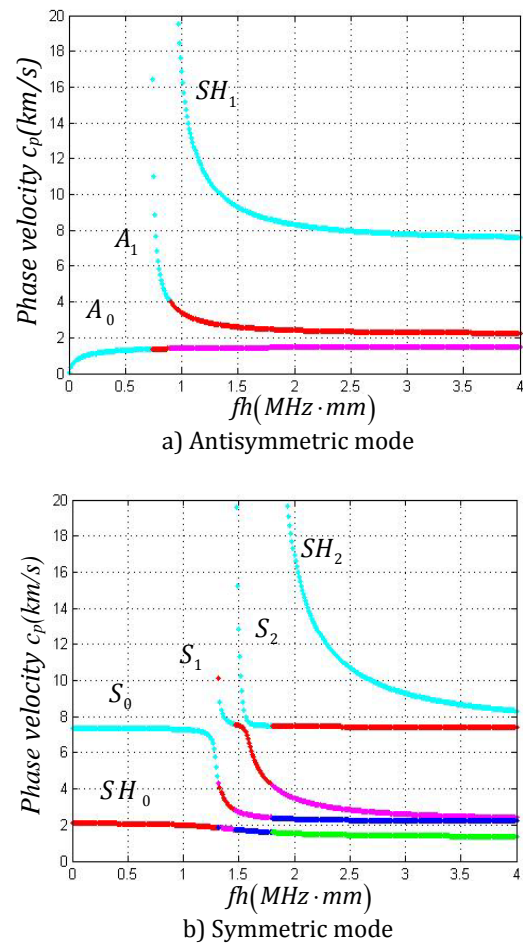


Fig. 2. Dispersion curves of wave propagation in a layer reinforced with one family of fibers at fixed angle of propagation $\phi=45^\circ$

The fundamental A_0 mode arises as a result of the coupling of all three antisymmetric modes, of which the bending mode is dominant. Bending mode A_1 occurs as a result of the coupling of quasi-bending mode qA_1 and horizontal shear mode SH_1 in which the bending mode is dominant. The third mode is the horizontal shear mode SH_1 and it has no mode coupling. It should be emphasized that in both mentioned cases all dispersion curves

asymptotically approach the maximum or minimum value on the ordinate with increasing value on the abscissa.

As said earlier, in case of $\mu_T = \mu_L$ and $\alpha = \beta = 0$ the material behaves like any isotropic material. In that case, pure wave propagation modes appear. For example, in the case of an antisymmetric wave mode the diagrams shown in Figure 3 are obtained.

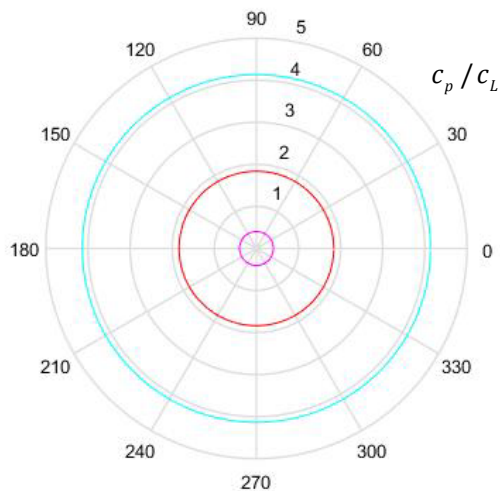


Fig. 3. Phase velocity diagrams of wave propagation in one layer at different values of the propagation angle and fixed value of ratio $fh/c_L = 0.25$

5. CONCLUSION

It is shown in the paper that during the propagation of Lamb waves due to the inhomogeneity of the material and a large degree of anisotropy, a geometric dispersion occurs. Phase velocity and dispersion curve were analyzed. The procedure of application of the second order shear deformation theories in the analysis of Lamb wave propagation through materials reinforced by one family of fibers was implemented.

Verification of the presented theory was performed on numerical examples. Materials whose constitutive matrix is defined through engineering constants were used and excellent matches with existing result obtained in papers [1, 12]. The verified theory provided an opportunity to analyze the propagation of Lamb waves through materials reinforced by a single family of fibers.

The dispersion relations of the phase velocity as a function of the product of the frequency and thickness of the laminate (fh) at a fixed value of

the propagation angle α as well as phase velocity at a fixed value of the ratio $fh/c_L = 0.25$ are analyzed.

The following conclusions were reached:

- By applying the second order shear deformation theory there are three curves (dispersion or phase velocities) corresponding to the antisymmetric propagation mode and five curves corresponding to the symmetric propagation mode.
- In both cases, there is no appearance of pure propagation modes, but quasi-modes have appeared in the form of quasi-bending qA , quasi-extension qS and quasi-horizontally polarized modes qSH .
- Quasi-horizontally polarized modes qSH occur in both clearly separated modes of propagation of symmetric and antisymmetric mode.
- Quasi-horizontally polarized modes occur in both clearly separated symmetric and antisymmetric propagation modes.
- In higher modes the deviations are slightly larger compared to lower modes.
- There are points on the diagram where the transition from one quasi mode to another is clearly seen. On the dispersion curves different colors show the exact transitions from one to another quasimode as well as the values of the frequency at which these transitions occur.

Acknowledgement

This investigation is a part of the projects TR 33015, TR 32036 and multidisciplinary project III 44007 of Technological Development of the Republic of Serbia. We would like to thank to the Ministry of Education and Science of Republic of Serbia for the financial support during this investigation.

REFERENCES

- [1] Wang, L., Yuan F. G. (2007). Group velocity and characteristic wave curves of Lamb waves in composites: *Modeling and experiments, Composites Science and Technology*, vol. 67, no. 7-8. p. 1370–1384.
DOI: 10.1016/j.compscitech.2006.09.023
- [2] Milosavljević, D., Bogdanovic, G., Veljovic L., Radakovic, A., Lazic, M. (2015). Wave propagation in layer with two preferred

- directions. *International Journal of Non-Linear Mechanics*, vol. 73, p. 94-99,
DOI: 10.1016/j.ijnonlinmec.2014.11.014.
- [3] Green, W., A. (1982). Bending Waves in Strongly Anisotropic Elastic Plates. *The Quarterly Journal of Mechanics and Applied Mathematics*, vo. 35, no. 4, p. 485-507.
DOI: 10.1093/qjmam/35.4.485
- [4] Green, W. A., Milosavljevic, D. (1985) Extensional Waves in Strongly Anisotropic Elastic Plates. *The International Journal of Solids and Structures*, vol. 21, no. 4, p. 343-353.
DOI: 10.1016/0020-7683(85)90060-5
- [5] Green, W. A., Rogerson, G. A., Milosavljević, D. I. (1992). Transient Waves in Six-Ply and Eight-Ply Fibre Composite Plates. *Composites Science and Technology*, vol. 44, no. 2, p. 151-158.
DOI: 10.1016/0266-3538(92)90108-F
- [6] Radaković, A., Bogdanović, B., Milosavljević, D., Veljović, Lj., Čukanović D. (2017). Using high-order shear deformation theory in the analysis of Lamb's waves propagation in materials reinforced with two families of fibers, *Acta Mechanica*, vol. 228, p. 187-200.
DOI: 10.1007/s00707-016-1707-1
- [7] Spencer A.J.M. (1984). *Constitutive Theory for Strongly Anisotropic Solids*. In: Spencer A.J.M. (eds) *Continuum Theory of the Mechanics of Fibre-Reinforced Composites*. International Centre for Mechanical Sciences (Courses and Lectures), vol: 282. Springer, Vienna.
DOI: 10.1007/978-3-7091-4336-0_1
- [8] Spencer, A.J.M., (1972). *Deformations of Fibre Reinforced Materials*, Clar. Press, Oxford.
- [9] Milosavljević, D.I., (1986). *Prostiranje talasa u elastičnim pločama ojačanim sa dve familije vlakana*, Univerzitet u Beogradu, Prirodno-matematički fakultet, Institut za mehaniku, Beograd.
- [10] Bogdanović, G., (2011). *Dinamičko ponašanje kompozitnih laminate*. Doktorska disertacija, Univerzitet u Kragujevcu, Mašinski fakultet u Kragujevcu, Kragujevac.
- [11] Radaković, A., Milosavljević, D., Bogdanović, G., Milanović, M., Čukanović, D. Application Of Analytical Methods In Bending Analysis Of Cross Ply Symmetric Laminates, *Proceeding of 14th International Conference on Accomplishments in Mechanical and Industrial Engineering DEMI 2019*, 24 - 25 May 2019, Banja Luka, p.397-402.
- [12] Wang, L. (2004). *Elastic waves propagation in composites*. Phd thesis, North Carolina State University.



Banja Luka
28–29 May 2021.

DEMI 2021

15th International Conference on Accomplishments in Mechanical and Industrial Engineering

www.demi.mf.unibl.org



Solving nonlinear problems in mechanics using simulation

I. Terzic^a, M. Todorovic^b, S. Aleksandrov^b, G. Miodragovic^b

^aFaculty of Engineering, University of Kragujevac, Sestre Janjica 6, 34000 Kragujevac, Serbia

^bAcademy of Vocational and Professional Studies – Sumadija, department in Trstenik, Radoja Krstica 19, 37240 Trstenik, Serbia

Abstract

When, by applying the law of dynamics, the motion of a body is described by a mathematical model, in some cases nonlinear differential equations are obtained that cannot be solved analytically. In the literature, such a model is often linearized, which limits the scope of its application. In addition, an individual solution can be obtained by applying other laws of mechanics, but only for a selected set of given data.

The application of the simulation on the already formed mathematical model, using Simulink from the MATLAB software package, enables the problem to be solved and the solutions to be obtained in the form of diagrams or a family of diagrams for different input data. Visualization of the solution enables reading of the required quantities (position, angle, velocity, acceleration) at any time and further analysis of the influential parameters.

The paper presents examples of simulation of body motion along rectilinear and curvilinear paths, through a resistant medium or along a rough path, whose mathematical models are in the form of nonlinear differential equations. The results are given in the form of diagrams for one group of numerous data, but the formed simulation model can be used for any other input data, by simply changing the numerical value in the appropriate block.

Keywords dynamics, nonlinear differential equations, simulation

1. INTRODUCTION

By applying the dynamic laws, one or a system of differential equations is set that describe the motion of the body, giving a connection between the dependent variable and time. The obtained equations have a form that can be easily integrated only in individual cases. If the body moves through a medium that provides

resistance to movement, the resistance forces (resistance force of air or fluid, friction force of a rough surface) must be taken into account, and then nonlinear differential equations are usually obtained. Solving nonlinear differential equations is demanding and complicated, and on the other hand, linear analysis is very developed and easily applicable. This is the reason why, whenever possible, linearization of the model is resorted to, most often by developing nonlinear members in the Taylor series and neglecting higher-order members in the developed form. However, the scope of the linearized model is limited. The application of modern software packages enables the numerical solution of nonlinear differential equations, but also the

Corresponding author

Phd student, Ivana Terzic
ivana.aa.terzic@gmail.com

Faculty of Engineering, University of Kragujevac
Sestre Janjica 6
34000 Kragujevac, Serbia

determination of the error that occur using linearized models, which defines the applicability of simplified analysis.

In this paper, using the Simulink from the MATLAB software package, kinematic quantities were determined in several examples of rectilinear and curvilinear body motion under the action of resistive forces. The solutions are shown in diagrams from which the coordinates of the position and values of velocity and acceleration can be read at any time. The obtained graphical representation can be used for the analysis of the degree of influence of individual parameters on the kinematic characteristics of the movement.

2. RECTILINEAR MOTION WITH THE RESISTIVE FORCE

When moving in the Earth's gravitational field, the body, which can be considered a material point, is affected by the force of gravity and the force of resistance of the medium (air) opposite to the direction of movement. For higher speeds (but less than the speed of sound), the force of air resistance is proportional to the square of the speed: $F_o = kv^2$.

The proportionality factor k depends on the shape of the body, the density of the medium through which the body moves and the surface of the projection of the body on a plane perpendicular to the direction of movement [1]. In the case of a body falling from a given height h (Fig. 1b.), the differential equation of motion is:

$$\ddot{y} = g - \frac{k}{m}v^2 \tag{1}$$

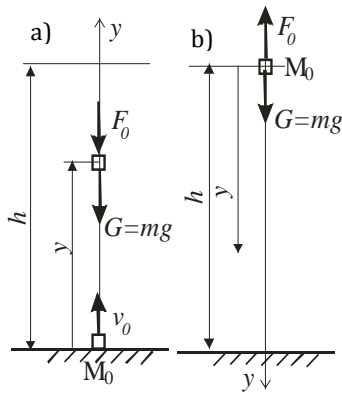


Fig. 1 The motion of a body in the Earth's field gravitates with a resistive force
The nonlinear differential equation (1) can be analytically integrated, but it is far simpler to

solve by applying simulation. Simulink is often used to simulate dynamical systems, as in this paper [2], [3]. The simulation model formed based on equation (1) is shown in Figure 2, with numerous data: $m=10\text{ kg}$, $k=0.2$, $h=100\text{ m}$, $v_0=0$. The movement ends when the body crosses a path equal to the initial height, so the simulation ends when this condition is reached.

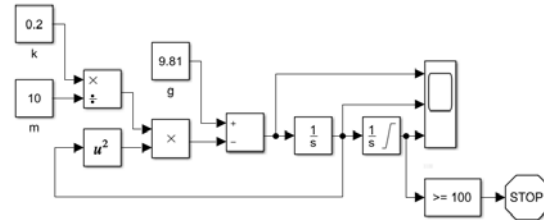


Fig. 2. A simulation model for body fall

The body begins to move without an initial velocity, with the gravitational acceleration and falls to the ground after 6.1 with a velocity of 22.15 m/s (Fig. 3). The movement is accelerated but the intensity of acceleration is constantly decreasing. The maximum speed that the body can reach in a free fall in a resistant environment is the same $\sqrt{mg/k}$ [4]. In this case, a body of mass 10 kg with a coefficient of resistance $k = 0.2$ reached its maximum speed. If the coefficient of resistance of the medium were reduced to $k = 0.02$, the body would fall to the ground at a speed of 41 m/s after 4.75 s , not reaching its maximum speed.

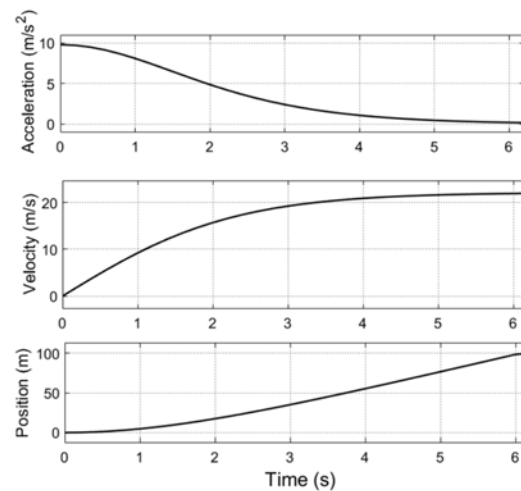


Fig. 3. Body fall – acceleration, velocity, position

The differential equation of motion for a vertical shot (Figure 1a.) is represented by the following expression:

$$\ddot{y} = -g - \frac{k}{m}v^2 \quad (2)$$

In Simulink, a simulation model was formed (Fig. 4) with numerous data $m = 10 \text{ kg}$, $k = 0.02$; for initial velocity $v_0 = 50 \text{ m / s}$. The model predicts that the resistance force will change direction at the highest point of the path, i.e., when the speed direction changes (Fig. 5). Diagrams of acceleration, velocity, and distance travelled in a vertical shot are shown in Figure 6.

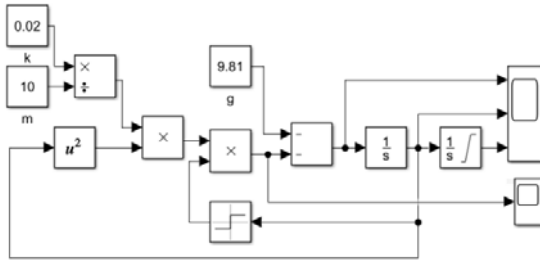


Fig. 4. A simulation model for a vertical shot

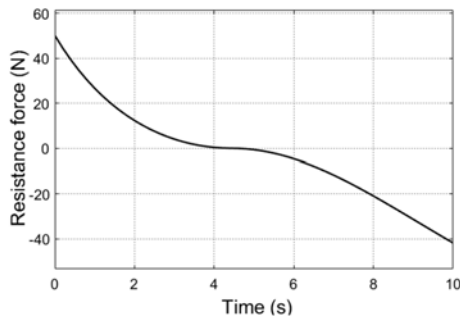


Fig. 5. The force of resistance to movement

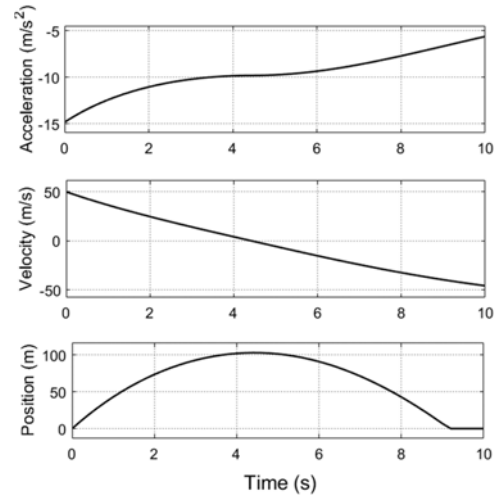


Fig. 6. Vertical shot – acceleration, velocity, position

The diagram in Figure 6 shows that the body reaches a maximum height of 103 m after 4.4 s and falls to the ground at a speed of 41 m / s at 9.2 s . By increasing the coefficient of resistance of the medium to $k = 0.2$, the maximum height reached is reduced to 45 m (by 2.6 s) and the body falls to the ground at a speed of 20.5 m / s after 6.2 s .

3. CURVILINEAR MOTION WITH THE RESISTIVE FORCE

3.1 Mathematical pendulum

On the mathematical pendulum (Figure 7), as an abstract representation of the physical pendulum, only the force of gravity of the Earth and the tensile force of the twine act, so the differential equation of free harmonic oscillations of the mathematical pendulum reads:

$$ml\ddot{\varphi} = -mg \sin \varphi$$

The motion of a mathematical pendulum is often described in the literature as a simple harmonic oscillator for small angles of deviation from the equilibrium position when it can be assumed that $\sin \varphi \sim \varphi$ [5], [6]. If the oscillation angles of the pendulum are larger, the linearized model gives large errors and becomes unusable. After arranging the equations, we obtain a nonlinear (1) and a linearized model (2):

$$\begin{aligned} \text{model (1): } \ddot{\varphi} &= -\frac{g}{l} \sin \varphi \\ \text{model (2): } \ddot{\varphi} &= -\frac{g}{l} \varphi \end{aligned} \quad (3)$$

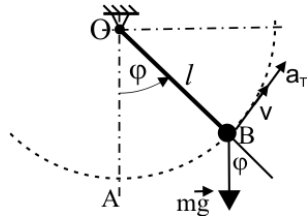


Fig. 7. Mathematical pendulum

Based on equations (3), a simulation model (Fig. 8) was formed to determine the law of motion of the mathematical pendulum. The data were used in the simulation: $l = 1 \text{ m}$ and the initial angle $\varphi_0 = 60^\circ$ and the results are shown in figure 9. The diagram shows that the linearized model gives a shorter period of oscillation, and this error is added over time.

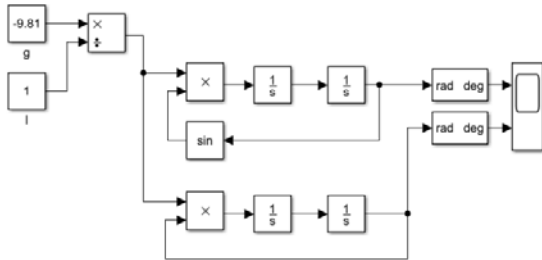


Fig. 8. The mathematical pendulum simulation model

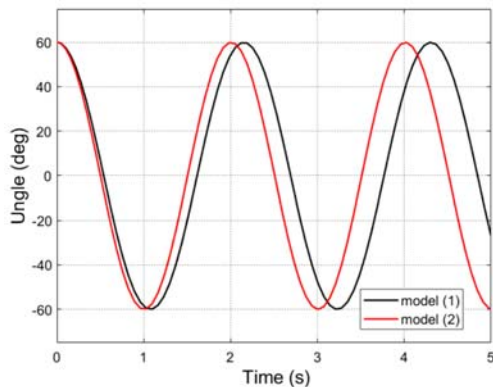


Fig. 9. Laws of motion of nonlinear and linearized model of mathematical pendulum

When a mathematical pendulum is subjected to a resistance force collinear with velocity, but in the opposite direction (Figure 10), whose

intensity is $F_o = kml\dot{\varphi}$ (where k is the damping coefficient), the differential equations of the nonlinear and linearized model are obtained:

$$\begin{aligned} \text{model (3): } \ddot{\varphi} &= -\frac{g}{l} \sin \varphi - k\dot{\varphi} \\ \text{model (4): } \ddot{\varphi} &= -\frac{g}{l} \varphi - k\dot{\varphi} \end{aligned} \quad (4)$$

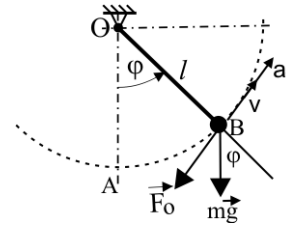


Fig. 10. The mathematical pendulum on which a resistance force acts

Using data $l = 1 \text{ m}$; $k = 0.6$; $\varphi_0 = 60^\circ$, according to equations (4), a simulation model of a mathematical pendulum with damping was made (Fig. 11).

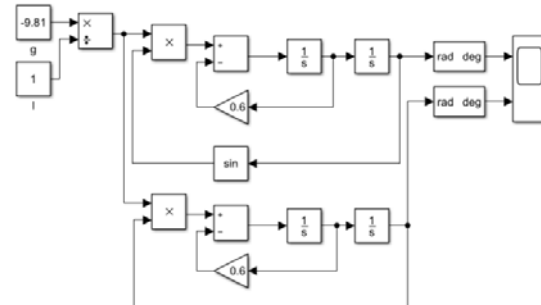


Fig. 11. Simulation model of a mathematical pendulum with damping

The results of the work for models (3) and (4) are shown in Figure 12, for two values of the damping coefficient. If the coefficient is lower ($k = 0.6$) the oscillation will last longer (Fig. 12a) and if the damping coefficient increases to $k = 1.2$ the oscillation lasts shorter (Fig. 12b).

In any case, the linearized model of the mathematical pendulum with damping (4) gives a shorter period of oscillation than the nonlinear model (3).

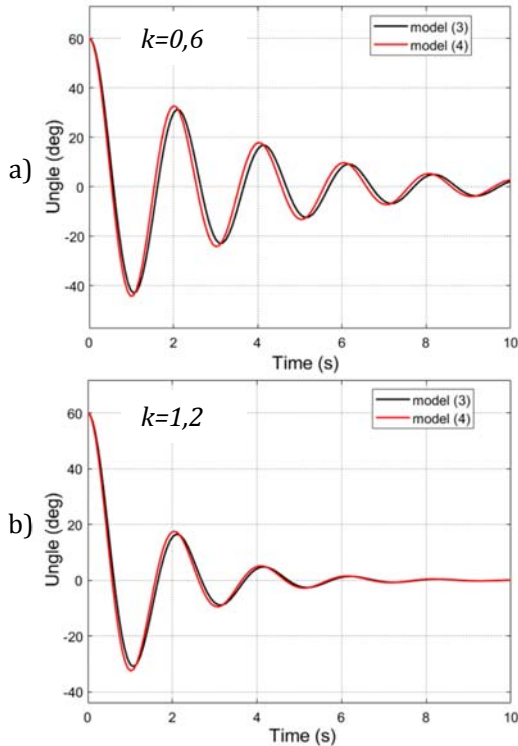


Fig. 12. Damped oscillation of a mathematical pendulum

3.2 Movement of the body along a roughly circular path

A body of mass m , ring-shaped, begins to move from position O along a circularly bent rough wire lying in a horizontal plane (Fig. 13).

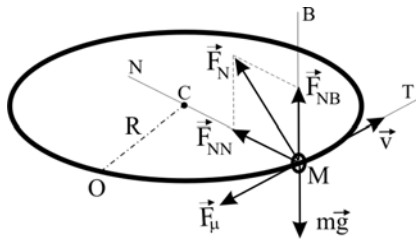


Fig. 13. Moving on a roughly circular path

The substrate reaction has components in the normal \vec{F}_{NN} and bi-normal \vec{F}_{NB} directions, so the friction force will be defined by the expression:

$$F_{\mu} = \mu \sqrt{F_{NN}^2 + F_{NB}^2}$$

The projective equations on the axes of the natural coordinate system (Fig. 13) are:

$$ma_T = m \frac{dv}{dt} = -F_{\mu}$$

$$ma_N = m \frac{v^2}{R} = F_{NN}$$

$$0 = F_{NB} - mg$$

When these equations are obtained, a nonlinear differential equation is obtained that describes the motion of the ring along a roughly circular path:

$$\frac{dv}{dt} = \dot{s} = -\frac{\mu}{R} \sqrt{v^4 + R^2 g^2} \quad (5)$$

The simulation model formed based on equation (5) is shown in Figure 14. Data for radius $R = 0.3 \text{ m}$, coefficient of friction $\mu = 0.3$ and initial velocity $v_0 = 10 \text{ m/s}$ are given.

In the literature [6], this problem is solved analytically only for certain data. Also, the solution can be obtained by applying programming in one of the software packages [7]. The simulation approach allows solutions to be obtained for any values of diameter R and coefficient of friction μ and any initial velocity, by simply substituting the values in a given block. The simulation stops when the speed becomes zero. The simulation results (displacement, velocity and acceleration diagrams) are given in Figure 15.

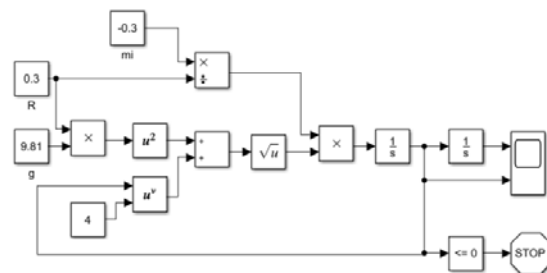


Fig. 14. Simulation model of movement on a roughly circular path

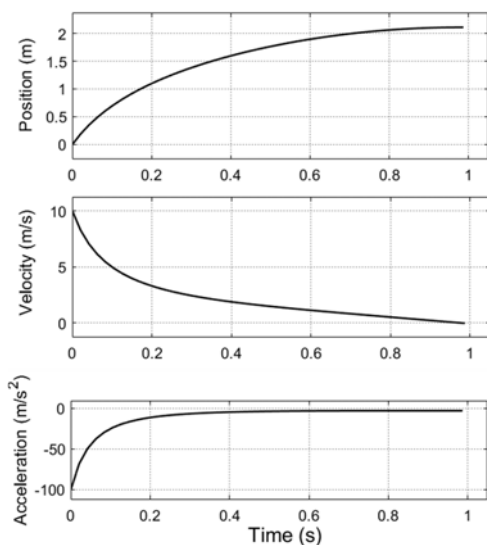


Fig. 15. Moving on a roughly circular path - position, velocity, acceleration

The nonlinear change in position, speed and acceleration of the ring over time is obvious. The values of speed and acceleration fall sharply in the initial period of movement. In Figure 15 it can be seen that for the given input data the ring stops after a distance of 2.1 m at 0.96 s. With a reduced initial velocity $v_0 = 2 \text{ m/s}$ the ring will stop after 0.65 s crossing a path of 0.555 m.

If the coefficient of friction is reduced to 0.15 and the initial velocity remains at 10 m/s, the ring circumvents the circular path twice during 2 s and stops after 4.2 m. As can be seen from expression (5), the kinematic characteristics of the motion are proportional to the coefficient of friction.

4. CONCLUSION

The paper presents the possibilities of the application of simulation in solving nonlinear differential equations that describe rectilinear and curvilinear motion under the action of resistive forces.

From the diagram of the dependence of position, speed and acceleration on time, the required quantity can be read for any time moment. Each of the formed simulation models provides an opportunity to easily obtain results for other input data or modified initial motion conditions. This approach allows you to see the impact of individual parameters on speed, distance travelled or travel time. Errors that occur using

linearized models that describe body motion can also be determined in this way.

REFERENCES

- [1] Vujanović, B. (1976). *Dinamika*. Naučna knjiga, Beograd.
- [2] Karris, S. (2007). *Signals and Systems with MATLAB® Computing and Simulink® Modeling*. Orchard Publications.
- [3] *MATLAB Simulink® 7, User's Guide*. (2015). Copyright 1990–2015 by the MathWorks, Inc.
- [4] Andrejev, V. (1971). *Mehanika III. deo, Dinamika*. Tehnička knjiga, Zagreb.
- [5] Rašković, D. (1965). *Teorija oscilacija*. Naučna knjiga, Beograd.
- [6] Targ, S. M. (1971). *Kratki kurs teorijske mehanike*. Građevinska knjiga, Beograd.
- [7] Todorović, M., Čajetinac, S. (2016). *Mehanika kroz inženjersko programiranje*. Visoka tehnička mašinska škola strukovnih studija, Trstenik.



Banja Luka
28–29 May 2021.

DEMI 2021

15th International Conference on
Accomplishments in Mechanical and
Industrial Engineering

www.demi.mf.unibl.org



Gears Replacement of Minuteman Cover Drive Planetary Gear Train

J. Stefanović-Marinović^a, S. Troha^b, Ž. Vrcan^b, K. Marković^b, A. Šoljić^b

^aUniversity of Niš, Faculty of Mechanical Engineering, Niš, Serbia

^bUniversity of Rijeka, Faculty of Engineering, Rijeka, Croatia

Abstract *The paper deals with the transmission ratio and efficiency determination of a Minuteman cover drive planetary gear train for gears replacement. Two methods are predicted for transmission ratio determination: The Willis method and the alternative torque method. The transformation procedure of one-carrier planetary gear train into the equivalent two-carrier gear train to which the torque method can be applied is explained, concluding that the two methods lead to the same results. This procedure may be applied to other types of planetary gear trains with three central gears. The efficiency was calculated by using reference from literature.*

Keywords *the torque method, Minuteman cover drive, efficiency, transmission ratio*

1. INTRODUCTION

The Minuteman cover drive planetary gear train is a type of 3K gear trains, i.e., planetary gear trains with three central gears (according to Russian classification). There are not many papers dealing with this transmission. The expressions for the basic calculations of the Minuteman-cover drive are given in [1]. The application of this transmission is significant in systems of heavy machinery, such as cranes [2]. This paper is a result of an application of this transmission on a crane. In the process of diagnosing a shipyard crane malfunction, it was concluded that the problem was gearbox failure. Further analysis has shown that the gearbox was in fact the Minuteman cover drive. Since the carrier was not damaged, the intention was to reuse it after repairs. The task

was to replace the gears without decreasing transmission ratio and changing centre distance. The problem was solved, and this paper is a result of the work at problem solving procedure.

2. MINUTEMAN COVER PLANETARY GEAR TRAIN

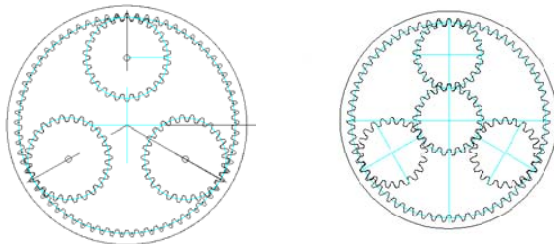
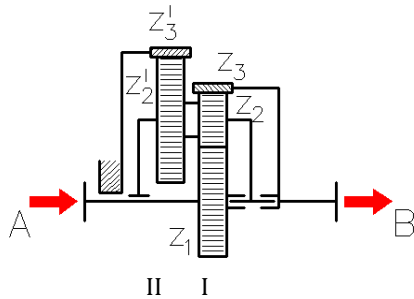
The Minuteman cover drive planetary gear train is a type of 3K planetary gear trains (according to Russian classification), i.e., a planetary gear train with three central gears, shown in Fig. 1. As can be seen in the Fig. 1 there are three central gears: two ring gears, marked as z_3' and z_3 , and one sun gear marked as z_1 . The satellites consist of two external gears z_2' and z_2 . The input element is sun gear z_1 , the output element is ring gear z_3 , while immovable element is ring gear z_3' . No load is transmitted though the planet carrier, and the planet gears rotate around shafts in the carrier spider.

Corresponding author

Assist. Prof. Željko Vrcan, D. Sc. M. E.
zeljko.vrcan@riteh.hr
University of Rijeka, Faculty of Engineering, Rijeka, Croatia
Vukovarska 58, Rijeka, Croatia

This type of planetary gear transmission is used for crane rotation.

When the crane malfunction occurred, the goal was to repair the gearbox without decreasing the transmission ratio, or at least with the transmission ratio remaining within the permissible range.



a) The second component planetary gear train at kinematic scheme - II b) The first component planetary gear train at kinematic scheme - I

Fig. 1. Minuteman cover drive planetary gear train

At the beginning of the process of the gear recovery it was necessary to identify the kinematic scheme.

The numbers of teeth were determined by examination: $z_1 = 24$, $z_2 = 21$, $z_2' = 26$, $z_3 = 66$, $z_3' = 71$. The centre distance with the original numbers of teeth was $a = 47,66$ mm. It was not possible to determine the module and shift coefficients due to severe gear damage. As the intention is to use the original carrier, the centre distance must be at the same value with replacement gears.

It is necessary to determine the transmission ratio and efficiency in both cases to select the appropriate replacement transmission: with original gears and with replacement gears. As This transmission type is rarely used, so the Willis method was applied to determine the transmission ratio first, and after that the

torque method. The expression from [1] was used for efficiency determination.

In the process of gears replacement, it is required to consider that the original gears have been made by diametral-pitch based tooling. On the other hand, the replacement gears must be made by module based metric tooling. Therefore, the module should be chosen according to ISO 54-DIN 780.

The requirements related to centre distance ($a = 47,66$ mm) and transmission ratio can be achieved with the following parameters: $z_1 = 21$, $z_2 = 21$, $z_2' = 26$, $z_3 = 63$, $z_3' = 69$, $m = 2,25$ mm.

The assembly conditions are satisfied by the adopted numbers of teeth [3].

The design of the repaired Minuteman cover drive planet gear is given in Fig. 2.

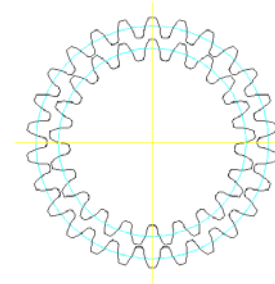


Fig. 2. Replacement satellite design

It can be noticed that the planets have two external gears, and that there are three planet gears with the same phase shift as shown in Fig 2.

The profile shift coefficient must be calculated to satisfy the demand related to centre distance [4].

3. THE WILLIS METHOD APPLICATION TO THE MINUTEMAN COVER DRIVE

As the transmission concerned is not often used, it was necessary to make equations for the Willis method to determine the transmission ratio.

The initial equality is:

$$\frac{n_1 - n_v}{n_2 - n_v} = -\frac{z_2}{z_1} \quad (1)$$

where n_1 , n_2 and n_v are speeds of sun gear, satellite, and carrier.

Also, an equation which determines the relation of planet speed and ring gear speed is necessary:

$$\frac{n_2 - n_v}{n_3 - n_v} = -\frac{z_3}{z_2} \quad (2)$$

Since ring gear z_3 is immovable, the speed is:

$$n_3 = 0$$

Then:

$$n_2 = \frac{z_3}{z_2} n_v + n_v \quad (3)$$

$$n_2 = \left(\frac{z_3}{z_2} + 1 \right) n_v \quad (4)$$

$$n_2 = \frac{z_3 + z_2}{z_2} n_v \quad (5)$$

By substituting the planet speed in equation (1) with equation (5) it is obtained:

$$\frac{n_1 - n_v}{\frac{z_3 + z_2}{z_2} n_v - n_v} = -\frac{z_2}{z_1} \quad (6)$$

$$\frac{n_1 - n_v}{\left(\frac{z_3 + z_2}{z_2} - 1 \right) n_v} = -\frac{z_2}{z_1} \quad (7)$$

and the equation for carrier speed calculation is:

$$n_v = \frac{z_1 z_2}{z_1 z_2 - z_2 z_3} n_1 \quad (8)$$

By substituting the carrier speed in equation (5) with equation (8) it was obtained:

$$n_2 = \frac{z_1 (z_3 + z_2)}{z_1 z_2 - z_2 z_3} n_1 \quad (9)$$

By including equations (8) and (9) into equation (2) it was obtained:

$$\frac{n_1}{n_3} = \frac{z_3}{z_1} \cdot \frac{z_1 z_2 - z_2 z_3}{z_3 z_2 - z_3 z_2} \quad (10)$$

where values for ring gears are considered as negative values.

Also, it is possible to write the corresponding equation to avoid possible mistakes:

$$\frac{n_1}{n_3} = \frac{|z_3|}{z_1} \cdot \frac{z_1 z_2 + z_2 |z_3|}{|z_3| z_2 - |z_3| z_2} \quad (11)$$

By including the numbers of the teeth of all gears in equation (11), the transmission ratio of the original Minuteman cover drive planetary gear train was obtained:

$$\frac{n_1}{n_3} = 25,848$$

By including the numbers of the teeth of the replacement gears in equation (11), the transmission ratio of the replacement Minuteman cover drive planetary gear train was obtained:

$$\frac{n_1}{n_3} = 31,667$$

The transmission ratio in this case is greater than the transmission ratio with original gears. As the goal was to repair the malfunction without regard to productivity, the slower rotation of the crane is not the problem.

4. THE TORQUE METHOD APPLICATION TO THE MINUTEMAN COVER DRIVE

The application of the torque method to 3K planetary gear trains supposes that 3K planetary gear trains change with equivalent two-carrier planetary gear train [2], since the application of torque method is possible to the two-carrier planetary gear trains.

4.1 The equivalent two-carrier planetary gear train

According to the procedure in [2], the Minuteman cover drive with one unloaded carrier shown in Fig. 1, should be replaced with an equivalent two-carrier planetary gear train, as shown in Fig. 3, because the direct application of the torque method to the Minuteman cover drive is not possible.

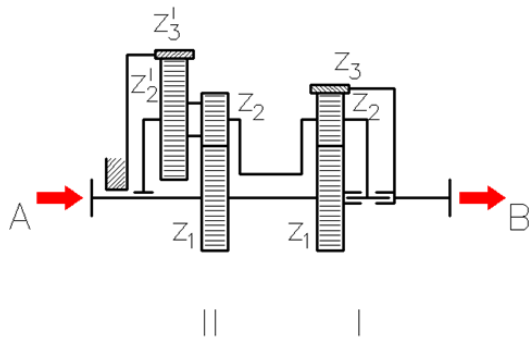


Fig. 3. Equivalent two-carrier planetary gear train

Both the component planetary gear trains (marked with I and II) consist of two central gears: sun gear and ring gear. The difference between the two component gear trains is in the planet gear design which causes different equations for torque ratio determination. The first component planetary gear train is type 2K-H, variant A (i.e., 1A1), and the second component gear train is type 2k-H, variant B (i.e., 2A1).

The equivalent transmission is also presented by Wolf-Arnaudov symbol in the Fig. 4 [5].

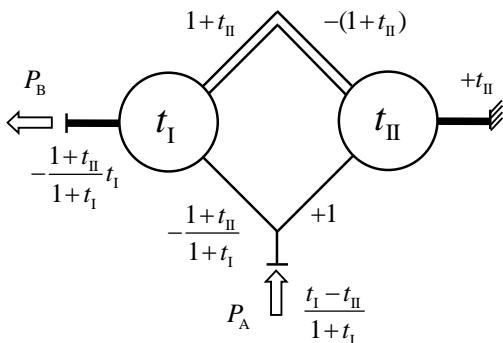


Fig. 4. Wolf-Arnaudov symbol of equivalent two-carrier planetary gear train

Application of the torque method makes possible the comparison of results obtained by this method and the results obtained by using the Willis method.

In the first case, the transmission ratio using the original gears can be obtained by using the ideal torque ratios:

$$t_1 = \frac{|z_3|}{z_1} = \frac{66}{24} = 2,75$$

$$t_{II} = \frac{|z_3'|}{z_2'} \cdot \frac{z_2}{z_1} = \frac{71}{26} \cdot \frac{21}{24} = 2,389423$$

$$i = \frac{1+t_{II}}{t_1-t_{II}} t_1 = \frac{1+2,3894}{2,75-2,3894} \cdot 2,75 = 25,848$$

The ideal torque ratios using the suggested numbers of teeth of the replacement gears are:

$$t_1 = \frac{|z_3|}{z_1} = \frac{63}{21} = 3$$

$$t_{II} = \frac{|z_3'|}{z_2'} \cdot \frac{z_2}{z_1} = \frac{69}{26} \cdot \frac{21}{21} = 2,65385$$

and the transmission ratio is:

$$i = \frac{1+t_{II}}{t_1-t_{II}} t_1 = \frac{1+2,65385}{3-2,65385} \cdot 3 = 31,667$$

The coincidence between two methods is obvious.

5. EFFICIENCY

The efficiency was calculated by using equation (12) from [1]:

$$\eta = \frac{1 - \left[\frac{z_2 z_3'}{z_1 z_2 + z_2 z_3'} \right] (1 - \eta_{12})}{1 + \left[\frac{-z_2 z_3'}{z_3 z_2 - z_2 z_3} - \frac{z_2 z_3'}{z_1 z_2 + z_2 z_3} \right] \left(\frac{1}{\eta_{3'2}} - 1 \right) + \left[\frac{z_2 z_3'}{z_1 z_2 + z_2 z_3} \right] \left(\frac{1}{\eta_{23}} - 1 \right)} \quad (12)$$

where η_{12} , η_{23} , $\eta_{3'2}$ are the partial efficiencies. As it can be seen, partial efficiencies have great influence on efficiency.

In this regard, the calculation with different values for partial efficiency and the same numbers of teeth was done. The quality of gear manufacturing has a significant influence on efficiency, as can be seen in the Table 1 for original gears and in the Table 2 for replacement gears. The partial efficiencies have a significant effect due to power losses in gear meshing.

It can be concluded that efficiency significantly grows as with partial efficiencies rise. The decrease in efficiency due to gear replacement is negligible and can be avoided by increased

quality of gear manufacturing. Also, it is another confirmation that the replacement gears were chosen correctly.

Table 1. Dependence efficiency of partial efficiencies for original gears

η_{12}	η_{23}	$\eta_{3'2'}$	η
0.97	0.97	0.97	0,603535
0.98	0.98	0.98	0,701855
0.99	0.99	0.99	0,829107
0.995	0.995	0.995	0,907819
0.997	0.997	0.997	0,942893
1	1	1	1

Table 2. Dependence efficiency of partial efficiencies for replacement gears

η_{12}	η_{23}	$\eta_{3'2'}$	η
0.97	0.97	0.97	0,58582
0.98	0.98	0.98	0,685991
0.99	0.99	0.99	0,818088
0.995	0.995	0.995	0,901221
0.997	0.997	0.997	0,938623
1	1	1	1

6. CONCLUSION

The application of the Minuteman cover drive is not frequent, and it is generally limited to construction machines, like cranes. Also, there are not many papers based on research of this transmission.

This paper is based on a real problem with this kind of transmission application on the crane.

In this case of gearbox failure, it was necessary to replace only the gears, while the planet carrier could be retained. The original gearbox was not manufactured with metric module tools (ISO/EN), and therefore it was not possible to recreate the same gears.

The broken gears were replaced with gears made using metric module (ISO/EN) based tools i.e., the module and numbers of teeth are different from the broken gears, but the centre distance has remained the same and the transmission ratio is within reasonable range of the original value.

The Willis method was applied to the Minuteman cover drive, and the results crosschecked by the torque method. The torque method application was possible by changing transmission with equivalent two-carrier planetary gear train. As both methods have led

to the same value, it can be concluded that both methods can be applied to the Minuteman cover drive planetary gear trains.

The gear replacement does not significantly influence the efficiency, but the gear roughness must be as small as possible, therefore meaning that the gears must be manufactured in high quality.

These facts indicate that the replacement was correctly made.

Acknowledgement

This research was financially supported by the Ministry of Education, Science and Technological Development of the Republic of Serbia (Contract No. 451-03-9/2021-14/200109)

REFERENCES

- [1] Parmley, R. O. (2006). *Illustrated sourcebook of mechanical components*. McGraw-Hill, USA.
- [2] Muller, H. (1997). *Die Umlaufgetriebe*. Springer-Verlag Berlin Heidelberg.
- [3] Kudriavtsev, V. N., Kirdyashev, I. N. (1977). *Planetary gears*. Handbook, Mashinostroenie, Leningrad.
- [4] Niemann, G., Winter, H. (1989). *Maschinenelemente*. Band II, Springer-Verlag Berlin.
- [5] Arnaudov, K., Karaivanov, D. (2017). *Planetary Gear Trains*. Under the auspices of the Balkan Association of Power Transmission, BAN „Prof. Marin Drinov“, Sofia.



Banja Luka
28–29 May 2021.

DEMI 2021

15th International Conference on
Accomplishments in Mechanical and
Industrial Engineering

www.demi.mf.unibl.org



Estimation of the Remaining Life of the High Pressure Pipeline in the Thermal Power Plant

K. Maksimović^a, S. Posavljak^b, M. Maksimović^c, I. Vasović Maksimović^d

^aSecretariat for Utilities and Housing Services Water Management, Kraljice Marije 1, Belgrade, Serbia

^bUniversity of Banja Luka, Faculty of Mechanical Engineering, Vojvode Stepe Stepanovića 75, Banja Luka
Republic of Srpska, Bosnia and Herzegovina

^cBelgrade Waterworks and Sewerage, Kneza Miloša 27, Belgrade, Serbia

^dLola Institute, Kneza Višeslava 70a, Belgrade, Serbia

Abstract *This paper deals with the estimation of the lifespan of high pressure pipelines within a thermal power plant GACKO. Primary attention is focused on the pipe elbow of the steam line. For this purpose, a precise analysis of stress states as well as thermo-mechanical characteristics of the material is required. The finite element method (FEM) was used to determine the stress in the pipe elbow and to determine critical location zone of the stress concentration at high pressure pipeline in thermal power plant. The material of the pipe elbow is steel 15H1M1F. For the life assessment, "in-house" software was used, which is based on the combined effect of the stress state in the structural element and the thermo-mechanical characteristics of the material. This computation estimate determined that the analyzed elbow under the code CL3 within the high pressure pipeline meets the conditions that its life can be extended, which satisfies the necessary condition between two overhauls.*

Keywords *thermal power plant, high pressure pipeline, pipe elbow, FEM, remaining life*

1. INTRODUCTION

Thermal Power Plants in its working life preoccupy lot of energy sources and costs to produce more energy for distribution to the customers.

Important item in working life of Thermal Power Plant is analysing and prediction of failures and stagnations in system, because, that can prevent lot of problems, stopping the work process and large costs, behind unplanned expenditure of energy. In this paper was

considered the critical zones in terms of stress state and determine procedure for prediction of life assessment and overhaul period. This is one prevent approach, which can save the hours of repairing, energy and money. Structural elements as a part of whole system is exposed to complex stress state and loading, because of complex working conditions.

There are mechanical stress and thermomechanical stress. The subject of this paper is focused on the assessment of the remaining life of structural elements on the high pressure steam pipeline in the Gacko thermal power plant. The entire calculation procedure is shown on the pipe elbow under the code CL3. It should be noted that the high pressure pipeline operates at the temperature of 545 °C and under the

Corresponding author

Dr Strain Posavljak
strain.posavljak@mf.unibl.org
University of Banja Luka, Faculty of Mechanical
Engineering, V. S. Stepanovica 75, 78000 Banja Luka,
Republic of Srpska, Bosnia and Herzegovina

pressure of 250 bar. Therefore, high-pressure steam pipelines are critical components of thermal power plants, which have a significant influence on the reliability and availability of thermal power plants, as well as on safety in service operation. In order to avoid steam pipeline failures, it is necessary to know the stress state under the influence of all expected loads: internal pressure, disturbed thermal expansion, flow, weight of the steam line, concentrated forces, mechanical prestressing loads. In these working conditions, the steam lines the considered pipe elbow should perform its function in the period between two overhauls and not cause damage. Certainly, when it comes to estimating the remaining life, it is necessary to use NDT methods to determine that there is no damage to the considered structural elements. The material of the high pressure pipeline is steel 15H1M1F (GOST) [1]. This material has been used for a long time to make the elements of thermal power plants, and its thermomechanical characteristics have been investigated in detail. High-pressure steam pipelines are basically critical components of thermal power plants, which have a significant impact on the reliability and availability of thermal power plants, as well as on operational safety. To estimate the life of structural elements, it is necessary to know the thermomechanical characteristics of the material as well as the precise analysis of stress states. The finite element method (FEM) within the ANSYS [2] software package was used for the analysis of stress conditions under thermomechanical loading. It is well known that FEM, within the software package ANSYS, is a reliable method for accurate analysis of stress conditions under the action of thermomechanical loads.

Components working at high temperatures, such as elements of high pressure turbines, are exposed to extreme operating conditions and a complex temperature-stress state during exploitation [3-6]. High pressure pipelines are vital parts of thermal power plant systems. Basically, pipelines represent the connection between boilers and turbines in power plants or boilers in power plants and customers in heating plants. They are key

components in power plants and heating plants and have a significant impact on the reliability and availability of power plants and heating plants. Damage to the elements of the steam line can occur even earlier than expected, not only as a result of internal pressure and temperature, but also as a consequence of the load that occurs due to poor design and inadequate maintenance. Also, damage to the elements of the steam lines can occur due to numerous switching on and off of the boiler. Therefore, the analysis of the stress state in steam pipelines is extremely important both for the analysis of the static strength itself and from the aspect of estimating the remaining life. The practice of service life extending is common around the world, not only for economic reasons, but also because the risks are generally reduced with the advancement of knowledge in the areas of metallurgy, strength, dynamics and fracture mechanics. Also, significant contribution to safe maintenance and work of older turbine facilities is provided by data about exploitation of these and similar facilities. Components working at high temperatures, such as elements of high pressure turbines, are exposed to extreme operating conditions and a complex temperature-stress state during exploitation [2-4].

2. STRESS ANALYSIS OF THE PIPE ELBOW ON HIGH PRESSURE PIPELINE

Here is already mention that for structural analyse in the term of remaining life assessment have been used Finite Element Method (FEM). In addition to the geometric characteristics of the pipe elbow, it is necessary to precisely define the material characteristics under thermomechanical loads. Taking into consideration that here is analysed the high pressure pipeline with a large thickness, the pipe elbow is modelled with 3D finite elements. The base parameters for structural analyses of the pipe elbow are pressure $p = 250 \text{ bar} = 25 \times 10^6 \text{ Pa}$, temperature $t = 545 \text{ }^\circ\text{C}$, as well as the time of previous exploitation expressed in working hours.

The geometrical characteristic of the pipe elbow is presented in Table 1.

Table 1. Geometrical characteristic of pipe elbow CL3

Element	Dimension	Radius of elbow [mm]	Thicknesses [mm]
Pipe elbow CL3	Ø325x60	R1370	61.2-65.7

Exploitation time in the previous period: 126.077 h. Steel 15H1M1F has been in use for a very long time (in the 1960s it was already widely used for the production of parts operating at temperatures up to 565 °C and pressures up to 25.5MPa [1]), so there is a large amount of data from real exploitation, for all pipe dimensions used; for example, for very large thicknesses (for diameters 377-530 mm and thicknesses 65-90mm) the time strength at 500 °C for 100 000 h.

Reliable determination of the remaining life of high-pressure steam pipelines requires determination of the stress state, whereby not only the influence of internal pressure and temperature, but all operating loads should be taken into account. Therefore, it is necessary to apply numerical methods of calculation and analysis of the stress state. This paper presents the possibilities of the finite element method in steam line stress analysis. Finite Element Method (FEM) is used to determine critical location, zone of the stress concentration at high pressure pipeline. The main advantage of FEM, unlike analytical and experimental methods, is that it can model all geometric shapes and boundary conditions [7-9]. The governing equation can be used to study the linear/nonlinear static and eigenvalue buckling analysis [12,13]

$$[[K]-[K_T]+[K_G]+\frac{1}{2}[N_1(\delta)]+\frac{1}{3}[N_2(\delta)]]\{\delta\} = \{F_M\}+\{F_T\} \quad (1)$$

where [K] is the linear stiffness matrix, [N₁] and [N₂] are nonlinear stiffness matrices linearly and quadratically dependent on the field variables, respectively, [K_T] and [K_G] are the geometric stiffness matrices due to thermal and initial stress resultants. {F_M} and {F_T} are mechanical and thermal load vectors, δ is the vector of degrees of freedom associated to the displacement field in a finite element

discretization. The governing equation (1) can be used to study the linear/nonlinear static analysis by neglecting the appropriate terms as:

a) Linear static analysis:

$$[K]\{\delta\} = \{F_M\} + \{F_T\} \quad (2)$$

b) Nonlinear static analysis:

$$[[K]-[K_T]+\frac{1}{2}[N_1(\delta)]+\frac{1}{3}[N_2(\delta)]]\{\delta\} = \{F_M\} + \{F_T\} \quad (3)$$

In this analysis, the complete results of the calculation of pipe elbow stress states are given, under the designation, CL 3 (Primary steam flow B: Pipe arc CL3): R = 1370 mm, Ø325x60 mm, p = 25×10⁶ Pa, t = 545 °C, Material 15X1M1F. In order to accurately calculate the stress state in the pipe elbow, only the pipe elbow is modelled with three-dimensional (3-D) finite elements. Figures 1 to 3 show the complete results of the stress state in the pipe elbow.

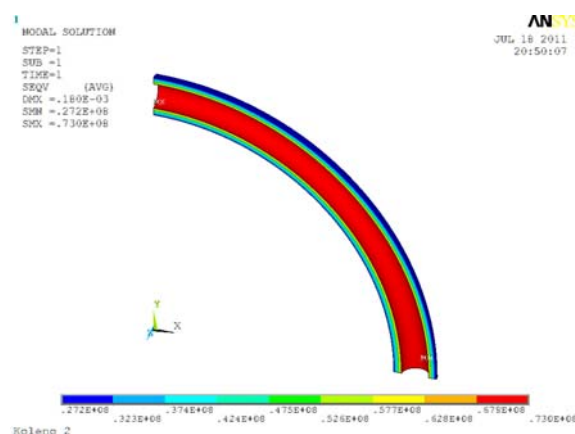


Fig. 1 Equivalent Von-Mises stresses in the pipe elbow [Pa], at the global level (R=1370 mm, Ø325x60)

The maximum equivalent stress that occurs in the pipe elbow is:

$$\sigma_{ekv,max} = 73\,000\,000.00 \text{ Pa (=73.0 MPa)}$$

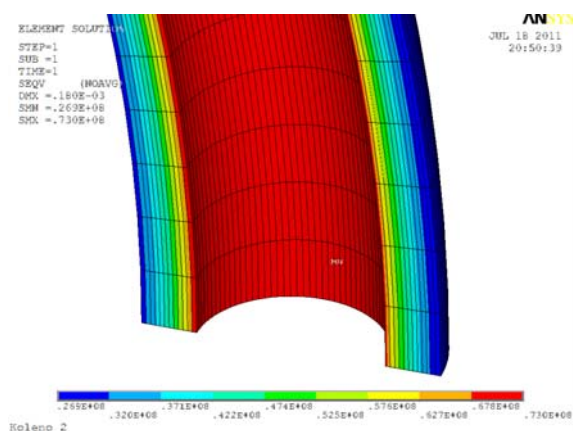


Fig. 2 Equivalent Von-Mises stresses in the pipe elbow detail 1 [Pa]

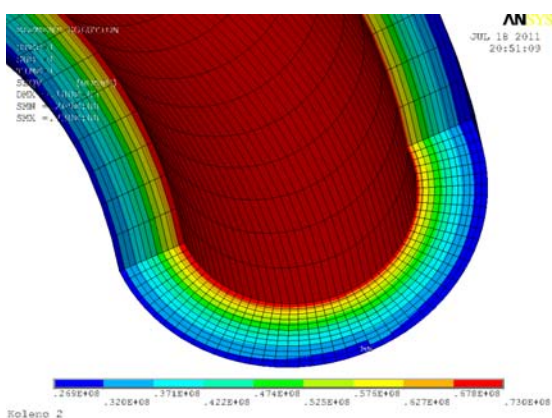


Fig. 3 Equivalent Von-Mises stresses in the pipe elbow detail 2 [Pa]

3. ESTIMATION OF THE REMAINING LIFE UNTIL THE NEXT GENERAL OVERHAUL OF THE PIPE ELBOW

It is well known that during service life, operating conditions may be established that differ from designed conditions. Component overload then occurs due from exceeding designed thermal, fatigue or dynamic loads, as the result of inconvenient steam line configuration, improper function of the supporting system and measuring instrumentation, regulation and control, faulty dimensioned injection system, incorrect component design solution (especially shaped configurations), gasodynamic shock and vibration, especially in transition regimes. In the previous chapter is presented values of the maximal stress that occurs in the knee (pipe elbow) under thermomechanical loads for

working loads. For the purpose of life assessment, the working stresses were increased from the aspect of structural safety (reserve strength factor, RSF) and the maximum obtained value of stresses for the pipe elbow were considered above. That stress is:

$$\sigma_{\max} = \sigma_{\text{ekv,max}} \times \text{RSF} = 73 \times 1.5 = 109.5 \text{ MPa.}$$

For this stress value as well as for the thermomechanical characteristics of the material 15X1M1F using "in-house" software, the results are given in Table 2.

Steel 15X1M1F is used for a long period for the production of thermoenergetic structural elements and has proven to be reliable during very long exploitation time that exceeded 250000 h [1,10]. Therefore, all important thermomechanical characteristics of the material are available, which were used in this case in the development of "in-house" software for estimating the remaining life of the pipe elbow.

This approach based on the used FEM for precise analysis of stress state and definition of critical locations in structural elements together with thermomechanical characteristics of materials can be used for estimates of the remaining life of other structural elements of thermal power plants.

Table 2. Estimation of the remaining life of the steam pipeline

15X1M1F			
Temperatura	Izaberite vrstu napona:	NaponMin	106
540	Donji napon	NaponMax	110
		Korak	1
Analiticko resenje		Izracunaj	Brisi
Napon	tr	Pt	
106	0.000121509	19509.46347	
107	0.000105763	19483.04942	
108	0.000092081	19456.69837	
109	0.000080189	19430.40991	
110	0.000069851	19404.18364	
*			

As mentioned, using the software package for the calculation of the lifetime of structures under thermomechanical load for stress $\sigma_{\max} = 109.5 \text{ MPa}$ and the characteristics of the pipe

elbow material (15X1M1F), the lifetime for the considered pipe elbow is around **19404.00** hours, i.e. the total lifetime of the pipe elbow:

$$N_f \geq 146\,000,00 \text{ h}$$

For the obtained stress values, the computed lifetime estimate satisfies the conditions to allow extension of the CL3 pipe elbow life to about 20000.00 h (where the second condition is included as a time limit between two overhauls should be more than 3 years).

4. CONCLUSION

In practical extension life of structural elements it is necessary to establish conditions for a reliable, safe operation and sustainable development of the energy system. By application of the new reliability model, efficiency is significantly increased by reducing failures in the work of the power plant. The goal of implementation of model recognition emergency sheet is increase system reliability reducing the number of failures. Thus increasing operational safety of plants in energy sector, which is in accordance with the provision of energy security by applying measures of Directive EU. According to directive is necessary to ensure: a reliable, safe, efficient and quality power supply.

This paper presents a computation procedure for estimating the remaining life, i.e. estimating the life of a structural element or pipe elbow of a high pressure steam line. The computation estimate of the remaining life is based on a precise analysis of the stress state on the one hand and the thermomechanical characteristics of the material on the other. Structural analysis, i.e. stress state analysis, was performed using the ANSYS software package. The stress state obtained by the finite element method is more realistic and represents an improvement in relation to the application of stress concentration (intensification) coefficients, obtained empirically. FEM provides a more detailed explanation of in-service behaviour of steam line elements. Finite Element Method (FEM) is used to determine critical location, zone of the stress concentration at high pressure pipeline. The performed stress

analysis of the whole steam line structure and of individual components enables to determine critical locations for stress increase, requiring special attention in the procedure for steam line remaining life assessment. In addition to precise stress analysis using FEM for reliable estimation of the remaining life, well-documented mechanical characteristics of 15X1M1F material at elevated temperatures were used.

This computation estimate determined that the analyzed pipe elbow CL3 within the high pressure pipeline meets the conditions that its life can be extended by 20000.00 h, which satisfies the necessary condition between two overhauls. Precise the life estimation of the structural elements in the thermal power plants is of the crucial importance for defining the period between two overhauls and that is significant for saving the time and money. Unnecessary interruption in working of the plant for overhauls or late inspection of structural elements can lead to the costs that can be avoid using proper analyze presented in this paper.

The extension of the pipe elbow life, in turn, contributes to increasing the reliability and thus the safety of the thermal power plant.

Acknowledgment:

This reseelbow has been supported by the reseelbow grants No. 451-03-9/2021-14/200066, of the Serbian Ministry of Education, Science and Technological Development.

REFERENCES

- [1] Бугай, Н. В., Березина, Т. Г., Трунин, И. И. (1994). *Работоспособность и долговечность металла энергетического оборудования*, Энергоатомиздат, Москва.
- [2] ANSYS: Software packages code based on FEM.
- [3] Jovičić, G., Grabulov, V., Maksimović, S., Živković, M., Jovičić, N., Bošković, G., Maksimović, K. (2009). Residual life estimation of a thermal power plant component: The high-pressure turbine housing case. *Thermal Science*, Vol. 13 no. 4, p. 99-106, DOI:10.2298/TSCI0904099J
- [4] Bakic, G., Sijacki, V., Đukic, M., Maksimović, S., Plesinac, D., Rajacic, B. (2011). Thermal History and Stress State of a Fresh Steam-Pipeline Influencing Its Remaining Service Life. *Thermal Science*. Vol. 15, no. 3, p. 691-704.
- [5] Bakic, G., Sijacki, V., Đukić, M., Maksimović, S., Plešinac, D., Rajčić, B., Andelić, B. (2012). 1.25Cr1Mo0.3V Steel Properties Responsible For Reliable High Temperature Application. Int. Conf. Power Plants. p. 2012-2042, Zlatibor, Serbia: printed on CD
- [6] Vasovic Maksimovic I., Maksimovic S., Stamenkovic D., Stupar S., Maksimovic M., Bakic G. (2014). Fracture Mechanics Analysis of Damaged Turbine. *Thermal Science*, Vol. 18, Suppl. 1, p. S107-S112
- [7] Maksimovic S., Posavljak S., Maksimovic K., Nikolic V., and Djurkovic V. (2011). Total Fatigue Life Estimation of Notched Structural Components Using Low-Cycle Fatigue Properties. *STRAIN an International Journal for Experimental Mechanics*. Vol. 47 (Suppl. 2), p. 341-349.
- [8] Maksimović S., Vasović I., Maksimović M., Đurić M. 2011. Residual Life Estimation of Damaged Structural Components Using Low-Cycle Fatigue Properties. *Proceeding of The Third International Congress of Serbian Society of Mechanics*, 1, p. 605-617. Vlasina lake, 5-8 July (Serbia)
- [9] Ognjanović O., Maksimović K., Stamenković D. (2013). The Effects of Thermal Gradients on Stress Distributions, *Proc. Fourth International Congress of Serbian Congress of Serbian Society of Mechanics*, p. 365-70. Vrnjačka Banja, Serbia, 4-7 June.
- [10] Крутасова, Е. И. (1981). *Надежность металла энергетического оборудования*, Энергоиздат, Москва
- [11] Dhutti, A., Tat-Hean, G. (January 10th 2019). Pipeline Health Monitoring to Optimise Plant Efficiency, Edited by Tolga Taner, *Power Plants in the Industry*, , IntechOpen, DOI: 10.5772/intechopen.80844, Available from: <https://www.intechopen.com/books/power-plants-in-the-industry/pipeline-health-monitoring-to-optimise-plant-efficiency>
- [12] Maksimović, S., Kojić, M. (1995). Geometric and material nonlinear analysis of layered fiber reinforced composite structures: Numerical and experimental study, *Proceeding of the 4th International Conference on Computational Plasticity*, 3-6 April, Barcelona, Spain.
- [13] Maksimović, S. (1996). Instability analysis of layered composite structures using shell finite elements based on the third order theory, *J. Applied Composite Materials*, Vol. 3, p. 301-309.



Banja Luka
28-29 May 2021.

DEMI 2021

15th International Conference on Accomplishments in Mechanical and Industrial Engineering

www.demi.mf.unibl.org



Influence of Cycloid Disk Profile Correction on Contact Force

T. Mačkić^a, N. Marjanović^b, G. Jotić^a, M. Tica^a, Ž. Đurić^a

^aMechanical Faculty of Banja Luka, Bulevar Vojvode Stepe Stepanovića 71, 78000 Banja Luka, Bosnia and Herzegovina

^bFaculty of Engineering University of Kragujevac, Sestre Janjic 6, 34000 Kragujevac, Serbia

Abstract

It is impossible to assemble cycloid drive if there is no certain gap between the cycloid disk and the housing rollers. Due to the existence of these clearances, significant deviations of the contact force in relation to the ideal distribution can occur. During coupling, deformations also occur, which reduce these clearances and enable simultaneous coupling of several teeth. The change in contact force on the produced cycloid disk was examined and compared with a disk with a constant offset. Nikon MCx20+ measuring arm and 3D Nikon MMDx100 scanner were used for scanning profile. The deviation values on the cycloid disk tooth are entered into the contact force calculation program. The most unfavourable case is if the profile correction is constant, where there can be a significant increase in the contact force relative to the ideal distribution. This value can be several times higher, which can lead to high values of contact pressure and tooth wear.

Keywords cycloid drive, contact forces, clearance, deformation

1. INTRODUCCION

Compared with conventional drives, which use the involutes gear teeth, cycloid drives possess a number of advantages, such as compactness, high transmission ratio, high efficiency, quiet operation with no vibration, lower weight, etc.

Lehmann described in detail [1] the procedure for force distribution at cycloid speed reducer for theoretical case (when friction doesn't exist). Chen and others defined complete geometric and kinematic relations of cycloid disc tooth profile, with correct meshing condition and distribution of forces [2].

The influence of the sizes of the clearances and

deformations between the cycloid disk and the rollers is significant, due to the provision of normal and reliable operation of the gearbox. D.C.H Yang and J.G Blanche [3] set out the first significant steps in determining the impact of technological gaps and derived mathematical expressions and numerical methods.

The authors L. Lixing [4] and M. Blagojević [5] dealt with the clearances and deformations of cyclo gears, taking into account the aspect of gear meshing condition.

The existence of technological clearances is very important due to the aspect of simpler assembly, but too large clearances can affect significantly increased contact forces, reduce the percentage of meshing and lead to noisy operation of the transmission.

This paper presents the impact of the clearances, deformations and profile modification on the distribution of contact forces between cycloid disk and housing rollers. An actual model of the cycloid disk was

Corresponding author

MSc Tihomir Mačkić
tihomir.mackic@mf.unibl.org

Mechanical Faculty of Banja Luka
Bulevar Vojvode Stepe Stepanovića 71
Banja Luka, Bosnia and Herzegovina

fabricated, to measure deviations from the produced, nominal and ideal profiles. Nikon MCAx20+ measuring arm and 3D Nikon MMDx100 scanner were used for scanning profile.

2. GEOMETRIC PARAMETERS AND LOADS

The cycloid drive train consists of many parts, which are in contact with each other. The main design parameters of cycloid reducer are (Figure 1) [6]: pitch radius of housing rollers (r), pitch radius of output mechanism rollers (R_{oiz}), diameter of housing pins (d_o) and rollers (D_o), diameter of output mechanism pins (d_{vk}) and rollers (D_{vk}), eccentricity (e), number of housing rollers (z_2) and number of output mechanism rollers (u).

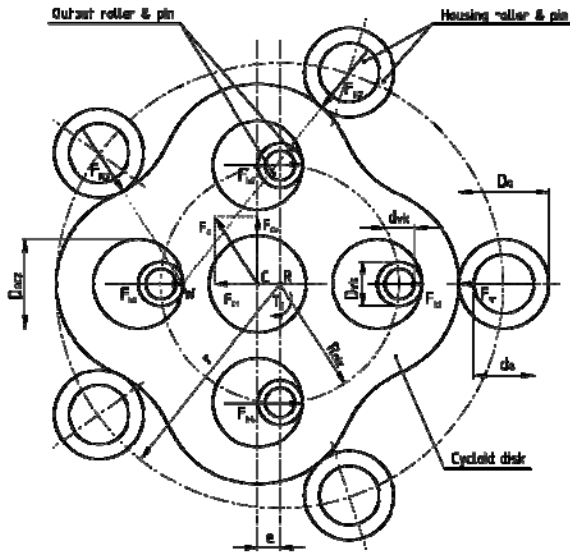


Fig. 1. Design parameters and loads of cycloid disk

Equivalent radius of curvature of coupled profiles is calculated on the basis of the expression [7]:

$$R_e = \frac{r_o \rho_c}{r_o + \rho_c} \tag{1}$$

where:

- $r_o = D_o/2$ - radius of the housing rollers,
- ρ_c - radius of curvature of the inner gear,

$$R_c = \frac{ez[1 + \lambda^2 + 2\lambda \cos \beta]^{3/2}}{z + \lambda^2 + \lambda(z + 1) \cos \beta} - r_o, \tag{2}$$

λ - coefficient of cycloid profile.

For the calculation of contact force between cycloid disk and housing rollers (Figure 2) at the current contact point, the expression can be written [7, 8]:

$$F_{Nt} = \frac{M_{FN}(e) \sin \alpha_{nt}}{e(z-1) \sum_{j=p}^q \sin^2 \alpha_{nt}} \tag{3}$$

where:

p and q - the serial numbers of the starting and ending tooth of the outer gear, which transmit the load,

$M_{FN}(e)$ - the total moment of the normal forces, and it is equal to the sum of the moments of the normal forces, on the individual pairs of teeth, around the center of the gears.

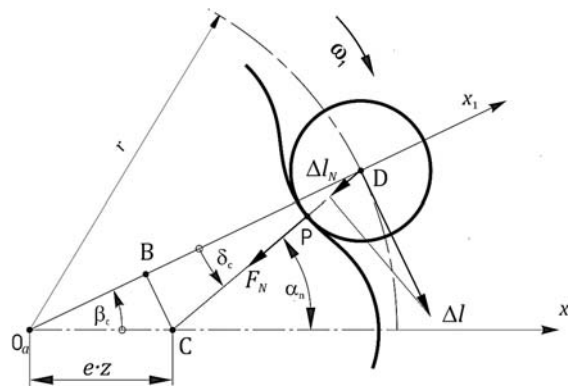


Fig. 2. Force between housing rollers and disc

Force F_{Kj} between output roller j and cycloid disc is calculated based on the following expression (Figure 3) [6]:

$$F_{Kj} = (c_K \cdot \Delta \beta) \cdot r_{Kj} \cdot \sin \psi_{Kj} \tag{4}$$

where:

- c_K - stiffness of roller,
- $\Delta \beta$ - small angle of displacement.

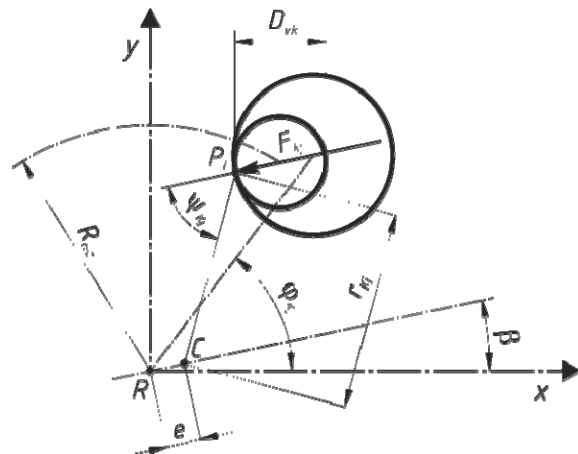


Fig. 3. Force between output roller and disc

If clearances and deformations are neglected, then the contact forces constantly act on the rollers. In Figure 4, the change of the contact force on the housing roller F_N and the contact force on the output roller is shown, where the basic input parameters are:

$r_c=3$ mm, $e=2$ mm, $\lambda=1,5$, $R_{oiz}=14,2$ mm, $T_1=13$ Nm, $n_1=314$ min⁻¹.

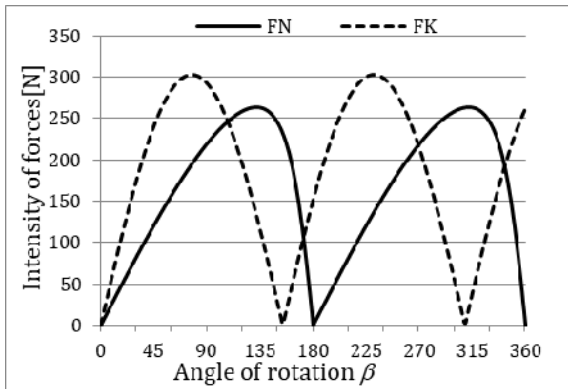


Fig. 4. Force between housing rollers and disc

3. CLEARANCES AND DEFORMATIONS

If it is assumed that the outer ring race of the bearing are tightly fitted into the disk, then the size of the clearance between the roller and the cycloid disk (at the i -th contact point) can be determined based on the following formula [4, 5]:

$$k_{iD} = \delta_{rzs} \left\{ 1 - \frac{\lambda \sin(\pi - \alpha_{ri})}{\sqrt{1 + \lambda^2 - 2\lambda \cos(\pi - \alpha_{ri})}} \right\}, \quad (5)$$

where:

δ_{rzs} - profile correction value.

Total deformation at the i -th contact point between the cycloid disk and housing roller can be calculated as [4, 5]:

$$W_{iD} = \frac{\lambda \sin(\pi - \alpha_{ri})}{\sqrt{1 + \lambda^2 - 2\lambda \cos(\pi - \alpha_{ri})}} W_{max}, \quad (6)$$

where:

W_{max} - the value of the total deformation.

The formulas and procedure for calculating the total deformation are explained in detail in the papers [4, 5].

3.1 Geometrical inspection

An approach which involves a comparison of a digitized model of the produced object (a cloud of spots - real geometry) with a CAD model (nominal geometry) is commonly known as CAD to part [9].

The offset distance between theoretical profile and CAD profile of cycloid disk is 0,05 mm. This offset is needed due to easier mounting of the cycloid disc.

Nikon MCAx20+ measuring arm and 3D Nikon MMDx100 scanner were used for scanning. Presentation of results in the color map region (Fig. 5) implies the generation of a color region based on calculated deviation levels, where the green color signifies regions with a zero-deviation level or a very close to zero level, and the red regions are with the greatest deviations in the positive direction (from the measuring object), and blue regions with the greatest deviations in the negative direction.

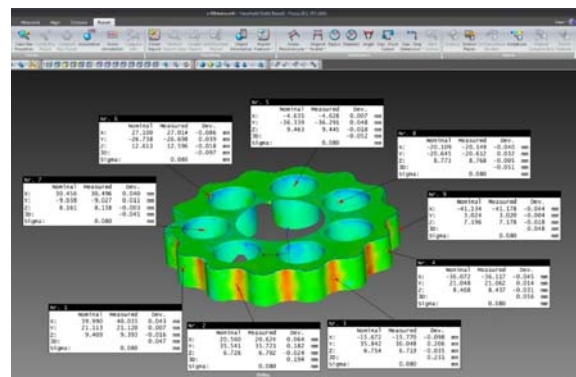


Fig. 5. Presentation of deviation

The difference in the deviation of the produced and CAD model, can be shown in the cross section, as a 2D model (Fig. 6). The deviation was measured at several points on the half of the tooth. The profile correction value or the clearances between the theoretical and produced model, can be calculated as:

$$\delta_{rzs} = \delta_C - \delta_M, \quad (7)$$

where:

δ_C - offset between theoretical profile and CAD profile,

δ_M - deviation between nominal and measured profile.

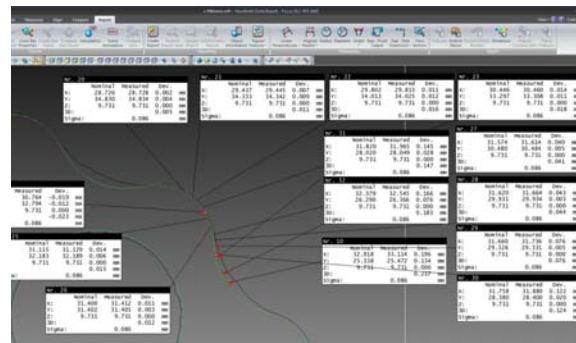


Fig. 6. Deviation on the half tooth profile

4. RESULTS

For the tested cyclic disk, the basic parameters are shown in Table 1.

Table 1. The basic parameters of cycloid disk

Symbol	Parameters	Value	Unit
e	Eccentricity	2	mm
λ	Coefficient of cycloid profile	1,45	
r_c	Radius of the housing rollers	6	mm
z	Number of tooth of cycloid gear	14	
δ_z	Profile correction value	0,05	mm
b	Width of gear	14	mm
P	Input power	750	W
n	Input speed	2800	rpm

If the cycloid disk were made with a constant offset of 0,05 mm, then the difference between the ideal and contact force with constant offset would look like in the Figure 7. The maximum force would increase from 340 [N] to 961 [N].

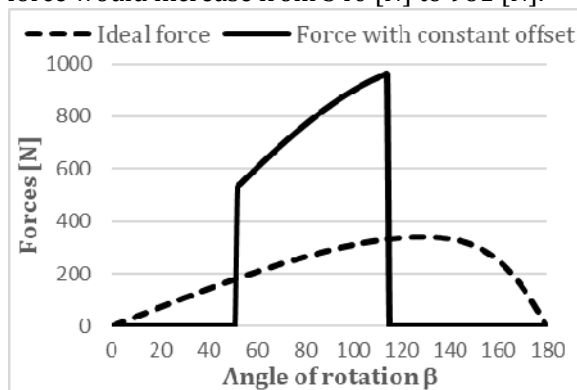


Fig. 7. Contact forces of ideal and offset profiles

The measured (actual) profile (Fig. 8) has certain corrections, ie. less offset in the second coupling phase, so that the maximum force is 347 [N].

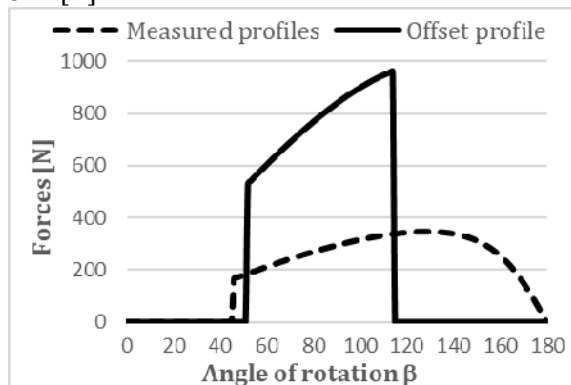


Fig. 8. Contact forces of actual and offset profiles

5. CONCLUSION

Correction of the cycloid disk profile has a significant effect on the magnitude of the contact force. The most unfavourable case is if the profile correction is constant, where there can be a significant increase in the contact force relative to the ideal distribution. This value can be several times higher, which can lead to high values of contact pressure and tooth wear.

REFERENCES

- [1] Lehmann, M. (1976). Calculation and Measurement of Forces Acting on Cycloidal Speed Reducer (in German). PhD Thesis, Technical University Munich, Germany.
- [2] B.K. Chen, T.T. Fang, C.Y. Li, S.Y. Wang, Gear Geometry of Cycloid Drives, Science in China Series E: Technological Sciences, Vol. 51, No. 5, pp. 598-610, (2008).
- [3] D.C.H Yang, J.G Blanche, Design and application guidelines for cycloid drives with machining tolerances, Mechanism and Machine Theory, Volume 25, Issue 5, 1990, Pages 487-501, ISSN 0094-114X, 10.1016/0094-114X(90)90064-Q
- [4] Lixing, L., Xin, L., Weidong, H., Yuanmei, Q., 1999, Profile Modification and Accurate Force Analysis on Cycloid Drive, World Congress on Gearing and Power Transmission, March16-18, Paris, France, pp. 1141-1146.
- [5] Blagojević, M. Analysis of clearances and deformations at cycloid disc, Machine design, 2014, pp. 79-84.
- [6] Mačkić, T., Babić, Ž., Blagojević, M. An analysis of lubrication regime between the contact elements of cycloid reducer. DEMI 2013, Banja Luka, Bosnia and Herzegovina, 30 May-1 June 2013, pp.77-82.
- [7] L. Ivanović, T. Mačkić, B. Stojanović, Analysis of the instantaneous coefficient of friction of the trochoidal gear pair, Journal of the Balkan Tribological Association, Vol.22, No.1, pp. 281-293, ISSN 1310-4772, 2016,
- [8] Ivanović, L. (2007). Identification of the optimal form of the trochoidal tooth profile of the rotary pumps elements. Ph.D. Thesis, University of Kragujevac, Faculty of Mechanical Engineering in Kragujevac, Kragujevac, Serbia (in Serbian)
- [9] Budak, I., Hodolič, J., Bešić, I. i dr. (2009): Koordinatne mjerne mašine i CAD inspekcija, Fakultet tehničkih nauka Novi Sad, Tempus projekat br. IB_JEP-41120-2006, Novi Sad.



Banja Luka
28–29 May 2021.

DEMI 2021

15th International Conference on Accomplishments in Mechanical and Industrial Engineering

www.demi.mf.unibl.org



Upright and frame protective components of pallet racking

R. Vujanac^a, N. Miloradovic^a, L. Petrovic^b, P. Zivkovic^b

^aAssociate professor, Faculty of Engineering University of Kragujevac, Sestre Janjic 6, 34000 Kragujevac, Serbia

^bPhD student, Faculty of Engineering University of Kragujevac, Sestre Janjic 6, 34000 Kragujevac, Serbia

Abstract Adequate protection of pallet racking system depends on a number of parameters, to be defined as a part of a risk assessment. Minimizing the possibility of damage to pallet racking structure is one of the important challenges facing the specifier, designer, supplier and user in the warehouse industry. Protection of the pallet racking against collision from a material handling equipment is of great importance. The purpose of upright and frame protectors are to absorb and disperse impact forces generated by material handling equipment. In addition to the most important safety at work, the important fact is that the replacement of one protective component will always be much cheaper than the replacement of the structural component of the racking system. This paper provides information on the requirements, design and use of basic upright and frame protection of pallet racking. In the practice a number of basic protectors are available and for specific applications dedicated protectors have been developed. Rack protectors are designed and manufactured in accordance with current regulations and standards.

Keywords pallet racking, protection, standards

1. INTRODUCTION

Adjustable pallet racking is the most represented universal system for storing palletized goods. Wide range of its modular components and variety of accessories make the racking adjustable to storage of goods of various sizes and weights enabling direct and easy access to any loading unit using mechanical handling equipment (MHE). That is why they are perfect for warehouses with many articles. Adjustable pallet rack system can be installed in

two configurations: wide aisle or narrow aisle pallet racking [1]. Wide aisle solutions enable a full turn of a fork lift truck within aisle while narrow aisle solutions need induction or solid guides. In both solutions some protective components of pallet racking (rack protectors) are necessary even they are not mandatory equipment. Adequate protection depends on a number of parameters, to be defined as part of a risk assessment. Two basic types of protective components considered within this paper are: upright protectors and side frame protectors [2]. There are a number of different types of other protective components like guide rails and guide-ins, safety and buffering backstops, handrails and stair rails, wire decks, etc. that will not be discussed. Protective components for pallet racking have been designed, manufactured and applied in accordance with current EN standards & FEM regulations:

Corresponding author

PhD Rodoljub Vujanac
vujanac@kg.ac.rs

Associate professor
Faculty of Engineering University of Kragujevac
Sestre Janjic 6
Kragujevac, Republic of Serbia

- Structural design in accordance with EN 15512. Steel static storage systems - Adjustable pallet racking systems - Principles for structural design [3].
- Parameters for application in accordance EN 15620. Steel static storage systems - Adjustable pallet racking - Tolerances, deformation and clearances [4].
- In terms of basic applications and installation locations of column and frame protectors EN 15629. Steel static storage systems - Specification of storage equipment [5].
- In terms of dimensions, construction and required resistance to damage FEM 10.2.16. The Design and Use of Rack Protection for Adjustable Pallet Racking - Upright and Frame Protection [6].

2. RACK PROTECTION TYPES

The main role of the upright and frame protectors are to eliminate mechanical damage to warehouse racks caused by impacts from material handling equipment, usually order picker or fork lift truck. The new generation of forklifts are equipped with modern control and security systems that make them easier and safer to use. They are designed to operate at low speeds which are not critical in terms of occupational safety [7]. However, common practice says that it is inevitable that a forklift driver in a quick operation will eventually hit the racking upright [8]. According to the FEM 10.2.16 location of the racking protection shown in Figure 1 has been defined as following:

- Each corner uprights where is crossroads.
- On the rear upright and frame bracing where goods are stored at the ends outside of a run.
- On the rear uprights and frame bracing at each side of a passageway through the rack configuration.
- Protection of internal uprights within an aisle is optional and shall be based on the risk assessment [8].

Rack protections can be classified according to several criteria:

- Position in the racking configuration:
 - Upright protection
 - Frame protection
- Method of installation:
 - Floor fixed

- Upright fixed
 - Type of material: steel, plastic, foam rubber, rubber or combination of materials.
- Each type of above-mentioned solution has advantages and disadvantages and shall be installed according to the risk assessments by designer, supplier or/and user [8].

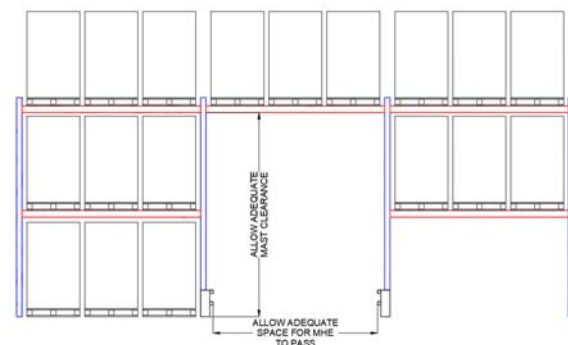
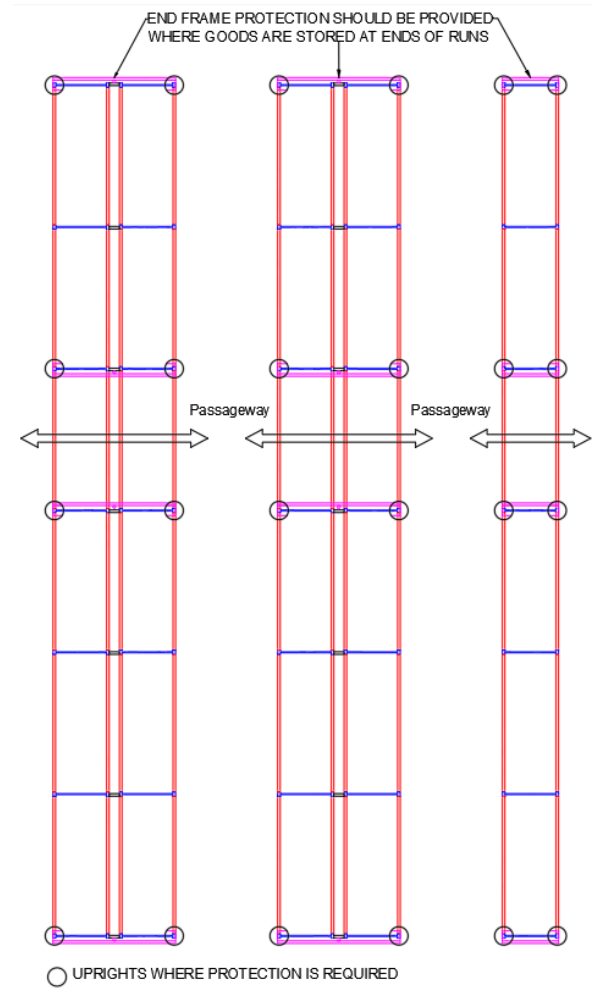


Fig. 1. Location of racking protection [6]

2.1 Upright protection

Upright protectors according to the position of the upright in the racking structure can be realized in form of the corner as shown in Figure 2. a) or in-aisle protector shown in Figure 2. b). For both solutions a minimum of 300 mm high from the floor level is required. Taking into account the position relative to the upright, protectors can be floor or upright mounted. The first and most popular type is freestanding steel rack protectors mounted on the floor in front of each upright in a rack aisle. If fork lift truck hits protector, it transmits the load into the floor slab and not into the racking structure [6]. So, floor fixed protectors may lead to floor damage or disruption of the anchoring due to excessive and repeated impacts without disturbing the rack structure [6].

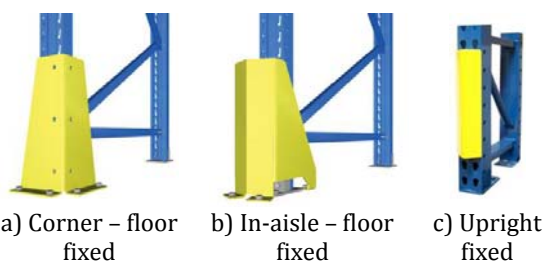


Fig. 2. Upright protectors [9-10]

The second type of protector is upright fixed protectors (Figure 2. c). These protectors don't try to stop a forklift or pallet when it hits a rack. Instead, they try to absorb the impact. Therefore, their advantage comparing the first type is in terms of easier installation and replacement after damage.

2.2 Frame protection

Frame protector shown in Figure 3 provides protection to the corner and rear uprights with frame bracing. According to their position in the racking structure they can be performed as single row protectors or double row protectors. Taking into account the position relative to the end frames they can be performed in two types, too [6]. The first type of frame protectors shown in Figure 4 is located close to the end frame. They protect at the same time complete line of end frames, i.e. their uprights and bracing. They usually consist of two edge upright protectors connected with one or two horizontal rails. This

rail or rails shall, as minimum, extend between 50 mm and 300 mm from the floor level.



Fig. 3. Frame protector [9]

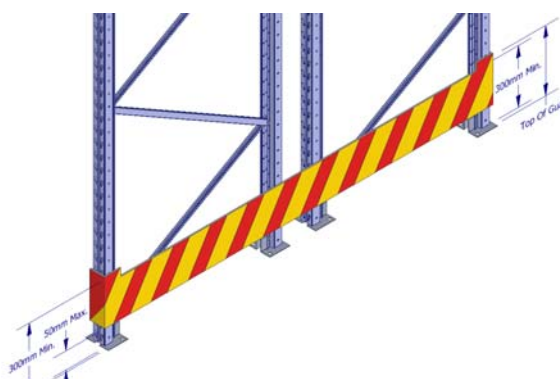


Fig. 4. Type 1 frame protector [6]

The second type of frame protector as shown in Figure 5 are located a minimum of 200 mm from the end frame and provide clearance to minimise frame impact. The ends of the frame protector, which act as a guard to the front upright, shall be minimum of 300 mm high from the floor level. The barrier shall be at any height between 100 mm from the floor and the top of the guard to the front upright [6].

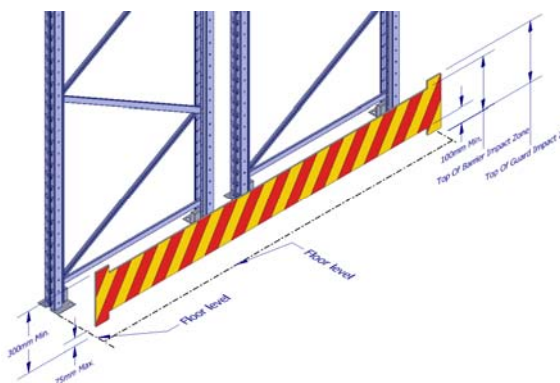


Fig. 5. Type 2 frame protector [6]

3. DESIGN REQUIREMENTS

Standard EN 15620 defines allowed clearance within a bay, dimension "A", between pallet or load and upright. For the freestanding upright protectors according to the FEM 10.2.16 clearance "Δ" between the edge of the column protector is less than or equal to 40 mm from the side of the upright, shown in Figure 6. a). If this clearance "Δ" is greater than 40 mm total clearance "C" shall increase for the additional dimension "B", as shown in Figure 6. b).

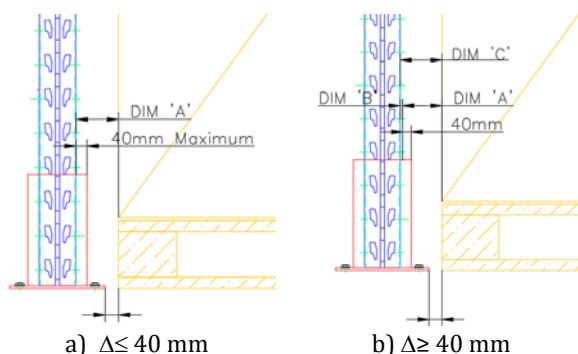


Fig. 6. The minimum distance from the upright to the protector [6]

For the attached upright protectors clearance between the edge of the column protector is less than or equal to 15 mm from the side of the upright, shown in Figure 7. a). If this clearance is greater than 15 mm total clearance "C" shall increase for the dimension "B", as shown in Figure 7. b).

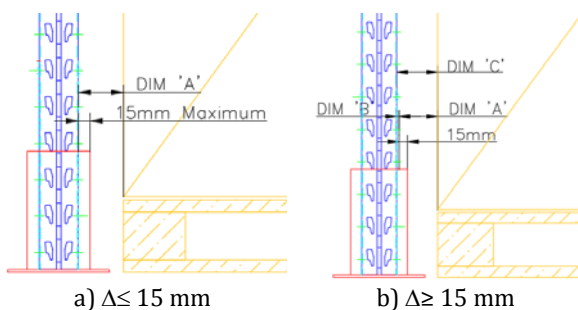


Fig. 7. The minimum distance from the upright to the protector [6]

For the frame protectors, length of the barrier shall be equal or greater than single frame or double frames as shown in Figure 8. The second limit is that barrier and baseplates should not extend past pallet and load overhang. The position in front of the frame

from 200 mm up to 600 mm depends on corridor necessary for MHE passage.

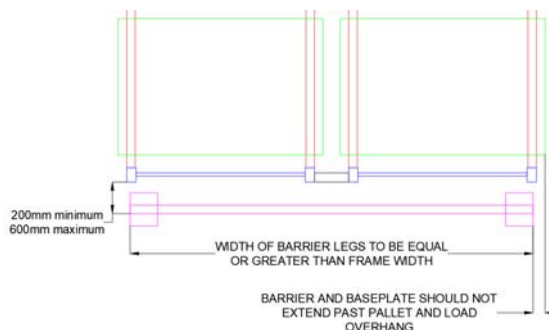


Fig. 8. Location of Type 2 frame protection [6]

Upright protection shall be designed in accordance with FEM 10.2.16 where the minimum horizontal energy absorption is defined in Table 1 and Figure 9 according to the "Key" E4→400J and E2→200J.

Table 1. Minimum design criteria of upright protection [6]

Protection type	Energy absorption to front face (J)	Energy absorption to side face (J)	Impact zone
Corner	400	400	75 mm to top of protector
In-aisle	200	200	75 mm to top of protector

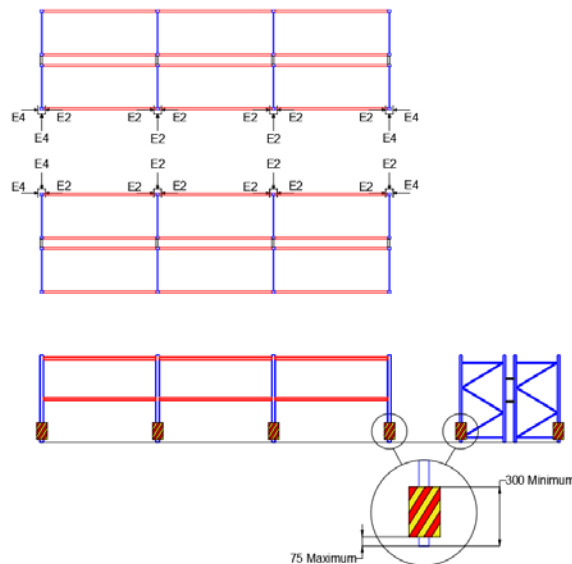


Fig. 9. Upright protection types [6]

End frame protection shall be designed in accordance with FEM 10.2.16 where the minimum horizontal energy absorption of 400 J in direction specified in Figure 10.

Table 2. End frame protection impact zone [6]

Protector rating	Impact zone
Type 1	
Front upright protection	75 mm to top of protector
Rear upright and bracing	75 mm to top of protector
Type 2	
Front upright protection	75 mm to top of protector
Rear upright and bracing	At top of barrier

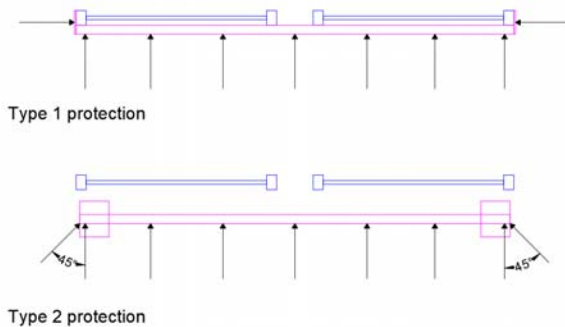


Fig. 10. Frame protection types [6]

4. CONCLUSIONS

Pallet rack damage can be extremely costly and dangerous. Damaged racks are more likely to collapse or drop down their loads, so avoiding that damage is important. Minimising the possibility of damage to pallet racking is one of the important challenges facing the storage industry. There are plenty of reasons of racking damage and one of them as most common is when MHE impact them. Replacing a single protective component will always be much cheaper, easier and faster than replacing an entire upright. Within application and maintenance of storage equipment it is not always necessary but fully recommended to take the most basic protective measures. Protectors range from simple steel protector that anchors to the floor to upright fixed protector that surrounds the upright to absorb potential impact. Their design and application in combination with many other safety accessories according to EN standards and FEM

regulations is of great importance for safe and long term usage of storage equipment.

REFERENCES

- [1] Vujanac, R. (2007). *Razvoj metodologije za projektovanje i proračun nosećih elemenata skladišnih sistema*. (In Serbian). MSc thesis. Mašinski fakultet u Kragujevcu Univerziteta u Kragujevcu.
- [2] MGL. Rack protectors. From: <https://mgltechnika.com/racking-accessories/rack-protectors>, accessed on: April 22, 2021.
- [3] EN 15512 (2009). *Steel static storage systems - Adjustable pallet racking systems - Principles for structural design*. European Committee for Standardization. Brussels.
- [4] EN 15620 (2008). *Steel static storage systems - Adjustable Pallet Racking - Tolerances, deformations and clearances*. European Committee for Standardization. Brussels.
- [5] EN 15629 (2008). *Steel static storage systems - Specification of storage equipment*. European Committee for Standardization. Brussels.
- [6] FEM 10.2.16 (2017). *The Design and Use of Rack Protection for Adjustable Pallet Racking Upright and Frame Protection*. European Racking Federation. Hitchin.
- [7] Vujanac, R., Miloradovic, N., Djordjevic, M. Design of fork lift speed limit control system for warehouse. *Proceeding of 7th Int. Congress Motor Vehicles & Motors MVM 2018*, October 2018, Kragujevac, p. 393 - 397.
- [8] EN 15635 (2008). *Steel static storage systems - Application and maintenance of storage equipment*. European Committee for Standardization. Brussels.
- [9] Stow. Rack protection. From: <https://www.stow-group.com/en/products/pallet-racking/pallet-protection>, accessed on: April 22, 2021.
- [10] Cisco-Eagle. Comparing Pallet Rack Frame Protectors. From: <https://www.cisco-eagle.com/blog/2016/01/21/comparing-pallet-rack-frame-protectors>, accessed on: April 22, 2021.



Banja Luka
28-29 May 2021.

DEMI 2021

15th International Conference on Accomplishments in Mechanical and Industrial Engineering

www.demi.mf.unibl.org



Structural FEM analysis of an aircraft piston engine cylinder assembly at elevated temperature

N. Vučetić^a, R. Antunović^a, B. Krstić^b, D. Jeremić^a

^aUniversity of East Sarajevo, Faculty of Mechanical Engineering, Vuka Karadžića Street 30, East Sarajevo

^bUniversity of Defense in Belgrade, Military Academy, Generala Pavla Jurišića Šturma 33, Belgrade

Abstract

In this paper the numerical structural analysis of the cylinder assembly of an aircraft piston engine at elevated temperature is presented. The considered cylinder assembly failed during the flight of the aircraft due to the appearance of a crack on the cylinder head. The connection of the cylinder body to the cylinder head, as well as the connection of the cylinder body to the engine housing is simulated numerically and the mechanical load that occurs during operation is applied. Based on the analysis performed at elevated temperature, the distribution of equivalent stress on the cylinder head and on the cylinder body was determined and the areas with minimum and maximum stress values were shown. The main goal of this paper is to determine the zones with the highest stress values that represent potential locations of fatigue crack initiation. The obtained results showed a non-uniform distribution of the stress field per cylinder assembly. Based on the above research, it can be concluded that thermal stresses are dominant during the numerical structural analysis of the cylinder assembly.

Keywords FEM analysis, cylinder assembly, crack, Von-Misses stress, thermal analysis

1. INTRODUCTION

The finite element method (FEM) is one of the numerical methods on the basis of which, with satisfactory reliability, a quality structural analysis of machine elements or structures can be performed. In order to obtain reliable results during the analysis, it is necessary to set the appropriate loads as realistically as possible. Boundary conditions must be defined so as to simulate real constraints as closely as possible [1-5].

Since the cylinder assembly, analyzed in this paper, has a very complex geometry, consists of two different materials and is exposed to a combined thermomechanical load, it was not possible to perform a structural analysis analytically. The mentioned cylinder assembly failed during the flight due to the appearance of a crack on the cylinder head.

Cylinder heads are components that are exposed to multiaxial thermomechanical loads leading to fatigue.

In paper [6] a 3D model of the cylinder head was created and a structural FEM analysis of the area between the intake and exhaust valve was performed in order to determine the strength and reliability of the mentioned construction. The failure analysis of the cylinder head made of aluminum concluded that the crack was caused by the appearance of high pre-stressing [7]. In papers [8-10] the locations with the

Corresponding author

PhD, Nikola Vučetić, Assistant Professor
nikola.vucetic@ues.rs.ba

University of East Sarajevo, Faculty of Mechanical
Engineering
Vuka Karadzica Street 30
East Sarajevo, Bosnia and Herzegovina

highest stress values on the cylinder heads were determined by structural FEM analysis.

The aforementioned papers have provided research on aluminum alloys and aluminum cylinder heads related to the automotive industry. For the aluminum alloys from which the cylinder heads in mentioned research are made, a sufficient number of data can be found in the literature and they have been the subject of several studies to date. The research in this paper addresses the problems related to the failure of the cylinder head of an aircraft piston engine. So, it is about aviation industry with very strict requirements for the safety of all aircraft components for reasons of increased safety of passengers and the aircraft itself.

Research in this paper includes the structural FEM analysis of the cylinder assembly exposed to high cycle mechanical and thermal loads that failed due to a crack appearance on the cylinder head. A 3D cylinder assembly model was created. Using structural FEM analysis zones with the highest stress values, both mechanical and thermal, that represent potential locations of fatigue crack initiation were determined.

2. CYLINDER ASSEMBLY MODEL AND BOUNDARY CONDITIONS

The Lycoming IO-360-B1F engine cylinder assembly was modeled in Catia V5-6R2013, Fig. 1. The cylinder assembly is air-cooled and it consists of cylinder body (the lower part) and cylinder head (the upper part).

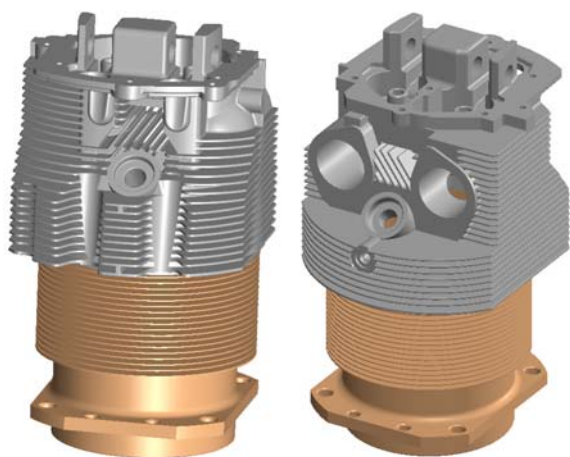


Fig. 1. Cylinder assembly 3D model

The assembly 3D model was imported into Ansys Workbench for further structural

analysis. The cylinder body is made of CrNiMo steel with AISI 4140 designation. The material properties of the cylinder body have been taken from the literature [11]. The inside of the cylinder body is sanded and honed and the outside has deep cooling fins.

The cylinder head is made of cast aluminum alloy 242.0. Mechanical properties of aluminum alloy 242.0 that are going to be used as input values in structural FEM analysis were determined in earlier research [12].

The connection between the cylinder body and the cylinder head is achieved by heating the cylinder head to a temperature of approximately 350°C and so warmed up it fastens to the cylinder body by a threaded connection formed by threads on the outside of the cylinder body and the inside of the cylinder head. By cooling of the cylinder head an extremely rigid connection is being realized, both in the threaded area and between the corresponding smooth cylindrical surfaces above the threaded joint. Therefore, the connection of the cylinder body to the cylinder head is numerically modeled as a rigid connection „Bonded“, Fig. 2.

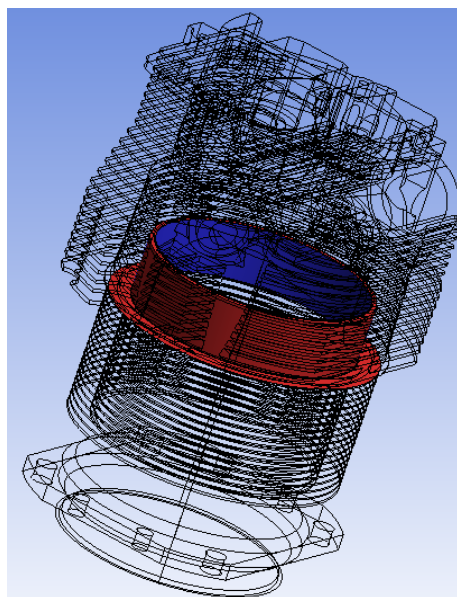


Fig. 2. The cylinder head to the cylinder body connection

The cylinder body is connected to the engine housing by eight screws. Thus, the base of the cylinder body is numerically presented as fixed, Fig. 3.

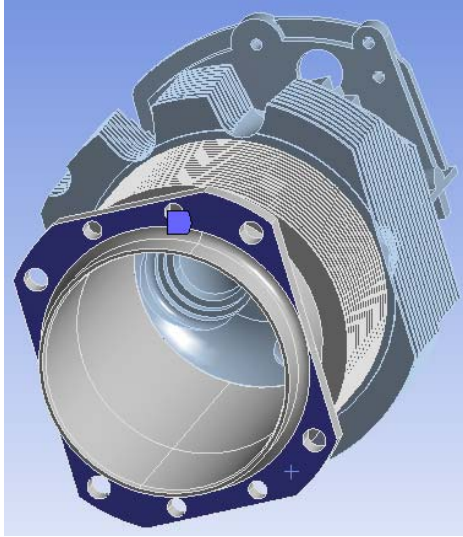


Fig. 3. The cylinder body to the engine housing connection

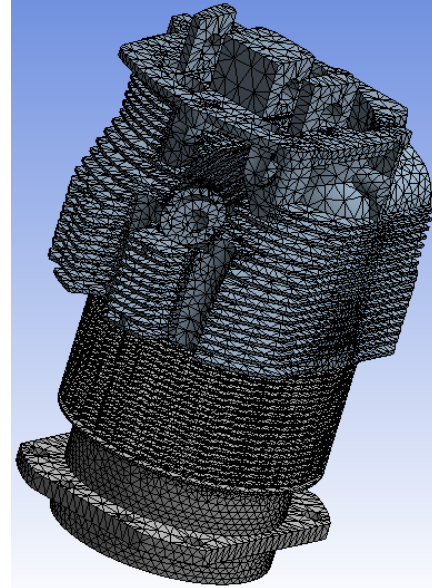


Fig. 4. Tetrahedral finite element mesh

3. COUPLED THERMOMECHANICAL STRUCTURAL FEM ANALYSIS OF THE CYLINDER ASSEMBLY

The main aim of structural analysis of the cylinder assembly using Steady-State Thermal and Static Structural modules is to identify the locations that represent sources of the stress concentration as potential locations for crack appearance and to determine the stress values, both mechanical and thermal.

Tetrahedral finite elements with midside nodes SOLID187 will be used for structural FEM analysis of the cylinder assembly. The SOLID187 finite element consists of 10 nodes with three degrees of freedom each and is suitable for creating an irregular finite element mesh due to the possibility of good adjustment. Tetrahedral finite elements with midnodes are suitable because they easily fill volumes and can be generated automatically, unlike hexahedral finite elements which, for a large number of engineering problems, require appropriate skills to be generated. Tetrahedral finite elements enable easier finishing of the local finite element mesh compared to hexahedral finite elements which are much more difficult to achieve if the good quality of the mesh is to be maintained [13,14].

The mesh of tetrahedral finite elements with midside nodes was generated on the 3D model of the Lycoming IO-360-B1F aircraft engine cylinder assembly, Fig. 4.

The finite element mesh consists of 145604 elements and 277367 nodes. The minimum finite element size was 0.062 mm and the maximum was 12.3 mm.

The analysis of the stress state of the cylinder assembly at operating temperature, first, requires a thermal analysis of the assembly using the Steady-State Thermal module in Ansys Workbench.

Thermal loading is the most important loading in the thermomechanical analysis of cylinder heads [15]. At very beginning of analysis it is necessary to calculate the heat that occurs in the cylinder assembly, as well as the heat losses defined by convection over individual surfaces. Based on the energy content of gasoline [16]:

$$E_g = 33 \cdot 10^6 \left[\frac{J}{L} \right]$$

and aircraft piston engine average consumption:

$$A_{con} = 25 \left[\frac{L}{h} \right],$$

total consumed power is:

$$P_{tot} = E_g \cdot A_{con} = 229.17 [kW].$$

The share of thermal energy in the total is defined by the coefficient [17]:

$$k_t = 0.75,$$

wherein the total thermal energy is:

$$P_t = k_t \cdot P_{tot} = 171.875 [kW].$$

The share of thermal energy going to the engine is defined as:

$k_{mt}=0.5$,

on the basis of which the thermal energy that goes to the engine is:

$$P_e = k_{mt} \cdot P_t = 85.937[\text{kW}].$$

Thermal energy per engine cylinder is:

$$P_c = \frac{P_e}{4} = 21.483[\text{kW}].$$

The energy distribution in the cylinder assembly is determined in proportion to the size of the components [18]:

$$P_{ch} = 0.2 \cdot P_c = 4.297[\text{kW}], \text{ Fig. 5.}$$

$$P_{ce} = 0.3 \cdot P_c = 6.445[\text{kW}], \text{ Fig. 6.}$$

$$P_{cc} = 0.05 \cdot P_c = 1.074[\text{kW}], \text{ Fig. 7.}$$

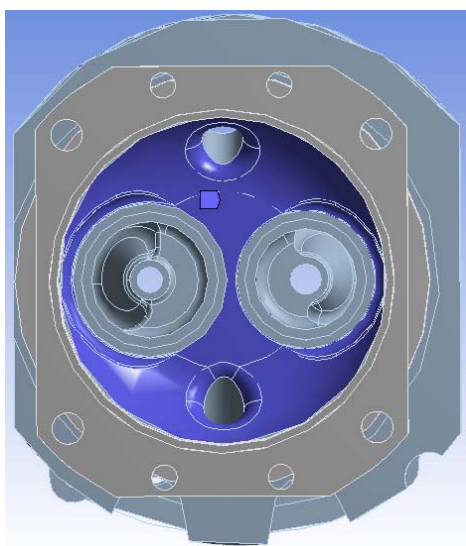


Fig. 5. Energy distribution in cylinder head

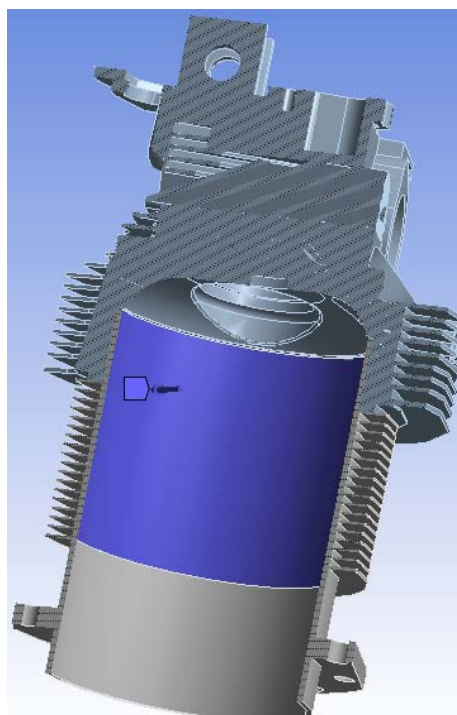


Fig. 6. Energy distribution in cylinder body walls

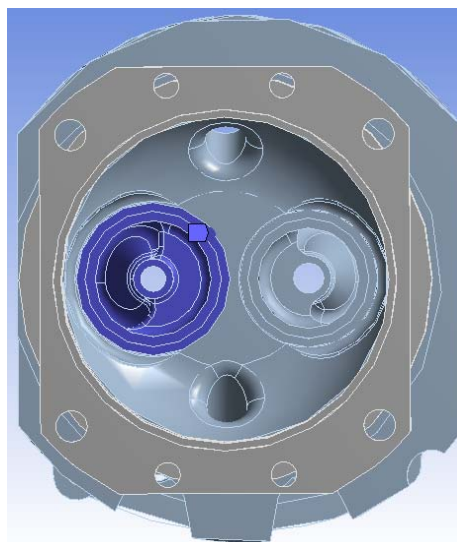
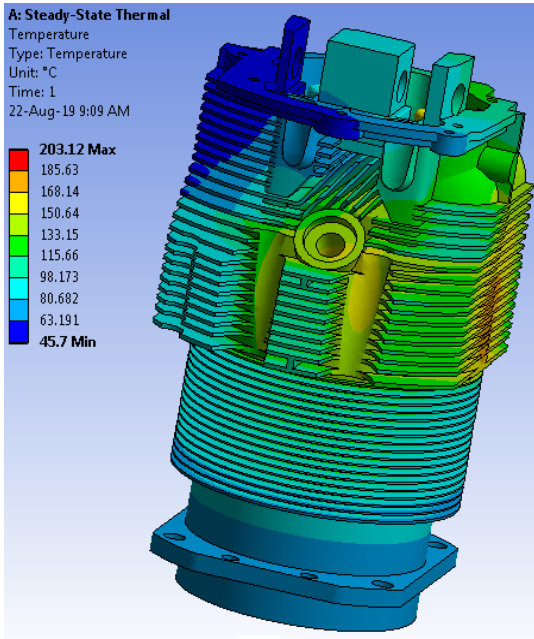


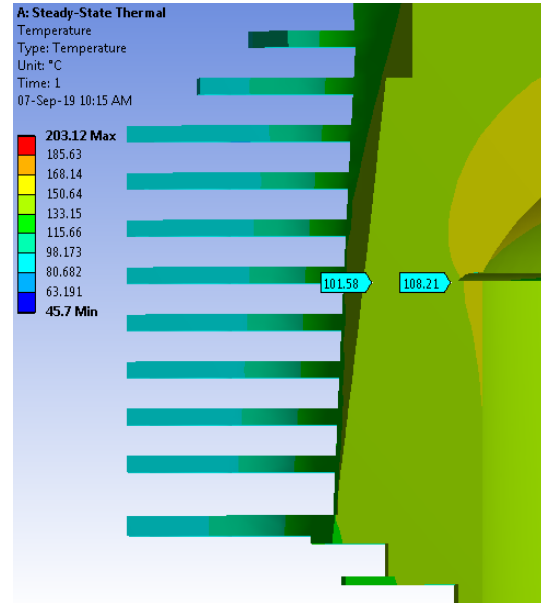
Fig. 7. Energy distribution in exhaust valve

Convection of the outer surfaces of the assembly exposed to airflow and convection of upper cylinder head surface (under camshaft cover) were defined [12].

As a result of the Steady-State Thermal analysis the temperature field distribution of the cylinder assembly was obtained, Fig. 8 a-c.

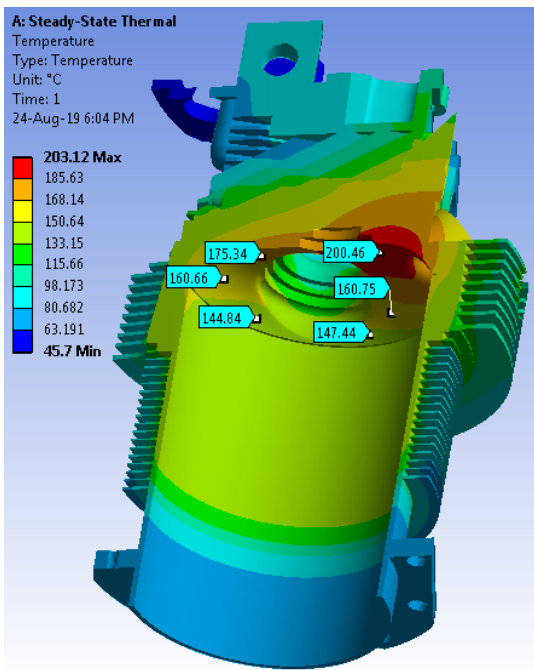


a)



c)

Fig. 8. Temperature field - results of Steady-State Thermal analysis: a) cylinder assembly; b) cylinder assembly cross section; c) values at crack location



b)

Steady-State Thermal and Static Structural analysis in Ansys Workbench have been coupled in order to define the stress state of the cylinder assembly resulting from combined thermomechanical load [12].

Within the analysis, the load is modeled as mechanical, that is, the pressure on the cylinder head that occurs during operation, Fig. 9.

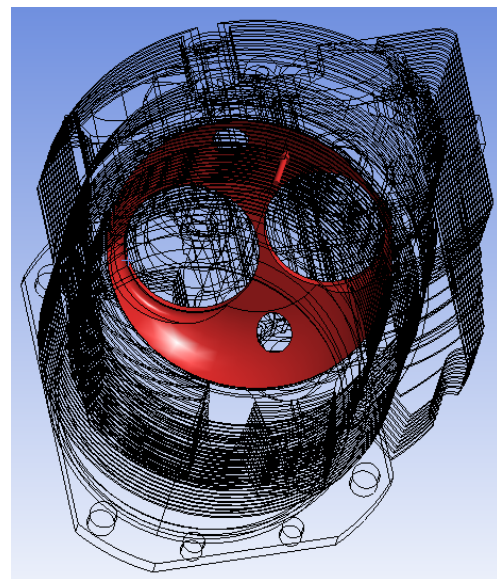
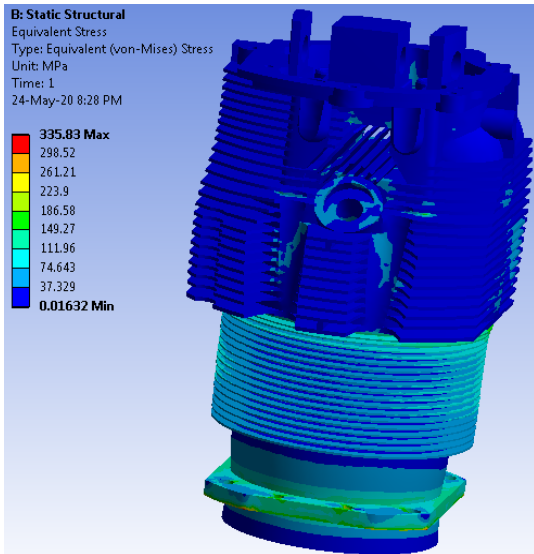


Fig. 9. The applied mechanical load

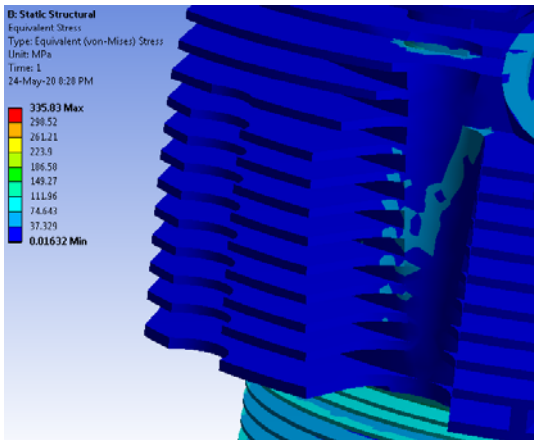
The cylinder head workload is presented by a mean effective pressure of 998 kPa obtained from the expression [12]:

$$p = \frac{P \cdot n_R \cdot 10^3}{V \cdot n}$$

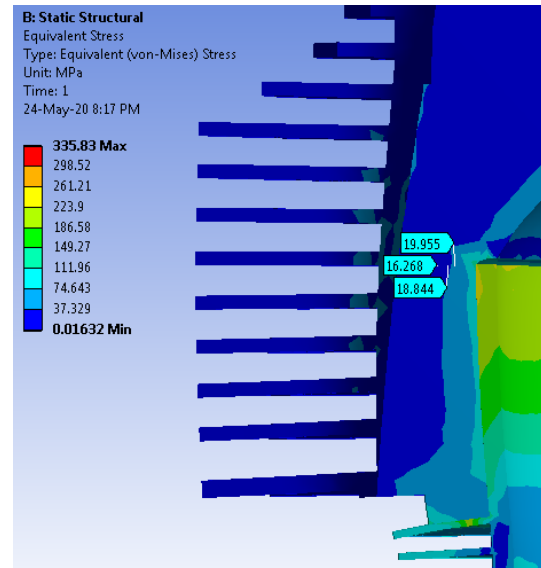
Fig. 10 a-c shows the distribution of the stress field on the cylinder assembly resulting from combined thermomechanical load.



a)



b)



c)

Fig. 10. The distribution of the stress field resulting from coupled thermomechanical load: a) cylinder assembly; b) cylinder head; c) values at crack location

4. RESULTS AND DISCUSSION

The distribution of temperature field per cylinder assembly was obtained by Steady-State Thermal analysis. Since the crack appeared on the cylinder head between the fifth and sixth cooling fins from the bottom, the discussion will be focused on that location. The obtained results show that the minimum temperature during operation is 45.7°C, while the maximum temperature is 203.13°C and occurs near the hole of the exhaust valve. According to the Operator's Manual Lycoming, cylinder head temperatures are no more than 224°C at high engine performance or 205°C at optimal cruising [19]. Based on the above fact it can be concluded that none of the obtained temperatures exceeds the stated values.

The coupled thermomechanical stress-strain state of the cylinder assembly, with the aforementioned thermal load, shows a nonuniform stress distribution per cylinder assembly in the range from 0.02 to 335.83 MPa. The maximum stress value is localized at the sharp edge at the very bottom of the cylinder body at the part where the cylinder body attaches to the engine housing. This value may be considered to be due to the neglect of the radius of curvature at said edge, although its

current value is within the permissible limits given both the tensile and fatigue strength of AISI 4140 steel.

The stress values at the cylinder head in the cross-section where the crack occurred are in range from 16.21 to 19.96 MPa. The values obtained are far below the tensile strength of the head material and are within the fatigue strength of said material obtained experimentally [12].

Based on the conducted research, it can be concluded that there are very small values of stress on the cylinder assembly originating only from mechanical load which would be appropriate for the case of analysis at room temperature, i.e. before the engine is warmed up. Thus, it can be concluded that thermal stresses, that must be taken into account in the analysis, are dominant. Including thermal stresses the stress on the cylinder assembly reaches a value of 335.83 MPa.

5. CONCLUSION

During the research of the considered problem, the complex, or combined, mechanical and thermal stresses to which the cylinder assembly is exposed during operation had to be taken into account. On the basis of the energy that occurs inside the cylinder assembly the distribution of the temperature field per cylinder assembly was obtained on the basis of Steady-State Thermal analysis. It was found that the values of the obtained temperatures correspond to the operating temperature during exploitation. By defining the pressure, that is, the mechanical load occurring in the cylinder assembly, the cylinder assembly stress state distribution was, also, obtained. The maximum stresses are within the limits of the tensile and fatigue strength. Based on the obtained results, a non-uniform distribution of the stress field across the cylinder assembly is observed. Maximum stress values occur at sharp edges resulting from the removal of tiny radii from the model in order to reduce the time required for simulation processing. At the crack initiation location low values of the obtained stress can be noticed.

REFERENCES

- [1] Kojić, M., Slavković, R., Živković, M., Grujović, N. (2010). *Metod konačnih elemenata 1 – Linearna analiza*. Mašinski fakultet, Kragujevac.
- [2] Bathe, J.B. (1982). *Finite element procedures in Engineering analysis*. Prentice-Hall, New Jersey.
- [3] Zienkiewicz, O.C., Taylor, R.L. (2000). *Finite Element Method*. Vol. 1, Elsevier Butterworth-Heinemann.
- [4] Zienkiewicz, O.C., Taylor, R.L. (2000). *Finite Element Method*. Vol. 2, Elsevier Butterworth-Heinemann.
- [5] Liu, G.R. (2003). *Finite Element Method: A practical course*. Elsevier Butterworth-Heinemann.
- [6] Shixiong, L., Jinlong, M., Shumao, W. (2007). Cylinder Head FEM Analysis and its Improvement. *International Conference on Computer and Computing Technologies in Agriculture*, Vol. 2, August 18-20, Wuyishan, China, p. 761-768.
- [7] Azadi, M., Mafi, A., Roozban, M., Moghaddam, F. (2012). Failure Analysis of a Cracked Gasoline Engine Cylinder Head. *Journal of Failure Analysis and Prevention*, Vol. 12, No. 3, p. 286-294, DOI: <https://doi.org/10.1007/s11668-012-9560-6>.
- [8] Tripathi, P.M., Prakash, S., Singh, R., Dwivedi, K.S. (2014). The Finite Element Analysis and Improvement on a Single Cylinder Head of Spark Ignition Engine. *International Journal of Engineering and Science*, Vol. 4, No. 3, p. 20-26, DOI: 07.4721/044020026.
- [9] Pinca, C. (2011). The Finite Element Analysis of a Cylinder Head of a Spark Ignition Engine. *Annals of Faculty Engineering Hunedoara – International Journal of Engineering*, Vol. 9, No. 3, p. 239-242.
- [10] Lee, C.C., Chiang, K.N., Chen, W.K., Chen, R.S. (2005). Design and analysis of Gasket Sealing of Cylinder Head under Engine operation conditions. *Finite Elements in Analysis and Design*, Vol. 41, p. 1160-1174, DOI: <https://doi.org/10.1016/j.finel.2004.12.007>.
- [11] MakeItFrom.com. From: <https://www.makeitfrom.com/material-properties/Normalized-4140-Cr-Mo-Steel>, accessed on: 26.04.2019.
- [12] Vučetić, N. (2020). *Razvoj metodologije za procjenu integriteta vazdušno hladenog avionskog klipnog motora izloženog visokocikličnom mehaničkom i termičkom opterećenju*. (In Serbian). PhD thesis. Fakultet inženjerskih nauka Univerziteta u Kragujevcu.

- [13] Sorić, J. (2004). *Metoda konačnih elemenata*. Golden Marketing, Zagreb.
- [14] Abbas, M.A. (2018). Comparison of convergence rate of higher order tetrahedral and hexahedral elements for Linear Static Structural FEA. *International Journal of Pure and Applied Mathematics*, Vol. 119, No. 10, p. 1927-1933.
- [15] Ashouri, H. (2015). Finite element analysis of thermo-mechanical stresses in diesel engines cylinder heads using a two-layer viscoelasticity model. *International Journal of Automotive Engineering*, Vol. 5, p. 2054-2064.
- [16] The Physics Factbook - Energy density of Gasoline. From: <https://hypertextbook.com/facts/2003/ArthurGolnik.shtml>, accessed on: 25.04.2019.
- [17] Are Airplane Engines so Inefficient. From: <https://michaelsoroka.com/2014/03/26/are-airplane-engines-inefficient/>, accessed on: 25.04.2019.
- [18] Abdala, I.A.A. (2012). *Internal Combustion Engine Heat Transfer-Transient Thermal Analysis*. (In English). PhD thesis, University of Southern Queensland, Faculty of Engineering & Surveying.
- [19] Operator's manual (2005). *Lycoming O-360, HO-360, IO-360, AIO-360, HIO-360 & TIO-360 series aircraft engines*, Part No. 60297-12, Rev. No. 60297-12-5, Lycoming, Williamsport, PA.



Banja Luka
28–29 May 2021.

DEMI 2021

15th International Conference on Accomplishments in Mechanical and Industrial Engineering

www.demi.mf.unibl.org



Fatigue endurance analysis of a surface stress raiser

Slobodanka Boljanović^a, Strain Posavljak^b, Stevan Maksimović^c

^aMathematical Institute of the Serbian Academy of Sciences and Arts, Kneza Mihaila 36, Belgrade, Serbia

^bUniversity of Banja Luka, Faculty of Mechanical Engineering, Vojvode Stepe Stepanovića 71, Banja Luka, Republic of Srpska, Bosnia and Herzegovina

^cMilitary Technical Institute, Ratka Resanovića 1, Belgrade, Serbia

Abstract *Fatigue-induced flaws play an important role in safety-integrity performances of large moving systems. Therefore, the present research work proposes a computational model to gain insight into such surface stress raisers. The analysis shows that a combination of damage-tolerance design with fracture mechanics-based concept is a key to generating relevant relationships between fatigue life and stress intensities.*

Keywords *fatigue design, residual life, stress intensity analysis, surface flaw*

1. INTRODUCTION

Surface flaw phenomenon is one of the major deterioration mechanisms in existing large moving systems, causing considerable costs for maintenance and repair. In this context the development of reliable computational models to localize and characterize such part-through damage represented as quarter-elliptical and semi-elliptical crack is essential to assess the load bearing capacities of structural components.

Under cyclic loading, the stability of quarter-elliptical crack at a pin-loaded hole has been analyzed by Rigby and Aliabadi [1] using J -integral method and the boundary element method. Further, Yamashita et al. [2] have explored the driving mode caused by semi-elliptical crack through the Paris' crack growth

concept together with the finite element method.

In order to evaluate the propagation of quarter-elliptical crack coupled with the pin-loaded effect Antoni and Gaisne [3] have suggested the analytical concept whereas Mikheevskiy et al. [4] have employed the crack growth concept proposed by Noroozi et al. [5]. The behaviour of the same failure-relevant configuration has been evaluated by Boljanović et al. [6] through the crack growth concept proposed by Zhan et al. [7] and the J -integral method. Further, Boljanović et al. [8] have used the stress ratio dependant crack growth model [9] and the finite element method to assess the fatigue performances of quarter-elliptical corner crack at semicircular edge notch.

The present research work discusses the computational model recommended for fatigue assessments of plate-type configurations with quarter-elliptical crack-like flaw. Such fracture mechanics-based analytical tool is aimed at evaluating of structural responses and defining safety levels. Furthermore, several cases of technical interest are treated in detail, varying

Corresponding author

Ph.D. Slobodanka Boljanović
slobodanka.boljanovic@mi.sanu.ac.rs

Mathematical Institute SANU
Kneza Mihaila 36
Belgrade, Serbia

both the crack shape characteristics and parameters of loading profiles.

2. SURFACE FLAW PROGRESSION

At operating loads, surface flaws become sources of fatigue damages as a result of complex load-environment interactions. Therefore, the safety and long-term operation of large moving systems requires the inclusion of fracture mechanics-based concepts for analyzing the progression of these stress raisers [3-9]. In this context, the driving mode due to a quarter-elliptical crack (Fig. 1) is herein theoretically examined through the crack growth model proposed by Walker [10], expressed as follows:

$$\frac{da}{dN} = \frac{C_A (\Delta K_A(a,b))^{m_A}}{(1-R)} \quad (1a)$$

$$\frac{db}{dN} = \frac{C_B (\Delta K_B(a,b))^{m_B}}{(1-R)} \quad (1b)$$

where da/dN , db/dN and a , b are the crack growth rate and crack length in depth and surface crack growth direction, respectively, R is the stress ratio, ΔK_A and ΔK_B are the stress intensity factors for two critical crack growth directions.

In the frame of the fatigue endurance analysis the number of loading cycles N may be evaluated, integrating relevant crack growth rates (Eq. (1a) and (1b)) from initial a_0 , b_0 to final a_f , b_f crack lengths with respect to depth and surface crack growth direction, i.e.

$$N = \int_0^N dN = \int_{a_0}^{a_f} \frac{(1-R)}{C_A (\Delta K_A(a,b))^{m_A}} da \quad (2a)$$

$$N = \int_0^N dN = \int_{b_0}^{b_f} \frac{(1-R)}{C_B (\Delta K_B(a,b))^{m_B}} db \quad (2b)$$

Additionally, it is worth to be mentioned that the structural durability is herein estimated through novel software in which the Euler's algorithm is used for solving complex-valued functions.

3. STRESS INTENSITY EVOLUTION

The fatigue performance of quarter-elliptical corner crack (Fig. 1) is assessed employing the stress intensity factor [11], expressed as follows:

$$\Delta K = M_{qe} \Delta S \sqrt{\frac{\pi a}{Q}} \quad (3)$$

where ΔS and ΔK are applied stress range and stress intensity factor range, respectively, a is crack length in depth direction and Q represents the ellipse shape factor.

Through the stress raiser evaluations the boundary conditions related to the crack shape, the crack size, thickness and width of the plate are taken into account by means of the correction factor M_{qe} , defined by

$$M_{qe} = \left(M_1 + M_2 \left(\frac{a}{t} \right)^2 + M_3 \left(\frac{a}{t} \right)^4 \right) g_1 g_2 f_\phi f_w \quad (4)$$

$$M_1 = \sqrt{\frac{b}{a}} \left(1.08 - 0.03 \frac{b}{a} \right) \quad (5)$$

$$M_2 = 0.375 \left(\frac{b}{a} \right)^2 \quad (6)$$

$$M_3 = -0.25 \left(\frac{b}{a} \right)^2 \quad (7)$$

$$g_1 = 1 + \left(0.08 + 0.4 \left(\frac{b}{t} \right)^2 \right) (1 - \sin \phi)^3 \quad (8)$$

$$g_2 = 1 + \left(0.08 + 0.15 \left(\frac{b}{t} \right)^2 \right) (1 - \cos \phi)^3 \quad (9)$$

where b is crack length in surface direction, t and w are thickness and width of the plate, respectively, and ϕ is the angle location.

Further, the interaction between the ellipse crack shape effect ($a/b > 1.0$), and the effects of angle location and width of the plate are theoretically examined via the correction factors Q , f_ϕ and f_w , expressed as follows:

$$Q = 1 + 1.464 \left(\frac{b}{a} \right)^{1.65} \quad (10)$$

$$f_\phi = \left(\left(\frac{b}{a} \right)^2 \sin^2 \phi + \cos^2 \phi \right)^{1/4} \quad (11)$$

$$f_w = \sec \left(\frac{\pi b}{2w} \sqrt{\frac{a}{t}} \right)^{0/5} \quad (12)$$

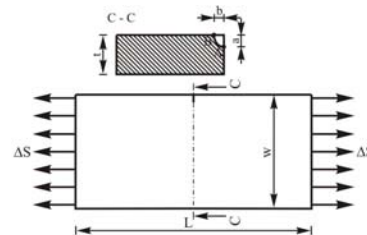


Fig. 1. Cyclically loaded plate with corner crack.

4. FATIGUE DURABILITY EVALUATIONS

4.1 Residual life analysis

The present Section examines the fatigue performances of the plate with quarter-elliptical corner crack (Fig. 1), made of 2024 T3 aluminium alloy. Such failure evaluations are performed adopting the applied maximum stress equal to $S_{max}= 310.63$ MPa and 240.79 MPa with $R = -1$, and the following geometrical and material parameters: $w = 76.2$ mm, $t = 2.3$ mm, $C_A=C_B=1.2 \times 10^{-11}$, $m_A = 3.02$, $E = 73.1$ MPa, $\nu=0.33$. The initial part-through crack is characterized by relevant lengths equal to $a_0 = b_0=20$ μm in the case of depth and surface direction.

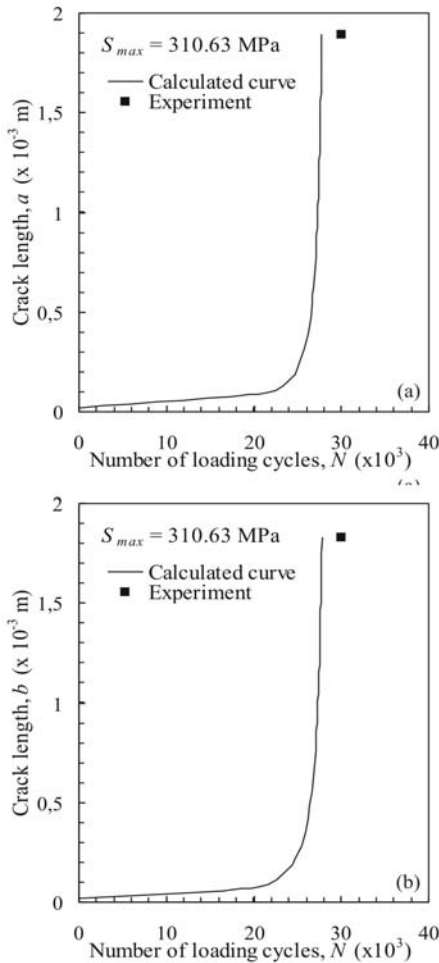


Fig. 2.

Fatigue life evaluation for the plate with a quarter-elliptical crack ($S_{max}= 310.63$ MPa): (a) $a - N$ and (b) $b - N$ (calculated curves are the present results and experiments are reported in Ref. [12])

Under cyclic loading the stability of damaged plate is estimated through the stress intensity factor and residual life, using Eq. (3)-(12) and Eq. (2a)-(2b), respectively. The evaluated number of loading cycles, as a function of crack length in depth and surface directions, are shown in Fig. 2a, 2b and Fig. 3a, 3b for maximum stress equal to $S_{max}=310.63$ MPa and $S_{max}= 240.79$ MPa, respectively.

In order to verify the life evaluations, experimentally tested data available in the literature [12] are reported in the same figures. By examining different comparisons, it can be deduced that safety-relevant results are in a quite good agreement for two critical directions.

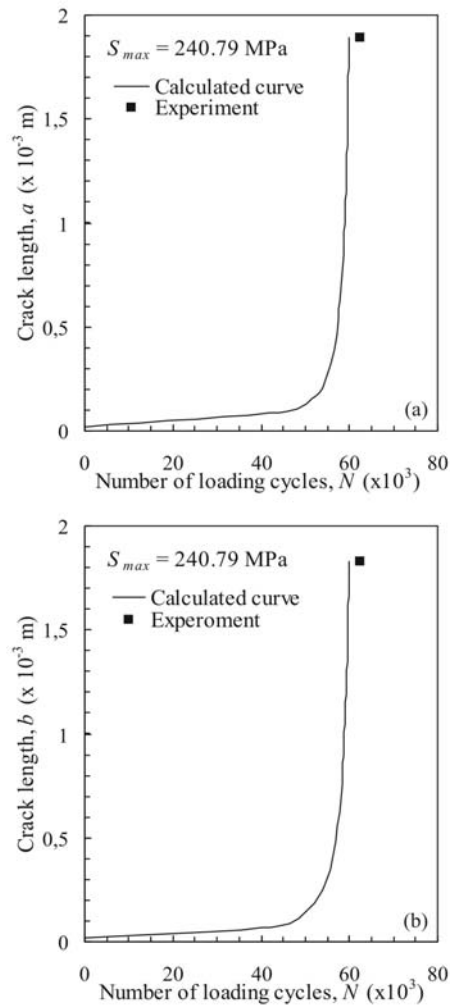


Fig. 3. Fatigue life evaluation for the plate with a quarter-elliptical crack ($S_{max}= 240.79$ MPa): (a) $a - N$ and (b) $b - N$ (calculated curves are the present results and experiments are reported in Ref. [12])

4.2 Effects of stress ratio and thickness on the residual strength under cyclic loading

Now, through the stability evaluations the effect of applied load is examined in the case of surface corner flaws (Fig. 1). In this regard, the fatigue endurance of a plate made of 2024 T3 aluminium alloy (assuming the following applied maximum stress and geometrical parameters: $S_{max}=300$ MPa, $t=8$ mm, $w=50$ mm, $a_0=1.85$ mm, $b_0=2.1$ mm) is explored for three values of stress ratio ($R=0.1, 0.25$ and 0.625).

According to the developed fracture mechanics-based analytical model, the driving mode due to quarter-elliptical crack is herein analyzed through Eq. (3)-(12) and Eq. (2a)-(2b), respectively.

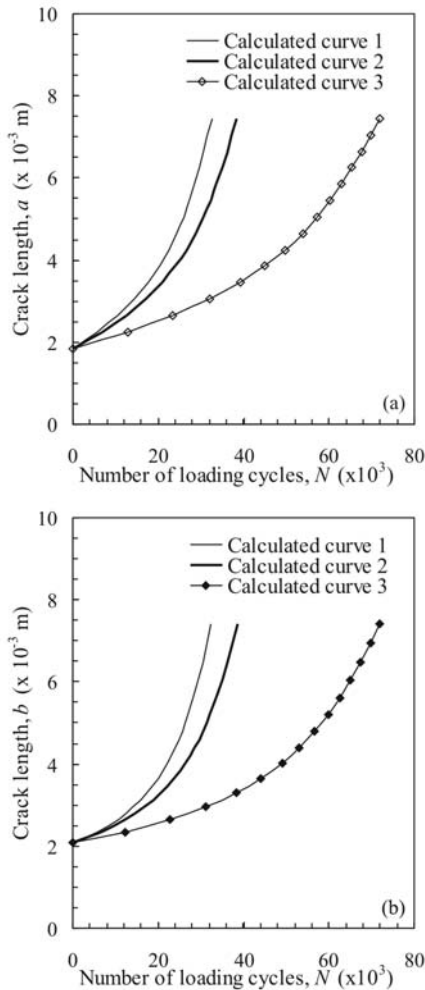


Fig. 4. Fatigue life evaluation for the plate with a quarter-elliptical crack ($S_{max}=300$ MPa): (a) $a - N$ and (b) $b - N$ ($1 - R = 0.1, 2 - R = 0.25, 3 - R = 0.625$, calculated curves are the present results)

Fatigue life and stress intensity factor which are evaluated as a function of crack length in depth and surface direction respectively, are shown in Fig. 4a, 4b and Fig. 5a, 5b for three values of the stress ratio, assuming the same material parameters as those mentioned in Section 4.1.

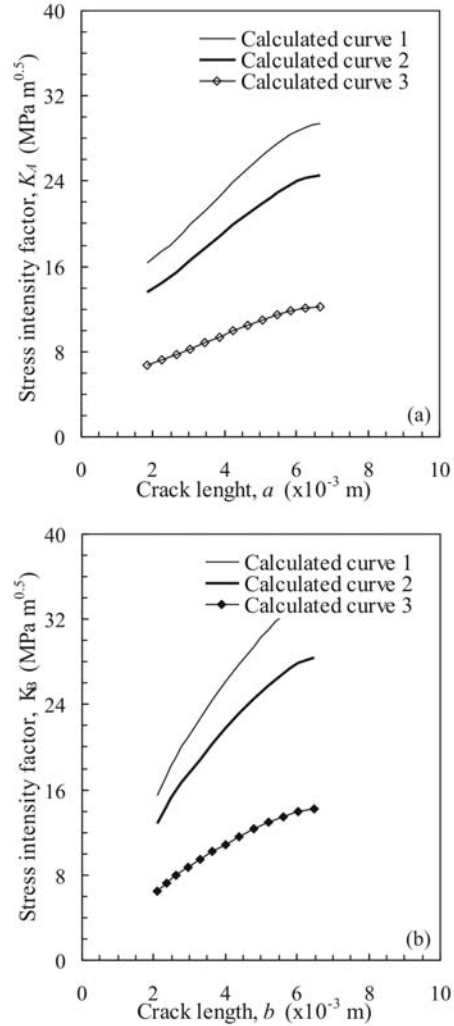


Fig. 5. Stress intensity evaluation for the plate with a quarter-elliptical crack ($S_{max}=300$ MPa): (a) $K_A - a$ and (b) $K_B - b$ ($1 - R = 0.1, 2 - R = 0.25, 3 - R = 0.625$, calculated curves are the present results)

Moreover, the stress raiser analysis examines the fatigue behaviour of three plates ($w=60$ mm, $a_0=b_0=1.85$ mm, $S_{max}=250$ MPa and $R=0.1$), made of 2024 T3 aluminium alloy. Such plates with a quarter-elliptical crack are characterized by the following thicknesses: $t=6$ mm, 7.5 mm and 9 mm, respectively. Relevant fatigue evaluations for the number of loading

cycles, as a function of crack length in depth and surface direction, are shown in Fig. 6a and 6b, respectively.

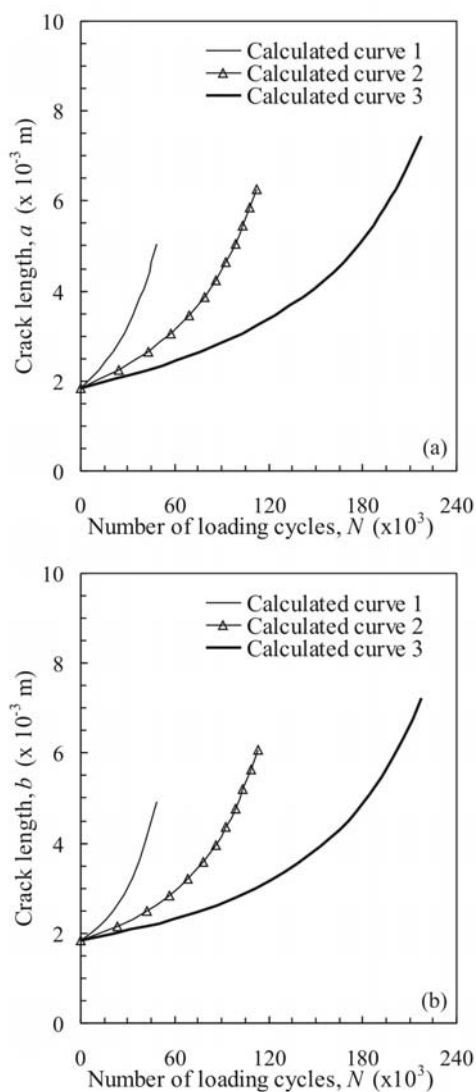


Fig. 6. Fatigue life evaluation for the plate with a quarter-elliptical crack ($S_{max}=250$ MPa): (a) $a - N$ and (b) $b - N$ ($1 - t = 6$ mm, $2 - t = 7.5$ mm, $3 - t = 9$ mm, calculated curves are the present results)

From theoretical outcomes presented in Fig. 2 to 5, it can be deduced that the effects of applied loads can seriously compromise the structural durability under cyclic loading. Also, relevant comparisons shown in Fig. 6 indicate that the thickness is a factor that can have an important impact on the safe functioning of plate-type systems.

5. CONCLUSIONS

Improving the understanding of surface flaw mechanisms is a relevant task that can prevent the onset of sudden fatigue failure in large moving systems. Therefore, in the present research work a novel analytical model is proposed, in which the Walker's crack growth model is extended to quantify the progression of surface stress-raiser due to cyclic loading. Furthermore, novel relationships for the life assessment are presented, and the estimated results demonstrate that the developed computational tool can be successfully applied for evaluating the fatigue stability of plate-type structural components with a quarter-elliptical flaw.

Acknowledgement

This research work is supported by the Serbian Ministry of Education, Science and Technological Development through the Mathematical Institute of the Serbian Academy of Sciences and Arts, Belgrade and the COST (European Cooperation in Sciences and Technology) Organization under the Action CA 18203, Brussels, Belgium.

REFERENCES

- [1] Rigby, R., Aliabadi, M.H. (1997). Stress intensity factors for cracks at attachment lugs, *Engineering Failure Analysis*, vol. 4, no. 2, p. 133-146.
- [2] Yamashita, Y., Shinozaki, M., Ueda, Y., Sakano, K. (2004). Fatigue crack growth life prediction for surface crack located in stress concentration part based on the three-dimensional finite element method, *ASME Journal of Engineering for Gas Turbines and Power*, vol. 126, no. 1, p. 160-166.
- [3] Antoni, N., Gaisne, F. (2011). Analytical modelling for static stress analysis of pin-loaded lugs with bush fitting, *Applied Mathematical Modelling*, vol. 35, no. 1, p. 1-21.
- [4] Mikheevskiy, S., Glinka, G., Alegria, D. (2012). Analysis of fatigue crack growth in an attachment lug based on the weight function technique and the UniGrow fatigue crack growth model, *International Journal of Fatigue*, vol. 42, p. 88-94.
- [5] Noroozi, A.H., Glinka, G., Lambert, S. (2007). A study of the stress ratio effects on fatigue crack growth using the unified two-parameter fatigue

- crack driving force, *International Journal of Fatigue*, vol. 29, p. 1616-1633.
- [6] Boljanović, S., Maksimović, S., Carpinteri, A., Jovanović, B. (2017). Computational fatigue analysis of the pin-loaded lug with quarter-elliptical corner crack, *International Journal of Applied Mechanics*, vol. 9, no. 4, 1750058:p.1-17.
- [7] Zhan, W., Lu, N., Zhang, C. (2014) A new approximate model for the *R*-ratio effect on fatigue crack growth rate, *Engineering Fracture Mechanics*, vol. 119, p. 85-96.
- [8] Boljanović, S., Maksimović, S., Carpinteri, A., Čosić, M. (2019). Fatigue endurance design of plates with two semicircular edge notches and one quarter-elliptical corner crack or through-the-thickness crack. *International Journal of Fatigue*, vol. 127, p. 45-52.
- [9] Huang, X., Moan, T. (2007). Improved modeling of the effect of *R*-ratio on crack growth rate, *International Journal of Fatigue*, vol. 29, no. 4, p. 591-602.
- [10] Walker, E.K. (1970). The effect of stress ratio during crack propagation and fatigue for 2024-T3 and 7075-T6 aluminum. In: *Effect of environment and complex load history on fatigue life*, ASTM STR vol. 462, p. 1-14, ASTM Philadelphia, Pa, United States.
- [11] Newman Jr., J.C., Raju, I.S. (1984). *Stress-intensity factor equations for cracks in three-dimensional finite bodies subjected to tension and bending loads*, NASA TN-85793, Langley Research Center, Hampton, Virginia, United States.
- [12] Grover, H.J., Hyler, W.S., Kuhn, P., Landers, C.B., Howell, F.M. (1953). *Axial-load fatigue properties of 24S-T and 75S-T aluminium alloy as determined on several laboratories*, NACA TN-2928, Battelle Memorial Institute, Langley Aeronautical Laboratories, United States.

Mechatronics



Banja Luka
28-29 May 2021.

DEMI 2021

15th International Conference on
Accomplishments in Mechanical and
Industrial Engineering

www.demi.mf.unibl.org



UPGRADING OF THE HYDRAULIC SYSTEM BY INSTALLING A FREQUENCY CONVERTER

J. Eric Obucina^a, S. Stankovski^b, G. Ostojic^b, S. Aleksandrov^a

^aShumadia Academy of Professional Studies, Department in Trstenik, Radoja Krstica 19, 37240 Trstenik, Serbia

^bFaculty of Technical Sciences, University of Novi Sad, Dositeja Obradovica 6, 21000 Novi Sad

Abstract This paper will present the use of the frequency converter in the hydraulic system. Application of a hydraulic gear pump with a constant capacity in a hydraulic system that should satisfy the achievement of different pressure values and displacement of the piston, i.e. to realize a variable flow during the working cycle, is completed by applying a frequency converter. The frequency converter, changing the speed of the electric motor, allows the gear pump at the output to provide a variable flow. The development of hydraulics and electronics is aimed at rationalizing the structural modalities of hydraulic components and in efforts to improve the hydraulic system energy efficiency coefficient and minimize the total installed power of the drive motors of the pumps. Thus, in a particular area of application, pumps with hydraulic-electronic regulators are replaced with pumps of constant specific volume of variable speed (frequency converter control). The result of the development of electronics is the improvement of the construction of frequency converters that are installed in systems with hydraulic pumps with the task of regulating pump capacity by changing the number of revolutions according to the predefined program in the processor unit.

Keywords hydraulic gear pump, frequency converter

1. INTRODUCTION

The hydraulic system as used for more than one hundred years and during that lifetime has experienced a large number of structural transformation. Classic distribution valves with end positions of the working piston is adapted to the requirements of construction and manufacturing mobile machines so they are reducing the volume and weight, and increasing operating pressures, flow, speed and accuracy of response time, service life, reliability and efficiency ratios. At the moment when this and

other improvements can not be successful and/or rational to meet the requirements, there are new structural forms of hydraulic components.

Development of electronics creates new spaces for the development of hydraulics, not only in the field of construction components but also management systems. [4]

Converting hydraulic energy into mechanical and vice versa takes place in the components of the hydraulic system - hydraulic pumps and motors.

The transfer of power to the hydraulic systems is done using fluid, incompressible fluid. For incompressible fluid is true that his volume will change significantly under the influence of external forces. [3]

In the context of the basic functions of the hydraulic system, the transformation of energy, construction of the hydraulic system must meet

Corresponding author

MSc, Jelena Eric Obucina
jelena.obucina@vtmsts.edu.rs

Shumadia Academy of Professional Studies, Department in
Trstenik, Radoja Krstica 19
37240 Trstenik, Serbia

other important requirements. The requirement is that the energy losses in the way of the transformation of energy must be minimal.

From the known relationship of fluid power failure, pressure and flow, the ratio of the total, useful and power loss due to loss of fluid power pressure and flow is displayed in the form of diagrams ($P = p \cdot Q$).

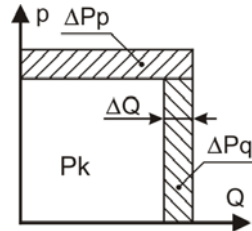


Fig. 1. Total available capacity hydraulic pumps

The total amount of pump power is distributed to usable power, which is marked with P_k , and the loss of power that is lost power due to falling pressure - ΔP_p and lost power due to the loss of flow - ΔP_q .

The pressure drop and flow in the hydraulic system are the result of losses in the hydraulic components and for them we can say that they are within acceptable limits, normal.

However, if the inside of the hydraulic system reduces the damping the flow of oil, at unchanged requires pump pressure is increased to a level that is adjusted to the pressure limiting valve.

The resulting excess oil is drained to the tank and increase:

- total power fluid current (or pumps):

$$P_{fs} = p_{vp} \cdot Q,$$

- power losses pump $P_{gfs} = p_{vp} \cdot \Delta Q$

where: p_{vp} - pressure set on relief valve; ΔQ - oil flow which goes through the pressure limiting valve drains into the reservoir.

Described losses reduce the coefficient of utilization of the hydraulic system as a whole. If the hydraulic system, instead of a constant pump capacity installed variable volume pump (vane or piston-axial) and its capacity to comply with the necessary, power fluid stream is reduced to $P_{fs} = p_r \cdot Q_r$, where: p_r - working pressure; Q_r - regulated pump flow.

The mechanism described alignment capacity pumps belong to the group control the flow line (Figure 2, flow control "a").

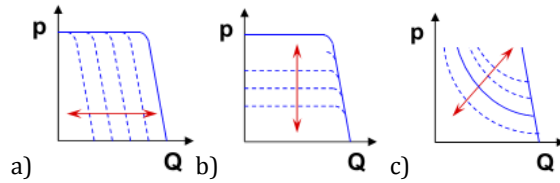


Fig. 2. Principles of regulation capacity volumetric pump capacity per line, pressure and power curve

When we talk about the basic principles of the regulation should be pointed out that in addition to the line of flow there and the line pressure control (Figure 2, b) and power curve (Figure 2, c) the capacities pump changes as a function of pressure, but so that the power always maintained at a level of the calculated values.

The losses are due to the pressure drop can be reduced constructions of hydraulic components that provide the required pressure in the system. When reducing the volume of losses in the hydraulic system, in fact, an adjustment to the pump with the requirements that occur in the system. This means that at any moment should follow the work of the hydraulic system and meets the requirements that are necessary in this moment.

This paper presents a hydraulic system driven by an asynchronous motor with speed adjustment. This adjustment is made possible by a frequency converter which will, as a result, also give a variable flow pump with a constant capacity.

Since the advent of the first frequency inverter is contained within it self the appearance of thyristors today's microprocessor-controlled inverter exceeded the long development time. Due to the increasing participation of automation in industry, constant need for automatic control and increasing production speed, continuously develop methods for improvement of electrical drives.

Electric motors are very important in standard industrial production and constitute the inevitable part of the vast majority industrial process.

These motors are designed to operate at a constant speed so that the control of their speeds, implementation of control algorithms and control themselves device issue of great importance to optimize and attached themselves industrial processes.

2. U/f CONTROL FOR VARIABLE SPEED THREE-PHASE AC MOTOR IN HYDRAULIC SYSTEM

Variable-speed electro-hydraulic drives, an electric motor with a frequency converter in combination with a constant-volume hydraulic pump, are a good solution, because in addition to higher energy efficiency, they also provide better system safety and a wider speed range. This can be deduced from a comparison with the drives provided by an electric motor with a variable displacement hydraulic pump. [6,7]

However, the main disadvantage of variable speed drives is the time response and lack of precision due to the high inertia of the electric motor and hydraulic pump.

In hydraulic systems where it is possible to replace the variable capacity pump with a constant capacity pump and a frequency regulator, the dominant influence on the application of the pump capacity control system has the ratio of price and energy savings.

In the late 1960s, frequency converters began to be used first in water transport systems, using the well-known property of centrifugal pumps to move the $p - Q$ characteristic along the pressure line (p) when changing the number of revolutions of the impeller, thus changing its capacity. With the development of pump performance control applications, systems have been obtained to maintain the required pump capacity as a function of changing the pressure and / or the set flow to be kept constant. [6, 7]

Capacity management of constant capacity volumetric pumps is rarely found in hydraulic drive structures. Only in the last twenty years, in parallel with the development of the construction, the improvement of the technical characteristics and the fall of the price per kW of power, the frequency converters are modestly, but more and more often found in the constructions of hydraulic systems. Such a trend required the development of the construction of gear pumps, in fact their penetration into the area of higher operating pressures (250 to 300 bar) and higher capacities.

The good characteristics of frequency regulators are known: a) programming of continuous speed control at constant torque; b) the possibility of programming ramps; c) defining the take-off time; d) a relatively high degree of accuracy of the repeated state; e) allowed short-term load up to 50%; f) increase

in the number of revolutions and capacity of the pump in relation to the nominal and others.

2.1 Basic principles of application of frequency inverter

Frequency converters are electronic devices that enable speed control of induction motors turning the input supply voltage and frequency, which are fixed values in the variables. In addition to the basic functions of speed control AC motors, drives integrate a number of other functionalities such as: motor protection, alarm systems, process control in closed loop and a switchable speed and control work through a variety of interfaces. [9]

Frequency converter control along output frequency and the voltage according to Figure 3, maintaining a constant ratio of volt/hertz. Momentum generated is directly proportional to this ratio, which means that at all speeds (up to nominal speed) torque constant and equal to the nominal time. This means that the engine at all speeds and can deliver full torque.

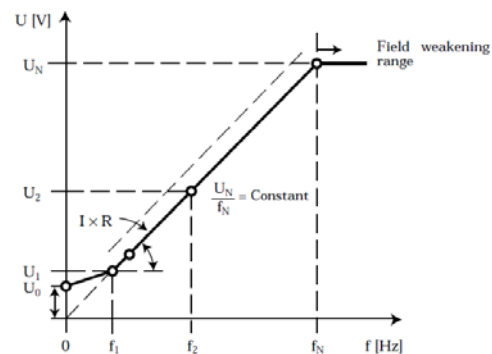


Fig. 3. Control frequency converter [5,9]

The speed control of three-phase AC motors has developed in recent years on the basis of two different control principles with normal V/f or scalar control or flux vector control. [5,9]

The controller can be operated motor with frequency above the nominal (50 or 60 Hz), but in this case it is not possible to further increase the voltage. In this case, the torque decreases, and there is a possibility that the engine at higher speeds can not deliver enough torque to launch a given load. [4]

Today, the development of fast and powerful energy semiconductors has provided a wide standard application of frequency converters for the regulation of AC motors in a large

number of automated processes and drives. The development of energy semiconductors ensured the conversion of electricity with small losses, without delay, while the development of electronic processing elements enabled the performance of complex control systems with very high properties. Thanks to significant technological progress in the production of cheap, powerful and compact microcomputers, the possibility has been created for the realization of economical frequency converters, which provide the required accuracy in combination with very accurate analog / digital converters for speed and position (speed and angle).

3. UPGRADING OF FREQUENCY REGULATOR IN HYDRAULIC SYSTEM FOR REGULATING CAPACITY GEAR PUMPS

Gear pumps belong to the group pumps with a constant working volume. [6, 7]. They belong to the group of volume pump in which the operating means for the suppression of the working liquid two coupled gears. One of the drive gear and receives torque of the drive unit, usually an electric motor, and the second driven gear. Volume of fluid to be pushed depends on the speed and the size of place between the tooth.

Gear pump is a kind of displacement pumps where it is not possible to regulate the capacity of the regulator installation capacity. [3, 5]

Due to the inability installation of hydraulic controller and regulating capacity that makes this pump, the paper presents the application of the frequency converter for the purpose of regulating the number of revolutions of the engine. In this way we achieve that, a simple and reliable hydraulic pump, the hydraulic system may provide variable flow rate as a function of the number of revolutions.[4]

The following figure shows a hydraulic system with gear pump, hydraulic energy source and frequency converter, as well as an electronic component that regulates the pump capacity. The system works so that, when starting, includes an electric motor as a power source, and the frequency at which the regulator sets the reference pressure value that he wants to maintain the system. By activating the command that the system is put into operation hydraulic pump is started and in accordance with the desired output, ie. reference value to

be reached at the executive body ie. hydraulic cylinder, maintains the set value.[3, 4, 5]

Frequency converter, which serves as the controller has in it integrated PID regulator that maintains a reference pressure. Frequency converter, slightly run-up pump, and then change the speed to pressure remained on the set value.

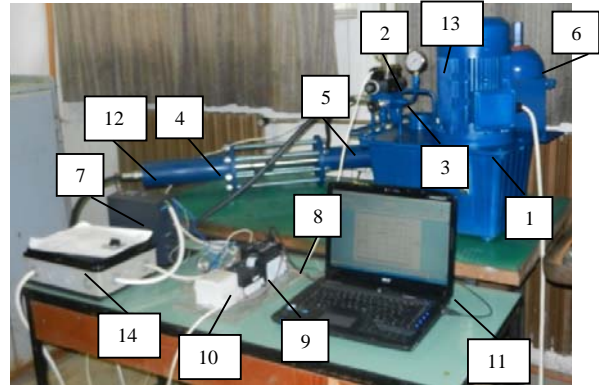


Fig. 4. Figure of experimental hydraulic system of regulation capacity gear pump frequency converter [3, 4, 5]

Components of the hydraulic system are:

1 hydraulic power pack, 2 - hydraulic valve, 3 - safety valve, 4 - hydraulic cylinder, 5 - hydraulic cylinder for load, 6 - hydraulic accumulator, 7 - frequency converter, 8- PLC CP1L, 9 - a module for acquisition CP1W-MAD11, 10 - DC module 24V, 11 - computer, 12 - pressure transmitter, 13 - manometer, 14 - clutch.

Data on the actual value of the pressure supplied via pressure transmitter mounted on a hydraulic cylinder, precisely at the point where the pressure measured in the hydraulic cylinder, and is directly connected to the frequency converter.

In the event of a major higher the required force, the frequency converter will be changed over speed electric motors and thus will increase the pump flow rate, as it will be needed and higher pressure value that is directly related to the force of the hydraulic cylinder.

Also, in case that is needed less force, the hydraulic pressure on the executive body that would, through feedback, respond frequency regulator that will reduce the number of revolutions of the drive shaft has a hydraulic pump and it will give a smaller flow.

Another variant of this experimental work is that the frequency converter is controlled via

PLC, which would then pressure value received from the transmitter and sending a command to the frequency converter.

The results that have been generated during the experimental part of the city are shown in Fig. 5 and determine the dependence of the number of revolutions of the electric motor and the pressure in the hydraulic system.

From the diagram, it is seen that when changing speed electric motor and changing the pressure in the hydraulic system. [3, 4, 5]

In the case of the first variant, ie. when done directly manage frequency converter which still regulates the necessary force to the hydraulic cylinder, PLC has a role for data acquisition. Which means that the PLC and the module for acquisition connected to a computer, and custom set values and compares them with the reference signal in a closed loop. [3, 5]

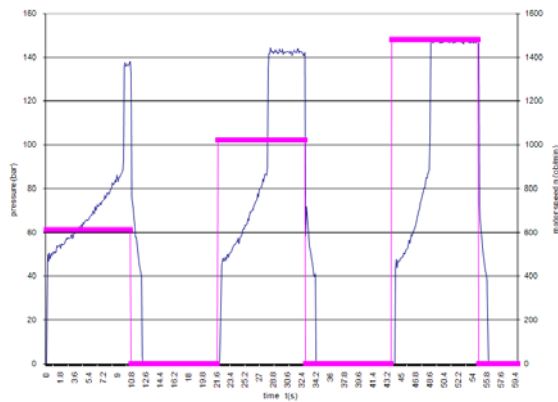


Fig. 5. Diagram depending on the pressure in the hydraulic system and the number of revolutions of electric motors [3, 4, 5]

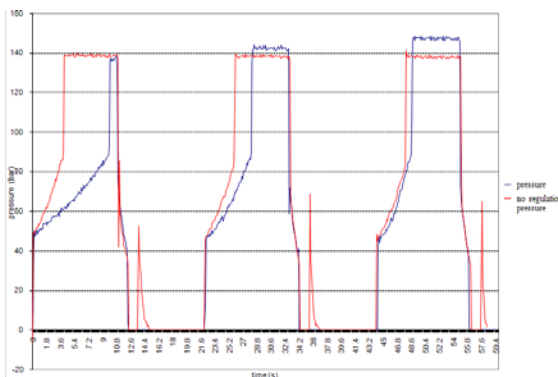


Fig. 6. Pressure with and without speed control motors [3, 4, 5]

In the context of this paper I criteria and recorded the results of which indicate the energy savings in the hydraulic system.

Saving energy is very important in hydraulic systems because the system itself is not working at maximum pressure for each load and no-load pumps. [3, 4]

These savings are automatically mirrored to the application of the frequency converter, for comparing the system with and without regulation it can be read. For this kind of experiment give measurement of engine power consumed, as well as of the electricity required for operation of the hydraulic system.

The diagram shows the pressure difference of pressure with and without regulation.

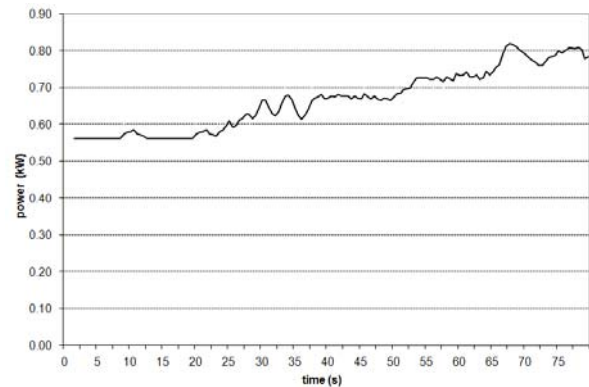


Fig. 7. Diagram depending on input power electric motors in relation to time and the required reference value [3, 5]

4. CONCLUSION

In this study, data analysis and experimental data show that the use of the frequency converter in the hydraulic system useful. Designed hydraulic system in which the pump is replaced by a variable capacity pump whose capacity is altered by changing the number of revolutions, removes all doubt about a possible replacement of conventional hydraulic controllers with frequency converters. [3, 4, 5] When the hydraulic system in which it is possible to substitute the variable capacity pump with a constant pump capacity and frequency converter, a dominant influence on the application of the system of regulation of pump capacity has a price-performance ratio and energy conservation. Energy saving is confirmed by experimental results obtained in this paper and shown graphically in Fig. 7. [4, 5]

A frequency converter can be used to regulate the flow of a constant capacity pump such as a gear pump by regulating the speed of the AC electric motor that drives the pump. This system is more reliable and cheaper than traditional methods such as the use of variable speed electric motors or variable flow pumps.

By using a frequency converter to reduce the piston speed with increasing piston load instead of using a flow control valve, a reduction in the maximum rated power, weight, size and price of the drive motor is achieved.

This system can be used to meet certain operating conditions such as certain piston speed values with appropriate piston loads. The required pump flow values can be predicted using a theoretical model and stored in a program that supports this control method. These values are used to regulate the flow of the pump without opening the safety valve and without exceeding the rated power of the motor, which reduces energy losses and increases the efficiency of the system. To achieve this concept, only a frequency converter and a theoretical model are needed. So, this is a simple, flexible and cheap method of saving energy.

REFERENCES

Journal papers:

- [1] Lovrec D., Ulaga S. (2007). Pressure control in hydraulic systems with variable or constant pumps?, *Experimental Techniques*, Vol. 31, No. 2, 33-41.

Proceedings papers:

- [2] Savic V., Eric Obucina J., Knezevic D., Ivanisevic A., Balovic B., Kizic S., Technical-economic view of the replacement of pumps with variable volume pumps a constant volume of the frequency converter, *12th International Conference on Accomplishments in Mechanical and Industrial Engineering DEMI*, University of Banja Luka, Faculty of Mechanical Engineering, 29-30. May 2015. Banja Luka
- [3] Eric Obucina J., Cajetinac S., Stankovski S., Ostojic G., Modern solutions management capacity hydraulic pumps using frequency regulation, *XIII International SAUM Conference on Systems, Automatic Control and Measurements*, November 09th-11th, 2016., Niš, Serbia.

- [4] Eric Obucina J., Stankovski S., Savic V., Ostojic G., Cajetinac S., Energy savings using frequency regulation in the hydraulic system with a pump of constant displacement, *13th International Conference on Accomplishments in Mechanical and Industrial Engineering DEMI*, University of Banja Luka, Faculty of Mechanical Engineering, 26-27. May 2017. Banja Luka
- [5] Eric Obucina J., Stankovski S., Ostojic G., Aleksandrov S., Application of frequency converter in hydraulic system, *XIV International Conference SAUM 2018*, 14-16. November 2018 in Nis, Serbia.

Books:

- [6] Savic V. (2014). *Uljna hidraulika 4, deo 1, IKOS Novi Sad*.
- [7] Savic V. (2014). *Uljna hidraulika 4, deo 2, IKOS Novi Sad*.
- [8] Merritt, H. E. (1967). *Hydraulic control systems*, John Wiley & Sons Inc., New York.
- [9] Bose B. K. (1996). *Power Electronics and Variable Frequencies Drives*, IEEE Press.
- [10] Andersen T., Hansen R. (2007). *Fluid Power Circuits - System Design and Analysis, 3rd Edition*, AALBORG University.

Internet links:

- [11] Danfoss, From: [https:// www.danfoss.com](https://www.danfoss.com), accessed on: March 25, 2021.
- [12] Bosch Rexroth, From: [https:// www.boschrexroth.com](https://www.boschrexroth.com), accessed on: March 18, 2021.



Banja Luka
28-29 May 2021.

DEMI 2021

15th International Conference on
Accomplishments in Mechanical and
Industrial Engineering

www.demi.mf.unibl.org



A new concept of robotic plant protection in greenhouses

B. Z. Knezevic^a, A. Gojkovic^a, Z. Gajic^b, S. Mitric^c

^aUniversity of Banja Luka, Faculty of Mechanical Engineering, vojvode Stepe Stepanovica 71, Banja Luka, RS, B&H

^bHoloSCOPE, Jevrejska 50, 78000, Banja Luka, RS, B&H

^cUniversity of Banja Luka, Faculty of Agriculture, vojvode Petra Bojovića 1A, Banja Luka, RS, B&H

Abstract

Intensive use of pesticides in modern agriculture is trying to be minimized but the use of chemicals in plant protection is still irreplaceable and widespread. Proper application of pesticides is crucial to their effectiveness but protecting the health of people who perform chemical plant protection is imperative. In greenhouses, pesticides are usually applied with back or trailed sprayers. Due to the small distance between the rows, the farmer who applies pesticides is in direct contact with small dispersed solutions of chemical agents, which are most often classified in the third group of poisons.

Robotic plant protection indoors without the presence of humans would be an excellent solution that would improve the protection of farmers' health and increase the quality of plant protection, which would reduce the use of pesticides.

The paper presents just such a solution through a new conceptual design of robot control and guidance that has not been applied in practice so far. The presented solutions are the result of a wider research aimed at the development, design and practical implementation of robots with autonomous functioning in greenhouses. The robot is intended for the application of pesticides completely independently without the presence of a man in the greenhouse.

Keywords robotics, greenhouses, pesticides, autonomous vehicle

1. INTRODUCTION

Mechatronic approach, robotics and automation systems have changed a significant number of industrial applications in previous years and even decades. This type of modern technologies is increasingly entering the agricultural sector, as a predominantly labour-intensive sector with relatively low productivity, especially in the region.

Works in agriculture, physically demanding, repetitive in nature, with a great influence of the environment and weather conditions, are

gradually being improved and automated by applying a wide range of technologies. The introduction and use of agricultural robots for various purposes in advanced countries and industries around the world are increasingly taking on various tasks such as land preparation, sowing, fertilization, plant protection and harvesting.

From the point of view of agricultural production, it is important to point out the necessity of implementing protection measures in order to prevent yield losses of cultivated plants, and due to the harmful effects of insects, phytobagous mites and phytopathogenic microorganisms. Plant protection as such, must ensure the reduction of yield loss due to the action of harmful organisms and at the same time ensure that the agricultural product is of high quality and safe. By applying robotics, expectations are that effective plant protection

Corresponding author

PhD, Bojan Z. Knezevic
bojan.knezevic@mf.unibl.org

Faculty of Mechanical Engineering Banja Luka
vojvode Stepe Stepanovica 71, 78000
Banja Luka, RS, B&H

would be achieved at all stages of plant growth. The production of health-safe food is a condition that must be met in agricultural production. At the same time, the safe and sustainable use of pesticides must be ensured, in which farmers' exposure to pesticides must be minimized.

Safe application of pesticides in greenhouses, with reduced exposure of workers, is very difficult to achieve because the worker is directly exposed to both droplets and vapours of pesticides. Namely, in greenhouses, pesticides are usually applied with backpack sprayers or trailed sprayers. In such an application, the exposure of workers is quite large, because there is almost no distance from the working fluid of the pesticide, unlike working in the open field with tractors with special cabins. When a farmer works with pesticides, the temperature in greenhouses is often high, so workers are reluctant to use protective equipment, which further contributes to exposure to pesticides. When applying pesticides with backpack sprayers, an additional source of contamination of workers are the exhaust gases of internal combustion engines.

With the use of an autonomously controlled electrically powered robot, the danger to the health of farmers disappears completely. The farmer would be out of the greenhouse during the application of pesticides thanks to a robot that would independently perform the application of pesticides. At the same time, the quality of plant treatment would increase, so the number of treatments, i.e. the amount of applied pesticides would decrease.

2. STATE OF THE ART

Currently, the most commonly used robots in greenhouses are spraying robots (24.7%), planting and harvesting robots (22.2%) and packaging (11.7%) and stacking (3.7%) [1]. There are different variants of robotic systems for agriculture. Some of them are on the market as products, and some are at the research level. NAIIO technologies is one of the first manufacturers of commercially available robots. They provide support to farmers after the purchase of the robot and additionally adapt the robot to the user (Fig. 1.) [3].

OZ, DINO and TED, Naio robots, are not the only robots that aim to reduce the share of human

labor. Solutions such as AGROINTELLI [4], AVO [5], Meropy [6], Rhoban [7], ROVITIS [8], Trektor [9], Vinescout [10] and ViTiBOT [11] are solutions that are under development and which would could soon appear on the market. A comparison of these robots is given in Table 1.



Fig. 1. OZ robot from Naio in greenhouse, sowing application [3]

SITIA provides an interesting solution for viticulture with a hybrid drive. The design allows you to adjust the height and width depending on the distance between the plants. It can work on the ground, above the vines or at the height of the trees in the orchards (Fig. 2) [9].

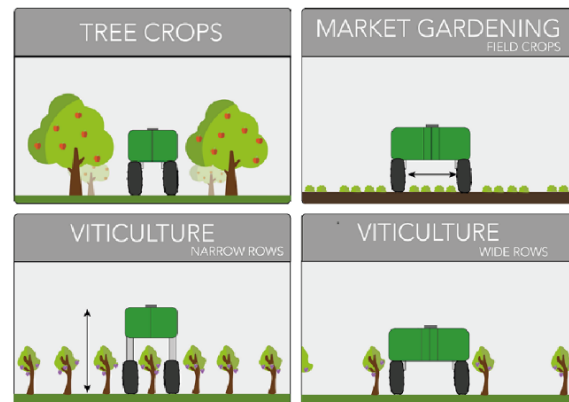


Fig. 2. SITIA robots, multifunctional approach for wide spectrum of applications [9]

The Bakus robot from ViTiBOT has an electric drive and includes various position sensors, 8 infrared 3D cameras and 2 RTK GPS to achieve a robust solution that will be able to work in a natural environment. The electrically powered platform is environmentally friendly, preserves soil and air quality and does not produce much noise (Fig. 3) [11].



Fig. 3. Bakus robot from ViTiBOT for applications in vineyards [11]

ROVITIS 4.0 is also a vineyard robot made with the support of the Italian project EIP AGRI. Rovitis 4.0 autonomous robot for vineyards is the last stage of prototype development. He can drive himself from the garage to the plot, do the work and return even if he loses the GPS signal (Fig. 4) [8].



Fig. 4. Rovitis 4.0 for applications in vineyards, in development [8]

SAGA Robotics was established as a company committed to delivering autonomous services for the agricultural industry. They have few types of robot platforms: a three-wheeled version, a low, narrow version for greenhouses, a differential drive version, a tall phenotyping version, a standard version. The most interesting application of their robots is for UV treatments. Weekly exposure of strawberries to

shortwave UV light is highly effective in suppressing powdery mildew, but the treatments must be applied at night to avoid damaging the plants. That creates a labour issue. No one wants to drag a UV light array behind a tractor all night long. That's where modern agricultural robots excel: they can carry the relatively lightweight lamp arrays, and they don't mind working all night (Fig. 5) [14].

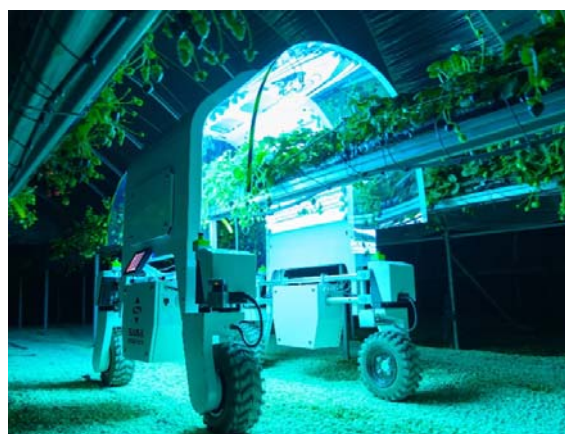


Fig. 5. Thorvald by SAGA, robot for UV treatment of strawberries [14]

Robots are not the only solutions to replace human labor in agriculture. Attachments for existing agricultural machines are one of the possibilities. For example, the Lettuce bot from Blueriver technology was made at the request of John Deere, in order to detect and remove weeds [12]. Or RowCropPilot, developed by Robotmakers GmbH, which provides the ability for farmers to automate their machines with little investment [13].

3. CONCEPT DESCRIPTION

It is clear that automation in agriculture is an interdisciplinary problem that as such needs to be addressed. Only the synergistic action of researchers in the field of mechanical engineering, mechatronics, robotics, software technologies, artificial intelligence and plant protection can give an adequate result.

The innovative solution that is the goal of the research presented in this paper implies a unique case of the possibility of pesticide application without the presence of man in the greenhouse. It is a fully automated plant protection during which there is not a single person in a closed greenhouse.

Table 1. Comparison of the characteristics various types of agriculture robots [2]

Company - Robot	Intended for	Format	Drive	GPS	LIDAR	Vision
SITIA - Trektor	Vineyards, Orchards, Fields	Big	Hybrid	YES, RTK	NO	NO
Ecorobotis - AVO	Fields	Big	Electric	YES	NO	YES
AGROINTELLI - Robotti	Fields	Big	ICE	YES, RTK	YES, multichannel	YES
Instar - Trooper	Horticulture, logistika	Small	Electric	YES	NO	YES
Bakus - ViTiBOT	Vineyards, Orchards, Fields	Big	Electric	YES	NO	YES
VineScout	Vineyards	Small	Electric	YES	YES	YES
Naio – TED, Dino, OZ	Vineyards, Orchards, Fields	Big, Big, Small	Electric	YES, RTK	YES	YES
Meropy - SentiV	Fields	Small	Electric	YES	NO	YES
Rhoban - E-Tract	Fields	Big	Electric	YES, RTK	YES	NO
Ag. Giorgio Pantano - ROVITIS	Vineyards	Big	ICE	YES, RTK	YES, multichannel	YES, visual odometry
Farmbeast	Fields	Small	Electric	NO	YES, multichannel	YES, weed detection

In addition to the above, the research should provide an innovative solution of a multifunctional and flexible robot that can be easily adapted to various applications in plant production in a protected area. Also, the robot must be cheap and based on components that already exist and are not expensive.

Unlike traditional solutions of agricultural machines, which, regardless of power and purpose, are powered by internal combustion engines, the robot will be powered by electricity, which introduces ecologically superior and energy efficient electric machines into agriculture.

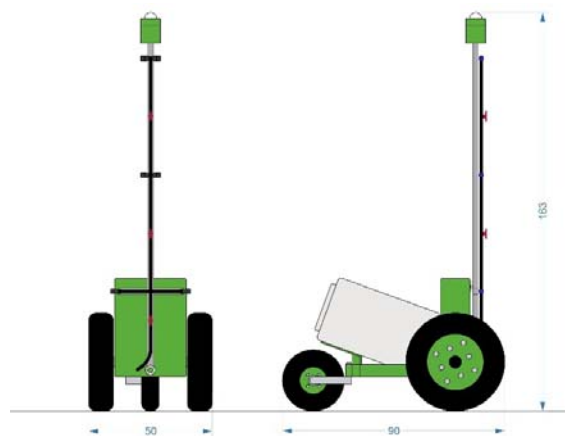
The application of robotic plant protection in the way proposed in this paper is most useful in plant crops such as tomatoes, peppers and cucumbers due to their height, duration of vegetation and density of the assembly.

4. FUNCTIONAL SUBSYSTEMS OF AUTONOMOUSLY GUIDED ROBOT

4.1 Drive subsystem and mechanical design

The mechanical design of the robot is based on three wheels. Two wheels are for propulsion. The control of the robot direction is realized by differential control of the drive wheels. The

third wheel has two degrees of freedom (Fig. 6). Such a construction ensures the contact of the drive wheels with the ground in all cases of terrain configuration. The drive of the drive subsystem, as well as all other subsystems, is electric due to the indoor operation. Electric drive motors, gearboxes, brakes, drivers and position and angle sensors are an integral part of the drive subsystem. The rechargeable batteries are of the Li ion type and provide sufficient robot autonomy for the smooth operation of the one-day protection treatment.

**Fig. 6.** Drive subsystem and mechanical design

The complete robot is 50 cm wide and less than one meter long. Small dimensions are necessary due to the small space between the rows in the greenhouses. It is a great challenge to place the complete device in such small dimensions and only with an innovative design can it be achieved (Fig. 6).

4.2 Control subsystem

Autonomous driving through the greenhouse is realized by a camera with an integrated graphics processor that monitors the objects on the ceiling of the greenhouse. It is placed high, above the treatment subsystem (Fig. 6). To ensure proper positioning of the camera view with the vehicle axis, the camera and nozzles holder is maintained in a vertical position regardless of the vehicle position. Thanks to this, the nozzles are always directed perpendicular to the plants, too. The three-axis gyroscope is used as a feedback sensor in the control loop in which the linear motor is the actuator.

An integral part of the control subsystem is the control software of a high level of mathematical complexity for the analysis of objects and the determination of paths and trajectories.

In addition to automatic operation, the robot also has manual control by the user via a wireless interface.

4.3 Treatment subsystem

It is possible to mount various application systems on the robotic platform. First and foremost, the robot carries a pesticide application system, with a solution tank, pump, filters, pressure sensor, piping and nozzles with supporting fittings. The drive of the pesticide application system is electric and powered by shared rechargeable batteries. The pressure in the system is kept constant in the control structure which includes the nozzles, the pump with the driver, the pressure sensor and the microcontroller-based regulator. It is possible to switch off individual nozzles, depending on the height of the plants, while keeping the pressure unchanged. This gives the optimal treatment of plants in all possible cases.

The complete pesticide application system together with the tank can be easily removed, thus turning the robot into a mobile multifunctional platform with a variety of

applications in agriculture, including applications outside the greenhouse.

5. DESIGN OF THE AUTONOMOUSLY GUIDED ROBOT

The functionality of the robot must be accompanied by an adequate design that will make the robot as a product attractive on the market without a negative impact on functionality or price.

The mechanical structure that is the base of the robot (Fig. 6) is closed with two covers made by thermoforming technology. The material is ABS plastic (Fig. 7). The final appearance was obtained with heat-shrinkable printed foil (Fig. 8 and 9).

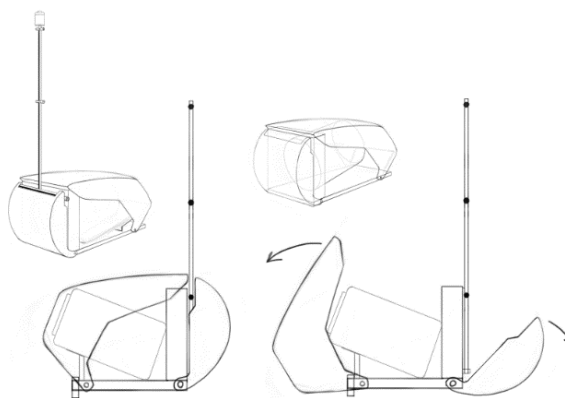


Fig. 7. Design of ABS covers



Fig. 8. Final design of the autonomous guided robot for applications in greenhouses

6. FUTURE RESEARCH

The described concept is the starting point for future work that will be directed towards the development of new solutions that will be applied in outdoor agriculture, both in vegetable production and in farming and fruit growing.

Future development will aim not only at the safety and health of farmers but also at reducing the use of pesticides through selective spraying as well as the development of techniques that would enable the complete exclusion of pesticides in crop production of the most economically important crops.

The plan is to continue the development cycle from this starting point, which would last from 3 to 5 years. The goal is to get a multifunctional robot that can be adapted to different uses in agriculture by developing various attachment subsystems, based on the identified needs of farmers.



Fig. 9. The autonomous guided robot in operation – virtual presentation

One of the challenges in the long-term development cycle will be the development of computer vision, which will enable it to perform more complex tasks, such as recognizing weeds and destroying them mechanically or by spraying them with a minimum controlled dose of herbicide. Also, other types of extension of robot functionality (transport, harvesting assistance, etc.) as well as improvement of the treatment subsystems for more efficient application of pesticides with the aim of

reducing pesticide and water consumption. Energy efficiency and the use of renewable energy sources is a special field for further research.

7. CONCLUSION

The robotization of agriculture is a process that is inevitable and that is coming. The application of robots in agriculture is not a simple problem and requires very specific solutions. Many scientists and companies around the world are working on the development of robots for agriculture. In addition to the development of robots, it is necessary to work on educating users who will be ready for new technologies and for investments in unconventional agricultural machines.

The concept presented in this paper, on which the authors' research team is working, is a solution that should be a link between new technology and traditional users. The presented system is a high-tech solution, but it is not too demanding to use and which users will be able to easily get used to and adopt in application.

Acknowledgement

This paper presents the initial part of the research conducted through a project funded by the Ministry of Agriculture of the Republic of Srpska. The implementers of the project are Holoscope, Faculty of Mechanical Engineering and Faculty of Agriculture of the University of Banja Luka.

REFERENCES

Technical reports:

- [1] Clave, H., (2019). *Use of robots in greenhouse horticulture increasing*, Future farming, <https://www.futurefarming.com/Machinery/Articles/2019/12/Use-of-robotsin-greenhouse-horticulture-increasing-508761E/>, accessed on: January 4, 2021.
- [2] Rakun J., Stajanko D., Rihter E., (2021). *Use of robotics in agriculture*, Practical guide for the use of ICT in AET.

Internet links:

- [3] Naio Technologies, <https://www.naiotechnologies.com/en/>, accessed on: December 5, 2020.
- [4] AGROINTELLI, Robotti, <https://www.agrointelli.com/>, accessed on: December 5, 2020).
- [5] Ecorobotix, AVO, <https://www.ecorobotix.com/en/>, accessed on: December 25, 2020).
- [6] Meropy, SentiV, <https://meropy.com/robot.html>, accessed on: February 15, 2021.
- [7] Elatech, Rhoban, <https://www.rhoban-project.fr/post/e-tract>, accessed on: February 6, 2021.
- [8] Giorgio Pantano, ROVITIS, <https://www.aziendapantano.it/rovitis40.html>, accessed on: March 20, 2021.
- [9] SITIA, Trektor, <https://www.sitia.fr/en/home/>, accessed on: April 2, 2021.
- [10] Vinescout, <http://vinescout.eu/web/>, accessed on: April 2, 2021.
- [11] Bakus, ViTiBOT, <https://vitibot.fr/>, accessed on: April 2, 2021.
- [12] Blue river technology, <http://www.bluerivertechnology.com>, accessed on: April 3, 2021.
- [13] Robotmakers, RowCropPilot, <https://robotmakers.de/en/blog/2018/01/15/rowcroppilot-autonomy-kit-for-row-crops/>, accessed on: February 22, 2021.
- [14] SAGA robots, <https://sagarobotics.com/pages/thorvald-platform>, accessed on: April 6, 2021.

*Automotive and
Transportation Engineering*



Banja Luka
28–29 May 2021.

DEMI 2021

15th International Conference on Accomplishments in Mechanical and Industrial Engineering

www.demi.mf.unibl.org



Experimental determination of thermal stresses disk brakes in depending from the braking pressure and vehicle speed

N. Stojanović^a, I. Grujić^a, J. Glišović^a

^aUniversity of Kragujevac, Faculty of Engineering, Department for Motor Vehicles and Motors, 6 Sestre Janjić STR., 34000 Kragujevac, Serbia

Abstract *The goal is that during the process of braking stopping distance as short as possible, which is one of the important parameters of braking. During the braking process itself, a certain heat is generated on the brake disc and brake pads, which depends on the speed of movement that the vehicle had at the time of the brakes, as well as from the realized pressure in the brake installation. The purpose of this work is to find optimal braking parameters, in order to generate as less heat as possible on the disc brakes. The paper presents experimental research on a test rig BRAKE DYNO 2020, for a simulated vehicle speed of 100 km/h when the braking pressure of 2.8 MPa and 5 MPa. It is concluded that higher temperatures occur in the case when the braking pressure is 2.8 MPa, because it takes more time to stop. The results of this research can be applied in practice, in defining braking pressure.*

Keywords *braking parameters, heat, experimental research, BRAKE DYNO 2020*

1. INTRODUCTION

During the exploitation from vehicle is expecting to achieve the fastest possible desired speed, as well as to slow down or to stop for shortest possible time, all depending from road conditions. Because of this reason, the system that is the most exposed to the stresses, is the braking system. The braking system should do three basic tasks and that:

- Emergency braking – characteristic for critical situations;
- Easy long-term braking – vehicle

movement on long downhills, and

- Easy short-term braking – characteristic for city situations.

During the braking process, the entire kinetic energy transforms into the heat energy, on disc brakes. The heat energy generates in the contact between the braking disc and braking pads, as the consequence of the friction appearing. The tendency is, that the friction coefficient during the braking process be as great is possible, in order to provide as shortest possible stopping distance. However, the undesirable consequence of friction is the heat generation in the braking system.

With the temperature increment, the friction coefficient value falls [1]. However, this happens, when the temperature value on the contact surfaces passes value of 250 °C. In the case, when the temperature on the contact

Corresponding author

M.Sc., Ivan Grujić
ivan.grujic@kg.ac.rs

University of Kragujevac, Faculty of Engineering,
Department for Motor Vehicles and Motors
6 Sestre Janjić STR.
Kragujevac, Serbia

surface of the braking disc is 150 °C, the friction coefficient is biggest [2]. Important parameters from which depends, the amount of heat that generates on the contact surfaces are coefficient of heat transfer, heat flux, specific heat and heat dissipation into the environment [3].

Braking pads, during the braking process acting on the braking disc with determined force. Due this, it comes to the deformations of elements, which are in contact, which further causes the appearance of wear on the same elements. On the wear size, as well as on the size of contact temperatures are influencing loads that appear in observed moment [4], where are separating three different wear types and that:

- Slight wear;
- Moderate wear, and
- Hard wear

In more researches, the same conclusions have been obtained, that is that the temperature that was generated on the contact surfaces is not uniform [5, 6]. Because of this it comes to greater wear of contact elements. When the sliding speed is high, the temperatures that are generating on the contact surfaces are very high, which can cause the disturbances in the material [7]. The shape of hot surfaces that appearing during the braking process (Figure 1), can be separated on five types [8]:

1. Asperity – the heating appears on discrete points on the contact surface of the braking disc, are short-term character.
2. Gradients on hot bands – its appearing one long contact track, with interruptions.
3. Hot bands – are consequence of reduced contact between the braking disc and braking pads, can be present more bands.
4. Macroscopic hot spots – are representing hot spots that are deployed on the contact surface of the braking disc. Due such generated temperature on the braking disc, it can come to the braking disc twisting.
5. Regional hot spots – on the contact surfaces are appearing lower temperatures that are characteristic for nonhomogeneous cooling

By observing all five heating types, Figure 1, the greatest damages of the braking disc are appearing in the cases 2., 3. and 4. types of heating.

The aim of the paper is the investigation of the influence of the braking pressure on the size of the generated temperature on the braking disc

and braking pads, all with reason to find optimal braking parameters.

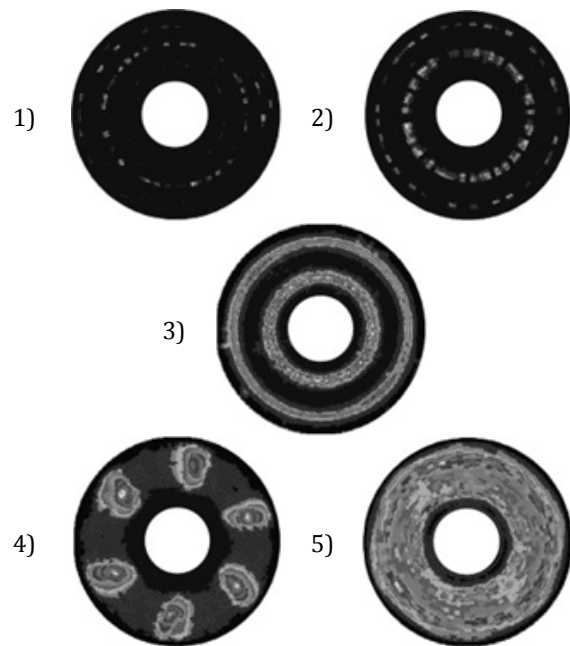


Fig. 1. Types of braking disc surface heating: 1) asperity, 2) gradients on hot bands, 3) hot bands, 4) macroscopic hot spots, and 5) regional hot spots [8]

2. THE TEST RIG WITH APPLIED DEVICES/SENSORS FOR MEASUREMENT

The experimental investigation for this paper was performed on the test rig BRAKE DYNO 2020, on the Faculty of Engineering University of Kragujevac. The scheme of the test rig for investigation of the disc brake thermal stresses can be seen on the Figure 2.

The test rig control is performing by application of the PC (11), from which command signals are sent through A/D converter 6353, to the actuators. By command signals is performing the activation of the electric motor (29) start. Also the same electric motor is controlled by AC drive (13), which also receives command signal from the PC. At the end, the signal for the activation and deactivation of the electromagnetic clutch (2), also is also sent form the PC. The activation of the brake caliper (27), is performing by braking cylinder (12), which activates by application of the pneumatic installation (9), Figure 3. The air supply for pneumatic installation is from compressor (10), which can provide maximal pressure 10 bar. The electromagnetic clutch is on one side in

rigid connection with electric motor and on other side, with the flywheel mass shaft (5). The flywheel mass is on the both side with two bearings placed on the carrying construction (22) of the test rig. While the position of the electric motor is defined by vertical adjusters (23) in order to achieve axis adjustment

between the shaft of the electric motor, and shaft of the flywheel mass. On the other side of the flywheel mass shaft is mounted braking disc (6). Where the braking calliper is in rigid connection with the calliper carrying plate (28), which is with other side relying on a force sensor (19).

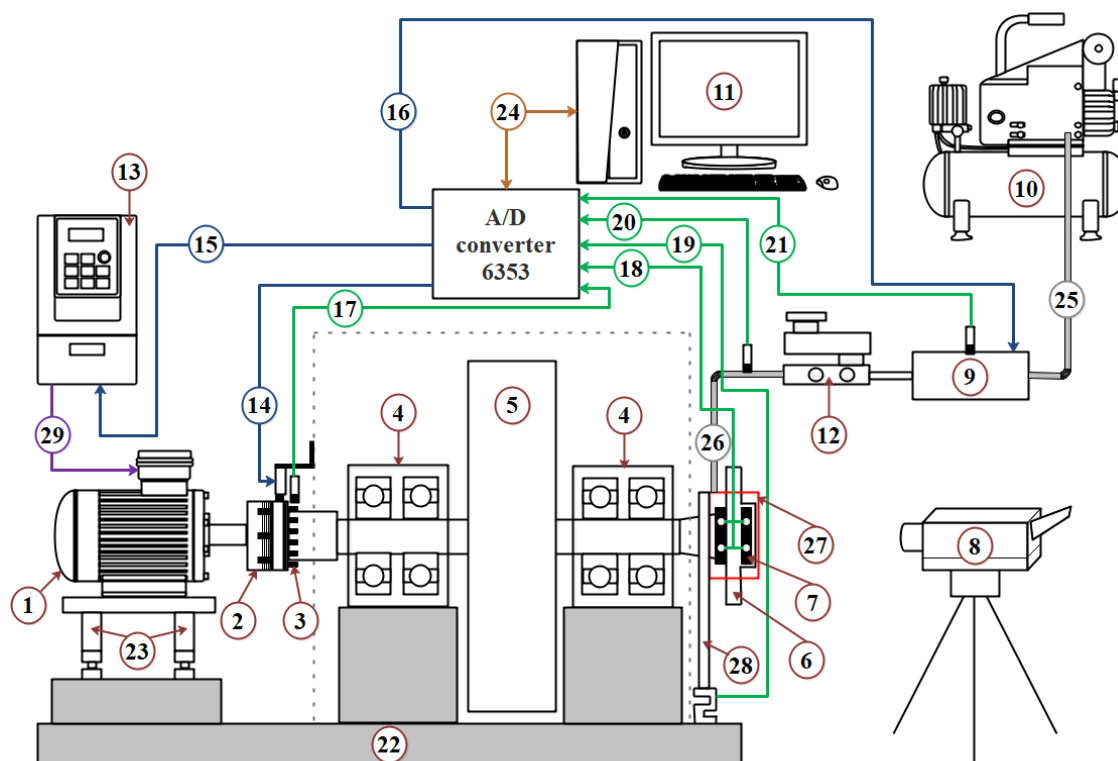


Fig. 2. The scheme of the test rig

Also, by A/D converter 6353 are collecting the measured signals from mounted sensors, which are mounted on the test rig. On the test rig, during the experimental work, are measured next parameters:

- The angular speed of the flywheel mass/braking disc (14).
- The pressure in the pneumatic installation (Figure 2 – position 21, Figure 3 – position 7).
- The pressure in the braking installation (20).
- Braking torque (19).
- Temperature in the braking pads (18).

While the temperature on the contact surfaces of the braking disc is measured by application of thermal imager TESTO 868 (8). Inside each

braking pad are located two temperature probes at 2 mm depth, from the contact surface. One is located on the entering side of the braking pad and the other on the exiting side of the braking pad

Pneumatic installation (Figure 3) consists from air conditioning group (1 and 2), 5/2 electromagnetic valve (3), with which is performing activation of the pneumatic cylinder (8). The air pressure is controlling by pressure regulator (4), while by flow control valves (5 and 6) are controlled activation and deactivation speed of the pneumatic installation.

The test rig for the investigation of the disc brake thermal stresses BRAKE DYNO 2020, is shown on the Figures 4 and 5. The Figure 4 represent the 3D model of the test rig that was

created in the CATIA software package, while Figure 5 illustrates the realized test rig.

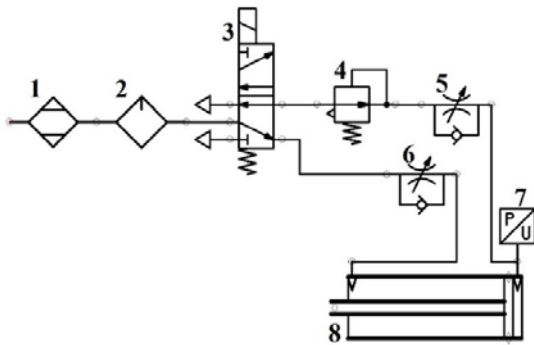


Fig. 3. The pneumatic installation for the braking system activation

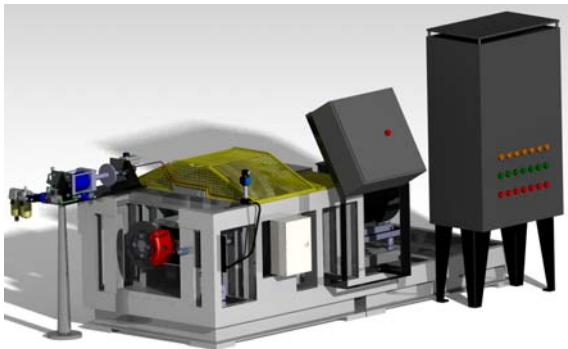


Fig. 4. 3D model of test rig BRAKE DYNO 2020



Fig. 5. The appearance of test rig BRAKE DYNO 2020

3. TESTING PROCEDURE

How the aim is to determine how the size of the braking pressure influences on the value of the generated temperature on the disc brake, is was defined testing procedure, Figure 6. First step is to define the testing conditions such are value of the braking pressure, the vehicle quarter mass

(the test rig simulates one quarter of the vehicle) and desired vehicle speed. After that are defining values which are observing during the investigation process – output parameters. The output parameters are the temperatures on braking pads and on the braking disc, deceleration, friction coefficient, the pressure changes during the stopping period and braking torque.

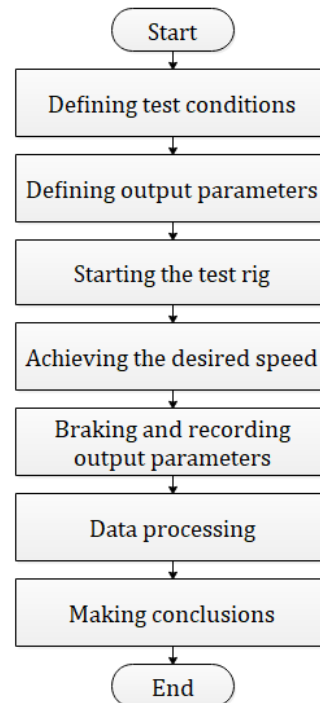


Fig. 6. Testing procedure

Next step after defining input and output parameters is the test rig starting, and after achieving the desired speed, the simulated vehicle is stopping and during the braking process are recorded the input and output parameters. After that, the measured data is processing and showing by charts, from where are coming conclusions, about thermal stresses that occurred during the braking process. While the temperature obtained by application of the thermal imager, are showing in the shape of thermal images.

4. RESULTS AND DISCUSSION

In this chapter are shown the obtained results by experimental work, according to the defined testing procedure on the test rig BRAKE DYNO 2020.

In the moment of achieving the maximal speed, the brake activates and it starts the stopping process of the simulated vehicle. According to the defined braking conditions, at the moment when starts the braking process, the electromagnetic clutch deactivates and

separates the electric motor from the flywheel mass. The maximal braking pressure in both cases was achieved after 1 s, Figures 7 and 8, and it stays almost constant during entire braking process.

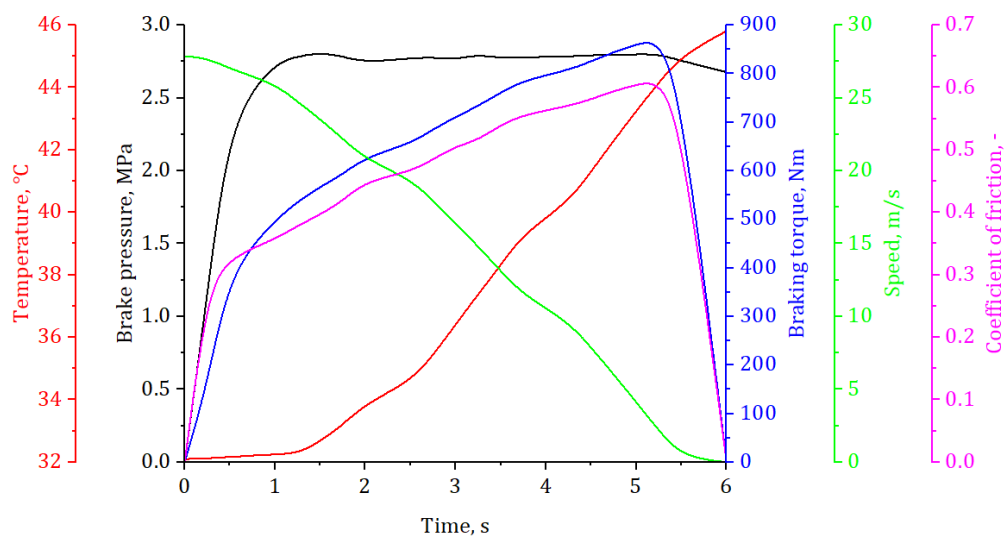


Fig. 7. Changes of braking pressure, temperature, braking torque, speed and friction coefficient in the function of time, when the maximum pressure in braking installation is 2.8 MPa

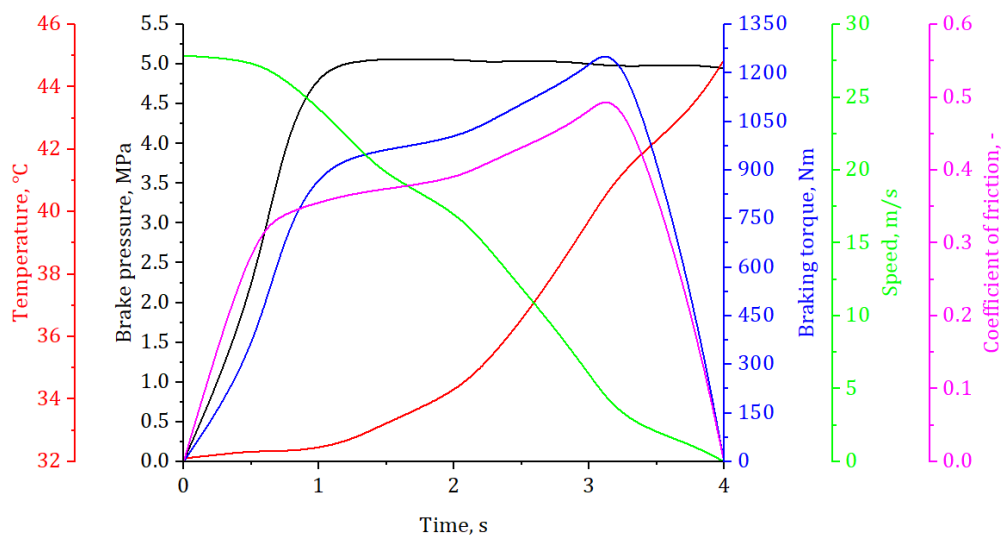


Fig. 8. Changes of braking pressure, temperature, braking torque, speed and friction coefficient in the function of time, when the maximum pressure in braking installation is 5 MPa

Maximal values of braking torque and friction coefficient are appearing when the speed of the simulated vehicle falls under 3 m/s. The temperature that was observed, is the temperature on the external braking pad, on the side that first enters in contact with the braking disc, from reason, because on it are appearing

highest values. In the first period, while vehicle speed don't falls under 20 m/s, the temperature changes are insignificant, more accurately its grown for 1.5 °. After the speed falls under the 20 m/s, the temperature change is significantly greater. In the case when is defined 5 MPa braking pressure, the temperature it's grown

for 9.7 \square . While in the case when the braking pressure is 2.8 MPa, it has grown for 11.22 \square . The reason for higher temperature in the case when the maximal braking pressure is 2.8 MPa, is because the braking time is longer, Figures 7 and 8.

The thermographic representation of the braking disc and braking pads is shown on Figures 9 and 10. Different from braking pads, greater temperatures are appearing on the braking disc. Which is very good, because only the braking disc can dissipate heat into the environment, because during the braking process, the greatest part of the braking disc rotates free in space, where on it acts only the air. How the testing was performed in stationary conditions, without air that flows around disc, the heat dissipates only because the temperature difference of the braking disc and air. Higher values of temperature on the braking disc are consequence of higher pressure in the braking installation, which is proven and in earlier researches [9, 10].

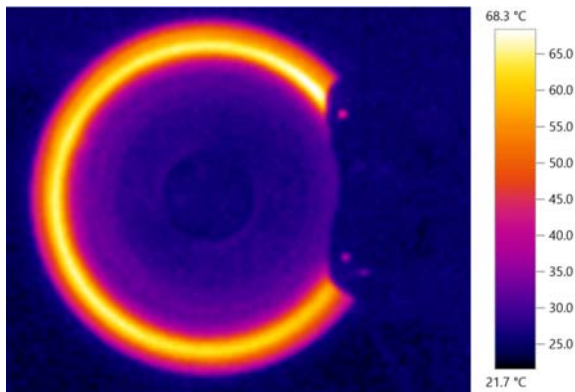


Fig. 9. The thermographic representation of the braking disc for braking pressure 2.8 MPa

the braking disc for braking pressure 5 MPa
During the braking process, when the braking pressure is 2.8 MPa, on the braking disc can be noticed hot band on the entire contact surface of the braking disc. This is not good from the aspect of the gratest damages appearing of the braking disc, which further have shorter life as the consequence [8].

However in the case when the braking pressure is 5 MPa, on the contact surface of the braking disc, can be noticed two hot bands. Which also is not good from the aspect of gratest damages appearing of the braking disc.

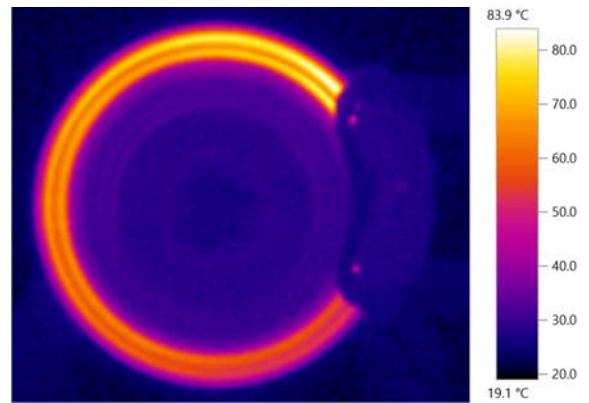


Fig. 10. The thermographic representation of

On the braking disc can be noticed that the contact surface heats more than hub, which further can cause appearance of the uneven temperature expansion, which further can led to the appearance of deformations, and at the end to breaking.

5. CONCLUSION

The stopping process is followed with appearance of temperatures generation on the braking disc and braking pads. Which further as consequence have appearance of deformations and damages. The braking pressure is very important parameter how from the aspect of traffic participants safety, where the tendency is that the stopping distance be as less as possible in the case of some critical situation, so and from the aspect of disc brake stresses. How the final temperature that was generated on braking pads is different only for 1.52 \square , the pressure in the braking installation can be 5 MPa.

Future research should include analysis of braking disc and braking pads made from alternative materials, and to investigate their influence how in normal conditions of exploitation, so in the extreme exploitation conditions.

ACKNOWLEDGEMENT

This paper was realized within the framework of the project "The research of vehicle safety as part of a cybernetic system: Driver-Vehicle-Environment", ref. no. TR35041, funded by the Ministry of Education, Science and Technological Development of the Republic of Serbia.

REFERENCES

- [1] Breuer, B., Karlheinz, H. B. (2012). *Bremsenhandbuch – Grundlagen, Komponenten, Systeme, Fahrdynamik, Springer Fachmedien Wiesbaden.*
- [2] Ahmed, I., Leung, P., Datta, P. (2000). Experimental Investigations of Disc Brake Friction. *SAE Technical Paper*, 2000-01-2778, DOI: [10.4271/2000-01-2778](https://doi.org/10.4271/2000-01-2778).
- [3] Ostermeyer G.P., Graf M. (2013). Influence of wear on thermoelastic instabilities in automotive brakes. *Wear*, vol. 308, iss. 1-2, p. 113-120. DOI: [10.1016/j.wear.2013.09.009](https://doi.org/10.1016/j.wear.2013.09.009)
- [4] Riahi, A.R., Alpas, A.T. (2003). Wear map for grey cast iron. *Wear*, vol. 255, iss. 1-6, p. 401-409. DOI: [10.1016/S0043-1648\(03\)00100-5](https://doi.org/10.1016/S0043-1648(03)00100-5)
- [5] Barber, J.R. (1967). The influence of thermal expansion on the friction and wear process. *Wear*, vol. 10, iss. 2, p. 155-159. DOI: [10.1016/0043-1648\(67\)90087-7](https://doi.org/10.1016/0043-1648(67)90087-7)
- [6] Hartsock, D.L., Dinwiddie, R.B., Fash, J.W., Dalka, T., Smith, G.H., Yi Y.B. (2000). Development of a high speed system for temperature mapping of a rotating target. *Proc. SPIE 4020*, p. 2-9. DOI: [10.1117/12.381533](https://doi.org/10.1117/12.381533)
- [7] Anderson, A.E., Knapp R.A. (1990). Hot spotting in automotive friction systems. *Wear*, vol. 135, iss. 2, p. 319-337. DOI: [10.1016/0043-1648\(90\)90034-8](https://doi.org/10.1016/0043-1648(90)90034-8)
- [8] Panier, S., Dufrénoy, P., Brunel, J.F., Weichert, D. (2004). Progressive waviness distortion: a new approach of hot spotting in disc brakes. *Journal of Thermal Stresses*, vol. 28, iss. 1, p. 47-62, DOI: [10.1080/01495730490498638](https://doi.org/10.1080/01495730490498638)
- [9] Stojanović, N.R., Glišović, J.D., Abdullah, O.I., Grujić, I.Lj., Vasiljević, S.Ž. (2020). Pressure influence on heating of ventilating disc brakes for passenger cars. *Thermal Science*, vol. 24, no. 1A, p. 203-214. Doi [10.2298/TSCI190608314S](https://doi.org/10.2298/TSCI190608314S)
- [10] Stojanović, N., Abdullah, O.I., Schlattmann, J., Grujić, I., Glišović, J., (2020). Investigation of the penetration and temperature of the friction pair under different working conditions. *Tribology in Industry*, vol. 42, no. 2, p. 288-298. DOI: [10.24874/ti.849.02.20.05](https://doi.org/10.24874/ti.849.02.20.05)



Banja Luka
28–29 May 2021.

DEMI 2021

15th International Conference on
Accomplishments in Mechanical and
Industrial Engineering

www.demi.mf.unibl.org



Possibility of implementing the Lean Six Sigma concept on logistics processes

N. Simić^a, A. Stanković^b, I. Mačuzić^a, G. Petrović^b

^aFaculty of Engineering, University of Kragujevac, Serbia.

^bFaculty of Mechanical Engineering, University of Niš, Serbia.

Abstract *Modern trends in the economy, the current crisis caused by the pandemic, as well as the demands made by relentless customers, have caused changes in the organizational structures of companies in both administrative and excellent processes. There was a need for new philosophies, the most advanced of which were those developed in Japan. Lean, as a business philosophy was developed in Toyota Motor Manufacturing during the 1960s, and Six Sigma developed in the 1980s at Motorola. Lean simplifies and speeds up the process while reducing or eliminating waste, while Six Sigma is focused on neutralizing defects that slow down and increase the cost of the production process. These two ideas currently in practice form a unique unbreakable Lean Six Sigma concept. This paper presents the methodology of implementing the Lean Six Sigma concept on the processes of a logistics company through the definition and description of a mega process, which aims to reduce waste, stocks, and excessive transport as well as the number of communication channels in administrative processes. The ultimate goal is to show the application of a possible way to improve the processes and to show the advantages of the implementation.*

Keywords *Lean Six Sigma concept, mega process, implementation, logistics.*

1. INTRODUCTION

The long-term economic crisis, along with the current situation caused by the COVID-19 pandemic, has brought unpredictable and unstable business conditions that require changes in the production process. The changes are reflected in the transition from traditional mass production to a new business philosophy. Many companies have realized that the demands of the global market, with an emphasis on increasingly demanding and sensitive customers, set new standards for production flexibility, which condition the

development of new production systems with better and more convenient services. For companies to maintain their market presence, they must adapt their structure to meet the requirements of customers with lower high-quality prices as well as short delivery times at the lowest possible cost. Delivery and costs, as well as the scope of work, staff effort, and response time, are a research problem of this paper, which presents the possible practical application of the Lean Six Sigma concept to logistics processes to gain time, reducing employee stress, increasing the quality of information and efficient design and management of logistics. The aim of the paper is not to repeat in detail the theory that can be found in the wilds of the Internet but to try to show the possibility and way of the practical application of the Lean Six Sigma concept to logistics processes.

Corresponding author

MSc Nikola Simic
nikolasimicva@hotmail.com

Faculty of Engineering, University of Kragujevac
Kragujevac, Serbia

2. PHILOSOPHIES OF MODERN PRODUCTION

Among the business philosophies of modern production are those created in mass production, of which the following stand out. Lean concept of business philosophy was created in Toyota as reengineering to save the company from bankruptcy resulting in the production of products with minimal energy, materials, and labor waste. In doing so, the products must be of the highest quality for customers to accept products from a country with a bad tradition and reputation. Toyota's gradual growth from a "small player" to the largest company in the automotive industry has caused a great deal of public attention and interest, which has made the Lean concept a hot topic in management at the beginning of the 21st century. On the other hand, Six Sigma (6σ) was developed by Motorola in the mid-1980s, when in its business it adopted the then-new philosophy of "zero flaws" [10]. This concept is based on the understanding that a company can ensure competitiveness by reducing defects, which occur in the daily implementation of processes and activities. In doing so, Six Sigma is primarily process-oriented rather than results-oriented, because results are determined by what happens during the process. According to Pešić [6], by creating effective processes and increasing their efficiency, the possibility of the occurrence of defects is reduced or even eliminated. In modern academic circles, these two concepts are inconceivable without each other and together they are called Lean Six Sigma (LSS). The problem with using only Lean is that it is difficult to statistically control the process (say, in the control of defective products), while Six Sigma alone cannot increase process speed or reduce costs. Applied in combination, they help reduce costs and complexity production. Lean and Six Sigma are similar because they have a wide-angle and telescopic lens. Lean thinking allows you to see the big picture, and Six Sigma focuses on complex issues. As Damjanovic and others point out [11] combining the best of both processes and enabling the transition from traditional to LSS production (Table 1).

Table 1. Comparison of traditional and Lean Six Sigma production [3]

Elements	Traditional manufacturing	Lean Six Sigma manufacturing
Beat the competition	Company goals	Gain Customers
Results	Priorities	Processes
Company managers	Production initiators	Consumers
Operating costs	Employee treatment	A Condition of Competitiveness
Inventory	Yes	No
Transfer batch size	Large series	Small Series
Troubleshooting	Business culture	Preventing Problems
Find the culprits	Problem treatment	Finding the Cause of Problems
Beat the competition	Company goals	Gaining Customers

Unlike the traditional approach, the Lean Six Sigma concept requires a decentralized approach to organizing, in terms of transferring responsibility to those workers who possess high abilities and skills. The first step in the Lean Six Sigma transformation is for people to see waste and become aware that these are unnecessary losses for everyone. At the heart of Lean Six Sigma, the concept is a people-based system. The success of any Lean Six Sigma transformation depends on the engagement of each employee in the process of continuous business improvement. All employees must be ready and able to solve all complex problems. Those who are in higher positions, who make decisions, are the most responsible and they have the strength and authority to initiate change [3].

3. LEAN SIX SIGMA CONCEPT

Lean Six Sigma production is a set of methods and techniques and is guided by the following principles [4]:

- Value - value for customers (it is necessary to determine what contributes to value creation and what is not excluded from the customer's perspective, not from the perspective of companies).
- Value Stream - value map (it is necessary to identify all the necessary production steps throughout the value chain, with emphasis on activities that do not add value).

- Value Flow - value flow (activities that create value should be realized without interruption and waste).
- Pull Value - withdrawal of value (produced by customer orders).
- Pursue Perfection - strive for perfection (continuously eliminate unnecessary wear and tear - waste and waste).




The most important goals derive from the defined principles, among which is the elimination of waste, ie. activities that do not add value, where according to Jeremić et al., [1]; (in Japanese terminology) waste can be represented by three M's (Fig. 1.):

- Overload (Japanese: Muri 無理) is an unnecessary job of a worker that occurs as a result of poor organization.
- Unevenness (Japanese: Mura 斑) is a loss that occurs due to the uneven production process, uneven load on workers and machinery.
- Loss (Japanese: Muda 無駄) represents all other activities that do not create new value.







Fig. 1. Illustrated representation of three types of losses

In the modern literature, different classifications of waste causes are encountered, in the sense that seven, eight, or even nine different types are listed. Although very similar, these classifications deserve special attention. According to the most widely accepted approach, there are seven types [7] of unnecessary spending [5]:

1. *overproduction*, means overcapacity, which results in a surplus of stocks in each case; it is not initiated at the request of consumers and represents a fundamental loss; 
2. *scrap, malfunctions and errors in administration*, poor product delivery performance or waste generation during processing; 
3. *excessive stocks of materials*, unfinished production or parts, 

which causes high costs of their maintenance;

4. *inadequate processes*, due to the use of wrong instruments, procedures; 
5. *excessive transport* of materials or products, which results in waste of time and high costs; 
6. *waiting*, ie periods of inactivity of the workforce, idling of equipment, waiting for information or materials due to production bottlenecks and 
7. *unnecessary movements* caused by poor organization of the working space. 

This systematization of types of waste causes can be applied in any system, so the possibility of the practical application of small changes to the presented types of waste in logistics processes will be presented below, which together give greater value to the user to create a lossless organization.

4. IMPLEMENTATION PROCESS

LeanSixSigma organization is maximally effective in what it does, consuming the minimum necessary resources while delivering the best possible quality of products or services [2]. For the organization to function in this way, it is necessary to meet all the requirements and principles of the LSS philosophy. Then in such an organization "everyone gets everything", ie [5]:

- employees: - better process and ideas for change ("to hear me and allow me to shape the process in which I work"),
- organization: - improved key indicators (quality, cost, safety, morale) and
- customer (end-user) : - increased satisfaction (better quality, lower costs).

There is no universal recipe for applying the LSS concept to all systems, so there are no two organizations where the same LSS could be implemented, due to their specificity. The possibility of applying the LSS concept can be shown using the MEGA process (Fig. 2). The following principles were applied in the process design:

- the director of the organization must approve the LSS vision of the system. - "LSS thinking": step-by-step approach,

- by applying a process approach and structural analysis of a real system, a process model is obtained, which is a unique basis for design, development, and implementation of this concept,
- process model provides continuous improvement of product quality, which is the main motto of the LSS concept,
- final review after a suitable period,
- “LSS business culture” - an essential condition for the success of the project.

The logistics process design model should be based on the philosophy of cyclic or spiral design models. Continuous verification of the results of improvement ensures the cyclical nature of the procedure. Therefore, the MEGA process diagram (Fig. 2.) does not specify the end of the process, because, in the LSS concept, this is an “endless process”.

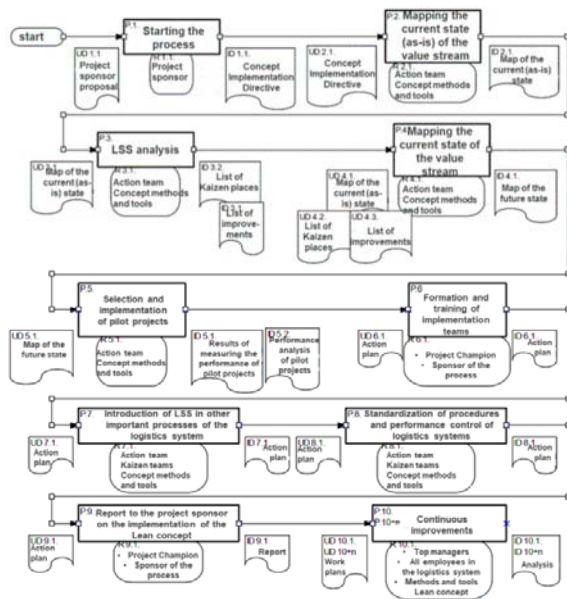


Fig 2. Mega process of LSS concept implementation

When starting the MEGA process and the start itself, the first step is to determine the action team, the necessary work plans, ie directives (P.1.) is made. Mapping the current flow of system values, ie observing the current state of the system, is done by taking a walk through the entire system from the beginning to the end (P.2.). During processes of the walk, information from all levels of the organization is collected and analyzed. The problem with mapping the current state of a value stream is the tendency (of the mapping one) to idealize

procedures. When designing - mapping, it should be borne in mind that designers are also people of habit, so they tend to resist change, which can be characteristic of employees. Therefore, it is necessary to show exactly what is happening, and not allow mapping to present the processes as they should look. It is necessary to show the processes and connections between them. For mapping, it is necessary to be done in the system itself. Mapping the value flow begins from the perspective of the end-user, from the moment he submits a request to perform the service [5]. Creating a value flow map is practically done by asking the right questions. The answers to these real questions copied in the value flow map best show the current state of the system, but they are also the basis for mapping its desired state (P.4.). "Today's problems stem from yesterday's solutions", is the first message of the well-known management expert [12]. Therefore, after creating a flow chart of the current situation, the next step is its LSS analysis (LSS criticism (P.3.)) Because it is one of the main tools of the LSS methodology that will show the current state of the system. Only when we find out where we are at the moment can we think about where we want to go, and only then can we initiate change according to that desired state. If we have not analyzed the current situation well, then our conclusions will be wrong, so we will have wrong goals, and therefore the methods of achieving those goals will be wrong. After the LSS analysis (critique) of the as-is state value flow map, we need to get answers to questions, such as:

- What activities in the logistics process are at the level of LSS quality, which should be improved and which should be eliminated,
- What new activities should be included in the process to achieve the desired quality,
- Whether to change the order of activities or change the way of engaging resources in the process.

LSS analysis of the root cause of the problem indicates activities that cause harmful steps (scattering) during the value and those that do not bring value to the end-user. Because “Every problem represents a new opportunity for improvement,” the problem areas in the LSS methodology are called Kaizen sites. Kaizen places, ie the list of improvements, allow us to

generate possible and then to choose the right (optimal) solution [6]. "Today's solutions are often tomorrow's problem. What are the possible consequences of the proposed solution and why we think that the proposed solutions would enable the achievement of the desired goal, are questions that we must constantly ask ourselves when we create the desired situation", is the second position of the already mentioned Peter Senge, identification of potential improvements and Kaizen places as well as the choice of the right solution to achieve the desired goal [6]. After analyzing the flow chart of the value of the current (as-is) state, the flow of values of the future (desired - ideal) to-be state is created. When mapping the value flow of the future state of the organization's system, it is necessary to constantly look for answers to two questions [5]:

- Why do we think that the proposed solution would enable the achievement of the desired goal?
- What are the possible long-term consequences of the proposed solution?








The idea of an LSS value stream is to create only what is needed when needed. Kaizen places are specially marked on the map of the future situation. When drawing a map of the future state, we should try to divide it into segments or loops, because the implementation process usually cannot be done in one phase. In this way, this map will become a good basis for the development of the implementation plan and the implementation of the process (P.5.). The implementation plan describes the specific ways in which the map of the future situation will be realized. No organization has enough resources to make mistakes. Therefore, the next step, LSS implementation is the selection of improvement processes. In the system, the implementation of a pilot project is a good base to start. With the implementation of the pilot project, the action team and top management continue with the implementation of the implementation plan (P.6.). The implementation plan identifies significant processes, their priorities, and the order of implementation. At this stage of implementation, all that remains is to appoint Kaizen teams (P.7) and to continue the introduction of LSS in other important logistics processes according to the same methodology

and with lessons learned from the implementation of the pilot project at the start of the LSS concept. The implementation process ends with the stabilization of positive results and the incorporation of new standards into the system and all work areas (P.8.). After stabilization, the changes are insured. This is realized by drafting appropriate regulatory documents in the form of rules and instructions. Also, a report is prepared to the project sponsor on the implementation of the LSS concept (P.9.) Which will also serve for further continuous improvements of the logistics system (P.10.).

5. POSSIBILITY OF APPLYING THE CONCEPT TO LOGISTICS PROCESSES

By applying the MEGA project and the stated principles to logistics processes, it is possible to simplify business, create additional capacity, reduce costs and improve the performance of the logistics system. Organizational logistics processes are often hampered by the waste in their systems that affect not only the financial costs but also the performance and overall performance of the organization. Table 2 shows seven types of LSS waste and their equivalents in a large logistics company.

Table 2. Types of waste in the organization

<i>overproduction</i>		It refers to excessive storage that is necessary due to insufficient or poor inventory management.
<i>errors in administration</i>		Double record-keeping or damaged / incorrectly sent administrative material.
<i>excessive stocks of materials</i>		Excessive supplies in the supply chain as a result of poor visibility of the system.
<i>inadequate processes</i>		Work more than necessary. Process overlap.
<i>excessive transport</i>		Lost effort to deliver supplies, parts, or equipment between warehouses or units by priority of use.
<i>waiting</i>		Delivery time or time spent cargo in loading and transport.
<i>unnecessary movements</i>		Any unnecessary maneuver to pick up, pack, or move material in storage.

Based on the table shown, it can be seen that there are many opportunities to improve the speed and performance of logistics processes that can be done in a short time and can offer significant cost savings in terms of staff required amount of inventory stored and reduced overall load. Other improvements may require more investment in information systems to turn existing data pockets into integrated knowledge of logistics processes all to neutralize waste. In the continuation of the work, possible solutions for each type of waste will be presented.

5.1 Administration errors and inadequate processes

The easiest way to dispose of waste is to remove unnecessary tasks or processes in the system. Action teams redirect processes based on their relationship to other required processes, seeking to shorten the overall system requirement. The time associated with the overall system reflects the critical path of the system. For example, the graph (Fig. 3.) shows the sequence of processes that are performed sequentially. Completion of these processes, sending the request, in the current configuration results in a total system time of 32 hours for the request to arrive for execution via electronic communication.

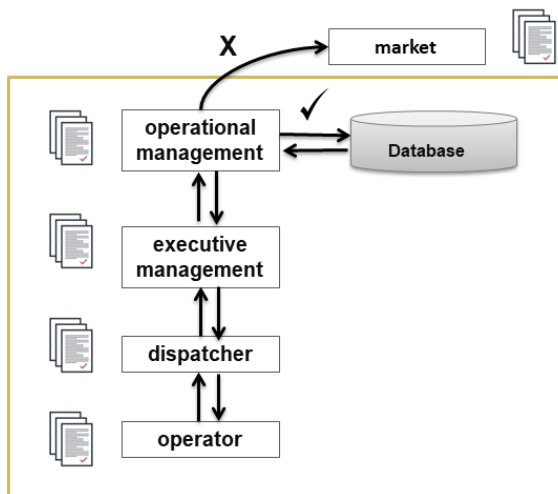


Fig. 3. Graph of processes running consecutively.

Although a system consists of five processes (nodes), changing the relationship between these processes - so that some processes can run simultaneously - would reduce system time. Once the optimal sequence of processes

and relationships is determined, the focus shifts from critical path management to “system crash” (reducing the processing time associated with each activity along the critical path). Breaking a critical path is usually achieved by combining tasks in processes or adding more resources to shorten process cycle times. The same concept can be applied to the design of large supply chains as one of the logistics processes. With supply chains, removing a single node can save millions of dollars in unnecessary infrastructure and additional costs. For many operations, this can result in the release of critically needed space for other purposes, by reducing labor requirements and creating additional system capacity. Unfortunately, the supply chain is much more complex than shown in the chart. Reducing the number of processes, tasks, or communication channels as a whole can have a positive effect on improving the efficiency and quality of the system. For example, if 5 people or “nodes” are involved in the process and each has to call the other for coordination, the result will be a total of 10 communication channels (Fig. 4.). This result was derived using the formula:

$$[n \times (n - 1)] / 2 \tag{1}$$

where n is the number of persons/nodes in the system. If one of the 5 people involved in the process is removed and all the remaining parties are still able to communicate with each other, the number of channels is reduced from 10 to 6. From 5 nodes, using the formula (1) the result is:

$$[5 \times (5 - 1)] / 2 = 10 \text{ channels.}$$

With 4 nodes, the result is:

$$[4 \times (4 - 1)] / 2 = 6 \text{ channels.}$$

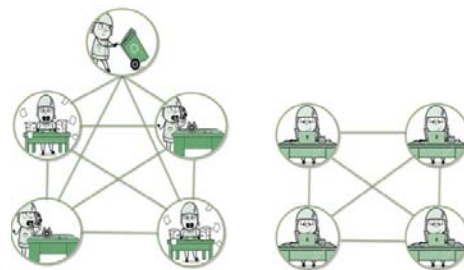


Fig. 4. The number of communication channels in a five- and four-node system.

At each of these physical or virtual nodes, material transit or electronic data exchange takes place (Fig. 5.). Each of these compounds provides an opportunity to make mistakes. Engineers call this the "Rolled Throughput Yield" (RTY).



Fig. 5. The success rate of the system is five and four nodes.

The figure above shows an example of an overall quality output based on four or five process nodes. For example, system 1 has five processes in the system. Despite the relatively high success rate at each node, combining success rates for each process results in a total system yield of only 59%: $(0.9 \times 0.9 \times 0.9 \times 0.9 \times 0.9 = 0.59)$. Reducing only one process node increases the output yield to 66%. More activity means more room for error and a lower production yield. Decreasing a single node can significantly reduce the number of system channels and activities, resulting in a significant increase. For example, for manual systems in which orders are printed, prepared, packaged, documented, and shipped, many steps must be achieved by human effort. Human performance in this case is far from perfect and often results in errors.

5.2 Excessive production, transport, and unnecessary movements

When the principles of LSS management are applied, the value of inventory reduction is obvious. Reducing the amount of storage material means that less capital is tied up in inventories. If less inventory space is needed, a smaller facility is needed and thus less equipment for storage and inventory management. Reducing inventory reduces storage costs, increases inventory turnover, and can reduce overall costs. The MEGA project requires the selection of the required number of facilities for the storage of stocks, by considering the best possible location to reduce transport costs. The implementation of a pilot project for the selection of warehouses can significantly remove waste from

overproduction (storage). Also, the choice of location will greatly contribute to reducing transportation costs. Excessive transport is perhaps the biggest waste that the supply system generally faces there is certainly room for additional improvements related to transport, but they also require improvements in other areas, such as manipulation processes (Fig. 6.).



Fig. 6. Location selection + transport binding + integral transport = LSS

The system of palletizing and integral transport greatly affects the speed of loading and as such is indispensable in the transformation process. The palletizing system proportionally affects the process of reducing excessive transport.

5.3 Excessive stocks of materials and waiting

Reducing the time required to incorporate knowledge of requirements shortens the time required to integrate this information into inventory recovery forecasts. Reliable inventory location information in the supply chain also allows supply managers to accurately determine the status and availability of incoming refill items. This knowledge can reduce the number of safety supplies required. These improvements can reduce total inventory, reduce storage space needs, result in higher inventory turnover ratios, and lead to significant cost savings. Because inventory typically comes from different suppliers, through different transportation hubs, and in many configurations, organizations must look beyond the walls of individual warehouses and validate operations in their respective supply chains. Of course, maintaining inventory

accuracy is a basic prerequisite for improving inventory management. Therefore, efforts to ensure accurate current balances should precede improvement initiatives to achieve better visibility in transit or accelerate the speed at which inventory flows. One of the solutions may be the availability of information at the very beginning, i.e. an information solution that will provide access to the database at the beginning of the process (Fig. 7). This would save time for feedback and reduce waiting.

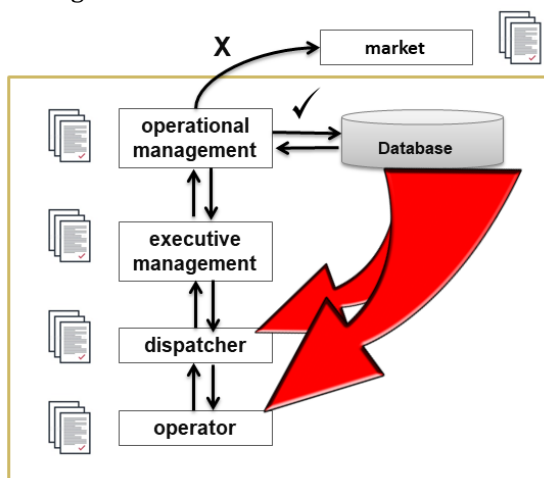


Fig. 7. Possibility to skip excess processes and nodes

Time savings can also be gained by resolving internal issues in the warehouse, such as moving objects through a given warehouse. For example, stockpiling, consolidation, packaging, and preparation for shipment can take days. Internal storage improvements that increase the speed at one node can add time to another. Take together the selection and packaging of all similar items. This can increase the speed at which these items travel through the warehouse. However, items may need to be separated at another location and moved to another means of transport before heading to their final destination. The initial modification of the packaging of all similar items only transfers the separation load to another place in the system and can slow down the whole process. So, the basic challenge is to create an integrated system for bringing items from the place of origin to the place of consumption with the least time. As already mentioned in the paper, the LSS concept is an "endless process" and the paper presents only some of the solutions that can be further upgraded.

6. CONCLUSION

Defects or losses are common features of organizational systems. They are the ones that cause waste, additional work of employees, an increase in costs, etc. The answers to these problems can be found in the Lean Six Sigma concept, which is a synthesis and upgrade of management in the most important elements of the organizational system. It is concluded that if organizations can harmonize their activities with the principles of the LSS concept, then they can also strive for the gradual achievement of business excellence. The concept enables progress in the development of the logistics process, which represents superiority for the side that manages to recognize and use it, while the one that does not does so leads to inferiority. If an organization strives for the highest standards and wants a partnership with other world organizations, its logistics system must be modernized, among other things, so that it is interoperable with the logistics system of other organizations. All these improvements can be done as we see it if we start immediately or wait for the moment when the solutions will be imposed and when the whole system will have to adapt to the imposed solutions. This paper, among other things, had the task of pointing out that fact as well. Applying the LSS concept is not easy. Decision-makers should be aware that without this concept, there is no, not only the much-desired cooperation, but also a common future, which we certainly strive for, both in the environment and beyond. The LSS concept provides a solid basis for escaping inferiority to which, despite the lack of money and the current COVID-19 pandemic, we do not have to be condemned. Possible improvements related to administration and unnecessary processes are presented, show that the omission of unnecessary nodes can contribute to reducing the stress of the logistics staff and faster response to requests. The presented analysis shows that omitting only one node in the request process increases the possibility of the successful execution of the request by 7%. It is also concluded that with a smaller number of nodes, the possibility of error decreases exponentially, which automatically fulfills the condition of the LSS concept in reducing errors. In the analysis and proposal to improve the losses of overproduction, transport, and unnecessary movement, it can be concluded

that it is necessary to revise the existing storage infrastructure by location and thus reduce the number of people needed for warehousing operations, reduce transport distances and minimize and limit manipulation within the warehouse as well as speed up the delivery process by palletizing the funds. During the analysis of the last two losses of excessive stocks of materials and waiting, a conclusion is drawn regarding the availability of information to the end-user, ie the transparency of stocks in the entire system. To implement the LSS concept, problems arise in inexperience in the application of scientific methods and in determining specific goals, which is why the help of consultants is necessary. This seems to be the only approach for companies if they want the current crisis to be overcome as quickly and with less pain. The dynamics of events do not allow silence but encourage that in the field of quality, it must be constantly re-created, upgraded, and improved. The scientific contribution of this project lies in a new theoretical approach, defining the place, role, and significance of the LSS concept in logistics processes, where the possible way of applying the concept in the form of reducing costs and improving the logistics culture among the logistics staff is presented in one place. Besides, the professional contribution of the project is reflected in the practical fields of application of the LSS concept implementation process, with increased effectiveness and loss reduction, and a special contribution would be reflected in situations where information availability and accuracy of information is invaluable for decision making. As a final effect of the work, the contribution of the implementation of the LSS concept can be singled out by the emergence of a new style and culture of living among employees among the logistics processes.

Acknowledgment

This research was financially supported by the Ministry of Education, Science, and Technological Development of the Republic of Serbia.

REFERENCES

- [1] Jeremic, B., Todorovic, P., Macuzic, I., Djapan, M., Milosevic, M., Radenkovic, M. & Vuckovic, Dj. (2013). *Basics of Lean production - Lean production*. Faculty of Engineering, Kragujevac.
- [2] Kostic, M. (2009). Lean Six Sigma on sale. *Profit Magazine* no.19, Novi Sad.
- [3] Macuzic, I., Djapan, M., (2016). *The lean concept in production management*. Faculty of Engineering, Kragujevac.
- [4] Mowen, M. M., Hansen, R. D. (2011). *Introduction to Cost Accounting*. Mason, South-Western Cengage Learning, OH, USA.
- [5] Pesic, P., Marinkovic, Z. (2011). Implementation of the Lean concept in the logistics organization system of the military organization, *Transport, and logistics*, no. 4, 27 May 2011, Faculty of Mechanical Engineering, Nis, p. 95-102.
- [6] Pesic, P. (2015). Kaizen concept and its application in logistics, *Military Technical Courier*, vol.63, no.2, p. 161-178, DOI: 10.5937/vojtehg63-6068.
- [7] Shingo, S., Dillon, A. (1989). *A Study of the Toyota Production System: From an Industrial Engineering Viewpoint (Produce What Is Needed, When It's Needed)*. CRC Press, USA.
- [8] Liker, J. K. (2004). *The Toyota Way: 14 Management Principles from the World's Greatest Manufacturer*. McGraw-Hill, New York.
- [9] Kubiak, T.M. and Benbow, D. (2016). *The Certified Six Sigma Black Belt Handbook*. ASQ Quality Press, USA.
- [10] The Council for Six Sigma Certification, (2018). *Six Sigma Reference Manual*. Harmony Living, Buffalo.
- [11] Damnjanovic, R., Tomasevic, M., Mihajlovic, M. (2016). Possibilities of using the lean six sigma methodology in program budgeting of the defense system, *Vojno Delo*, no.5, p. 306-313, DOI: 10.5937/vojdela1605306D.
- [12] Senge, M. P., Dyer, K., (2004). Face to face: Living and learning: A conversation with Peter M. Senge, *Wiley Periodicals, Inc.*, vol. 24, no.3, <https://doi.org/10.1002/lia.1072>.



Banja Luka
28-29 May 2021.

DEMI 2021

15th International Conference on Accomplishments in Mechanical and Industrial Engineering

www.demi.mf.unibl.org



AN OVERVIEW OF NON-EXHAUST BRAKE EMISSION MEASURING METHODS

S. Vasiljević^a, J. Glišović^b, N. Stojanović^c, I. Grujić^c

^a M.Sc., Teaching assistant, Academy of Professional Studies Šumadija, Department in Kragujevac, Kosovska 8, 34000, Kragujevac, Serbia

^b Ph.D., Assoc. prof., University of Kragujevac, Faculty of Engineering, Sestre Janjic 6, 34000 Kragujevac, Serbia

^c M.Sc., Teaching assistant, University of Kragujevac, Faculty of Engineering, Sestre Janjic 6, 34000 Kragujevac, Serbia

Abstract Non-exhaust emission is the type of particle emission that is not caused by a combustion process, but by the wear of different parts of a vehicle's systems. One of the sources of non-exhaust particulate emission is the braking system where the wear of friction pairs is present. There is growing number of studies that analyse brake wear with reference to the size and concentration of non-exhaust emissions, especially PM₁₀ and PM_{2.5} particles. An overview of various measuring techniques and devices for measuring the concentration of the formed particles by brake wear was performed in this paper. Pin-on-disc tribometers and brake inertial dynamometers are most commonly used for such tests. It is important to mention that for testing the emission of particles caused by brake wear, it is necessary to make certain modifications and design additional housings that retain the emission product. The authors have used different methods for measuring or collecting particles, which is also shown in the paper. In addition to laboratory testing methods, some authors used real vehicles whose brakes were also inserted into the housing, which prevents the entry of particles from the environment. The paper also presents a newly proposed inertia dynamometer for measuring non-exhaust particles who is development on the Faculty of Engineering.

Keywords Brake, emission, dynamometer, measurement, non-exhaust.

1. INTRODUCTION

The problem of particles caused by brake wear is one of the current problems today after solving the problem of particle formation by combustion of fuel in the engine [1]. Modern technology of electric vehicles today does not

emit particles by combustion in the engine, but one of the particles' source is certainly the braking system. The braking system belongs to the so-called non-exhaust group of particle sources, bearing in mind the fact that these particles are not emitted by combustion of fuel or some other substance, but purely by wear of friction pairs of brakes. Particle emission is very harmful because these particles contain various materials that are harmful to human health and the environment [2, 3]. Particles can be classified according to their size. So the most commonly measured particles that are formed by brake wear are PM₁₀ and PM_{2.5}, but the concentration of formed PM₁ particles is also

Corresponding author

M.Sc., Saša Vasiljević
vasiljevic.sasa036@gmail.com

Teaching assistant
Academy of Professional Studies Šumadija, Department in
Kragujevac, Kosovska 8,
34000, Kragujevac, Serbia

increasingly measured. The reason is that the harmfulness of particles is higher if their diameter is smaller, i.e. PM_1 particles are more harmful than particles of larger diameters, such as PM_{10} and $PM_{2.5}$ particles [4, 5].

Today, when this is a current problem, as well as air pollution and therefore, more and more authors are researching this area. In their research, the authors use several methodologies, but also different devices that have been modified in order to be able to measure the particles formed by the wear of a friction pair of brake pad and brake disc.

The aim of this paper is the analysis and presentation of measuring devices used by different authors with the aim of measuring the concentration of particles generated by brake wear. An installation for measuring particles, which is in the development phase at the Faculty of Engineering, University of Kragujevac, is also presented in the paper.

2. THE MOST COMMONLY APPLIED METHODS AND THEIR FEATURES

Numerous authors who have examined brake wear have applied different test methods. The most commonly used methods or better said devices are pin-on-disc tribometers, inertial brake dynamometers and road testing. Devices or methodologies used to test the particle concentration are shown in Figure 1. It is important to note the fact that tribometers and inertial dynamometers belong to laboratory test methods, while road tests are performed on the road and on a real vehicle. However, some authors investigating the concentration of the formed particles use real vehicles with the aim of testing the formation of particles by brake wear in laboratory conditions.

It is important to note that each of the applied methods has specifics, i.e. test conditions differ in each case. When a pin-on-disc tribometer is applied for testing brake wear and particle formation, it is not possible to apply a pad on the tribometer that would have the same dimensions as on a real vehicle, while the disc could certainly be made of brake disc material. However, such devices may have different combinations of test conditions in terms of different pin and disc contact speeds and pressures.

Compared to the pin-on-disc tribometer, inertial brake dynamometers represent a much more

realistic type of testing the formation of particles by brake wear. Such devices also belong to the laboratory type of devices with the use of brake pads and disc brakes that are actually applied to the vehicle. Brake dynamometers can very well simulate real vehicle braking and can even simulate different braking conditions (temperature, speed, pressure, air flow, etc.).

Road tests are the most realistic type of test; however the test itself is very complex. This type of testing, when it comes to particles caused by brake wear, is especially complex because there are other sources of particles on the road, so it is necessary to separate the particles generated by the braking system. This problem is much easier to solve in the case of tribometers and a brake dynamometer.

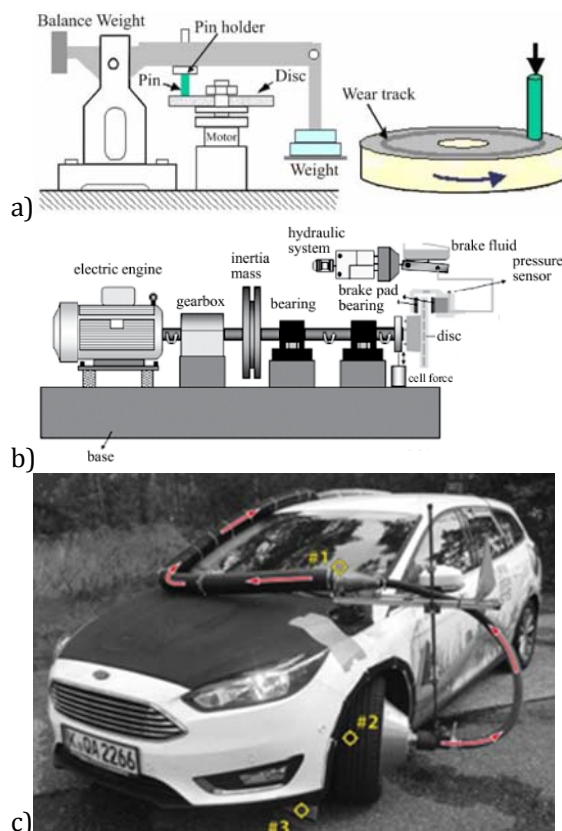


Fig. 1. Different methods for testing the concentration of particles formed by braking, a) pin-on-disc tribometer, b) inertia brake dynamometer, c) road measurement [5-8]

Having in mind the problem of the presence of particles that do not occur due to brake wear, during the test it is necessary to enable the measurement of only the particles formed by

the brakes. This is solved by isolating the brake itself in a closed housing from which the particle measuring device draws air with brake wear particles. In this way, the particle measuring device retracts and measures only the particles formed during the braking process, while the other particles remain outside the housing and the device does not retract those particles. The appearance of the housing itself is different depending on the experimental installation used for measurement. Of course, as it is necessary for air to enter the housing, at the very beginning where the air enters from the outside, there is an element for purifying the air from particles, mainly an HEPA (High Efficiency Particulate Air) filter.

When it comes to the characteristics of the device used, it mostly depends on the author himself, i.e. what is the topic of his research and what are the possibilities of the installation itself. Thus, most measuring installations can measure the rotation speed of the disc, the contact pressure between elements of the friction pair, individual temperature of the brake disc and the brake pads, the temperature in contact surface, pressure in the measuring installation, deceleration of the disc, different loads, etc. Furthermore, other devices can be connected to the measuring installation, such as the humidity control device inside the housing in which the disc brake is located, but again depending on what is being tested and what conditions the researcher wants to achieve during the test.

The most important device during such tests when particles are the subject of research is certainly the device for measuring the concentration of particles. Mostly different authors use different devices, although all devices have in common that they are intended for analysis and measurement of particle concentration. Different authors also use different measurement methodologies, i.e. different modes of particle measurement. Thus, some authors use measuring devices, i.e. modes for measuring the number of formed particles classified according to their sizes or particle concentration $\mu\text{g}/\text{m}^3$. Some research also uses multiple devices to measure particles in multiple modes.

Some of the solutions used in measuring and testing brake wear, as well as various solutions used by other authors are presented later in this paper.

3. APPLICATION OF TRIBOMETER IN MEASUREMENT OF PARTICLES FORMED DURING BRAKING

Numerous authors use various constructive solutions of tribometers to test the wear rate, especially of new materials in brake pads and their behavior in terms of the stability of the coefficient of friction.

Wahlström et al. applied a tribometer solution shown in Figure 2 to test brake wear and particle formation. In this case, in order to collect only the particles that are formed by the wear of the pin and the disc, the tribometer is located inside the housing (marked with a black bold line) and thus prevents the measurement of non-wear particles. In order to inject air from the outside into the housing, i.e. outside the housing, an HEPA filter of class H13 EN 1822 is placed at the inlet, as well as the compressor before the filter itself, while the air flow was measured using the TSI® air velocity transducer model 8455. Three devices were used for particle measurement and analysis, namely Dekati® Electrical Low Pressure Impactor (ELPI +), TSI® Optical Particle Sizer (OPS) model 3330 and TSI® Condensation Particle Counter (CPC) model 3772.

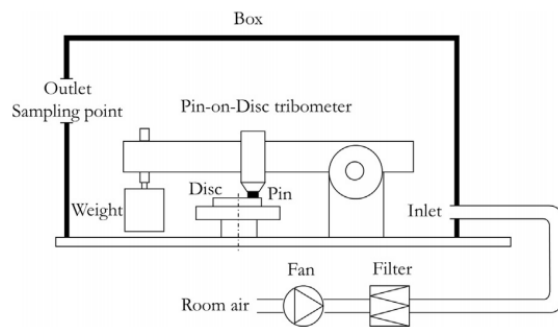


Fig. 2. Example of a solution for a device for testing the formation of particles using a pin-on-disc tribometer [9]

A similar solution of the measurement installation as before, in order to use a pin-on-disc for measuring particles caused by brake wear, was used in the study by Dizdar et al. [10]. Also, three particle analysis devices were used here: optical particle sizer (TSI® Optical Particle Sizer (OPS) model 3330), condensation particle counter (CPC) and electrical low-pressure impactor (ELPI).

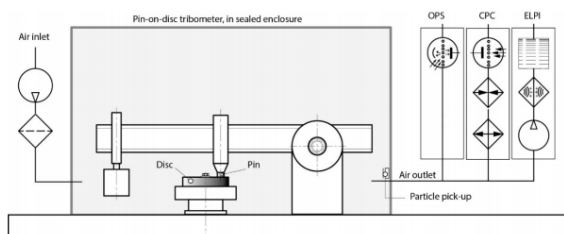


Fig. 3. Example of a solution for testing the particle formation using a pin-on-disc tribometer [10]

Mirzababaei and Filip [11] examined the effect of humidity on brake wear. Figure 4 shows the appearance of such an experimental installation. An ultrasonic Cool Mist Humidifier was used to control the humidity inside the housing.



Fig. 4. Example of a solution for testing brake wear and the influence of humidity on wear [11]

In [12], Djafri et al. presented an example of a tribometer for testing the influence of humidity on brake wear and particle formation. Figure 5 shows the installation where the housing in which the disc and pin are closed is marked with 3. Humidity and temperature are controlled in the housing itself. Meaning of the labels in Figure 5: (1) measurement unit with a display data panel, (2) adjustment unit of test conditions (humidity and ambient temperature), (3) essay chamber, (4) disc-pin couple, (5) display screen [4].

Tribometer used to test brake wear by Cuev [13] is shown in Figure 6. An interesting aspect

in this installation is the way of measuring the temperature inside the brake pads, or specifically inside the pin. In this case, the thermocouple sensor is placed inside the pin, so the temperature inside the pin is measured.

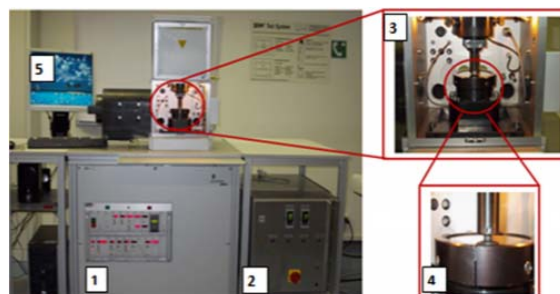


Fig. 5. Example of solution for testing particle formation using pin-on-disc tribometer under humidity and temperature control conditions [12]

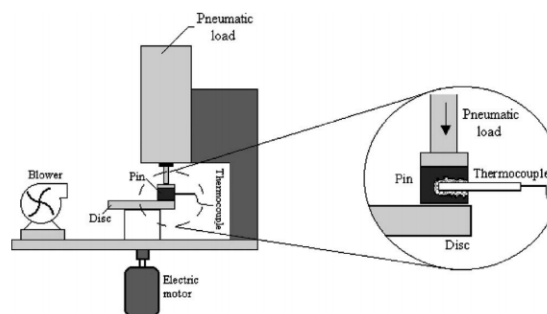


Fig. 6. Example of a solution for testing brake wear and the effect of humidity on wear [13]

4. LABORATORY TESTS OF REAL VEHICLE BRAKES

Bearing in mind the fact that Chapter 2 mentions tests performed using real brakes that are normally installed on vehicles and in the form of an inertial brake dynamometer and real vehicles only in laboratory conditions, this chapter presents such solutions that were used in testing.

4.1 Measurement of particle formation using an inertial brake dynamometer

A schematic representation of the inertial brake dynamometer in the examination of the formed particles, which is shown in [14], is specifically given in Figure 7. In this case, too, it is noticeable that the brake is located inside the housing from which the particles are collected and measured.

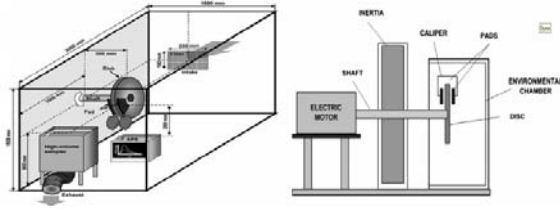


Fig. 7. Schematic representation of the dynamometer and brake housing [14]

In their study, Niemann et al. [15] applied the measuring installation shown in Figure 8. In this study, too, the disc brake is located inside the housing, and the air entering the housing from the environment is purified using a HEPA filter. This measuring installation was developed by the Institute of Environmental and Energy Technology (IUTA e.V.). For particle measuring and their analysis, an Optical Particle Sizer (TSI OPS 3330), a Fast Mobility Particle Sizer (TSI FMPS 3091), and a Condensation Particle Counter (TSI CPC 3776) were used.

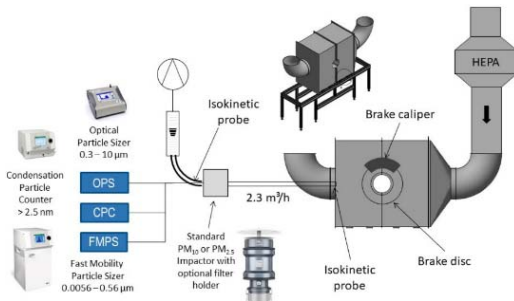


Fig. 8. Measuring installation applied in research [15]

Hagino et al. applied the installation shown in Figure 9 to investigate the concentration of the formed particles. The experimental installation is designed so that it is possible to monitor and record multiple parameters that can be analyzed and compare their impact on the formation of particles during braking.

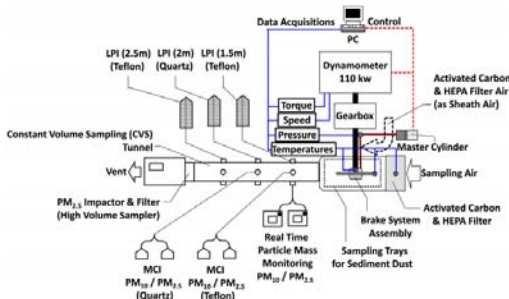


Fig. 9. Applied measuring installation in research of formed particles during braking [16]

In their study of particle formation by brake wear in the braking process, Matějka et al. applied the measuring installation shown in Figure 10. In this case, an electric low-pressure impactor ELPI+ (Decati) was used to measure the particles.

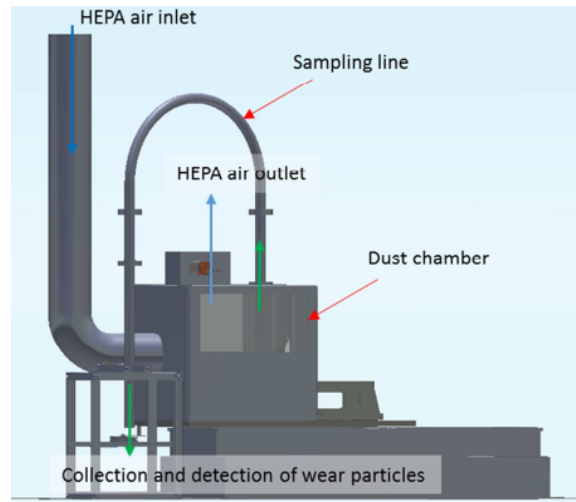


Fig. 10. Applied measuring installation for measuring particles formed during braking [17]

Figure 11 shows the measuring installation used in the research [18]. It can be seen from the figure that, in this case, clean-air flows through the brake disc which further pushes the particles towards the devices for measuring and analyzing the formed particles.

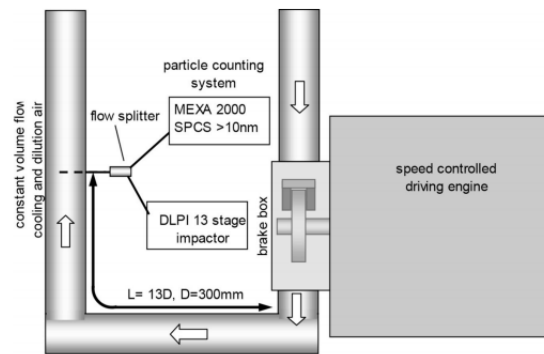


Fig. 11. Applied measuring installation for measuring particles formed during braking [18]

According to [19], the installation shown in Figure 12 can be used to measure the formed particles.

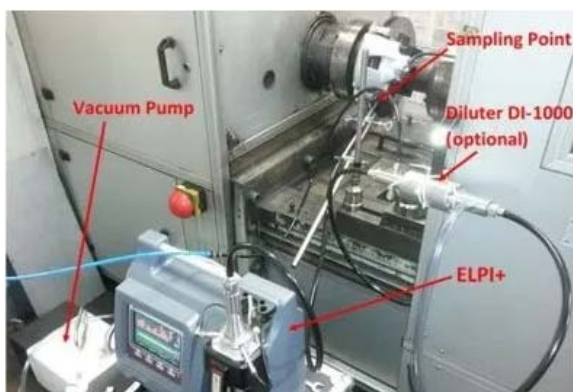


Fig. 12. Applied measuring installation for collecting the particles formed during braking [19]

One of the professional installations for brake particle emissions developed by LINK Engineering is shown in Figure 13. Such installations have a wide range of test possibilities. Such installations can simulate driving cycles, and also control conditions such as air temperature, humidity, brake cooling, and many more. Interesting in this case is the housing in which the brake is located and it is also shown in the figure.

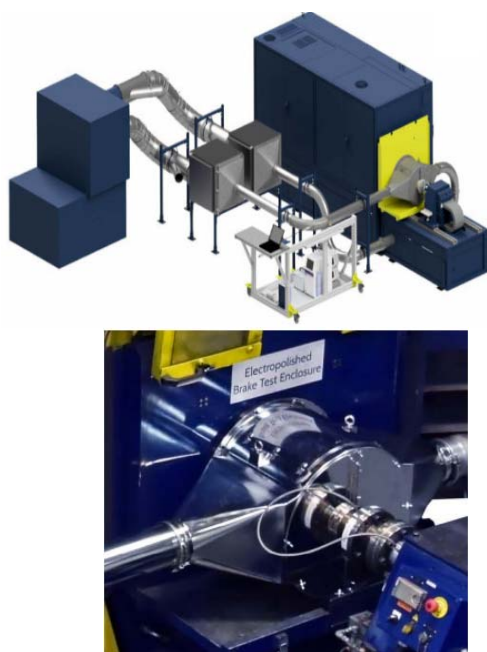


Fig. 13. Applied measuring installation for measuring particulate matter during braking [20]

Reference [13] shows a measuring installation that was also developed for measuring the concentration of particles generated by braking, but also for the analysis of particles. Figure 14

shows the disc brakes inside the housing as well as the construction of the housing, but also the construction of the air inlet and outlet to the housing.

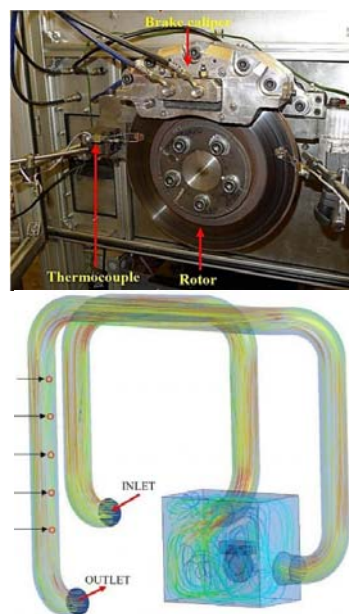


Fig. 14. Particle collection installation [21]

One of the methods for collecting particles according to [22] is shown in Figure 15. In this case, the particles created by wear are directly collected and withdrawn.



Fig. 15. Particle collection method [22]

A view of the housing in which the disc brake is located is shown in Figure 16. It can be seen in the figure that this housing is closed, as mentioned so far. This figure shows the way air escapes from the housing to the particle measuring devices.

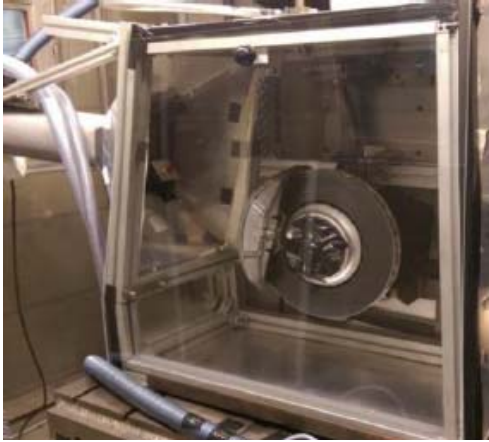


Fig. 16. Particle collection method [23]

Figure 17 shows another solution of the particle feeder. In this case, as can be seen, there is a profile that is connected to the device for measuring the concentration of particles, so with the help of this part, the formed particles are retracted and measured.



Fig. 17. Particle retraction method formed by brake wear [24]

4.2 Measurement of generated particles using real vehicles in laboratory conditions

Although research on real vehicles in laboratory conditions is very rare, at least from the aspect of particles generated during braking, Perrenoud et al. in a study [25] performed just such research. Six different vehicles were used in this research, but in laboratory conditions. An illustration of one vehicle on which the measurement of particle formation was performed is shown in Figure 18. In this case, it is noticeable that the housing is placed on the brake, i.e. on the vehicle in the part where the brake is located. Thus, only the measurement of particles created by brake wear is possible and

there is no entry of particles from the environment. According to [25], the labels in Figure 18 represent: A-exposure box; B - HEPA filter and pump system; C - water cooling pump; D - pumps for collection on filters; E - DMA-CPC particle sizer and counter. Wide Range Aerosol Sampler (Grimm Aerosol Technik GmbH & Co) and condensation particle counter (DMA-CPC, Vienna U-Type, model 5.400) were used for analysis and measurement of particles.

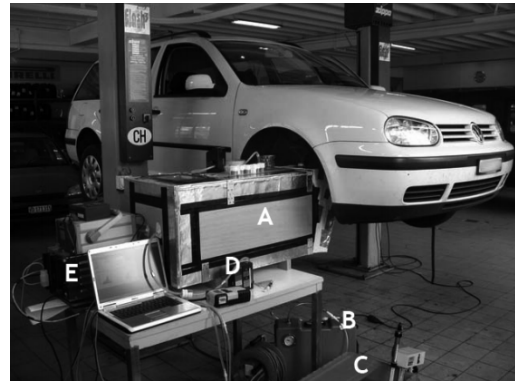


Fig. 18. Investigation of particle formation on a real vehicle in laboratory conditions [25]

A similar measurement installation was presented by Riediker et al. in his research [26]; however, he also gave an overview of some parts of the installation and the installation solutions shown in Figure 19. It is noticeable that an installation is shown in the housing that allows the retraction of particles, while the device for measuring concentration is outside the housing, but there are also sensors for measuring humidity of the air and body which enable the maintenance of a stable temperature.

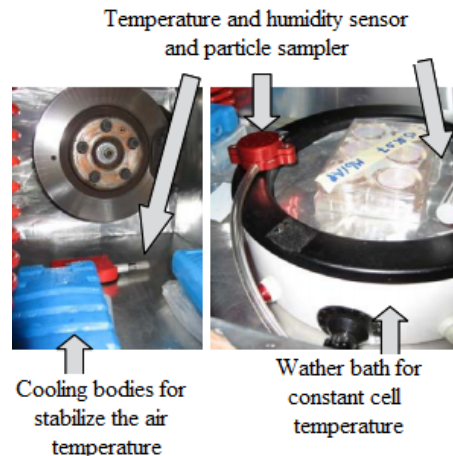


Fig. 19. Investigation of particle formation on a real vehicle in laboratory conditions [26]

5. MEASURING INSTALLATION PROJECT FOR BRAKE WEAR MEASUREMENT AT THE FACULTY OF ENGINEERING

The measuring installation at the Faculty of Engineering, University of Kragujevac will be based on the inertial brake dynamometer shown in Figure 20.

The installation is based on the fact that it is possible to change the loads during braking, which simulates different wheel loads. Thus, it is possible to simulate different types of vehicles and their axle loads, and to achieve different speeds, so different loads of one wheel of the vehicle and wheel's rotation speed can be combined as when the vehicle is on the road. At any time, it is possible to monitor the speed of rotation of the disc on the computer, i.e. the simulated speed of the vehicle. Braking with different pressures has been achieved so that it is possible to adjust the braking force. So the pressure in the brake system can be monitored on the computer too, and it is also possible to control the pressure. The installation is also equipped with sensors for measuring the temperature of the brake pads in different zones of contact.



Fig. 20. Inertial brake dynamometer at the Faculty of Engineering [27]

In order to measure the particles formed during braking, the dynamometer was upgraded with a housing in which the brake is located. The purpose of the housing is to collect the particles that were created by the wear of the brakes and to place a device for measuring the concentration of particles. It is certainly necessary for air to enter the housing from the environment in order not to create a vacuum when extracting air with the help of a device that measures the concentration of the formed particles. In order to prevent particles from entering from the environment and to avoid leading to erroneous measurement results, there is an HEPA filter at the inlet that purifies the air entering the housing.

The device used for measuring particles, i.e. particle concentration is TROTEC PC-220, which is shown in Figure 21. The device can measure the number of particles $PM_{0.3}$, $PM_{0.5}$, PM_1 , $PM_{2.5}$, PM_5 and PM_{10} . Bearing in mind that the device can measure particles in multiple modes, one possibility is to measure the mass of particles in $\mu\text{g}/\text{m}^3$; however such measurement is only possible for particles $PM_{2.5}$ and PM_{10} . The device enables the transfer of data from its internal memory to a computer, so it is possible to analyze data numerically or graphically using diagrams [28].



Fig. 21. Trotec PC-220

The entire projected installation is shown in Figure 22. The dashed line in the figure represents the housing from which the particles are extracted, and the concentration is measured using a Trotec PC-220. The red arrows represent the data that the researcher sets as the initial conditions, i.e. braking conditions, single wheel loads, speed and brake

pressure. The green line represents the data that is collected and controlled at the same time as the conditions that are set as the initial.

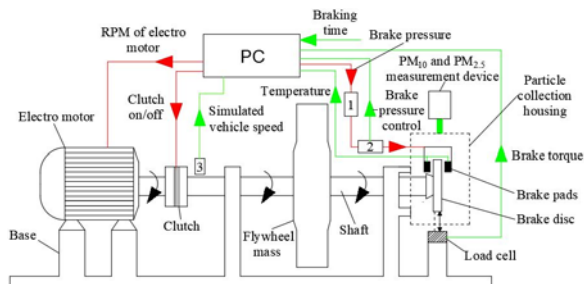


Fig. 22. Schematic representation of the proposed measuring installation for measuring particles generated by brake wear

6. CONCLUSION

Measurement installations for monitoring the concentration of particles differ from author to author, but the test method itself also differs. Measurement devices generally differ in their performance depending on what the author's aim of the research. Tribometers are most often used, but in a large number of studies, inertial brake dynamometers are also used. Certainly, different sensors are used on each installation, which can measure different parameters, but the most important devices are those for measuring and analyzing particles. These are the key devices in any installation.

The measured installation at the Faculty of Engineering, University of Kragujevac is a type of laboratory testing using an inertial brake dynamometer. The installation developed at the Faculty is a very complex installation that allows a number of different tests of vehicle brakes, but also has the possibility of different modes of operation and changing various parameters.

Acknowledgement

This paper was realized within the framework of the project "The research of vehicle safety as part of a cybernetic system: Driver-Vehicle-Environment", ref. no. TR35041 funded by the Ministry of Education, Science and Technological Development of the Republic of Serbia.

REFERENCES

- [1] OECD (2020), Non-exhaust Particulate Emissions from Road Transport: An Ignored Environmental Policy Challenge, OECD Publishing, Paris, <https://doi.org/10.1787/4a4dc6ca-en>.
- [2] Gasser, M., Riediker, M., Mueller, L., Perrenoud, A., Blank, F., Gehr, P., Rothen-Rutishauser, B. (2009). Toxic effects of brake wear particles on epithelial lung cells in vitro. *Particle and Fibre Toxicology*, vol. 6, no. 30. DOI:10.1186/1743-8977-6-30
- [3] Kelly, F. J., Fussell, J. C. (2012). Size, source and chemical composition as determinants of toxicity attributable to ambient particulate matter. *Atmospheric Environment*, no. 60, p. 504–526. doi:10.1016/j.atmosenv.2012.06.039
- [4] Topias, P., T. Uuppo, M., Niemi, S. (2013). Health effects of exhaust particles. Paper presented at the In Proceedings of the University of Vaasa, Reports Vaasa, Finland.
- [5] Particulate Matter and Outdoor Air Pollution-From: <https://www.healthlinkbc.ca/healthlinkbc-files/outdoor-air-pollution#:~:text=Generally%2C%20smaller%20particles%20are%20thought,respiratory%20tract%2C%20including%20the%20lungs.&text=The%20coarse%20particles%20tend%20to,as%20the%20nose%20and%20throat>, accessed on: February 17, 2021.
- [6] Li CX, Wear Testing and Wear Measurement, http://193.6.1.183/projektek/adveng/home/kurz/korsz_anyagtech/1_konzultacio_elemei/wear_testing_measurement.htm, accessed on: February, 09, 2021.
- [7] Triches Jr, M., Gerges, S. N. Y., & Jordan, R. (2004). Reduction of squeal noise from disc brake systems using constrained layer damping. *Journal of the Brazilian Society of Mechanical Sciences and Engineering*, vol. 26, no. 3. doi:10.1590/s1678-58782004000300011
- [8] Farwick zum Hagen, F. H., Mathissen, M., Grabiec, T., Hennicke, T., Rettig, M., Grochowicz, J., ... Benter, T. (2019). On-road vehicle measurements of brake wear particle emissions. *Atmospheric Environment*, 116943. doi:10.1016/j.atmosenv.2019.116943
- [9] Wahlström, J., Lyu, Y., Matjeka, V., & Söderberg, A. (2017). A pin-on-disc tribometer study of disc brake contact pairs with respect to wear and airborne particle emissions. *Wear*, no. 384-385, p. 124–130. doi:10.1016/j.wear.2017.05.011

- [10] Dizdar, S., Lyu, Y., Lampa, C., Olofsson, U. (2020). Grey Cast Iron Brake Discs Laser Cladded with Nickel-Tungsten Carbide—Friction, Wear and Airborne Wear Particle Emission. *Atmosphere*, vol. 11, no. 6, p. 621. doi:10.3390/atmos11060621
- [11] Mirzababaei, S., Filip, P. (2017). Impact of humidity on wear of automotive friction materials. *Wear*, no. 376-377, p. 717–726. doi:10.1016/j.wear.2017.02.020
- [12] Djafri, M., Bouchetara, M., Busch, C., Weber, S. (2014). Effects of humidity and corrosion on the tribological behaviour of the brake disc materials. *Wear*, no. 321, p. 8–15. doi:10.1016/j.wear.2014.09.006
- [13] Cueva, G., Sinatora, A., Guesser, W. L., Tschiptschin, A. P. (2003). Wear resistance of cast irons used in brake disc rotors. *Wear*, vol. 255 no.7-12, p. 1256–1260. doi:10.1016/s0043-1648(03)00146-7
- [14] Grigoratos, T., Martini, G. (2014). Brake wear particle emissions: a review. *Environmental Science and Pollution Research*, vol. 22, no. 4, p. 2491–2504. doi:10.1007/s11356-014-3696-8
- [15] Niemann H, Winner H, Asbach C, Kaminski H, Frentz G, Milczarek R. (2020). Influence of Disc Temperature on Ultrafine, Fine, and Coarse Particle Emissions of Passenger Car Disc Brakes with Organic and Inorganic Pad Binder Materials. *Atmosphere*, vol. 11, no. 10 p. 1060. <https://doi.org/10.3390/atmos11101060>
- [16] Hagino, H., Oyama, M., Sasaki, S. (2016). Laboratory testing of airborne brake wear particle emissions using a dynamometer system under urban city driving cycles. *Atmospheric Environment*, no. 131, p. 269–278. doi:10.1016/j.atmosenv.2016.02.014
- [17] Matějka, V., Metinöz, I., Wahlström, J., Alemani, M., Perricone, G. (2017). On the running-in of brake pads and discs for dyno bench tests. *Tribology International*, no. 115, p. 424–431. doi:10.1016/j.triboint.2017.06.008
- [18] Liati, A., Schreiber, D., Lugovyy, D., Gramstat, S., Eggenschwiler, P. D. (2019). Airborne particulate matter emissions from vehicle brakes in micro- and nano-scales: Morphology and chemistry by electron microscopy. *Atmospheric Environment*. doi:10.1016/j.atmosenv.2019.05.037
- [19] Particles Measurement of Brake Emissions. From: <https://envilyse.de/particles-measurement-of-brake-emissions/?lang=en>, accessed on: March 01, 2021.
- [20] Link engineering. Model 6330 Brake Emissions Testing. From: <https://www.linkeng.com/product/model-6330-brake-emissions-testing/>, accessed on: March 01, 2021.
- [21] University of Leeds Enters the Arena of Brake Dust Collection and Analysis. From: <https://thebrakereport.com/university-of-leeds-enters-the-arena-of-brake-dust-collection-and-analysis/>, accessed on: March 02, 2021.
- [22] Hosier, C. UN PMP Activities – Non-exhaust particles. From: https://a.storyblok.com/f/77802/x/24501b0bb8/cpm_hosier_2018_activities-of-the-un-pmp-particle-measurement-procedure-group-exhaust-and-non-exhaust-particle-emissions.pdf, accessed on: March 01, 2021.
- [23] Horiba, Brake dust measurements-selection of the most suitable sampling method, <https://wiki.unece.org/download/attachments/42041609/PMP-43-13%20Brake%20dust%20measurement%20Horiba%20full.pdf?api=v2>, accessed on: March 04, 2021.
- [24] Glišović, J., Pešić, R., Lukić, J., Miloradović, D. (2016). Airborne wear particles from automotive brake systems: environmental and health issues, 1. International Conference on Quality of Life, Kragujevac, 2016, 09-10 Jun, p. 289-296.
- [25] Perrenoud, A., Gasser, M., Rutishauser, B. R., Gehr, P., Riediker, M. (2010). Characterisation of nanoparticles resulting from different braking behaviours. *International Journal of Biomedical Nanoscience and Nanotechnology*, vol. 1, no. 1, p. 17-33. doi:10.1504/ijbnn.2010.034123
- [26] Riediker, M., Gasser, M., Perrenoud A., Gehr, P., Rothen- Rutishauser, B. (2008). A system to test the toxicity of brake wear particles. *12th International ETH-Conference on Combustion Generated Nanoparticles*, Zurich, Switzerland.
- [27] Stojanović, N., Grujić, I., Glišović, J., Taranović, D., Lukić, J. (2020) The development of the inertial dynamometer for disc brakes testing, *Tractors and power machines*, vol.25, no.3/4, p. 27-38.
- [28] Trotec, Operating manual particle counter PC 220, TRT-BA-PC220-TC-005-EN.



Banja Luka
28–29 May 2021.

DEMI 2021

15th International Conference on
Accomplishments in Mechanical and
Industrial Engineering

www.demi.mf.unibl.org



Application of hybrid composites based on ZA27 alloy in automotive industry

D. Miloradović^a, N. Miloradović^a, J. Glišović^a, B. Stojanović^a, R. Vujanac^a

^aUniversity of Kragujevac, Faculty of Engineering, Sestre Janjić 6, 34000 Kragujevac, Serbia

Abstract *The field of application of ZA27 alloy is very wide due to favourable combination of physical, mechanical and tribological properties. In automotive industry, it is used for the production of engine cylinders and pistons, engine blocks, plain bearings, pumps, brakes, etc. Composites based on ZA27 alloy were developed with the aim of obtaining materials with better mechanical and tribological characteristics compared to the original matrix alloy. In this paper, special attention is given to metal matrix composites developed from ZA27 alloy with a high content of aluminium. Based on experimental research, the paper presents the tribological characteristics of hybrid composites based of ZA27 alloy and reinforced with silicon carbide and graphite particles. Experimental tribological tests were performed on a tribometer under different test conditions, by varying normal loads and sliding speeds. The obtained composites retain good mechanical properties at elevated temperatures and have better tribological properties compared to the base alloy. Application of the tested composites in the automotive industry is justified by their lower weight and high wear resistance. It directly affects the reduction of vehicle weight and gives positive economic and environmental effects.*

Keywords ZA27, hybrid composites, automotive industry

1. INTRODUCTION

The automotive industry is one of the largest consumers of various kinds of raw materials. The process of material selection during product development in this industry presents a hard endeavour of balancing between demands of corporation, market and society. Modern needs for lightweight, compact and impact-resistant vehicle designs are the key factors inducing the use of alternative materials to metals in automotive applications.

Composite materials have been utilized in vehicle designs since 1945 (Stout Scarab vehicle's body structure with glass fibre reinforced plastic). Today, automotive producers are introducing new composite parts in their vehicles in order to meet the stringent emission norms, increase the fuel efficiency by reducing vehicle weight and increase the overall efficiency of vehicle manufacturing. Composites are commonly used to replace steel and other heavy materials because of their better structural and mechanical properties compared to other materials such as steel and aluminium. Use of automotive composites in Europe has increased dramatically in recent years due to the presence of the key automotive manufacturers in Germany, UK, Poland, France, and Spain. It is anticipated that Europe

Corresponding author

Ph.D. Danijela Miloradović, assoc. prof.
neja@kg.ac.rs

University of Kragujevac, Faculty of engineering
Sestre Janjić 6
Kragujevac, Serbia

automotive composites market share will grow at a compound annual growth rate (CAGR) of 6.6% from 2019 to 2026, Fig. 1 [1].

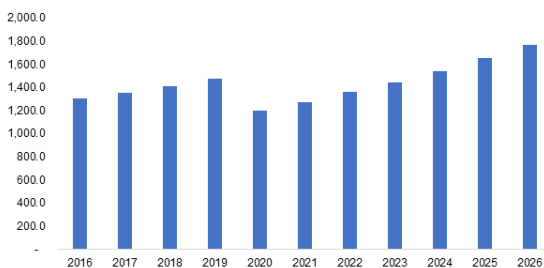


Fig. 1. Europe automotive composite market size, 2016 – 2026 (USD Million) [1]

Composite materials were majorly used for the exteriors of the vehicle (door frames, fenders, bumpers), but their application area has widened. Today, they are used in interiors, chassis, powertrain, under the hood parts and structural parts of the vehicle, Fig. 2, and provide distinct structural and weight advantages. In 2019, the biggest share in global automotive composite market (38.6%) belonged to exterior vehicle components, followed by interior components such as central console, carpets, steering wheels, cockpit modules, door panels, headliners and automotive seats [2].

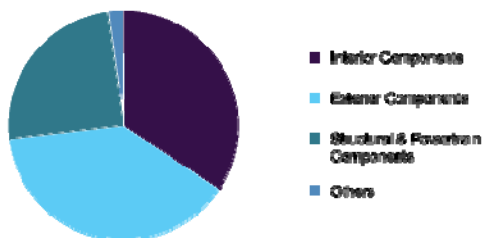


Fig. 2. Global automotive composite market share, by application, 2019 (%) [2]

Major types of composite materials which are used in automotive industry are: polymer matrix composites (PMC), metal matrix composites (MMC), ceramic matrix composite (CMC) and others (hybrid composites). In 2019, the biggest share of the automotive composite market (75.3%) had belonged to polymer matrix composites, followed by metal matrix composites and ceramic matrix composites. On the other hand, hybrid composites have gained

preference in the recent years due to their lower cost in regard to single fibre composites. Due to their low cost and easy fabrication method, polymer composites are most frequently used in inner door panels, roof modules, flaps, lids and dashboards. They are also known for improving the crash performance of vehicles.

Ground transportation (automotive and locomotive) segment dominates the metal matrix composites market, Fig. 3, with more than 50% share. Metal matrix composites for automotive applications are based on aluminium and its alloys. They are generally used for engine components (pistons, connecting rods, cylinder blocks, and valve train parts), brake components, fins, drive shafts and bearings.

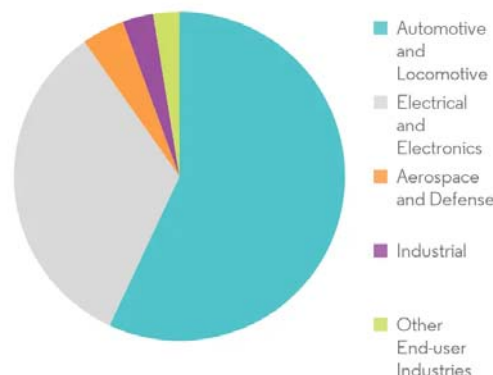


Fig. 3. Metal matrix composites market, Revenue (%), by end-user industry, global, 2020 [3]

Ceramic matrix composites have the high cost of production, but they are known for high strength, excellent corrosion and wear resistance and superior chemical and thermal resistance. Thus, their key applications in automotive industry are in brake disks, brake system components and clutches.

The largest end-use segment of hybrid composite materials market, the automotive and transportation segment, Fig. 4, is anticipated to register a CAGR of 13.9% from 2020 to 2027 [4]. Compared to automotive product made from traditional materials, hybrid composites offer higher strength, lower density, and higher impact resistance. Applications of hybrid composite materials in automotive industry include: seat backs, side and back door panels, boot liner, hat rack, spare tire lining,

windshield dashboard, business table, pillar cover panel, etc.

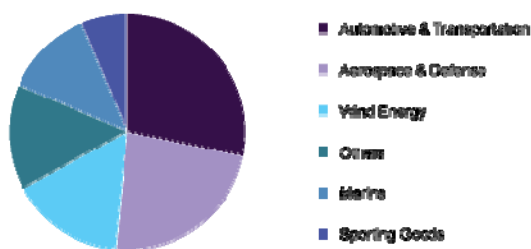


Fig. 4. Global hybrid composites market share, by end-use, 2019 [4]

2. APPLICATION OF ZA27 ALLOY AND COMPOSITES BASED ON ZA27 ALLOY

Zinc-aluminium alloys (ZA alloys) have higher concentrations of aluminium than traditional zinc alloys and have unparalleled bearing properties. Due to good mechanical characteristics (strength, hardness, toughness), ZA alloys are easy to machine and are especially suitable for the production of various types of bearings in the machine industry.

ZA27 alloy has the highest aluminium content of 27%. The basic alloying elements in ZA27 alloy are aluminium, copper and magnesium. The presence of aluminium has a favourable effect on strength and increases the fluidity of the alloy. The addition of small amounts of magnesium has a positive effect on corrosion resistance and on increasing the strength of ZA27 alloy. The presence of copper has a favourable effect on the hardness of the alloy and its tensile strength and creep resistance. ZA27 alloy is characterized by higher hardness and higher modulus of elasticity than aluminium alloy, which together with high strength provides high resistance of ZA27 alloy to abrasion and wear [5].

ZA27 alloy is also characterized by good technological properties, such as excellent castability, easy machining, good damping characteristics, the possibility of applying various surface protection procedures on castings, etc. It is very easy to machine, with minimal tool wear, resulting in items with clean and smooth surfaces.

Due to the favourable combination of physical, mechanical and technological properties, the field of application of ZA27 alloy is very wide.

ZA27 alloy has the lowest density of all ZA alloys, so its application can achieve a significant reduction in the total weight of structures (up to 60% if it replaces bronze products). In the automotive industry, grey cast iron components are increasingly being replaced by ZA27 alloy components, with a weight reduction of over 40%.

Castings made of ZA27 alloy are used in automobile engines and drive mechanisms, for the manufacture of machine tools, presses, pumps, household appliances, agricultural machinery, in the chemical, textile and construction industries, on railways, in refineries, in electric power plants, thermal power plants and foundries. Due to its good electrical and thermal conductivity, it is used in various cooling systems.

Many cast aluminium alloys are being replaced by ZA27 alloy which, in addition to high strength, also has high resistance to wear and atmospheric corrosion. This enabled the commercial application of this alloy as a significant tribo-material, primarily for the manufacture of plain bearings and sleeves.

ZA27 alloy is non-magnetic, which makes it suitable for use in electronic devices. Due to good vibration absorption, it is widely used for the manufacture of various housings.

ZA27 alloy is also acceptable from the ecological point of view, because, according to EU legislation, it is not classified as a hazardous material, which is important for its application in automotive industry.

Relatively low melting temperature of ZA27 alloys requires less energy for melting and casting, so the production costs are lower. However, the mechanical properties of the alloy deteriorate at elevated temperatures, i.e. its hardness and strength decrease. One way to reduce the deterioration of the mechanical properties of ZA27 alloy at elevated temperatures is to make composites based on this alloy.

A composite material is a compound of two or more materials with different characteristics, which has different properties with respect to the constituent components. The production of composite materials has been in continuous expansion since the 1970s. It is expected that this production will reach its maximum in the middle of the 21st century. Composites are used in the aerospace, automotive and electronic industries, medicine and construction [6].

Graphite is nontoxic and acts as a lubricant, so it is used to make composites with a ZA27 base, from which bearings, pistons of automobile and other engines and cylinder liners are produced, Fig. 5.



Fig. 5. Connecting rod and engine piston

Cheap and reliable housings of mechanisms for moving seats in vehicles, are shown in Fig. 6.

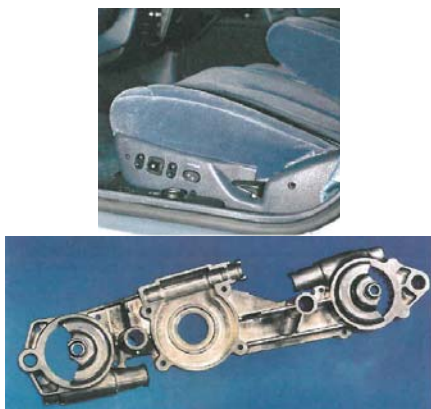


Fig. 6. Mechanism for moving the vehicle seats

The ZA27 alloy is also used for manufacture of plain bearings, gears, plain slats, worm wheels and similar parts, for which good tribological properties are required. The structural and mechanical characteristics of ZA27 alloy, which are extremely important for its application, can be influenced by heat treatment. Thus, the heat-treated ZA27 alloy can be used to make elements such as worm gears, gears, etc, Fig. 7.



Fig. 7. Manufacture of gears

High wear resistance is a consequence of the high hardness of ZA27 alloy and its natural lubricity. Thanks to this, ZA27 alloy plain bearings are increasingly used as a direct replacement for bronze bearings, especially when it comes to larger bearings, Fig. 8.



Fig. 8. Bearings for working machines

The best bearing characteristics of ZA27 alloy are found when used in conditions of high loads and low sliding speeds, with lubrication. The bearings also have improved wear characteristics, because deformation of the graphite particles results in the formation of a continuous graphite film, which provides self-lubrication of the component, allowing for improved component longevity.

3. PROPERTIES OF HYBRID COMPOSITES BASED ON ZA27 ALLOY OBTAINED BY EXPERIMENT

Due to its wide temperature range of solidification, ZA27 alloy is very suitable as a metal base for obtaining composites by the compocasting procedure.

The compocasting procedure is one of the most promising procedures for obtaining composites. This procedure is increasingly used in the commercial production of composite materials, given the savings in energy and material, as well as the relatively low temperature at which the process takes place [7].

The paper presents the results of testing the tribological behaviour of ZA27 alloy as well as the composite reinforced with SiC particles (ZA27+5%SiC) and the hybrid composite reinforced with SiC and Gr particles

(ZA27+5%SiC+3%Gr). Both composites are based on the ZA27 alloy. Tribological tests were performed using a block-on-disc tribometer. The dependences of the wear scar width on the sliding speed and the normal load for ZA27 alloy and the two observed composite materials are shown in Figs. 9 to 11, respectively.

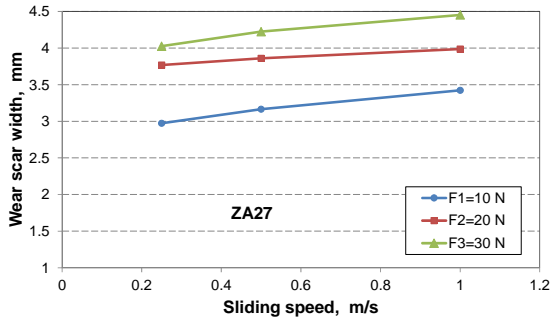


Fig. 9. Dependence of wear scar width on sliding speed for ZA27 alloy

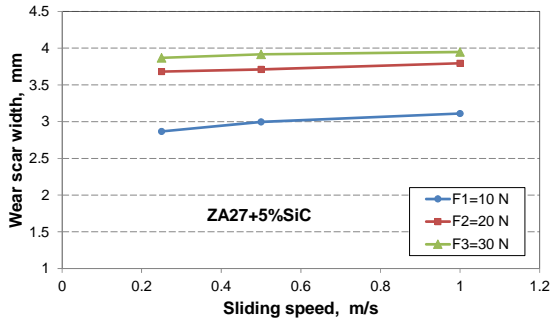


Fig. 10. Dependence of wear scar width on sliding speed for ZA27+5%SiC composite

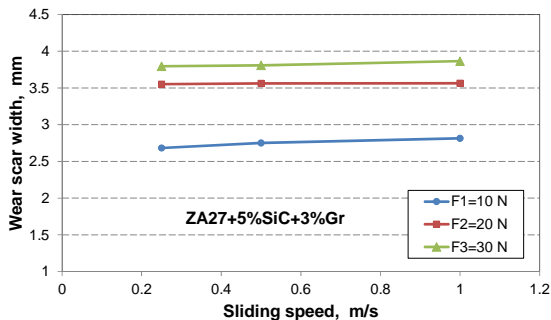


Fig. 11. Dependence of wear scar width on sliding speed for ZA27+5%SiC+3%Gr hybrid composite

The values of the wear scar widths given in the figures represent the mean values after three

tests were performed under the same operating conditions (dry sliding, normal loads of 10 N, 20 N and 30 N, sliding speeds of 0.25 m/s, 0.5 m/s and 1 m/s). It can be observed that the wear scar width increases with the increase in sliding speed and applied normal loads. This applies to all tested materials. Hybrid composite ZA27+5%SiC+3%Gr has the smallest values of wear scar widths, which means that it has the best tribological characteristics for all testing conditions.

Wear rates for all materials were obtained by calculation based on the known geometry of the contact pair and on the volumes of the worn material. Analytical and graphical dependences between the wear rate and the adopted parameters are presented in Figs. 12 to 14 [8].

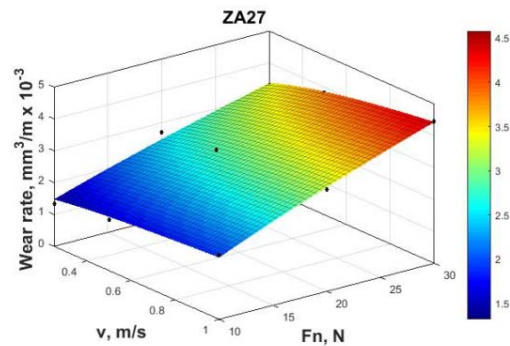


Fig. 12. The wear rate surface for ZA27 alloy

The wear rates of the tested composites are smaller than the wear rates of the ZA27 alloy for all the applied sliding speeds and normal loads.

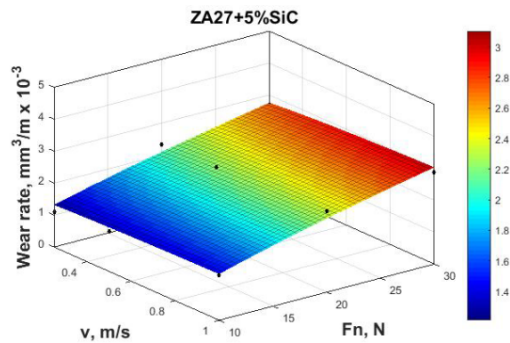


Fig. 13. The wear rate surface for ZA27+5SiC composite

Values of the wear rates of all tested materials increase with the increase of the normal load

and also increase with the increase in the sliding speed.

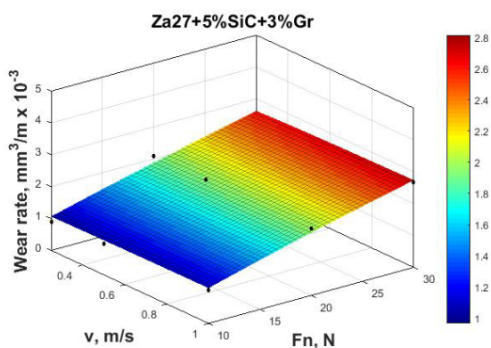


Fig. 14. The wear rate surface for ZA27+5SiC+3Gr hybrid composite

4. CONCLUSIONS

Modern automotive producers must face the challenges imposed by strict emission regulations and better fuel economy demands. Part of the solution to these problems is found in application of composite materials in vehicle design. Their properties like high-strength, wear-resistance and self-lubrication can be customized in order to obtain significant weight reductions and improved fuel efficiency of the vehicles.

Hybrid composites based on ZA27 alloy, which contain SiC particles and graphite, are materials with significant tribological potential for application in the automotive industry. Experimental research have shown that these composites are characterized with high hardness, high wear resistance and good overall tribological properties. Projections from market reports forecast the increase in use of this lightweight and high-strength alternative for traditional fiberglass and metal applications in the automotive industry.

Acknowledgement

Research presented in this paper was supported by the Ministry of education, science and technological development of the Republic of Serbia (grant TR35041).

REFERENCES

- [1] Graphical Research Report ID: GR1504. Europe Automotive Composites Market Share 2020-2026 – Covering trends. From: <https://www.graphicalresearch.com/industry-insights/1504/europe-automotive-composites-market>, accessed on: February 20, 2021.
- [2] Grand View Research Inc. Global Automotive Composite Market Size Report, 2020-2027. From: <https://www.grandviewresearch.com/industry-analysis/automotive-composites-market>, accessed on: February 20, 2021.
- [3] Mordor Intelligence. Metal Matrix Composites Market - Growth, Trends, COVID-19 Impact, and Forecasts (2021 - 2026). From: <https://www.mordorintelligence.com/industry-reports/metal-matrix-composites-market>, accessed on: February 20, 2021.
- [4] Grand View Research Inc. Hybrid composite market size - Industry report, 2020-2027. From: <https://www.grandviewresearch.com/industry-analysis/hybrid-composites-market>, accessed on: February 20, 2021.
- [5] Gangwar, S., Payak, V., Pathak, V.K., Jamwal, A., Gupta, P. (2020). Characterization of mechanical and tribological properties of graphite and alumina reinforced zinc alloy (ZA-27) hybrid metal matrix composites. *Journal of Composite Materials*, vol. 54, no. 30, p. 4889-4901. DOI: 10.1177/0021998320938442
- [6] Owoeye, S.S., Folorunso, D.O., Oji, B., Borisade, S.G. (2019). Zinc-aluminum (ZA-27)-based metal matrix composites: a review article of synthesis, reinforcement, microstructural, mechanical, and corrosion characteristics. *Int J Adv Manuf Technol*, vol. 100, p. 373-380. DOI:10.1007/s00170-018-2760-9
- [7] Miloradović, N., Stojanović, B., Nikolić, R., Gubeljak, N. (2018). Analysis of wear properties of Zn-based composites using the Taguchi method. *Materials Testing*, vol. 60, no.3, p. 265-272. DOI 10.3139/120.111142
- [8] Miloradović, N., Vujanac, R., Mitrović, S., Miloradović D. (2019). Dry Sliding Wear Performance of ZA27/SiC/Graphite Composites. *Metals - Special Issue: "Advances in Design by Metallic Materials: Synthesis, Characterization, Simulation and Applications"*, vol. 9, no. 7, p. 717. DOI: 10.3390/met9070717

Materials Science



Banja Luka
28–29 May 2021.

DEMI 2021

15th International Conference on
Accomplishments in Mechanical and
Industrial Engineering

www.demi.mf.unibl.org



Optimization of hybrid ZA-27 nanocomposites using ANOVA and ANN analysis

S. Gajević^a, S. Miladinović^a, O. Güler^b, H. Çuvalcı^b, N. Miloradović^a, B. Stojanović^a

^aFaculty of Engineering University of Kragujevac, Department of Mechanical Constructions and Mechanization, Sestre Janjic 6, 34000 Kragujevac, Serbia,

^bKaradeniz Technical University, Department of Metallurgical and Materials Engineering, 61080, Trabzon, Turkey

Abstract Nanocomposites based on graphite and aluminium oxide were synthesized via hot pressing process with pre-processing mechanical milling. Optimization of wear loss and coefficient of friction of the nanocomposites with ZA-27 alloy matrix, was performed through the analysis of the following influences: sliding speed (100, 150, 200, 250 rpm), reinforcement of Gr (1, 2, 3, 4 vol.%) and reinforcement Al₂O₃ (1, 2, 3, 4 vol.%). Percentual influence of factors on wear loss and coefficient of friction was determined by ANOVA analysis and is as follows: sliding speed 10.05% and 0.61%, reinforcement of Gr 30.30% and 19.37%, reinforcement of Al₂O₃ 52.99% and 69.01%, respectively. Validation of results using Artificial Neural Network (ANN) gave good correlation with experimental results. Based on this research, it can be observed that nanocomposites with reinforcement of Gr and Al₂O₃ can be potentially employed in many industries as a good substitute for the base alloy.

Keywords Hybrid nanocomposite, ZA27 alloy, wear loss, coefficient of friction, ANOVA, ANN

1. INTRODUCTION

Composites have a great influence in the development of today's industry, due to their different tremendous properties. Nanocomposites are combination of nanoreinforcement and base material. Nanoreinforcements can be nanoparticulates, nanotubes, nanowhiskers, nanofibers and nanoplates. Mostly used nanoreinforcements are nanoparticles which have a very small size. As base materials in metal matrix nanocomposites (MMNC) widely used are aluminum, zinc, magnesium, titanium and their alloys.).

Corresponding author

MSc, Sandra Gajević
e-mail: sandrav@kg.ac.rs

Faculty of Engineering University of Kragujevac
Sestre Janjic 6
Kragujevac, Serbia

Zinc aluminium alloy (ZA) are characterized by good combination of physical, mechanical and technological properties and low manufacturing costs. Alloy ZA27 has the highest tensile strength and wear properties compared to other ZA alloys, which makes this alloy a good material for a replacement of bronze bearings [1, 2, 3].

Experimental research of many authors is based on improvement of tribological and mechanical properties of ZA alloys by adding nanoreinforcements like SiC, Gr, Al₂O₃, ZrO₂ and others. In addition to the above these nanocomposites are characterised by easy machinability and low manufacturing costs.

Vencl et al. have conducted research of structural, mechanical and tribological properties of nanocomposites using Zn25Al3Si and Zn25Al3Si0.03Sr alloys as the matrices and nanoparticles of 1 wt.% Al₂O₃ as the reinforcement. Nanocomposites were fabricated by

compositing process [4]. After the extensive testing they concluded that there was improvement in mechanical and tribological properties of nanocomposites compared to the matrix alloy. Improvement in mechanical properties of nanocomposites with the base of ZA27 fabricated by compositing process have observed Bobic et al. They used different ceramic reinforcements more precisely Al_2O_3 (20–30 nm and 100 nm), and SiC (50 nm) nanoparticles [5]. Hybrid nanocomposites with ZA27 base and B_4C and Gr reinforcements were researched by Güler et al [6]. In process of fabrication the time of mechanical milling was varied and then it was followed by hot-pressing technique. Improvement in properties of these nanocomposites was observed. Application of optimization methods in all stages of research is constantly increasing. One of the optimization methods is Taguchi analysis which was applied by Shivakumar et al. in order to reduce wear volume loss of ZA27/ Al_2O_3 nanocomposite [7]. They used different weight percentage of Al_2O_3 (1, 3 and 5%) in stir casting followed by squeeze casting technique for fabrication of composites. Tribological test were done in dry conditions and the load, sliding speed and sliding distance were varied. With ANOVA analysis it was determined that the highest influence on wear loss has reinforcement content with 77.3% and determined optimal reinforcement content was 5 wt.% of Al_2O_3 . In this paper tribological properties of ZA27 based MMNC reinforced with ceramic and soft nanoparticles were investigated. Taguchi design of experiment was used to investigate dry sliding wear behaviour of the ZA27/ Al_2O_3 /Gr nanocomposite.

2. EXPERIMENTAL INVESTIGATION

For obtaining the optimum combination of factors, in this study, Taguchi experimental design was used. Taguchi method uses the orthogonal array and signal to noise ratio (S/N) for investigation of performance characteristics with the least number of experiments.

2.1 Materials and methods

For fabrication of nanocomposite ZA27 alloy was used as a base in which reinforcements of Al_2O_3 and Gr, with average particle size of 50 nm and 100 nm, were dispersed. These

nanocomposites were produced by mechanical milling process followed by hot pressing process, more details about this process can be found in previous studies [8, 9].

2.2 Design of experiments

In order to obtain the optimum combination for the nanocomposite with the lowest coefficient of friction (CoF) and wear loss (WL), three four-level factors were considered. These factors are: sliding speed (100, 150, 200 and 250 rpm), content of Gr (1, 2, 3 and 4 vol.%) and content of Al_2O_3 (1, 2, 3 and 4 vol.%). In table 1 are presented experimental results and S/N ratio obtained by using statistical software MINITAB19. With A is marked sliding speed, B is content of Gr, and C is content of Al_2O_3 . All experiments were done for constant load of 10 N.

Table 1. Experimental results and results of S/N analysis

No. exp.	A	B	C	WL (mg)	CoF	S/N for WL	S/N for CoF
1	100	1	1	9.8	0.343	-19.825	9.288
2	100	2	2	9.0	0.311	-19.085	10.143
3	100	3	3	10.0	0.336	-20.000	9.487
4	100	4	4	6.2	0.236	-15.848	12.561
5	150	1	2	9.1	0.323	-19.181	9.823
6	150	2	1	17.1	0.392	-24.660	8.138
7	150	3	4	9.3	0.306	-19.370	10.301
8	150	4	3	9.2	0.257	-19.276	11.807
9	200	1	3	6.0	0.23	-15.563	12.754
10	200	2	4	9.2	0.257	-19.276	11.806
11	200	3	1	21.4	0.388	-26.608	8.226
12	200	4	2	25.6	0.372	-28.165	8.600
13	250	1	4	4.5	0.202	-13.064	13.897
14	250	2	3	10.0	0.296	-20.000	10.567
15	250	3	2	16.9	0.359	-24.558	8.909
16	250	4	1	31.7	0.411	-30.021	7.725

Statistical analysis of wear loss and CoF of ZA27 nanocomposites are performed by S/N ratio analysis, ANOVA and Artificial Neural Network (ANN). In this paper S/N ratio analyses of wear loss and CoF by using smaller-the-better quality characteristic as responses have to be minimized [10]. Experimental results are converted with S/N ratio in order to perform a characteristic analysis.

3. RESULTS AND DISCUSSION

Analysis of the effect of each control factor on the tribological characteristics was performed with S/N analysis. Responses of S/N ratios for WL and CoF in table 2. Analysis of S/N ratios of the experimental results determined order of factor importance (Rank).

Table 2. Responses Table for S/N Ratios

Level	WL			CoF		
	A	B	C	A	B	C
1	-18.69	-16.91	-25.28	10.370	11.440	8.344
2	-20.62	-20.76	-22.75	10.017	10.163	9.369
3	-22.40	-22.63	-18.71	10.346	9.231	11.154
4	-21.91	-23.33	-16.89	10.274	10.173	12.141
Delta	3.71	6.42	8.39	0.352	2.210	3.797
Rank	3	2	1	3	2	1

Based on the table 2 it can be observed that the highest influence on wear loss and CoF has the content of Al₂O₃ followed by content of Gr and sliding speed. Optimal combination of factors can be seen on the figure 1 or determined from table 2 according to the highest S/N.

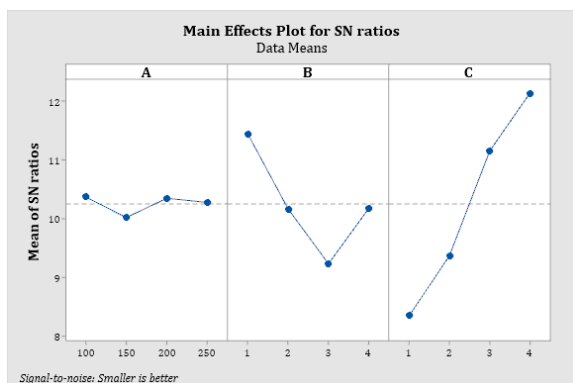
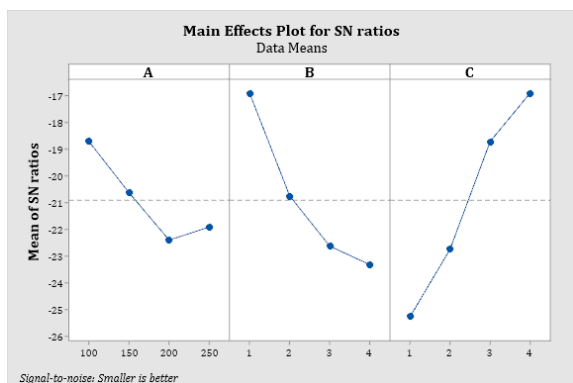


Fig. 1. Main effects plot for a) WL and b) CoF of nanocomposite

According to table 2 and figure 1 optimal factor combination for WL and CoF is A1B1C4, more precisely: sliding speed of 100 rpm, reinforcement content of 1 vol.% Gr and reinforcement content of 4 vol.% Al₂O₃.

Analysis of variance (ANOVA) is a statistical method for determining the impact of various input factors and for interpreting experimental data. Degrees of freedom (DF), mean square (MS), sum of squares (SS), F and P values and percent of contribution are all included in ANOVA analysis. The effect of sliding speed and reinforcement content of Gr and Al₂O₃ on tribological behaviour of nanocomposite was performed with a 95% confidence level and it is shown in the table 3.

Table 3. ANOVA for SN ratios WL and CoF

WL							
Source	DF	Seq SS	Adj SS	Adj MS	F	P	%
A	3	32.98	32.98	10.994	3.02	0.116	10.05
B	3	99.42	99.42	33.139	9.09	0.012	30.30
C	3	173.86	173.86	57.953	15.90	0.003	52.99
Residual Error	6	21.87	21.87	3.644			6.67
Total	15	328.13					100

CoF							
Source	DF	Seq SS	Adj SS	Adj MS	F	P	%
A	3	0.313	0.313	0.105	0.11	0.950	0.61
B	3	9.879	9.879	3.293	3.52	0.089	19.37
C	3	35.201	35.201	11.734	12.53	0.005	69.01
Residual Error	6	5.618	5.618	0.936			11.01
Total	15	51.01					100

The results of ANOVA for wear loss (table 3) show that the wear behaviour of nanocomposite is highly affected by Al₂O₃ reinforcement content with 52.99%, followed by reinforcement content of Gr with 30.30% while the sliding speed has the least influence with 10.05% on the wear loss of nanocomposites. CoF of nanocomposite is, also, highly affected by Al₂O₃ reinforcement content (69.01%), followed by reinforcement content of Gr (19.37%) while sliding speed (0.61%) has almost no influence on the CoF of nanocomposites. Figure 2 shows a 2D diagram of the dependence of the influencing factors on wear loss and coefficient of friction.

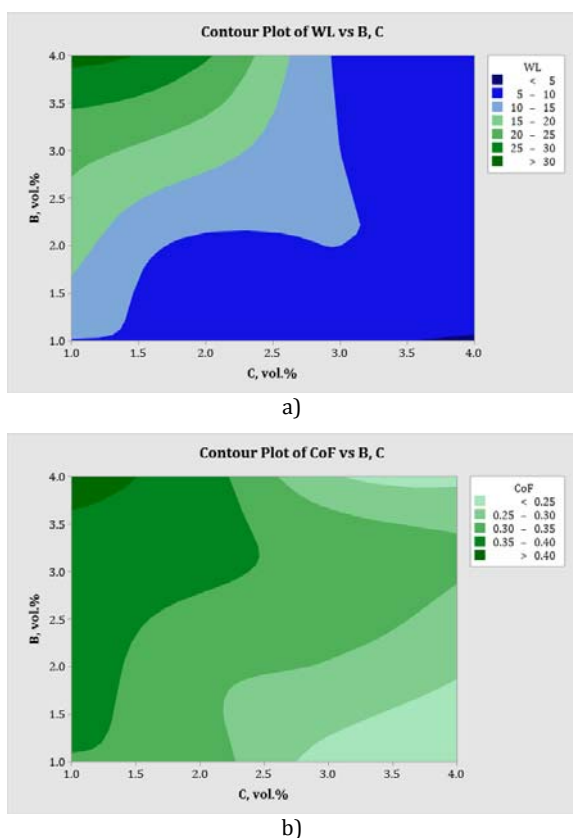


Fig. 2. Diagram of dependence of reinforcements Gr and Al₂O₃ on a) WL and b) CoF

The influence of factors A: reinforcement Gr and B: reinforcement Al₂O₃ was chosen because of their highest influence on wear loss (figure 2a). Minimal wear loss based on the diagram is indicated by blue colour. By following a light green colour (figure 2b) minimal CoF was obtained. It is possible to achieve the target value of wear loss and CoF by adjusting the factors to certain values.

In order to verify the results obtained by the Taguchi method prediction is performed by training experimental data using the ANN method. In this purpose neural network with 3 input factors, 15 neurons in hidden layer and 2 output values was created. The network trained with the help of the software Matlab R2016a is feed forward neural network.

On figure 3 is represented regression plot of trained network. Observing the values for the regression coefficients, it can be found that the coincidence of the results obtained by ANN training and experimental is very good, as indicated by the total regression coefficient of 0.99.

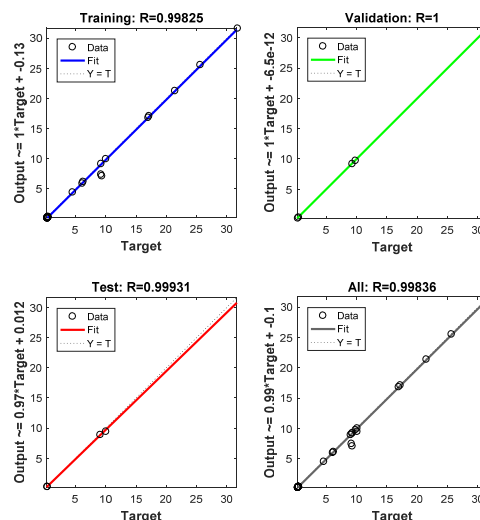


Fig. 3. ANN regression plot for WL and CoF

By observing regression coefficients for testing, validation, training and overall it can be concluded that the trained network can be used for prediction of responses with high reliability. Images for the worn surface, obtained for the different sliding speeds, of the ZA27 hybrid nanocomposites with the highest Al₂O₃ and the lowest Gr reinforcement amount are given in figure 3, since the greatest effect on the wear loss and friction coefficient values is caused by Al₂O₃ reinforcement. As can be seen in this figure, the abrasive lines on the eroded surfaces decrease and the surface becomes smoother until the sliding speed increases from 100 rpm (figure 3a) to 150 rpm (figure 3b) and then to 200 rpm. It has been previously noted that the wear losses are reduced until the sliding speed is increased to 200 rpm. With the effect of hard Al₂O₃ particles, the abrasive wear mechanism has become dominant, and the specific contact area decreases with the increase of the sliding speed (up to 200 rpm), so wear loss is decreased in ZA27 hybrid composites with hard Al₂O₃ additive. It is clear that the resulting abrasive lines narrow down to 200 rpm and the grooves have almost disappeared (figure 3c). With the increase of the sliding speed to 250 rpm and the increase in temperature during wear, material rupture zones were found at the edges of the grooves (figure 3d). While the abrasive wear mechanism is still preserved, it has been observed that materials with high sliding speed move away from the surfaces create pits. This situation can be attributed to

material detachment from the abrasive groove edges with continued sliding of the soft ZA27 matrix zones adhering to the abrasive disc by increasing the sliding speed to 250 rpm.

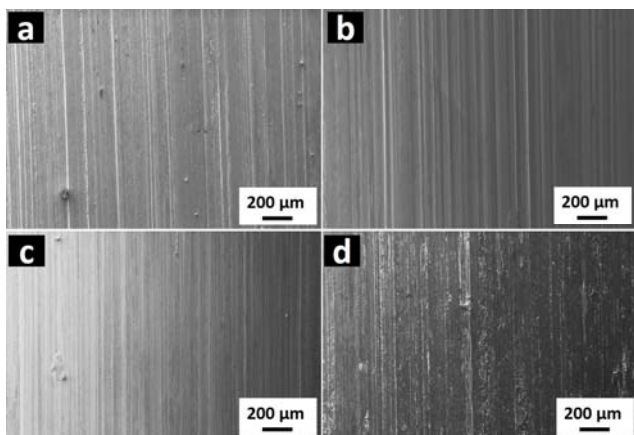


Fig. 3. SEM images of the worn surface of ZA27 composites reinforced 1 vol.% Gr and 4 vol.% Al₂O₃ under the sliding speed of (a) 100, (b) 150, (c) 200 and (d) 250 rpm

Figure 4 presents the mapping analysis of SEM image obtained from the worn surfaces as a result of the wear tests performed under 250 rpm sliding speed of ZA27 hybrid nanocomposites with 1 vol.% Gr and 4 vol.% Al₂O₃ reinforced. As a result of the increase in the sliding speed, the oxide density is noticeable at the edges of the grooves. In addition, the oxide from Al₂O₃ in the structure, can be attributed to the increase in temperature caused by the increase in shear rate causing the matrix material to oxidize. Also, the presence of C within the groove regions draws attention. In this case, it can be understood that the soft structure of the Gr regions is caused by pitting. This phenomenon supports that the effect of Al₂O₃ additive on wear performance in this study is higher than that of Gr. In addition, it is seen that the regions where iron elements are detected are the edges of the grooves.

Thus, it has been determined that the increase in the sliding speed causes adhesion on the abrasive disc and the transfer of Fe from the disc surface to the material worn surface has been determined.

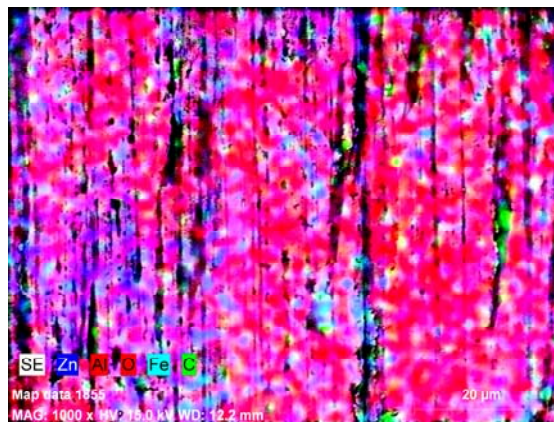


Fig. 4. EDS image of mapping for ZA27 composites 1 vol.% Gr and 4 vol.% Al₂O₃ under the sliding speed of 250 rpm

4. CONCLUSION

This study has presented an experimental investigation of WL and CoF of hybrid metal matrix nanocomposite.

Based on ANOVA and ANN the following conclusions can be made:

- The most influential factor on WL is reinforcement of Al₂O₃, followed by reinforcement of Gr and sliding speed with the least percent of influence.
- In analysis of CoF the most influential factor is reinforcement of Al₂O₃, followed by reinforcement of Gr and with the least influence is sliding speed.
- By observing the achieved results, it can be concluded that ANN can be successfully used to predict the tribological characteristics of hybrid nanocomposites with ZA27 base.
- Based on worn surfaces of hybrid ZA27 nanocomposite it can be seen that dominant mechanism is abrasion.

Acknowledgement

This paper presents the results obtained during research within the framework of the project TR 35021, supported by the Ministry of Education, Science and Technological Development of the Republic of Serbia. In addition, the authors would like to thank TÜBİTAK (The Scientific and Technological Research Council of Turkey) for the support in the carrying out of this study with project number 213M276.

REFERENCES

- [1] Bobić, B., Bajat, J., Bobić, I., & Jegdić, B. (2016). Corrosion influence on surface appearance and microstructure of compo cast ZA27/SiCp composites in sodium chloride solution. *Transactions of Nonferrous Metals Society of China*, vol. 26, no. 6, p. 1512-1521.
- [2] Shivakumar, N., Vasu, V., & Narasaiah, N. (2017). Processing and dry sliding wear behavior of Al₂O₃ nanoparticles reinforced ZA-27 composites. *Materials Today: Proceedings*, vol. 4, no. 2, p.4006-4012.
- [3] Miloradović, N., Vujanac, R., Stojanović, B., & Pavlović, A. (2021). Dry sliding wear behaviour of ZA27/SiC/Gr hybrid composites with Taguchi optimization. *Composite Structures*, vol. 264, no. -, p.113658.
- [4] Vencl, A., Bobić, B., Vučetić, F., Svoboda, P., Popović, V., & Bobić, I. (2018). Effect of Al₂O₃ nanoparticles and strontium addition on structural, mechanical and tribological properties of Zn25Al3Si alloy. *Journal of the Brazilian Society of Mechanical Sciences and Engineering*, vol. 40, no. 11, p. 1-13.
- [5] Bobić, B., Vencl, A., Ružić, J., Bobić, I., & Damjanović, Z. (2019). Microstructural and basic mechanical characteristics of ZA27 alloy-based nanocomposites synthesized by mechanical milling and compocasting. *Journal of Composite Materials*, vol. 53, no. 15, p. 2033-2046.
- [6] Güler, O., Çelebi, M., Dalmış, R., Çanakçı, A., & Çuvalcı, H. (2020). Novel ZA27/B₄C/Graphite Hybrid Nanocomposite-Bearing Materials with Enhanced Wear and Corrosion Resistance. *Metallurgical and Materials Transactions A*, vol. 51, no. 9, p. 4632-4646.
- [7] Shivakumar, N., Vasu, V., & Narasaiah, N. (2015). Synthesis and characterization of nano-sized Al₂O₃ particle reinforced ZA-27 metal matrix composites. *Procedia Materials Science*, vol. 10, no. -, p. 159-167.
- [8] Güler, O., Çuvalcı, H., Gökdağ, M., Çanakçı, A., & Çelebi, M. (2018). Tribological behavior of ZA27/Al₂O₃/graphite hybrid nanocomposites. *Particulate Science and Technology*, vol. 36, no. 7, p. 899-907.
- [9] Güler, O., Cuvalci, H., Canakci, A., & Celebi, M. Ü. S. L. İ. M. (2017). The effect of nano graphite particle content on the wear behaviour of ZA27 based hybrid composites. *Advanced Composites Letters*, vol. 26, no. 2, p. 30-36.
- [10] Stojanovic, B., Blagojevic, J., Babic, M., Velickovic, S., & Miladinovic, S. (2017). Optimization of hybrid aluminum composites wear using Taguchi method and artificial neural network. *Industrial lubrication and tribology*, vol. 69, no. 6, p. 1005-1015.



Banja Luka
28–29 May 2021.

DEMI 2021

15th International Conference on
Accomplishments in Mechanical and
Industrial Engineering

www.demi.mf.unibl.org



THERMAL PROPERTIES OF ARMOUR STEEL PROTAC 600

M. Lešnjak^{1,2}, B. Kosec^{1,3}, B. Karpe¹, G. Janjič⁴, M. Gojić⁵, J. Bernetič⁶, G. Kosec²

¹University of Ljubljana, Faculty of Natural Sciences and Engineering, Aškerčeva cesta 12, 1000 Ljubljana, Slovenia

²SIJ ACRONI d.o.o., c. Borisa Kidriča 44, 4270 Jesenice, Slovenia

³University of Ljubljana, Faculty of Mechanical Engineering, Aškerčeva cesta 6, 1000 Ljubljana, Slovenia

⁴University of Banja Luka, Faculty of Mechanical Engineering, vl. S. Stepanovića 71, 78000 Banja Luka, BiH

⁵University of Zagreb, Faculty of Metallurgy, Aleja narodnih heroja 3, 44103 Sisak, Croatia

⁶SAAT d.o.o., na Lipce 4, 4260 Bled, Slovenia

Abstract Steels from the group PROTAC are distinguished by good mechanical properties and excellent armour properties even at small thicknesses. The mechanical properties of PROTAC 600 steel are known, while data on thermal properties (thermal conductivity, specific heat and temperature conductivity) are not available, so in the frame of our work we determined its thermal properties. As the first part of the work, a study and evaluation of the operation of the device for determining the thermal properties of Hot Disk TPS 2200, today one of the more modern and high-quality instruments for determining thermal properties. In the second part of the work, we performed measurements of thermal properties in accordance with the standard ISO 22007-2 at ambient temperature. The values of thermal properties of PROTAC 600 steel at ambient temperature (approximately 22 °C) are: thermal conductivity 28.69 W/mK, specific heat 3.94 MJ/m³K, and temperature conductivity 7.29 mm²/s. We found that steel PROTAC 600 has more than 10% higher heat conductivity in comparison with the steel of previous generation PROTAC 500.

Keywords armour steel, properties, thermal properties, measurements

1. Introduction

Steel PROTAC 600 is the last generation of the steels from the family PROTAC. It belongs to the group of high strength low alloy (HSLA) steels. It is made in Slovenian steelwork ACRONI d.o.o. by the standard industrial procedures, and the relevant mechanical properties are achieved by quenching and tempering.

Corresponding author

Prof. Borut Kosec
borut.kosec@omm.ntf.uni-lj.si

University of Ljubljana Faculty of Natural Sciences and Eng.
Aškerčeva cesta 12
1000 Ljubljana, Slovenia

The selection of the appropriate armored material is crucial to ensure the adequate safety and mobility transport systems [1]. When selecting or developing the appropriate materials for the armor it is necessary to achieve the best possible compromise between the required mechanical properties of materials, minimizing the density and the final price of the product [2].

With the appropriate production technology, which includes synthesis, hot forming, heat treatment, etc. [3,4] high strength low alloy steel of good functional properties at affordable prices can be produced.

By improving the strength and toughness of the steel the required thickness and the weight

of the steel shell is reduced. Such steels are competitive to other materials for the armor [5].

2. BASIC MATERIAL PROPERTIES

Basic material properties of the armour steel PROTAC 600 are still well known. Chemical composition of the armour steel PROTAC 600 is represented in Table 1, mechanical properties are collected in Table 2, and microstructure is represented in Figure 1.

Tab 1. Chemical composition of steel PROTAC 600

Element	Mass %
C	0.42
Si	1.00
Mn	0.80
P	0.02
S	0.003
Cr	1.30
Ni	3.50
Mo	0.50
B	0.004

Tab 2. Mechanical properties of steel PROTAC 600

Thickness	6.5 – 60 mm
Hardness	570 – 650 HB
Yield strength $R_{p0.2}$	1500 MPa
Tensile strength R_m	2100 MPa
Elongation A_5	9 %
Impact toughness (at testing temperature - 20 °C)	20 J

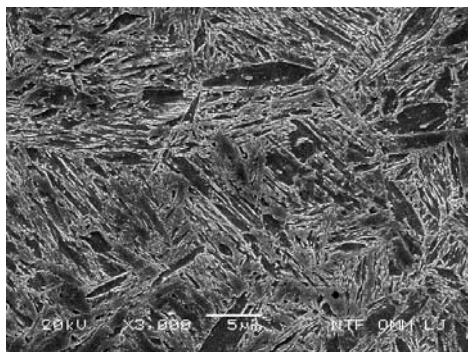


Fig 1. Martensitic microstructure of steel PROTAC 600 (SEM).

3. THERMAL PROPERTIES

In our research, we used one of the most advanced instruments for determining the thermal properties, Hot Disk TPS 2200, a product of Hot Disk AB company, Gothenburg, Sweden (Figure 2) [6].



Fig 2. Instrument Hot Disk TPS 2200.

The instrument can be used for determining thermal properties of various materials including pure metals, alloys, minerals, ceramics, plastics, glasses, powders and viscous liquids with thermal conductivity in the range from 0.01 to 500 W/mK, thermal diffusivity from 0.01 to 300 mm²/s and heat capacity up to 5 MJ/m³K. Measurements can be performed in a temperature interval between -50 °C up to 750 °C.



Fig 3. Measuring sensor sandwiched between two halves of a sample during measurement.

Hot disk measuring method is a transient plane source technique (TPS). Based on the theory of TPS, instrument utilizes a sensor element in the shape of 10 µm thick double

spiral (Figure 3), made by etching from pure nickel foil.

Spiral is mechanically strengthened and electrically insulated on both sides by thin polyimide foil (Kapton ®Du Pont) for measurements up to 300 °C or mica foil for measurements up to 750 °C (Figure 4).

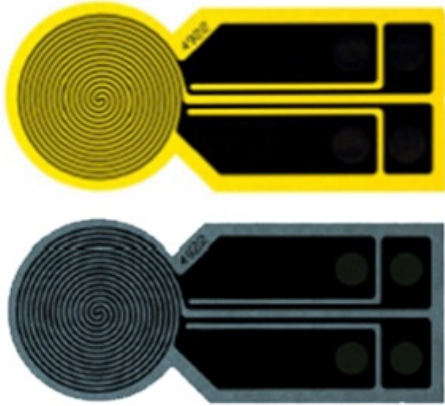


Fig 4. Sensor element (yellow-Kapton, gray-Mica).

Sensor acts both as a precise heat source and resistance thermometer for recording the time dependent temperature increase. During measurement of solids, encapsulated Ni-sensor is sandwiched between two halves of the sample and constant precise pre-set heating power is released by the sensor, followed by 200 resistance recording in a pre-set measuring time, from which the relation between time and temperature change is established. Based on time dependent temperature increase of the sensor, thermal properties of the tested material are calculated.

3.1 Experimental Work

Measurements and analysis of thermal properties of testing samples from the steel PROTAC 600 (Figure 5) were performed in accordance with ISO 22007-2 standard [7] in the Laboratory for Thermotechnical Measurements, Faculty of Natural Sciences and Engineering, University of Ljubljana.

In Figure 6 are presented results of thermal properties measurements.



Fig 5. Testing samples (40 x 40 x 14 mm).

Row	St	Description	Heating...	Mea	Thermal Conductivity	Thermal Diffus...	Specific Heat	Probing Depth	T...	Tem...	Total...	Total Te...	Time Correction	Mean Deviation	Sensor Resist...
4	R.	Average	650 mW	5s	29.897	5.5688	5.3716	10.822	0...	NaN	0.713...	2.5229	0.1	0.00039124	12.346
5	R.	Standard Devi...	0W	0s	0.077771	0.13951	0.12061	0.13523	0...	0	0.017...	0.35649	0	2.9374E-05	0.0060387
6	C.	Protac 600 R...	750 mW	5s	29.200 W/mK	6.554 mm ² /s	4.425 MJ/m ³ K	11.5 mm	0...	1.38...	0.610	4.16 K	0.0535 s	1.019e-003 K	12.343381 Ω
7	C.	Protac 600 R...	750 mW	5s	29.23 W/mK	5.887 mm ² /s	5.233 MJ/m ³ K	10.6 mm	0...	-2.4...	0.690	3.41 K	0.0793 s	3.999e-004 K	12.333143 Ω
8	C.	Protac 600 R...	750 mW	5s	29.57 W/mK	5.521 mm ² /s	5.336 MJ/m ³ K	10.6 mm	0...	-2.4...	0.682	3.41 K	0.100 s	3.632e-004 K	12.324826 Ω
9	R.	Average	750 mW	5s	29.269	5.8873	5.0046	10.919	0...	-0.0...	0.727...	3.6606	0.077605	0.00059419	12.334
10	R.	Standard Devi...	0W	0s	0.23243	0.47216	0.41261	0.43313	0...	0.00...	0.058...	0.35096	0.019031	0.00030111	0.0075887
11	C.	Protac 600 R...	850 mW	2.5s	29.67 W/mK	5.463 mm ² /s	5.431 MJ/m ³ K	10.8 mm	0...	-0.710	0.384 K	0.100 s	0.0796 s	5.495e-004 K	12.315903 Ω
12	C.	Protac 600 R...	850 mW	2.5s	29.33 W/mK	5.703 mm ² /s	5.142 MJ/m ³ K	11.0 mm	0...	-0.742	0.392 K	0.0796 s	0.0796 s	6.390e-004 K	12.307831 Ω
13	C.	Protac 600 R...	850 mW	2.5s	29.65 W/mK	5.489 mm ² /s	5.402 MJ/m ³ K	10.8 mm	0...	-0.714	0.388 K	0.1000 s	0.0796 s	4.752e-004 K	12.300614 Ω
14	R.	Average	850 mW	2.5s	29.546	5.5513	5.3249	10.888	0...	NaN	0.722...	3.8818	0.093215	0.00055159	12.308
15	R.	Standard Devi...	0W	0s	0.15576	0.10767	0.12959	0.10543	0...	0.014...	0.030585	0.0095952	0.0062036	6.6961E-05	0.0062036
16	C.	Protac 600 R...	850 mW	2.5s	28.96 W/mK	7.432 mm ² /s	3.896 MJ/m ³ K	8.63 mm	0...	-0.454	0.385 K	0.0294 s	0.0294 s	1.170e-003 K	12.291564 Ω
17	C.	Protac 600 R...	850 mW	2.5s	29.188	7.451 mm ² /s	3.887 MJ/m ³ K	8.64 mm	0...	-0.455	0.385 K	0.0293 s	0.0293 s	1.159e-003 K	12.283766 Ω
18	R.	Average	850 mW	3.3s	29.188	6.7904	4.395	9.3657	0...	NaN	0.540...	3.8613	0.05289	0.00093452	12.292
19	R.	Standard Devi...	0W	1.17	0.32487	0.92055	0.7189	1.033	0...	0.122...	0.016507	0.033312	0.0009348	0.0068843	
20	C.	Protac 600 R...	850 mW	2.5s	29.18 W/mK	6.973 mm ² /s	4.185 MJ/m ³ K	9.04 mm	0...	-0.498	0.385 K	0.0849 s	0.0849 s	1.152e-003 K	12.278778 Ω
21	C.	Protac 600 R...	850 mW	2.5s	28.76 W/mK	7.365 mm ² /s	3.905 MJ/m ³ K	9.10 mm	0...	-0.505	0.385 K	0.0293 s	0.0293 s	1.125e-003 K	12.142119 Ω
22	C.	Protac 600 R...	850 mW	2.5s	28.63 W/mK	7.249 mm ² /s	3.949 MJ/m ³ K	9.04 mm	0...	-0.497	0.382 K	0.0294 s	0.0294 s	1.140e-003 K	12.160608 Ω
23	C.	Protac 600 R...	850 mW	2.5s	28.69 W/mK	7.252 mm ² /s	3.956 MJ/m ³ K	9.04 mm	0...	-0.498	0.380 K	0.0294 s	0.0294 s	1.155e-003 K	12.183976 Ω
24	R.	Average	850 mW	2.5s	28.693	7.2889	3.9367	9.0599	0...	NaN	0.4999	3.8252	0.029347	0.0011388	12.162
25	R.	Standard Devi...	0W	0s	0.050194	0.053875	0.022297	0.030296	0...	0	0.003...	0.021504	3.456E-05	0.0017084	0.017084

Fig 6. Results of measurements.

In Table 3 are presented thermal properties (thermal conductivity, specific heat and temperature conductivity) of steel PROTAC 600 and steel PROTAC 500 (basic, main steel quality from the group PROTAC) [8,9] at ambient temperature (approx. 22 °C).

Tab 3. Thermal properties of steel PROTAC 600 and steel PROTAC 500 at ambient temperature

Steel	PROTAC 600	PROTAC 500
Thermal conductivity	28,69 W/mK	25,61 W/mK
Specific heat	3,94 MJ/m ³ K	3,76 MJ/m ³ K
Temperature conductivity	7,28 mm ² /s	6,81 mm ² /s

4. CONCLUSIONS

Steels from the group PROTAC are distinguished by good mechanical properties and excellent armour properties even at small thicknesses. The mechanical properties of PROTAC 600 steel are known, while data on thermal properties (thermal conductivity, specific heat and temperature conductivity) were not available, so in the frame of this work its thermal properties were determined.

As the first part of the work, a study and evaluation of We performed measurements of thermal properties in accordance with the standard ISO 22007-2 at ambient temperature. The values of thermal properties of PROTAC 600 steel at ambient temperature (approximately 22 °C) are:

thermal conductivity 28.69 W/mK,
specific heat 3.94 MJ/m³K, and
temperature conductivity 7.29 mm²/s.

We found that steel PROTAC 600 has more than 12% higher heat conductivity in comparison with the steel previous generation steel PROTAC 500.

REFERENCES

[1] Hu, C.J., Lee, P.W., Ballistic performance and microstructure of modified rolled homogeneous armor steel, *Journal of the Chinese Institute of Engineers*, 25 (2002) 1, 99 – 107.

- [2] Dobrzanski, L.A., *Technical and Economical Issues of Materials Selection*, Silesian Technical University, Gliwice, 1997.
- [3] Bernetič, J., Bradaškja, B., Kosec, G., Bricelj, E., Kosec, B., Vodopivec, F., Kosec, L., Centreline formation of Nb(C, N) eutectic in structural steel, *Metallurgy*, 49 (2010) 1, 29-32.
- [4] Thelning, E.K., *Steel and its Heat Treatment*, Butterworths, London, 1984.
- [5] Jocić, B., *Steels and Cast Irons*, BIO-TOP, Dobja Vas, 2008.
- [6] Kosec, B., Karpe, B., *Instrument for the thermal properties analysis Hot Disk TPS 2200, IRT3000*, 1 (2017), 67.
- [7] International standard ISO 22007 (2009). *Plastics – Determination of thermal conductivity and thermal diffusivity – Part 1: General principles*. Reference: ISO 22007:2009(E).
- [8] Børvik, T., Dey, S., Clausen, A.H., Perforation resistance of five different high-strength steel plates for ballistic perforation resistance, *International Journal of Impact Engineering*, 36 (2009) 7, 948–964.
- [9] Bernetič, J., Kosec, B., Kosec, G., Gojić, M., Burzić, Z., Nagode, A., Soković, M., Bizjak, M.. A new generation of armored steel plate. *Contemporary materials*. 7 (2016) 2, 137-141.

Acknowledgement

The authors want to thank professor Ladislav Kosec (University of Ljubljana), dr. Slavko Ažman⁺ (ACRONI d.o.o.), professor Franc Vodopivec⁺ (Institute of Metals and Technology), dr. Milan Rimac (Metallurgical Institute K. Kapetanovic Zenica), and professor Anton Smolej (University of Ljubljana) for mentorship at study armoured steels.



Banja Luka
28–29 May 2021.

DEMI 2021

15th International Conference on Accomplishments in Mechanical and Industrial Engineering

www.demi.mf.unibl.org



The material selection of the heating plates used in the vulcanization process obtained using different MCDM methods

J. Mihajlović^a, G. Petrović^a, D. Ćirić^a, M. Madić^a

^aFaculty of Mechanical Engineering, University of Niš, A. Medvedeva 14, 18000 Niš, Serbia

Abstract *The material selection problem is one of the most important steps in the development process of a part of any subassembly assembly, machine, product, etc. The material selection process needs a systematic and time-consuming approach to choose the optimal material to satisfy the product's requirements. That is to say, many confronting criteria and possible material types (alternatives) available, makes this problem Multi-Criteria Decision-Making problem (MCDM). This paper shows the applicability of the MCDM methodology in the material selection problem for steam heating plates for the vulcanization process used in the inner tube manufacturing process. Specifically, the criteria weights are obtained by CRITIC (Criteria Importance Through Intercriteria Correlation), ENTROPY and PIPRECIA (Pivot Pairwise Relative Criteria Importance Assessment) methods, while TOPSIS (Technique for the Order Preference by Similarity to Ideal Solution) method has been implemented in this process for evaluation and ranking of the possible alternatives (material types).*

Keywords *Material selection, CRITIC, ENTROPY, PIPRECIA and TOPSIS method*

1. INTRODUCTION

The material selection process represents one of the most challenging issues in the design and development of any structural element [1]. Generally, constructors-designers are choosing materials for their desired products based on their previous experience. That is to say, the recommendations from the textbooks or material suppliers added to important product's requirements, as well as desired material properties are also observed. Despite the engineers' experience and their knowledge

about the materials, the ability to select the proper material from the wide spectrum of available materials is a challenging and time-consuming task [2].

The oldest and the basic material selection principle remains the same and it is by trial and error methods [3] which follows substantial costs and time in the development process, because of the improperly chosen material. Consequently, this means that improperly selected material can negatively affect productivity and profitability [1, 4].

Thus the proper methods and tools have been created to overcome problems as such.

In recent years, one of the approaches in the material selection process is a multi-criteria decision-making approach (MCDM approach).

When applied, MCDM methods can help decision-makers with objective and systematic evaluation of alternatives on multiple criteria

Corresponding author

PhD student, Jelena Mihajlović
jelena.mihajlovic@masfak.ni.ac.rs

PhD student
Aleksandra Medvedeva 14
18000 Niš, Serbia

[5]. The MCDM methodology provides an easy way to observe a wide range of possible alternative solutions (different material types) in comparison with the multiple confronting criteria (material characteristics, costs, construction requirements, etc.) [6].

Specifically, this paper shows the applicability of different MCDM methods in the material selection process of the heating plates used for the vulcanization process of the inner tubes.

The heating plates are responsible for the pre-heating (preparation phase) and the heating (production phase) of the mould in which the inner tube profile gets vulcanized. The vulcanization process is the last in the production of the inner tubes. Thus, the heating plates must properly maintain the heat inside the mould in order not to produce scrap tubes.

Those plates are maintaining one of the most important vulcanization parameters which are the temperature-pressure characteristics of the steam. Steam is used to “power” the heating plates and it transfers heat through them to the mould. The mould is getting proper temperature (defined by the production process) which is then transferred to the inner tube.

After the vulcanization process is over, the production cycle of the inner tube is done.

For the present research, CRITIC (Criteria Importance through Intercriteria Correlation), ENTROPY and PIPRECIA (Pivot Pairwise Relative Criteria Importance Assessment) method have been applied for the determination of the criteria weights. Individually determined criteria weights from each method will be summarized in one joined criteria weights set. Criteria weights determined in the previous step are going to be used in TOPSIS (Technique for the Order Preference by Similarity to Ideal Solution) method for evaluation and selection of the proposed alternative solutions.

2. LITERATURE REVIEW

The MCDM methodology has been attracted by many researchers. Thus, a variety of MCDM methods have been developed and applied to numerous subjects. One of the topics was a combination of the MCDM methodology and the material selection problem.

In order to evaluate alternatives, the criteria weights must be objectively calculated. This

process represents the basic step for most MCDM methods. Some of them have the determination of the criteria weights embedded as one of the steps inside their methodology (e.g. AHP method). On the other hand, most of the MCDM methods combine with one (or more) methods which are applied only for the criteria weights determination. Those methods are: CRITIC, SWARA, AHP, ENTROPY, PIPRECIA, etc.

Since there is no specific MCDM method that should be applied for the material selection, many methods such as AHP, ANP, TOPSIS, VIKOR COPRAS, DEMATEL, ELECTRE, MOORA, PROMETHEE, etc. have been introduced.

The great majority of these methods have been used to material selection problem because of their user-friendly process [7, 8]. Although every MCDM method has its advantages and disadvantages, the most frequently used methods are TOPSIS, ELECTRE and AHP.

AHP is one of the most popular MCDM methods and it was successfully applied for reinforced composite materials material selection for automotive brake lever design [9]. Some researchers have made a comparative analysis of MCDM methods such as ELECTRE and PROMETHEE for pipe material selection in the sugar industry [1]. On the other hand, the TOPSIS method has been applied in comparison with the VIKOR method for the selection of microelectromechanical systems electrostatic actuators [10]. Also, a comprehensive MCDM-based approach using TOPSIS, COPRAS and DEA as an auxiliary tool for material selection problems was carried over [7].

3. MCDM METHODOLOGY

Decision analysis is concerned with the situations in which a decision-maker needs to make the best possible outcome among numerous possible solutions (specifically, material type) while considering a set of confronting criteria.

One of the most important steps in the material selection process is ranking and choosing the right material for a specific application.

MCDM methodology is rapidly growing in the material selection problem [1], because of their ability to evaluate and select materials by several involved factors rather than a single criterion [10].

Here, a brief description of the applied MCDM methods is given. In order to calculate criteria weights, the CRITIC, ENTROPY and PIPRECIA method are used, while TOPSIS method is used for the evaluation of alternatives.

3.1 CRITIC Method

In decision-making problems criteria can be viewed as a source of information. The importance weight of criteria could reflect the amount of information contained in each of them [11]. The criteria weights obtained this way are „objective weights“.

The CRITIC (Criteria Importance Through Intercriteria Correlation) method is a method for determining the objective criteria weights in the MCDM problem, introduced by Diakoulaki (1995) [12].

The criteria weights derived by this method combine the standard value deviation of the alternatives by each criterion and the correlation coefficient between those criteria [12].

The process of determining the criteria weights based on this method can be summarized in several steps.

Step 1. Calculate the transformations of performance values and obtain criteria vectors as follows (K^+ is the set of maximization criteria and K^- is the set of minimization criteria):

$$r_{ij} = \frac{x_{ij} - x_j^-}{x_j^+ - x_j^-}, \forall K_j \in K^+$$

$$r_{ij} = \frac{x_j^+ - x_{ij}}{x_j^+ - x_j^-}, \forall K_j \in K^-$$

where $x_j^+, j=1, \dots, n$ are the greatest values for each criterion, while $x_j^-, j=1, \dots, n$ are the lowest values for each criterion.

Step 2. Calculate the standard deviation σ_j of each criterion using the corresponding vector:

$$\sigma_j = \sqrt{\frac{\sum_{i=1}^m (r_{ij} - \bar{r}_j)^2}{m}}, j=1, \dots, n$$

Step 3. For each pair of the criteria, the correlation coefficient is calculated as an indicator of their mutual dependence:

$$\rho_{jk} = \frac{\sum_{i=1}^m (r_{ij} - \bar{r}_j)(r_{ik} - \bar{r}_k)}{\sqrt{\sum_{i=1}^m (r_{ij} - \bar{r}_j)^2 \sum_{i=1}^m (r_{ik} - \bar{r}_k)^2}}, j, k=1, \dots, n$$

Step 4. The amount of information C_j contained in the criteria j is determined in the following manner:

$$C_j = \sigma_j \sum_{k=1}^n (1 - \rho_{jk}), j=1, \dots, n$$

Step 5. Determine the criteria weights as follows:

$$w_j = \frac{C_j}{\sum_{j=1}^n C_j}, j=1, \dots, n$$

3.2 ENTROPY Method

The Entropy Method is a method for determining the objective criteria weights in the MCDM problem, introduced by Claude Shannon (1984) [13].

Determination of objective criteria weights according to the Entropy Method is based on the measurements of uncertain information contained in the decision matrix and directly generates a set of weights for given criteria based on mutual contrast of individual criteria values of variants for each criterion and then for all the criteria at the same time [14, 15].

Determination of criteria weights w_j according to the Entropy Method is carried out in four steps [13].

Step 1. Normalization of the values of alternatives according to each of the criteria.

For criteria that are maximized:

$$r_{ij} = \frac{x_{ij}}{\sum_{i=1}^m x_{iu}}, \forall K_j \in K^+$$

For criteria that are minimized:

$$r_{ij} = \frac{1/x_{ij}}{\sum_{i=1}^m 1/x_{ij}}, \forall K_j \in K^-$$

Step 2. The entropy E_j of all alternatives in terms of criteria k_j is calculated as follows:

$$E_j = \varepsilon \sum_{i=1}^m r_{ij} \ln r_{ij}, j = 1, \dots, n$$

where the constant is:

$$\varepsilon = \frac{1}{\ln m}$$

Step 3. The complement of entropy is called the degree of diversification d_j and is calculated as:

$$d_j = 1 - E_j, j = 1, \dots, n$$

Step 4. The weight coefficients suggest that the weights are directly proportional to the degree of diversification.

$$w_j = \frac{d_j}{\sum_{j=1}^n d_j}, j = 1, \dots, n$$

3.3 PIPRECIA Method

The Pivot Pairwise Relative Criteria Importance Assessment (PIPRECIA) Method for determining the weights of criteria was proposed by Stanujkic et al (2017) [16].

The process of determining the criteria weights based on this method can be summarized in several steps.

Step 1. Determine the set of relevant evaluation criteria and those in descending order, based on their expected significances.

Step 2. Determine the relative importance S_j of the criteria, in relation to the previous $j - 1$ criterion, and do so for each particular criterion.

$$S_j = \begin{cases} > 1, & \text{if } C_j > C_{j-1} \\ 1, & \text{if } C_j = C_{j-1} \\ < 1, & \text{if } C_j < C_{j-1} \end{cases}$$

Step 3. Calculate the coefficient k_j .

The coefficient k_j is being calculated for each criterion.

$$k_j = \begin{cases} 1, & j = 1 \\ 2 - S_j, & j > 1 \end{cases}$$

Step 4. Calculate the recalculated weight q_j .

$$q_j = \begin{cases} 1, & j = 1 \\ \frac{q_{j-1}}{k_j}, & j > 1 \end{cases}$$

Step 5. Calculate the relative weights of the evaluation criteria. The criterion weights reflecting the attitudes of each participant are obtained.

$$w_j = \frac{q_j}{\sum_{k=1}^n q_k}$$

3.4 TOPSIS Method

TOPSIS (Technique for the Order Preference by Similarity to Ideal Solution) method was introduced by Hwang and Yoon (1981). The ordinary TOPSIS method is based on the concept that the best alternative should have the shortest Euclidean distance from the ideal solution (positive ideal solution - PIS) and at the same time the farthest from the anti-ideal solution (negative ideal solution - NIS). It is a method of compensatory aggregation that compares a set of alternatives by identifying weights for each criterion [5, 17].

TOPSIS method can be implemented using the following steps:

Step 1. Develop the decision matrix (X):

$$X = [x_{ij}]_{m \times n}$$

Step 2. Determine the normalized decision matrix which elements are r_{ij} :

$$r_{ij} = \frac{x_{ij}}{\sqrt{\sum_{i=1}^m x_{ij}^2}}$$

Step 3. Obtain the weighted normalized decision matrix which elements v_{ij} are obtained by multiplying each column j of the normalized decision matrix by its associated weight w_j (obtained using the joint weights from CRITIC, ENTROPY and PIPRECIA methods for this paper purposes):

$$v_{ij} = r_{ij} \cdot w_j$$

Step 4. Determine the positive ideal and the negative ideal solutions:

$$V^+ = (v_1^+, v_2^+, \dots, v_n^+) = \{(\max_j \{v_{ij} | j \in B\}), (\min_j \{v_{ij} | j \in C\})\}$$

$$V^- = (v_1^-, v_2^-, \dots, v_n^-) = \{(\min_j \{v_{ij} | j \in B\}), (\max_j \{v_{ij} | j \in C\})\}$$

where B and C are associated with the maximization and minimization criteria sets, respectively.

Step 5. The distance from the ideal and anti-ideal solutions are calculated for each alternatives using the two Euclidean distances as follows:

$$S_i^+ = \sqrt{\sum_{j=1}^n (v_{ij} - V_j^+)^2}$$

$$S_i^- = \sqrt{\sum_{j=1}^n (v_{ij} - V_j^-)^2}$$

Step 6. Calculate the relative closeness of the *i*-th alternative *A_i* to the positive ideal solution:

$$P_i = \frac{S_i^-}{S_i^+ + S_i^-}$$

The higher values of *P_i* indicate that the rank is better.

4. CASE STUDY

The production of the inner tubes consists of a couple of phases. It begins with the preparation phase in which the rubber mixture is being specifically prepared for the tube production regarding the inner tube type. After the rubber mixture is prepared and inner tube profiles produced, the assembly phase starts.

The assembly phase is responsible for the creation of the inner tube rough shape (the joint of both ends of the inner tube profile is made as well as the application of the valve on the upper side of the profile – opposite side of the joint). Inner tubes prepared this way need to complete the final production phase in order to meet the process requirements.

That phase is the vulcanization phase. The vulcanization phase is done on the curing presses inside the vulcanization moulds. The inner tube profile is placed inside the mould and the specified pressure and temperature outside the tube with specified pressure inside the inner tube during the required period of time make the final perspective to the inner tube profile. Those process parameters regard the pressure/temperature of the steam, which obtain the proper temperature of the mould and the compressed air is applied through the valve from the inside of the inner tube. A medium that distributes the heat from the steam to the mould is heating plates (Fig. 1).

Heating plates must be manufactured specifically for the type of the mould with excellent heat distribution characteristic as well as durability in order to extend their life cycle. Thus, the selection of the optimal material is crucial.

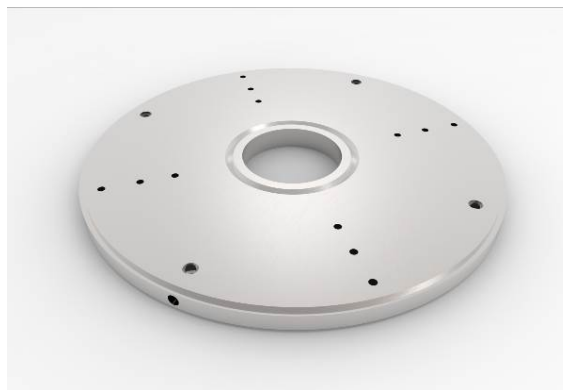


Fig. 1. Heating plate for the vulcanization process

4.1 Decision matrix

The most important step for the MCDM application on a selected problem is the proper definition of the decision matrix. A properly defined decision matrix could reduce input errors and provide reliable and objective output data.

The decision matrix represents a set of values for each alternative solution in comparison to each criterion.

The presented material selection problem involves a set of 5 criteria and 5 alternative solutions (materials) on which the decision matrix is formed (Table 1).

Table 1. The material selection of the heating plates problem decision matrix

Criteria	C ₁ [-]	C ₂ [MPa]	C ₃ [W/m-K]	C ₄ [J/g-°C]	C ₅ [GPa]
Alternatives	min	max	max	max	max
A₁	9	1000	45	480	210
A₂	3	360	49	470	190
A₃	6	570	53	470	190
A₄	7	590	58.6	460	210
A₅	4	370	47	470	190

The criteria set consist of 5 criteria (Table 2). Those chosen criteria are selected on the previous author’s experience – literature review, type of the problem, as well as the previous and existing experience of the heating plates in use.

C₁ – Cost criterion was intended to be expressed in RSD/kg, but it is numerically represented by marks from the basic Saaty’s scale. The reason for this was the intersection between wide price

ranges for each of the selected materials provided by the local steel suppliers.

Table 2. Steel material selection criteria

Properties of the steel material	Symbol
Cost [RSD/kg]	C ₁
Ultimate tensile strength [MPa]	C ₂
Thermal conductivity [W/m-K]	C ₃
Specific heat [J/g-°C]	C ₄
Modulus of elasticity [GPa]	C ₅

C₂ – Ultimate tensile strength [MPa] is used to refer to the maximum stress a material can handle before becoming elongated, stretched or pulled.

C₃ – Thermal conductivity [W/m-K] is defined as the rate at which heat is transferred by conduction through a unit cross-section area of a material when a temperature gradient exists perpendicular to the area [18].

C₄ – Specific heat [J/g-°C] is the amount of heat per unit mass needed to increase the temperature of a material by one degree Celsius.

C₅ – Modulus of elasticity [GPa] is defined as the slope of the straight-line portion of stress (σ) and strain (ϵ) curve.

Only the first criterion is the minimization criterion where the lower attribute values are performed. On the other hand, the rest four criteria are maximization criteria where higher attribute values are desired.

The proposed set of alternative solutions consists of 5 steel materials represented by the SRPS EN and DIN standards in use (Table 3).

Table 3. Steel material selection alternatives

Alternative solutions (steel materials)	
Standards: SRPS EN/DIN	Symbol
16MnCr5/1.7131	A ₁
S235J/1.0038	A ₂
E335/1.0060	A ₃
C15/1.0401	A ₄
S275N/1.0490	A ₅

4.2 Criteria weights

The criteria weights determination is one of the crucial steps in MCDM methodology.

Those weights are a significant source of subjectivity and they have a massive impact on the final solution. Thus, the sensitivity analysis must be performed to have a certain degree of consistency – objectivity.

The criteria weights for this paper’s purposes are determined by three methods. The CRITIC, ENTROPY and PIPRECIA method have been applied (Table 4).

The PIPRECIA method is declared as the subjective method in criteria weights determination because of the subjective evaluation of criteria importance between all selected criteria (every author has evaluated the criteria importance individually and those values are summarized for further calculations), while CRITIC and ENTROPY method does not determine the criteria weights on the same methodology.

Table 4. The criteria weights obtained by different MCDM methods

w _j	C ₁	C ₂	C ₃	C ₄	C ₅
CRITIC	0.264	0.155	0.189	0.168	0.224
ENTROPY	0.491	0.472	0.028	0.001	0.008
PIPRECIA	0.155	0.141	0.202	0.269	0.234

After the criteria weights are determined by each method individually, those weights could be summarized into one joint criteria weights. The average criteria weights values are represented in Table 5 and those values are applied in the final step – alternative evaluation.

Table 5. Joint criteria weights

	C ₁	C ₂	C ₃	C ₄	C ₅
w _j	0.303	0.256	0.140	0.146	0.155

4.3 Evaluation of alternatives

The final step in MCDM methodology describes the evaluation of alternatives and their preferences.

For the evaluation process of the alternative solutions – steel materials, the TOPSIS method has been applied.

Complete alternative evaluation and ranking obtained with TOPSIS method as described in

Section 3.3 and the assessment results are presented in Table 6.

Table 6. Complete rankings obtained by TOPSIS method

Alternatives	TOPSIS
A ₁	0.471
A ₂	0.526
A ₃	0.427
A ₄	0.355
A ₅	0.480

According to this table, preference is given as follows: Alternative A₂ > Alternative A₅ > Alternative A₁ > Alternative A₃ > Alternative A₄. The best choice is Alternative A₂, and the worst choice is Alternative A₅.

5. CONCLUSIONS

This research has demonstrated the applicability of the MCDM methodology in the material selection for the heating plates inside the inner tube production process. The final results have shown the best-ranking score which is Alternative A₂ (S235J/1.0038). This material represents the best possible evaluated alternative solution/ material for the heating plates.

That is to say, the selected material is proposed to the Company as the solution for the heating plates manufacturing. This way the experimental study would confirm the material selection process.

The improvement of this research from the MCDM point of view is in the better understanding of the problem and increasing the relative criteria and alternative sets.

Also, the thermal analysis could be obtained on the numerical model inside the finite element analysis (FEA). This way the behaviour of the heating plates under the same working conditions and different types of steel materials could be observed. The material selection could be tested virtually before the heating plates manufacturing and testing in real conditions.

Acknowledgement

This research was financially supported by the Ministry of Education, Science and Technological Development of the Republic of

Serbia (Contract No. 451-03-9/2021-14/200109).

REFERENCES

- [1] Anojkumar L., Ilangkumaran M., Sasirekha V. (2014). Comparative analysis of MCDM methods for pipe material selection in sugar industry. *Expert Systems with Applications*, vol. 41, p. 2964-2980.
- [2] Petković D. (2016). *Izbor biomaterijala – višekriterijumska analiza i razvoj sistema za podršku odlučivanju*. (In Serbian). PhD thesis. Mašinski fakultet Univerziteta u Nišu.
- [3] Shanin A., Savadogo O. (2006). TOPSIS multiple-criteria decision support analysis for material selection of metallic bipolar plates for polymer electrolyte fuel cell. *Journal of Power Sources*, vol. 159, p. 1095-1104.
- [4] Karande P., Chakraborty S. (2012). Application of multi-objective optimization on the basis of ratio analysis (MOORA) method for material selection. *Materials and Design*, vol. 37, p. 317-324.
- [5] Čojbašić Ž., Mihajlović J., Petrović G., Madić M., Marinković Z. Comparison of two fuzzy MCDM methods for supplier selection problem. *Proceedings of XIVth Int. Conference on Szstems, Automatic Control and Measurements SAUM 2018*, November 2018, Niš.
- [6] Čirić D., Mihajlović J., Mijajlović M. Transient Finite Element Analysis (FEA) in Material Selection Process: Introduction. *Proceedings of the 5th Int. Conference Mechanical Engineering in XXI Century MASING 2020*, December 2020, Niš, p. 161-166.
- [7] Mousavi-Nasab S. H., Sotoudeh-Anvari A. (2017). A comprehensive MCDM-based approach using TOPSIS, COPRAS, and DEA as an auxiliary tool for material selection problems. *Materials and Design*, vol. 121, p.237-253.
- [8] Das D., Bhattacharya S., Sarkar B. (2016). Decision-based design-driven material selection: a normative-prescriptive approach for simultaneous selection of material and geometric variables in gear design. *Materials and Design*, vol. 92, p. 787-793.
- [9] Mansor M. R., Sapuan S. M., Zainudin E. S., Nuraini A. A. (2013). Hybrid natural and glass fibers reinforced polymer composites material selection using Analytical Hierarchy Process for automotive brake lever design. *Materials and Design*, vol. 51, p. 484-492.
- [10] Yazdani M., Farokh Payam A. (2015). A comparative study on material selection of microelectromechanical systems electrostatic

- actuators using Ashby, VIKOR and TOPSIS. *Materials and Design*, vol. 65, p. 328-334.
- [11] Kashavarz M., Amiri M., Zavadskas K., Antuchevičiene J. (2017). Assessment of third-party logistics providers using a CRITIC-WASPAS approach with interval type-2 fuzzy sets, *Transport* 32 (1), 66-78.
- [12] Diakoulaki D., Mavrotas G., Papayannaki L. (1995). Determining objective weights in multiple-criteria problems: the CRITIC method, *Computer & Operations Research*, 22, 763-770.
- [13] Dimitrijević B. (2017). *Višekriterijumsko odlučivanje (In Serbian.)* University of Belgrade – Faculty of Transport and Traffic Engineering.
- [14] Srđević B., Medeiros Y., Faria A., Schaer M. (2003). Objective Evaluation of Performance Criteria for a Reservoir System, *Vodoprivreda*, Vol. 35, No. (3-4), pp. 163-176.
- [15] Vuičić M., Papić M., Blagojević M. (2017). Comparative Analysis of Objective Techniques for Criteria Weighing in Two MCDM Methods on Example of an Air Conditioner Selection, UDC: 005:519.226 519 816, DOI: 10.5937/tehnika1703422V
- [16] Bakir M., Akan S., Kiraci K., Karabasevic D., Stanujkic D., Popovic. (2020). Multiple-Criteria Approach of the Operational Performance Evaluation in the Airline Industry: Evidence from the Emerging Markets, *Romanian Journal of Economic Forecasting – XXIII (2)*.
- [17] Petrović G., Sekulić V., Madić M., Mihajlović J. (2018). A study of multi-criteria decision-making for selecting suppliers of linear motion guide, *Facta Universitatis*, 14(1), 1–14.



Banja Luka
28–29 May 2021.

DEMI 2021

15th International Conference on Accomplishments in Mechanical and Industrial Engineering

www.demi.mf.unibl.org



High strength low-alloy steels impact toughness assessment at different test temperatures

S. Bulatović^a, V. Aleksić^a, Lj. Milović^b, B. Zečević^c

^aInstitute for Materials Testing (IMS), Bulevar vojvode Mišića 43, Belgrade, Serbia

^bUniversity of Belgrade, Faculty of Technology and Metallurgy, Karnegijeva 4, Belgrade, Serbia

^cUniversity of Belgrade, Innovation Centre of Faculty of Technology and Metallurgy, Karnegijeva 4, Belgrade, Serbia

Abstract *In many production processes, as well as in the exploitation of machine components and structures, materials are exposed to impact loads. In structures made of welded joints of high strength low-alloy steels with their constituents (parent metal, weld metal and heat-affected-zone), the toughness test determines the tendency of steel to brittle fracture, respectively the tendency to increase brittleness during exploitation.*

The strain rate is high and the material manifests much more brittle behavior than is shown by tensile testing. Toughness as a mechanical property is an important factor that is defined as the energy that needs to be spent in order to achieve fracture. Parameters obtained by testing the properties of plasticity are the basis for the design of structures in order to achieve strengths under applied load.

The test results of high strength low-alloy steel toughness assessment at different test temperatures show that temperature significantly affects the impact toughness of steels and their alloys. At higher temperatures the impact energy on fracture is high (the material shows the properties of plasticity) while at lower temperatures the impact energy is small (the material is brittle).

Keywords *impact toughness, high strength low-alloy steel, welded joint*

1. INTRODUCTION

High-strength low-alloy (HSLA) steels or micro-alloyed steels are widely used structural steels for manufacturing of structures used in many industry branches such as process industry, shipbuilding and offshore structures, automotive industry, etc.

For many applications, the most important factor in the steel selection process is the favorable strength-to-weight ratio of HSLA

steels compared with conventional low-carbon steels.

For steel structures such as pressure vessels, ship constructions, transport vehicles and so on, the most common manufacturing process is welding. That is why HSLA steels, besides high strength, should also have good plasticity, sufficient toughness and high resistance to brittle fracture, satisfactory workability and good weldability [1].

The capability of forming is another substantial material property, and for HSLA steels the weldability is of particular significance. Since requirements for safe service are more and more strict, the testing of ductility and toughness parameters is specified, including fracture resistance tests. All cited parameters

Corresponding author

Phd Srđan Bulatović, Research Associate
srdjan.bulatovic@institutims.rs

Institute for Materials Testing (IMS)
Bulevar vojvode Mišića 43,
Belgrade, Serbia

are tested for the entire welded joint as well as for three joint constituents, parent metal (PM), weld metal (WM) and the heat-affected-zone (HAZ), since the requirement for service safety of welded structures, produced of HSLA steel has importance because of the consequences of eventual failure [2].

2. IMPACT TESTING OF HSLA STEEL

A large number of machine parts and structural parts are submitted to variable loads during exploitation. Properties of base material and especially welded joint that are submitted to impact load differ from the properties obtained in case of static force effect. Therefore, the need to determine them is understandable. Pre-cracked specimen testing by bending, performed by impact effect of force, can offer an explanation on the material behaviour in case of obstructed deformation, or three-dimensional stress state. Determination of the work needed for fracture, under certain test conditions, is most commonly used for the ongoing quality, material homogeneity and treatment control. Brittle fracture tendency and accordingly the brittleness increase during exploitation can be determined by this procedure [3].

The material used in the current experimental study was welded joint of high strength low-alloy steel (HSLA) Nionikral-70 (NN-70), designed for ship structures and pressure vessels.

The technology of manufacture and thermomechanical processing, of Nionikral-70 steel is the result of joint research from the Military Technical Institute in Žarkovo (VTI) and ironworks Jesenice from Jesenice, in the early 1990s. Steel is produced in the electric furnace, cast in plates, subsequently rolled into slabs and then into sheets of various thickness. Due to some of its characteristics, it is classified among fine-grained steels. The process of hardening is the combination of classical improvement (quenching and tempering) with grain refinement in accordance with selected chemical composition, by microalloying and appropriate deposition [4,5].

The chemical composition of NN-70 is given in Table 1.

Table 1. Chemical composition of NN-70 (% wt)

NN-70						
C	Si	Mn	P	S	Cr	Ni
0.106	0.209	0.220	0.005	0.017	1.258	2.361

Mechanical properties Nionikral-70 (NN-70) of welded joint are given in Table 2.

Table 2. Mechanical properties of NN-70

Yield strength (MPa)	Ultimate strength (MPa)	Elongation (%)
645	914	22.4

The specimens used in this experiment are standard Charpy specimens of rectangular cross section, with grinded and polished faces, taken from shielded manual arc butt welded 20 mm thick plates. Specimen dimensions are: length $L=55$ mm, width $W=10$ mm and thickness $B=10$ mm, with 2 mm deep notch, Fig. 1.

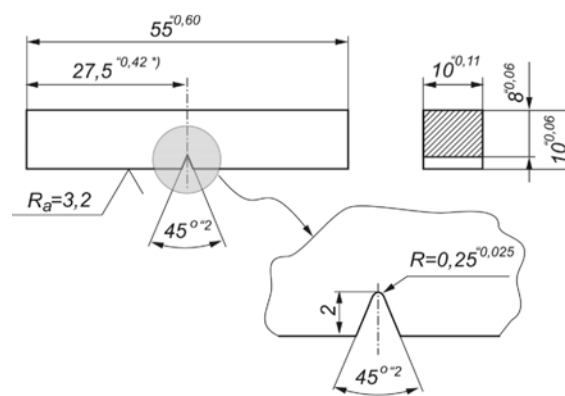


Fig. 1. Charpy specimen for impact energy testing

Impact tests of Charpy specimens with notches in parent metal, weld metal and the heat affected zone are performed in order to determine the total impact energy and its components - crack initiation and crack propagation energy. The test procedure and specimen sizes and shape, as shown in Fig. 1, are defined according to SRPS EN 10045-1 and SRPS EN 10045-2 or ASTM E23-02 [6-9].

Impact testing is performed on the SCHENCK TREBEL 150-300 J (Fig. 2), instrumented Charpy pendulum, at different temperatures (20 °C, -20 °C, -60 °C and -100 °C). The position of notch is according to EN 875 [10].



Fig. 2. SCHENCK TREBEL for impact testing

By testing the specimen with a notch on the instrumented Charpy pendulum, it is possible to obtain a force-time diagram (Fig. 3).

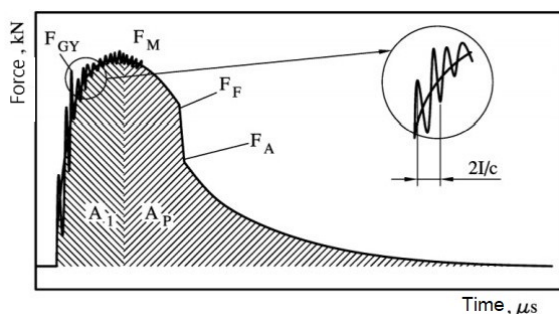


Fig. 3. Typical force-time diagram.

From the considered force-time diagram it is possible to calculate the impact total energy required for the specimen fracture. The total impact energy is broken down into the part of crack initiation energy A_i and the part of crack propagation energy A_p . Areas A_i and A_p , on the force-time diagram, Fig. 3, are proportional to crack initiation and propagation energies.

Examples of results from impact toughness testing are given in Table 3 for specimens with notch in parent metal of NN-70, in Table 4 for specimens with notch in weld metal NN-70 and in Table 5 for specimens with notch in heat-affected zone NN-70. More precisely, testing is performed for parent metal at 20 °C, -20 °C, -60 °C and -100 °C. For specimens with notch in weld metal and heat-affected zone, testing is performed at 20 °C, -40 °C and -80 °C temperatures. Results that refer to a few of tested specimens are shown in Tables 3-5.

Table 3. Impact test results for specimens with notch in parent metal (PM) of NN-70

Spec.	Test temper. °C	Total impact energy, A_T (J)	Crack initiation energy, A_i (J)	Crack propagation energy, A_p (J)
PM-1	20	97.08	39.07	57.90
PM-2	-20	96.89	41.59	55.30
PM-3	-60	60.78	41.44	19.34
PM-4	-100	52.91	46.21	6.7

Table 4. Impact test results for specimens with notch in weld metal (WM) of NN-70

Spec.	Test temper. °C	Total impact energy, A_T (J)	Crack initiation energy, A_i (J)	Crack propagation energy, A_p (J)
WM-1	20	78.24	24.60	53.64
WM-2	-40	53.69	21.85	31.85
WM-3	-80	18.28	0	18.28

Table 5. Impact test results for specimens with notch in heat-affected zone (HAZ) of NN-70

Spec.	Test temper. °C	Total impact energy, A_T (J)	Crack initiation energy, A_i (J)	Crack propagation energy, A_p (J)
HAZ-1	20	104.88	26.80	78.09
HAZ-2	-40	98.59	32.58	66.01
HAZ-3	-80	51.34	27.99	23.35

3. CONCLUSION

Comparing the values of force-time and energy-time for all three constituents of the welded joint (PM, WM and HAZ) of steel NN-70, it follows that the values of total impact energy and crack propagation energy are highest in tests at 20 °C, which means that as the temperature decreases, the toughness of the material decreases.

The location where specimens were taken has influence on the impact total energy value A_T , as well as the V-notch position. Welded joint structure heterogeneity, followed by different mechanical properties of some areas in the welded joint (parent metal, weld metal and heat

affected zone), has a crucial effect on impact properties, more precisely on the impact total energy value.

Thus, based on the obtained results of impact tests, it is clear that the total impact energy depends on:

- the location where specimens were taken (parent metal, weld metal and heat affected zone)
- test temperature

Therefore, it is obvious that a different microstructure in different regions of the welded joint NN-70 affects crack resistance more in dynamic than in static loading conditions. The test results of high strength low-alloy steel toughness assessment at different test temperatures show that temperature significantly affects the impact toughness of steels and their alloys. At higher temperatures the impact energy on fracture is high (the material shows the properties of plasticity) while at lower temperatures the impact energy is small (the material is brittle).

Acknowledgement

This research is supported by the Ministry of Education, Science and Technological Development of the Republic of Serbia (Contract No. 451-03-9/2021-14/ 200012).

REFERENCES

- [1] Aleksić, V., Milović, Lj., Blacic, I., Vuherer, T., Bulatović, S. (2019). Effect of LCF on behavior and microstructure of microalloyed HSLA steel and its simulated CGHAZ. *Engineering Failure Analysis*, Vol. 104, pp. 1094-1106. <https://doi.org/10.1016/j.engfailanal.2019.06.017>
- [2] Grabulov, V., Blačić, I., Radović, A., Sedmak, S. (2008). Toughness and ductility of high strength steels welded joints. *Structural integrity and life*, Vol. 8, no. 3, pp. 181-190.
- [3] Čamagić, I., Vasić, N., Ćirković, B., Cvetković, S., Vasić, Z. (2010). Variable and impact load testing of HSLA steel welds. *Structural integrity and life*, Vol. 10, no. 3, pp. 231-234.
- [4] Radović, N., Drobnjak, Đ. (2001). Development of steels for fabrication of welded constructions with improved safety. *Zavarivanje i zavarene konstrukcije*, Vol. 46, no. 3, pp. 81-92.
- [5] Das, A., Chowdhury, T., Tarafder, S. (2014). Ductile fracture micro-mechanisms of high strength low alloy steels. *Materials and Design*, Vol. 54, pp. 1002-1009.
- [6] Jovanović, M., Čamagić, I., Sedmak, S.A., Živković, P., Sedmak, A. (2020). Crack initiation and propagation resistance of HSLA steel welded joint constituents. *Structural integrity and life*, Vol. 20, no. 1, pp. 11-14.
- [7] SRPS EN 10045-1:1993. (1993). Mehanička ispitivanja metala - ispitivanje udarom po Šarpiju, Deo 1: Metoda ispitivanja.
- [8] SRPS EN 10045-2:1993. (1993). Mehanička ispitivanja metala - ispitivanje udarom po Šarpiju, Deo 2: Verifikacija uređaja za ispitivanje.
- [9] ASTM E 23-02. (2002). Standard Test Methods for Notched Bar Impact Testing of Metallic Materials, Annual Book of ASTM Standards, Vol. 03.01.
- [10] EN 875 (1995). Destructive tests on welds in metallic materials - Impact tests - Test specimen location, notch orientation and examination. Comite Europeen de Normalisation.



Banja Luka
28-29 May 2021.

DEMI 2021

15th International Conference on Accomplishments in Mechanical and Industrial Engineering

www.demi.mf.unibl.org



Cavitation erosion behavior of aluminium based alloys

M. Ćosić^a, S. Boljanović^b, M. Dojčinović^c

^aFaculty of Applied Ecology, Požeška 83a, Belgrade

^bMathematical Institute, SANU, Kneza Mihaila 36, Belgrade

^cUniversity of Belgrade, Faculty of Technology and Metallurgy, Karnegijeva 4, Belgrade

Abstract This paper provide description of cavitation damage and microstructural changes in two types of Al alloys – AlSi18 and AlMg4.5Mn. Aluminum foundry alloys were frequently applied for production of parts like diesel cylinder blocks, pistons, while Al-Mg alloys were widely used in various applications such as the pressure vessels, yachts and ships. These parts were exposed cavitation erosion phenomena during their working service. Cavitation erosion tests were performed on both types of samples according to ASTM G32-92 standard. The mass loss of each material, was investigated by measuring as a function of cavitation time. The damaged surfaces of all samples were analyzed using a optical and scanning electron microscope. The effect of cavitation erosion resistance of conventionally cast AlSi18 alloy was assessed and compared to rolled samples of Al Mg4.5Mn. The experimental results show better cavitation resistance for foundry alloys then rolled Al alloys.

Keywords cavitation erosion, Al alloys, SEM, microstructure

1. INTRODUCTION

The components such as propellers, blades of hydraulic pumps, turbines, piping are exposed to high-speed flow of liquid during their working service. In the same time these parts are exposed cavitation erosion damaging. In other to chose of material for producing hydraulic parts like previous mentioned, the evaluation of cavitation erosion resistance is fundamental. The cavitation erosion phenomenon represents of the rapid formation, growth and collapse of bubbles in a liquid. The reason for this phenomenon is related to presence of strong pressure fluctuations [1].

Corresponding author

Ph.D., Milena Ćosić, cosic.milena@gmail.com
Faculty of Applied Ecology, Požeška 83a,
Belgrade, Serbia

If the liquid is subjected to higher hydrostatic pressure, the bubbles can collapse and then they cause surface damage. Many authors investigated the behavior of different metals and alloys exposed to cavitation erosion. Several studies have been performed on mainly steel, cast iron, titanium, and other. Aluminium alloys such as Al-Cu, Al-Mg, Al-Si-Mg or Al-Zn-Mg have also been widely studied.

Studies on the cavitation erosion resistance of AlMgMn alloys are less common in literature than conventional casting AlSi alloys [2-9].

In this paper cavitation phenomenon was analyzed by modified ultrasonically cavitation test method. The present work shows the investigation of the cavitation erosion resistance of the conventional AlSi18 alloy in comparison with the behaviour of AlMg4.5Mn alloy.

2. EXPERIMENTAL ANALYSIS

The material used in this study was industrially produced. The experiments were carried out on a samples of hypereutectic AlSi18 (sample A) and AlMg4.5Mn (sample B) alloys. The chemical compositions of the alloys are given in Table 1.

Table 1. The chemical composition of alloys (mas%)

	Si	Cu	Mg	Ni	Fe	Zn	Mn	Al
AlSi18	18	0.8	0.8	0.8	-	0.7	0.2	Bal.
		-	-	-	0.7	0.2	0.2	
AlMg4.5Mn	0.13	0.04	3.95	-	0.2	0.03	0.66	Bal.

The modified vibratory cavitation test method was used for laboratory testing of the cavitation resistance. The setup consisted of a high-frequency generator of 360 W, electrostrictive transducer, transformer for mechanical vibrations, and water bath containing the test specimen [10]. The frequency of vibration and the peak-to-peak displacement amplitude of horn were 20 ± 0.05 kHz and 50nm, respectively, with separation of 0.5mm between the sample and horn tip.

The evaluation of the mass losses of the test specimens was performed using an analytical balance with an accuracy of 0.1mg. Before being weighted, the test specimens were dried in hot air. The measurements were performed after subjecting each test specimen to cavitation, every 60 min for test period of 240 min.

Samples were prepared for microstructural analysis by standard metallographic procedure. The initial microstructure of samples and microstructure after cavitation was characterized by optical microscopy (OM), as well as JEOL JSM 6460 LV scanning electron microscopy (SEM).

Some authors report the hardness as an indicator of the erosion resistance. The hardness of the alloys was measured in order to define the correlation between this mechanical property and the resistance to damage.

The average Vickers hardness of the samples was measured with a universal hardness tester

under 5N loads. The measurement was repeated 4 times for each alloy.

3. RESULTS AND DISCUSSION

The influence of the cavitation erosion on the microstructure of the conventional casted samples was studied and than compared to the cold rolled samples.

The results of the cavitation resistance of the test samples subjected to cavitation are shown in Fig.1 and Fig. 2.

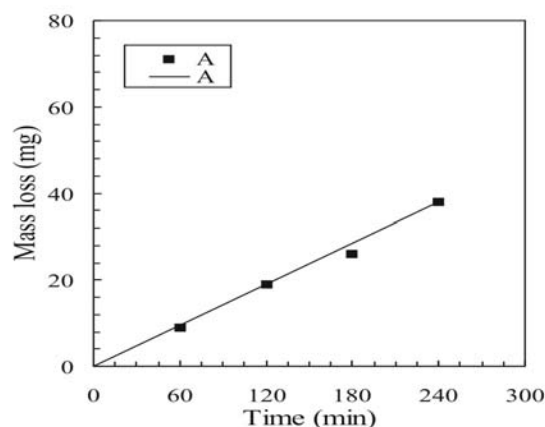


Fig. 1. Cavitation rate for sample A

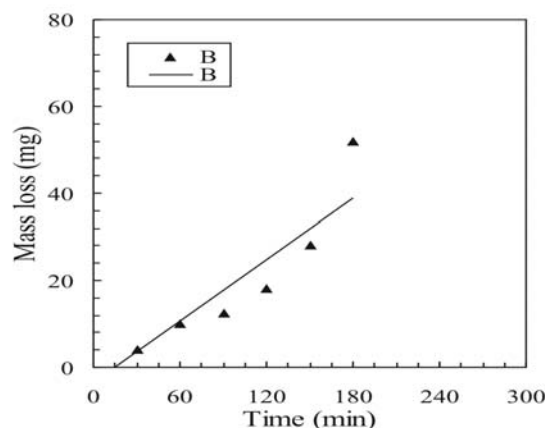


Fig. 2. Cavitation rate for sample B

The diagrams show mass loss as a function of test time for each studied alloy.

According to the ASTM G32 standard, the incubation period was quantitatively defined as point where the line intercepts the time axis.

The mass loss curves vs. time, Fig.2 during the first hour of exposure cavitation shows that the incubation period for the sample B was about 15 min. Mass loss was detected for sample A after 60 min effects of cavitation because there was no incubation period for this sample. Values of cavitation rate were 0.157 mg/min and 0.285 mg/min in case sample A and B, respectively. Microstructural characterization of the tested alloys was performed in order to understand the difference in cavitation properties of sample A and sample B.

The SEM microphotographs of samples after 60 min of cavitation testing are shown in Figs. 3 and 4 for sample A and sample B, respectively. The presence of undulation of the surface was noticed for the both samples (Fig.3 and Fig.4)

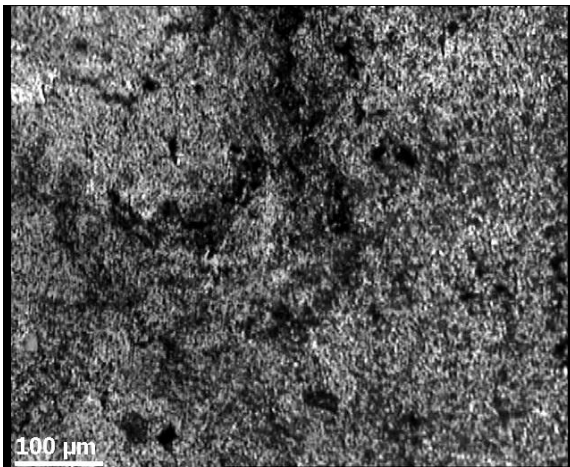


Fig.3. SEM image after 60 min cavitation (sample A)

By comparing two tested materials, it can be inferred that the damage was caused by plastic deformation in the surface layer.

The evolution of the eroded surfaces was observed again after 60 min of testing time. After that time, the damage of surface was more affected by plastic deformation than the previous step. Based on mass loss which was measured, it can be concluded that the large mass loss for sample B then the case in the sample A.

Number of pits on the surfaces of the sample B was higher as compared with sample A.

The microphotographs of the sample A and sample B were obtained by scanning electron microscopy (SEM) after 3h cavitation.

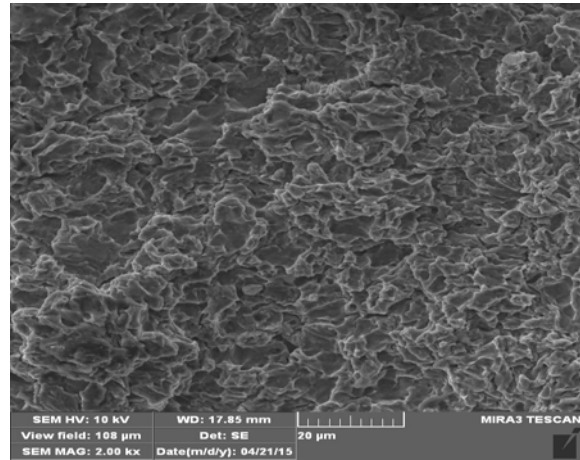


Fig.4. SEM image after 60 min cavitation (sample B)

These microstructures are given in Fig. 5 and Fig.6.

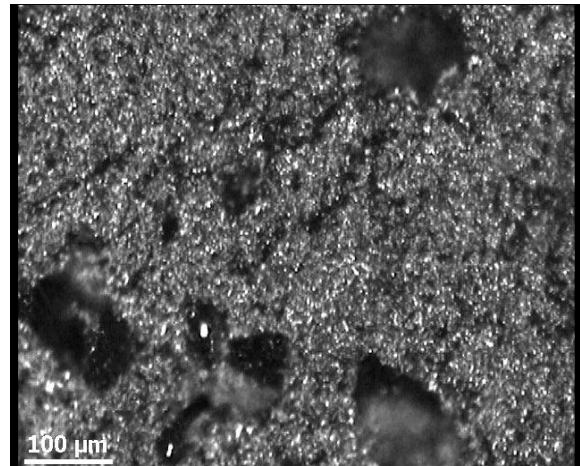


Fig.5. SEM image after 180 min cavitation (sample A)

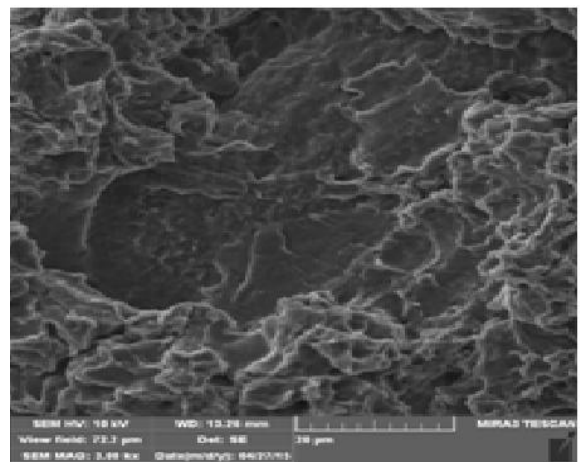


Fig.6. SEM image after 180 min cavitation (sample B)

The surfaces of sample A and sample B after 180 min, show pits and craters. The deepest erosion pits were detected on the sample B.

According to literature, the hardness was indicator of the erosion resistance, in this context the higher the hardness, the higher the cavitation resistance.

The average hardness values were 90 HV and 79 HV for the samples A and B respectively.

Also, the higher hardness for sample A may cause lower level of damage than in the case of sample B.

4. CONCLUSION

In this study, the cavitation resistance of samples A and B was analysed. The obtained conclusions can be summarized as follows:

- Based on mass loss measurement it can be inferred that there was no incubation period for sample A. After 60 min of testing for the same sample mass loss was recorded.
- The analysis of the eroded areas showed that the surface damage of sample B is higher than in the case of sample A.
- During cavitation testing, the damage in both of the tested materials is caused by plastic deformation in the matrix area.
- It was shown that the sample A has a higher cavitation resistance than the sample B.
- The cavitation rates were 0.157 mg/min and 0.285 mg/min in case of sample A and B, respectively.

REFERENCES

[1] Davis J.R., (1999). Corrosion of Aluminum and Aluminum Alloys, ASM International: Materials Park, OH, USA, p. 1-97.

[2] Feller H.G., Kharrazi Y., (1984). Cavitation erosion of metals and alloys, *Wear*, vol 93, p.249-260.

[3] Richman R.H., McNaughton W.P., (1990). Correlation of cavitation erosion behavior with mechanical properties of metals, *Wear*, vol. 140 p.63-82.

[4] Neville A., McDougall B.A.B., (2001). Erosion and cavitation corrosion of titanium and its alloys, *Wear*, vol. 250 p.726-735.

[5] Wu, S.K.; Lin, H.C.; Yeh, C.H. (2000). Comparison of the cavitation erosion resistance of TiNi

alloys, SUS304 stainless steel and Ni-based self-fluxing alloy. *Wear*, vol. 244, p.85-93.

- [6] S.J.Lee, K.H. Kim, S.J.Kim, (2011). Surface analysis of Al-Mg alloy series for ship after cavitation test, *Surf. Interface Anal.*, vol 44, p.1389-1392.
- [7] Li X.Y., Yan Y.G., L., Ma Z.M. Xu, Li J.G., (2004). Cavitation erosion and corrosion behaviour of copper-manganese-aluminum alloy weldment, *Mater. Sci. Eng. A - Struct.* vol.382 no. (1-2) p.82-89.
- [8] Richman R.H., McNaughton W.P., (1990). Correlation of cavitation erosion behavior with mechanical properties of metals, *Wear* vol.140 p.63-82.
- [9] Rao B.C.S., Buckley D.H., (1985) Erosion of aluminum 6061-T6 under cavitation attack in mineral oil and water, *Wear*, vol.105, p.171-182.
- [10] Standard Method of Vibratory Cavitation Erosion Test, G32-92. Annual Book of ASTM Standards.vol.03.02. Philadelphia: ASTM; 1992.



Banja Luka
28–29 May 2021.

DEMI 2021
15th International Conference on
Accomplishments in Mechanical and
Industrial Engineering
www.demi.mf.unibl.org



Influence of the polymer matrix type on cavitation resistance of composites

M. Dojčinović^a, M. Pavlović^b, S. Jezdimirović^a, B. Purić^a, A. Cvetković^c

^a University of Belgrade, Faculty of Technology and Metallurgy, Karnegijeva 4, Belgrade, Serbia, rina@tmf.bg.ac.rs

^b Kontrol Inspekt, D.O.O., Mladena Mitrića 12, Belgrade, Serbia,

^c University of Belgrade, Faculty of Civil Engineering, Bulevar Kralja Aleksandra 73, Belgrade, Serbia

Abstract Cavitation resistance of polymer matrix / basalt powder composites was determined in this work. Two types of composites were tested: epoxy resin / basalt powder composite and polyester resin / basalt powder composite. In both cases, a basalt powder was used as reinforcement in the resin (grain size 20µm, in the amount of 15 wt%). An ultrasonic vibration method with a stationary sample was used to test the cavitation resistance of composites in laboratory conditions. The change in sample mass with test time was monitored to define cavitation rate. Scanning electron microscopy was used to monitor the morphology of composites surface damage.

Keywords cavitation, composite, cavitation damage

1. INTRODUCTION

Composites are modern engineering materials of specific properties: low density and mass, good mechanical properties, corrosion resistance, wear resistance. Compared to other engineering materials (metal materials, polymers, ceramics) they are characterized by a range of positive application properties in different fields of technique. Significant application of composite materials is in the areas of production and application of high-temperature materials. Most composite materials have two components: matrix and reinforcement. Composite properties depend on

the properties of both constituents such as size, distribution, form, nature and the strength of connections between constituents [1, 2].

Ultrasonic vibration method with stationary sample according to ASTM G32 was applied for cavitation testing of two types of composite: epoxy resin/basalt powder composite and polyester resin/ basalt powder composite.

Epoxy resins are used to make coatings, adhesives and composite materials with carbon and glass fibers. Epoxy resins are mainly known for excellent adhesion, chemical and thermal resistance, excellent mechanical properties and very good electrical insulation properties. Polyester resins are often used due to the possibility of their application at temperatures up to 100°C.

The ultrasonic vibration method, applied to examine the properties of the obtained composites, is based on the creation and implosion of cavitating bubbles on the sample surface. Monitoring the formation and

Corresponding author

Dr Marina Dojčinović
rina@tmf.bg.ac.rs
University of Belgrade, Faculty of Technology and Metallurgy
Karnegijeva 4
Belgrade, Serbia

development of surface damage, and measuring the loss of sample mass during the time of exposure to the effects of cavitation enable assessment of applying the obtained composites for the production of parts of equipment that are exposed to the conditions of wear, corrosion, cavitation was evaluated [3-6].

2. EXPERIMENT

Synthesis and characterization of polymer matrix / basalt powder composites was done in this experimental research. Two types of composites were tested: composite epoxy resin/basalt powder (samples A) and composite recycled polyester resin/basalt powder (samples B). In both cases, a 20 μm basalt powder-sized reinforcement was applied, amounting to 15 wt% [7].

Basalt rocks from the "Vrelo"-Kopaonik deposit were used as a starting material for the production of reinforcements for composites. The basalt rocks were crushed and ground to a grain size of 20 μm in a vibrating mill with agate balls. The chemical composition of pyroxene-olivine basalt was: 56.21% SiO_2 ; 18.61% Al_2O_3 ; 1.15% Fe_2O_3 ; 2.97% FeO ; 3.40% MgO ; 7.78% CaO ; 4.73% Na_2O ; 3.37% K_2O ; 1.10% TiO [8].

Fig. 1 shows the SEM microphotograph of basalt powder used as a resin reinforcement for both series of composite samples (samples A and samples B).

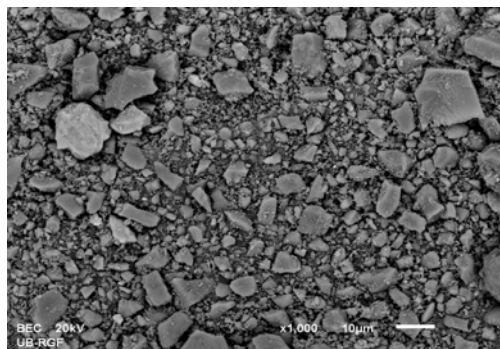


Fig. 1. SEM microphotography of basalt powder samples.

Mixtures of resin and basalt powder for each composite were put in a blender and mixed for 1 to 2 min. During the mixing, a magnet was placed in the pan to prevent the mixture from sticking to the walls of the dish. After that, the mixture was placed on the ultrasound bathroom

for 5 min to remove the bubbles from the mixture. For composite B, 2% of initiator (methyl-ethyl ketone peroxide, 0.15 ml) was added to the mixture. The mixture was stirred in an ultrasonic bath for 15 s, and then poured into teflon molds to obtain test samples. Samples B were left in the mold for 30-45 min at room temperature to harden, then dried into a laboratory dryer at 70°C / 2h. After that, the molds were removed from the dryer, left for 48h at room temperature, and then samples were removed from the mold. Composite based on epoxy resin (samples A) was polymerized faster. The basalt powder was involved in the composite matrix and mixed for 1 to 2 min, the mixture was poured into teflon moulds and polymerization was performed at room temperature

The mechanical properties were tested on the obtained samples of composites: tensile strength and hardness according to the Shore method. An ultrasonic vibration method (with a stationary sample) according to the ASTM G32 standard was used to test cavitation resistance of composites [3]. To assess cavitation resistance, the change in sample mass as a function of cavitation testing time was monitored. The sample exposure interval and the total testing time were adjusted to the behavior of the samples during the experiments (min): 15; 30; 45; 60.

After each test interval, the samples were dried at 110°C for 1h and then the mass of the samples was measured using an analytical balance with an accuracy of ± 0.1 mg. Measurements were performed individually for each sample after all cavitation test intervals, for a total test time of 60 min. Obtained results calculated for the coordinate system: mass loss (ordinate) and exposure time (abscissa). The diagram shows relation between mass loss and testing time, where the lines were drawn by least-square method and data can be expressed by a straight line. The slope of the straight line represents the cavitation rate. The change in the surface morphology of the samples with the testing time was monitored using scanning electron microscopy ("JEOL" model JSM 6610 LV).

3. RESULTS AND DISCUSSION

The test results of the obtained A composite showed that in the case of B composite, grouping and uneven distribution of reinforcements in the composite appear in some places. The examination revealed weak points in the structure of individual samples where cracks appear during deformation (Fig. 2.b), which also affected the lower values of mechanical properties of B composite. The testing results of the mechanical properties of A composite A and B composite are shown in Table 1.

Table 1. Mechanical properties of composite samples

Samples	Tensile strength (MPa)	Hardness Shore
A	19,97	96
B	18,61	95

Composites with epoxy resin matrix and unsaturated polyester resin and reinforcements based on basalt powder with a particle size of 20 µm (designations of composite series: A, B) were subjected to cavitation resistance testing using ultrasonic vibration method with a stationary sample according to ASTM G32.

Fig. 2 shows the samples of A composite and B composite at the end of the cavitation testing for 60 min.

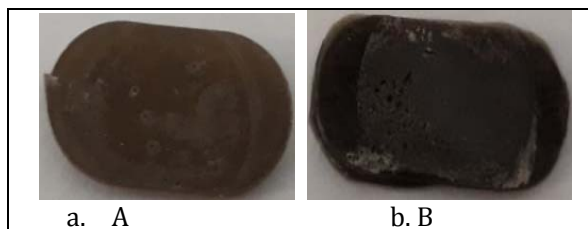


Fig. 2. Samples of A composite and B composite at the end of the testing time (60 min)

During the cavitation resistance test, the change in the mass of the composite as a function of the exposure time was monitored, Fig. 3. Based on the results of mass loss measurements during the test, cavitation rates were calculated as an indicator of the resistance of the samples to the action of cavitation. Cavitation rates were

calculated as the total mass loss at the time of cavitation testing. Composite samples tested for cavitation showed the following cavitation rates: $V_A=0.73$ mg/min and $V_B=0.91$ mg/min.

The results show that A composite has a significantly lower value of cavitation rate compared to B composite, which shows that this composite with epoxy resin matrix has higher resistance to cavitation compared to composite with polyester resin as matrix. It has been shown that the presence of larger grains of the reinforcements leads to its uneven distribution in the polymer matrix as well as the accumulation of grains in certain places in the matrix. These are potentially weak points, which reduce the resistance of composites to the action of cavitation. Formation and development of damage to the surface of samples under the action of cavitation are manifested in the form of shallow and deeper pits, located most often in places where the accumulations of reinforcements are located and where there is an unbalanced place in the composite, Fig. 2. Larger reinforcement grains prevent a higher proportion of reinforcements in the composite. It is considerably more favorable in case of smaller dimensions of grain. Then there may be higher proportions of reinforcements in the composite, which would contribute to obtaining composites with better characteristics.

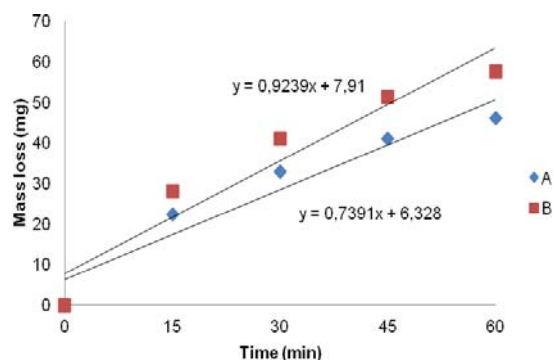


Fig. 3. Cavitation rate diagram of composite A and composite B

Fig. 4 and Fig.5 show SEM micrographs of the surfaces of the samples of A composite and B composite before the test (0 min) and at the end of the test (60 min) under the action of cavitation (magnification 500x).

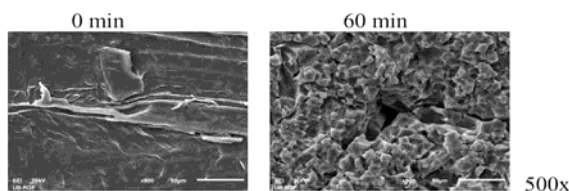


Fig. 4. SEM microphotographs of the A composite sample surface before (0 min) and after cavitation testing (60 min)

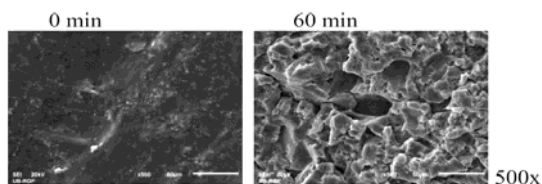


Fig. 5. SEM microphotographs of the B composite sample surfaces before (0 min) and after cavitation testing (60 min)

Composite A, epoxy resin/basalt powder show lower cavitation rate ($V_A = 0.73$ mg/min) compared to composite B, polyester resin/basalt powder where the cavitation rate was higher ($V_B = 0.91$ mg/min), shown in Figure 3. Also, samples A showed higher values of tensile strength and hardness than samples B with a polyester resin matrix, Table 1. This suggests that A composite have better cavitation resistance than B composite.

Both types of composites can be applied in conditions of lower cavity loads.

Analysis of SEM micrographs of composite samples shows that after 60 min of cavitation, the surface changes and pits are formed. In the case of A composite, shallower pits are formed, which indicates a lower level of damage to the surface of the samples after cavitation for 60 min, Fig.2a and Fig.4. In the case of B composite, larger and deeper pits are created, which join and thus increase the level of damage to the sample surface, Fig. 2.b and Fig.5.

Acknowledgement

This work was supported by the Ministry of Education, Science and Technological Development of the Republic of Serbia (Contract No. 451-03-9/2021-14/200135)

CONCLUSION

Based on the results of determining the cavitation resistance of two types of polymer matrix / basalt powder composites, it can be concluded that satisfactory properties of the resistance of composites to the action of cavitation have been obtained. Tests have shown that the properties of the obtained composites are greatly influenced by the matrix of the composite. In A composite the matrix was epoxy resin, while in B composite the matrix of the composite was recycled polyester resin. It has been shown that the matrix of epoxy resin affects the production of composites with better properties, both mechanical properties and properties of resistance to cavitation. Epoxy resin polymerized faster compared to polyester resin, which had an influence on the composite synthesis process.

REFERENCES

- [1] Chawla, K.K., (1998). *Composite materials science and engineering*, 2nd ed. New York, Springer-Verlag.
- [2] Akinci, A., (2009). Mechanical and morphological properties of basalt filled polymer matrix composites, *Archives of Materials Science and Engineering*, vol.35, no. 1, p. 29-32.
- [3] ASTM G32-10, Standard Test Method for Cavitation Erosion Using Vibratory Apparatus, ASTM International, West Conshohocken, PA, 2010, www.astm.org, n.d
- [4] Brennen, C. E., (1995). *Cavitation and Bubble Dynamics*, Oxford University Press, Inc., New York.
- [5] Dožinović, M., (2013). *Razaranje materijala pod dejstvom kavitacije*, Tehnološko-metalurški fakultet, Beograd.
- [6] Franc, J. P., Michel, J. M., (2004). *Fundamentals of Cavitation*, Kluwer Academic Publishers, Dordrecht.
- [7] Pavlovic, M., Dožinovic, M., Prokic- Cvetkovic, R., Andric, Lj., (2019). Cavitation resistance of composite polyester resin/basalt powder, *Structural integrity and life*, vol. 19, no. 1, p. 19–22.
- [8] Pavlovic, M., Dožinovic, M., Prokic- Cvetkovic, R., Andric, Lj., Ceganjac, Z., Trumbulovic, Lj., (2019). Cavitation wear of Basalt Glass Ceramic, *Materials*, vol.12, p.1552. DOI: 10.3390/mai12091552

Quality and Ecology



Banja Luka
28–29 May 2021.

DEMI 2021

15th International Conference on Accomplishments in Mechanical and Industrial Engineering

www.demi.mf.unibl.org



Energy Management System Application in Healthcare

Milena Rajić^a, Rado Maksimović^b, Peđa Milosavljević^a, Dragan Pavlović^a

^aFaculty of Mechanical Engineering, University of Niš, Address: Aleksandra Medvedeva 14, Niš, Serbia

^bFaculty of Technical Sciences, University of Novi Sad, Address: Trg Dositeja Obradovića 6, Novi Sad, Serbia

Abstract *The paper presents the application of an energy management system in healthcare institutions as the one with constant and strict demand for energy. Hospitals and healthcare facilities in general, need to manage energy use more effectively and setting targets to reduce the consumption of fossil fuels and electricity. Energy Management System (EnMS), with defined energy policy, energy goals and ways to achieve these goals, forms a system for monitoring energy performance and implements procedures for a continuous improvement of energy performance. The ISO 50001 standard for energy management systems considers the energy performance achieved by an individual institution. The standard proposes a management model that was used for presented research. As healthcare institutions consume large amounts of energy, ranking the second highest energy-intensive buildings in the commercial sector, the special focus should be in this sector. The analysis results provide data on the scientific level for the national policy improvement, as well as a developed model based on the Plan Do Check Act (PDCA) cycle for energy management system application. The aim was to determine the current situation regarding the application of energy management practices in such facilities.*

Keywords *energy management, ISO 5000, healthcare*

1. INTRODUCTION

Healthcare centres are considered to be large consumers of energy, even ranking the fifth highest energy-intensive buildings in the commercial sector [1-3]. The high energy intensity of building that belongs to healthcare system are subjected to energy-intensive system that are required to operate at full scale, with the full energy load, 24h a day. This continuous operational requirement has as a consequence high energy costs. Also, in the case if healthcare centres facilities, electricity loads are not constant, due to sensitive load requirements. Having that in mind, this can

result into substantial electricity costs while installed equipment operates through peak periods of time, with highest electricity costs [3-6]. Numerous researches had been done with the aim to improve energy efficiency of specific systems [7-8]. Even though, there are a few specific scientific papers about energy efficiency measures in healthcare facilities or buildings.

Energy management system is offering many benefits, such as optimizing energy consumption, reducing costs, reducing the negative impact on the environment. Having that in mind, organizations have developed other suitable approaches to energy management, having the goal to reduce energy losses [9-13]. Energy Management System (EnMS) begins with an energy policy, defines energy goals and ways to achieve these goals, forms a system for monitoring energy performance, and implements procedures for a continuous improvement of energy

Corresponding author

dr Milena Rajić
milena.rajic@masfak.ni.ac.rs

Faculty of Mechanical Engineering, University of Niš,
Address: Aleksandra Medvedeva 14, Niš, Serbia

performance [14]. The ISO 50001:2011 standard does not include specific energy performance criteria related to energy consumption and energy efficiency. But it proposes a management model that contributes development and implementation of the energy policy in order to achieve the defined objectives and action plans. With fully defined legal requirements and information resulting from the analysis and proper management of energy consumption.

The presented study includes the methodology based on the PDCA model from the ISO 50001 standard. It has the aim to identify the current state of EnMS implementation and energy management awareness in the medical sector in Serbia. The analysis was performed by using a questionnaire with ISO 50001 requirements, presented in [15]. The collected results of the questionnaire were evaluated according to the analytical framework that covers organizational characteristics and conditions. The presented study represents the basis of scientific data for improving the national energy policy as well as planning activities within the implementation of the ISO 50001 standard in terms of sustainability.

2. METHODOLOGY

Research was performed by using a questionnaire and data was collected from interviews also in hospitals and health centres that belong to the medical centres in Serbia. Seventeen healthcare centres participated in this research. The research sample used includes different territories of the Republic of Serbia. This kind of research of healthcare centres has never been done in Serbia so far. It is important to emphasize that the size of the organization, the level of its development (how many years has been present), influence different approaches to the energy management system. It was of great importance that managers, quality and facility managers and, where applicable, energy managers respond to the questionnaire. Statistical methods were applied for data processing. The average, standard deviation, and minimal and maximal values were calculated for the analyzed parameters. In the first part of the questionnaire, some basic information was collected. It is important to emphasize that not only public medical healthcare centres were

included in this research, but also private ones, with specific specialization in one field. It also represents the special contribution to the research. The majority of organizations in research sample are, in fact, micro organizations (up to 10 employees) 41.18%, followed by small organizations (from 11 to 50 employees) 35.29% and medium-sized organizations (from 51 to 250 employees) 17.65%, and finally large organizations (more than 251 employees) with only 5.88%. As it was mentioned, the first part of the questionnaire was related to the organizations' profile, but not only its size (number of employees), but also the centre surface area, with all accompanied facilities. The surface area of the organizations in the research sample is in the range from 100 m² to 180,000 m², with the average value 11,870.59 m², while the standard deviation of 43,353.29 m² indicated that the organizations had a large deviation of the area in the sample. It was important to have in mind that the organizations show any interest in and make efforts to apply current standards, and how many of them have a certified management system. The majority have implemented ISO 9001 (Quality Management System)—82.35% organizations, but also ISO 14001 (Environmental Management System)—64.71%, and ISO 45001 (Occupational Health and Safety)—64.71%. The number of organizations that have not implemented any management system is 3 (17.65%), which represents critical data for further analysis. The majority (70.59%) has been present more than 10 years, 5.88% of the organization 5-10 years and 17.65% 3-5 years, while 5.88% of the research sample has been present for only up to 3 years.

For the second part of the questionnaire, which represents the energy profile of organizations, it was important to obtain the data about the age of equipment installed. Old and non-serviced equipment was considered to be energy-inefficient. The largest number of organizations (52.94%) indicated that the average age of the installed equipment was between 5 to 10 years, 23.53% own new equipment up to 5 years old, while 23.53% operate with equipment that is older than 10 years. In order to define the energy profile of an organization that depends on the complexity of processes and equipment installed, a part of the questionnaire required data about the number of used energy sources,

such as electricity, natural gas, oil, compressed air, overheated water vapour, solar energy, wind energy, geothermal energy. The majority (76.47%) use only one or possibly two energy sources, while 17.65% of the enterprises use 3 and 5.88% 4 different energy sources. The interviewed organizations assessed how many significant energy consumers they had and what their average annual energy consumption was: 41.18% of organizations indicated that they have fewer than 5 critical or significant consumers, 23.53% between 6 and 10 crucial consumers, and 35.29% more than 11, while 11.76% of the researched organizations have the annual energy consumption less than 200TJ; 64.71% between 200 TJ and 2000 TJ; 5.88% between 2000 TJ and 10,000 TJ, and 17.65% more than 10,000 TJ. These data provide the basis for further energy audits and energy consumption monitoring, as well as control and monitoring of key energy consumers within the centres. In this part of the questionnaire, there was data concerning the number of people that are in charge and have any connection with energy management within the organization, in order to assess the willingness to implement the energy management system. According to the results, 64.71% of the research sample has only one person in charge of energy management. On the other hand, 11.76% of the research sample has 3 persons dealing with this issue, 11.76% of the sample has 2 persons, while 11.76% do not have any employed person who can in any way monitor the energy consumption or propose energy savings.

3. IMPLEMENTATION OF ENERGY MANAGEMENT SYSTEM IN HEALTHCARE

The ISO 50001 standard provides support to organizations regarding a more efficient energy use through the implementation and development of an energy management system (EnMS). The model of EnMS is based on the PDCA (Plan-Do-Check-Act) model cycle. The presented model was used, but also developed healthcare purposes and medical centers that are present in Serbia. It includes a model for systematic observation and measurement of the implementation level of energy management in an organization. It can be easily used for further research in other countries. It should be emphasize that if the organization does not have a certified energy management system, it

does not necessarily mean that it does not apply it in certain parts. The questionnaire that is used is given as the part of the research done in 2018-2020 [15].

3.1 Energy Planning and Identifying the Energy Management Organization Basis - The PLAN Phase of EnMs

The first phase of EnMS represents energy planning or the PLAN phase, and the whole EnMS base is considered to be defined in this phase. The researched organizations do not have a systematic energy management approach in general, but it is necessary to emphasize that achieving energy savings by reducing energy consumption requires time as one of the long-term goals. Namely, the average application of the PLAN phase in this research was 40.51%. This means that the organizations do not show willingness for energy planning. The average response about the implementation of the systematic approach was 34.56%. Having that in mind, it can be notated that special efforts are needed in order to inform and raise awareness, educate, and train employees. It is important also to have responsibility and managerial authorization in the organization to fulfill requirements of the energy management system. Within the systematic approach, 32.35% of the organization had implemented a system through which they monitor, document, and maintain energy consumption in processes. This group certainly includes organizations that have certified ISO 14001 as well. When it comes to the issue of the application area of the energy management system (whether it refers to the whole center, part of it), 32.35% of the organizations recognize which part of their building is the most significant from the aspect of energy use. The rules and procedures of an organizations are in the form of a documented procedure according to the requirements of EnMS. Data analysis shows that only 29.41% of organizations stated that there had been a document/procedure that somehow determines effective energy management (which may be an integral part of the rules of procedure, but it does not have to be). 44.12% of the research sample stated that they had an organizational system that includes a continuous improvement of the performance of the energy system, as well as energy efficiency. It implies that the existence

of a system is not enough, but it is necessary to constantly monitor and control energy indicators that are directly related to the rational use of energy and efficiency of the system. The system approach to energy management according to the ISO 50001 standard belongs to the systematization of the PLAN phase, which also includes the part referring to leadership, energy planning, requirements of standards and regulations related to energy, energy profile of the organization, as well as energy goals. The support of the organizations' management is crucial for the implementation of any management system in almost all organizations, regardless of size.

The average implementation level regarding leadership in EnMS is 63.73%. The results show that 58.82% of organizations clearly define and determine responsibilities as well as competences in order to ensure effective energy management. Support of the management to promote the importance of energy savings and energy efficiency, 64.71% of the researched organizations responded that the management emphasizes and promotes the importance of energy efficiency and effective energy management at all levels. Very significant share of researched organizations 67.65% responded that the management raises the awareness of energy efficiency among employees.

Energy planning or an energy consumption plan according to ISO 50001 contains regulations that are important for monitoring and eventual improvements in energy performance within an organization. The average level of the implementation of energy planning in organizations' activities is 32.35%. The plan of energy consumption represents a mandatory part of the reports made and submitted by individual organizations to the Ministry of Mining and Energy of the Republic of Serbia (especially the public property). The collected data related to energy planning indicate less than 50% of positive results of the research. Namely, 47.06% of the surveyed organizations include energy performance of the processes, procedures in long-term plans, while 14.71% of organizations have a full defined plan of energy use, energy savings, and system performance that is necessary to achieve in a defined period, and 35.29% define their plan of activities related to the energy performance of the system.

Regarding the legal requirements and regulations that are mandatory, organizations had different attitudes regarding legal requirements that do not have mandatory legal application, for example, standards such as ISO 50001. The average level of application of requirements of EnMS standards and regulations is 29.41%. The analysis of the research results, 26.47% of the researched organizations identified, applied and had access to the appropriate requirements defined by legislation (regulations, rules) related to energy use, energy consumption and energy efficiency. And 32.35% ensured that these requirements were respected and monitored at a certain period.

In this phase, the organizations defined their energy profile. The energy profile was determined by the implementation of energy audit procedures. An energy audit can be defined according to data given in [17] as a systematic control and analysis of energy use and energy consumption of the system or enterprise, with the aim of identifying energy flows and possibilities of improving energy efficiency. The researched organizations with defined requirements for the energy profile was 44.96%. The research data showed that 41.18% of organizations have energy audits, which indicates the extent to which the energy performance of the system within the organization is controlled and monitored. This data indicates the insufficient willingness of the organizations to include in their business processes the optional audits related to energy consumption, which is very discouraging, since 64.71% of the researched organizations had implemented ISO 14001, which implies monitoring of energy consumption and determination of critical consumers. Only 23.53% of organizations had clearly defined methodology and criteria for the development and implementation of energy audits. It means that there is no clear methodology or procedure for audits. Knowing that, in order to develop and improve energy audits, it is necessary to analyze the energy use and/or consumption within the enterprise and to have detailed measurement and identification of current energy sources. At this stage, 52.94% of the surveyed organizations showed willingness for it. Regarding the data on the current energy consumption, as well as the archives of old energy consumption data, the results are quite

satisfactory. Namely, 76.47% of organizations had records of energy consumption in the past, so that they can compare it with the current consumption; 50.00% of organizations document energy consumption and energy costs for a certain period; 50.00% of organizations considered possibilities for energy savings and energy efficiency at regular meetings (monthly, quarterly). One of the criteria for defining the organizations' energy profile is to determine the current state of the existing building and facilities using standard methodologies, such as building certification and obtaining a building energy passport. The information on the existence of a building energy passport that an organization owns or uses (administrative building, facility centers etc.) was present in only 20.59% of the researched organizations.

The researched organizations apply an average of 30.39% of requirements in terms of defining energy goals. In order to achieve certain organizational goals, the management should also define an action plan for achieving certain general or specific energy goals. For clearly defined goals and constraints related to energy consumption in an organization, 44.12% of the researched organizations responded that they have clearly defined goals and limitations related to energy consumption. When it comes to action plans that should result from the defined goals, 29.41% of organizations define the action plans for achieving energy consumption targets, in which specific tasks, necessary resources, deadlines, as well as responsibilities of employees regarding the fulfillment of those tasks are defined. The research data shows that only 17.65% of organizations actually implement previously defined action plans for energy savings, as well as monitor energy consumption. When defining energy goals in organizations, the limiting factor is definitely the lack of financial resources for the reconstruction and installation of equipment, machines, and devices, in order to achieve better energy performance. Medical organizations also stated that there are no corresponding supporting funds or proper budget planning from the state budget or any other available funds, in order to consider purchasing new equipment or planning reconstruction. This certainly influences defining and predicting action plans, because without adequate financial means it is

impossible to make important changes in the performance of production processes. Figure 1 represents the implementation of the PLAN phase in healthcare organizations in Serbia. Full implementation of planning in energy management is not present in any organization, and 11.76% of organizations apply at least some phase of the activities in the PLAN phase of energy management. The average implementation of the PLAN phase in the research sample is 40.51%, which means that energy management planning has been implemented, but still not present sufficiently.

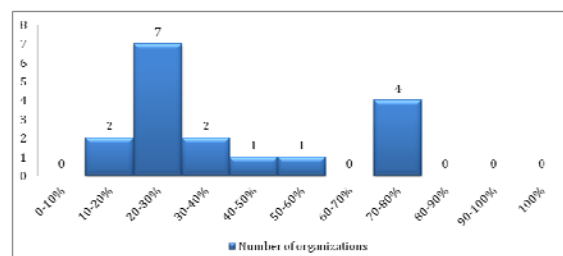


Fig. 1. Application of the PLAN phase in medical organizations in the research sample

From the histogram in Figure 1, can be concluded that 70.59% of the organizations have a level of application of requirements for the energy management system in the PLAN phase below average, while the percentage of organizations above average is 29.41%. With these results it can be concluded that most of the organizations in the sample are far below the average application of the PLAN phase requirements for the energy management system. The full implementation of the requirements for the energy management system was not found in the research sample.

3.2 Implementation of the Energy Management System - The DO Phase of EnMs

The second phase of the energy management model according to ISO 50001 is the DO phase, which represents the absolute inclusion of employees, communication within the organization, an energy-related documentation system, as well as a process approach to energy management. The entire documentation system can be divided into the one that can provide guidance on how to implement activities, and the other that confirms that an activity has been performed. For successful organizations, both

forms of reporting and communication are necessary. Also, without motivation and involvement of employees in energy management, there can be no significant improvement. Firstly, it is necessary to inform and then motivate employees to take part in improving energy efficiency. 24.96% of the researched organizations had the average level of applying the requirements that relate to the inclusion of employees according to the requirements of EnMS. If employees are not motivated and do not see the significance of it, they will not be able to achieve great improvements in the process itself, which will in turn result in possible savings. Therefore, employees need to be informed about the importance of energy performance and energy efficiency of processes and then motivated by the management to fully participate in the implementation of EnMS. Employee motivation should also be reflected in free communication and submission of proposals for energy efficiency.

The data related to whether employees in their annual/monthly/weekly reports include data related to energy consumption shows that 20.59% of the organizations in the sample responded positively. Also, 32.35% of the researched organizations motivate employees to have activities in which they monitor, measure, document, or report on energy consumption at any level. The data regarding employees training shows that only 20.59% of respondents provide employees the opportunity to attend or complete any training, course, or lecture related to effective energy use and energy management. Employee training is very important, both for organizations and themselves for the energy management system implementation, as well as for monitoring actual trends and news in that field. Less than one third of the organizations, or more precisely 23.53%, indicated their readiness to organize training and/or employee meetings regarding education on energy management and its significance. This result indicates the lack of leadership in terms of promoting the significance of energy performance of processes and organization in general.

Communication related to energy management gives possibility to managers and employees to be informed about all problems related to energy consumption, saving measures, and process improvements. In order to achieve

energy goals in advance, through defined action plans, it is essential that employees freely communicate on all relevant data. The researched organizations gave a very satisfactory response in this part of research. Namely, the average level of application of the requirements concerning communication within the enterprise in terms of energy management is 23.53%. According to the answers, it can be concluded that there is free communication in organizations and that the management encourages an exchange of information on energy management. The share of 18.82% of the researched sample exchange information related to energy consumption or energy use (in meetings, mail transcripts, etc.). It is significant that 25.29% of organizations encourage free communication related to energy savings, and that 26.47% of the surveyed organizations encourage employees to make suggestions and comments related to improving energy efficiency of individual processes.

Very often, the management exchanges its own experience of energy management with other similar organizations (through its associations, clusters, various fairs, etc.) and thus come up with ideas for possible energy savings and improvement opportunities. EnMS documentation points out the existence of procedures and rules for document management and is related to energy consumption, energy savings, and improvement proposals. Documentation system in organization can be divided into documents that indicate the execution of a certain activity, as well as the manner of execution, and documents that indicate performed activities, results, and measures for improvement. In addition to the existence of certain documentation, it is very important to prescribe the appropriate procedures for document management, archiving, reporting, traceability, and priority. In this part of the research, the average level of requirement applications was 32.06%. Medical organizations do not use enough written reports, procedures, etc. related to energy management. For individual answers, 41.18% of organizations stated that they had some sort of documentation related to energy management, referring to all procedures, plans, reports, activities, instructions, etc. Additionally, 22.94% of organizations have clearly defined procedures for managing documentation

related to energy management. For most organizations, the documentation related to energy management is part of the documentation related to the environmental management system, as well as the quality management system. The existence of documentation management procedures mainly relates to methods of issuing, authentication, archiving, or modification of documentation, which relate to energy management, but organizations do not possess any software that would manage this documentation system in any way.

To have proper monitoring of the operational processes within an organization, it is necessary to identify all processes, with all sub-processes, activities, necessary resources, and engaged personnel. All processes in an organization convert the input (raw material, information) into the output (product or/and service that is further allocated to the buyer). In order to identify and adequately describe and define business processes, it is also necessary to identify the energy flows in all processes, as well as those processes that have enviable or inadequate energy performance and thus significantly influence the energy efficiency of the process and the enterprise as well. The average level of application requirements within the process approach is 57.75% for the researched enterprises. Regarding the process approach to energy management, 53.53% of organizations know and can identify processes that significantly influence energy consumption. This data is very important because it shows that the management in these organizations is aware of energy consumption and energy performance in certain processes or parts of the process. It also indicates the readiness of the enterprise for optimum energy consumption. This is indicated by the fact that 36.35% of the researched organizations can identify processes where it is possible to increase energy efficiency. In order for machines, devices, units to work properly and without any losses in the production process, it is necessary to comply with all instructions for use, maintenance, and servicing. 76.47% of the researched organization have clearly defined procedures related to the operation and maintenance of machines, tools, and equipment.

Figure 2 shows the application of the DO phase in medical centres in Serbia. Full implementation of the activities of the

management system in the DO phase is not present in any researched centres. The average implementation of the DO phase is 43.68%, indicating that the implementation of the energy management definitely has potential for improvement. It can be observed that 29.41% of organizations have a level of application of requirements for the energy management system in the DO phase below average, while the percentage of organizations above average is 70.59%.

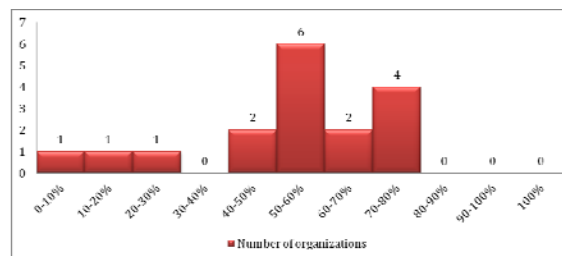


Fig. 2. Application of the DO phase in medical organizations in the research sample

3.3 Monitor, Measure and Analyze Business Process - The CHECK Phase of EnMs

Factual based decision-making represents an integral phase of the CHECK phase of the EnMS model according to ISO 50001. Factual based decision-making represents one of the eight principles of quality management. For an organizations' management to make a decision based on facts, there should be a developed system of data collection and processing, so that they can be available for comparison, analysis and forecasting. The researched sample stated positively in this part, namely, the average level of application that relates to factual based decision-making was 52.57%. The obtained data indicate the need for energy managers to educate themselves in the implementation of techniques and tools for collecting, processing data, and making trends and forecasting analysis, which would be easy to use for the organizations' management, on the basis of which they should make important business decisions, plan certain activities, and include them in the organizations' strategic plan.

It was quite significant that 67.65% of the researched organizations know and can define the largest consumers within their centre. But 58.82% of the research centres determine the current energy performance installed equipment, system, or processes, in order to

identify significant energy consumers. As far as cost prediction is concerned, 50.00% of the researched sample can estimate energy consumption, as well as expected costs in the future, based on their current costs, consumption, and predetermined plans and targets. In 58.82% of organizations, a list of priorities related to possibilities for improving the energy performance can be identified and is being made. Additionally, 61.76% of the researched sample follows the development of new devices, systems, and production lines that have better energy performance. In 58.82% of the researched sample, there is a person within the medical centre that deals with monitoring, recording, and reporting on energy consumption and system savings in a certain way. In 44.12% of organizations record of all significant accidents or deviations related to the variation in the expected energy consumption. Additionally, only 20.59% of organizations possess evidence of how much energy is spent on their each medical service. This data refers to the cost of service through the use of energy.

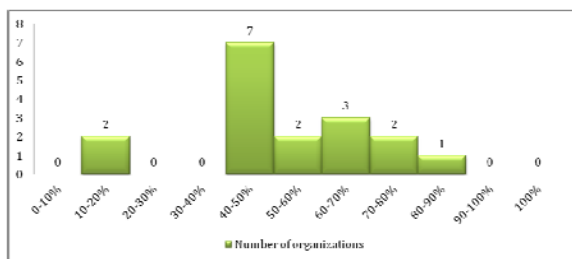


Fig. 3. Application of the CHECK phase in medical organizations in the research sample

Figure 3 shows the implementation of the CHECK phase in medical centres in Serbia. Full monitoring of the functioning and effecting of the energy management system is not present in any medical center and very low implementation is present in even 11.76% of research sample. The implementation of the CHECK phase is 52.57%, which shows that controlling and monitoring the energy management process is on the satisfactory level. From the histogram (Figure 3) it can be observed that 52.94% organizations have a level of application of requirements for the energy management system in the CHECK phase below average, while the percentage of enterprises above average is 47.06%. More than half of the enterprises are below the average

application of requirements of the verification phase, the monitoring or the functioning of EnMS.

3.4 Management Review and Continual Improvements - The ACT Phase of EnMs

Reviews and continuous improvements are the basis of the ACT phase of the energy management model according to the ISO 50001 standard. Internal audits and reviews of EnMS conducted by the management represent the opportunities to determine the current state regarding the energy performance as well as to consider possible ways of improvement. The average level of application within this requirement of energy management is 26.47%. The research results show that 29.41% of research sample conducted management reviews of energy management (spending, saving, increasing energy efficiency), while 47.06% of organizations defined corrective actions and/or plans related to the current problem of energy consumption at the quarterly and/or annual level. As for preventive measures, actions and/or plans related to energy management 38.24% of medical centres recognized their definitions as very important and implemented them in a certain period. However, 20.59% considered that the opinion of their patients was not formed based on the rational energy use within their enterprise. Additionally, 8.82% of organizations considered that energy savings in process activities are in direct relation to the satisfaction of consumers' expectation. The organizations are not engaged by independent auditors for energy management audits, only 3.82% employ external energy audit experts. Finally, 12.35% of organizations stated that their management defines the plans for the next period of actions, which will improve the process of production/provision of services in terms of energy management. Figure 4 shows the ACT phase in the medical centres in Serbia. A complete review and improvement of the energy management system is not present in any researched centre in the sample, while very low implementation of this phase is present in no fewer than 29.41%. The average application of the ACT phase is 26.47%, indicating that the review and improvement of the energy management system is insufficiently present in the research

sample and that it is necessary to concentrate further reviews at this stage.

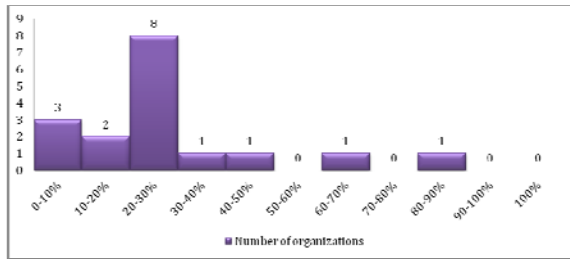


Fig. 4. Application of the ACT phase in medical organizations in the research sample

Regarding the distribution of the organizations in the research sample, the level of application of requirements for energy management system in the ACT phase is below average in 88.23% of the given sample, while the percentage of organizations above average is only 11.76%. A situation is quite different from the other stages of the application of the requirements of the management system. At this stage, additional efforts are needed to bring closer to the requirement of reviewing and improving energy management systems, thus completing the PDCA cycle.

4. DISCUSSION

Research results shows that the level of application of energy management in medical centres in the research sample, observing the international standard ISO 50001 requirements implementation, is in the range of 0 to 98 points, which is also the maximum number of points that organizations could get, counting all question groups that are used in the survey. The average points scored by the enterprises in the sample were 42.82. The average level of application, if the whole survey is taken into account, is 43.70%. The medical organizations in Serbia generally have a systematic approach to energy management, but it is not on a satisfactory level. It points to the not sufficient willingness of the management to implement this management system. However, energy planning is present in the strategic planning of organizations that had participated in the research. The documented system, as well as the involvement of employees is existent but not sufficient, and therefore there is no energy policy that would clearly define the directions

for the implementation and development of an energy management system, as well as the review of the system and the implementation of proposed improvements. In order to present the results on a scale of 0–100%, the analysis uses data of the percentage for the energy management system requirements application, which is calculated on the basis of the points obtained.

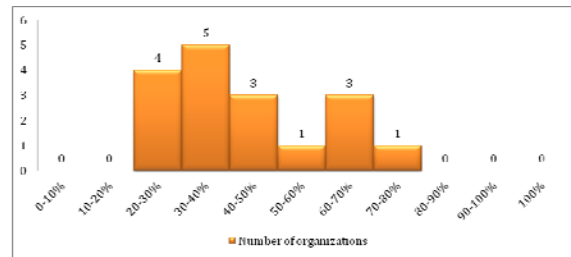


Fig. 5. Implementation of energy management systems in medical organizations in Serbia

From the histogram presented in Figure 5, it can be concluded that 70.59% of the organizations have a level of requirements application for EnMS below 50%, while the percentage above 50% is 29.41%. The full requirements implementation for the energy management system was not found in any organization in the sample. No similar study for medical organizations has been made, so that the results of the conducted research could be compared with. The presented model could represent the basis for future more detail research done in this field.

5. CONCLUSION

According to the presented results, it can be said that the average medical centre in Serbia, in terms of the energy management system, can be described as follows: The system approach is not implemented; top management is not completely committed to energy management and not sufficient measures are planned; energy policy is generally not defined; energy use is planned partly; employees are involved in energy management, but there is place for improvement; communication on energy management is not frequent enough; documentation system is not at satisfactory level; energy indicators serve to monitor the achievement of energy goals; the data collected through monitoring and measurement are

analyzed; data and trends are reviewed, but often not applied, as there is often no financial basis for implementing the improvements provided by the data from the analysis.

By having reduced energy costs and therefore reducing energy use, represent the priority for every organizations as well as the country. As the ISO 50001 standard was revised and harmonized three years ago, it is expected that in the forthcoming period, a package of laws and procedures regarding greenhouse gas emissions would be adopted in Serbia.

Acknowledgement

This research was financially supported by the Ministry of Education, Science and Technological Development of the Republic of Serbia (Contract No. 451-03-9/2021-14/200109).

REFERENCES

- [1] Pérez-Lombard, L., Ortiz, J., Pout, C. (2008). A review on buildings energy consumption information. *Energy Build*, vol. 40, p. 394–398. DOI: [10.1016/j.enbuild.2007.03.007](https://doi.org/10.1016/j.enbuild.2007.03.007)
- [2] Allouhi, A., El Fouih, Y., Kousksou, T., Jamil, A., Zeraouli, Y., Mourad, Y. (2015). Energy consumption and efficiency in buildings: Current status and future trends. *J. Clean. Prod.* vol. 109, p. 118–130. DOI: [10.1016/j.jclepro.2015.05.139](https://doi.org/10.1016/j.jclepro.2015.05.139)
- [3] Hohne, P.A., Kusakana, K., Numbi, B.P. (2020). Improving Energy Efficiency of Thermal Processes in Healthcare Institutions: A Review on the Latest Sustainable Energy Management Strategies. *Energies*, vol. 13, no. 3, p. 569. DOI: [10.3390/en13030569](https://doi.org/10.3390/en13030569)
- [4] Nour, M., Sindi, H., Abozinadah, E., Öztürk, S., Polat, K. (2020). A healthcare evaluation system based on automated weighted indicators with cross-indicators based learning approach in terms of energy management and cybersecurity. *International Journal of Medical Informatics*, vol. 144, p.1-11. DOI: [10.1016/j.ijmedinf.2020.104300](https://doi.org/10.1016/j.ijmedinf.2020.104300)
- [5] Mariano-Hernández, D., Hernández-Callejo, L., Zorita-Lamadrid, A., Duque-Pérez, O., Santos García, F. (2021). A review of strategies for building energy management system: Model predictive control, demand side management, optimization, and fault detect & diagnosis. *Journal of Building Engineering*, vol. 33, p.1-12. DOI: [10.1016/j.jobbe.2020.101692](https://doi.org/10.1016/j.jobbe.2020.101692)
- [6] Morgenstern, P., Li, M., Raslan, R., Ruyssevelt, P., Wright, A. (2016). Benchmarking acute hospitals: Composite electricity targets based on departmental consumption intensities? *Energy and Buildings*, vol. 118, p. 277-290. DOI: [10.1016/j.enbuild.2016.02.052](https://doi.org/10.1016/j.enbuild.2016.02.052)
- [7] Amowine, N., Ma, Z., Li, M., Zhou, Z., Azembila Asunka, B., Amowine, J. (2019). Energy Efficiency Improvement Assessment in Africa: An Integrated Dynamic DEA Approach. *Energies*, vol. 12, no.20, p.1-17. DOI: [10.3390/en12203915](https://doi.org/10.3390/en12203915)
- [8] Aydin, Y.C., Mirzaei, P.A., Akhavanasab, S. (2019). On the relationship between building energy efficiency, aesthetic features and marketability: Toward a novel policy for energy demand reduction. *Energy Policy*, vol. 128, p. 593–606. DOI: [10.1016/j.enpol.2018.12.036](https://doi.org/10.1016/j.enpol.2018.12.036)
- [9] Introna, V., Cesarotti, V., Benedetti, M., Biagiotti, S., Rotunno, R. (2014). Energy management maturity model: An organizational tool to foster the continuous reduction of energy consumption in companies. *Int. J. Clean. Prod.*, vol. 83, p. 108–117. DOI: [10.1016/j.jclepro.2014.07.001](https://doi.org/10.1016/j.jclepro.2014.07.001)
- [10] Capehart, B.L., Turner, W.C., Kennedy, W.J. (2006). *Guide to Energy Management*. The Fairmont Press, Inc: Lilburn, GA, USA.
- [11] Petrecca, G. (2012). *Industrial Energy Management: Principles and Applications*. Springer Science & Business Media: New York, NY, USA.
- [12] Piper, J.E. (2016). *Operations and Maintenance Manual for Energy Management*. Taylor & Francis Group: Boca Raton, FL, USA; Routledge: London, UK.
- [13] Rajić, M., Milovanović, M., Antić, D., Maksimović, R., Milosavljević, P., Pavlović, D. (2020). Analyzing energy poverty using intelligent approach. *Energy & Environment*, vol. 31, no. 8, p. 1448-1472. DOI: [10.1177/0958305X20907087](https://doi.org/10.1177/0958305X20907087)
- [14] ISO 50001:2011. (2011). *Energy Management*. International Organization for Standardization. Geneva.
- [15] Rajić, M., Maksimović, R., Milosavljević, P., Pavlović, D. (2019). Energy Management System Application for Sustainable Development in Wood Industry Enterprises. *Sustainability*, vol. 12, no.1, p. 1-16. DOI: [10.3390/su12010076](https://doi.org/10.3390/su12010076)
- [16] CEN/CLC. Report on the CEN/CLC TR 16103:2010. (2010). *Energy Management and Energy Efficiency - Glossary of Terms*. CEN/CLC: Brussels, Belgium.



Banja Luka
28–29 May 2021.

DEMI 2021

15th International Conference on Accomplishments in Mechanical and Industrial Engineering

www.demi.mf.unibl.org



DUST PARTICLES EMISSIONS AT STEEL CUTTING AND WELDING PROCESSES

L. Cigić^a, B. Kosec^{a,c}, M. Ilić Mićunović^b, D. Klobčar^c, Z. Tanasić^d, B. Karpe^a, A. Nagode^a

^a University of Ljubljana, Faculty of Natural Sciences and Engineering, Aškerčeva cesta 12, 1000 Ljubljana, Slovenia

^b University of Novi Sad, Faculty of Technical Sciences, Trg D. Obradovića 6, 21000 Novi Sad, Serbia

^c University of Ljubljana, Faculty of Mechanical Engineering, Aškerčeva cesta 6, 1000 Ljubljana, Slovenia

^d University of Banja Luka, Faculty of Mechanical Engineering, S. Stepanovića 71, 78000 Banja Luka, BiH

Abstract *Oxyfuel cutting, plasma cutting, and gas shielded arc welding are material processing technologies that are strongly associated with particulate matter emissions. These particles have a negative impact on the health of the operator because they penetrate deep into the lungs due to their small size. The impact is determined by measuring the amount of particulate matter emissions, particles morphology, particles chemical composition, and particles size and their size distribution. The methods for measuring and evaluating these parameters are regulated in the standard ISO 13322-1: 2014.*

In our study, the emitted particles generated during flame cutting and plasma cutting of S460 steel and manual arc welding of S460 and AISI 316 steel were analysed. The collection of the particles was performed with the personal particle sampler EGO PLUS TT, the weighing of the particles was performed on an electronic balance, while particle size, their morphology and chemical composition were determined with a field emission scanning electron microscope.

By comparing the measurement results, it was determined how the processing techniques, the processed material and the use of the extraction filter device affect the emission of fine dust to which the operator is exposed.

It was found that both cutting methods produced more particulate matter emissions than manual arc welding. Spherical particles and agglomerates were formed in all cutting and welding processes, consisting mainly of iron as well as other alloying elements oxides.

Keywords *Dust, particles, emissions, steel, cutting, welding*

1. Introduction

To achieve the desired shape of the product, it is necessary to choose the most suitable machining process. If we want to separate two metal parts, the easiest way to do this is to use

metal parts, the easiest way to do this is to use thermal cutting. Flame cutting is most commonly used, where an exothermic metal oxidation reaction is used to melt and cut the material [1]. We also know plasma cutting, which allows the cutting of materials that conduct electricity well, because here the material melts due to the electric arc. In the frame of our investigation work, we chose both the flame and plasma cutting process for cutting S460 structural steel.

Corresponding author

Prof. Borut Kosec
borut.kosec@omm.ntf.uni-lj.si

University of Ljubljana Faculty of Natural Sciences and Eng.
Aškerčeva cesta 12
1000 Ljubljana, Slovenia

In case we want to join two or more metal parts into a permanent, hard and inseparable connection, the welding process is most often chosen. Among all welding methods [2], manual arc welding with a coated electrode is most often used in practice. The only condition for such welding is the selection of a suitable current source and type of electrode coating. Among the types of coating, we know the cellulose electrode, which has been used in the investigation for manual arc welding of structural steel S460 and the rutile electrode, which was used to join AISI 316 stainless steel [3].

Both the flame and plasma cutting process and the manual arc welding process apply to machining technologies that are strongly related to dust particle emissions. These particles are dangerous from a health point of view as they can penetrate deep into the lungs of the operator performing these processes. Therefore, it is very important to determine the level of risk to the human respiratory system that is related to the nature, shape and size of the particles. The resulting particles can be of different sizes, the most dangerous being particles with a diameter of less than 10 μm , which are respiratory particles and due to their small size are most easily dispersed in the working environment [4].

2. PARTICLES FORMED DURING CUTTING AND WELDING PROCESSES

For cutting and welding processes, the resulting particles can be divided into two groups. Namely, these are particles larger than 20 μm . These are caused by metal injection. Another type of particle is represented by particles with a size of about 1 μm , which are the result of condensation of metal vapors. Upon closer analysis, it was found that ultrafine particles (less than 0.1 μm) are also present, representing only about 7% of the total mass of all formed particles.

Chemical analysis of the filters on which the particles were trapped showed that in the welding of aluminum the particles contain organic and elemental carbon, iron and aluminum. In steel welding, however, the particles contained iron, organic carbon, zinc, and copper. The presence of these elements can be attributed to organic coatings on metals, aluminum, galvanized steel or electrodes [5].

2.1 Effects on humans

Adverse effects on humans can be divided into three categories:

1. chemical hazard (caused by particulates and gases),
2. mechanical hazard (electricity, heat, noise, vibration),
3. danger due to radiation (electromagnetic radiation in the area of visible, ultraviolet and infrared waves).

Of all the above, the chemical hazard has the greatest impact, as the resulting flue gases and harmful gases have the most negative impact on human health. Epidemiological studies of full-time welders have shown that they developed febrile illness from inhaling metal fumes, respiratory tract irritation, changes in lung function, lung infections, and an increased likelihood of developing lung cancer [6].

2.2 Classification of particles by size

Basically, dust particles are classified as primary particles resulting from emissions from natural or artificial sources and secondary particles formed due to chemical and physical reactions once they are in the atmosphere. To facilitate the determination of the origin of the particles and the influence of the dust particles, we divide them into predetermined size classes. [20]

Particles can be quantitatively characterized by determining their geometry. After processing the image with the help of software, we get a set of geometric parameters that describe the size and shape of the particle [6].

2.3 ISO 13322 standard

ISO standard 13322, entitled Particle size analysis - Image analysis methods [7], consists of two parts, namely static image analysis and dynamic image analysis. For the purposes of the master's thesis, the first part of the standard describing static analysis will be considered and will be presented below.

The purpose of the first part of ISO 13322 is to recommend when captured images can be used for particle size analysis. The aim of this part of the standard is to give a standardized description of the technique used, whereby the obtained measurements correspond to the

recommendations of the standard and are traceable. This section does not describe the devices used to capture images, but the standard is limited to image sections that are relevant to the correctness of the results in the particle size analysis. The first part of the standard contains calibration verification methods and recommendations for using a certified standard as a reference. Throughout the analysis, errors are taken into account that contribute to the final uncertainty of the measurements. This part of ISO 13322 is useful for image analysis to determine the size distribution of stationary particles. The particles are arranged and fixed in the plane observed with the image capture device. The field of view changes by moving the support on which the particles are or by moving the camera, so it is necessary to ensure that there is no distortion of the captured images. The standard focuses on digital images generated by a light or electron detection system and considers only images that are analyzed using pixel counting methods.

2.4 Measurements

In accordance with ISO 13322, the projection area of each particle, given in pixels, is first measured. This is followed by determining the longest and shortest Feret diameters for each particle, which are also expressed in pixels.

Primary measured particle size parameters with appropriate labels:

- the area of each particle A_i ;
- the longest dimension of each particle, the largest Feret diameter, $X_{Fmax, i}$;
- the shortest dimension of each particle, the smallest Feret diameter, $X_{Fmin, i}$.

With the help of these parameters, the diameter of the equivalent circle x_{CE} and the design factor φ_i can be calculated, which enables an even better inventory of the measured particles.

3. EXPERIMENTAL WORK

The experimental part the work includes the measurement and analysis of particulate emissions produced by the welding and cutting process for structural and stainless steel. Table 1 presents the machining procedures that took place on the selected steels for the case of use and non-use of the suction device.

Tab 1. Machining procedures for selected steels

Steel	Process	Heat source	Type	Suction
S460	Cutting	Flame	Cutter gk TIP200/A	X
S460	Cutting	Plasma	Cutter Lincoln Electric INVERTEC PC100	X
S460	Manual arc welding	Cellulose electrode (arc)	Electrode CELEX E 35 2 C 21	✓
AISI 316	Manual arc welding	Cellulose electrode (arc)	Electrode INOX R 18/8/6 Fe	✓
AISI 316	Manual arc welding	Cellulose electrode (arc)	Electrode INOX R 18/8/6 Fe	X

All steel processing operations were carried out for 1 minute, during which time the produced particulate emissions were recorded with the measuring instrument ZAMBELLI EGO PLUS TT (Figure 1), which had to be pre-calibrated. We first weighed the emitted particles that were trapped on the filter of the device and then evaporated them with carbon. With this, we prepared them for observation under a ThermoFisher Scientific Quattro S scanning electron microscope, where we captured images of the particles on the filter and measured their chemical composition. At the very end, we used the computer program ImageJ to process the captured images and determine the geometry and size of the particles.



Fig 1. Components of measuring instrument ZAMBELLI EGO PLUS TT.

2.4.1 Cutting

The flame cutting process of S460 steel was performed for 1 minute with a gk TIP200 / A flame cutter on acetylene and oxygen. Plasma cutting of S460 steel was also performed for 1 minute with a Lincoln Electric INVERTEC PC100

plasma cutter connected to direct current and a three-phase voltage of 400 V.

2.5.1 Welding

The process of manual arc welding of S460 steel with cellulose electrode took place 1 minute at a current of 120 A and a DC voltage of 25 V. The process of manual arc welding of AISI 316 steel with a rutile electrode took 1 minute at a current of 160 A and a DC voltage of 28 V.

2.6 Sampling

Sampling with this meter can be done spatially or in person. In spatial sampling, the meter is fixed to a specific area in the room, which means that the average amount of dust particles in the measured area is measured. In personal sampling, the meter is located at the operator near his respiratory system.

I decided to choose personal sampling as I was interested in the direct impact of particulate emissions on the operator performing the cutting or welding process. To achieve the desired effect, the mouthpiece of the meter was attached under the airway, 30 cm away from the mouth as shown in Figure 2.



Fig 2. Operator with measuring instrument installed.

Before starting each measurement, it is necessary to calibrate the meter, determine the time of capture of particles and select the filter. Speed, temperature and relative humidity must also be measured during particle capture. The operation of the meter could be compared to the operation of a suction device, as the meter sucks air through a tube attached to a nozzle on which trapped dust particles accumulate that

are large enough to trap the filter. The parameters with the corresponding units and values are shown below and had the same values in all processing operations.

Measured constant parameters during measurements:

1. Room air velocity [m/s]: 0 m / s
2. Room air temperature [°C]: 21 ° C
3. Relative humidity in the room [%]: 50%

Selected parameters:

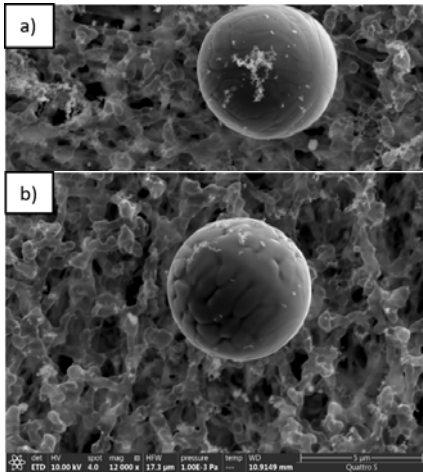
1. Calibration of air flow through the filter [l /min]: 3 l/min (simulates operators breathing)
2. Total particle capture time [min]: 1 min
3. Filter: Mixed cellulose ester filter (MCE).

The results of dust particle emissions showed that the steel cutting process causes about 7 times more emissions than the manual arc welding process. The highest emission of dust particles is produced by the flame cutting process of S460 structural steel, namely 0.096 g/h. At least among all processes, manual arc welding with rutile electrode, which produces 0.006 g/h of emissions. The choice of steel does not affect the change in particulate matter emissions. This can be seen in the case of manual arc welding of S460 structural steel with cellulose electrode and manual arc welding of AISI 316 stainless steel with rutile electrode. Welding of S460 steel produces 0.012 g/h of emissions and, for the case of AISI 316 steel, 0.016 g/h of emissions, indicating a very small difference of only 0.004 g/h.

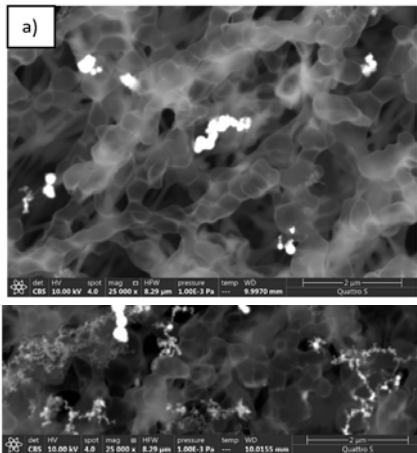
2.7. Analysis of captured dust particles

For particle analysis the ThermoFisher Scientific Quattro S SEM has been used. It is a field emission electron microscope (FEG SEM) that can operate in three different vacuum modes. It operates in low vacuum (up to 200 Pa), in high vacuum ($<6 \cdot 10^{-4}$ Pa) or in ESEM (Environmental Scanning electron microscope) mode (up to 4000 Pa). The highest resolution can be achieved in high vacuum mode by scanning electron microscopy (STEM), which in this case is 0.8 nm. With ESEM and low vacuum mode, a resolution of up to 1.3 nm can be achieved. For imaging, the FEG SEM Quattro S is equipped with secondary electron (SE), backscattered electron (PSE) detectors and transmission electron detectors. An energy-dispersive X-ray detector (EDXS) of the new generation Ultim® Max is installed for the analysis of the chemical composition.

In Figures 3 and 4 are presented results of dust analysis used field emission electron microscope (FEG SEM).



gh the use of
, for example:
plasma cutting of



ring manual
ile electrode
nification: a)

by analyzing all the obtained images, we came to the conclusion that the individual particles have the correct spherical shape in both the cutting process and manual arc welding for both types of steels. In all cases, clusters of particles or agglomerates were also present, which were composed of individual spherical particles and were clearly visible.

Flame cutting produces more particles with an equivalent diameter of less than 1.75 μm than plasma cutting. Plasma cutting produces particles with a diameter greater than 5.5 μm that cannot be detected by flame cutting. This means that, on average, smaller particles are obtained in flame cutting than in plasma cutting. All analyzed particles for both plasma and flame cutting are less than 10 μm , which means that they are classified as respiratory particles, as they reach the lower respiratory tract all the way to the alveoli. Manual arc welding with a cellulose electrode results in the formation of

particles larger than 8.6 μm . Approximately 80% of the analyzed particles have an equivalent diameter equal to or greater than 17.3 μm . Most of the analyzed particles thus do not reach the lower respiratory tract, but the lungs, as they are larger than 10 μm . Such particles are classified in the category of thoracic particles, which are less harmful to humans than respiratory particles. The manual arc welding process produces larger particles than the flame and plasma cutting process in the case of S460 steel processing, although both cutting processes produce more emissions than the welding process.

4. CONCLUSIONS

Prior to sampling (capturing) the emitted dust particles during the cutting and welding processes, care must be taken to ensure that the mixed cellulose ester filter on which the particles are trapped is not moistened. Moisture affects the initial mass of the filter and causes a change in its properties.

The amount of emissions is most influenced by the choice of machining process, which is evident in the case of machining steel S460, where the cutting process causes 7x more emissions than manual arc welding.

The use of a suction device also affects the amount of emissions. This is confirmed by the case of manual arc welding of AISI 316 steel, where the use of this device generates more emissions.

Due to suction, heavier dust particles that would otherwise settle are expected to rise high enough to be captured by the ZAMBELLI EGO PLUS TT sampling instrument (stimulates human respiration). Nevertheless, it is recommended to use a suction device, as this removes flue gases that lead to severe respiratory diseases.

The choice of steel and electrode does not affect the amount of emissions.

REFERENCES

- [1] Krajcarz, D., Comparison Metal Water Jet Cutting with Laser and Plasma Cutting, *Procedia Engineering*, 6 (2014), 838-843
- [2] Sacks, R.J., Bohnart, E.R., *Welding: principles & practices*; McGraw-Hill Education, 2018.

- [3] Jocić, B., Steels and Cast Irons, BIO-TOP, Dobja Vas, 2008.
- [4] Wahab, M.A., Comprehensive Materials Processing, Elsevier Ltd., 6 (2014), 49-76.
- [5] Dasch, M., Physical and Chemical Characterization of Airborne Particles from Welding Operations in Automotive Plants, Journal of Occupational and Environmental Hygiene 5, 2008
- [6] Nieuwenhuijsen, M.J., Exposure Assessment in Occupational and Environmental Epidemiology,
- [7] ISO 13322-1 (2014): Particle size analysis -- Image analysis methods -- Part 1: Static image analysis methods, International Standardization Organization
- [8] Ilić Mićunović, M., Model za evaluaciju rezultata merenja karakteristika praškastih materija zasnovan na elektronskoj mikroskopiji, Doktorska disertacija, Novi Sad, 2018



Banja Luka
28–29 May 2021.

DEMI 2021

15th International Conference on Accomplishments in Mechanical and Industrial Engineering

www.demi.mf.unibl.org



Analysis of energy saving opportunities in the building, transport and public lighting sectors in local communities

H. Muratović^a, S. Midžić Kurtagić^b, S. Arnaut^a, F. Ćorović^a, E. Manić^a

^aEnova d.o.o., Podgaj 14 Sarajevo, B&H

^bFaculty of Mechanical Engineering, Vilsonovo šetalište 9 Sarajevo, B&H

Abstract *The paper covers the calculation of energy consumption and emissions by sectors for 10 municipalities in B&H. The sectors covered are building, transport, public lighting and water supply. The calculation of energy consumption and CO₂ emissions was performed for 2019. Due to the lack of data, the water supply sector was excluded from the further analysis. The COPERT program, EU standard vehicle emissions calculator, was used to calculate energy consumption and emissions from the transport sector. The Typology of Residential Buildings in B&H and the Typology of Public Buildings in B&H were used for the calculation of energy consumption in building sector, while the Methodology for measuring and verifying energy savings using the bottom-up method was used for the calculation of energy savings and emissions. The analysis of energy consumption and emissions was done using the benchmarking method. In each of the local communities, a set of measures in these three sectors was selected, in order to achieve significant reduction of emissions by 2030 compared to the 2019. The results of the analysis show that a very ambitious program with a high level of investment is needed to achieve the goals.*

Keywords *energy efficiency, CO₂ emission reduction, benchmarking*

1. INTRODUCTION

The scientific evidence is overwhelming for the proposition that global warming is due in great measure to the increase in CO₂ levels in the atmosphere, as is the fact that the increase in CO₂ concentration is due to human activity. Climate change is currently one of the most pervasive and threatening problems. In many places, the changes in temperature are already placing ecosystems under stress and are also affecting human well-being [1]. Studies have shown that concentrations of carbon dioxide in the atmosphere have increased considerably over the last century, compared to the rather stable level of the pre – industrial era. It is evident that increasing population rate, energy consumption and economic development contribute to climate change [5]. Since environmental change is happening at a much

faster rate than previously, it is imperative that governments act now to reverse the damage that has been done to the planet [1].

Extreme climate events in Bosnia and Herzegovina have become more frequent. In the period 2003–2014, six of the 12 years (2003, 2007, 2008, 2011, 2012, and 2013) were either very dry or extremely dry. In 2001, 2002, 2009, 2010 and 2014, there were large to disastrous floods. April and May 2014 saw record rain (over 420 mm) in the northern part of the country, which caused disastrous floods in the catchment area of the Vrbas and Bosna Rivers, as well as in the area of Semberija. These extreme climate and weather episodes have caused substantial material and financial deficits, as well as casualties [9]. Accordingly, mitigation and adaptation to climate change have become topics of increasing attention in Bosnia and Herzegovina.

According to the latest available data, the sectors that produced the largest amounts of CO₂ in Bosnia and Herzegovina during 2016 were following [20]:

- Electricity and Heat,
- Transport,
- Manufacturing and Construction
- Buildings.

The sectors identified as having the greatest potential for reducing energy consumption, and therefore CO₂ emissions, through local authorities' actions are the transport, buildings, public lighting and water supply sectors.

2. METHODOLOGY

Calculations of energy consumption and corresponding CO₂ emissions were done for 10 municipalities in Bosnia and Herzegovina covering building, transport and public lighting sectors. Data for the water supply sector were available for only two municipalities, so those will not be discussed further in this paper.

In order to assess level of performance of the municipalities, the performance benchmarking method was used. According to Fong et al. (1995) benchmarking is a technique or a tool to improve performance and to establish quality process directed toward the best [2]. Due to its many benefits [6], the scope of application of benchmarking today is very diverse. Apart from its application in the private sector [7], benchmarking has become a key tool for measuring performance in the public sector too, e.g., in water supply and wastewater services[8], waste management [3], public transport [4], etc.

Depending on where the reference values are found, inside or outside the organization, internal and external benchmarking can be distinguished. Whether it is external or internal benchmarking, it is crucial to determine the measurable units through which the comparison is performed. Such units of measure are called indicators and are expressed as individual variables or as equations containing two or more measurable variables [12]. In

Corresponding author

Prof. Sanda Midžić Kurtagić, PhD
midzic@mef.unsa.ba

Faculty of Mechanical Engineering
 Vilsonovo šetlište 9
 Sarajevo, Bosnia and Herzegovina

addition to comparing the values of indicators over the years, which is the case when it comes to internal benchmarking, it is possible to make comparisons with the values of other organizations engaged in the same activity or with the values that are considered reference.

A total of five indicators were selected, two for the transport sector and the building sector, and one for the public lighting sector (Table 1). The main criterion in selecting the indicators was the availability of data needed for their calculation and the availability of data for comparison.

Table 1. Selected indicators for the benchmarking analysis

Indicator	Formula	Unit
Transport sector		
Percentage of diesel cars in total vehicle fleet	$(\text{Number of diesel cars} / \text{Total number of vehicles}) * 100$	%
Average number of vehicles per household	$\text{Number of cars and motorbikes} / \text{Number of households}$	vehicles/household
Building sector		
Electricity consumption in residential buildings	$\text{Electricity consumption in residential buildings} / \text{Residential surface}$	MWh/m ²
Heat consumption in residential buildings	$\text{Heat consumption in residential buildings} / \text{Residential surface}$	MWh/m ²
Public lighting sector		
Energy consumption per light point	$\text{Energy consumption} / \text{Number of light points in the system}$	MWh/light point

The benchmarking of the calculated indicators from the transport and building sector was performed in comparison to reference values set in the Green City Benchmarking Approach. The OECD together with ICLEI – Local Governments for Sustainability developed a Green City Benchmarking Approach in 2016 (EBRD, 2016). The benchmarks corresponding to the traffic light thresholds (“green”; “yellow”; “red”) is developed where the “red” light of a certain indicator indicates low performance, in need of critical attention, “yellow” means insufficient performance, cause for concern,

while "green" means good performance, in line with international standards (Table 2, Table 3). Various international institutions contributed to defining the benchmarking scale including World Health Organization (WHO), Chartered Institution of Building Services Engineers (CIBSE), International Energy Agency (IEA), European Environment Agency (EEA), etc. [10]

Table 2. Reference values of the selected transport indicators

Indicator	Benchmarks		
	Green	Yellow	Red
Percentage of diesel cars in total vehicle fleet	<20%	20-30%	>30%
Average number of vehicles per household	<0.5	0.5-1	>1

Table 3. Reference values of the selected building sector indicators

Indicator	Benchmarks		
	Green	Yellow	Red
Electricity consumption in residential buildings	<0.021	0.021-0.026	>0.026
Heat consumption in residential buildings	<0.096	0.096-0.126	>0.126

Benchmarking analysis of the public lighting sector involves comparing the municipalities' values of selected indicators with the values of five European cities **Error! Reference source not found.** We found limited availability of data for public lighting energy consumption at the local community level. The available data are from 2010, 2011, and 2014.

Benchmarking values of the selected cities are obtained from the Tool for Rapid Assessment of City Energy (TRACE), which was first developed in 2008 by ESMAP's Energy Efficient Cities Program to help cities expand their municipal services through energy efficiency [21].

2.1 Calculation of energy consumption and CO₂ emissions

In order to develop calculations for 2019, first calculations were made for the base years for each municipality (Table 4). The main criterion when selecting a base year was the availability of data required for the calculation of energy consumption and CO₂ emissions for all considered sectors.

Table 4. Selected base years for each subject municipality

Municipality	Base year
1	2010
2	2010
3	2013
4	2014
5	2011
6	2008
7	2014
8	2010
9	2008
10	2012

Inventories of CO₂ emissions were prepared according to the instructions and methodology of the IPCC protocol [24]. The IPCC Protocol for the Determination of Emissions of Pollutants into the Atmosphere is a protocol of the Intergovernmental Panel on Climate Change (IPCC) as the executive body of the United Nations Environment Program (UNEP) and the World Meteorological Organization (WMO) in implementation of the United Nations Framework Convention on Climate Change (UNFCCC).

CO₂ emissions include emissions from electricity and heat consumption and emissions from fuel combustion. Emissions are calculated through standard emission factors, except when it comes to electricity, where specific national emission factor was used. All emission factors are presented in Table 5.

Table 5. Emission factors used for the calculation of CO₂ emissions in 10 B&H municipalities [17, 18, 24]

Fuel	Emission Factor tCO ₂ /MWh _{el}
Electricity	0.760
Diesel	0.268
Gasoline	0.250
Liquid gas	0.227
Natural gas	0.202
Heating oil	0.268
Lignite	0.365
Coal	0.349
Biomass	0.007

2.2 Calculation of energy consumption and CO₂ emissions from the transport sector

The software tool COPERT 5.3 [25], EU standard vehicle emissions calculator, was used to calculate energy consumption and emissions from the transport sector. The software uses the structure and number of vehicles, the annual distance travelled, the average speed on different sections of the road, as well as data on the outside temperature and humidity, all in order to calculate emissions according to European standards. The necessary data for the calculation of energy consumption and emissions are i) number and structure of vehicles, ii) average age, iii) vehicle category and iv) emission standard.

The source of data was the database of the Agency for Identification Documents, Registers and Data Exchange (IDEEAA) related to registered vehicles in Bosnia and Herzegovina; average annual distance travelled, amount of fuel consumed, and climate data.

2.3 Calculation of energy consumption and CO₂ emissions from the building sector

The calculation of energy consumption and corresponding CO₂ emissions for the building sector was performed for public buildings and for residential buildings.

Energy consumption calculations for public buildings for the base year were made considering the year of construction and purpose of the building. Based on these data, the type of building was obtained, according to

the Typology of Public Buildings in BiH from 2017 [13]. The Typology defines the specific energy required for heating the building per unit area $Q_{\text{hnd,spec}}$ (kWh/m²) which is multiplied by the actual heated area of the building A_k (m²) and thus obtained the actual energy required for heating $Q_{\text{hnd,item}}$ (kWh). The actual and reference heating degree days were included and the final (delivered) energy was calculated. Energy consumption of public buildings for 2019 was calculated taking into account data on implemented energy efficiency measures on public buildings built before the base year and data on new buildings built in the period from the base year to 2019. The Methodology for Measurement and Verification of Energy Savings by the Bottom-Up Method (MVP) [19] and data from the Typology of Public Buildings in BiH [13] were used to calculate energy savings.

Data on the specific energy required for heating and the heated area of residential buildings by type and period of construction were used from the Typology of residential buildings [14], while the Household Energy Consumption Survey from 2015 was used to obtain data on electricity consumption in households [15]. From the 2013 Census of Population, Households and Dwellings in BiH [16], data regarding number of households and residential buildings by type and method of heating, as well as the data on energy used for heating were used.

For 2019, the analysis of energy consumption of residential buildings was performed on the basis of data collected from the surveys on energy consumption in households. Surveys' samples for subject municipalities with confidence levels and error margins are presented in the Table 6.

Surveys collected data on implemented construction measures and changes in the heating system in residential buildings in the period from the base year to 2019. The calculation of savings for residential buildings was performed in accordance with the already described method of calculating savings for public buildings.

Table 6. Energy consumption in households' surveys' samples for 10 subject municipalities

Municipality	No. of households	Confidence level	Error margin
1	700		
2	227	95%	6%
3	34	90%	13%
4	368	95%	6.8%
5	355	95%	5%
6	321	95%	
7	371	95%	5%
8	365	95%	6%
9	95	95%	9.6%
10	386	95%	

Based on the total annual energy consumption for public and residential buildings, which was divided according to different energy sources, the calculation of CO₂ emissions was performed by taking into account corresponding emission factor of each source (Table 5).

2.4 Calculation of energy consumption and CO₂ emissions from the public lighting sector

The calculations for the public lighting sector were made according to the data obtained from the municipal departments in charge of communal affairs. These data included information on average daily working hours, total number of luminaires in the system taking into account type of light source and control mode, and annual electricity consumption of the system.

As input data for the calculation of indirect CO₂ emissions, data on total annual electricity consumption (calculated / bills) were used. Current CO₂ emission factor was taken from the relevant legislation [17, 18], and it was obtained from the ratio of electricity produced from hydropower and thermal power plants depending on the used fossil fuels' structure (and other renewable sources) and amounts to 0.760 tCO₂/MWh.

3. RESULTS AND BENCHMARKING ANALYSIS

3.1 Transport sector

Energy consumption and corresponding CO₂ emissions from the transport sector in 2019 in 10 subject municipalities are presented in Table 7.

Table 7. Energy consumption and corresponding CO₂ emissions from the transport sector in 10 subject municipalities

Municipality	Energy consumption (MWh/year)	CO ₂ emissions (tCO ₂ /year)
1	136,399	36,244
2	52,325	13,729
3	3,678	972
4	66,983	17,771
5	50,669	13,374
6	140,700	36,960
7	47,894	12,643
8	76,043	20,066
9	5,533	1,466
10	73,324	19,262

The value of the first indicator, Percentage of diesel cars in total vehicle fleet (Fig. 1), for all observed municipalities exceeds the reference value of 30% and indicates low performance and need of critical attention.

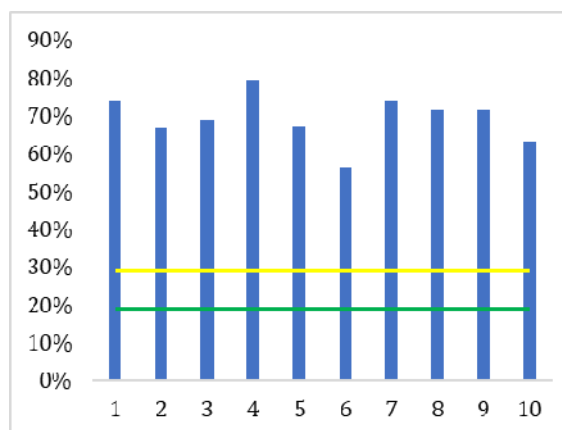


Fig. 1. Percentage of diesel cars in total vehicle fleet

Regarding the indicator Number of cars per household (Fig. 2), six municipalities have a

"yellow" value which indicates insufficient performance, and only one municipality has the value that is in line with international standards. Municipalities 1, 2 and 6 have the "red" value of the observed indicator. Common to all of them is good geo-traffic position and the population that travels daily from their place of residence due to work obligations and therefore needs more cars in one household.

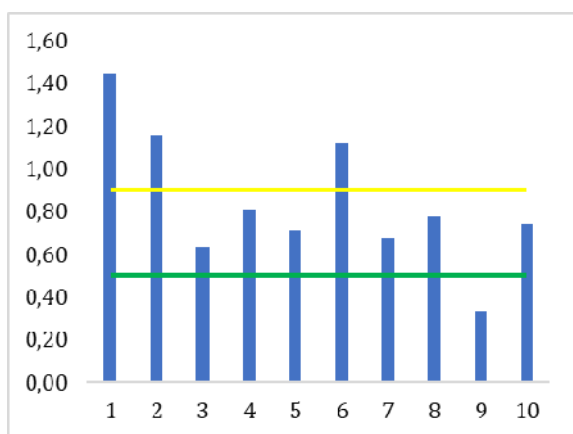


Fig. 2. Number of cars per household

3.2 Building sector

In 2018, building sector accounted for the largest share of both global final energy use and energy-related CO₂ emissions [11]. This trend is also present in the observed municipalities where the average share of the building sector in total energy consumption and CO₂ emissions is 65% and 60%, respectively.

Results of the calculations of energy consumption and generated CO₂ in the building sector in 2019 are shown in the Table 8.

Table 8. Energy consumption and corresponding CO₂ emissions from the building sector in 10 subject municipalities

Municipality	Energy consumption (MWh/year)	CO ₂ emissions (tCO ₂ /year)
1	49,619	18,521
2	48,158	19,585
3	8,677	1,406
4	186,923	31,141
5	116,313	21,467
6	246,793	41,256
7	144,735	39,289

Municipality	Energy consumption (MWh/year)	CO ₂ emissions (tCO ₂ /year)
8	120,613	27,931
9	19,780	3,588
10	330,492	58,233

Table 9. Energy consumption and corresponding CO₂ emissions from the building sector in 10 subject municipalities

Municipality	Shares in total energy consumption in building sector	
	Residential buildings	Public buildings
1	94%	6%
2	94%	6%
3	94%	6%
4	94%	6%
5	93%	7%
6	96%	4%
7	96%	4%
8	93%	7%
9	95%	5%
10	96%	4%

Each municipality has electricity consumption in residential buildings over 0.026 MWh/m², which indicates the low performance (Fig. 3). Heat consumption in residential buildings also indicates low and unsatisfactory performance except for municipalities 1 and 2 (Fig. 4).

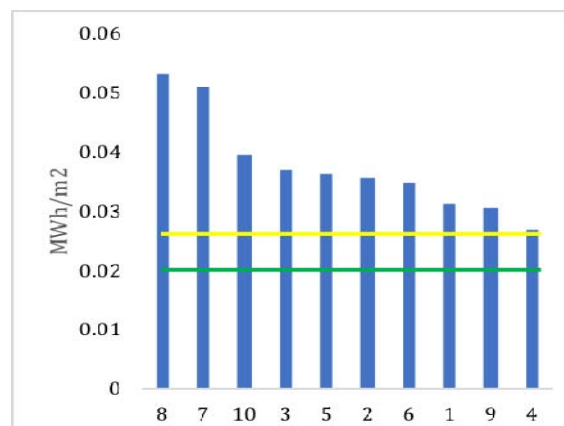


Fig. 3. Electricity consumption in residential buildings [MWh/m²]

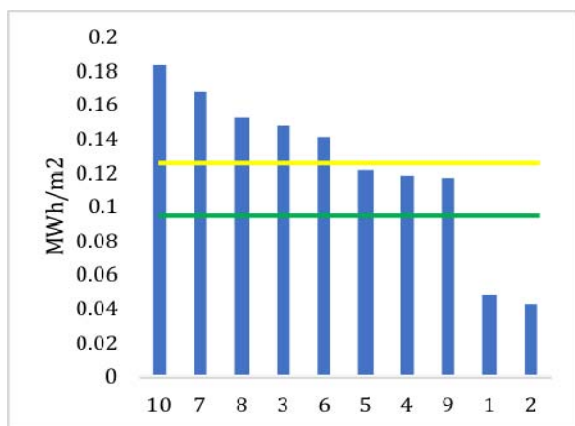


Fig. 4. Heat consumption in residential buildings [MWh/m²]

3.3 Public lighting sector

The public lighting sector has a very small share in total energy consumption and CO₂ emissions and does not exceed 2% in the analyzed municipalities. The calculated energy consumption and corresponding CO₂ emissions from this sector in 2019 are presented in the Table 10.

Table 10. Energy consumption and corresponding CO₂ emissions from the public lighting sector in 10 subject municipalities

Municipality	Energy consumption (MWh/year)	CO ₂ emissions (tCO ₂ /year)
1	695	528
2	562	427
3	62	47
4	727	553
5	1,046	795
6	1,941	1,475
7	628	477
8	675	513
9	196	149
10	1,800	1,368

The highest energy consumption was recorded in the Municipality 10 (Fig. 5). The reason for this is that 75% of public light sources in this municipality are mercury, sodium and metal-halogen, which, in addition to high energy consumption, also results in poor lighting of public areas.

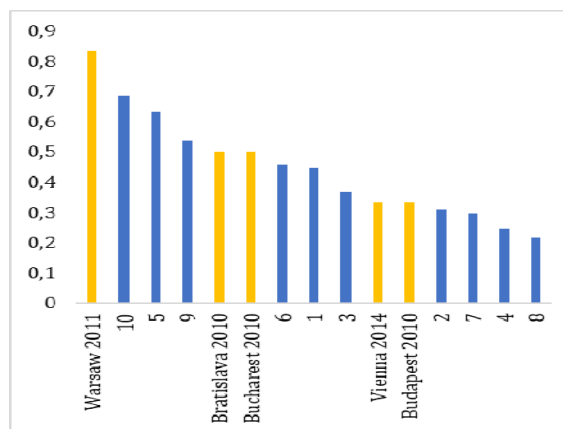


Fig. 5. Energy consumption per light point [MWh/light point]

Good performance in energy consumption for public lighting have municipalities 2, 7, 4 and 8. In the last 5 years, they made significant investments in public lighting, which include the replacement of inefficient lamps with LED lamps and improvements related to the control of public lighting by analogue time relays.

4. PROPOSED MEASURES

The performance analysis has indicated the areas for improvement and directed the proposal of measures for the reduction of energy consumption and CO₂ emissions in transport, building and public lighting sectors. The transport is second highest energy consumer. The number of cars per household and percentage of diesel cars in in total vehicle fleet indicates low and insufficient performance. Therefore, the municipalities proposed measures to increase number of vehicles in public transport on natural gas as well as to increase non-motorised transport (Table 11). Selected measures in the transport sector will result in a reduction of CO₂ emissions by an average of 41%, with the exception of municipalities 2 and 10 where the expected reduction is minimal (2%, 6%, Table 12) due to the limited scope of selected measures.

The building sector, as the largest energy consumer, offers the most opportunities for savings. The municipalities have chosen measures related to improving the energy efficiency of public buildings, the efficiency of lighting in buildings and the production of heat from renewable sources (biomass and heat pumps). Two proposed measures in the two

municipalities are related to the connection to the district heating system whose installation is planned in the future. Only in one case replacement of heating oil boilers with gas boilers was proposed. (Table 11). This measure will not result in energy savings but will contribute to CO₂ reductions due to replacement of oil with gas.

Higher energy consumption in some municipalities indicates the need to invest in efficient lighting and to pay special attention to

regular maintenance (Table 11). The proposed measures are applicable to all analysed municipalities. Increase of CO₂ emission related to public lighting in some municipalities is related to the expansion of lighting systems, to a greater extent than in others, depending on the current coverage by public lighting (Table 12). The level of investment costs is high and ranges from 1,027 to 3,358 KM per ton of CO₂ (Fig. 6).

Table 11. Proposed measures for 10 subject municipalities by sectors

Municipality	1	2	3	4	5	6	7	8	9	10
Measure										
TRANSPORT SECTOR										
Renewal of the vehicle fleet under the jurisdiction of the Municipality	x	x	x	x	x	x	x	x	x	x
Replacement of existing dilapidated buses with natural gas buses	x	x	-	x	x	x	x	x	-	x
Promotion of the public transport as a cheap and efficient mode of transport	x	x	-	x	x	x	x	x	-	x
Education of citizens in the field of traffic	x	x	x	x	x	x	x	x	x	x
Promotion and improvement of cycling	x	x	x	x	x	x	x	x	x	x
Construction, reconstruction and maintenance of local and uncategorized roads	-	-	-	-	-	-	-	x	-	-
BUILDING SECTOR										
Thermal insulation of the outer envelopes of buildings under the jurisdiction of the Municipality	x	x	x	x	x	x	x	x	x	x
Replacement of lighting in public buildings under the jurisdiction of the Municipality	x	x	x	x	x	x	x	x	x	x
Installation of pellet boilers in public buildings under the jurisdiction of the Municipality	x	-	-	x	x	-	x	-	x	x
Installation of natural gas boilers and central heating systems in facilities under the jurisdiction of the Municipality	-	x	-	-	-	-	-	-	-	-
Installation of heat pumps in public buildings under the jurisdiction of the Municipality	x	x	-	x	x	x	x	x	x	x
Connection of public buildings under the jurisdiction of the Municipality to the future district heating system	-	-	-	-	-	-	x	-	-	x
Installation of pellet boilers and central heating system in the central building of the Municipality	-	-	x	-	-	-	-	x	-	-
Thermal insulation of the outer envelopes of buildings that are not under the jurisdiction of the Municipality	x	x	x	x	x	x	x	x	-	x
Replacement of lighting in public buildings that are not under the jurisdiction of the Municipality	x	x	x	x	x	x	x	x	-	x
Installation of heat pumps in public buildings that are not under the jurisdiction of the Municipality	-	x	x	-	x	x	-	x	-	x
Installation of pellet boilers and central heating systems in facilities that are not under the jurisdiction of the Municipality	-	-	x	-	x	x	x	x	-	-
Installation of natural gas boilers and central heating systems in facilities that are not under the jurisdiction of the Municipality	-	x	-	-	-	-	-	-	-	-
Connection of public buildings that are not under the jurisdiction of the Municipality to the future district heating system	-	-	-	-	-	-	x	-	-	-
Raising the awareness of citizens about the benefits of using renewable energy sources and ways to achieve energy efficiency, as well as training on the possibilities of achieving this	x	x	x	x	x	x	x	x	x	x
Thermal insulation of the outer envelopes of residential buildings	x	x	x	x	-	x	x	x	x	x
Connection of residential buildings to the future district heating system	-	-	-	-	-	-	x	-	-	x
Replacement of existing heating systems in residential buildings that use fossil fuels with systems that use RES	x	x	x	x	x	x	x	x	x	x
Replacement of existing heating systems in residential buildings that use electricity with heating systems using heat pumps	x	x	x	x	x	x	x	x	x	x
Replacement of existing lighting fixtures in residential buildings with LED bulbs	x	x	x	x	x	x	x	x	x	x
Replacing home appliances with more energy efficient appliances	x	x	x	x	x	x	x	x	x	x
Installation of solar systems for domestic hot water preparation	x	x	x	x	x	x	x	x	x	x
PUBLIC LIGHTING SECTOR										

Municipality	1	2	3	4	5	6	7	8	9	10
Replacement of low-efficiency lamps with high-efficiency ones (LEDs) and expansion of the public lighting system with LEDs	x	x	x	x	x	x	x	x	x	x
Improving the public lighting control system	x	x	x	x	x	x	x	x	x	x

Table 12. Percentage difference in CO₂ emissions in 2030 compared to 2019

Municipality	Buildings	Transport	Public lighting	Total
1	-49%	-45%	19%	-45%
2	-44%	-6%	-5%	-28%
3	-36%	-57%	-57%	-45%
4	-44%	-33%	5%	-40%
5	-39%	-47%	-44%	-42%
6	-57%	-28%	-62%	-44%
7	-37%	-34%	-13%	-37%
8	-43%	-41%	-16%	-41%
9	-40%	-46%	-55%	-42%
10	-44%	-2%	-52%	-34%

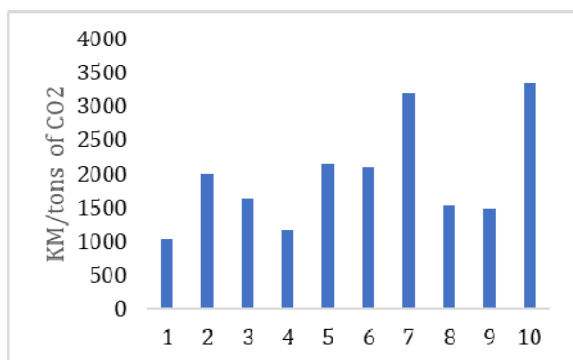


Fig. 6. Investment costs per tons of CO₂ savings [KM/tons of CO₂]

Significant variations in investment costs per tons of CO₂ savings are due to differences in the size, number and current state of buildings covered by the proposed measures. Particularly large investments were recorded in municipalities 7 and 10, which is a consequence of the connection of facilities to the district heating system whose installation is planned in the future. In addition, the investments of municipalities in the transport sector are different depending on the number of vehicles that need to be replaced, those in the municipal fleet, as well as the public transport vehicles.

4.1 Conclusion

Performance analysis of energy consumption and corresponding CO₂ emissions from the transport, buildings and public lighting sectors of 10 subject municipalities in Bosnia and Herzegovina indicate the need to implement strategic measures in order to comply with European cities and international standards.

All analysed municipalities can achieve a significant reduction of CO₂ compared to the 2019. However, in order to achieve this, very ambitious program with a high level of investment is needed.

Benchmarking is a useful tool for recognizing one's own shortcomings and identifying best practices applicable in a particular sector. However, an aggravating circumstance is the unavailability of recent data, both for Bosnia and Herzegovina and regional local communities and municipalities, as well as for European and global ones. Transparency of data would enable the calculation of a number of indicators and provide insight into the complete state of a particular sector and municipality.

REFERENCES

Journal papers:

- [1] Flavio, R., Arroyo, M., Luis, J. Miguel. (2019). The Trends of the Energy Intensity and CO₂ Emissions Related to Final Energy Consumption in Ecuador: Scenarios of National and Worldwide Strategies. *Sustainability*, vol. 12, no. 1, DOI: [10.3390/su12010020](https://doi.org/10.3390/su12010020)
- [2] Kosar, Lj. (2014). Benchmarking method for quality evaluation in hotel industry. *exclusive e-JOURNAL*, vol. 3, no. 1
- [3] Ilic, M., Nikolic, M. (2016). Waste Management Benchmarking: a case study of Serbia. *Habitat International*, vol. 53, p. 453-460, DOI: [10.1016/j.habitatint.2015.12.022](https://doi.org/10.1016/j.habitatint.2015.12.022)
- [4] Georgiadis, G. (2012). The role of benchmarking in public transport: The case of Thessaloniki, Greece. *Procedia – Social and Behavioural Sciences*, vol. 48, p. 2577-2587, DOI: [10.1016/j.sbspro.2012.06.1228](https://doi.org/10.1016/j.sbspro.2012.06.1228)

Proceedings papers:

- [5] Ntanos, S., Arabatzis, G., Miliotis, K., Chalikias, M., Lalou, P. Energy Consumption and CO₂ Emissions on a Global Level. *Proceeding of 4th International Conference on Quantitative and Qualitative Methodologies in the Economic and Administrative Sciences*, May 2015, Technological Educational Institute of Athens.

Books:

- [6] Meade, P. (1998). *A Guide to Benchmarking*. University of Otago, Dunedin. ISBN 0-473-05568-6

Theses:

- [7] Cirkic, M., Ökvist, A. (2016). *Managing Profit Oriented Key Performance Indicators*. Bachelor Thesis. School of Business, Society and Engineering, Mälardalen University.
- [8] Milutinović, B. (2013). *Benchmarking and Performance Indicators in Water Supply and Wastewater Services*. Master Thesis. Faculty of Civil Engineering, University of Belgrade.

Technical reports:

- [9] Nunes, A. (2018). *Third Environmental Performance Reviews of Bosnia and Herzegovina*. United Nations, New York and Geneva, Review report, no. 48. ISBN: 978-92-1-117168-6
- [10] (2016). *Green City Action Plan methodology*. European Bank for Reconstruction and Development. United Kingdom.
- [11] Abergel, T., Dean, B., Dulac, J., Hamilton, I. (2019). *Global Status Report for Buildings and Construction: Towards a zero-emission, efficient and resilient buildings and construction sector*. International Energy Agency. Global Status Report. ISBN: 978-92-807-3729-5
- [12] Stave, S.E. (2010). *Monitoring Peace Consolidation United Nations Practitioners' Guide to Benchmarking*. United Nations.
- [13] Nišandžić, M., at all (2017). *Typology of public buildings in Bosnia and Herzegovina*. UNDP.
- [14] Arnautović-Aksić, D., at all (2016). *Typology of Residential Buildings in Bosnia and Herzegovina*. GIZ, Sarajevo. ISBN 978-9958-691-51-5
- [15] Mrgud, D. (2018). *Household Consumption Survey for 2015*. Agency for statistics of Bosnia and Herzegovina, Sarajevo.
- [16] Jukić, V. (2016). *Census of Population, Households and Dwellings in Bosnia and Herzegovina, 2013, Final Results*. Agency for statistics of Bosnia and Herzegovina, Sarajevo.

Standards:

- [17] Official Gazette of Republika Srpska (2015). *Rulebook on minimum requirements for energy performance of buildings*. Official Gazette of Republika Srpska, 30/15. Banja Luka.
- [18] Official Gazette of the Federation of Bosnia and Herzegovina (2019). *Rulebook on minimum requirements for energy performance of buildings*. Official Gazette of the Federation of Bosnia and Herzegovina, 81/19, p. 3-63. Sarajevo.
- [19] Official Gazette of the Federation of Bosnia and Herzegovina (2019). *Rulebook on energy efficiency information system in the Federation of BiH*. Official Gazette of the Federation of Bosnia and Herzegovina, 02/19, p. 2-279. Sarajevo.

Internet links:

- [20] Our World in Data. CO₂ emissions by sector, Bosnia and Herzegovina. From: <https://ourworldindata.org/grapher/co-emissions-by-sector?tab=chart&stackMode=absolute&time=earliest.latest&country=~BIH®ion=World>, accessed on: March 9, 2021.
- [21] ESMAP. Tool for Rapid Assessment of City Energy (TRACE): Helping Cities Use Energy Efficiently. From: <https://esmap.org/node/235>, accessed on: March 24, 2021.
- [22] Agency for statistics of Bosnia and Herzegovina. Electricity and natural gas price statistics. From: http://www.bhas.gov.ba/data/Publikacije/Saopštenja/2019/ENE_02_2019_H1_0_BS.pdf, accessed on: 24 March, 2021.
- [23] Statista. Electricity prices for households in the European Union (EU-28) from 2010 to 2018, semi-annually. From: <https://www.statista.com/statistics/418049/electricity-prices-for-households-in-eu-28/>, accessed on: 24 March, 2021.
- [24] IPCC. 2006 IPCC Guidelines for National Greenhouse Gas Inventories. From: <https://www.ipcc-nggip.iges.or.jp/public/2006gl/index.html>, accessed on: 4 April, 2021.
- [25] emisia. COPERT The industry standard emission calculator. From: <https://www.emisia.com/utilities/copert/>, accessed on: 4 April, 2021.



Banja Luka
28–29 May 2021.

DEMI 2021

15th International Conference on
Accomplishments in Mechanical and
Industrial Engineering

www.demi.mf.unibl.org



Strategic analysis of the possibility of starting the production of fast - growing Paulownia tree

G. Janjić^a, M. Radaković^b, Z. Tanasić^a, B. Kosec^c, D. Kardaš Ančić^a

^a University of Banja Luka, Faculty of Mechanical Engineering, S. Stepanovića 71, 78 000 Banja Luka, BiH

^b University of Banja Luka, Faculty of Architecture, Civil Engineering and Geodesy, S. Stepanovića 77/3, 78 000 Banja Luka, BiH

^c University of Ljubljana, Faculty of Natural Sciences and Engineering, Aškerčeva cesta 12, 1000 Ljubljana, Slovenia

Abstract *Increasing energy needs and demands to reduce environmental impact have expanded interest in exploring sustainable alternative energy sources. The purpose of the article is to analyse the cost-effectiveness of starting the production of fast-growing Paulownia tree, which is characterized by low concentration of ash, sulphur, and nitrogen, as well as high calorific value and absorption of CO₂ from the air. Also, Paulownia is suitable for carving and insulation and it is an excellent raw material for ethanol production. Through the given strategic analysis, it is necessary to observe all-important external and internal factors that affect the success of the production of a quality product and its placement on the market. The paper also provides an assessment of the risks of identified threats arising from the environment and weaknesses related to the observed product.*

Keywords *strategic analysis, Paulownia, profitability*

1. INTRODUCTION

Wood production through the planting of fast-growing energy crops leads to the preservation of natural ecosystems that are partly disturbed by unsustainable deforestation. Among many fast-growing woody crops, Paulownia is considered a “magic tree” because of its fast-growing rate and a large amount of wood mass delivered in such a short time [1]. Each part of the Paulownia plant, as an energy source, can be exploited for the production of pellets [2].

Paulownia, because of its high percentage of cellulose, can be used for the production of ethanol [3]. In addition to renewable energy, Paulownia has found its purpose in building construction, furniture manufacturing, musical

instruments and veneers production, and etc. because of its good insulating characteristics and natural fire resistance.

Additionally, the Paulownia plant has the following characteristic: lightness, firmness, dry quickly, pleasant unchangeable colour, ease to process, and resistance to diseases and insect attacks.

It dries naturally for about 35 to 45 days and does not require storage to dry. Paulownia wood can be installed alone or mixed with particles of other materials (e.g., in plywood production to improve their strength properties) [4].

Paulownia has a low concentration of sulphur, nitrogen, and ash during combustion (by burning one cubic meter of wood, which is about 280 kilograms, as low as half a kilogram of ash will occur) [5]. Paulownia uses highly efficient photosynthesis to fix carbon [6] where one adult tree absorbs an average of about 22 kilograms of CO₂ and emits 6 kilograms of O₂ in a year [7]. After cutting, plants regenerate quickly. The estimated lifespan of the roots is about 70 years,

Corresponding author

Prof. Goran Janjić, PhD
goran.janjic@mf.unibl.org

University of Banja Luka, Faculty of Mechanical Engineering
Vojvode Stepe Stepanovića 71
78 000 Banja Luka, Republic of Srpska, BiH

and they can support about 8 to 9 cuttings with a vegetative cycle of 8 years [1]. After the third year of growth tree almost does not require any care.

One of the crucial factors that benefit the Paulownia wood production is the *European Green Deal* from 2014 related to climate change and the energy framework. This document sets ambitious goals for the European Union countries by 2030, whose legislation in this area country Bosnia and Herzegovina accepted through the *Stabilisation and Association Agreement* which came into force in 2015. To this date, the given objectives, to a certain extent, have been revised. These objectives are as follows [8]:

- At least 40 % reduction of greenhouse gases emission compared to the 1990 level (the European Commission proposed in September 2020 the goal of reducing greenhouse gases emissions by 2030 by raising it to at least 55 %),
- At least 32 % share of renewable energy sources,
- Improve energy efficiency by at least 32,5 %.

The cost-benefit analysis of the production of the fast-growing Paulownia trees in Bosnia and Herzegovina, used as raw material for different types of products, was analysed in this paper.

The external environment, in which complex changing factors operate, imposes on the company the obligation of a strategic way of thinking and timely decision making. It is necessary to establish the firm's and its business units' strategic positions and their environmental factors. Strategic management is a continuous process whose purpose is to optimally prepare the organization for responding to changes coming from the surroundings. Its task is to create a solid strategic position in those markets in which the organization has decided to operate.

2. PHASES OF STRATEGIC MANAGEMENT

There are no large differences in defining the phases of strategic management among well-known authors in this field. In his book *Strategic Management in Action*, Coulter talks about situational analysis, formulation, implementation, and evaluation of strategy as phases of strategic management whose result is

a series of strategies that an organization applies in its business (Fig. 1.) [9].

Ansoff, a well-known researcher in the strategic management field, suggests that environmental variability and dynamism, strategy and company open-mindedness to conditions of the environment represent the essence of strategic management. The relationship between listed components of strategic management determines the strategic position of the organization. According to Ansoff, strategic management includes strategic planning (strategic analysis and strategic choice) and strategic action (strategic implementation and control) [10].



Fig. 1. Phases of strategic management

Defining the company's strategy implies setting strategic goals and measures for their realization. It includes the development of long-term plans for managing opportunities and threats from the environment concerning the strengths and weaknesses of the company. There are several types of strategy, according to its design for appropriate hierarchical level: for an entire organization (basic strategy), for the business unit (which is independent within budgeting, target market, marketing mix), and the level of products and services (lowest level of strategy). Above mentioned strategies of the company should be implemented and shaped in compliance with the principle of hierarchical superiority. The product and service strategy, often called the product marketing strategy, should be in with the business unit strategy, and it should be in line with the company strategy.

The marketing strategy, above all, must take into account the needs of the market and the potential of the company to create competitive advantages and overcome the competition strategy. It requires a detailed strategic analysis of the external environment and internal factors of the company.

3. STRATEGIC ANALYSIS

The strategic analysis includes the following (Fig. 2) [11]:

- the forecasting of various trends and events in the external environment in which the company should operate. Analysis of external factors involves customers, markets and competition analysis, and a wide range of other environmental factors,
- analysis of the internal factors that affect the company's agility and ability to respond to environmental changes.

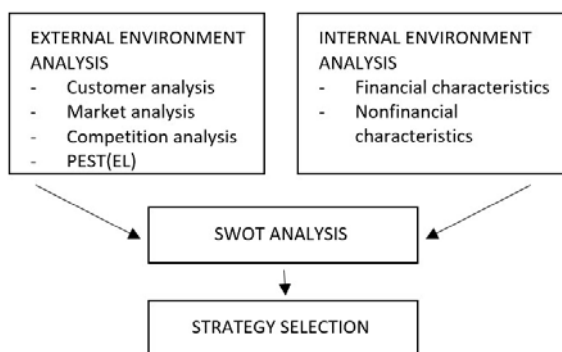


Fig. 2. The process of developing and designing marketing strategy

3.1 External environment analysis

Customer analysis. Customer satisfaction with parallel profit-making is the fundamental imperative of every company. The aim of the customer analysis is to provide market segmentation on relatively homogeneous groups of customers, identify customer's profiles (number of customers, their needs, behavior patterns, loyalty levels), and to detect unsatisfied needs.

Market analysis. This type of analysis aims to determine the market potential (maximum demand estimation) and the size of the market, or total sales.

Competition analysis. The competition analysis should determine who are the leading competitors and which part of the target market they capture, the strengths and weaknesses of the competition, their goals, sales volume, product quality, their technologies, development intentions and opportunities, etc.

Macro-environmental analysis – PEST(EL). This environment contains a wide range of social forces, which significantly affect the organization

and consist of demographic, natural, technological, economic, legal-political, and socio-cultural factors.

3.2 Internal environment analysis

Internal environment analysis aims to identify the strengths and weaknesses of the company. It includes financial analysis (like the total sale and profitability measured by ratios such as return on sales, return on assets, etc. to decide whether or not to launch a new product). Internal environment analysis considers staff, organizational structure, information system, crucial business portfolio process and the allocation of, potentially, successful and unsuccessful products.

4. FEASIBILITY ANALYSIS OF LAUNCHING THE PRODUCTION OF FAST-GROWING PAULOWNIA TREES

"M&M PAULOWNIA" LLC, the company for the production of fast-growing trees, plans to produce Paulownia plants for sale. Sales range includes quarterly seedlings (obtained by "in vitro" technology), sawmill wood products (uses in construction and wood industry for furniture production), wood biomass as a heating fuel (biomass can be used by other companies for the production of pellets and briquettes) and investment cultivation on an area of one hectare. An additional product, coming from the production process, is biomass generated mainly from the waste during the shredding of leaves and branches after pruning trees, which can be used to heat buildings or make briquettes and pellets. The planned location of the plantation is Aleksandrovac, the municipality of Laktaši in Bosnia and Herzegovina.

4.1 Analysis of the external environment of the company

The market research process identifies potential buyers and competitors, as well as possibilities of market expansion.

Customer analysis. On the domestic market, there is not a dominant presence of Paulownia plant culture. This culture can replace most of our woody species in terms of quality, so a gradual increase of new customers is expected. The most important identified buyers of the company's products (seedlings, biomass, sawmill wood,

investment cultivation packages) are those from sector of wood processing (sawmills, furniture factories, and other companies engaged in primary and final wood processing), and companies for the production of pellets and briquettes in the Banja Luka region (thirty companies have been identified of which eleven companies have expressed their interest in business cooperation). There is a possibility of selling products to construction companies (in the form of rafters, slats, planks, beams, etc.), to individual buyers and sales intermediaries.

Market analysis. The forestry sector is very significant for the Republic of Srpska and includes the business of the company “M&M PAULOWNIA” LLC. This sector employs 3,11 % of the total working population of the Republic of Srpska [12]. At the annual level, about 1.958.000,00 cubic meters of various wood assortments produced in the forests of the Republic of Srpska. The production of forest assortments in 2019 was lower by 19,81 % compared to the year 2018 according to the Agency for Statistics of Bosnia and Herzegovina. Some of the main problems in the forestry sector are forest fires and illegal logging. Insect damage and plant diseases did not have a growth trend for a long-time period.

Market segmentation has done according to territorial criteria (Table 1.):

Table 1. Market segmentation

Market segment	Area
Banja Luka region	Area 1
Bosnia and Herzegovina except for the Banja Luka region	Area 2
Region except Bosnia and Herzegovina	Area 3

Competition analysis. In the Banja Luka region and the whole of Bosnia and Herzegovina, there are no Paulownia plantations, but there are only trial plantations on very small areas. There is significant competition in companies that places other types of wood, that can be used for the same purposes as Paulownia. The most significant competitors on the main market of the company (Area 1 – Banja Luka region) are PFE “Šume Republike Srpske” (Forests of the Republic of Srpska) and the owners of private forests. In this market, the company “M&M PAULOWNIA” LLC should be able to position

itself due to the high demand for wood assortments. Besides that, the company would be able to take advantage of reduced transportation costs due to the proximity of customers.

In Area 2, there is greater competition due to the import of wood assortments from neighbouring countries, especially in border municipalities, but in this market, the company has great opportunities. There is a lot of competition in the regional market (Area 3) and positioning can be a real challenge. The Republic of Serbia and the Republic of Croatia have the most modern Paulownia plantations and the most modern technology in the region.

The company “M&M PAULOWNIA” LLC seeks to single out and primarily be better than the competition through the offer of investment cultivation, through several sales packages, on a plot of one hectare on which would be planted 500 seedlings of fast-growing Paulownia trees obtained “in vitro” technology of high genetic quality. The presence of strong competition in the region tells us that the market in Bosnia and Herzegovina will experience an expansion of Paulownia trees production.

PEST(EL). Population migrations to Western Europe had an unfavourable impact on the number of inhabitants, the number of customers and the choice of the labour force.

The economy in Bosnia and Herzegovina is far behind the economy of neighbouring countries and European Union countries. In recent years, banks have eased the conditions for obtaining loans, and now it is easier for companies to get more favourable loans. Due to the bad rating of the state, the insurance system is quite expensive.

The company has no problems in procuring seedlings and equipment for its products.

In recent years, the weather conditions have been very changeable.

4.2 Internal Analysis of the company

Purchase. Due to the insufficient presence of fast-growing Paulownia trees in our area, the supplier choice is small. The company decided to buy seedlings from supplier “AGROPLAN” nursery garden located in the City of Bijeljina for 6,50 BAM per piece with VAT included. If a larger quantity of seedlings is taken, it is possible to agree on a discount, when for purchase of 1.500,00 seedlings the supplier gives a price of

4,00 BAM per piece without VAT. The distance between our company and the supplier is 220,00 kilometres, which should be taken into account when agreeing on the delivery of purchased seedlings.

Finances. After the establishment of the company "M&M PAULOWNIA" LLC, the key focus will be to purchase: high-quality planting material, drip irrigation system, purchase ten hectares of land (after production stabilise buy additional ten hectares of land), three containers for offices with associated furniture and equipment, connections to electricity grid and water supply network. Previous activities follow terrain preparation works, installation of irrigation systems, planting, procurement of system for hail protection, weather conditions, insects, and purchase of a stationary chipboard machine with a protective canopy, for what is estimated to provide a total of 145.700,00 BAM. This amount of money includes equipment that is not completely necessary for launching the business. According to this, the sum of 132.300,00 BAM is enough to start a business.

After three years of growth from its planting, one Paulownia tree reaches a market value from 80,00 to 120,00 BAM. After eight years of growing the Paulownia tree (when the tree is best for lumbering), it can provide from 0,50 to 0,70 cubic meters of usable material worth from 280,00 to 1.000,00 BAM depending on its quality.

The company plans to plant 1.500,00 seedlings every year, and to do lumbering according to the recommended periods. After three years of production, after planting the first seedlings, we can expect plant growth to value between 120.000,00 and 180.000,00 BAM, depending on the quality. Every following year company would have the arrival of new 1.500,00 three-year-old trees. In the income statement (Table 2.), the total projected revenues after eight years of company operation are 956.550,00 BAM with total expenses for the same period of 627.982,40 BAM.

The payback period of investment, determined according to economic flow, is estimated to be at *five years and 143 days* (Table 3.). Also, a net present value represents a positive value.

Employees. A team of young and dedicated people with the required level of expertise makes up the company "M&M PAULOWNIA" LLC. The director manages the company. The operational section of the company includes

forestry and agricultural technician who is in charge of the preparation, planting, and maintenance of the plantation. Besides him, the company needs two wood technicians for felling and chopping of wood.

Table 2. Income statement

(BAM)	YEAR			
	1.	2.	3.	4.
NET PROFIT "+" (NET LOSS "-")	-25.069,4	-29.109,0	14.661,9	32.031,9
BUSINESS REVENYE	18.750,0	51.100,0	98.200,0	120.000,0
BUSINESS EXPENSES	43.819,4	80.209,0	81.909,0	84.409,0
	YEAR			
	5.	6.	7.	8.
NET PROFIT "+" (NET LOSS "-")	45.711,9	59.301,9	79.731,9	113.031,9
BUSINESS REVENYE	135.200,0	150.300,0	173.000,0	210.000,0
BUSINESS EXPENSES	84.409,0	84.409,0	84.409,0	84.409,0

Table 3. Income statement The payback period of investment (economic flow)

Year	Total investment (BAM)	Net receipts (BAM)		
		By years	Cumulative	Uncovered investment part
1	2	3	4	5 (4-2)
1	132.300,00	0	0	-132.300,00
2	132.300,00	0	0	-132.300,00
3	132.300,00	10.346,90	10.346,90	-121.953,10
4	132.300,00	27.716,90	38.063,80	-94.236,20
5	132.300,00	41.396,90	79.460,70	-52.839,30
6	132.300,00	54.986,90	134.447,60	2.147,60
7	132.300,00	75.416,90	209.864,50	77.564,50
8	132.300,00	108.716,90	318.581,40	186.281,40

4.3 SWOT analysis

By analysing the internal and external environment of the company, key elements are determined and classified: strengths, weaknesses, opportunities, and threats (Table 4.).

Table 4. SWOT analysis matrix

<p style="text-align: center;">Strengths</p> <ul style="list-style-type: none"> - Low product prices - Sale of investment cultivation – an innovative product - Experience and qualification of workers - Quality of equipment - Seed quality - Market potential - Cheap labour - Providing technical support to customers from the moment of planting to felling 	<p style="text-align: center;">Weaknesses</p> <ul style="list-style-type: none"> - Low information about the product by customers - Exploitation period - Satisfying market demand - Relatively long investment repayment period - Insufficient experience in growing Paulownia trees
<p style="text-align: center;">Opportunities</p> <ul style="list-style-type: none"> - Lack of Paulownia plantations in the Banja Luka region (Area 1), which is the primary market - Weak competition in Bosnia and Herzegovina - Subsidies - Availability of skilled labour - Quality of the finished product - High demand for wood assortments - In Bosnia and Herzegovina and the region, there is a large number of companies for final wood processing - In recent years, banks have eased the conditions for obtaining loans 	<p style="text-align: center;">Threats</p> <ul style="list-style-type: none"> - Big competition in the region, especially in the Republic of Croatia - Occurrence of pests (insects) - Uncontrolled import of wood assortments - Entry of new competitors - Weather trouble - Presence of coronavirus pandemic (COVID-19) - Small number of suppliers in Bosnia and Herzegovina - Population decline in Bosnia and Herzegovina and the region due to migrations - Due to the bad rating of the state, the insurance system is quite expensive

4.4 Vision and mission of the company

“M&M PAULOWNIA” LLC company vision is to become a leader in Bosnia and Herzegovina in the production of quarterly seedlings of fast-growing Paulownia trees, raw materials for the sawmills, and the sale of investment cultivation with the ambition to expand the product range and increase production in each subsequent year. To grow from good roots into a firm and stable organization.

“M&M PAULOWNIA” LLC company mission is to provide the more affordable offer of raw materials for the sawmills, which would affect the prices of final products in economic branches with which the company cooperates. Special emphasis is dedicated to stimulating the use of land suitable for planting the Paulownia trees in Bosnia and Herzegovina.

The company will have a special aspect of monitoring customer satisfaction, market demand, attracting new customers and retaining existing ones, continuous improvement of technologies and personnel in order to obtain higher quality products compared to the competition.

4.5 Strategy of the company

The strategy of the company “M&M PAULOWNIA” LLC is based on the idea that by combining resources and existing opportunities, with a view to the challenges and environment limitations, find the best way for achieving the strategic goals, mission, and vision of the company.

Strategic goal 1: Offer of innovative products – purchase of investment cultivation.

Measures:

- At the plantation in Aleksandrovac, parcel the land intended for investment sale on plots of one hectare with a capacity for planting about 500 seedlings of fast-growing Paulownia trees obtained by “in vitro” technology.
- As part of the business, the company will offer several sales packages on one-hectare plots:
 - PACKAGE 1: Purchase of investment cultivation after three years of growth and independent continuation of work and maintenance until the moment suitable for logging (next 4-5 years);
 - PACKAGE 2: Purchase of investment cultivation after three years of growth

- with continued maintenance by the company “M&M PAULOWNIA” LLC (irrigation, pruning, and all other actions prescribed by the profession);
- PACKAGE 3: Independent work on the formation of the plot from planting, through plucking after the first year of growth, and further monitoring of growth until the moment suitable for logging. As part of this packaging company “M&M PAULOWNIA” LLC offers a plot of one hectare, all its knowledge and skills and transfers it to the investor for necessary education. The acquired knowledge and skills can be used by the investor later for independent cultivation and starting a business.
 - PACKAGE 4: Giving the investor opportunity to create the contents of the package where all combinations of the Package 1, 2 and 3, which are already mentioned, are allowed with the possibility of adding new elements (e.g., between rows of Paulownia trees other plant species can be planted [13]; usage for beekeeping during the flowering of Paulownia trees [1] and other).

Strategic goal 2: Strengthening marketing activities

Measures:

- Create a company's website to improve the visibility in the market, better inform customers, and reach new customers easier,

- In addition to on-site sales, the company will offer the possibility of selling through the online store on the company's official website,
- Developing a network of distributors in strategic locations in the country (and later in the region) to deliver products faster to customers.

Strategic goal 3: Placing products on the European Union market

Measures:

- After gaining the necessary experience and work references, the company plans to expand the scope of its activities to the market of the European Union countries,
- To achieve this ambitious strategic goal, it is necessary for planting material and other products of the company to pass all strict phytosanitary inspections and successfully meet all the required conditions for export to the European Union countries.
- To find an adequate business partner and exclusive distributor for our company's products in the European Union.
- Find new suppliers to ensure a constant supply of planting material and better prices.

4.6 Risk assessment

Table 5. provides an excerpt of the risk analysis for the identified hazards coming from the environment and weaknesses of the company with the necessary risk mitigation measures.

Table 5. Excerpt from the risk assessment for identified hazards and weaknesses

RISK	RISK ASSESSMENT		
	POSSIBILITY	CONSEQUENCES	MEASURES
Insect appearance	Low, to 10 %	Partial or complete damage to seedlings; Repeated planting	Application of insecticides from verified manufacturers
Natural disasters	Unable to determine	Partial or complete damage to seedlings; Repeated planting	Installation of protective structure
Irrigation system failure	Low, to 5 %	Slow plant growth	Preventive control and regular maintenance
Theft of plantation	Low, to 5 %	Reduced sales; Repeated planting	Hiring security worker
Low demand for products	Low, to 8 %	Reduced sales; Financial problems	Appropriate promotion and advertising

5. CONCLUSION

The production of fast-growing energy crops, which includes Paulownia trees observed

through this paper, can play a major role in increasing the share of renewable energy sources in the Republic of Srpska and Bosnia and Herzegovina. Also, their impact on reducing

global warming by absorbing greenhouse gases should not be ignored. Before starting the production of Paulownia trees all important external and internal factors, that may have an impact on the placement of products on target markets should be considered because all areas where the Paulownia tree production is present have a specific business environment.

The analysis that has been done for starting the production of Paulownia trees in the Banja Luka region showed good profitability and great opportunities for its placement on the Bosnia and Herzegovina market. It is necessary to strengthen product innovation and marketing activities in order for the customer to become better acquainted with its characteristics and advantages.

REFERENCES

- [1] Icka, P., Damo, R., Icka, E. (2016). Paulownia Tomentosa, a Fast-Growing Timber. *Annals "Valahia" University of Targoviste – Agriculture*, vol. 10, no. 1, p. 14-19. DOI: <https://doi.org/10.1515/agr-2016-0003>
- [2] Rodríguez-Seoanea, P., Beatriz Díaz-Reinosob, B., Mourea, A., Domíngueza, H. (2020). Potential of Paulownia sp. for biorefinery. *Industrial Crops & Products*, vol. 155, p. 1-15 DOI: 10.1016/j.indcrop.2020.112739
- [3] Woods, V. (2008). Paulownia as a novel biomass crop for Northern Ireland?: a review of current knowledge, Hillsborough, Co. Down: Agri-Food and Biosciences Institute, Global Research Unit, Occasional Publication, no. 7
- [4] Nelis, P., Michaelis, F., Krause, K., Mai, C., (2018). Kiri wood (Paulownia tomentosa): can it improve the performance of particleboards? *European Journal of Wood and Wood Products*, vol. 76, p. 445-453. DOI: <https://doi.org/10.1007/s00107-017-1222-7>
- [5] Qi, Y., Yang, C., Hidayat, W., Jang, J. H., & Kim, N. H. (2016). Solid bioenergy properties of Paulownia tomentosa grown in Korea. *Journal of the Korean Wood Science and Technology*, vol. 44, no. 6, p. 890-896. DOI: <https://doi.org/10.5658/WOOD.2016.44.6.890>
- [6] Ferreira, A., Paiva, J. Evaluation of Paulownia's biomass in a pelletized form, *23rd ABCM International Congress of Mechanical Engineering*, December 6-11, 2015, Rio de Janeiro. DOI: 10.20906/CPS/COB-2015-0720
- [7] Angelov, B. (2010). "Paulownia the tree of future", Velboy Ltd. Bulgaria
- [8] https://ec.europa.eu/clima/policies/strategies/2030_en, accessed on: March 20, 2021.
- [9] Coulter, M. (2008). *Strategic Management in Action*. Prentice Hall, Upper Saddle River, New Jersey
- [10] Martinović, S., Nićin, N. (1995). *Menadžment danas*, Ulixes marketing, Novi Sad
- [11] Kukić, S. (2007). *Marketing*, Ekonomski fakultet Sveučilišta u Mostaru, Mostar
- [12] The Republic of Srpska Institute of Statistics, <http://www3.rzs.rs.ba:8080/rzs/faces/indicator.s.xhtml>, accessed on: March 31, 2021.
- [13] Yin, R., & He, Q. (1997). The spatial and temporal effects of paulownia intercropping: the case of northern China. *Agroforestry Systems*, vol. 37, no. 1, p. 91-109. DOI: <https://doi.org/10.1023/A:1005837729528>



Banja Luka
28–29 May 2021.

DEMI 2021

15th International Conference on
Accomplishments in Mechanical and
Industrial Engineering

www.demi.mf.unibl.org



BUSINESS PROCESS IMPROVEMENT IN THE AUTOMOTIVE INDUSTRY - QUALITY METHODS AND TOOLS

Z. Tanasić^a, A. Jokić^b, G. Janjić^a, M. Bobrek^a, B. Kosec^c

^aFaculty of Mechanical Engineering, University of Banja Luka, V. Stepe Stepanovića 71, 7800 Banja Luka, BiH

^bMAHLE Electric Drives Bosnia, Nemanjina 63a, 78250 Laktaši, Bosnia and Herzegovina

^cFaculty of Natural Sciences and Engineering, University of Ljubljana, Aškerčeva cesta 12, 1000 Ljubljana, Slovenia

Abstract *The development of global economy has forced many companies to introduce and apply modern approaches, models, and initiatives for rapid and long-term business improvement. Achieving business excellence and creating world-class products and services are a basic prerequisite for the survival, growth, and development of the company. It is not the job of just one organizational unit, but the result of synchronized action of all processes in the organization according to clearly defined business goals.*

This paper includes and elaborates tools and methods of a quality management system in the automotive industry. As statistical process control and the occurrence of non-compliance are indispensable, only organizations that continuously improve the level of product quality and reduce costs survive in the market. Therefore, it is very important to establish an efficient system for managing the quality of processes and products, which means the efficient application of quality tools and the commitment of all employees in the organization.

Keywords *quality standards, automotive industry, quality tools*

1. Introduction

The automotive industry has made a huge contribution to the overall development of mankind, especially in the area of quality. It was the first to realize that in order to achieve the development and improvement of the competitive position on the market, it is not enough to be good, but it is necessary to be in the group of the best, where those who are equal in terms of technology compete. [1].

In order to assure that the desired quality of the products is achieved, there are several

standards that are used in the automotive industry. ISO 9000 defines the quality standards and general rules on quality management for all industries. QMS is based on five pillars of quality, which are [2].

- Advanced Product Quality Planning (APQP) and Control Plans
- Failure Mode and Effect Analysis (FMEA)
- Statistical Process Control (SPC)
- Measurement System Analysis (MSA)
- Production Part Approval Process (PPAP).

However, ISO/TS 16949 is specific for the automotive industry in terms of quality management systems.

Today, the world's leading companies are increasingly using the term “business excellence”, which claims that providing high quality is a unique and right path to efficiency and effectiveness.

Corresponding author

Prof. Zorana Tanasić, PhD
zorana.tanasic@mf.unibl.org

University of Banja Luka Faculty of Mechanical Engineering
Bulevar vojvode Stepe Stepanovića 71
78 000 Banja Luka, BiH

APQP is a structured method for defining and executing the steps necessary to ensure that the product meets the requirements of the customer /consumer. APQP is a team approach required of all systems, subsystems, production processes, and suppliers. This method was first applied by Ford, to be later integrated as a major element of ISO / TS 16949. Compared to earlier systems, the progressive quality plan covers several influencing factors, systematizes them and prescribes clear rules.

The goal of the quality system according to ISO / TS 16949 is the development of a quality management system that provides continuous improvement, failure prevention, and reduction of variations and defects in the supply chain. It is applied in the design (development), production, assembly, and servicing of products in the automotive industry and represents the harmonization of the requirements of the European (German, French, and Italian), American (GM, Ford, and Dodge / Chrysler) and Japanese automotive industries [2, 3].

Figure 1. shows the historical development of the quality management system (QMS) standard from 1970, until the establishment of the ISO / TS 16949: 2002 standard and its revision in 2009.

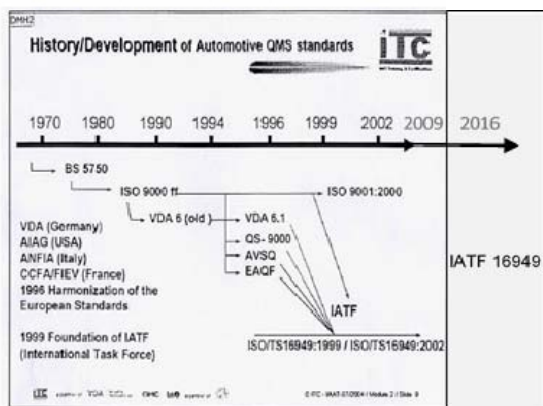


Fig. 1. Development of standards for the quality management system in the automotive industry

From October 2016, ISO / TS 16949 became IATF 16949, based on the ISO 9000 standard. Nevertheless, IATF declares in the History chapter of IATF 16949:2016 that „The IATF maintains strong cooperation with ISO by continuing liaison committee status ensuring continued alignment with ISO 9001” (IATF, 2016). IATF 16949:2016 is linked with ISO 9001:2015, and cannot be considered a

standalone QMS standard. It is a supplement to ISO 9001:2015 and must be used in conjunction with [3].

2. METHODS AND TOOLS OF THE QUALITY SYSTEM

Tools for improving quality in the automotive industry are known as: concepts, techniques, methods, studies, tools, or, more generally, all efforts aimed at improving quality. Quality policy covers the basic directions and goals of the organization in terms of quality, so it is one of the elements of the general policy of the company and must be in accordance with the strategy, goals, and mission of the organization. Also, the full effect of the application of quality tools (the tools of the quality management system), requires the correct choice of tools and their mutual coordination.

This paper presents only some of the quality tools used in the observed company, namely:

1. PPAP analysis,
2. a process flow chart,
3. FMEA analysis,
4. a Control plan, and
5. MSA/SPC analysis.

2.1 PPAP and MSA/SPC analysis

PPAP in the automotive industry represents a process that is required to ensure mutual trust between the customer and the supplier. The buyer / customer is the one who sets out his requirements, and the supplier needs to find the most favourable and easiest way to meet the requirements set by the customer.

Every supplier aims to conquer new markets and make a profit in the most competitive way possible. Therefore, the proper process of approving the first samples is paramount for ensuring deliveries for serial production with risks, in terms of quality, minimized, but also ensuring the delivery of the required quantity of products.

The customer submits to the supplier the technical documentation of the requested product / part, with defined dimensions and permitted deviations. The key characteristics and potential places (positions) where the risks of failure may occur are the positions that are processed in MSA/SPC analysis. According to the customer's requirements, the supplier must

submit the first samples, DFMEA analysis, flow chart as well as control plans with MSA / SPC analysis. PPAP ensures that the supplier can meet the customer's requirements in terms of production and quality, engineering design as well as the requirements and specifications defined in the technical documentation. Also, the analysis shows that the selected technological process of production can produce a part that complies with all the set requirements. Through PPAP analysis the customer requires a detailed process of analysis of his requirements and needs from the supplier. This analysis involves making the first samples and sending them to the customer for approval.

The PPAP analysis process is quite complex and long lasting, but, as such, it defined requirements that must be provided in order to confirm that the production process will produce a quality product. The elements that are required depend exclusively on the customer, which is most often defined in the offer for the production of a certain product [4]. The PPAP process is detailed and time consuming, but, as such, it provides customers with adequate information and confirmation that all processes from design to production and control will be inspected in detail and, thus, ensure that only high quality products will always be delivered.

2.2 FMEA analysis

The FMEA methodology was developed to systematically monitor and analyze process failures. This method belongs to the methodology of building business processes, and was developed in the 1950s. FMEA is one of the most reliable methodologies for monitoring and analyzing failures in management systems and it includes many factors to identify failures and their causes.

Today, many methodologies are used in business process management and construction systems, for example: IDEF0 (International Definition for Function Modelling), SIPOC (Supplier Input Process Output Customer), UML (Unified Modelling Language) and others. All of the above methodologies are useful for a quality management system. The FMEA was first used in the U.S. military industry and at the NASA. Due to good results it has shown, it has started to be applied in other areas of industry as well.

2.3 The Control plan

The control plan defines the method of assessing functional characteristics throughout the entire process of manufacturing semi-finished products and products, in order to meet the specific requirements of the process.

The process of making a control plan implies a detailed analysis of the process and place of occurrence of risks that affect the quality of products through the definition of control characteristics (control-points). Defining control points implies:

- Determining the type of quality characteristics (numerical or attributive), the form and specifications of failures, the availability of means and methods for measurement as well as the importance of quality characteristics,
- Defining the scope and frequency of quality control,
- Determining the holder of control (worker, process controller, or leader).

The results of the measurements are entered in the form "Taking over the process" on the basis of which it is possible to identify the deviation of the controlled measure from the measure prescribed by the control plan.

3. APPLICATION OF QUALITY METHODS AND TOOLS – a case study

The company was founded in 1994, and its main activity is the production of stator windings for motors and starters for customers of the automotive industry, Figure 2. The production line combines winding elements with soldering, which are impregnated with electrical insulating varnish immersion process. The installation of the protective layer elements takes place on an automatic line with dedicated devices.



Fig. 2. The finished product

In accordance with the procedures of the company that is under research, specific data (numerical values) will not be visible in this paper because they are secret, but they can always be available and presented to a potential customer.

3.1 PPAP – customer requirements

This paper presents a part of the PPAP analysis that is performed in the observed company, as a process of approving the first parts for a specific project of production and assembly of the final product.

In order to make the first parts and send them for approval, all the requirements stated in the technical documentation must first be realized. The first step in accepting and developing the first PPAP samples is to form a team, which will follow and support the whole process of making the first parts and develop an APQP plan, based on their knowledge and skills. This plan facilitates communication between all participants in the process and ensures that all required steps are implemented on time. The benefits expected from the application of the APQP are:

- directing resources to achieve customer satisfaction,
- enabling early identification of necessary changes,
- avoiding delayed changes,
- providing a quality product, on time, with minimal costs [3].

As shown in Figure 3, the customer submits a request stating all the necessary analysis, or specific requirements, for the first product samples to be approved, which are:

- three reference samples,
- the dimensions of the samples must be within the tolerances shown in the drawing,
- performing analysis of materials that are part of the stator,
- FMEA process analysis,
- a process flow diagram, and
- a control plan.

Also, the request provides key measures:

- inner diameter (during further installation, this dimension is one of the key functional characteristics),
- breakdown (100% control, value >2s/750V),
- water resistance (air release test), etc.

Figure 4. shows the measurement report. The analysis and production of the first samples is given on the example of stator assembly.

Fig. 3. PPAP requirements

Fig. 4. A measurement report

3.2 MSA/SPC analysis

Since most customers have certain dimensions on their products that are defined as key process characteristics (KPC), for such dimensions / measures during the production process, continuous statistical monitoring is performed.

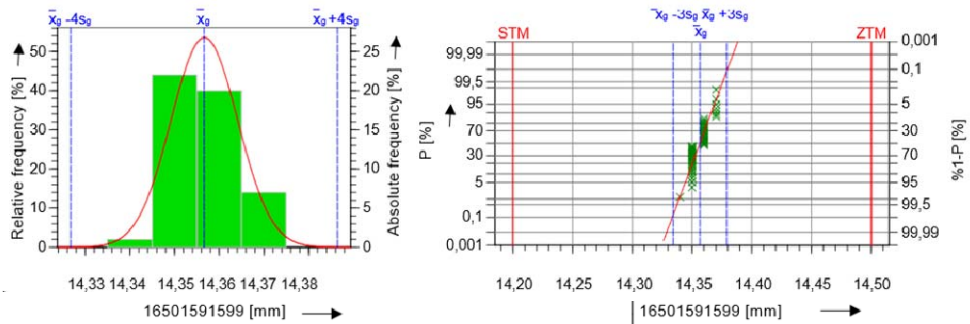
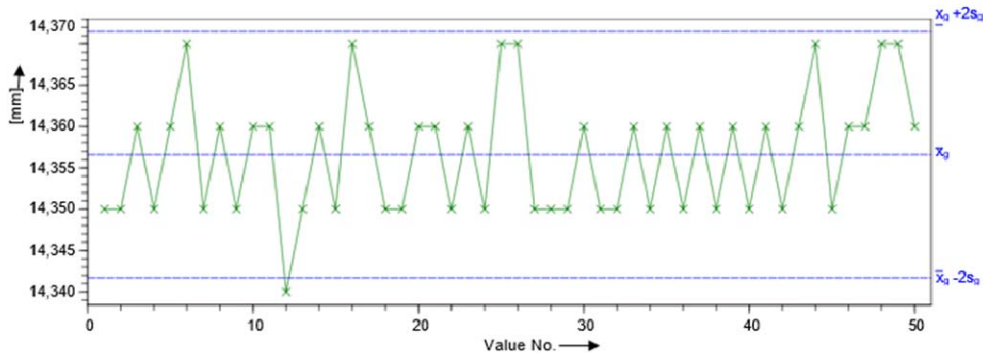
Figure 5 shows the samples on which the measurement was performed. Measurement

results can be presented in two forms, a process under statistical control and a process not under statistical control. A total of fifty samples were tested, of which forty-nine are within the prescribed limits, while sample number twelve goes beyond the set limits, which means that the samples meet the set tolerance limits. It is crucial that the process is under statistical control, if 2/3 of the values of the controlled parameters are within the central third of the

control chart, in a width $\pm \sigma$ around the central line. The values of C_g and C_{gk} are indicators of the process ability, and as $C_g = 2.01$ and is in the range ($1.62 < 2.01 < 2.41$), the results show that the possibility of scrap is reduced.

This ensures that the most important measures are under constant control and that potential errors are detected as soon as possible, which allows us to stabilize the process and reduce production costs.

Measurement System Analysis				Page 1 / 1	
Odd. po NN	Odd./SM/izd.	NN	Op. Name:	Đokić, Jokić	Date/time 09.10.2020.
Part no. 1	Char.Descr. 16501591599			Obv. dok. ne	
Mach.Descr.	Ozn. karakt. 16501591599			ZTM	XX
Mach. No.	Char.No. 1			Unit mm	STM XX
Char.Type variable	Char.Class significant	Rec.type. manual	Decimal Pl. 3		
Plant Sector	Gage Grp.		Gage Descr		
Tool Number	Gage No.		Gage Res.		
Evaluation	from 09.10.2020. 12:06:41	to 09.10.2020. 12:06:41			
Remark					



Drawing Values		Collected Values		Statistics	
$X_{m+U} \cdot 1 \& l$	---	$X_{max\ g}$	= 14.370	$X_g + 3S_g$	=
X_{m-}	---	$X_{min\ g}$	= 14.340	X_g	=
$X_{m-U} \cdot 1 \& l$	---	T_{kg}	= 0.030	$X_g - 3S_g$	=
$0.28T$	= 0.06000	n_{kisp}	= 50	G_{Sg}	= 0.04472
T	= 0.300			S_g	= 0.00745
	Bias			n_{ef}	= 50

Resolution	%RE =	---	0	5	
$\%EV = \frac{EV}{T}$	=	14.91%	0	15	$T_{min} (\%EV)$ = 0.298
$C_g = \frac{0.28T}{4\sigma_s}$	=	$1.62 \cdot 2.01 \cdot 2.41$	0	1.33	$T_{min} (C_g)$ = 0.199
$C_{gk} = \frac{0.14T - X_{m+U} - X_{m-U} }{2\sigma_s}$	=	---	0	1.33	

Fig. 5. MSA analysis for the product (winding)

Figure 6 shows the SPC analysis of the windings and based on a hundred values tested, they were all in the prescribed tolerance field. Process capability index $C_p = 3.45$ as well as long-term study of a stable process $C_{pk} = 1.56$

shows us that the process is stable, as shown in the diagram, both parameters are green and are within the allowable limits ($C_p \rightarrow 2.95 < 3.42 < 3.90$); ($C_{pk} \rightarrow 1.33 < 1.56 < 1.79$).

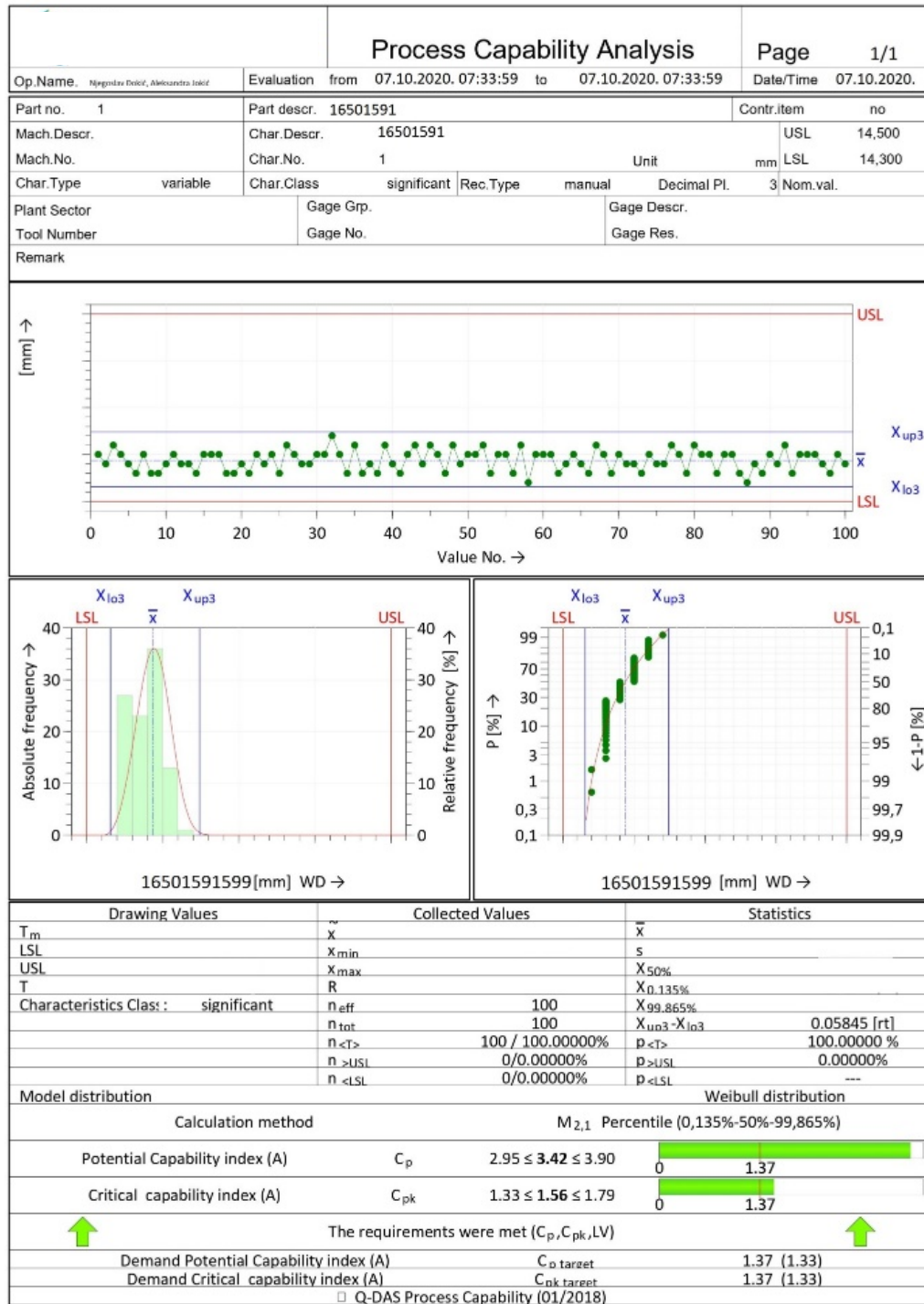


Fig. 6. Statistical monitoring of critical measures (winding)

specific requirements must also be harmonized with the existing technologies of manufacturing individual components, whereby new technologies are often approached and applied in order to achieve competitiveness in the market. New technologies, new suppliers, and projects represent a huge set of risks for the successful placement of products on the market while achieving appropriate competitiveness.

The revision of the standard, ISO / TS 16949: 2009 and the transition to IATF 16949: 2016 aims to develop a quality management system that provides continuous improvement highlighting the lack of prevention and reduction of waste and variation in the supply chain. The incorporation of ISO 9001: 2015 and IATF 16949 requirements includes specific requirements: employee competence (awareness and training), design, development, production and provision of services, control and monitoring of measuring devices and measurements, analysis, and improvement. All of this aims to get products and services that satisfy customers.

Quality control is performed by process controllers at all stages of production. In order to make a product of satisfactory quality, it is important that the production process is stable. Constant investment in new technologies, modernization of production, education, and training of employees at all levels improve the quality system in the company

Continuous improvement of the quality of the production process, based on increasing the productivity and knowledge of each employee in the organization, is crucial for the realization of the mentioned preconditions. Competition and the globalization of all flows are forcing companies to find increasingly successful management approaches using quality management tools in all business processes. The main goal of every company is to strive to always deliver improved value to the customer and user, as a result of improving the overall performance of the business system as well as capabilities and success in the market.

REFERENCES

- [1] Tanasić Z., Janjić G., Bobrek M. (2016). *Organizacija i menadžment*. Univerzitet u Banjoj Luci, Mašinski fakultet, Banja Luka.
- [2] Kušar, K., Rihar, L., Duhovnik, J., Starbek, M. (2014). Concurrent realisation and quality assurance of products in the automotive industry. *Concurrent engineering: Research and Applications*. Sage Publications. vol. 22 (2), p. 162-171.
- [3] <https://www.researchgate.net/publication/320356880> *Quality Management Requierements in the Automotive Sector a Structured System*, accessed on: March 20, 2021.
- [4] Bobrek, M., Sokovic, M. (2005). Implementation of APQP concept in design of QMS. *Journal of Materials Processing Technology*, vol. 162-163. p. 718-724.
- [5] Ebrahimi, M., Baboll, A., Rother, E. (2019). The Evolution of World Class Manufacturing Toward Industry 4.0: A Case Study in the Automotive Industry, *IFAC-Papers On Line*, vol. 52, p. 188-194.
- [6] IATF 16949:2016 - Automotive Quality Management System. International Organization for Standardization. Geneva.
- [7] <https://www.svijet-kvalitete.com/index.php/upravljanje-kvalitetom/878-fmea-metodologija>, accessed on: March 20, 2021.
- [8] Belu, N., Ali, A., Khassawneh, N. (2013). Application of Control Plan - PPAP Tool in Automotive Industry. *Production QUALITY access to success*, vol. 14 (136), p. 5-12.
- [9] Doshi Jigar A., Desai Darshak A. (2018). Role of Production Part Approval Process in Continuous Quality Improvement and Customer Satisfaction. *International Journal of Engineering Research in Africa*, ISSN: 1663-4144, vol. 22, p. 174-183, doi:10.4028/www.scientific.net/JERA.22.174
- [10] Chiarini, A., Vagnoni, E. (2018). Can IATF 16949 certification facilitate and foster Lean Six Sigma implementation? Research from Italy, *Total Quality Management & Business Excellence*. ISSN: 1478-3363 (Print) 1478-3371 (Online), vol. 31, Issue 7-8, p. 887-906. From <https://doi.org/10.1080/14783363.2018.1456330>, accessed on: February 25, 2021.



Banja Luka
28–29 May 2021.

DEMI 2021

15th International Conference on Accomplishments in Mechanical and Industrial Engineering

www.demi.mf.unibl.org



COMPARATIVE STUDY OF DIFFERENT OPTICAL COORDINATE MEASUREMENT SYSTEMS

G. Jotić^a, B. Štrbac^b, S. Tešić^a, M. Hadžistević^b

^aFaculty of Mechanical Engineering Banja Luka, V. Stepe Stepanović 71, 78000 Banjaluka, BiH

^bFaculty of Technical Science Novi sad, Trg Dositeja Obradovića 6, 21102 Novi sad, Serbia

Abstract Geometric inspection of complex parts is of great interest in industrial production. Coordinate measuring machines (CMM) are widely used because they are flexible and have a high accuracy. They are often used for inspection of prismatic parts and freeform surfaces. The CMMs are relatively slow and allow generating a certain number of points at the surfaces. Faster measurement can be achieved with non-contact optical measurement systems (OMS), 3D scanners. These measurement systems offer several advantages like fast acquisition of points at the surface of the part, high density of points, independence of measurement results from rigidity of part, fast and easy access to the surfaces of the complex part. Compared to coordinate measuring machines, these measurement systems are less accurate. Also, the procedures of accuracy test for non-contact measurement systems and shape of standards are not strictly defined. The aim of this paper is to present a comparative analysis of two 3D portable and handheld scanners based on laser triangulation. For this purpose, two calibrated artefacts were used and two test parts were designed. The result of this analysis can be used for the selection of an optimal measurement system for a specific measuring task.

Keywords accuracy, digitalization, contactless measurement systems

1. INTRODUCTION

Striving to reduce the total production costs, strict requirements are set for coordinate metrology. Coordinate measuring machines (CMMs) are the most common measurement systems in industrial metrology, especially in aerospace, automotive, die/ mold industry [1]. The CMMs with contact probes can measure up to 200 points/s with the maximum speed of 150 mm/s [2]. The CMMs are relatively slow and

allow generating a certain number of points at the surfaces.

Faster measurement can be achieved with non-contact coordinate measurement systems. These measurement systems offer several advantages like fast acquisition of points at the surfaces of the part, high density of points, independence of measurement results from rigidity of part, fast and easy access to the surfaces of the complex part [3]. Inspection of complex parts and freeform surfaces requires high performance of scanners, accuracy first of all. Optical measurement systems reduce measurement time, but, in comparison to CMMs, these measurement systems are less accurate [4]. The process of determination of laser scanner accuracy is not clearly defined and it is necessary to perform various comparison tests.

Corresponding author

Senior teaching assistant, Goran Jotić
goran.jotic@mf.unibl.org

Faculty of Mechanical Engineering Banja Luka,
V. Stepe Stepanović 71,
78000 Banjaluka, BiH

Giganto et al. [5] compared different measurement systems based on laser triangulation, conoscopic holography, and structured light techniques for Geometric Dimensioning and Tolerancing (GD&T) verification of selective laser melting parts. Barbero and Ureta [6] analyzed the accuracy of different optical measurement systems based on the surfaces obtained from point clouds. Five digitization systems are considered with three calibrated artefacts and two test parts. Al-Ahmari and Alam [7] focused their study on two laser triangulation scanners mounted on a CMM and an Articulated measuring arm. Design of Experiment (DOE) is used to optimize surface parameters in the process of reconstruction of complex parts. Toth and Živčák [8] compared the quality of scanned data at two different scanners. A comparative study included a dimensional and geometrical inspection of the special design of a test part. The part was produced by additive technology. Guerra et al. [9] compared a structured light scanner, a photogrammetry based scanner, and a laser scanner. Additionally produced step gauges were used for comparison of these measurement systems.

This paper presents a methodology of comparative analysis of two 3D portable and handheld scanners based on laser triangulation. For this purpose, two calibrated standards were used and two test parts were designed. Result of this study can be used to analyze dimensional and geometric accuracy of the analyzed measurement systems.

2. MATERIAL AND METHODS

Optical measurement systems were divided into five categories, i.e., the systems based on triangulation, ranging, interferometry, structured light, and image analysis [10]. 3D laser scanners based on triangulation method are the most commonly used for laboratory research and modern industry inspection. In this research two portable handheld laser scanners were analyzed (Figure 1-2).

The MMDx100 laser line triangulation scanner is integrated at a Nikon MCAX portable coordinate measuring arm (CMA) with six degrees of freedom (DOF). A portable arm can be mounted at the magnetic stand or tripod. The Creafom Handyscan scanner is a manual scanner without a stand. This scanner with

seven red laser lines and a camera identifies target points placed near the object. The advantage of these scanners is the ability to generate high density point clouds at the surfaces of complex parts for a short time.



Fig. 1. An MMDx100 laser scanner integrated at articulated measuring arm



Fig. 2. An Creafom Handyscan 700 laser scanner

Table 1 indicates the major configurations of the scanners compared.

Table 1. Specification of scanners

MMDx100	
Accuracy	10 μm
Min. point resolution	65 μm
Max. frame rate	150 Hz
Stripe width	100 mm
Max. points per stripe	1000
Accuracy comb. with MCAX arm	48 μm
Light source	1 laser crosses
Handyscan 700	
Accuracy	30 μm

Resolution	50 μ m
Scanning area	(175x250) mm
Measurement rate	480 000 measur./s
Volumetric accuracy	0,02 mm+0,06 mm/m
Light source	7 laser crosses

Calibrated artefacts like a gauge block, a cylinder, and a sphere are widely used in the industry. Comparison process and evaluation of scanners is based on the verification of two calibrated artifacts and two test parts (Figure 3). Chosen artefacts and test parts with set geometric features and freeform surface represent samples which cover a series dimensional and geometrical tolerances. Also, the scanned surfaces of test parts were compared to CAD models. Anti-reflection coat in spray form was applied to shiny surfaces of analyzed objects.



Fig. 3. Objects to be measured

A calibration process of used scanners was performed before digitization of objects. Because of the manual nature of the digitizing process, it is difficult to maintain consistency, even if the process is performed by the same operator. However, dispersion of values is bigger if scanning is done by a different operator. Considering this influence, analyzed objects are digitized by the same operator

under the same strategy of scanning and the same alignment process. After the digitization process, raw point clouds are cleaned. Also, this process includes manually removing point clouds which do not belong to a part of object surfaces. Software Focus inspection and Geomagic control were used for processing point clouds and analyzing deviations. The digitization process was performed under controlled laboratory conditions.

3. RESULT AND COMPARISON

The calibrated artefacts were defined with their corresponding certified values and uncertainties. Their accuracy is much higher than accuracy of analyzed measurement systems and serves as reference. A gauge block and a sphere (Fig. 2) were used for determination of a systematic error of scanners and enabled to compare their accuracy. The obtained deviation is presented as the difference between the measured value and value accepted as a reference (Table 2). The digitization of artefacts was repeated three times and obtained values presented a mean.

Table 2. Values of dimensional deviations

Digitization systems	Gauge block length deviation (mm)	Sphere diameter deviation (mm)
MMDx100	0.0259	-0.0105
HandyScan 700	0.0484	-0.0367

Dimensions of the complex test part are not established and they are not calibrated. These test parts are used to test scanners in real conditions in practice. A digitized surface of test parts was compared to CAD models. Comparison results are shown in Figures 4-7. Comparison of scanned surfaces and the CAD model was performed by the best-fit algorithm of alignment. Comparison based on numerical form deviation and global deviation using color maps allows quick and easy analysis of generated deviation by both scanners (Figure 4). Form deviations in the cross-section enable a better insight into the value of deviations in certain areas (Figure 5).

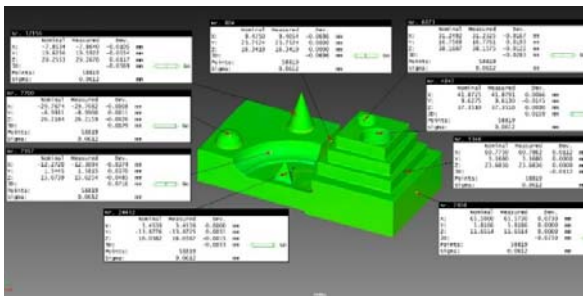


Fig. 5

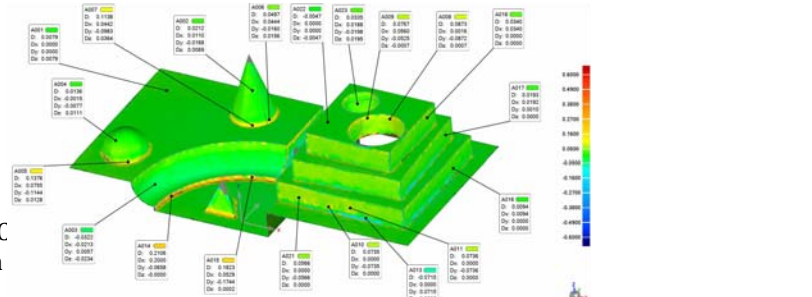


Fig. 6

Fig. 7

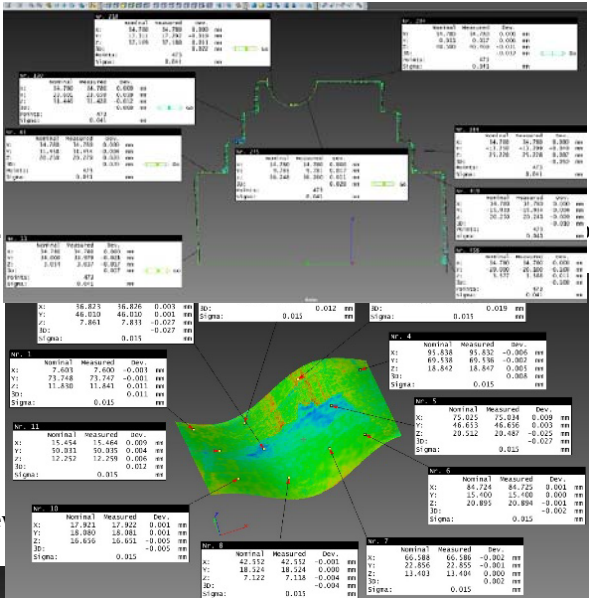


Fig. 8

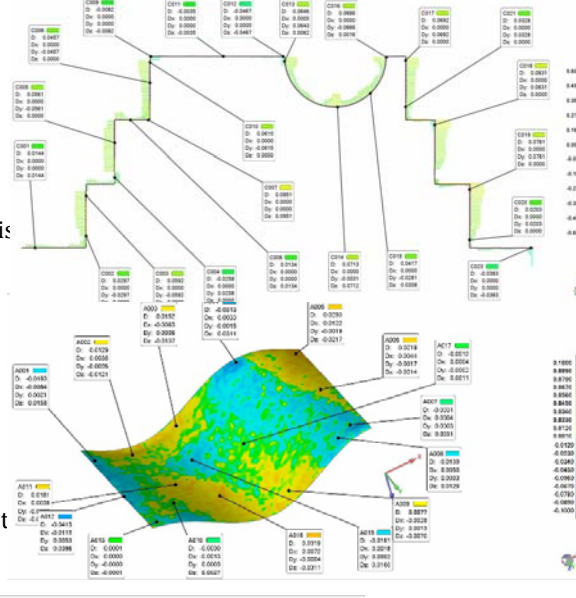


Fig. 9

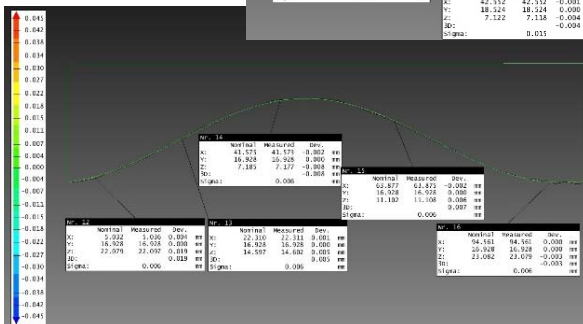
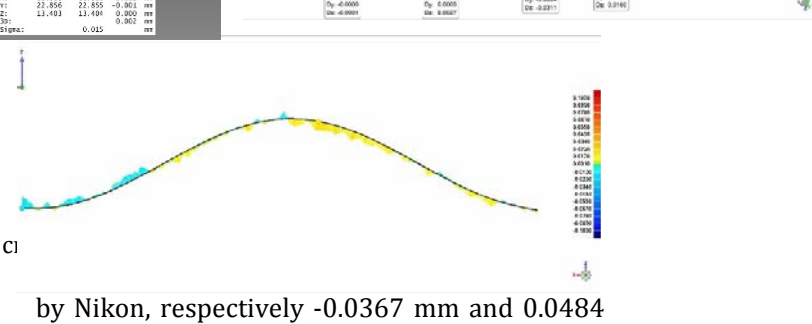


Fig. 10



on a variety of factors. Some of them come from the scanner (sensitivity of sensor, calibration), then from the object (geometry, rigidity, roughness of surface, shiny surfaces), then from ambient conditions (lighting, dust, temperature, humidity) and the operator's ability. Both scanners were used at the same laboratory conditions by the same operator. Deviations obtained at the calibrated artifacts can be used for determination of systematic error of scanners. Based on the deviation obtained at the two difference scanners (Table 2), it can be concluded that the MMDx100 scanner has shown smaller deviations. The values of these deviations range between -0.0105 mm and 0.0259 for MMDx100 scanner

by Nikon, respectively -0.0367 mm and 0.0484 mm for Handyscan 700 by Creaform. The test parts with a set of geometric features and a freeform surface are not calibrated. They can serve for comparison of scanners in terms of distribution of points, quality of mesh, digitization in the area of edges and holes. Deviations obtained at the test parts are shown in table 3.

Table 3. Deviations obtained at the test parts

	MMDx100	HandyScan 700
Prismatic test part	(-0.07 ± 0.07) mm	(-0.07 ± 0.09) mm
Test part with freeform	(-0.03 ± 0.02) mm	(-0.04 ± 0.03) mm

4. CONCLUSION

The inspection process in different areas has encouraged the development of different measurement systems. The main goal of digitization systems is to generate and save object information for the purpose of dimensional and geometric analysis. The contactless digitization systems have their own standards and verify accuracy in accordance with manufacturers' procedures. To compare the performance process of different measurement systems and their accuracy is demanding. Metrological performance of contactless measurement systems is presented with different parameters which are difficult to compare with each other. In the case of an unambiguous approach, it is possible to make comparison of characteristics.

In this study two different laser scanners were compared. A comparison was performed in terms of accuracy and quality of digitalization of complex parts. For this purpose, two calibrated artefacts and two complex test parts were used. Based on the result, it can be concluded that the MMDx100 laser scanner demonstrated better accuracy than the Handyscan 700. Compared to MMDx100, the Handyscan 700 has better acquisition speed. Some of the surfaces of complex parts are difficult to access and they require more passes for scanning, which increases the noise in the point cloud. Based on the surface optimization algorithm, the Handyscan 700 scanner avoids the creation of multiple scans at the same area.

REFERENCES

- [1] Magdziak, M., Ratnayake, C. (2018). Investigation of best parameters' combinations for coordinate measuring technique. *Procedia CIRP*, vol.78, no. 4, p. 213-218.
- [2] Barini, E., Tosello, G., De Chiffre, L. (2010). Uncertainty analysis of point-by-point sampling complex surfaces using touch probe CMMs: DOE for complex surfaces verification with CMM. *Precision Engineering*, vol.3, no. 1, p. 16-21.
- [3] Ameen, W., M. Al-Ahmari, A., Hammad Mian, S. (2018). Evaluation of Handheld Scanners for Automotive Applications. *Applied sciences*, vol.8, no. 2, p. 217-232. DOI: [10.3390/app8020217](https://doi.org/10.3390/app8020217)
- [4] Cuesta, E., Alvarez, B.J, Martinez-Pellitero, S., Barriero, J., Patino, H. (2019). Metrological evaluation of laser scanner integrated with measuring arm using optical feature-based gauge, *Optics and Lasers in Engineering*, vol. 121, no. 2, p. 120-132.
- [5] Giganto, S., Martinez-Pellitero, S., Cuesta, E., Meana, V., Barreiro, J. (2020). Analysis of Modern Optical Inspection Systems for Parts Manufactured by Selective Laser Melting, *Sensors*, vol. 20, no. 11, p. 120-140. DOI: [10.3390/s20113202](https://doi.org/10.3390/s20113202)
- [6] Ramos Barbero, B., Santos Ureta, E. (2011) Comparative study of different digitization techniques and their accuracy. *Computer-Aided Design*, vol. 43, no. 2, p. 188-206.
- [7] Al-Ahmari, A., & Aalam, J. (2015). Optimizing parameters of freeform surface reconstruction using CMM. *Measurement*, vol. 64, p. 17-28. DOI: [10.1016/j.measurement.2014.12.031](https://doi.org/10.1016/j.measurement.2014.12.031)
- [8] Živčák, J., Toth, T. (2014). A Comparison of the Outputs of 3D Scanners. *Procedia Engineering*, vol. 69, p. 393-401. DOI: [10.1016/j.proeng.2014.03.004](https://doi.org/10.1016/j.proeng.2014.03.004)
- [9] Guerra, M.G., De Chiffre, L.; Lavecchia, F.; Galantucci, L.M. (2020). Use of miniature step gauges to assess the performance of 3D optical scanners and to evaluate the accuracy of a novel additive manufacture process. *Sensors*, vol. 20, no. 3. DOI: [10.3390/s20030738](https://doi.org/10.3390/s20030738)
- [10] Várady T, Martin R.R, Coxt J. (1997). Reverse engineering of geometric models—an introduction. *Computer-Aided Design*, vol. 29, no 4, p. 255-268.



Banja Luka
28-29 May 2021.

DEMI 2021

15th International Conference on Accomplishments in Mechanical and Industrial Engineering

www.demi.mf.unibl.org



Knowledge management as a tool for management quality improvement

M. Bobrek^a, Z. Tanasic^a, G. Janjic^a, K. Macanović^b

^aUniversity of Banjaluka, Faculty of mechanical engineering

^bTelekomunikacije Republike Srpske a.d., Banjaluka

Abstract *The transition from “quality management” to “management quality”, (quality of management) in recently management theory and practice appears as a crucial approach in creating and realizing organization objectives oriented to achieve sustained success. The notions of “quality” and “sustainable success” imply the processes of measuring carefully selected performances. Organizations are faced with the problem of their correct choice, and the launch of adequate projects for their improvement. The main goal of this paper is the intention of the authors to properly understand and further explain the categories of “effectiveness” and “efficiency” as sets of different performances of the organization. This creates a prerequisite for the proper selection and application of appropriate management methods that will give a measurable result in increasing the quality of functioning of the organization. This approach is strongly related to the implementation of methods for creating and managing organizational knowledge, for which the basic responsibility belongs to the managerial structure of the organization. In this way, the application of these methods becomes the main indicator of the quality of management.*

Keywords *Knowledge management, Quality of management, Effectiveness, Efficiency*

1. TRANSICION FROM QUALITY MANAGEMENT TO MANAGEMENT QUALITY

If started with the definition of quality as set in ISO 9000:2015 Standard: “The degree to which a set of inherent characteristics of an entity fulfils the requirements” and the term ‘entity’ is replaced by ‘management’, management quality will be defined as follows: “The degree to which a set of inherent characteristics of a management fulfils the requirements”.

In organisations that have successfully implemented ISO 9001:2015 there is often a question raised what to do next. In such situations it is necessary to answer two questions, one is the issue of the goal to be realised and the other one is how to realise that goal. Analysing the business excellence EFQM model from 2013 and ISO 9004:2018 standard “Quality management - Quality of an organisation - Guidance to achieve sustained success” it has been concluded that sustainably successful organisation is the goal to strive for. The implementation of the quality management was directed to meeting the needs and expectations of goods and services’ users in the first place, whereas sustainably successful organisations direct efforts towards meeting

Corresponding author

Prof. dr Miroslav Bobrek
bobrek.miroslav@gmail.com

University of Banjaluka, Faculty of mechanical engineering
Stepe Stepanovića 75. Banjaluka, RS - BiH

needs and expectations of all stakeholders. In those efforts management of organizations can use a huge amount of management standards and guidelines such as series ISO 14000, 22000, 17025, 55000, 56000, ... which include theoretical concepts and principles referring to specific focus of management. These multiple needs and expectations of stakeholders elaborated and explained in management standards require a higher level of management maturity, i.e. management quality [1].

2. UNDERSTANDING - THE MAIN CONCEPT OF KNOWLEDGE CREATION

As a crucial way to avoid aforementioned misunderstandings there is conducting knowledge management initiatives in organizations by implementing suitable knowledge management concepts. Contemporary knowledge management literature affirms some of key concepts and issues on theoretical (etymological) level as well as on development of practical methods and tools for implementing in organizations.

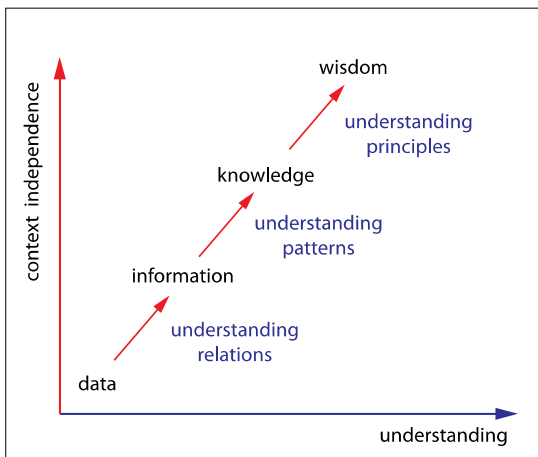


Fig. 1. The main relations of knowledge

Concept on Figure 1., in detail explained in [2], presents knowledge creation through the level of understanding considered problem (relations, patterns, principles). Emphasizing the significance of “understanding”, the author of this scheme stresses: “a collection of data is not information, a collection of information is not knowledge, a collection of knowledge is not wisdom and a collection of wisdom is not truth”. To put in other words, collecting data, information and knowledge has to be integrated

through learning process in order to achieve understanding, wisdom and truth.

3. EFFECTIVENESS AND EFFICIENCY – THE MAIN FOCUS OF MANAGERS IN ORGANIZATION

Owing to the fact that there are a number of varieties of management in the process of corporate management, it is necessary to recognize the structure and interconnections of the individual steps in the management process. Corporate governance is related to the structure of ownership and supplies the structure through which the goals of the organization and the means for achieving goals and monitoring performance are set. The representatives of the capital, together with the corporate management (executive directors) define the strategy of how to achieve the set goals. Since the strategic goals of the organization are definitely adopted by the corporate management bodies, it means they are assigned to the corporate executive management to implement. According to different mechanisms used in different types of management processes, managing staff should use appropriate knowledge and competences to effectively execute their goals. The authors of this paper have described in detail in literature the concepts and the methods of knowledge generation following the sequence: data – information – knowledge – wisdom, as well as the processes and the model of the integrated system of knowledge and quality management, respectively.

Peter Drucker’s concepts ‘effectiveness’ and ‘efficiency’ have been adopted in the professional literature for the purpose of the evaluation of management. As he puts it, effectiveness implies “do the right things” and efficiency means “do things in the proper way”. A more concrete meaning of this can be explained in the following way: The term ‘effectiveness’ should be understood as the ability to choose the right goals and ‘efficiency’ as realizing goals by using minimum resources. The main thesis in this paper is that for evaluation of organization performance level achieved related to effectiveness and efficiency depends on level of knowledge and competence of managing staff generated on relation: data - information – knowledge – wisdom. Figure 2. illustrates the main relations.

Effective application and integration of selected methods into organizational behavior should be formally incorporated into the designed and implemented management system, whose supervision through evaluation processes ensures its effectiveness and sustainable functioning of the organization [3].

In order to emphasize the recognition and correct choice of management methods, the following will illustrate the concept of "design thinking" as a typical set of methods aimed at increasing effectiveness and the concept of "lean thinking" as a set of methods to achieve efficiency parameters.

4.1 Design thinking to improve effectiveness

Design thinking [4] refers to the cognitive, strategic and practical processes by which design concepts (proposals for products, buildings, machines, communications, etc.) are developed. Many of the key concepts and aspects of design thinking have been identified through studies, across different design domains, of design cognition and design activity in both laboratory and natural contexts.

Design thinking is also associated with prescriptions for the innovation of products and services within business and social contexts. Some of these prescriptions have been criticized for oversimplifying the design process and trivializing the role of technical knowledge and skills. Design thinking encompasses processes such as context analysis, problem finding and framing, ideation and solution.

4.2 Lean thinking to improve efficiency

Lean thinking is a way of thinking about an activity and seeing the waste inadvertently generated by the way the process is organized. The aim of lean thinking is to create a lean enterprise, one that sustains growth by aligning customer satisfaction with employee satisfaction, and that offers innovative products or services profitably while minimizing unnecessary over-costs to customers, suppliers and the environment. The basic insight of lean thinking is that if you train every person to identify wasted time and effort in their own job and to better work together to improve processes by eliminating such waste, the resulting enterprise will deliver more value at less expense while developing every employee's

confidence, competence and ability to work with others.

5. CONCLUSION

With this paper, the authors intended to point out the importance of knowledge management in organizations, as the main approach in improving the management of the organization, and thus ensuring its sustainable functioning. In this way, they wanted to contribute to modern trends in management as a science, in the field of measuring or evaluating the quality of management. By doing so, they emphasize the need to properly understand the parameters of effectiveness and efficiency that are applied to measure the performance of the organization and its parts. Proper understanding of these categories of success leads to the correct choice of management methods, which explicitly leads to the recognition of the necessary competencies of managers at different levels of the organization. Thus, this approach indicates the directions for planning and programming of education, training and coaching structure in organizations. It can also point out to the top management the appropriate commitments in cooperation with educational institutions and organizations that provide consulting and training services.

REFERENCES

- [1] Ivanović, M., Bobrek, M. (2020). *Kako poboljšati kvalitet menadžmenta - Menadžment kao saznajna disciplina*. PD Q-Expert, Beograd.
- [2] Bobrek, M., Ivanović, M., (2017). *Upravljanje znanjem u sistemu kvaliteta*, Univerzitet u Banjaluci, Mašinski fakultet. Banjaluka.
- [3] Janjić, G., Tanasić, Z., Soković, M., (2021). *Upravljanje kvalitetom*, Univerzitet u Banjaluci, Mašinski fakultet. Banjaluka.
- [4] Bobrek Macanović K., Lukić, M. Uticaj "milenijalaca" na promjene u organizacijama. *CMZ Postignuća i perspective nauke u XXI vijeku*, vol. 6, no. 2, 12. feb. 2018. Banjaluka, p. 66-73. DOI: [10.7251/ZND1802066B](https://doi.org/10.7251/ZND1802066B)



Banja Luka
28–29 May 2021.

DEMI 2021

15th International Conference on
Accomplishments in Mechanical and
Industrial Engineering

www.demi.mf.unibl.org



Contaminants in used engine oil and their impact on the environment and human health

S. Rațiu^a, A. Josan^a, V.G. Cioată^a, I. Kiss^a

^a Politehnica University of Timișoara, Faculty of Engineering Hunedoara, Department of Engineering and Management, Revoluției Street 5, 331128 Hunedoara, Romania

Abstract *Degradation of engine oil occurs as a result of contamination with various substances that cause changes in its properties. This process has a number of negative effects, both on the operation of the engine, causing its wear, and on the environment, as used oils contain a high degree of toxic compounds. Contaminants in used engine oil, such as heavy metals, polycyclic aromatic hydrocarbons, glycol or polychlorinated biphenyls can have serious consequences once they reach nature, and their removal is a costly and time-consuming process. In order to avoid their spread in the environment, constant monitoring of the used oil and knowledge of these harmful substances is required. This paper presents an overview of the contaminants in used engine oil from an ecological perspective, highlighting their impact on the environment.*

Keywords *contaminants, environment, used engine oil, internal combustion engine*

1. INTRODUCTION

For optimal operation, the internal combustion engine needs constant lubrication of its components. This is done with the help of engine oil. Its importance is given by the fact that it creates a film between the moving parts of the engine, thus stopping the loss of mechanical work by friction. Also, the use of lubricants prevents the wear and heating of engine components and ensures their cleaning and sealing [1].

The quality of the engine oil determines the efficiency of the lubrication process. An increase in the level of contaminants in the oil will worsen its properties and, consequently,

decrease the performance of the lubricant. Thus, it can be considered that the lubrication efficiency is inversely proportional to the degree of contamination of the engine oil. In order to ensure a correct lubrication, a constant monitoring of the oil quality and its contaminants must be performed. In this way, not only can it be determined whether the oil needs to be changed, but potential engine problems can also be identified.

Due to the high degree of pollution that contaminants cause on the environment, used engine oil is considered hazardous waste. These substances affect both the optimal operation of the engine, causing the wear of its components, and the environment, as a result of improper disposal of oil. The aim of this paper is to provide a theoretical study on contaminants in used engine oil, exemplifying them and emphasizing their impact on the environment, as well as possible effects on human health.

Corresponding author

Assoc.Prof. PhD. Eng. Sorin Aurel Rațiu
sorin.ratiu@fih.upt.ro

Politehnica University of Timișoara, Faculty of Engineering
Hunedoara, Department of Engineering and Management,
Revoluției Street 5, 331128 Hunedoara
Romania

2. CLASSIFICATION OF CONTAMINANTS

Contaminants that cause engine oil degradation come from a wide variety of sources and can be classified according to several criteria. A first separation can be made depending on the nature of the substance. Thus, the following are distinguished [2]:

- Organic contaminants: represent approximately 75% of the total amount of contaminants present in used engine oil. This type of contaminant contains all the by-products of combustion, such as soot, fuel, glycol and other products that create organic sludge which, in turn, generates oil thickening, engine wear and filter plugging.
- Inorganic contaminants: consists of sand, dust and metal particles, as well as various inorganic acids. They cause all types of wear that occur in the engine.

Contaminants can also be differentiated depending on the state of the matter [3]. This classification is illustrated in Fig. 1.



Fig. 1. The three phases of contaminants in used engine oil [4-6]

There are several ways in which engine oil becomes contaminated [7-8]. Depending on these, contaminants can be categorized according to Fig. 2.

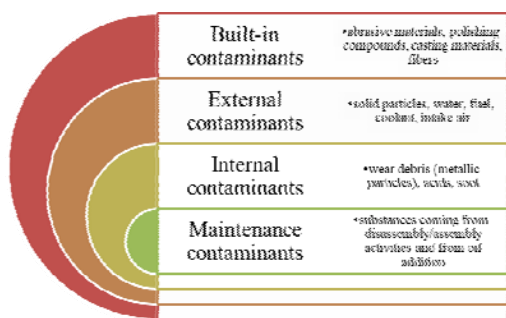


Fig. 2. Contaminants in used engine oil according to the mechanism of contamination

3. IMPACT OF CONTAMINANTS ON THE ENVIRONMENT

Used engine oil is a worrying contaminant due to its high content of heavy metals and polycyclic aromatic hydrocarbons. These substances are generally adsorbed by airborne particles, which are eventually deposited in the soil and water. Also, the used oil can reach the water due to improper disposal or can penetrate the soil, under the action of gravity, eventually reaching groundwater and spreading laterally due to capillary forces and soil heterogeneity [9].

3.1 Heavy metals

As a result of the wear of engine components, the lubricant picks up metallic particles, such as arsenic, cadmium, chromium, copper, lead or zinc [10]. Their impact on the environment and human health is presented in Table 1.

Table 1. Environment and health impact of metal contaminants in used engine oil

Metal contaminant	Environment impact	Human health impact
Arsenic (As)	Lethality, inhibition of growth, photosynthesis and reproduction, and behavioral effects for both plants and animals [11].	Various types of cancer (bladder, kidney, skin, and liver cancer) [12], cardiovascular and peripheral vascular disease, developmental anomalies, neurologic and neurobehavioral disorders, diabetes, hearing loss, portal fibrosis, hematologic disorders [13].
Cadmium (Cd)	Kidney damage, lung emphysema and hypocalcaemia for animals, elimination of some species of microorganisms [14].	Lung cancer, DNA damage, kidney and bone damage [15], depression, reproductive and teratogenic effects, death after ingestion [13].

Chromium (Cr)	Irritation and ulcers in the stomach and small intestine, anemia, male reproductive system damage and tumors for animals [13]; reduction in root growth, leaf chlorosis, inhibition of seed germination and depressed biomass for plants [16].	Stomach tumors, severe respiratory, cardiovascular, gastrointestinal, hematological, hepatic, renal, and neurological effects [13].
Copper (Cu)	Improper function of the gills, olfactory disorders, reproductive system damage for aquatic animals; death of algae [17].	Copper compounds, such as CuCl_2 , CuSO_4 , $\text{Cu}(\text{NO}_3)_2$, $\text{Cu}(\text{CH}_3\text{COO})_2$, ingested, cause digestive and nervous disorders, in large quantities can cause paralysis and cardiac and respiratory arrest [18].
Lead (Pb)	Anemia, lethargy, weakness, muscle wasting, emaciation, ataxia, blindness, head tremors, head tilt, paralysis, neurologic effects, death for animals [19]; damage of chlorophyll and photosynthetic processes, inhibition of growth for plants [16].	Brain damage, kidney damage, gastrointestinal diseases, reproductive system damage, adverse effects on the blood, central nervous system, blood pressure, and vitamin D metabolism [13].
Zinc (Zn)	Digestive system damage, reproductive system damage for animals [20]; biomass decline and growth inhibition for plants [21]	Digestive tract burns, nervous disorders, decreased pulse, extremity paralysis [18].

3.2 Polycyclic aromatic hydrocarbons

The group of polycyclic aromatic hydrocarbons (PAHs) includes all compounds that are composed of two to seven rings of carbon and hydrogen atoms. These substances are produced by incomplete combustion of fuel during engine operation. PAHs pose a particular danger to the environment and human health, as they are at the same time persistent,

bioaccumulative, and toxic to humans and other organisms. Studies have shown that many PAHs are carcinogenic, mutagenic, and/or toxic for reproduction [22]. Table 2 highlights the main PAHs in used engine oil and their effects.

Table 2. The main polycyclic aromatic hydrocarbons in used engine oil and their effects [23]

Name	Molecular formula	Environment impact	Human health impact
Benz[a]anthracene	$\text{C}_{18}\text{H}_{12}$	Toxic to aquatic life with long lasting effects	Carcinogen
Benzo[a]pyrene	$\text{C}_{20}\text{H}_{12}$	Very toxic to aquatic organisms, with long-term effects	Carcinogen, mutagen, fetotoxic, neurotoxic
Chrysene	$\text{C}_{18}\text{H}_{12}$	Very toxic to aquatic organisms, with long-term effects	Carcinogen, mutagen
Dibenz[a,h]anthracene	$\text{C}_{22}\text{H}_{14}$	Toxic to aquatic life with long lasting effects	Carcinogen
Naphthalene	C_{10}H_8	Very toxic to aquatic organisms, with long-term effects	Carcinogen, irritant of the digestive system

3.3 Polychlorinated biphenyls (PCBs)

PCBs represent a category of organic chemical compounds consisting of carbon, hydrogen and chlorine atoms. Environmental agencies, such as the European Environment Agency or the U.S. Environmental Protection Agency, include these substances in the category of Persistent Organic Pollutants (POPs). This is because PCBs are considered human carcinogens and produce a wide spectrum of adverse effects in animals and humans, including reproductive toxicity, teratogenicity and immunotoxicity [24].

The amounts of PCBs in used engine oil usually do not exceed $50 \mu\text{g/g}$, thus allowing the recycling of the lubricant [25]. But the presence of these contaminants is enough to classify used engine oil as hazardous waste. The effects of these compounds on the environment and human health are shown in Fig. 3.

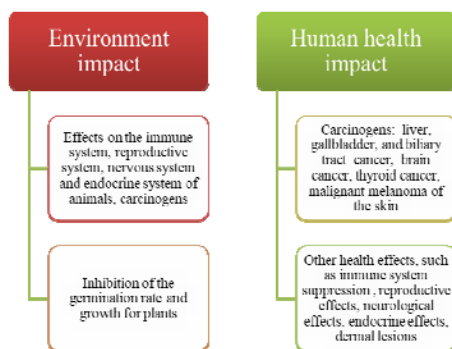


Fig. 3. Environment and human health impact of polychlorinated biphenyls [26-28]

3.4 Glycol

Glycol is the main ingredient in coolant, which is used in the automotive industry to lower the freezing temperature or and raise boiling point temperature or as a heat transfer fluid. There are two types of glycol used in coolant formulations: propylene glycol and ethylene glycol. Propylene glycol is less toxic, but ethylene glycol is far more widely used, due to its higher heat transfer properties and lower cost [29].

Glycol finds its way into the engine oil through several ways, such as deteriorated seals, blown head gaskets, damage of cylinder liners etc. Once it reaches the lubricant, it leads to the formation of acids and precipitates that damage engine components, destroy lubricant additives and create acidic sludge [29]. Thus, glycol is a major contaminant for engine oil. In addition to deteriorating the properties of the oil, glycol also has an unfavorable impact on the environment, as shown in Fig. 4.

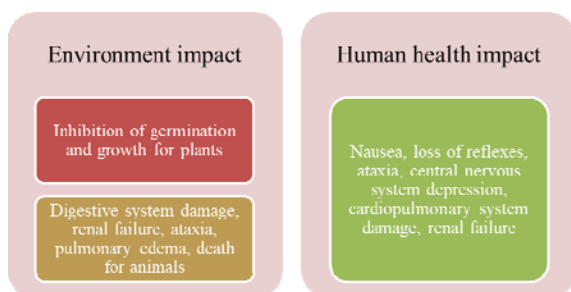


Fig. 4. Environment and human health impact of glycol [30-31]

4. CONCLUSIONS

Depending on different classification criteria, contaminants in used engine oil can be separated into several categories to facilitate their identification and potential neutralization. Among these contaminants, those that have the most severe impact on the environment and human health are heavy metals, polycyclic aromatic hydrocarbons, polychlorinated biphenyls and glycol. Their effects on the environment include: pollution of water and soil, reduction of germination and plant growth, harmful impact on animals (various types of cancer, malformations and diseases of the animal's body systems, mutagenic or teratogenic effects, neurological changes or even death).

The effects of contaminants in used engine oil on human health are at least as worrying as the impact on the environment. Thus, heavy metals can cause cancer of various organs, nervous disorders, damage to human body systems, diabetes, paralysis or even death from intoxication. Polycyclic aromatic hydrocarbons are recognized for their carcinogenicity and mutagenicity. They are also powerful neurotoxins and cause a number of other diseases of the human body's systems. Polychlorinated biphenyls are responsible for causing cancer in most organs, such as the liver, gallbladder, stomach, brain, thyroid or skin. PCBs also have other effects, such as immune system suppression or reproductive, neurological and endocrine systems damage. Glycol causes intoxications that can lead to kidney failure and even death. Due to all these particularly harmful effects, used engine oil is considered a hazardous waste and requires rigorous and specialized management, avoiding its improper storage or disposal.

REFERENCES

- [1] Rațiu, Sorin; Alexa, Vasile; Josan, Ana; Cioată Vasile; Kiss, Imre, Study of temperature dependent viscosity of different types of engine used oils. J. Phys.: Conf. Ser. Vol. 1426, pp. 2-9, 2020
- [2] Fleetguard, <https://www.cumminsfiltration.com/sites/default/files/MB10046.pdf>
- [3] Ali, Mohamen Kamal; Ezzat, Fawzy; El-Gawwad, K.A. Abd; Salem, M.M.M., Effect of Lubricant Contaminants on Tribological Characteristics

- During Boundary Lubrication Reciprocating Sliding, Appl. Phys. Cornell Uni. Vol. 1710, pp. 1-16, 2017
- [4] XS650, <http://www.xs650.com/threads/metal-shavings-on-oil-filter.48161/>
- [5] Danny's Engine Portal, <https://dannysengineportal.com/antifreeze-in-oil-can-be-catastrophic-if-not-dealt-with-quickly/>
- [6] ATA, <https://www.advancedta.com/blog/2016/2/16/what-is-aeration-why-should-we-care>
- [7] Addison, James; Needelman, William, Diesel Engine Lubricant Contamination and Wear. Scientific and Laboratory Services Department Pall Corporation. New York, 1986
- [8] Woodstock Power Company, <https://woodstockpower.com/blog/what-is-engine-blow-by/>
- [9] Mahaney, Patricia Ann, Effects of freshwater petroleum contamination on amphibian hatching and metamorphosis. Environmental Toxicology and Chemistry. Vol. 13 (2), pp. 259-265, 1994
- [10] National Geographic, <https://blog.nationalgeographic.org/2015/08/03/heavy-metals-in-motor-oil-have-heavy-consequences/>
- [11] INCHEM, <http://www.inchem.org/documents/ehc/ehc/ehc224.htm#1.8>
- [12] Tchounwou, Paul B.; Patlolla, Anita K.; Centeno, Jose A., Carcinogenic and systemic health effects associated with arsenic exposure-a critical review. Toxicol Pathol. Vol. 31(6), pp. 575-588, 2003
- [13] Tchounwou, Paul B.; Yedjou, Clement G.; Patlolla, Anita K.; Sutton, Dwayne J., Heavy Metal Toxicity and the Environment. Molecular, Clinical and Environmental Toxicology, Experientia Supplementum. Vol. 101, pag. 133-164, Springer, Basel, 2012
- [14] Cadmium Review. Nordic Council of Ministers. Report 1(4). 2003
- [15] World Health Organization, <https://www.who.int/ipcs/features/cadmium.pdf>
- [16] Jaishankar, Monisha; Tseten, Tenzin; Anbalagan, Naresh; Mathew, Blessy B.; Beeregowda, Krishnamurthy N., Toxicity, mechanism and health effects of some heavy metals. Interdiscip Toxicol. Vol. 7(2), pp. 60-72, 2014
- [17] Solomon, Frances, Impacts of Metals on Aquatic Ecosystems and Human Health. Environ. Communities. Vol. 25(8), pp. 25-28, 2009
- [18] Micle, Valer; Neag, Gheorghe, Procedee și echipamente de depoluare a solurilor și a apelor subterane. Editura U.T.Press. Cluj-Napoca. 2009
- [19] Today's Veterinary Nurse, <https://todaysveterinarynurse.com/articles/management-strategies-lead-toxicity-a-threat-to-wildlife/>
- [20] Eisler, Ronald, Zinc Hazards to Fish, Wildlife, and Invertebrates: A Synoptic Review. U.S. Department of the Interior Fish and Wildlife. Biological Report 10. 1993
- [21] Tsonev, Tsonko; Lidon, Fernando, Zinc in plants - An overview. Emir. J. Food Agric. Vol. 24(4), pp. 322-333, 2012
- [22] Crone, Timothy J.; Tolstoy, Maya; Magnitude of the 2010 Gulf of Mexico oil leak. Science. Vol. 330(6004), pp. 634, 2010
- [23] German Federal Environment Agency, <https://www.umweltbundesamt.de/en/publikationen/polycyclic-aromatic-hydrocarbons>
- [24] European Commission, <https://ec.europa.eu/environment/waste/pCBS/index.htm>
- [25] Lulek, Janina, Levels of polychlorinated biphenyls in some waste motor and transformer oils from Poland. Chemosphere. Vol. 37(9-12), pp. 2021-2030, 1998
- [26] Case Studies in Environmental Medicine: Polychlorinated Biphenyls (PCBs) Toxicity. Agency for Toxic Substances and Disease Registry. WB 2460. 2014
- [27] EPA, <https://www.epa.gov/pCBS/learn-about-polychlorinated-biphenyls-pCBS#healtheffects>
- [28] Subramanian, Srishty; Schnoor, Jerald L.; Van Aken, Benoit, Effects of Polychlorinated Biphenyls (PCBs) and Their Hydroxylated Metabolites (OH-PCBs) on Arabidopsis thaliana. Environ Sci Technol. Vol. 51(12), pp. 7263-7270, 2017
- [29] Machinery Lubrication, <https://www.machinerylubrication.com/Read/193/oil-glycol>
- [30] MSD Manual, <https://www.msdsmanual.com/toxicology/ethylene-glycol-toxicity/overview-of-ethylene-glycol-toxicity>
- [31] Sciencing, <https://sciencing.com/info-8573984-effects-antifreeze-environment.html>

*Maintenance of
Engineering Systems and
Occupational Safety Engineering*



Banja Luka
28–29 May 2021.

DEMI 2021

15th International Conference on
Accomplishments in Mechanical and
Industrial Engineering

www.demi.mf.unibl.org



The influence of the application of technical diagnostic on the efficiency of the industrial system

D. Branković^a, Z. Milovanović^a

^aFaculty of Mechanical Engineering Banja Luka, Stepe Stepanovića 71, 78000 Banja Luka, Bosnia and Herzegovina

Abstract To produce a business system in an increasingly competitive global market means constantly finding ways to improve the process. Maintenance, as an integral part of production processes, plays a significant role in achieving the final business result. The application of technical diagnostic systems within industrial production systems can be used in a positive way at the level of plant efficiency. This research shows the impact of the installation and application of a modern on-line diagnostic system on the final production results on the example of a technical system of paper machines. The analysis and calculation refer exclusively to the impact of the maintenance service on the overall efficiency of the plant by monitoring the number of hours in failure at the observed intervals before and after the installation of the diagnostic system. As it is a continuous production process with a larger volume of production based on hourly performance, even a relatively small % of the increase in efficiency brings a significant economic business result.

Keywords maintenance, industrial system, Overall Equipment Effectiveness

1. INTRODUCTION

Continuous improvement of the process of production industrial systems is the only guarantee of the survival of business industrial systems in the increasingly demanding world market. The development of the Lean concept of business systems management in the second half of the XX century enables methodological monitoring of production process parameters, defining all potential anomalies in processes, identifying places for potential improvements and specifying measures to achieve

improvements that significantly increase business results. One of the tools used by the Lean concept is the method of measuring and valorizing the total efficiency of production plants - OEE (Overall Equipment Effectiveness). According to the creators of the Lean concept (Taiichi Ohno [1]) OEE is a product of achieved availability, performance and achieved quality and can be represented by the form [2]:

$$OEE = EA \cdot PE \cdot RQ \quad (1.1)$$

where:

- EA – Equipment Availability,

$$EA = \frac{\text{total availability time} - \text{downtime}}{\text{total availability time}} \quad (1.2)$$

- PE – Performance Efficiency,

$$PE = \frac{\text{realized production} - \text{ideal production time}}{\text{total availability time} - \text{downtime}} \quad (1.3)$$

Corresponding author

PhD Dejan Brankovic, Assistant Professor
University of Banja Luka, Faculty of Mechanical Engineering
Banja Luka
dejan.brankovic@mf.unibl.org

University of Banja Luka, Faculty of Mechanical Engineering
Banja Luka
Stepe Stepanovića 71
Banja Luka, Bosnia and Herzegovina

- Ideal production time - I_{pt}

$$I_{pt} = \frac{\text{total availability with max.production}}{\text{max.production}} \quad (1.4)$$

- RQ – Rate of Quality

$$RQ = \frac{\text{realized production-waste}}{\text{realized production}} \quad (1.5)$$

In other words, good indicators of the effectiveness of production processes mean the realization of a quality product, in the shortest possible time with the elimination of all possible setbacks in the production process. Maintenance, as an integral part of the production system, with its activities can significantly affect the degree of effectiveness.

2. RESEARCH OF THE EFFICIENCY OF THE PAPER MACHINE PRODUCTION SYSTEM

In order to analyze the impact of maintenance methods and concepts on the effectiveness of the production process, the achieved results of the production of the technical system of the paper machine within the production system for the production of toilet paper from Banja Luka will be used. The basic idea is to check whether the installation of an online system of technical diagnostics at critical positions of the paper machine has an impact on changing or increasing the degree of effectiveness and what is the

assessment of its quantitative value. To assess the effectiveness of the paper machine system, the following recorded data from the production process were analyzed:

- number of hours of downtime caused by device failure,
- total availability,
- total net production of paper machine,
- waste.

2.1 Efficiency of a real system before the installation of technical diagnostics

To calculate the effectiveness of the production system of the paper machine, a database was formed, which included monitoring and recording of operating parameters during the production process. The key factors are defined as: net realized production, failure hours, time utilization and planned plant downtime.

Total downtime that occurs in the production process can be divided into:

- Technological downtime (cleaning, production program transitions,...),
- Downtimes due to failure (paper machine in complete failure - requires the intervention)
- other downtimes (external outages caused by lack of media).

The calculation of the effectiveness up to the date of technical diagnostics installation was performed by analyzing the data - Table 1, [3]:

Table 1. Production process data up to the date of installation of technical diagnostics

Paper machine performance indicators 2014 - 2015 (up to the date of installation of technical diagnostics)							
Month	Total availability (hours)	Planned maintenance downtimes (hours)	Total working hours (hours)	Maintenance downtimes (hours)	Production (tons)	Waste (tons)	
2014	August	744	18	724,25	11,5	3316	26,41
	September	720	19	643,25	43,25	2942,5	17,51
	Oktober	744	14	698	18,5	3130,5	46
	November	720	14	621,75	62,25	2847,5	13,95
	December	744	21	700,25	20	3250,1	26,61
2015	January	744	42	704,25	10,5	3269,7	23,91
	February	672	18	534	76,25	2450	27,7
	March	744	18	729,5	6,5	3226,5	15,79
	April	720	18	664	23,5	2975,8	39,5
	May	744	19	717,75	2,75	3395	19,83
	June	720	18	696,5	1,25	3281,6	17,87
	July	744	157	718,25	4	3198,3	16,4
	August	744	18	719	6,5	3221,6	21,76
	September	720	19	664	25,5	2921,9	14,66
	October	744	19	694	21,75	2995,1	30,71
	November	720	18	689	11,25	2999,3	10,8
Total:	11688	450	10917	345,25	49421,4	369,4	

In the analysis of the efficiency of the paper machine plant, only downtimes directly caused by the activities of the maintenance service will be taken into account in order to obtain an assessment of the impact of a certain activity, in this case the installation of a new diagnostic system, on the overall efficiency of the production system.

Total effectiveness up to the date of installation of technical diagnostics:

$$OEE_1 = EA_1 \cdot PE_1 \cdot RQ_1 \quad (2.1)$$

$$EA_1 = \frac{10918-345,25}{10918} = 96,83\% \quad (2.2)$$

$$PE_1 = \frac{49421,4 \cdot 0,211}{10918-345,25} = 98,63\% \quad (2.3)$$

Ideal production time:

$$I_{pt1} = \frac{717,75}{3395} = 0,211 \quad (2.4)$$

$$RQ_1 = \frac{49421,4-369,41}{49421,4} = 99,25\% \quad (2.5)$$

According to the results of expressions 2.2, 2.3 and 2.5, the total effectiveness is:

$$OEE_1 = 96,83 \cdot 98,63 \cdot 99,25 = 94,78\% \quad (2.6)$$

In order to get an idea of the significance and relatively small increases in efficiency, we will

Table 2. Production process data after installation of technical diagnostics

Paper machine performance indicators 2015 - 2017 (after installation of technical diagnostics)							
	Month	Total availability (hours)	Planned maintenance downtimes (hours)	Total working hours (hours)	Maintenance downtimes (hours)	Production (tons)	Waste (tons)
2015	December	744	19	590,5	20,75	2710,8	21,33
	January	744	18	622,25	10,25	2811,9	12,70
	February	696	17	643	15,5	2785,8	20,15
	March	744	21	710	9,75	3147,7	22,24
	April	720	16	640,5	48	2927,2	10,8
2016	May	744	19	699,75	4,75	3130,9	13,07
	June	720	15	691,75	14,25	3138,5	17,54
	July	744	16	705,75	14,25	3201,5	19,77
	August	744	18	724,75	5	3305,8	15,14
	September	720	19	630,25	59,75	2852,8	14,04
	October	744	233	609	8,5	2749,9	9,7
	November	720	18	672,25	25,75	3088,2	16,6
	December	744	19	732,5	2,5	3412,9	14,7
2017	January	744	18	693,75	22,75	3085	12
	February	672	18	631	8,75	2880	13
	March	744	19	740	2,5	3489,6	11,4
	Total:	11688	503	10736	273	48718,5	244,2

assume that the efficiency of the production system increases by 0.1%. If the average production of a paper machine for an hour of 4.8t and the total daily availability of the plant of 22 hours is known, the annual increase in production (T_g) would be:

$$T_g = 0,1 \cdot 22 \cdot 4,8 \frac{t}{hour} \cdot 12mon. = 127 \frac{t}{Year} \quad (2.7)$$

which represents the average one-day production of a paper machine and a clear quantitative indicator of the importance and possibility of investing in systems that raise the efficiency indicators of technical production systems that are in continuous operation.

2.2 Efficiency of real system after installation of technical diagnostics

For the period of monitoring the indicators of the production process of the paper machine after the installation of the technical diagnostic system, a time period of 16 months and the same procedure were taken. The calculation of effectiveness after the installation of technical diagnostics was performed by analyzing the data recorded during the production process, which are shown in Table 2, [3]:

The specificity of this time period were two longer overhauls of the paper machine plant (in December 2015 and January 2016) which referred to the implementation of investment activities that are not directly related to the activities of the maintenance service to ensure the continuity of the production process plants were not taken into analysis.

Total effectiveness after the term of installation of technical diagnostics:

$$OEE_2 = EA_2 \cdot PE_2 \cdot RQ_2 \quad (2.8)$$

$$EA_2 = \frac{10736,5-273}{10736,5} = 97,46\% \quad (2.9)$$

$$PE_2 = \frac{48718,5-0,212}{10736,5-273} = 98,70\% \quad (2.10)$$

Ideal production time:

$$I_{pt2} = \frac{740,75}{3489,6} = 0,212 \quad (2.11)$$

$$RQ_2 = \frac{48718,5-244,2}{48718,5} = 99,49\% \quad (2.12)$$

According to the results of expressions 2.9, 2.10 and 2.12, the total effectiveness is:

$$OEE_2 = 97,46 \cdot 98,70 \cdot 99,49 = 95,70\% \quad (2.13)$$

According to the previous budget, the total efficiency after the realization of investment activities is 95.70%, which in relation to the total efficiency before the realization of 94.78% is the difference ΔOEE of:

$$\Delta OEE = OEE_2 - OEE_1 = 95,70 - 94,78 = 0,92\% \quad (2.14)$$

i.e., increase in the total efficiency of the production system by 0.92%. If we observe the effect of increasing efficiency on an annual basis (T/god), we get:

$$T = 0,92 \cdot 21,7 \cdot 4,8 \frac{t}{hour} \cdot 12mon. = 1150 \frac{t}{Year} \quad (2.15)$$

where:

- 21,71 hours is - monthly average of the total number of working hours in one day (period of 16 months of observation of the production system with installed online diagnostic system),
- 4,8 tons is - the average production of a technical paper machine system for one hour of operation.

Given the diversity of the product range, if we assume the average gross margin - GM (Gross Margin) of 290 € / ton of paper produced, the potential annual savings (U) of costs are obtained:

$$U = GM \cdot T = 290 \frac{\text{€}}{t} \cdot 1150t = 333.616 \frac{\text{€}}{Year} \quad (2.16)$$

which represents a respectable degree of increasing efficiency in relation to the invested funds for the installation of technical diagnostics at a critical position in the production system.

3. CONCLUSION

Investing funds in modern technical diagnostic systems, which are an integral part of maintenance concepts according to the state of modern production systems of the continuous work process, today does not mean unnecessary allocation of significant investment funds in a certain process control comfort because relatively small positive effects can provide significant financial savings in businesses that are very quickly economically justified. Modernization of technological systems and investment in the effectiveness of the maintenance process reduces the likelihood of failure, increase hourly effects and enable better competitiveness of the business system in the market.

REFERENCES

- [1] Popović, B., Papić, Lj. (2020). *Filozofija nauke i prakse o upravljanju kvalitetom*, Istraživački centar za upravljanje kvalitetom i pouzdanošću, DQM, Prijedor.
- [2] Majdandžić, N. (1999). *Strategije održavanja i informacijski sustavi održavanja*, Sveučilište Josipa Jurja Strossmayera u Osijeku – Strojarski fakultet u Slavonskom Brodu, Slavonski Brod.
- [3] Branković D, Milovanović Z., Papić LJ. (2021). Analysis of the technical system reliability assessment with the application of technical diagnostics, Kumar A., Ram M. *The Handbook of Reliability, Maintenance, and System Safety through Mathematical Modeling*, Elsevier, p. 373-416.



Banja Luka
28–29 May 2021.

DEMI 2021

15th International Conference on
Accomplishments in Mechanical and
Industrial Engineering

www.demi.mf.unibl.org



Occupational injury analysis according to the injured part of the body in the function of risk management

Msc Mile Vajkić^a, PhD Biljana Vranješ^b, PhD Evica Stojiljković^c

^aSchool of Mechanical Engineering Prijedor, Nikole Pašića 4, 79101 Prijedor, Republic of Srpska-B&H, m.wajkic@gmail.com

^bUniversity of Banja Luka, Faculty of Mechanical Engineering, Stepe Stepanovića 71, 78000 Banja Luka, Republic of Srpska-B&H, biljana.vranjes@mf.unibl.org

^cUniversity of Niš, Faculty of Occupational Safety, Čarnojevića 10a, 18000 Niš, Serbia, evica.stojiljkovic@zrnrfak.ni.ac.rs

Abstract

Occupational injuries are a basic indicator of the influence of adverse working conditions on the production process participants, as a form of damage to their life and health. And they represent major health, economic and industrial problem of modern society. The consequences of occupational injuries directly affect the worker and his work potential, and indirectly they affect his family, work organization, and society as a whole.

The dynamics of the events negative consequences in the analyzed period is one of the most favorable ways of analyzing working conditions in a company. Occupational injury analysis according to the injured part of the body allows us to determine the severity of the injury, proper selection of preventive measures, and it indicates the importance and magnitude of problems related to occupational safety in the organization. Therefore, a graphical interpretation of the occupational injury analysis according to the injured part of the body was conducted in this paper. This analysis was the first applied in the Republic of Srpska (BIH) in companies that are considered as high-risk companies: forestry and mining, for the period 2011-2019. The guidelines for improving the risk management process have been provided.

Keywords

occupational injury, injury according to the injured part of the body, prevention measures, risk management.

1. INTRODUCTION

The system of recording data on occupational injuries and the circumstances in which they occur, as well as processing of the same, is a good basis for obtaining an explanation regarding the job risk and what measures can be taken to prevent negative consequences. The number of occupational injuries, registered in a certain period of time, indicates the importance and magnitude of the problem of occupational safety and health in one organization.

Therefore, the statistics of occupational injuries are highly needed in order to prevent those injuries, as well as for later control of the effectiveness of measures taken to prevent the occurrence of occupational injuries, i.e. to consider the negative economic consequences. In the theory and in the Republic of Srpska (BIH) legislation as well as in the neighboring countries legislation, there are several definitions of occupational injuries, which do not differ significantly, except in their form and the way they are presented. According to the

Law on Pension and Disability Insurance in the Republic of Serbia, an occupational injury is considered to be an injury to the insured that occurs in spatial, temporal and causal connection with the work on which he is insured; the injury caused by direct and short-term mechanical, physical or chemical effects, by a strong body movement, sudden body overload or other changes in the physiological state of the organism. By an occupational injury is also considered an injury caused while performing the job to which the employee is not assigned, but which is performed in the interest of the employer. Injury caused by actions taken in order to perform official duties and actions taken to start the work is also considered an occupational injury, as well as an injury that occurred in other cases determined by law [1]. The Law on Safety and Health at Work in the Republic of Serbia states that "occupational safety and health is providing such working conditions which, as far as possible, reduce occupational injuries, occupational diseases and diseases related to work, and the conditions which mostly create a precondition for full physical, mental and social well-being of the employees" [2].

Occupational injury in the Law on Pension and Disability Insurance of the Republic of Srpska is defined in the same way as in the Republic of Serbia, only: "An occupational injury is also: a disease of an insured which occurred directly or exclusively as a result of an accident or some higher force during job performance which is the basis of insurance" [3].

The Law on Occupational Safety in the Republic of Srpska states that "occupational safety and health is a set of organized measures and activities aimed at creating conditions that ensure: safety at work, prevention and elimination of dangers and harms that can cause occupational injuries, occupational and other diseases and damage to the health of workers at work and protection of workers health and working ability" [4].

In the theory of occupational safety, an occupational injury is defined as a violation of

human physical integrity in the work environment, which manifests itself in damage (or destruction) of certain parts, of a body-organic being that is followed by disruption of harmonious functioning of individual body parts or person's death [5]. From the point of view of occupational medicine, the consequences of occupational injuries and occupational diseases can be: sickness, temporary incapacity for work, reduction of working ability, loss of working ability, physical disability, and death [6]. In the world, occupational injuries are the leading cause of death for people under the age of 37, and for the entire population it is in third place, after cardiovascular and malignant diseases [7]. The occupational injury analysis, according to the injured part of the body, in an organization should enable, above all, the correct choice of the most adequate means of personal protection in terms of designing measures of protection at the workplace. Classification of injuries according to this criterion also enables the detection of deficiencies in work procedures or in the constructions of machines and devices that are used. In order to take measures to prevent occupational injuries in companies in the field of forestry and mining, in the Republic of Srpska (BIH), an analysis of occupational injuries for the period 2011-2019 was conducted in this paper.

2. OCCUPATIONAL INJURY ACCORDING TO THE INJURED PART OF THE BODY

The occupational injury analysis according to the injured part of the body is the most important parameter in assessing the degree of endangering physical integrity of the worker and the harmful effects of occupational injuries on his health. Classification of occupational injuries according to the injured part of the body can be conducted in several ways. The basic classification of occupational injuries according to the injured part of the body includes health injuries of head, neck, torso, arms, and legs [8].

The broader classification implies the classification of occupational injuries into eight groups: head, neck, torso, arms, legs, multiple places, general injuries, and non-specific location [9].

The legislation in the Republic of Srpska states that in the case of an occupational injury, the data on the injury are written in the Report on the occupational injury, and the degree of bodily injury resulting from the occupational injury is determined according to the Rulebook. According to this Rulebook, bodily injury is the loss, significant damage or inability of certain organs or body parts with the consequence of limited mobility, problems in the normal functioning of the organism and causing greater efforts to meet life needs, with or without disability. The Rulebook determines the minimum individual bodily injuries of 30% and the total percentage of bodily injuries. The injuries were classified into eleven groups with a more detailed classification within the group:

- head, oral cavity, and neck;
- cranial nerves, sense of sight and sense of hearing;
- brain, brainstem, and spinal cord;
- spinal nerves, neuromuscular system, and skin;
- lungs and heart;
- upper extremities;
- lower extremities;
- disfunction, reduction or loss of spinal function;
- digestive organs;
- urogenital organs and
- two or more bodily injuries.

By analyzing the literature that deals with this issue, we can conclude that the most common injured parts are arms, legs, head, but other parts of the body too. The importance of hands and head to productive work and safety at work imposes the need to pay special attention to these injuries. Injuries of some other parts of the body, such as eye injuries, and even milder forms of injuries, cause long sickness and more

severe disabilities than injuries of some other parts of the body, which are often significantly larger.

2.1. Graphical representation of injuries according to the injured part of the body

Figure 1, shows a graphic illustration made in the Solidworks software program with the percentage of injured body parts, where certain body units (head, neck, torso, arms, and legs) are shown by rectangles of certain areas. This graphic interpretation is based on the representation of the normal proportional relation of the average person's body parts. The body height of the model was 178 cm and the width of the torso was 45 cm, the volume of the model was neglected in this display.

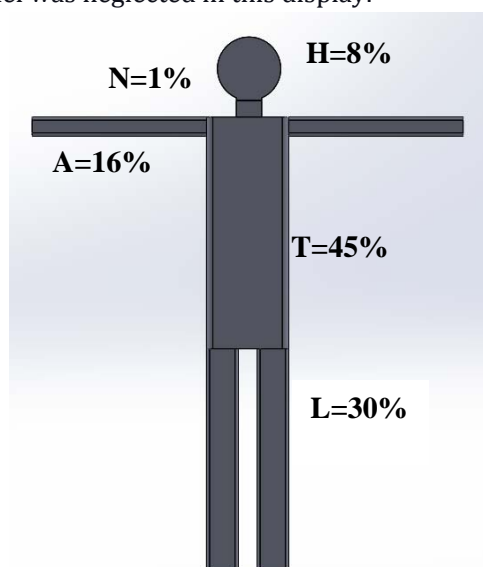


Fig. 1. The percentage ratio of body surface areas of the average person

If the same total size is retained, and the rectangles that symbolize certain body parts change the size, according to the proportional relative frequency of injuries of certain body parts, we get the representation as in Figure 2.

In the surrounding countries, the competent institutions conduct occupational injury analysis according to etymological parameters, including the injured part of the body.

According to the occupational injury analysis for 2018 conducted by the Croatian Institute of

Public Health, the most common injuries are injuries of the upper extremities (38.19%), in which the fingers make up 20,26%¹.

In Serbia, when analyzing occupational injuries for 2018 according to the injured part of the body, injuries of the hand (45.03%) most often occur, followed by injuries of the leg (30.69%) and head (6,92%)².

In the Republic of Srpska, according to the results of the research on nonfatal injuries that was conducted on the sample of 2512 recorded injuries for the period 2012-2014, it was found that the lower extremities (hip, leg, foot) were most often injured 37.3%, followed by the injuries of upper extremities (shoulder, hand, fist) 36.6%. Injuries to both extremities accounted for 73.9%, head injuries 10.8%, chest injuries 3.5%, and eye injuries 3.6% of all the injuries [10].

Figure 2 displays the analysis of injuries in the Republic of Srpska according to the workers' injured part of the body for 2015.

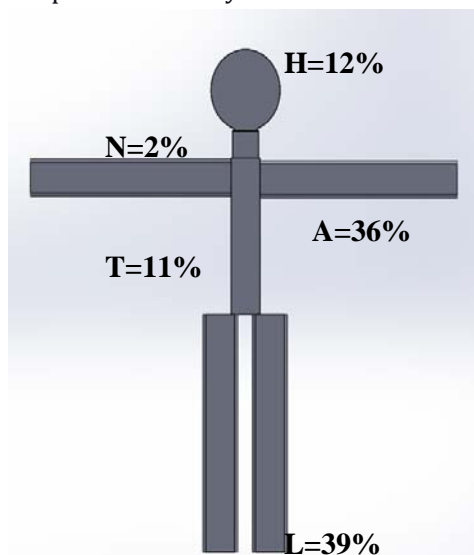


Fig. 2. Graphic interpretation of occupational injury analysis in the Republic of Srpska (BIH) according to the workers' injured part of the body in 2015.

Based on the data analysis and the graphical display, we can conclude the following:

- legs are mostly injured (39%), ankle joint and foot the most,
- hands are injured in 36% of all injuries, mostly fingers and hands, followed by shoulder,
- head injuries account for 12%, and of head injuries the most common are eye injuries,
- the torso is injured in 11% of cases, most often the back and chest,
- the neck injuries account for 2% of the total number of injuries.

In 2015, 16% of recorded multiple injuries are not included in the graphical display.

3. OCCUPATIONAL INJURY ANALYSIS IN FORESTRY AND MINING IN THE REPUBLIC OF SRPSKA (BIH)

Injury analysis and graphical display were done for two companies in the field of forestry and mining. The company in the field of forestry is a public company that employs an average of 4,500 workers, and in the analyzed period 2011-2019, 1369 occupational injuries occurred. The company in the field of mining is a private company, engaged in the production and processing of iron ore, that employs an average of 800 workers, and in the same analyzed period, there were 110 occupational injuries.

Table 1 shows the number of injuries according to the injured part of the body in these companies for the analyzed period 2011-2019, and Figure 3 shows the graphical interpretation.

¹ <http://www.hzzo.hr/zastita-zdravlja-na-radu/ozljeda-na-radu/>

² Report on the work for 2018 of the Directorate for Occupational Safety and Health of the Ministry of Labour, Employment, Veterans and Social Affairs of the Republic of Serbia, Belgrade, 2019

Table 1. Occupational injuries according to the injured part of the body in forestry and mining companies

The company in forestry											
Injured body part	2011	2012	2013	2014	2015	2016	2017	2018	2019	Total	
										No.	%
Head	29	34	35	29	21	16	24	24	22	232	16,95
Torso	16	30	16	16	11	17	11	14	14	145	10,59
Hands	41	34	61	52	43	50	43	49	59	432	31,56
Legs	47	53	48	48	93	69	93	52	57	560	40,91
Total	133	151	160	145	1268	152	171	137	152	1369	100
The company in mining											
Injured body part	2011	2012	2013	2014	2015	2016	2017	2018	2019	Total	
										No.	%
Head	2	0	2	3	2	2	0	4	0	15	15,46
Torso	0	1	2	0	2	2	1	2	2	12	12,37
Hands	5	5	4	5	1	4	5	7	1	37	39,18
Legs	5	2	1	5	4	2	3	8	2	32	32,99
Total	12	9	9	13	9	10	9	21	5	97	100
Multiple inj.	1	2	2	0	1	1	1	3	2	13	11,82
Total	13	11	11	13	10	11	10	24	7	110	100

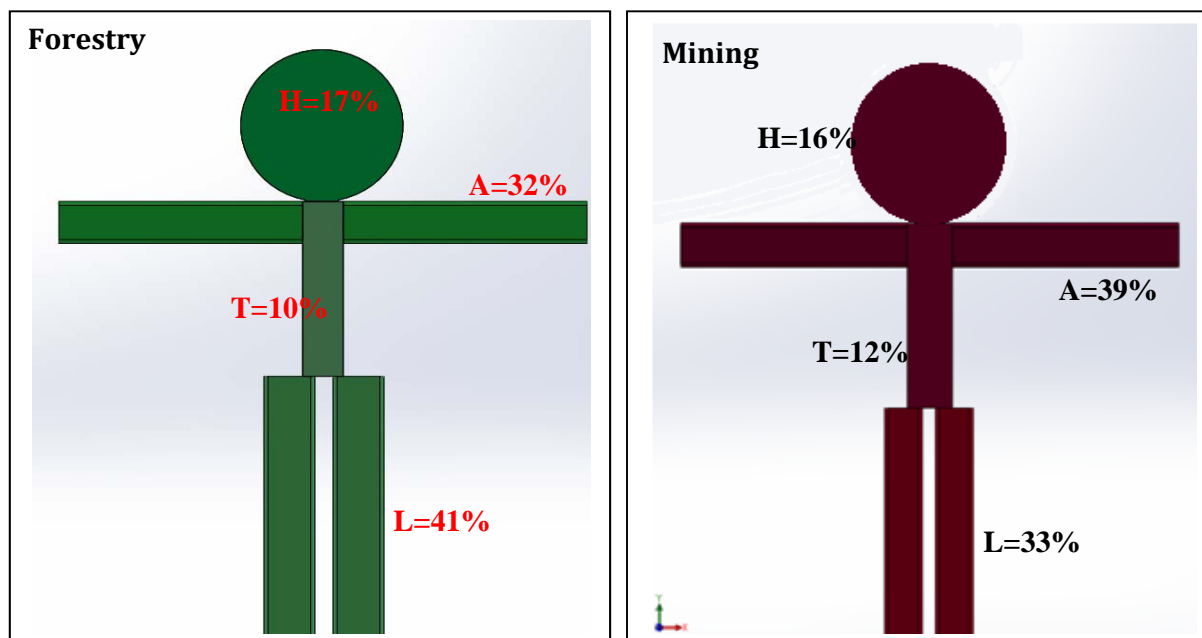


Fig. 3. Graphical interpretation of occupational injuries in forestry and mining companies according to the workers' injured part of the body for the period 2011-2019

In the company in the field of forestry, legs were injured the most (40.91%), and a similar situation is with the companies in the countries of the region, which perform jobs in forestry [9, 11]. Extremities injuries in this company (arms and legs) make up about 73% of injuries, and together with head injuries make 90% of all injuries that occur. The most common injuries of the extremities occur during operations of cutting, felling, extracting and loading wood using the means of work, and as a consequence of falls. In the system of occupational safety in forestry, the proper selection and providing adequate personal protective equipment, such as work shoes (shoes or boots with a steel cap), protective gloves, helmets and work clothes, should be used as a measure to reduce the frequency of injuries to the riskiest parts of the body and mitigate their negative effects.

In the company in the field of mining, hands are mostly injured (39.18%), fingers the most; followed by leg injuries (33%), most often an ankle. Previous researches on occupational safety and health in the mines of the Republic of Srpska for the period 2005-2009 gave similar results: the most commonly injured parts of the body were the extremities: arms and legs (64%), head (16%), eyes (5%), back (3%), and 9% of workers suffered multiple injuries [12]. In Croatia, in mining and quarrying in 2018, hands were injured the most (41.67%), followed by legs injuries (29.17%) and head injuries (8.33%). The data obtained by other authors are similar. Injuries most often affected the extremities (60%) in the brown coal mine, according to research in [13]. Hands are mostly affected because, in mines, part of the work related to maintenance of mining plants and mechanization, is done manually and by using inadequate tools; and there are also structural defects in machines and devices. Legs are most often injured due to falling objects and moving on slippery and icy surfaces, as well as on surfaces that are not secured by protective fences. The data lead to the conclusion that within the measure of selection of personal protective equipment, special attention should

be given to the hand protection equipment and means, and to the adequate choice of final date for their replacement.

Within the occupational safety measures, it is necessary to insist on following the safety procedures when performing works in mining and forestry and following safety rules when moving in the working environment.

Legislation in the Republic of Srpska stipulates that the Act on Risk Assessment for all workplaces, which is the result of the implemented risk assessment methodology, determines the means and equipment for personal protection at work, given the identified hazards and harms in the work environment, and the employer has an obligation to provide these means, and organizes their maintenance and testing, as part of a measure to prevent, eliminate or reduce risks.

4. CONCLUSION

In many companies in the Republic of Srpska (BIH) and the surrounding countries, a large number of occupational injuries occur. The reason for this is the fact that in these companies, in the previous period, not enough attention was paid to risk management in the workplace and work environment. Occupational risk assessment, a retrospective obtained through epidemiological data and a prospect obtained through analysis, aims to determine critical places and points, i.e. states and processes in which injuries can occur. For these reasons, it is necessary to review the long-term movement of occupational injuries, with the aim of assessing and managing risk, i.e. taking appropriate measures to reduce risk to an acceptable level.

Injury analysis by injured part of the body is an important indicator of the state of occupational safety and health, as well as useful information in the process of risk assessment, in order to determine hazards and harms, and accordingly to that to plan and procure adequate personal protective equipment. In the following period,

in the analyzed companies, due to the implementation of the research results and implementation of adequate occupational health and safety measures, it is expected to reduce the number of occupational injuries, the number of lost working days, prevent family tragedies, the productivity drop, respond quickly and accurately in emergencies, as well as reducing economic losses.

Also, by reducing the number of occupational injuries, workers in their organizations feel safe at their workplace, and that a strong motivating factor for more productive work results.

REFERENCES

- [1] *Law on Pension and Disability Insurance* "Official Gazette of RS" no. 34/2003, 64/2004 - the decision of the USRS, 84/2004 - law, 85/2005, 101/2005 - law, 63/2006 - the decision of the USRS, 5/2009, 107/2009, 101/2010, 93/2012, 62/2013, 108/2013, 75/2014, 142/2014, 73/2018, 46/2019 - decision US and 86/2019.
- [2] *Law on Safety and Health at Work* "Official Gazette of RS" no. 101/2005, 91/2015 and 113/2017 - the law.
- [3] *Law on Pension and Disability Insurance of the Republic of Srpska*, "Official Gazette of the Republic of Srpska", no. 106/05, 134/11, 82/13 and 96/13.
- [4] *Law on Occupational Safety*, "Official Gazette of Republic of Srpska", no. 1/08 and 13/10.
- [5] Anđelković, B. (2010). *Osnovi sistema zaštite*. Fakultet zaštite na radu Univerziteta u Nišu, Niš.
- [6] Arandelović, M., Jovanović, J. (2009). *Medicina rada*. Medicinski fakultet, Niš.
- [7] Babović, P. (2009). Povrede na radu kao indikatori neadekvatnih uslova rada i radne sredine, *Acta Medica Medianae*, vol.48, no.4, p. 22 - 26.
- [8] Spasić, D. (2001). *Ekonomika zaštite na radu*. Grafičko preduzeće SVEN, Niš.
- [9] Spasić, Ž., Spasić, D., Radisavljević, D. Povrede na radu prema povređenom delu tela kao indikator stanja zaštite na radu, *Proceedings of the 15th International Conference "Kontinuirano usavršavanje osnov unapređenja zaštite na radu"*, Kladovo, Serbia, 18 -22.9.2018, p. 159-166.
- [10] Šormaz, V., Paleksić, V., Popović, M. Karakteristike nefatalnih povreda na radu u Republici Srpskoj, *Journal of the Society of Medical Doctors of the Republic of Srpska and the Medical Faculty of the University of Banja Luka Scripta Medica*, vol. 46, no. 2, October 2015, p. 131-136.
- [11] Musić, J., Halilović, V., Lojo, A., Šporčić, M., Đonlagić, A. (2019). Analiza sigurnosti pri radu u šumarstvu Federacije BiH – studija slučaja, *Nova mehanizacija šumarstva: časopis za teoriju i praksu šumarskoga inženjerstva*, vol. 40, p. 31 - 41. doi.org/10.5552/nms.2019.4
- [12] Government of the Republic of Srpska, Republic Administration for Inspection Affairs, (2010). *Occupational Safety and Health in the Mines of the Republic of Srpska*, Banja Luka.
- [13] Jašarević, S., Karić, M. Uticaj radnog dana, smjene i perioda u smjeni na broj povreda na radu – primjer rudnika Abid Lolić Bila, *Proceeding of 11th Research/Expert Conference with International Participations, "QUALITY 2019"*, Neum, B&H, June 14 - 16, 2019, p. 363 - 371.



Banja Luka
28–29 May 2021.

DEMI 2021

15th International Conference on Accomplishments in Mechanical and Industrial Engineering

www.demi.mf.unibl.org



Exposure of production workers to stress

K. Mijanović^a, M. Jukić^b, J. Mijanović-Jukić^c, J. Kopač^d

^aInternational University of Travnik, Aleja Konzula bb, Travnik, Bosnia and Herzegovina

^bJajce Alloy Wheels Ltd., Divičani bb, Bosnia and Herzegovina

^cHoldina Ltd., Azize Šaćirbegović 4B, Sarajevo, Bosnia and Herzegovina

^dFakulteta za strojništvo, Univerza v Ljubljani, Aškerčeva cesta 6, Ljubljana, Slovenia

Abstract *The increased demand for many products for all types of production, and the creation of conditions for the establishment of production flexibility in the short term has caused a change in the production strategy of hyper production management. Adjustments to the new range and dynamics, in conditions that require quality and reduced costs with increased added value, cause stress to workers on production lines. It is a ubiquitous phenomenon encountered by many professions exposed to its significant influence. Stress and strain at work occurs in all production operations. The importance of studying stress is especially relevant in situations of social and economic crisis characteristic of the existing business environment.*

This paper is an attempt to theoretically interpret stress at work through the identification of sources of stress, the role of management in coping with stress, and to point out the procedures for managing the organization in conditions of increased stress of production workers, taking appropriate organizational measures. The starting point is the assumption that the sources of stress of production workers should be sought in the organization, established relations, work and technological discipline, and conflicts and their resolution by the ethics commission.

Keywords *stress in production, identification of sources of stress, prevention of stress in production*

1. INTRODUCTION

Effective management of safety and security at work affects the ability to work, business and the results of socially useful work in general. This is especially important in times of economic uncertainty when it is important for business to maintain productivity and when working under pressure to meet production plans and when injuries at work are most common.

It is more important than ever to be aware of workplace risk and to manage production facilities by assessing it by investigating hazards and the likelihood of occurrence. The aim of the paper is to help employers, management, workers and workers representatives to identify stress and psychosocial risks in the workplace and incorporate its reflections into the management method. Addressing psychosocial risks creates a healthy work environment in which workers feel important and in which the technological culture is positive.

Corresponding author

Doctor of Engineering, Krsto Mijanović
krsto.mijanovic@unmo.ba

University of Travnik
Aleja Konzula bb
Travnik, Bosnia and Herzegovina

2. THEORETICAL INTERPRETATION OF STRESS AT WORK

Stress at work is a consequence of a poor psychosocial environment in which work takes place, ie it occurs due to the exposure of workers to negative psychological, social and physical influences in the work environment, ie. psychosocial risks.

Daily exposure to psychosocial risks increases the level of stress which can manifest as physical, mental and social dysfunction in workers. Stress at work is the result of the interaction of the worker and his work environment. It arises from an imbalance between job requirements and working conditions and the knowledge, skills, physical and mental characteristics of workers. If the demands that the job places on the worker exceed his capacities and abilities to actively cope, the worker will experience a subjective feeling of stress, schematically shown in Fig. 1.

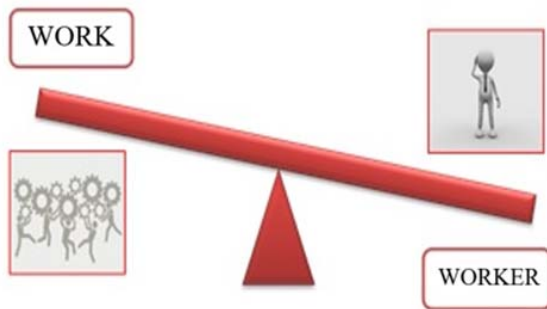


Fig. 1. Subjective feeling of stress in relation to work

Slightly elevated levels of stress (positive stress) can have a beneficial effect on the worker because they will direct his attention, increase motivation and readiness to face challenges. However, if the worker is exposed to elevated levels of stress for a long time, there will be a feeling of overload, fatigue, exhaustion, accompanied by numerous negative consequences.

In the I2I literature, it was pointed out that the solution is in an effort to reduce production from year to year and keep it at a sustainable level. This demonstrates concern for the environment, which is partly related to nature, but involves a proper burden on workers and other stakeholders. With this action, it is believed that the concept of sustainable development, which includes workers and their

social needs, would lead to the same or better standard of living as it is now, and the avoidance of crises and stress, Figure 2.

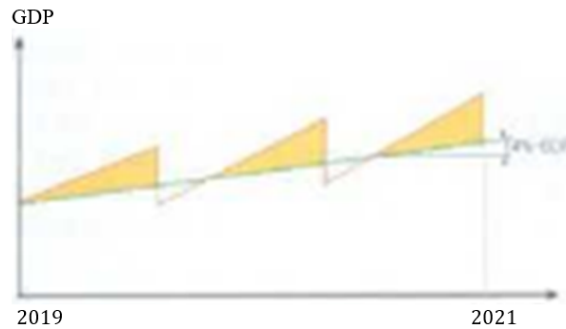


Fig. 2. Fluctuations in production

3. IDENTIFICATION OF SOURCES OF STRESS

Psychosocial sources of stress at work relate to negative influences from the psychosocial work environment such as poor planning, organization and management of work and the poor social climate in which work takes place. They can arise from the content of the work, ie the nature of the work and the conditions in which the work is performed, or from the characteristics of the work organization, or the overall work context, as systematized in the table 1.

Table 1. Sources of psychosocial risks [4]

Content and Nature of work
<p>Content of work: With clients, patients, students; lack of diversity of work tasks, short work cycles; meaningless and monotonous jobs; unused abilities and skills of workers; too much or too little workload; time pressures, unrealistic or unattainable deadlines</p>
<p>Work schedule: Shift work, night work; overtime work; inability to influence the work schedule; unpredictable working hours</p>
<p>Working conditions: Inadequate working conditions (noise, temperature, light); inadequate work equipment</p>
Relationships and characteristics of the work of the organization
<p>Organizational culture: Lack of control over work tasks and process; inability to decide on the manner and time of performing tasks; insufficient participation in decision making</p>

Control in work: Lack of control over work tasks and process; inability to decide on the manner and time of performing tasks; insufficient participation in decision making

Work role ambiguity: Not getting enough information to do a quality job

Work role conflict: Inconsistent or conflicting work requirements (work tasks, values, rules); high degree of responsibility for people, property

Relationships: Bad or conflicting interpersonal relationships; poor relationships with managers and superiors; lack of social support, isolation, harassment, threats, violence

Possibility of professional development: Career stagnation; inability to progress; low salary; job insecurity; low social value of the job

Work-family balance: Inability to reconcile private and business obligations; low level of support at home; the impact of a partner's career on family life

Stress is manifested in workers through stress reactions that can occur on an emotional, cognitive, physical or behavioral level. These reactions do not in themselves constitute damage to health, but are the first sign that some factor in the work environment causes a physically and emotionally harmful response in workers, as shown in table 2.

Table 2. Manifestation of stress through reaction [4]

Types of reaction to pressure at work

Physical reactions: sweating, headache, heartburn, chest pain, difficulty sleeping, development of mental and physical difficulties, psychosomatic reactions

Cognitive reactions: difficulty concentrating and remembering, indecision, constant anxiety, difficulty learning new knowledge and skills

Emotional reactions: irritability, restlessness, anxiety, irritability, mood swings, indifference or hypersensitivity, overload, inability to relax

Behavior, reactions: changes in appetite, increased consumption of coffee, alcohol, tobacco, destructive behavior, isolation or excessive dependence in social relationships

Stress at work is a consequence of the poor psychosocial environment in which the work takes place, ie it occurs due to the exposure of

workers to negative psychological, social and physical influences in the work environment, ie psychosocial risks. Daily exposure to psychosocial risks increases the level of stress which can manifest as physical, mental and social dysfunction in workers. Stress at work is the result of the interaction of the worker and his work environment. It arises from an imbalance between job requirements and working conditions and the knowledge, skills, physical and mental characteristics of workers. If the demands that the job places on the worker exceed his capacities and abilities to actively cope, the worker will experience a subjective feeling of stress.

4. THE ROLE OF MANAGEMENT IN COPING WITH STRESS AND ENSURING SUSTAINABLE DEVELOPMENT

Prolonged exposure to elevated levels of stress can in the long run result in impaired mental and/or physical health and well-being of workers and negative organizational outcomes. Workers who experience high levels of stress in the workplace are more likely to have physical and mental health problems, are less motivated and effective, and their safety in the workplace is compromised. As a result, the number of mistakes, accidents and injuries at work increases, workers are more often absent from work, the efficiency of the work organization decreases, while its costs increase. Therefore, management must monitor and record stress records as quality records, analyse them, make suggestions for improvement and subsequently take corrective actions.

5. MANAGEMENT'S ATTITUDE TOWARDS THE WORKER AND TOWARDS THE ORGANIZATION

Stress at work leaves numerous consequences on the worker's health, as well as on his subjective well-being. In addition to health consequences, impaired physical and mental health, stress at work leads to other negative outcomes and psychological consequences:

- Burnout at work
- Decreased job satisfaction
- Reduced work motivation
- Problems at home

At the organizational level, the following phenomena are present:

- More frequent absence of workers from work (absenteeism)
- Presence of workers in the workplace without the ability to function at full capacity (presentism)
- Increased rate of errors in work, accidents and injuries
- Reduced safety at work
- Prolonged sick leave
- Increased employee turnover
- Decreased employee loyalty to the organization
- Unproductive organizational behaviors, such as problematic behavior of workers and disturbed interpersonal relationships, irresponsible attitude towards organizational assets (alienation, destruction), etc.

Overall, these phenomena result in:

- Reduced work efficiency,
- Poorer business results,
- Increased costs,
- Endangered reputation of the organization.

The role of management is given and monitors the execution of technological operations in accordance with the organization, records omissions and "idle runs", makes proposals and correctively applies them, to ensure reduced entropy in the functioning of system cells, and thus establish a steady increase in efficiency.

Sustainability has now become an important policy issue being pursued in order to achieve concrete and long-term development. It is a process that characterizes development and commands all aspects of human life, including the provision of living conditions. Sustainability means resolving the conflict between sustaining human life and the integrity of nature. Therefore, sustainability encompasses at the same time methods for ensuring economic growth, environmental quality, energy efficiency and waste management, together with health and social equality. Basically, sustainability is the ability to sustain social and global development that seeks to change resource exploitation, the direction of investment, the orientation of technological development, and lead to institutional change to ensure consistency. Sustainable development initiatives are common at the political level

within the UN, OECD, EU and other national levels. However, the idea of sustainable development is well defined and implemented at the production macro level, but there is a serious lack of implementation practice at the applied or practical level, which puts additional pressure on managers and immediate executors of operations. Therefore, the gap between science, policy making and its implementation must be bridged, which is achieved with a previously developed strategy, Fig. 3.

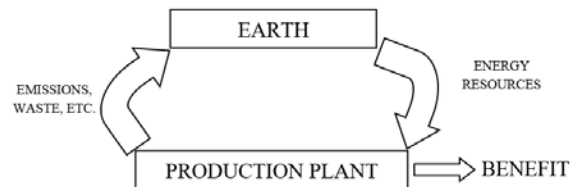


Fig. 3. Schematic presentation of sustainable development strategy [2]

6. MANAGEMENT OF THE ORGANIZATION IN CONDITIONS OF INCREASED STRESS OF PRODUCTION WORKERS

Work-related stress occurs when the demands of a job exceed the ability of a worker to continually cope with it. This is one of the most important consequences of a poor psychosocial work environment - among other things because workers who are exposed to long-term stress at work can develop a serious mental and physical health problem. Psychosocial risks related to negative psychological, physical and social outcomes resulting from unfavorable organization and management in the workplace, as well as from an inappropriate social context at work include:

- increased requirements for operations and short deadlines;
- conflicting demands and ambiguities about the role of workers;
- mismatch between the requirements and competence of workers (underestimation of workers' skills can be a source of stress, as well as their overestimation);
- non-involvement in making decisions that affect the worker and the inability to influence the way work is performed;
- independent work, especially when working with the public and clients (being a victim of third-party violence can take the form of verbal aggression, unwanted sexual

attention or threats of physical violence, or actual physical violence can be a source of stress);

- lack of support from management and colleagues and poor interpersonal relations;
- psychological or sexual harassment in the workplace (constant torture, humiliation, insult or threatening behavior of superiors or colleagues towards a worker or group of workers);
- unfair distribution of work, rewards, promotions or career opportunities;
- inefficient communication, poor management of organizational change and business insecurity;
- difficulties in reconciling business and private obligations.

It is important to emphasize that psychosocial risks should not be confused with a healthy and challenging work environment that provides support, stimulates workers and encourages their development and performance in the best possible way. [3] Why is stress and psychosocial risk management so important? Although many factors contribute to the mental health and well-being of workers, there is evidence that the workplace environment also plays a significant role. In a good psychosocial environment, work can be beneficial to workers' mental health, providing them with support in life and giving them a stronger sense of social inclusion, identity and status, an opportunity for development and increasing trust. In contrast, a poor psychosocial work environment can have significant negative effects on worker health. The process of stress depends on the perception of the situation, ie the assessment of the stress of the situation. Stress reactions occur when a person estimates that the intensity of the source of stress outweighs their coping capabilities. The term stress is avoided in the literature, and the term pressure is used because stress is seen as a negative consequence of pressure. [1]

The Pressure Management Indicator (PMI), Table 3, is a revised version of the OSI offering questions applicable to the entire working population and improving psychometric characteristics. As with other transactional models, due to complexity, empirical support is needed in order for the effects of pressure to be monitored, formula (1).

$$P = I_p \times I_r \dots\dots\dots (1)$$

P – Consequences of pressure

I_p – Sources of pressure

I_r – Individual differences

Table 3. Pressure indicators for management

Sources of pressure	Individual differences	Consequences of pressure
Workload	Striving for achievement	Loyalty to the organization
Relationships	Patience	Job satisfaction
Recognition	Personal influence	Mental well-being
Organizational climate	Control	The level of mental well-being
Personal responsibility	Coping	Resistance
Manager service	Problem-oriented coping	Concern
The balance of family business life	Balance of private and business life	Physical health
Daily difficulties	Social support	Working energy

Stress management involves assessing psychosocial risks and implementing prevention measures.

Managing stress at work generates profits at all levels.

Worker: preserved health, subjective well-being and job satisfaction

Manager: healthy, motivated, productive workers

Organization: improved overall efficiency, greater employee involvement

Society and the national economic organization: reduced costs of health care and pension system.

7. CONCLUSION

In a good work environment, workers show a high level of job satisfaction and feel encouraged and motivated to prove their potential. For the company, this results in good business efficiency and low absenteeism and worker turnover rates. The key factors that contribute to a good psychosocial work environment are:

- trained workers who have sufficient time to complete their tasks;

- minimized or divided monotonous tasks and workers encouraged to take over their jobs;
 - workers who understand exactly what is expected of them and who regularly receive constructive feedback (positive and negative);
 - workers involved in decision-making relating to their work who are encouraged to contribute to development, such as working methods and schedules;
 - fair distribution of work, awards, promotions or career opportunities;
 - a friendly and encouraging work environment that provides support and makes additional resources available when needed;
 - open and two-way communication, and workers are informed about developments, especially in times of organizational change.
- [3] Lundberg, U. Cooper, C.L. (2011). *The Science of Occupational Health: Stress, Psychobiology and the New World of Work*. Wiley-Blackwell
- [4] Brošura „Upravljanje stresom za zdrava radna mjesta” za razdoblje 2014.–2015. Evropska agencija za sigurnost i zdravlje na radu (EU-OSHA).

For an individual, the negative effects of poor psychosocial risk management include experiencing work-related stress, low mental health, increased work costs, difficulty concentrating, causing more mistakes, problems at home, drug and alcohol abuse, and poor physical health. For the organization, negative effects include poor overall business performance, more frequent absences from work, presentism (when workers come to work and when they are sick and unable to meet their obligations), and increased accident and injury rates. Absences are generally longer than those caused by other causes, and work-related stress can contribute to increased early retirement rates. Estimates speak of significant costs for business and society, and at the national level they are growing to a worrying level.

REFERENCES

- [1] Kenny, D. T. McIntyre D. (2005). Constructions of occupational stress: Nuance or novelty? In A-S.G. Antoniou and C.L. Cooper (Ur.) *Research Companion to Organizational Health Psychology*. Edward Elgar Publishing, Cheltenham, United Kingdom, p. 20-58.
- [2] Kopač, J., Pusavec, F. (2012) Benefit of Sustainable Machining, *MIT – SLIM*, Conference Fiesio, Slovenia



Banja Luka
28–29 May 2021.

DEMI 2021

15th International Conference on Accomplishments in Mechanical and Industrial Engineering

www.demi.mf.unibl.org



Analysis of the Causes of Occupational Injuries in a Production System – a Case Study

A. Helvidaa, L. Haznadarevićb, B. Vranješc, D. Adamovićd, E. Stojiljkoviće

^aArcelorMittal d.o.o Zenica, Bulevar Kralja Tvrtka I 17, Zenica, Bosnia and Herzegovina

^bCollege "Logos Centar" Mostar, Bišće polje bb, Mostar, Bosnia and Herzegovina

^cUniversity of Banja Luka, Faculty of Mechanical Engineering, Stepe Stepanovića 71, Banja Luka, Republic of Srpska–B&H

^dUniversity of Novi Sad, Faculty of Technical Sciences, Trg Dositeja Obradovića 6, Novi Sad, Serbia

^eUniversity of Niš, Faculty of Occupational Safety in Niš, Čarnojevića 10a, Niš, Serbia

Abstract *To increase the safety and reliability of production systems, it is essential that an occupational injury analysis be performed. Practice has shown that few companies, use the systems approach to analyze occupational injuries and human errors as a part of system safety assessment. Therefore, this paper discusses the efficiency of using methods for the analysis of the causes of human errors and occupational injuries in the production systems of ArcelorMittal Zenica LLC, Bosnia and Herzegovina.*

The results of the study are presented as a case study, which considers the actual scenario of regular maintenance of a high-voltage power facility in the company's energy department, when an employee suffered a severe physical trauma due to electric shock. Numerous errors and failures were identified in the said scenario and they were analyzed by means of a synergistic application of the 5 Whys method and the Ishikawa diagram.

The synergistic methodological framework for analyzing and identifying the causes of human errors and occupational injuries, whose efficacy has been confirmed in practice at ArcelorMittal Zenica LLC, is also applicable to other industrial activities.

Keywords *Occupational injury, Human error, Production system, 5 Whys method, Ishikawa diagram, Occupational safety and health.*

1. INTRODUCTION

It is imperative that any modern company should strive toward high productivity, while simultaneously creating conditions for a safe and healthy work of each employee. The best production systems are reliant on qualified and skilled workforce an on well-conceived jobs and

workplaces that are suited to the abilities of specific individuals. Accordingly, occupational safety and health is achieved through the interaction of technical, organizational, and individual (human) factors, whose proper functioning requires the application of available scientific knowledge and the integration of technology, organization, and management.

A production system is a set of technological systems and other technical, informational, and energy structures, which follow specific procedures to accomplish the set goals of the production process. It contains a multitude of

Corresponding author

Evica Stojiljković, PhD, Associate Professor
evica.stojiljkovic@znr fak.ni.ac.rs

University of Niš, Faculty of Occupational Safety in Niš,
Čarnojevića 10a, Niš, Serbia

different elements interconnected to form an integrated unit.

An occupational injury is a type of bodily harm at the level of organs due to acute exposure to energy (mechanical, thermal, electric, chemical, or radiant energy) interacting with the body and due to an amount of energy that exceeds the threshold of physiological tolerance [4]. Occupational injury refers to [10]

- any injury of the insured person caused by direct and short-term mechanical, physical, or chemical action, abrupt changes of the body's position, sudden overload of the body, or other changes in the physiological condition of the body, if such an injury is causally related to the performance of the job that forms the basis of insurance,
- any injury incurred by the insured person during the regular commute for the purpose of performing the work on the basis of which they are insured.

Examination and understanding of the causes of accidents are important for any type of improvement in the occupational safety and health management system. The causes leading to accidents can be classified as follows:

- *Direct causes*: equipment, tool, or agent that causes an injury or damages health (sharp edge, harmful substance, dust, etc.);
- *Indirect causes*: unsafe acts and unsafe conditions (absence of protective device, ventilation turned off, etc.);
- *Root causes*: failure leading to all the other deficiencies, often temporally and spatially removed from the undesired event (e.g., failure to recognize the need for training and competence assessment of employees, low risk assessment priority, etc.).

In the past, analyses of the causes of accidents focused solely on the investigation of people, even the people who were completely unrelated to the actual causes of accidents [6]. A more recent approach in accident analysis focuses on the error within the system. It is a proactive approach that primarily concerns the human factor. Instead of waiting for the accident to happen, the attention is devoted to unsafe behaviors and conditions that lead to near misses and do not result in any injury. Tremendous efforts have been made to promptly identify such errors and events, whereby workers are encouraged to actively

participate in reporting them, after which all errors are analyzed in detail in order to establish the main causes and to adopt efficient corrective measures.

This paper analyzes the production system at ArcelorMittal LLC in Zenica, Bosnia and Herzegovina, with the aim of determining the influence of human errors on the occurrence of occupational accidents and injuries.

2. PRODUCTION SYSTEM BACKGROUND

The town of Zenica is traditionally well-known for its steel production. This production process has its origins in 1892, and has been going on continuously, save for a few periods of halted production. The Zenica Ironworks truly flourished only during the 1980s, when it numbered 24,000 employees and when it reached the highest annual output of 1,870,000 metric tons of steel.

The process of integrated steel production was interrupted in the early 1990s, and the first attempts to revive production were made in September 1998 with the establishment of a joint venture, BH Steel LLC, between the Zenica Ironworks and the Kuwait Investment Authority (KIA), subsequently joined by Mittal's then LMN Group in 2004. After the merger of Mittal Steel and Arcelor in 2006, BH Steel was incorporated into the ArcelorMittal group and the integrated production process was successfully initiated two years later. ArcelorMittal Zenica LLC currently employs a little over 2,400 workers and for years it has been one of the most successful companies in Bosnia and Herzegovina, as well as one of the country's top exporters.

ArcelorMittal Zenica LLC specializes in the production and sales of steel billets and rolled steel products (multi-purpose wire rods, ribbed and round rebars as bars and coils, reinforcement mesh panels, lattice girders, and traditional construction reinforcement), made in its coke plant, sinter plant, blast furnace for molten iron, and steel plant, which also generate coal tar, ammonium sulfate, and slag as by-products. Its long tradition as a steel manufacturer, its recognizable quality of products, and its firmly established customer trust over other competitors have made the company the biggest manufacturer of long steel products in the region.

ArcelorMittal Zenica LLC is home to integrated production of iron, which comprises the primary portion of the metalworking process, specifically the coke plant, ore preparation, agglomeration, and the blast furnace, as well as the secondary portion, involving the steel plant and the rolling mills (Figure 1).

Many operations and processes within the integrated production are categorized as jobs with higher risk of injury or illness. They include numerous hazards that warrant a systems approach and the involvement of all employees in order to ensure safe work conditions.

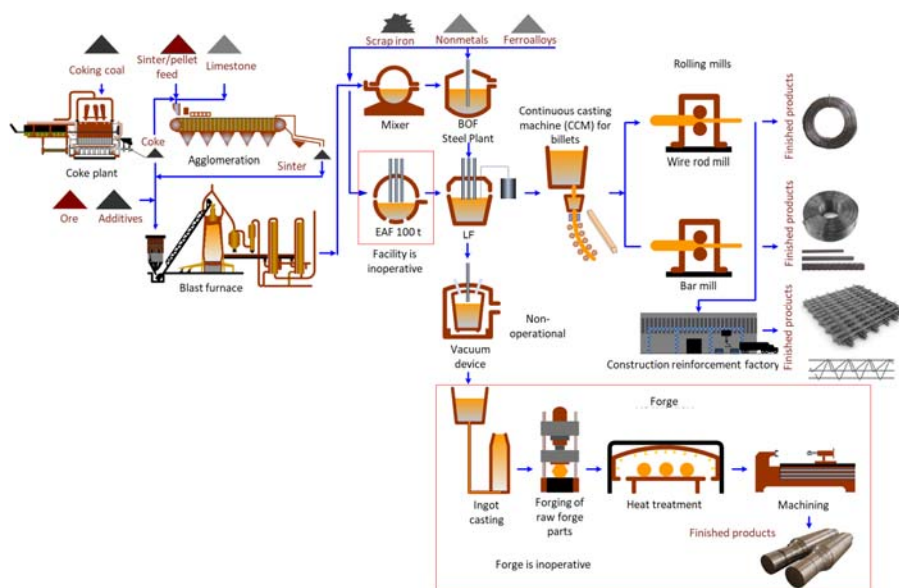


Fig. 1. Technological production lines at ArcelorMittal Zenica LLC [2]

Employees of ArcelorMittal Zenica LLC are one of the company’s most important assets, as they directly or indirectly impact the quality of products and services. Therefore, methods of managing human resources, headed by the company management, have been established. Human resource management activities have primarily been focused on establishing the capabilities of employees in terms of specific job requirements, so that every operation could be matched to a proper operator who complies with the requirements defined by the company, the customers, and the law. Accordingly, based on the system procedures and work instructions, work task descriptions have been formulated for every job within the company. This clearly defines the responsibilities and authorizations of both the management and other laborers.

Turbulent and dynamic developments in the labor market affected the hiring selection process in the company. Concerning the technical and craft occupations, the personnel

have primarily been recruited from external sources, while the high-skill personnel were recruited equally from external and internal sources. Upon analysis of the hiring process and the organizational structure of the company, particularly of the portion pertaining to occupational safety, it can be concluded that in recent years the internal sources have become dominant for recruitment, as numerous advantages over the external source have been identified, such as the following:

- the candidates are better acquainted with the technological process,
- less time is required to train and educate them for independent work,
- selection costs are lower,
- the candidates are more familiar with the risks and hazards having spent some time at jobs within the production facilities,
- motivation is improved and more positive work environment is created.

3. APPROACHES TO OCCUPATIONAL INJURY ANALYSIS

There are a number of approaches, theories, and techniques used in the analysis of occupational accidents and injuries, including the iceberg theory, the SHELL model, the domino theory, the 5 Whys method, the Ishikawa diagram, etc. (for more, see [7]).

According to the iceberg theory, unsafe work is the key component, which, combined with other unfavorable circumstances or omissions, results in an accident. That is why an analysis of such omissions and unsafe work can significantly help to reduce and prevent accidents. On the other hand, the interrelation between the technical and the human aspect also has a considerable impact on the safety of technological systems, as does their shared relation to the organizational structures of these systems [8].

This paper will describe in detail the principles of the 5 Whys method and the Ishikawa diagram, which were used in the analysis of occupational injuries at ArcelorMittal Zenica LLC.

3.1 The 5 Whys method

The 5 Whys method is an iterative technique used to investigate cause-and-effect relationships underlying any given problem. The primary purpose of this technique is to determine the cause of the problem by repeatedly asking *why* (Figure 2). Each answer leads to another question, whereby the researcher should theoretically reach a palpable solution after five simple questions [5].

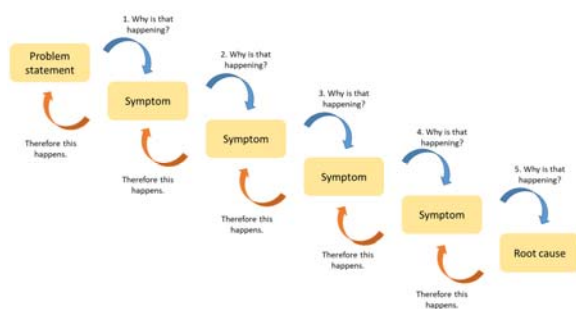


Fig. 2. The principle of the 5 Whys method

The technique was first developed by the Japanese inventor and industrialist Sakichi

Toyoda and it was used by the Toyota Motor Corporation during the development of their manufacturing methodologies. Today, it is widely used in various industry branches, as well as in risk management and causation of occupational accidents and injuries.

There are three key elements to efficient use of the 5 Whys method:

- accurate and comprehensive problem statements,
- complete honesty in answering the questions,
- resoluteness to get to the core of the issues and resolve them.

To properly implement the 5 Whys analysis, specific guidelines need to be followed:

- Get the management involved in the 5 Whys analysis. The analysis itself requires choosing a suitable number of employees or, for the more difficult cases, even involving external experts;
- Use paper or a whiteboard instead of a computer;
- Write down the problem and make sure that everyone understands it;
- Distinguish the causes from the symptoms;
- Consider the logic of a cause-and-effect relationship;
- Search for the cause, step by step, without rushing to conclusions;
- Make sure that the statements rely on facts and knowledge;
- Assess the process, not the people;
- Never leave “human error”, “worker’s inattention”, and the like as the root cause;
- Create an atmosphere of trust and sincerity;
- Keep asking *why* until the root cause has been established, i.e., the cause whose elimination will prevent the error from recurring.

3.2 The Ishikawa diagram

The fishbone diagram or the Ishikawa diagram (also the cause-and-effect diagram), is a tool for visualizing and categorizing potential causes of accidents/incidents in order to identify the root causes according to their degree of importance and form the hierarchy of events (Figure 3).

The initial concept was first used in the 1920s and it is considered one of the seven basic tools of quality control. The diagram was popularized

during the 1960s by Kaoru Ishikawa, who introduced quality management processes in the Kawasaki shipyards, thus becoming one of the pioneers of modern management [9]. It soon became widely used in other industry branches, including risk management and occupational safety.

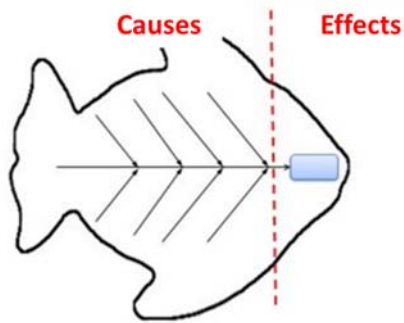


Fig. 3. Ishikawa diagram basic template [9]

The left side of the diagram is usually where the causes of an accident are shown. The identified causes are then categorized. The right side of the diagram shows the effect, which is defined as the problem for which the cause is to be identified.

The cause-and-effect diagram is formed over six steps [3]:

- *Defining the problem to be examined* – when the problem is properly defined, it is written inside the box on the right-hand side of the diagram;
- *Defining the main categories of the problem causes* – after the problem statement is placed in the diagram, the main categories of the causes are defined on the left side and connected to the “backbone” in the diagram. A production environment includes the following categories: machine/equipment, method, material, and people. A service-providing organization would thus include the categories of policy, procedure, facility, and people;
- *Brainstorming* – consideration of the causes is a phase that requires the most effort in the formation of an Ishikawa diagram. Some people prefer generating a list of all causes before any other steps so as to enable a flow of ideas without limiting the main categories of the causes. However, sometimes the main categories of the causes are used as catalysts for new ideas.

This is particularly useful when the idea flow begins to slow down;

- *Categorizing the causes of the problem* – when the list of causes has been generated, they are placed within the corresponding category in the diagram. Ideally, every cause should be placed within a single category, but there are causes, such as “people” that can belong to multiple categories;
- *Determining the underlying causes* – each cause in the diagram is further analyzed to determine if there is a root cause for a given aspect. This is achieved by asking the question: “Why is that happening?” This step may be repeated multiple times until the root cause has been identified;
- *Identifying the root causes* – this is the final step in the formation of a fishbone diagram. The step can be completed in several ways: searching for recurring causes, choosing the causes by means of a group consensus, choosing the causes according to their frequency of occurrence, etc.

4. THE CASE STUDY

A combination of the 5 Whys method and the Ishikawa diagram was used to identify human errors and analyze occupational injuries at ArcelorMittal Zenica LLC. The analyzed scenario involves the case of routine maintenance of a high-voltage (HV) power facility, specifically a 6.3 kV 2/III load cell installed inside the “Jug” substation, Energy Department, during which a severe physical trauma occurred due to electric shock.

An internal investigation of the occupational injury established that the planned tasks of inspection and cleaning of the 6.3 kV 2/III load cell were performed by employees from the company’s Energy Department according to the issued work order. The tasks are considered as regular and routine and, according to the internal procedures, they do not require additional risk assessment, because all risks and hazards are already included in the risk assessment for the positions of assistant substation operator and substation operator (‘switchman’), whose duties include the said tasks [1].

Preparations were made to secure the work location and to ensure safe operations in keeping with the current legislation and the

internal codes of ArcelorMittal Zenica LLC. The procedure went as follows [11]:

- a work order was issued defining the tasks and designating the crew leader and the crew,
- an order was issued for manipulation in the HV power facility,
- the busbar section disconnecter was switched off from the 2/III load cell and the auxiliary power was turned off,
- voltage check was performed on the 2/III load cell and it was determined that the cell was not live,
- the load cell's section disconnecter was locked,
- busbars were short-circuited to earth using jumpers,
- the substation operator placed the keys to the locked isolation points inside the isolation locks and key storage box,
- the crew members secured the storage box with their personal locks.

After the preparation procedures, the crew leader received the permission to fulfil the work order from the dispatcher and notified the other crew members, upon which they began performing their tasks.

The 2/III cell was originally designed by a company called Energoinvest in 1975. It contains two separate parts – one for the power cell and another for the load cell. In the normal operating mode, the two parts are separated by a protective panel that prevents voltage transfer between the two parts.

On the day of the accident, the 2/III load cell was the item to be worked on, and its power was turned off, as confirmed by a light-emitting indicator. The workers performing the task, who had been employed at the company for 10 months at the time (5 months on low voltage jobs and 5 months on high voltage jobs), did so under the supervision of an experienced crew leader – the substation operator, who had been at the company for 12 years. Since the power cell was not to be worked on, it was separated from the 2/III load cell by a protective panel while under a constant voltage of 6.3 kV, which was in keeping with the procedure. However, due to insufficient understanding of the work task, the soon-to-be-injured worker initiated the removal of the protective panel, thus creating unsafe work conditions that resulted in an occupational injury. Due to the specific

construction of the protective panel, the worker asked for the assistance from the substation operator, who complied by mistake.

After the removal of the protective panel, no one checked if the section busway inside the power cell was live. With the intention to clean the HV isolator, the soon-to-be-injured worker touched the section busway at 6.3 kV, receiving an electric shock and severe physical trauma.

Following the accident, an investigative team was formed, which conducted an analysis by observing the actual state in the field, collecting the facts from the accident site, interviewing the workers, and inspecting the following internal and external documents:

- the permit to enter the HV power facility,
- the work order,
- the order for the manipulation inside the HV power facility,
- work license,
- instructions for the manipulation and provision of no-voltage conditions,
- the single-line diagram, the work order records, and the daily reports,
- the "Isolation and Lockout" procedure of the quality system,
- the reports on safe work knowledge tests,
- the reports of periodical medical examinations of the employees involved in the accident,
- Regulation on Occupational Safety during the Use of Electric Current, "Official Gazette of the socialist republic of Bosnia and Herzegovina", no. 34/88,
- Law on occupational Safety, "Official Gazette of the socialist republic of Bosnia and Herzegovina", no. 22/90.

Occupational safety and health management at ArcelorMittal Zenica LLC is regulated, among other things, through the implementation of the corporate Fatality Prevention Standards (FPS). "Incident Investigation" is one of the more prominent standards, which is implemented in the event of an occupational injury, either severe or fatal.

After the investigation team was formed, the investigation of the occupational injury in "Jug" substation involved the following steps:

- collecting information,
- asking questions and conducting interviews,

- identifying the root causes using root cause analysis (RCA) and critical decision analysis (CDA),
- defining efficient preventive and corrective measures.

The present approach to the analysis of occupational accidents and injuries is based on the abovementioned elements of an accident investigation, whereby human error analysis is seen as a part of critical decision analysis, as an integral part of the investigation and not as a separate element that requires detailed analysis. A critical decision is a decision (or

action) made in hazardous or emergency situations. When the root cause analysis determines that a critical decision has been made, the next follow-up question to ask is “What did the person plan to do?” This helps to understand the type of decision or action that caused the effect and that can lead to a further analysis of the main behavioral factors.

The design of the cause-and-effect diagram (Figure 4) ensued after the accident investigation team had collected all the relevant facts concerning the occupational injury and after an interview with the employees involved in the accident.

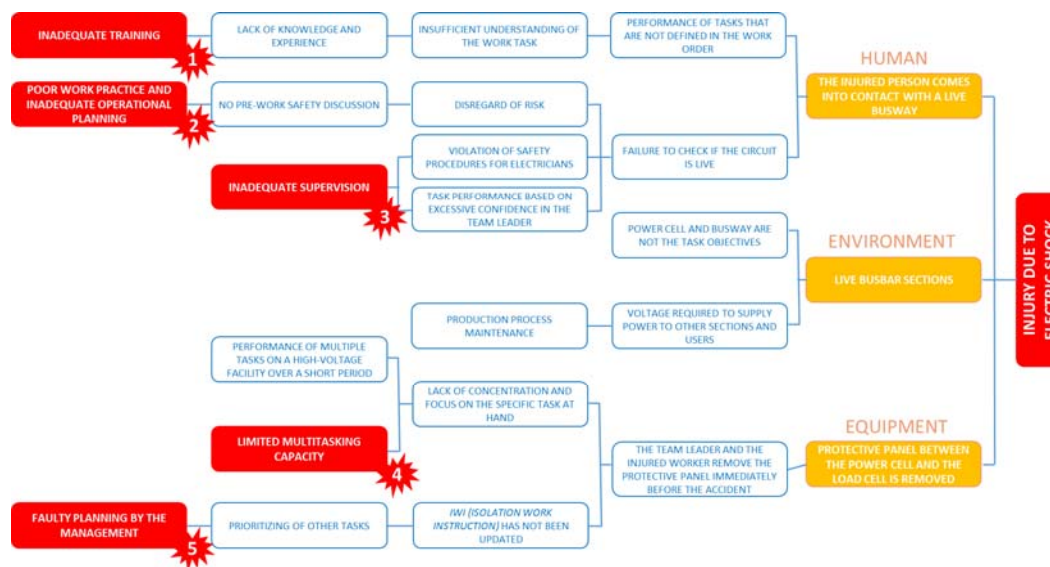


Fig. 4. Cause-and-effect diagram and the results of accident investigation [11]

The first element to be defined was the research problem, i.e., the effect – severe physical trauma due to electric shock (shown on the far right of the diagram). After that, the three direct causes of the occupational injury were determined within the three categories:

- *HUMAN* (the injured person comes into contact with a live busway);
- *ENVIRONMENT* (live busbar sections);
- *EQUIPMENT* (protective panel between the power cell and the load cell is removed).

The following step in the analysis of the cause of occupational injury involved the use of the 5 Whys method, whereby the root cause for each of the three aforementioned categories was identified by asking the question *why* (the left portion of the diagram).

After the analysis, the following causes were identified:

- inadequate training,
- poor work practice and inadequate operational planning,
- inadequate supervision,
- limited multitasking capacity, and
- faulty planning by the management.

According to the results of this study, it can be concluded that the root causes in the *human* category include inadequate training, poor work practice, inadequate operational planning, and inadequate supervision. Analysis of the *environment* did not reveal any root causes that could have led to the operator error, whereas the analysis of *equipment* indicated that there were errors concerning limited capacity of the

operators for multitasking as well as faulty operational planning by the management.

5. CONCLUSION

Human error cannot be seen solely as the lack of operator's attention that can result in an accident, but as a phenomenon that is a reflection of deeper issues in the system and a result of relations within the system between humans, tools, tasks, and the work environment. There is also the fact that people do not only manage buildings, facilities, and processes – it is they who also designed, built, and maintained them in the first place. Thus, there is ample room for people to contribute to the occurrence of accidents. This is why various technical solutions, business models, corporate strategies, rules, and regulations can help improve any specific work process. Therefore, a complete understanding of the multitude of roles people occupy in the work process and of the factors that contribute to people's decision making is crucial for accident prevention and operational efficiency through reduction of risk, elimination of any shortcomings, and successful maintenance of the production process.

Bearing in mind the previous discussion, it becomes apparent that the choice of methodology for the analysis, identification, and reduction of human error is a vital aspect of managing a production system. In order to gain insight into the efficiency of the methods and their applicability in the production system, we conducted a study at ArcelorMittal Zenica LLC steel company in Bosnia and Herzegovina, applying the 5 Whys method and the Ishikawa diagram.

The obtained results showed that the analysis of an occupational injury using the said methods provides a good graphical representation of the relationship between the causes and the effects, which facilitates the understanding of all factors leading to the accident. The approach based on team work and discussion can help distinguish the symptoms from the causes, which in turn simplifies the definition of corrective measures. The main drawback of these methods is that they do not offer a predefined classification of human errors and require considerable implementation time, which can prove particularly tiresome for the investigators. In addition, these methods analyze the role of the human factor primarily through the example of

an injured worker, whereas they only partially consider the involvement of other workers who directly perform the work tasks. Another issue is the fact that there are no registries or records of human errors (based on the analyses of previous injuries) to create a clearer picture of the causes of occupational accidents and injuries and, consequently, to provide quality guidelines on how to prevent future accidents.

Acknowledgement

The authors would like to express gratitude to the Ministry of Education, Science and Technological Development of the Republic of Serbia for financial support to these researches.

REFERENCES

- [1] Helvida, A. (2020). *Analiza uzroka ljudskih gresaka i povreda na radu u proizvodnom sistemu*. (In Serbian). MSc Thesis. Univerzitet u Nišu, Fakultet zaštite na radu u Nišu.
- [2] Interni dokument kompanije ArcelorMittal d.o.o Zenica: *Poslovnik sistema upravljanja kvalitetom, okolinom, zdravljem i zaštitom*.
- [3] Ishikawa, K. (1976). *Guide to Quality Control*. Asian Productivity Organization, Tokyo.
- [4] Krug, E. (1999). *Injury: A Leading Cause of the Global Burden of Disease*. Geneva: A WHO Monograph. From: http://www.who.int/violence_injury_prevention/index.html, accessed on: November 29, 2010.
- [5] Olivier, S. (2009). *The Five Whys Technique*. Knowledge Solutions, Manila.
- [6] Petz, B. (1987). *Psihologija rada*. Školska knjiga, Zagreb.
- [7] Stojiljković, E. (2011). *Metodološki okvir za procenu ljudske greške*. (In Serbian). PhD Theses. Univerzitet u Nišu, Fakultet zaštite na radu u Nišu.
- [8] Stojiljković, E. (2020). *Procena ljudske pouzdanosti*. (In Serbian). Monografija nacionalnog značaja. Univerzitet u Nišu, Fakultet zaštite na radu u Nišu.
- [9] Tague, N. (2014). *Seven Basic Quality Tools*. American Society for Quality, Milwaukee, Wisconsin.
- [10] Zakon o penzijskom i invalidskom osiguranju Federacije BiH 13/2018.
- [11] Zapis o internom uviđaju povrede na radu u TS „Jug“, departman Energetika, ArcelorMittal d.o.o Zenica.

CIP - Каталогизација у публикацији
Народна и универзитетска библиотека
Републике Српске, Бања Лука

621.3(082)(0.034.2)
621(082)(0.034.2)

INTERNATIONAL Conference on Accomplishments in Mechanical and Industrial Engineering (15 ; 2021 ; Banja Luka)

Proceedings : DEMI 2021 / [15th international conference on accomplishments in mechanical and industrial engineering, Banja Luka, May 2021 ; editor in chief Stevo Borojević]. - Onlajn izd. - El. zbornik. - Banja Luka : Faculty of Mechanical Engineering, 2021. - XVIII, 472 str.

Način pristupa (URL): <https://demi.mf.unibl.org/wp-content/uploads/2021/06/ZBORNIK-RADOVA-DEMI-2021-PROCEEDINGS.pdf>. - Насл. са насл. екрана. - Опис извора дана 11.06.2021. - Библиографија уз сваки рад.

ISBN 978-99938-39-92-7

COBISS.RS-ID 132978433



ISBN 978-99938-39-92-7